Author:
Apostolaki, Naomi

Title:
The evolution of pneumaticity in Sauropodomorpha and its correlation to body size

Author:
Apostolaki, Naomi

Title:
The evolution of pneumaticity in Sauropodomorpha and its correlation to body size

The evolution of pneumaticity in Sauropodomorpha and its correlation to body size

Naomi-Eva Apostolaki

A dissertation submitted to the University of Bristol in accordance with the requirements of the degree of Doctor of Philosophy in the Faculty of Science.

Department of Earth Sciences
University of Bristol
October 2018

Supervisor
Prof. Michael J. Benton

Word count: 105,881

Abstract

The superfamily Sauropodomorpha comprised some of the largest terrestrial herbivorous vertebrates that have ever walked on this planet. The study of these fascinating beings has been at the forefront of palaeontological research throughout the years. Especially in the last 20 years, due to the advent of modern techniques and technologies, significant steps have been made towards our understanding of their physiology. One of the sauropodomorphs' central morphological characteristics is the expression of postcranial skeletal pneumaticity (PSP), a condition that is also expressed in the other superfamily of the order Saurischia, the Theropoda, as well as in their extant relatives, the Avians. This condition remodels the vertebrae and, occasionally the girdles and appendicular elements, producing perforations, depressions, excavations, cavities and internal chambers. This is a result of bone invasion and resorption from the development of the lung-air sac diverticula of the respiratory system. The various forms of this expression have been addressed across all subfamilies of sauropodomorphs mostly from an evolutionary aspect and, recently, from a developmental scope too. The resulting hypotheses state that PSP may have acted as a mechanism for weight reduction, allowing for sauropods to attain large sizes without having to suffer analogous gravitational constraints from equally attained masses. Any possible associations, though, between the expression of pneumaticity and body size have not been put under test. Through this study, a method of quantification and categorisation of PSP, and therefore, classification of the sauropodomorphs which express it, is created from the data retrieved from 61 taxa across all subfamilies, permitting us not only to trace any correlation between PSP and metric size data (body mass and body length) but also to visualise the evolution of PSP throughout Sauropodomorpha. This classification scheme from highest to lowest expression of PSP, 'Alpha', 'Beta', 'Gamma', 'Delta', and 'Epsilon' stems from the numerical estimate of pneumaticity in terms of a percentage, called the Pneumaticity Degree Index (PDI%). The revised scheme, Pneumaticity Degree Index (PDI%), takes account of the number of vertebral elements that are pneumatized in a single vertebra, the nature of pneumaticity traits, as well as the intensity of pneumatization in different body regions of interest (e.g. vertebral column), resulting in an integral and comprehensive measure of PSP. The proposed method ranks each pneumaticity trait with a value from 1 to 5 with 1 (100%) representing the most invasive unambiguous trait (e.g. camellae) and 5 (~ 10%) the least invasive and most ambiguous trait (i.e. fossa). By adding and dividing by their number all of the observed traits of every available vertebra of a region we retrieve a decimal numeric outcome and this outcome is translated to a percentage. The total average pneumatization of any taxon is calculated by retrieving the total average of the pneumaticity from all available body regions. In this study, only vertebral and pelvic elements were used for the retrieval of

pneumaticity data since they are the most frequently exhibiting pneumatic traits in comparison to pectoral and appendicular elements. Results show that the total average PDI% range of basal Sauropodomorpha is 0%-59%, of the non-neosauropod Eusauropoda is 23%-90%, of Diplodocoidea is 45%-73%, of Macronaria is 45%-92% and of Somphospondyli is 46%-94%. The most pneumatized vertebral landmarks are the centrum, neural arch and neural spine. The vertebral regions most commonly pneumatized are the cervicals and dorsals. No genus or subfamily of sauropodomorphs ever reaches 100% pneumatization in all vertebral regions. Furthermore, PSP is not always positively correlated with mass, rather its expression is mostly correlated with length. Taxa with low or high masses may exhibit either low or high PDI's. In addition, increasing progression of the extent and expression of PSP occurs mostly on a subfamilial level and less throughout the entire lineage. Finally, modelling calculations result in an Ornstein-Ulenbeck with an early burst progress of the expression of pneumatisation in sauropodomorphs. After that, the expression proceeds relatively steadily throughout the entire superfamily. The biotic causes of PSP are still unclear, as it could be an artefact of inheritance and genetic drift throughout speciation events. The pneumatization degree index (PDI%) is a means of quantifying and categorising pneumatization in any archosaurian taxon that is faster and cheaper, though less accurate, than CT scanning. It is more precise than the Pneumaticity Index since it integrates a wider selection of the qualities and osteological characteristics of pneumaticity we want to measure, provided that the bone under study is at least 50% free of matrix.

Dedicatory

I dedicate this PhD thesis and its journey to my beloved parents, Kalliopi Voikou and Theocharis Mike Apostolakis, to whom I am immensely grateful for their enormous dedication and precious support towards the fulfilment of my childhood dream to become a dinosaur palaeontologist.

Acknowledgements

First and foremost, I want to wholeheartedly thank my dear supervisor and mentor, Mike Benton, for his untiring patience in providing me with advice, guidance, aid, feedback and support whenever I needed it most. His exemplary presence was inspirational to my academic ‘upbringing’ throughout my years of studying in the University of Bristol. I am grateful to Mary Benton, Ember Kelly and Guy Molloy for their aid and support, especially in giving me the opportunity to work in a rewarding part-time job as a Disabilities Support Worker which enabled me to cover my expenses during the course of my studies in Bristol. I also want to thank the people in the Exams Office for providing me with additional work opportunities as an examinations invigilator. I am also grateful to Emily Rayfield, Manabu Sakamoto and Gavin Thomas as well as to my progress reviewers Phil Donoghue, Phil Anderson and Davide Pisani for their helpful input as well as for driving me to develop confidence and skills as a ‘growing’ academic. Some important parts of this thesis would not have been completed without the aid of my colleagues Mark Puttick, David Button, Max Stockdale, Tom Stubbs, Albert-Prieto Marquez, Graeme Lloyd, Mathew Wedel, Jeffrey Wilson, Blair McPhee and Adam Yates. Special thanks to Paul Barrett (Natural History Museum, London), Niels Knotscke (DinoPark in Münchehagen, Hannover), Daniela Schwarz, Oliver Wings (both in Humboldt Museum für Naturkunde, Berlin) and Claudia Hildebrandt (University of Bristol) for their hospitality and for providing me with access to specimens needed for the completion of this project. In addition, I am grateful for the constructive comments made by my examiners Emily Rayfield and Paul Upchurch which greatly improved the final version of this thesis. Furthermore, I feel much obliged to the authors and journals for permitting the re-use of their published material (Figs. 1, 2, 6–8), namely Mathew Wedel and Jeffrey Wilson, as well as *PLoS ONE* and *Acta Paleontologica Polonica* which act under CCBY 4.0 protocol. Also, the completion of this journey would not have been successful without the support of my friends Stavros, Stefania, Thomas, Alexis, Akis, Richard, John, Giuseppe, Guillermo, Ioanna, James, Michalis and Mary. Last but not least, the inspiring music of the gifted composers Steve Jablonsky, John Williams, James Horner, Hans Zimmer, James Newton Howard, Vangelis, Trevor Jones, Michael Giacchino, Lorne Balfe,

Howard Shore, Danny Elfman, Brad Fiedel, Enya, Ramin Djawadi, Blake Neely, John Paesano, Trevor Morris and Klaus Badelt has given me strength and empowered me to overcome the daily difficulties in Bristol for the past seven years.

Author’s declaration

I declare that the work in this dissertation was carried out in accordance with the requirements of the University's Regulations and Code of Practice for Research Degree Programmes and that it has not been submitted for any other academic award. Except where indicated by specific reference in the text, the work is the candidate's own work. Work done in collaboration with, or with the assistance of, others, is indicated as such. Any views expressed in the dissertation are those of the author.

20/10/2018

Table of Contents **page no.**

Author's contact: Naomi.Apostolaki@bris.ac.uk

List of Figures

Chapter 2

Chapter 3

Chapter 4

Chapter 5

List of Tables

Chapter 1

Chapter 2

Chapter 3

Chapter 4

Chapter 5

Chapter 1 – Introduction to postcranial skeletal pneumaticity in Sauropodomorpha and its correlation to body size

1.1) Introduction to avian and dinosaurian postcranial skeletal pneumaticity (PSP)

Pneumaticity has long being recognised as a key attribute of the bones of birds, and classic accounts by early anatomists, such as Hunter (1774) and Müller (1908), addressed the differences that distinguish pneumatised from non-pneumatised bones. These researchers focused on recognising the characteristics of osteological pneumaticity in extant birds and stated the traits that do not fossilize, such as the vascular system, the oily nature and the colour. During the ontogeny of most extant birds, the air sac diverticula that originate from their lungs and air sacs, expand, attach and invade elements of their postcrania, resulting in aeration, resorption and restructuring both the exterior and interior aspects of the bone, namely, the cortical and the cancellous (Witmer, 1990; O'Connor, 2004; Apostolaki et al., 2015). This postcranial skeletal pneumaticity (PSP) is expressed and characterised by the variable levels of pneumatisation of particular sets of bones of the postcranial skeleton like the vertebrae, girdles and appendicular elements by specific air sac diverticula. The air sacs in the neck region pneumatise the cervical and thoracic vertebrae and their associated ribs (O'Connor, 2004, 2009). The air sac in the clavicular region pneumatises the humerus, sternum, sternal ribs and pectoral girdle, whereas the air sacs in the abdominal region pneumatise the posterior thoracic vertebrae, the pelvis, and the hind limbs. On the contrary, the anterior air sacs of the thoracic region do not invade, and thus do not pneumatise, any skeletal parts of the postcrania (Carrier and Farmer, 2000; Wedel, 2003). As the embryo develops, the newly-formed pneumatic diverticula penetrate the bone through osseous sutures in the cortical bone (O'Connor, 2004, 2006). As the diverticula invade in the medullary cavity, they replace the bone marrow with air sac epithelium. (O'Connor, 2004). This process is well documented in the literature but the biotic drivers behind it have not been clarified yet (O'Connor, 2009).

Britt's (1993, 1997) work was paramount in listing the characteristic pneumatic features identifiable in both avian bones and dinosaurian fossil bones. These include foramina with prominent lips that are distinguishable from vascular openings, foramina that lead into large internal chambers, fossae with crenulated feel, soft or crenulated furrows and bones with thin cortices. In modern birds, there is an association between the aforementioned pneumatic features and the air sac diverticula (Britt 1993; O'Connor, 2009). The presence of the aforementioned pneumatic features in the bones of

sauropods, theropods, and pterosaurs is considered to be unequivocal evidence of pneumaticity (Seeley, 1870; Cope, 1877; Marsh, 1877a; Janensch, 1947; Romer, 1966; Britt, 1993, 1997; O'Connor, 2006).

The vertebrae and girdles of the ornithischian dinosaurs do not, usually, bear evidence of PSP (Britt, 1993, 1997; Wedel, 2007). However, Butler et al. (2012) noticed laminated fossae and foramina in the neural arches of the dorsal vertebrae of both *Erythrosuchus,* an Early Triassic archosauromorph, as well as in the Lower Jurassic thyreophoran ornithischian *Scelidosaurus harrisonii.* Butler et al. (2012) also noted the existence of multiple foramina lying within the postzygapophyseal-centrodiapophyseal fossa. Norman (1986) and Norman and Barrett (2002) have observed similar features in the iguanodontoid *Mantellisaurus atherfieldensis* from the Early Cretaceous. In particular, its dorsal vertebrae exhibit laminated fossae with foramina which are walled dorsally by the postzygodiapophyseal laminae and anteroventrally by a posterior centrodiapophyseal lamina. These observations are similar to those found in *Erythrosuchus* and *Scelidosaurus harrisonii* (Butler et al., 2012).

The thoracic vertebrae of the Late Triassic theropod taxa *Herrerasaurus* and *Staurikosaurus* possess laminated fossae while their vertebrae in the cervical and caudal regions are not pneumatic. Workers such as Britt (1993, 1997) and Apostolaki et al. (2015) have suggested that the existence of pneumatic diverticula may be deduced by the presence of laminae, although, when found alone, fossae and laminae are not unambiguous proof of an animal possessing an avian-style respiratory system (Wedel, 2003; Butler et al., 2012). PSP has also been found and studied in many members of Neotheropoda (Britt, 1993; O'Connor & Claessens, 2005; O'Connor, 2006; Sereno et al, 2008; Benson et al, 2012) and the extent of its expression has been thoroughly addressed by Britt (1993) and Benson et al. (2012). PSP appears to have been present within Neotheropoda (Britt, 1993; O'Connor & Claessens, 2005; Benson et al, 2012) as well as in Triassic theropods such as *Coelophysis bauri* (Colbert, 1989; Britt, 1993) and *Liliensternus liliensterni* (O'Connor & Claessens, 2005), although Benson et al. (2012) cast doubt on the pneumatic nature of the features found in *L. liliensterni*. *Tawa,* described by Nesbitt et al. (2009) and positioned as the sister taxon to Neotheropoda, was observed to possess pneumatic pleurocoels in its cervical vertebrae. Based on its phylogenetic position and pneumatic characters, the researchers concluded that PSP must have evolved prior to the origin of Neotheropoda. Most theropods like *Abelisaurus* and *Allosaurus* possess advanced pneumatic traits in their vertebrae such as laminated fossae and foramina as well as foraminous fossae (Sereno et al., 2008). Benson et al. (2012) has demonstrated the gradual expression of vertebral pneumatisation throughout phylogeny, which begins in the dorsal vertebrae and expands anteriorly to the cervical vertebrae and

posteriorly to the sacral and caudal vertebrae. This pattern is also recognized in sauropods, as discussed throughout this present study.

1.1.1) Studies on PSP in Sauropodomorpha

In Sauropodomorpha, the presence and extent of pneumaticity has been thoroughly documented (e.g. Britt, 1993; Britt, 1997; Wedel, 2003a; Wedel, 2003b; Wedel, 2005, 2007, 2009). Early sauropodomorphs (termed as basal sauropodomorphs) have never been found to possess unambiguous evidence of pneumaticity (Britt, 1993). Nevertheless, the blind excavations (fossae) found on the basal sauropodomorph vertebrae may have been initially pneumatic or that they may be evolutionary precursors of pneumatic cavities such as pleurocoels (Britt, 1993; Wedel et al., 2000a,b; Wedel, 2003a; Wedel, 2003b; Wedel, 2005). Pneumaticity features are poorly expressed in basal sauropodomorphs, if present, and become more elaborate in eusauropods. Evidence for PSP in basal sauropodomorphs was reviewed by Wedel (2007) and he noted that the prezygapophyseal-centrodiapophyseal, postzygapophyseal-centrodiapophyseal and centrodiapophyseal fossae (Wilson et al., 2011) of the neural arches of their presacral vertebrae were laminated but blind. These bony ridges that usually 'connect' two vertebral landmarks are often associated with pleurocoels, foramina and fossae (e.g. Wedel et al., 2000; Wedel, 2009; Wilson et al., 2011; Apostolaki et al., 2015). The vertebrae of sauropods, theropods and occasionally of birds may possess laminae that have anterior, middle and posterior expressions, create lattice-like forms and interconnections, or the vertebrae may even have isolated laminae (Wilson, 1999; Wilson et al., 2011). Such examples include the pre-and postspinal laminae while other similar isolated laminae may exist on the centra of avian and dinosaurian vertebrae (Apostolaki et al., 2015).

Many basal sauropodomorphs (e.g. *Plateosaurus, Thecodontosaurus,* and *Eucnemesaurus*) bear laminated fossae in their posterior cervical and anterior dorsal vertebrae, which increase in complexity and expression as we approach the Sauropoda proper (Yates et al., 2012). Most basal sauropodomorphs do not bear unambiguously pneumatic postcrania (Britt, 1993; Wedel, 2007) like *Pantydraco* which possesses prominent depressions on its cervicals; a rather ambiguous piece of evidence of PSP (Galton et al., 2007; Wedel, 2007). The majority of the vertebral fossae in basal Sauropodomorpha are not invasive and, thus, are not a certain indication of pneumatization (Wedel, 2007). The early sauropodomorphs *Panphagia protos* and *Eoraptor* lack evidence of PSP (Martinez & Alcober, 2009; Martinez et al., 2011). Yates et al. (2010, 2011, 2012) corroborated many such observations by documenting the presence of PSP in many taxa spanning from non-sauropod sauropodomorphs to basal

sauropodomorphs as well as the eusauropods and neosauropods. The vertebrae of most derived macronarians and somphospondylans are almost completely camerate and camellate, respectively. Wedel et al. (2000a,b) and Wedel (2003) discussed extensively the nature of these pneumatic features, including their variant forms (semicamerate, semicamellate) among sauropod lineages. The internal structure of a camerate vertebra is composed of few and large air-filled chambers separated by thick walls whereas a camellate vertebra possesses a 'honeycomb' - like internal structure composed of many and small air-filled chambers separated by thin walls. King (1957), Hogg (1980, 1984) and Wedel et al. (2000*a,b*) have proposed that the possible reason for this extensive intraosseous pneumatisation lies in the ontogenetic remodelling of the internal structure of the bone by the pneumatic diverticula. Large chambers, often called “pleurocoels”, as well as various combinations among foramina, fossae, laminae and pleurocoels (see Figures 1-6 and Table 3 in Chapter 2) are evident in cervical, dorsal and even in sacral and caudal vertebral regions of sauropods such as *Apatosaurus* and *Diplodocus*. (Upchurch, 1993; McIntosh et al., 1996; Taylor and Wedel, 2013).

In addition, sauropods not only possess pneumatic vertebrae, but also pneumatic ribs (Seeley, 1870*a*; Cope, 1877; Marsh, 1877a; Janensch, 1947, 1950; Romer, 1966; Wilson, 1999). Vertebral and costal PSP (Wilson, 1999; Lovelace et al., 2007; Sereno et al., 2008) has been independently developed in many diplodocoids, macronarians and somphospondylans, in their precaudal (Wedel, 2003*b*; Schwarz & Fritsch, 2006) as well as their caudal (Britt, 1997; Sanz et al., 1999; Wedel, 2003*a*) regions. Even non-neosauropod eusauropods such as *Jobaria* (e.g. Poropat et al., 2016) possess pneumatic presacral vertebrae (Sereno et al, 1999; Wedel, 2003*b*). Pneumatic girdles are rare. However, some somphospondylans (Powell, 1992; Sanz et al., 1999) like *Saltasaurus* (e.g. Powell, 1992; Cerda, Salgado & Powell, 2012; Zurriaguz & Powell, 2015; Zurriaguz & Cerda, 2017) possess ilia with a camellate internal structure and the diplodocoid rebbachisaurid *Amazonsaurus* has been noted to have a camerate ilium (Carvalho, Avilla & Salgado, 2003). Wedel (2005) proposed a method to calculate the air proportion within a vertebra, called Air Space Proportion (ASP), and estimated that highly pneumatised sauropod vertebrae could be comprised of at least 50% air, and this estimation was found to be similar to that of avian limbs and vertebrae. The ASP is a measure of the volume of an individual bone occupied by air space in proportion to the whole bone, estimated from a cross section or CT slice of the element. The ASP method could be used to calculate the entire pneumaticity of a vertebra if a 3D reconstruction is available. Practical drawbacks, though, lie in the assumption that the vertebra under examination is complete and easy to handle and transport. Most fossil vertebrae are fragmented by taphonomic processes during burial. Further, the internal surfaces and chambers that are pneumatic

may not be symmetrical, smooth, or isolated. Initial hypotheses regarding the evolution and function of such an aerating mechanism in the bones of sauropods revolved around the lightening of the skeleton which, in turn, would pave the way for them to acquire gigantic sizes without the consequential analogous increase in gravitational pull due to the increase in mass. So, PSP would allow the increase in body size while maintaining the mass at lower than expected levels (Cope, 1877; Janensch, 1947; Britt, 1993; Schwarz et al., 2007). It has also been suggested that penetration of the bones by the pneumatic diverticula could act as an adaptation to reduce the animal's weight as well as to support and stabilise the evolution of very elongated necks (Wedel, 2003*b*; Schwarz et al, 2007a; Sander et al., 2011; Taylor and Wedel, 2013), though more rigorous biomechanical tests need to be performed to test this suggestion. Researchers now believe that weight reduction was probably not the main driver for the evolution of PSP (Wedel, 2003a, 2006) and that PSP have been exapted as a means of weight-saving in these giant dinosaurs. However, this supposition has not been tested and, indeed, current methods of quantifying PSP have only assessed the total volume of such spaces in the vertebrae or other elements in a handful of sauropodomorph taxa (e.g. *Diplodocus*; Wedel, 2005).

PSP has been the only skeletal evidence thus far to indicate the presence of pneumatic diverticula in sauropodomorphs (Britt, 1993 & 1997; Wedel, 2003a, 2009; O'Connor & Claessens, 2005; O'Connor, 2006; Benson et al., 2012; Butler, Barrett & Gower, 2012; Yates, Wedel & Bonnan, 2012). Recently, Lambertz, Bertozzo & Sander (2018) demonstrated that the histology, on a microscopic level, of the secondary trabecular and endosteal tissue of the pneumatic vertebrae of sauropods and birds reveals a particular form of bone (termed 'pneumosteum') that is affiliated with pneumatic diverticula. This work and the evidence it provided could be the basis of a complete reappraisal of pneumaticity in sauropodomorphs, carried out in future studies. PSP appeared multiple times across the phylogeny (e.g. Upchurch, 1998), in variable expressions of form but also in locations in the skeleton (e.g. Wedel, Cifelli & Sanders, 2000a, b; Wedel, 2003a, b; Schwarz & Fritsch, 2006; Schwarz, Frey & Meyer, 2007; Wedel & Taylor, 2013).

This variable occurrence of PSP has been observed in other clades, including avian and non-avian theropods (O'Connor, 2004, 2006, 2009; O'Connor & Claessens, 2005; Benson et al., 2012), pterosaurs (e.g. Claessens, O'Connor & Unwin, 2009). The highest expression of PSP is seen in pterosaurs, where Martin & Palmer (2014) CT scanned limb bones of nine pterosaurs and compared them with the limb bones of birds and the vertebrae of sauropods. They discovered that pterosaur limb bones have higher ASP than the bones of the other archosaur groups. Pterosaurs were usually larger than birds, so, they probably experienced higher flight pressures compared to those of birds.

Thus, the higher expression of pneumaticity in their wing bones must have acted primarily in favour of bending stiffness and secondly in reducing weight. The least expression of osteological pneumatization is seen in crocodilians, namely the presence of blind fossae, which may have housed air sacs and/or adipose tissue, cartilage and muscles (e.g. Britt, 1993). These fossae have weakly developed margins and are 'blind', in that they do not 'lead' further inside the bone.

1.1.2) Selection of the 61 sauropodomorph taxa

In this study, 61 taxa were selected across Sauropodomorpha, listed here, and with specimens examined and measured first-hand indicated in bold. The chosen taxa were: 10 basal Sauropodomorpha [*Efraasia minor* Huene, 1908; Galton, 1973 (SMNS 12354, 12684), *Plateosaurus engelhardti* Meyer, 1837 (AMNH 6810, SMNS F65, BSPG 1912 VIII 61) and ***Plateosaurus longiceps* Jaekel, 1914 (HMN MB.R.4402.24; MB.R.4398.119.1; MB.R.4398.119.2; MB.R.4398.120; MB.R.4398.102; MB.R.4398.84; MB.R.4402.12; MB.R.4402.7)**, ***Ruehleia bedheimensis* Galton, 2001 (HMN MB.R.4718.41; MB.R.4718.70; MB.R.4718.72; MB.R.4718.32; MB.R.4718.38; MB.R.4718.55; MB.R.4718.20; MB.R.4718.41-43; MB.R.4718.46; MB.R.4718.27; MB.R.4719.4; MB.R.4771)**, *Eucnemesaurus fortis* Van Hoepen, 1920 (BP/1/6107, TM 119), ***Thecodontosaurus antiquus* Morris, 1843 (BRSUG 26629, 28124, 28133, 26621, 28131, 23969, 26645, 26589, 28122),** *Camelotia borealis* Galton, 1985 (OUMNH J13605-13613, 13615-13616, 13619-13688, 13899), *Massospondylus carinatus* Owen, 1854 (BP/1/4934, 5143, 5241), *Aardonyx celestae* Yates et al., 2010 (BP/1/6644, BP/1/6513, 6615, 6662, 6681,BP/1/6287, 6323, 6591, 6642, 6666; BP/1/6261, 6324, 6613, BP/1/6566,BP/1/5379, 6309,BP/1/6241), *Seitaad ruessi* Sertich & Loewen, 2010 (UMNH VP 18040), and *Antetonitrus ingenipes* Yates & Kitching, 2003 (BP/1/4952)], 12 non-neosauropod Eusauropoda [*Vulcanodon karibaensis* Raath, 1972 (QG24)*, Tazoudasaurus naimi* Allain et al., 2004 (CPSGM To1-38; To1-129, To1-103, To1-239, To1-354, To1-64, To1-69, To1-38 A-C, To1-156, Tol-100, To1-303 A-C, To1-288, To1-88, To1-317, To1-357), *Klamelisaurus gobiensis* Zhao, 1993 (IVVP V9492)*, Barapasaurus tagorei* Jain et al., 1975 (AMNH 5760)*, Kotasaurus yamanpalliensis* Yadagiri, 1988 (IA 12/S1Y/76)*, Spinophorosaurus nigerensis* Remes et al., 2009 (GCP-CV-4229 & NMB-1698-R)*, Jobaria tiguidensis* Sereno et al., 1999 (MNN TIG3), *Rhoetosaurus brownei* Longman, 1926 (QM F1695), *Cetiosaurus sp*. Owen, 1841 (OUMNH J13644/2)*, Shunosaurus lii* Dong et al., 1983 (IVPP V.9065)*, Omeisaurus tianfuensis* He et al., 1984 (ZDM T5703 / T5701 / T5704 / BMNH 28632)*, Patagosaurus fariasi* Bonaparte, 1979 (PVL 4170, PVL 4116, PVL, 4615, PVL 4171, PVL 4172 and MACN-CH935, MACN-

CH932, MACN-CH933) and *Mamenchisaurus jingyanensis* Zhang et al., 1998 (CMNH JV002)], 13 Diplodocoidea [*Haplocanthosaurus s*p. Hatcher, 1903 (CM 897-7), *Amphicoelias sp.* Cope, 1877 (AMNH 5764)*, Apatosaurus sp.* Marsh, 1877 (OMNH 0138, 01380, 1251, 1217; YPM 1980)*, Suuwassea emilieae* Harris & Dodson, 2004 (ANS 21122)*, Barosaurus lentus* Marsh, 1890 (AMNH 6341)*, Seismosaurus halli* Gillette, 1991 (NMMNH 3690)*, Diplodocus sp.* Marsh, 1878 (DMNH 1494, USNM 10805, CM 11161)*,* ***Tornieria africana*** **Fraas, 1908 (HMN MB.R.3816; MB.R.2957; MB.R.2956.1; MB.R.2733)*, Dicraeosaurus sattleri*** **Janensch, 1914 (HMN MB.R.3677-3680; MB.R.3681-3687; MB.R.3688; MB.R.2711; MB.R.2714; MB.R.2731-2732)***,* *Amargasaurus cazaui* Salgado & Bonaparte, 1991 (MACN-N 15)*, Nigersaurus taqueti* Sereno et al., 1999 (MNN GAD513, GAD 515-518)*, Amazonsaurus maranhensis* Carvalho et al., 2003 (MN 4558-V; UFRJ-DG 58-R/9; MN 4559-V; MN s/n(-V); UFRJ-DG 58-R/7; MN 4555-V; MN 4560- V; MN 4556-V; UFRJ-DG 58- R/10; UFRJ-DG 58-R/1; MN s/n(-V) MN 4558-V; UFRJ-DG 58-R/9; MN 4559-V; MN s/n(-V); UFRJ-DG 58-R/7; MN 4555-V; MN 4560- V; MN 4556-V; UFRJ-DG 58- R/10; UFRJ-DG 58-R/1; MN s/n(-V), MN 4558-V; UFRJ-DG 58-R/9; MN 4559-V; MN s/n(-V); UFRJ-DG 58-R/7; MN 4555-V; MN 4560- V; MN 4556-V; UFRJ-DG 58- R/10; UFRJ-DG 58-R/1; MN s/n(-V)) and *Cathartesaura anaerobica* Gallina & Apesteguia, 2005 (MPCA - 232)], 11 Macronaria and basal titanosauriforms [*Tehuelchesaurus benitezii* Rich et al., 1999 (MPEF-PV 1125), *Camarasaurus* sp. Cope, 1877 (OUMNH J13605-13613, 13615-13616, 13619-13688, 13899)*, Euhelopus zdanskyi* Wiman, 1929 (PMU 233, IVPP 10601)*,* ***Europasaurus holgeri*** **Sander et al., 2006 (DFMMh - FV 652.1, FV 652.4, FV 019, FV 896.1, FV 1084, FV 862, FV 890.5, FV 569, FV 719, FV 866, FV 495.3, FV 863.2, FV 863.1)***,* *Brachiosaurus altithorax* Riggs, 1903 (DMNH 39045/BYU 12866)*,* ***Giraffatitan brancai*** Janensch, 1914 (HMN SI 70 - SI 71/WN-V6; **MB.R.2738; MB.R.2921-2939; MB.R.2712; MB.R.2189.87; MB.R.3824**)*, Ornithopsis hulkei* Seeley, 1870 (BMNH 28632)*,* *Eucamerotus foxi* Blows, 1995 (BMNH R2522, BMNH R91*), Pleurocoelus sp.* Marsh, 1888 (USNM 5678, 4968, 4946; UMNH VP900)*,* and ***Janenschia robusta*** **Fraas, 1908 (HMN MB.R.2091.31; MB.R.2094],** and 15 Somphospondyli [*Erketu ellisoni* Ksepka & Norell, 2006 (MPC/IGM 100/1803), *Huanghetitan liujiaxiaensis* You et al. (2006) (HGM 41HIII-0001)*, Sauroposeidon proteles* Wedel et al., 2000 (OMNH 53062), *Australodocus bohetii* Remes, 2007 (HMN MB.R.2455 [G 70] and MB.R.2454 [G 69]), ***Tendaguria tanzaniensis*** **Bonaparte et al., 2000 (HMN MB.R.2092.1, MB.R.2092.2)**, *Phuwiangosaurus siridhornae* Martin et al., 1994 (SM-PW1-0001 to SM-PW1-0022/SM - K11-0001 to SM-K11-0167)*, Malawisaurus dixeyi* Haughton, 1928 (MAL 89-78)*,* *Andesaurus delgadoi* Calvo & Bonaparte, 1991 (MUCPv 132)*, Dongyangosaurus sinensis* Lu et al., 2008 (ZMNH DYM 04888)*, Futalognkosaurus dukei* Calvo et al., 2007 (MUCPv-

323), *Neuquensaurus australis* Lydekker, 1893 (MLP Ly1-6 / MLP-Cs, MC S-5/17, MCS-Pv 180 / MCS-Pv 5-12 / MLP-CS 1434), *Saltasaurus sp.* Bonaparte & Powell, 1980 (PVL 4017-137), *Puertasaurus reuili* Novas et al., 2005 (MPM 10002), *Rapetosaurus krausei* Curry Rogers & Forster, 2001 (FMNH PR 2209) and *Alamosaurus sanjuanensis* Gilmore, 1922 (TMM 43598)].

The chosen taxa are classified according to current phylogenetic understanding (Table 1 in Chapter 2), with some alternative placements. By 'Eusauropoda' or 'eusauropods' we mean 'non-neosauropod eusauropods' and by 'Macronaria' or 'macronarians' we mean both 'basal Macronaria' and 'basal titanosauriform' taxa. The author acknowledges the following facts: a) some generic placements under these categories are not completely unambiguous since their position is not stable in every phylogenetic study that has been undertaken by various workers (e.g. *Pleurocoelus*), b) lack of completeness for most of these taxa which results in the situation presented in (a) and also many characters being marked as unknown ('?') and c) the '*sp.*' implies that more than one species have been examined and the pneumaticity score for 'presence' corresponds to its presence found in any, or all, of the species within the genus. Therefore, if a pneumatic character occurs in one of the two or more species in a genus, then the character is recorded as present. Therefore, unless stated otherwise, these genera will be utilised for the purposes of this study and its analyses.

1.1.3) Previous work on body size in sauropodomorphs - Body mass, body length and femur length estimates

The body size of an organism is profoundly associated with its body plan, metabolism and ecological interactions (Clutton-Brock and Harvey, 1983; Peters, 1983; Schmidt-Nielsen, 1984; Alexander, 1998; Hunt & Roy, 2006; Makarieva, Gorshkov & Li, 2005; Bonner, 2006). There are natural minimum and maximum thresholds to body size in which every animal's body plan can function within. Body size evolution, its drivers and implications have received increasing attention recently due to the realisation that many biotic factors are linked to body size evolutionary innovations. Sauropods were a highly successful radiation of terrestrial herbivores from the Late Triassic, and became the dominant megafauna and thrived until the end of the Mesozoic (Wedel, 2005; Tidwell & Carpenter, 2005). Their gigantic body size in combination to high expression of vertebral pneumatisation marks sauropods as a unique superfamily within Dinosauria (Sander et al., 2011). The early evolution of large body size signified it as a fundamental characteristic of sauropods throughout their evolution (Dodson, 1990). Biotic functions are inherently associated with an animal's mass (rather than with its length) but body mass of extinct taxa cannot be determined without making a number of assumptions. Body mass

is positively correlated in linear dimension to every skeletal feature (Sander et al., 2011). The difference in the uppermost limits of body size between sauropods and other large representatives of dinosaurian and mammalian families, has been reviewed in light of many developed techniques of mass derivation. Metrics for body size can be estimates of mass, length, height, a combination of them, or even proxies such as femur length (Carrano, 2006; Sander et al., 2011). These mass estimates can be the result of volume measurements based on laser-scanning photogrammetry of mounted skeletons (e.g. Gunga et al., 2007, 2008), of scientific reconstructions (e.g. Paul, 1994, 1995, 1997; Henderson, 1999, 2004, 2006; Seebacher, 2001), or by using any of the other methods also mentioned above, suggesting that most sauropods fall within the 5–45 tonne range (Table 1). The largest somphospondylan sauropods such as *Sauroposeidon* and *Argentinosaurus*, respectively, are estimated to have even larger body masses (Wedel et al., 2000*a*, *b*; Mazzetta et al., 2004; Benson et al., 2014). The Lower Jurassic *Europasaurus holgeri* (Sander et al., 2006) and the Upper Cretaceous *Magyarosaurus dacus* (Stein et al., 2010) from palaeo-islands of Germany and the Hateg Basin of Romania, respectively (Weishampel et al., 1991; Grigorescu, 1992; Jianu and Weishampel, 1999; Curry-Rogers, 2005; Sander et al., 2006; Benton et al., 2010) are examples of sauropods with very small adult body size and thus they are classified as dwarfs, since their mass is estimated to not have exceeded the tonne threshold.

In terrestrial vertebrates, body mass and appendicular (femur or humerus) circumference are correlated (Anderson et al., 1985). It is generally convenient to use this method with the femur as a proxy for body-mass estimation since it is generally the largest limb bone in a skeleton and it is commonly well preserved (Carrano, 2006). However, less than half of the sauropod taxa considered here have a femur (or a humerus) attributed to them, leading us to also obtain estimated size (primarily mass) measurements from other methods such as polynomial volume (e.g. Seebacher, 2001) and scale models (e.g. Christiansen, 2002). Long bone circumference (e.g. Colbert, 1962; Anderson et al., 1985), femur length and pelvic height determination (e.g. Peczkis, 1995), femur diameter (e.g. Galton, 1985), femur length (e.g. Jain & Chatterjee, 1979) and humerus diameter (e.g. Anderson et al., 1985; Raath and McIntosh, 1987) methods are used when there is a lack of more sophisticated techniques for deriving the estimated mass of a given taxon (Table 1). Femur length cannot be used as an extra proxy for size in this study due to its scarcity in our data set. It will only be used for comparative and statistical reasons in phylogenies in Chapter 5. Therefore, when conducting comparative analyses between size estimates and pneumaticity degree, they are restricted to pneumaticity and body mass, body length as well as vertebral length regions. More recently, body masses of Mesozoic reptiles have been recently retrieved by volume-based techniques (Motani, 2001; Seebacher, 2001) or

by 3D computer reconstructions (e.g. Henderson, 1999, 2006; Seebacher, 2001; Mazzetta et al., 2004). In the latter technique, the animal's body is reconstructed by means of digital slicing and its size (in terms of volume) is derived by the sum of the individual volumes of the slices. Newer studies on body mass estimate techniques (Bates et al., 2009; Campione & Evans, 2012; Sellers et al., 2012; Benson et al., 2014; Brassey & Sellers, 2014; Campione et al., 2014; Bates et al., 2015; Brassey et al., 2015) have given us clearer approaches with respect to calculating the body mass of extant animals as well as minimising the levels of uncertainty when trying to estimate the mass of extinct taxa such as non-avian dinosaurs. Needless to say that different methods apply to different circumstances, depending on the condition of the specimen and the level of completeness of the skeleton. For example, when the described taxon is known only from few skeletal remains, the preferred method is the predictive regression approach which correlates the linear dimensions of the long weight-bearing bones (midshaft circumferences of humerus and femur) of an animal with its mass in a form of bivariate equation that incorporates measurements of density or specific gravity (density of animal with respect to water density; Campione & Evans, 2012; Lacovara et al., 2014). This method only requires the most commonly preserved skeletal elements, which are the limb bones and has been shown that their measurements strongly correlate with body mass (Campione & Evans, 2012). In general, predictive regression and bivariate equation approaches are fast, practical and objective (Sellers et al., 2012). However, they may be inappropriate when applied to specimens with uncertain ontogenetic stage as they may lead to inaccurate mass estimates due to the allometric scaling of the limb bone measurements with the taxon's age as the animal grows (Kilbourne & Makovicky, 2010; Brassey et al., 2015). In addition, they also produce highly variable results and require a new dataset of measurements for each case (Sellers et al., 2012). Alternatively, if the taxon is known from near complete (e.g. at least 40-50%) to complete skeletal material, volumetric approaches can be employed such as laser 3D scanning computer imaging photogrammetry (Gunga et al., 2007; Bates et al., 2009) and convex hulling (Sellers et al., 2012; Brassey et al., 2015; Bates et al., 2015). Laser scanning and imaging as well as convex hulling are non-destructive methods that allow for the creation of digital reconstructions of extinct animals (Bates et al., 2009). Such reconstructions can be used to extrapolate masses of body segments by adjusting their volumes and incorporating values of density, thus calculating an overall estimate of body mass for the entire animal (Bates et al., 2009; Sellers et al., 2012). Volumetric methods utilise every detail from the mounted specimen and their calculations are not affected by extreme morphologies of the skeletal elements (e.g. unusually large limbs in an individual or a species) nor do they

need to employ data from regression analyses derived from other than measured body mass data (Sellers et al., 2012; Brassey et al., 2015).

However, they are prone to errors due to the user-subjective nature of the reconstruction process, and thus, sensitivity analyses have to be performed so as to rule out any implausible outcomes of mass allocation and estimation. Such outcomes stem from uncertainties with respect to the anatomical distribution of the body parts of the animal e.g. limb posture, incorrect mounting, tissue distribution, tissue density, etc. (Bates et al., 2009, 2015; Brassey et al., 2015). In addition, volumetric methods require a good proportion of the skeleton to exist in order to recreate as accurately as possible the three-dimensional image and are time-consuming since the user has to manually create the digital form around the skeleton (Sellers et al., 2012). In order to bypass the issue of anatomical inaccuracies, the method of convex hulling tightly covers the 3D image of the skeleton with convex polytopes and calculates the body mass by correlating the volume of the convex hull and the body mass of similarly shaped extant animals (Brassey et al., 2015). As Brassey et al. (2015) has demonstrated, convex polytopes are units of volume similar to the voxels (volume pixels) in Finite Element Analysis (Rayfield et al., 2001; Rayfield, 2005) but it is like 'wrapping the skeleton in cling film'. Unfortunately, only few mounted dinosaurian skeletons have been scanned and had their masses estimated by convex hulling, and out of them only one sauropod (*Dreadnoughtus*) which is not included in this study.

In this study, various methods of mass estimates were chosen for the 61 sauropodomorph taxa, depending on the availability of the specimens for which different methods were implemented by previous workers. For example, laser photogrammetry was used whenever a near-complete mounted skeleton was present whereas stylopodial (i.e. femur and/or humerus bones) measurements were used in specimens with few skeletal elements available. Specifically, for *Plateosaurus*, *Thecodontosaurus*, *Massospondylus, Shunosaurus*, *Omeisaurus*, *Patagosaurus*, *Mamenchisaurus*, *Haplocanthosaurus*, *Amphicoelias, Apatosaurus, Barosaurus, Brachiosaurus, Diplodocus, Seismosaurus* and *Amargasaurus*, the author chose to use the mass estimate based on the polynomial volume from which the 'polynomial mass' (Seebacher, 2001) is derived. Body mass estimation based on such allometric equations of polynomial volume fairly agrees with masses retrieved by independent methods of e.g. actual weighing of an animal, as was demonstrated with extant mammals (Seebacher, 2001). This method utilises polynomial equations whereby mass is the sum of many voluminous parts (e.g. cylinders) that the examined animal is segmented into (Seebacher, 2001). For *Camarasaurus* and *Europasaurus* the body mass estimation method and result for each animal were chosen to be the measurement of long bone (femoral or humeral) circumference, for its ease

regarding specimen availability, speed and reasonable accuracy (Anderson et al., 1985; Sellers et al., 2012). Furthermore, laser scanning and photogrammetry was performed in the mounted skeletons of *Dicraeosaurus* and *Giraffatitan,* a method preferred for its accuracy, wherever applicable (Gunga et al. 2008; Sellers et al. 2012). The femoral (or humeral) length-to-diameter ratio method (Cooper, 1984; Galton, 1985) is the only method used and, therefore, chosen for *Camelotia*, *Vulcanodon*, *Tornieria*, *Phuwiangosaurus*, *Neuquensaurus*, *Saltasaurus* and *Rapetosaurus*. Like the previous ones, this method also produces plausible mass estimates for extinct animals and can be used when limited skeletal material is available, usually restricted to limb bones. The femur diameter over pelvic height ratio (Galton and Cluver, 1976) is another reliable proxy for body mass estimation because it utilises both stylopodial and entire limb measurements and was used and chosen in *Euhelopus*. The disadvantage of this method is its requirement of the entire limb to have been preserved. The only body mass estimate method used for *Cetiosaurus* was the method that utilised humeral and femoral circumferences (different mass estimate in each case of measurement) by Anderson et al. (1985). The body mass resulting from the femoral circumference yields an implausible value (39,100 Kg) and thus for this study the estimate based on humeral circumference is preferred, as it produces a more reasonable mass value (15,800 Kg) with respect to is body length (16 m). Similarly, the only method for mass estimation that was used to determine the body mass of *Suuwassea* was the one based on its humeral circumference (this method was firstly introduced by Anderson et al., 1985) which yielded a realistic estimate. A less accurate method is often used when no other available choice exists, due to scarcity of skeletal material and that is the production of a scale model that imitates the hypothesised body proportions of an animal. From this model, and with high levels of uncertainty, a probable body mass estimate is calculated. This method was used and chosen for *Tendaguria*. The proxy of femur length in association with the probable body length of an animal (Yates & Kitching, 2003) was the only method used to derive an estimate of body mass for *Efraasia*, *Antetonitrus*, *Aardonyx*, *Barapasaurus*, *Kotasaurus*, *Klamelisaurus*, *Cathartesaura*, *Jobaria*, *Janenschia* and *Tehuelchesaurus*. Estimates based on their closest relatives were used to derive the body mass of the basal sauropodomorphs *Ruehleia*, *Eucnemesaurus* and *Seitaad*, the eusauropods, *Tazoudasaurus*, *Spinophorosaurus* and *Rhoetosaurus*, the diplodocoids *Nigersaurus* and *Amazonsaurus*, the macronarians *Ornithopsis*, *Eucamerotus* and *Pleurocoelus* and the somphospondylans *Australodocus*, *Sauroposeidon*, *Huanghetitan*, *Malawisaurus*, *Andesaurus*, *Dongyangosaurus*, *Futalognkosaurus*, *Puertasaurus* and *Alamosaurus* (see Table 1 below).

Concerning the choice for body lengths for the sauropodomorph taxa, this study relied upon the literature of the documented taxa and the estimates derived from their skeletal reconstructions (e.g. McIntosh et al., 1997; Seebacher, 2001 – see Table 1 below). Body length is a less ambiguous size parameter, compared to body mass, when research involves extinct taxa because its derivation depends directly on the presence of skeletal material. Thus, the estimated values of body lengths are less prone to an error, as is the case with body mass estimates which rely on proxies of appendicular measurements, regression equations, scaling and machine algorithms.

The caveat with volume-based estimates is that they produce high values because their derivation is founded in the value of 0.9–1 kg* L^{-1} (L= Litres), which is the body density of extant crocodilians (Wedel, 2005). That may not be the case, though, since sauropods, unlike crocodilians, possessed pneumatised postcrania, just as birds do, and, therefore it would be reasonable to assume they would have a body density analogous to that of birds (0.73 kg * L^{-1} to 0.8 kg * L^{-1} (Hazlehurst & Rayner, 1992; Perry, 2001; Henderson, 2004; Wedel, 2003*a*, *b*, 2005, 2009; Schwarz & Fritsch, 2006). Wedel (2005) also suggested that the mass estimates derived from volume-based methods that predate the consensus on sauropod pneumatisation should be reduced by 10%. The author of this study would agree to the latter statement and probably implement it if the focus of the research was to establish a new method of body mass derivation. Since this is not the case in this current project, the author chose the most appropriate, based on method and specimen availability, body mass estimates for the sauropodomorphs examined in this study. The body mass and body length estimates for the 61 taxa of this study are summarised in Table 1, and for comparative reasons, a column of femoral lengths was added too. Femoral length measurements will only be used in the analyses conducted in Chapter 5.

Table 1. List of body masses and body lengths of the sauropodomorph taxa. List of the selected and examined 61 sauropodomorph taxa with body mass, body length and femur length estimates along with their supporting references.

Sauropodomorph taxa						
Basal Sauropodomorpha	Body Masses (Kg)	Methods	References	Body Lengths (m)	References	Femur lengths (m) (Carrano, 2006)
Efraasia	700	estimate from femoral length	Yates, 2003	6.5	Galton, 1973	0.226
Plateosaurus	1073	polynomial volume	Seebacher, 2001	8.5	Galton, 1986	0.75
Ruehleia	1000	estimate based on other related basal sauropodomorphs	Yates et al., 2011	10	Galton, 2001	N/A
Eucnemesaurus	500	estimate based on other related basal sauropodomorphs	Yates, 2007	6	Van Hoepen, 1920	N/A
Thecodontosaurus	24.6	polynomial volume	Seebacher, 2001	2.6	Benton et al., 2000	0.28
Camelotia	2500	femur length-over-diameter ratio	Galton, 1985c	10	Galton, 1985	0.98
Massospondylus	136.7	polynomial volume	Seebacher, 2001	4	Paul, 1990	0.33
Antetonitrus	5000	estimate from femoral length	Yates & Kitching, 2003	12.2	Yates & Kitching, 2003	0.794
Aardonyx	1000	estimate from femoral length	Yates et al., 2010	6.5	Yates et al., 2010	0.68
Seitaad	80	estimate based on other related basal sauropodomorphs	Yates et al., 2011	2.8	Sertich & Loewen, 2010	N/A
Eusauropoda						
Tazoudasaurus	5000	estimate based on relative eusauropods	Yates et al., 2011	9.5	Allain et al., 2004	N/A
Vulcanodon	3500	femur length-over-diameter ratio	Cooper, 1984	6.5	Raath, 1972	1.1
Barapasaurus	7000	estimate from femoral length	Jain et al., 1979	12	Jain et al., 1975	1.36
Kotasaurus	5000	estimate from femoral length	Yadagiri, 1988	9	Yadagiri, 1988	1.13
Spinophorosaurus	7000	estimate based on relative eusauropods	Remes et al., 2009	13	Remes et al., 2009	N/A
Jobaria	16000	estimate from femoral length	Sereno et al., 1999	24	Sereno et al., 1999	1.8
Rhoetosaurus	9000	estimate based on relative eusauropods	Longman, 1926	15	Longman, 1926	N/A
Cetiosaurus	15800	humerus circumference	Anderson et al., 1985	16	Anderson et al., 1985	1.61
Shunosaurus	4793.5	polynomial volume	Seebacher, 2001	8.7	Zhang, 1988	1.25
Omeisaurus	11796	polynomial volume	Seebacher, 2001	20	He et al., 1998 / Paul, 1990	1.31
Patagosaurus	9435	polynomial volume	Seebacher, 2001	15	Bonaparte, 1979	1.54
Mamenchisaurus	18169.7	polynomial volume	Seebacher, 2001	21	McIntosh et al., 1997	1.86
Klamelisaurus	5000	estimate from femoral length	Zhao, 1993	15	Zhao, 1993	1.2
Diplodocoidea						
Haplocanthosaurus	14528.6	polynomial volume	Seebacher, 2001	14	McIntosh et al., 1997	1.74
Amphicoelias	18170	polynomial volume	Galiano & Albersdorfer, 2010	25	Galiano & Albersdorfer, 2010	1.77
Apatosaurus	22407.2	polynomial volume	Seebacher, 2001	21	Christiansen, 1997	2.5
Suuwassea	5950	long bone (humerus) circumference	Anderson et al., 1985	15	Harris & Dodson, 2004	N/A
Barosaurus	20039.5	polynomial volume	Seebacher, 2001	26	McIntosh et al., 1997	1.44
Seismosaurus (Diplodocus)	49275.5	polynomial volume	Seebacher, 2001	40	Gillette, 1994	N/A
Diplodocus	19654.6	polynomial volume	Seebacher, 2001	25.7	Holland, 1910	1.54
Tornieria	20000	humerus length-over-diameter ratio	Raath and McIntosh, 1987	25	Sternfeld, 1911 / Raath & McIntosh, 1987	1.36
Dicraeosaurus	5700	laser scanning photogrammtery of mounted skeleton	Gunga et al., 2007	12	McIntosh et al., 1997	1.22
Amargasaurus	6852.9	polynomial volume	Seebacher, 2001	10.3	Salgado & Bonaparte, 1991	1.05
Nigersaurus	2000	estimate based on other related diplodocoideans	Sereno et al., 1999	9	Sereno et al., 1999	N/A
Amazonsaurus	5000	estimate based on other related diplodocoideans	Carvalho et al., 2003	12	Carvalho et al., 2003	N/A
Cathartesaura	5000	estimate from femoral length	Gallina & Apesteguia, 2005	12	Gallina & Apesteguia, 2005	1.38
Macronaria						
Janenschia	10000	estimate from femoral length	Bonaparte et al., 2000	17	Wild, 1991 / Bonaparte et al., 2000	1.33
Tehuelchesaurus	9000	estimate from femoral length	Rich et al., 1999	15	Rich et al., 1999	1.53
Camarasaurus	18413	long bone circumference	Foster, 2005	15.4	McIntosh et al., 1996	1.8
Euhelopus	4000	femur diameter & pelvic height determination	Wilson & Upchurch, 2009	11	Romer, 1956 / Wilson & Upchurch, 2009	0.95
Europasaurus	800	long bone circumference	Sander et al., 2006	6.2	Sander et al., 2006	0.316
Brachiosaurus	28264.6	polynomial volume	Seebacher, 2001	21	Riggs, 1903	2
Giraffatitan	38000	laser scanning photogrammtery of mounted skeleton	Gunga et al., 2008	24	Paul, 1988	1.91
Ornithopsis	8000	estimate based on other related macronarians	Blows, 1995	15	Seeley, 1870 / Blows, 1995	N/A
Eucamerotus	8000	estimate based on other related macronarians	Blows, 1995	15	Blows, 1995	N/A
Pleurocoelus	12000	estimate based on other related macronarians	Salgado et al., 1995 / Carpenter & Tidwell, 2005	15	Marsh, 1888 / Lull, 1911	N/A
Somphospondyli						
Australodocus	4000	estimate based on other related titanosaurids	Remes, 2007	17	Remes, 2007	N/A
Sauroposeidon	50000	estimate based on other related titanosaurids	Wedel et al., 2000	27	Wedel et al., 2000	N/A
Tendaguria	48000	scale model	Bonaparte et al., 2000	30	Bonaparte et al., 2000	N/A
Erketu	5000	estimate based on other relative titanosaurids	Ksepka & Norell 2006	15	Ksepka & Norell 2006	N/A
Huanghetitan	32000	estimate based on other related titanosaurids	Lu et al., 2007	22	You et al., 2006	N/A
Phuwiangosaurus	17000	femur length-over-diameter ratio	Suteethorn et al., 2009	19	Martin et al., 1994	1.25
Malawisaurus	10000	estimate based on other related titanosaurids	Jacobs et al., 1993 / Gomani et al., 1999	16	Jacobs et al., 1993	N/A
Andesaurus	7000	estimate based on other related titanosaurids	Calvo & Bonaparte, 1991	18	Calvo & Bonaparte, 1991	1.55
Dongyangosaurus	7000	estimate based on other related titanosaurids	Lu et al., 2008	15	Lu et al., 2008	N/A
Futalognkosaurus	45000	estimate based on other related titanosaurids	Calvo et al., 2007	30	Calvo et al., 2007	N/A
Neuquensaurus	3500	femur length-over-diameter ratio	Salgado et al., 2005	7.5	Powell, 1992 / Salgado et al., 2005	0.7
Saltasaurus	4000	femur length-over-diameter ratio	Bonaparte & Powell, 1980	12	Bonaparte & Powell, 1980	0.87
Puertasaurus	50000	estimate based on other related titanosaurids	Novas et al., 2005	30	Novas et al., 2005	N/A
Rapetosaurus	8000	femur length-over-diameter ratio	Curry-Rogers & Forster, 2001	15	Curry-Rogers & Forster, 2001	0.68
Alamosaurus	16000	estimate based on other related titanosaurids	Bakker, 1980	20	Gilmore, 1922	N/A

1.1.4) Ambiguous and unambiguous traits of postcranial skeletal pneumatisation

Differentiation between pneumatic and non-pneumatic (e.g. openings for vessels and nerves) vertebral foramina in birds and sauropods has been based upon on a set of characteristics (O'Connor, 2004; Wedel, 2005). The invading diverticulum creates a pneumatic aperture that has soft margins, an almost oval shape, and is larger in size (usually twice or more) than a non-pneumatic hole, allowing for the pneumatic foramen to be easier to spot than a non-pneumatic opening. Pneumatic foramina can be found to occupy almost every vertebral part (from the centrum up to the spine) while the number of the non-pneumatic holes is far less than that of the pneumatic apertures (O'Connor, 2004; Wedel, 2005, Apostolaki et al., 2015).

It is harder to determine whether fossae are pneumatic or not, because they can contain a variety of tissues. Such cavities may house diverticula as well as soft tissues like nerves and vessels (Apostolaki et al., 2015). Extant crocodilian vertebrae bear fossae that do not possess pneumatic features but contain adipose tissue instead; furthermore, these excavations also serve as origination points for the animal's musculature (O'Connor, 2006). Identified fossae in the vertebrae of the birds have been observed to possess both pneumatic and non-pneumatic tissues (O'Connor, 2006). Avian pneumatic fossae in birds are deep and wide, usually walled by laminae and their margins are smooth (O'Connor, 2006, Gutzwiller et al., 2013). Such fossae may often bear small foramina that lead into the cancellous bone or they may enclose a group of smaller interconnected fossae that further excavate the bone (O'Connor, 2006; Gutzwiller et al., 2013; Apostolaki et al., 2015). Based on our observations (Apostolaki et al., 2015), we established the laminated fossa as a different trait from a simple fossa justified on previous personal and literature experimental observations (Wilson, 1999; Wilson, 2002; Wilson et al., 2011; Apostolaki et al., 2015). These observations, based on the affinities between pneumatic diverticula and cortical vertebral bone showed the frequent presence of a lamina in the area where the diverticulum was invading the bone. Therefore, having a laminated fossa on a vertebral compartment indicates higher probability of the presence of a pneumatic diverticulum being attached and possibly penetrating the bone than if it was a mere fossa. When the only evidence of pneumaticity in a sauropod is the presence of fossae, the determination of its pneumaticity is questionable. Therefore, pneumatisation in such taxa would be weakly supported and, thus, limitedly expressed. Caution is advised when assuming that all observed fossae are pneumatic while to reject any fossae from being pneumatic unless they contain pneumatic foramina is equally false because the cavity may have served as

either being an adipose tissue reserve or a remodelled cavity due to bone resorption from the invading pneumatic diverticulum.

An indication that a fossa is unambiguously and strongly pneumatic is when it houses pneumatic foramina. *Giraffatitan* vertebrae possess pneumatic foramina within fossae with prominent margins and pleurocoels on its centra (Janensch, 1950; Wilson, 1999). Highly pneumatic features such as those aforementioned above can also be found in *Diplodocus* (Hatcher, 1901), *Tendaguria* (Bonaparte et al., 2000) and *Sauroposeidon* (Wedel et al., 2000). The larger cervical diverticula of the ostrich (*Struthio camelus*) expand into smaller diverticula (Wedel, 2003a) that, in turn, invade the vertebrae via foramina (Apostolaki et al., 2015). The result of a contact between the diverticula and the vertebra, and the subsequent bone modification, is the formation of a fossa. Inside the fossa, the diverticulum would further reform the interior of the bone, creating a ‘subfossa’. This hypothesis can only be verified by computed tomography (CT) studies on as many sauropod and theropod vertebrae as possible. In my database, I do not enlist the term 'subfossa' for reasons of simplicity, therefore, the simple presence of a fossa is sufficient to mark its presence unless it is enclosed within a pleurocoel, where it would be marked as a fosseous pleurocoel’. In addition, if a pleurocoel houses pneumatic foramina, this characteristic is called ‘pleurocoelous foramina’. Finally, if a pneumatic trait is bordered by laminae then it is recorded as such, e.g. ‘laminated pleurocoel’. For a more detailed account concerning the definitions, descriptions and illustrations of the basic pneumaticity features of this study see ‘Materials and Methods’ in Chapter 2.

1.1.5) Current project statement and its significance

In theory, the overall volume of pneumaticity in a vertebra could be calculated by the sum of the air volume for each compartment for every part of the vertebra. One must calculate the percentage of the compartment's volume with respect to the overall vertebral volume, then estimate how much of this volume is actually pneumatic (air space proportion), and finally, derive the percentage of the compartment's pneumaticity with respect to the overall vertebral volume. By doing this for every compartment, the overall pneumaticity for a particular vertebra would be easily derived. The practical drawbacks, though, for this technique lie in the assumption that the vertebra under examination will be complete and easy to handle and transport. Most recovered vertebrae are fragmented by various taphonomic processes during burial. Of course, being partially fragmented would allow us to observe the internal design and extent of pneumatisation, if present, inside the vertebrae or other skeletal elements. Another drawback is that the internal surfaces and chambers that are pneumatic may not be symmetrical, smooth, or isolated. Therefore, it is

almost impossible to measure the internal volume of a vertebra without the aid of a CT scanner, and CT scanning every vertebra in every taxon would be a punishing task.

As a result, the creation of a more practical, but less accurate method to measure the degree of pneumatisation in a vertebra, would seem more appropriate. O'Connor (2006) introduced a simple method (Pneumaticity Index) by dividing the number of pneumatised vertebrae over the overall number of vertebrae. This method, though, does not estimate the percentage of pneumaticity explicitly in a vertebra. The method proposed here, is far more accurate and accounts for a single vertebra; for simplicity, the pneumatisation of the vertebra is a proxy for the entire vertebral region it belongs to. Intervertebral variability with respect to the expression of pneumatisation does occur but due to the scarcity and incompleteness of fossils it would be hard to reveal the complete pneumatisation of a region, let alone an entire column of a sauropod. It would also be out of the scope of this project, since the primary goal is to create a method to quantify the degree of pneumatisation and produce a classification scheme of pneumatisation that can be applied to any archosaur specimen. The method proposed here is the 'Pneumatisation Degree Index' (PDI%), measured as a percentage, and it is based on a ranking scheme which results in a classification system that is composed of five stages (conditions), Alpha, Beta, Gamma, Delta, and Epsilon, each corresponding to a particular degree of generalised expression of pneumaticity, where Alpha > Beta > Gamma > Delta > Epsilon (see ‘Methods’ below and in Chapter 2). This method can be a good 'modus operandi' because it is (a) repeatable, and (b) is not entirely arbitrary because it is inspired by previous works of O’Connor (2006), Wilson (1999), Wedel (2000, 2003, 2007), Wilson et al. (2011) and Benson et al. (2012).

Despite many studies on postcranial skeletal pneumaticity in sauropods, little effort has been devoted to understanding the phylogenetic significance of these traits. There are two reasons for wishing to explore the evolutionary patterns of dinosaurian pneumaticity: (1) this is a key character of sauropods, and it would be good to know how and when it evolved, as well as how it was associated with body size evolution, and (2) such a study must be carried out in a phylogenetic comparative framework in order to distinguish the phylogenetic inheritance from independent adaptive signal.

The proposed study will consider the intergeneric phylogenetic relationships from a pneumaticity point of view emanating from the various factors that affect body size, namely, pneumaticity as well as metabolism and rate of growth in continental and insular taxa. The research will also focus on the pneumatic similarities and differences between 'dwarf', ‘juvenile’ and 'normal gigantic' taxa and discuss the reasons that result in such extremes of size. The interpretation of these affinities will mainly revolve around the various theories of endothermy or 'gigantothermy' and suggest which of these metabolic

cases might have applied to Sauropodomorpha in relation to their levels of pneumaticity (Sander et al., 2011; Perry et al., 2009). The project will also result in a more clear understanding of the development of the various pneumatic elements in the vertebral columns of the Sauropodomorpha.

1.1.6) Aims and objectives of this project

The key notions I need to test are that: a) the degree of pneumaticity measured across the skeleton increases as body size increases, b) the relationship between body size and pneumaticity is contingent with the body size metrics (e.g. neck length, tail length and body mass of dwarf and juvenile case studies and c) the expression of pneumaticity in sauropodomorphs increases through phylogeny and time. The expected notion is that there is analogous expression of pneumaticity with sauropod size and/or evolution as well as similar expressions and degrees of postcranial skeletal pneumaticity between the 'dwarf' sauropods and their larger mainland relatives. Lastly, I hypothesize that different phylogenetic lineages do not share parallel paths in the evolution of their pneumaticity.

The first hypothesis (Chapters 2 & 3) aims to test if high degrees of pneumaticity are associated with large body size in sauropods or if the expression of pneumaticity is irrelevant to body size.

The objectives are:

- **i)** To test if the relationship between body size and pneumaticity is contingent on the body size metrics (i.e. body mass, body length).
- **ii)** To test if pneumaticity measured across the vertebral column correlates proportionately (positive), inversely proportionately (negative) or neutrally variable with body size.
- **iii)** To shed light on how pneumaticity varies throughout vertebral regions.

It also aims to verify if pneumaticity varies differently in different families (positive, negative or neutral correlation) and vertebral regions. The alternative scenario would be that all major clades have the same degree of pneumaticity, thus concluding that the pneumaticity degree remains stable when comparing the same vertebral regions of different taxa.

The objectives are:

- **i)** To test if the correlation of the Pneumaticity Degree Index (PDI) with length is found consistently when pneumaticity is measured within vertebral regions.

ii) To test if and how the degree of pneumaticity varies across taxa using genus as the operational taxonomic unit.

iii) To show if different regions of the vertebral column are pneumatised differently among taxa of the same and of different families.

The second hypothesis (Chapter 4) explores pneumaticity in a dwarf sauropod to further shed light on any association between body size and degree of pneumatisation. It also aims to test this relationship in a juvenile sauropod and show if, during ontogeny, pneumaticity patterns change and the PDI expression increases with age or if pneumaticity patterns form early in life and remain stable throughout ontogeny without variation.

The objectives are:

i) To record pneumaticity patterns in the vertebral column of one dwarf sauropod specimen and compare it with related 'normal' sized sauropods.

ii) To record and compare the ontogenetic expression and transition of vertebral pneumaticity of the juvenile taxon with the pneumaticity of hypothetical (probable) adult taxa that this taxon might develop into.

The third hypothesis (Chapter 5) aims to test if pneumaticity has phylogenetic signal, thus affecting the phylogenetic interrelationships of Sauropodomorpha when incorporated into existing phylogenies. Alternatively, the interrelationships are not affected, i.e. there is no phylogenetic signal.

The objectives are:

i) To use comparative phylogenetic methods to inspect the evolution and distribution of discrete and continuous pneumaticity characters in existing phylogenies (via *Mesquite*).

ii) To incorporate pneumaticity discrete characters into accepted morphological matrices of existing phylogenies in order to inspect intergeneric interrelationships of sauropods so as to test if pneumaticity has a phylogenetic signal (via *PAUP, RStudio* and *TNT*). In addition, to independently assess the fitness and phylogenetic signal in a small sample of pneumaticity characters, their scores were compared with those of dental characters, in *TNT*.

1.2) Materials and Methods

1.2.1) Database contents – sauropod vertebral anatomy and pneumaticity

To objectively assess the distribution of the pneumatic characters on the postcranial skeleton of sauropodomorphs, documentation from the literature as well as personal observations of specimens were undertaken regarding the pneumaticity elements on the vertebral column and the pelvic bones. In order to construct the list of pneumaticity characters, all aspects of the extent of pneumaticity, such as detected marks, foramina, fossae, laminae, and other structures on the skeleton were recorded. The pneumatic elements (found at least once to be present) chosen for this study are distinguished as: pleurocoel (or, pneumatocoel), foramen, fossa, camerae, camellae, fossa with foramina, laminated pleurocoel, laminated foramen, laminated fossa, foraminous pleurocoel [foramen (-mina) inside a pleurocoel], fosseous pleurocoel (pleurocoel with fossa(e) inside), septated foramen, subdivided fossae, as well as the semicamerated and semicamellated conditions (for more details concerning the characteristics of these features go to section 2.2 in Chapter 2).

This covers the vertebral column including the pelvic bones wherever applicable. A taxon versus character data matrix in *Excel* was compiled, using all the metrics, and entering values, where possible, for all sauropodomorph taxa that can be coded. A character was assigned as a combination of a pneumatic element with a vertebral compartment, resulting to a total of 182 characters accounting for each vertebral region and another 27 for the pelvic region (see a small sample in 'Table S1' in Appendix 2; due to its form and extremely large size, the *Excel* spreadsheet of the pneumaticity matrix is stored as a separate file, Appendix 3). It has been recognised by the current scientific community that a sauropod (and bird) vertebra is composed of these compartments: centrum, condyle, cotyle, prezygapophyses, postzygapophyses, diapophyses, parapophyses, transverse processes, neural canal, neural arch, neural spine, and occasionally, epipophyses and hypapophyses. Any of these landmarks may bear fossae, foramina, some of them pleurocoels/pneumatocoels, any combination of them as well as laminated versions of these features (Figs. 1-6 and Table 3 in Chapter 2).These different landmarks / compartments have been marked with respect to their association with any pneumatic trait(s) and have been assigned accordingly as '1' if present, '0' if absent and '?' if unknown. The 'unknown' condition may result from a) absence of fossil material, b) absence of description of the bone with respect to pneumaticity (when, for example, the focus of the description is on morphometry and general morphology), c) unpublished data or d) unprepared material. The significant limitation of the incomplete fossil record leads to

the recovery of more data from cervical and dorsal vertebrae, both regions being the most frequently discovered, and less from sacral and caudal vertebrae.

1.2.2) Methodological approach for the current project objectives

Chapters 2 and 3 required the derivation of the Pneumaticity Degree Index (PDI) based on the occurrence of the pneumatic characters in each examined region (cervical, dorsal, sacral, caudal and pelvic) based on the numerical ranking of each observed character with respect to its extent of ostial invasiveness (i.e. “highly pneumatic” for e.g. a pleurocoel or “least pneumatic’ for e.g. a fossa). The PDI is a percentage while the ranking of the characters is stated by the integers from one to five with one being the highest pneumatic trait and five being the lowest. The rankings of the characters of each region were added together and divided by their number to give us the mean pneumaticity ranking for that region. The percentage scale was then correlated with the numbers existing from one to five, in one-tenth intervals (i.e. 1, 1.1, 1.2…5) in order to derive the PDI as a percentage (Tables 4- 6 in Chapter 2). As mentioned earlier, this ranking was also put under a classification scheme from A to E which included ranges of percentages of pneumatisation, thus making it easier to classify the sauropodomorphs based on their degree of pneumaticity (see ‘Materials and Methods’ in Chapter 2). Records of phylogenetic classification as well as the evolutionary time bins of the examined 61 taxa are also provided in Chapter 2 (see Tables 1 & 2). Estimates of body mass, body length and body segment length values (neck, trunk and tail) of each taxon were also summarised in Table 7 (Chapter 2). Information was retrieved from the literature and museum observations. Calculation of the body segment lengths of each taxon was made by deductive reasoning, again based on both the literature and museum observations and the process is described in Chapter 2. Linear regression analyses were carried out in *PAST3* showing how pneumaticity of all examined taxa as well as of each vertebral region of all taxa vary with evolutionary time and with body size metrics.

Chapter 3 contains the aforementioned plots in *PAST3* and discusses the results of these analyses on a temporal and phylogenetic context.

In Chapter 4, I performed the same logistic and comparative tests as in Chapter 3 in the dwarf basal titanosauriform (macronarian) sauropod *Europasaurus* and in an unnamed juvenile (SMA 0009) in order to derive their pneumaticity degrees. These data along with their size, location and time were put into context and discussed with regard to their continental and adult forms.

Chapter 5 required the assembly of morphological matrices and phylogenetic trees, encompassing sauropodomorph taxa from various subfamilies, merging some of

them into ‘supertrees’, mapping the pneumaticity characters on them and performing various phylogenetic analyses in *Mesquite, PAUP*, *RStudio* (GUI version of R) and *TNT* software programmes in order to reconstruct the ancestral states of the pneumaticity characters as well as to test for phylogenetic signal.

Finally, Chapter 6 summarises all of the chapters’ derived conclusions about the expression of pneumaticity in Sauropodomorpha and its correlations to body size, phylogeny and time.

Anatomical abbreviations

CD = caudal vertebra(e)
CL = camellae
CM = camerae
CV = cervical vertebra(e)
DV = dorsal vertebra(e)
F = fossa
FRF = foraminous fossa
FPL/PLF = fosseous pleurocoel
FRPL = foraminous pleurocoel
LF = laminated fossa
LFR = laminated foramen
LPL = laminated pleurocoel
NCL = neural canal
PF = pneumatic foramen
PL = pleurocoel / pneumatocoel
POZ = postzygapophysis
PRZ = prezygapophysis
SCL = semicamellate
SCR = semicamerate
SF = subdivided/septated fossa(e)
SFR = septated foramen
SV = sacral vertebra(e)
TRP = transverse process
VF = vascular foramina

Institutional abbreviations

AMNH = American Museum of Natural History, New York, USA; **ANS** = Academy of Natural Sciences, Philadelphia, USA; **BMNH** = Natural History Museum, London, UK; BP = Evolutionary Studies Institute - formerly Bernard Price Institute for Palaeontological Research, University of the Witwatersrand, Johannesburg, South Africa; **BRSUG** = University of Bristol, Department of Earth Sciences, UK; **BSPG** = Bayerische Staatssammlung für Paläontologie und Geologie, Munich, Germany; **CM** = Carnegie Museum of Natural History (CMNH), Pittsburgh, Pennsylvania, USA; **CMNH** = Chongqing Museum of Natural History, Chongqing, Sichuan, China; **CPSGM** = Collections

Paléontologiques du Service Géologique du Maroc, Direction de la Géologie, Ministère de l'Energie et des Mines, Rabat, Morocco; **DFMMh** = Dinosaurier-Freilichtmuseum Munchehagen/ Verein zur Forderung der Niedersächsischen Paläontologie, Germany; **DMNH** = Dallas Museum of Natural History, Dallas, Texas, USA; **FMNH** = Field Museum of Natural History, Chicago, USA; **GCP-CV** = Grupo Cultural Paleontologico de Elche, Museo Paleontológico de Elche, Spain; **HGM**, Henan Geological Museum, Zhengzhou, Henan, China; **IA**, Geological Survey of India, Hyderabad, India; **MCS** = Museo de Cinco Saltos, Rio Negro Province, Argentina; **MPC/IGM** = Paleontological Center, Mongolian Academy of Sciences, Ulaanbaatar, Mongolia; **MPCAPv** = Colección de Paleovertebrados de la Museum Provincial de Cipolletti 'Carlos Ameghino', Cipolletti, Rio Negro Province, Argentina; **IVPP** = Institute of Vertebrate Paleontology and Paleoanthropology, Beijing, China; **MACN** = Museo Argentino de Ciencias Naturales "Bernardo Rivadavia", Buenos Aires, Argentina; **MAL** = Malawi Department of Antiquities Collection, Liongwe and Nguludi, Malawi; **MB.R (HMN-MB)** = Humboldt Museum fur Naturkunde-Universität zu Berlin, Berlin, Germany; **MLP- Cs/Ly** = Museo de la Plata, Lydekker collections, La Plata City, Argentina; **MNN** = Musée National du Niger, Niamey, Republic of Niger; **MN** = Museu Nacional, Rio de Janeiro, Brazil; **MPEF-PV** = Museo Paleontologico Egidio Feruglio, Trelew, Argentina; **MPM** = Milwaukee Public Museum, Vertebrate Zoology, Milwaukee, Wisconsin, USA; **MUCPv** = Museo de Geologia y Paleontologia de la Universidad Nacional del Comahue, Neuquen Province, Argentina; **NMB** = Staatliches Naturhistorisches Museum Braunschweig, Germany; **NMMNH** = New Mexico Museum of Natural History, Albuquerque, New Mexico, USA; **OMNH** = University of Oklahoma, Sam Noble Oklahoma Museum of Natural History, USA; **OUMNH** = Oxford University Museum of Natural History, United Kingdom; **PMU** = Paleontological Museum, Uppsala, Sweden; **PVL** = Instituto-Fundacion "Miguel Lillo", Tucuman, Argentina; **QG** = Zimbabwe Natural History Museum, Bulawayo; **QM** = Queensland Museum, Geoscience collection, Brisbane, Queensland, Australia; **SMNS** = Staatliches Museum für Naturkunde, Stuttgart, Germany; SM = Sirindhorn Museum, Phu Wiang area, Changwat Kalasin, Thailand; **TM** = Ditsong National Museum of Natural History (formerly Transvaal Museum), Pretoria, South Africa; **TMM** = Vertebrate Paleontology Laboratory of the Texas Memorial Museum, Austin, Texas, USA; **UFRJ-DG** = Universidade Federal do Rio de Janeiro, Departmento de Geologia, Brazil; **UMNH** = Utah Museum of Natural History, Utah, USA; **USNM** = United States National Museum, Smithsonian Institution, Washington D.C., USA; **YPM** = Yale University, Peabody Museum of Natural History, New Haven, Connecticut, USA; **ZDM** = Zigong Dinosaur Museum, Zigong, Sichuan, China; **ZMAU** = Zoological Museum, Faculty of Science, Andhra University, Visakhapatnam, Andra Pradesh, India; **ZMNH** = Zhejiang Museum of Natural History, Hangzhou, Zhejiang, China.

Chapter 2 – Correlation of pneumaticity with body size and variation throughout vertebral regions

2.1) Introduction to the body size of Sauropodomorpha and its evolution with respect to vertebral pneumaticity

The body plan of any organism is fundamentally associated with other parameters like size, ontogeny, metabolic type and ecology (Clutton-Brock and Harvey, 1983; Peters, 1983; Schmidt-Nielsen, 1984; Alexander, 1998; Hunt & Roy, 2006; Makarieva, Gorshkov & Li, 2005; Bonner, 2006). The formation of the body plan during ontogeny is guided by the body's specific allometry (positive or negative), 'written' in the genetic code of a given organism. Major evolutionary changes occurring in animal lineages are linked with changes in their body size and form. Sauropods were a highly successful superfamily of herbivorous dinosaurs that dominated the terrestrial ecosystems on a global scale from the Late Triassic to the Late Cretaceous (Curry-Rogers & Wilson, 2005; Tidwell & Carpenter, 2005; Sander et al., 2011). During that time they radiated into many forms and sizes, from the dwarf-sized island dwellers *Magyarosaurus* and *Europasaurus* to the gigantic continental forms of *Brachiosaurus* and *Giraffatitan* and, probably, even some armoured forms like the medium-sized lithostrotian somphospondylan *Saltasaurus*, as well as the eusauropods *Shunosaurus, Mamenchisaurus and Omeisaurus* which had modified their distalmost caudal vertebrae into an osseous mass (He et al., 1988; Lida et al., 2009). Depending on its ecological niche, every body plan has specific upper and lower limits of growth and, thus, needs to be examined from a different evolutionary perspective. The factors of size such as length and mass play a crucial role in most biological processes, and, although their nature and estimation may be considered narrow and inaccurate, the scope of this study is to assess any association between size factors and osteological pneumatisation.

Terrestrial quadrupeds of more than 5-10 kg are graviportal and are distinguished from other animals; the length of their forelimbs is close to, equal, or sometimes longer than the hindlimbs (Noto and Grossman, 2010). Conversely, the bipedal vertebrates have hindlimbs that are longer than their forelimbs. An additional category incorporates facultative bipedal animals that can facilitate locomotion on two as well as four limbs like some iguanodontoids and basal sauropodomorphs (Christian & Preuschoft, 1996; Wright, 1999). Quadrupedalism in sauropods evolved as a secondary trait from the previous state of bipedalism, a characteristic of their basal sauropodomorph ancestors. Sauropods retained their characteristic 'small head-long neck-robust trunk-long tail' body plan since the emergence of *Camelotia* and *Vulcanodon*, establishing quadrupedalism in the

sauropod lineage, although the first steps towards this evolutionary path can be seen in the basal sauropodomorph clade of melanorosaurids which is considered to be a closer sister group of sauropods than the more distantly related plateosaurids (Benton et al., 2000). Sauropodomorpha, though, is the unanimously accepted term that includes Sauropoda plus Basal Sauropodomorpha, uniting all sauropods in a monophyletic group (Upchurch, 1998; Wilson, 2002).

For the purposes of tabulation and analyses in this study, the taxa have been grouped into five categories: Basal Sauropodomorpha, Eusauropoda, Diplodocoidea, Macronaria and Somphospondyli, referring to the groups chosen above and following the latest phylogenetic classification update from the literature and PBDB (see Table 1). Table 1 contains the latest two phylogenetic placements for each of the 61 taxa in order to give a broad perspective to the reader. However, the author considers the last entry for the assignment of the taxa within the five broad, aforementioned categories. For the analyses of this project and for reasons of clarity, concerning the phylogenetic positions of the taxa and wherever there are two different classifications assigned to a taxon, from different authors but the same year of publication, the author resolved the disputed relationships regarding the somewhat ambiguous placement of some taxa: *Vulcanodon* (Vulcanodontidae; Sekiya, 2011) is assigned here as a eusauropod, *Antetonitrus* as a basal sauropodomorph, *Tazoudasaurus* as a eusauropod, *Haplocanthosaurus* as a diplodocoid, and *Huanghetitan* and *Sauroposeidon* as somphospondylans. The reasoning behind the decision for *Vulcanodon* is that the subclade Vulcanodontidae is defined by characters neither too primitive for it to be placed within 'basal sauropodomorphs', nor too derived to be placed in Neosauropoda (Sekiya, 2011). According to Allain & Aquesbi (2008), the subclade Vulcanodontidae belongs to Gravisauria and Gravisauria are some of the earliest members of Sauropoda (i.e. Eusauropoda; see PBDB). Thus, for convenience, the author places within 'Eusauropoda' every non-basal sauropodomorph as well as every non-neosauropod sauropod, including gravisaurian ones. *Tazoudasaurus* was recently placed within 'Sauropoda' (Otero & Pol, 2013) and it is considered to be a vulcanodontid (Allain & Aquesbi, 2008), thus placing it in Eusauropoda (within Sauropoda but outside Neosauropoda). *Pleurocoelus* has vague taxonomic affinities but Salgado et al. (1997) has identified it as macronarian. For this study, any taxa belonging to the subclades of Sauropodiformes, Plateosauridae, Riojasauridae and Massospondylidae are placed within Basal Sauropodomorpha (McPhee et al., 2015). Also, Dicraeosauridae and Rebbachisauridae are placed in Diplodocoidea (Tschopp et al., 2015; Wilson & Allain, 2015; Xing et al., 2015) and Camarosauromorpha in Macronaria (Mannion et al., 2013; Carballido et al., 2015; Xing et al., 2015). Finally, any taxa belonging to the subclades Titanosauria, Saltasaurinae, Lognkosauria and Lithostrotia are placed within

Somphospondyli (e.g. Mannion et al., 2013; Mocho et al., 2014; Poropat et al., 2016; Gonzalez Riga et al., 2016; Mannion et al., 2017). The estimated evolutionary time bin of each taxon is also provided here (Table 2) based upon the latest updates from the literature (e.g. Poropat et al., 2016) and Palaeobiology Database (PBDB).

Table 1. Phylogenetic classification of the 61 sauropodomorph taxa. The classification is based upon the latest literature/PBDB. The second column contains the last two placements of each taxon, separated by a semicolon, in order to provide a broad perspective of the changes that have been made over time by different workers. Unless otherwise stated in the text, the author has assigned the 61 examined taxa into the five broad categories used in this study (Basal Sauropodomorpha, Eusauropoda, Diplodocoidea, Macronaria and Somphospondyli) based on the second entry of the 'Phylogenetic classification' column of this table.

Genus	Phylogenetic classsification / Latest Reference; Source: PBDB
Efraasia minor	Sauropodomorpha / McPhee et al. 2015
Plateosaurus sp.	Sauropodomorpha / Xing et al. 2015; Plateosauridae / McPhee et al. 2015
Ruehleia bedheimensis	Sauropodomorpha / Otero & Pol, 2013; Plateosauridae / McPhee et al. 2015
Eucnemesaurus fortis	Plateosauria / Apaldetti et al. 2011; Riojasauridae / McPhee et al. 2015
Thecodontosaurus sp.	Sauropodomorpha / Xing et al. 2015
Camelotia borealis	Sauropoda / Apaldetti et al, 2011; Sauropodiformes / Otero & Pol, 2013
Massospondylus carinatus	Sauropodomorpha / Barrett, 2009; Massospondylidae / McPhee et al. 2015
Aardonyx celestae	Sauropoda / Apaldetti et al, 2011; Sauropodiformes / McPhee et al. 2015
Seitaad ruessi	Sauropodomorpha / Apaldetti et al. 2011; Massospondylidae / Otero & Pol, 2013; Sauropodiformes / McPhee et al. 2015
Vulcanodon karibaensis	Sauropoda / Moser et al. 2006; Vulcanodontidae / Sekiya, 2011
Barapasaurus tagorei	Eusauropoda / Xing et al. 2015
Antetonitrus ingenipes	Sauropoda / Otero & Pol, 2013; Sauropodiformes / McPhee et al. 2015
Tazoudasaurus naimi	Vulcanodontidae / Allain & Aquesbi, 2008; Sauropoda / Otero & Pol, 2013
Kotasaurus yamanpalliensis	Sauropoda / Bandyopadhyay et al. 2010; Sekiya, 2011
Spinophorosaurus	Sauropoda / Remes et al. 2009; Eusaropoda / Xing et al. 2015
Rhoetosaurus brownei	Sauropoda / Wilson, 2002; Eusauropoda / Upchurch et al. 2004
Cetiosaurus sp.	Eusauropoda / Otero & Pol, 2013
Shunosaurus lii	Sauropoda / Li et al. 2010; Eusauropoda / Xing et al. 2015
Omeisaurus tianfuensis	Mamenchisauridae / Suteethorn et al. 2013; Eusauropoda / Mocho et al. 2014
Jobaria tiguidensis	Macronaria / Xing et al. 2015; Eusauropoda / Mannion et al. 2017
Patagosaurus fariasi	Eusauropoda / Mocho et al. 2014
Klamelisaurus gobiensis	Eusauropoda / Upchurch et al. 2004
Mamenchisaurus sp.	Eusauropoda / Mocho et al. 2014; Mamenchisauridae / Xing et al. 2015
Tehuelchesaurus benitezii	Camarasauridae / Mocho et al. 2014; Camarosauromorpha / Carballido et al. 2015
Haplocanthosaurus priscus	Eusauropoda / Xing et al. 2015; Diplodocoidea / Tschopp et al. 2015
Amphicoelias altus	Diplodocidae / Tchopp et al. 2015; Apatosaurinae / Tschopp & Mateus, 2017
Apatosaurus sp.	Diplodocoidea / Xing et al. 2015; Apatosaurinae / Tschopp et al. 2015
Suuwassea emilieae	Dicraeosauridae / Tschopp et al. 2015; Diplodocoidea / Xing et al. 2015
Barosaurus lentus	Diplodocoidea / Xing et al. 2015; Diplodocinae / Tschopp et al. 2015
Seismosaurus hallorum	Diplodocinae / Tschopp et al. 2015; Diplodocoidea / Xing et al. 2015
Diplodocus sp.	Diplodocinae / Tschopp et al. 2015; Diplodocoidea / Xing et al. 2015
Tornieria africana	Diplodocinae / Tschopp et al. 2015; Diplodocoidea / Xing et al. 2015
Dicraeosaurus sp.	Dicraeosauridae / Mocho et al. 2014; Diplodocoidea / Xing et al. 2015
Amargasaurus cazaui	Dicraeosauridae / Mocho et al. 2014; Diplodocoidea / Xing et al. 2015
Nigersaurus taqueti	Diplodocoidea / Xing et al. 2015; Rebbachisaurinae / Fanti et al. 2015
Amazonsaurus maranhensis	Diplodocoidea / Ibiricu et al. 2012; Rebbachisauridae / Wilson & Allain, 2015
Cathartesaura anaerobica	Limaysaurinae / Wilson & Allain, 2015; Rebbachisauridae / Motta et al. 2016
Janenschia robusta	Titanosauriformes / D'Emic, 2012; Macronaria / Mannion et al. 2013
Camarasaurus sp.	Camarasauridae / Moco et al. 2014; Macronaria / Xing et al. 2015
Australodocus bohetii	Neosauropoda / Ibiricu et al. 2012; Titanosauria / Mannion et al. 2013
Euhelopus zdanskyi	Camarosauromorpha / Carballido et al. 2015; Somphospondyli / Xing et al. 2015
Europasaurus holgeri	Camarosauromorpha / Carballido et al. 2015; Brachiosauridae / Mannion et al. 2017
Tendaguria tanzaniensis	Titanosauria / Mannion & Calvo, 2011; Somphospondyli / Carballido et al. 2015
Brachiosaurus altithorax	Titanosauriformes / Xing et al. 2015; Brachiosauridae / Mannion et al. 2017
Giraffatitan brancai	Titanosauriformes / Mocho et al. 2014; Brachiosauridae / Mannion et al. 2017
Erketu ellisoni	Euhelopodidae / D'Emic, 2012; Somphospondyli / Carballido et al. 2015
"Pleurocoelus"	Macronaria / Xing et al. 2015
Ornithopsis hulkei	Titanosauriformes / Mannion, 2010
Eucamerotus foxi	Neosauropoda / Sanchez-Hernandez et al. 2007; Macronaria / Xing et al. 2015
Huanghetitan liujiaxiaensis	Titanosauriformes / Mannion & Calvo, 2011; Somphospondyli / Mannion et al. 2013
Sauroposeidon proteles	Titanosauriformes / Mannion & Calvo, 2011; Somphospondyli / Mannion et al. 2017
Phuwiangosaurus sirinhornae	Euhelopodidae / D'Emic, 2012; Somphospondyli / Mocho et al. 2014
Malawisaurus dixeyi	Titanosauria / Mannion & Calvo, 2011; Lithostrotia / Mocho et al. 2014; Somphospondyli / Xing et al. 2015
Andesaurus delgadoi	Titanosauria / Gonzalez Riga & Ortiz David, 2014
Dongyangosaurus sinensis	Titanosauria / Poropat et al. 2016
Futalognkosaurus dukei	Lognkosauria / Gonzalez Riga & Ortiz David, 2014; Lithostrotia / Poropat et al. 2016
Neuquensaurus australis	Saltasaurinae / Gonzalez Riga & Ortiz David, 2014
Saltasaurus loricatus	Somphospondyli / Xing et al. 2015; Saltasauridae / Poropat et al. 2016
Puertasaurus reuili	Titanosauridae / Novas et al. 2005; Lognkosauria / Navarrete et al. 2011
Rapetosaurus krausei	Somphospondyli / Xing et al. 2015; Lithostrotia / Gonalez Riga et al. 2016
Alamosaurus sanjuanensis	Somphospondyli / Xing et al. 2015; Saltasauridae / Poropat et al. 2016

Table 2. Estimated evolutionary time bins of the 61 examined sauropodomorph taxa. The evolutionary time of each taxon is given as First Appearance Dates (FADs) and Last Appearance Dates (LADs). The average value of each FAD and LAD is also derived, which is used for the linear regression analyses in Chapter 2. Source of information was retrieved by the literature/PBDB.

Taxa	Evolutionary time bins (FADs-LADs in MYA)	Stratigraphic stages	Average time	Period	References
Efraasia minor	215.5-212	Norian	213.5	Upper Triassic	PBDB / Yates, 2003
Plateosaurus sp.	215.5-201.3	Norian-Rhaetian	208.4	Upper Triassic	PBDB / Yates, 2003
Ruehleia bedheimensis	228-208.5	Norian	218.25	Upper Triassic	PBDB / Galton, 2001
Eucnemesaurus fortis	228-201.3	Norian-Rhaetian	214.65	Upper Triassic	PBDB / Yates, 2007
Thecodontosaurus sp.	208.5-190.8	Rhaetian-Sinemurian	199.65	Upper Triassic-Lower Jurassic	PBDB
Camelotia borealis	208.5-201.3	Rhaetian	204.9	Upper Triassic	PBDB / Galton, 1985
Massospondylus carinatus	228-190.8	Norian-Sinemurian	209.4	Upper Triassic-Lower Jurassic	PBDB
Aardonyx celestae	201.3-190.8	Hettangian-Sinemurian	196.05	Lower Jurassic	PBDB / Yates et al. 2010
Seltaad ruessi	190.8-174.1	Pliensbachian-Toarcian	182.45	Lower Jurassic	PBDB / Sertich & Loewen, 2010
Vulcanodon karibaensis	201.3-199.3	Hettangian	200.3	Lower Jurassic	PBDB / Raath, 1972
Barapasaurus tagorei	199.3-182.7	Sinemurian-Pliensbachian	191	Lower Jurassic	PBDB / Jain et al. 1975
Antetonitrus ingenipes	201.3-182.7	Hettangian-Pliensbachian	214.65	Lower Jurassic	PBDB / McPhee et al. 2014
Tazoudasaurus naimi	190.8-174.1	Pliensbachian-Toarcian	182.45	Lower Jurassic	PBDB / Allain et al. 2004
Kotasaurus yamanpalliensis	199.3-182.7	Sinemurian-Pliensbachian	191	Lower Jurassic	PBDB / Yadagiri, 1988
Spinophorosaurus nigerensis	174.1-163.5	Aalenian-Callovian	168.8	Middle Jurassic	PBDB / Remes et al. 2009
Rhoetosaurus brownei	170.3-168.3	Bajocian	169.3	Middle Jurassic	PBDB / Bonaparte, 1986
Cetiosaurus sp.	171.6-122.4	Bajocian-Aptian	147	Middle Jurassic-Lower Cretaceous	PBDB
Shunosaurus lii	168.3-166.1	Bathonian-Callovian	167.2	Middle-Upper Jurassic	Zhang, 1988 / Chatterjee & Zheng / Poropat et al. 2016
Omeisaurus tianfuensis	168.3-163.5	Bathonian-Oxfordian	165.9	Middle-Upper Jurassic	Tang et al. 2001 / He et al. 1998Poropat et al. 2016
Jobaria tiguidensis	174.1-145	Aalenian-Berriasian	159.55	Middle-Upper Jurassic	PBDB / Sereno et al. 1999
Patagosaurus fariasi	166.1-163.5	Callovian	164.8	Middle Jurassic	PBDB / Bonaparte, 1979
Klamelisaurus gobiensis	163.5-157.3	Oxfordian	160.4	Upper Jurassic	PBDB / Zhao, 1993
Mamenchisaurus sp.	163.5-152.1	Oxfordian-Tithonian	157.8	Upper Jurassic	Ouyang & Ye, 2002 / Young & Zhao, 1972 / Poropat et al. 2016
Tehuelchesaurus benitezii	157.3-150.8	Kimmeridgian-Tithonian	154.05	Upper Jurassic	Cuneo et al. 2013 / Poropat et al. 2016
Haplocanthosaurus sp.	157.3-145	Kimmeridgian-Tithonian	151.15	Upper Jurassic	PBDB / Upchurch, 1995
Amphicoelias altus	157.3-150.8	Kimmeridgian	154.05	Upper Jurassic	PBDB / Wilson & Smith, 1996
Apatosaurus sp.	157.3-150.8	Kimmeridgian-Tithonian	154.05	Upper Jurassic	Kowallis et al. 1998 / Poropat et al. 2016
Suuwassea emilieae	155.7-145	Kimmeridgian-Tithonian	150.35	Upper Jurassic	PBDB / Harris & Dodson, 2004
Barosaurus lentus	157.3-145	Kimmeridgian-Tithonian	151.15	Upper Jurassic	PBDB
Seismosaurus hallorum	157.3-145	Kimmeridgian-Tithonian	151.15	Upper Jurassic	PBDB /Gillette, 1991 / Lucas et al. 2006
Diplodocus sp.	157.3-150.8	Kimmeridgian-Tithonian	154.05	Upper Jurassic	Kowallis et al. 1998 / Poropat et al. 2016
Torvisaurus africana	155.7-145	Kimmeridgian-Tithonian	150.35	Upper Jurassic	PBDB
Dicraeosaurus sp.	163.5-150.8	Oxfordian-Tithonian	157.15	Upper Jurassic	PBDB
Amargasaurus cazaui	129.4-122.4	Barremian-Aptian	125.9	Lower Cretaceous	PBDB / Salgado & Bonaparte, 1991
Nigersaurus taqueti	118-110	Aptian-Albian	114	Lower Cretaceous	Taquet, 1976 / Sereno et al. 1999 / Poropat et al. 2016
Amazonsaurus maranhensis	125-100.5	Aptian-Albian	112.75	Lower Cretaceous	PBDB / Carvalho et al. 2003
Cathartesaura anaerobica	99.6-89.8	Cenomanian-Turonian	94.7	Upper Cretaceous	PBDB / Gallina & Apesteguía, 2005
Jainosaurus robusta	152.1-145	Tithonian	148.55	Upper Jurassic	Aberhan et al. 2002 / Bussert et al. 2009 / Poropat et al. 2016
Camarasaurus sp.	157.3-150.8	Kimmeridgian-Tithonian	154.05	Upper Jurassic	Kowallis et al. 1998 / Poropat et al. 2016
Australodocus bohetii	152.1-145	Tithonian	148.55	Upper Jurassic	Remes, 2007 / Bussert et al. 2009 / Poropat et al. 2016
Euhelopus zdanskyi	129.4-112	Barremian-Aptian	120.7	Lower Cretaceous	Wilson & Upchurch, 2009 / Poropat et al. 2016
Europasaurus holgeri	157.3-152.1	Kimmeridgian	154.7	Upper Jurassic	Carballido & Sander, 2014 / Sander et al. 2006 / Marpmann et al. 2015 / Poropat et al. 2016
Tendaguria tanzaniensis	152.1-145	Tithonian	148.55	Upper Jurassic	Aberhan et al. 2002 / Bussert et al. 2009 / Poropat et al. 2016
Brachiosaurus altithorax	157.3-150.8	Kimmeridgian-Tithonian	154.05	Upper Jurassic	Kowallis et al. 1998 / Poropat et al. 2016
Giraffatitan brancai	157.3-150.8	Kimmeridgian-Tithonian	154.05	Upper Jurassic	Aberhan et al. 2002 / Bussert et al. 2009 / Poropat et al. 2016
Erketu ellisoni	100.5-96.3	Cenomanian-Santonian	93.4	Lower Cretaceous	Ksepka & Norell, 2010 / Poropat et al. 2016
"Pleurocoelus"	166.1-125	Callovian-Aptian	145.55	Middle Jurassic-Lower Cretaceous	PBDB / Salgado et al. 1997
Ornithopsis hulkei	164.7-122.4	Callovian-Aptian	143.55	Middle Jurassic-Lower Cretaceous	PBDB / Mannion, 2010
Eucamerotus foxi	164.7-122.4	Callovian-Aptian	143.55	Middle Jurassic-Lower Cretaceous	PBDB / Mannion, 2010
Huanghetitan liujiaxiaensis	100.5-96.3	Cenomanian-Santonian	93.4	Lower Cretaceous	Lu et al. 2007 / Poropat et al. 2016
Sauroposeidon proteles	125-113	Aptian-Albian	119	Lower Cretaceous	Wedel et al. 2000 / Poropat et al. 2016
Phuwiangosaurus sirindhornae	129.4-112	Barremian-Aptian	120.7	Lower Cretaceous	Racey & Goodall, 2009 / Poropat et al. 2016
Malawisaurus dixeyi	125-113	Aptian	119	Lower Cretaceous	Gomani, 2005 / Gorscák et al. 2014 / Poropat et al. 2016
Andesaurus delgadoi	100.5-93.9	Cenomanian	97.2	Upper Cretaceous	Leanza et al. 2003 / Poropat et al. 2016
Dongyangosaurus sinensis	100.5-88	Cenomanian-Turonian	94.25	Upper Cretaceous	Lu et al. 2008 / Yu et al. 2010 / Poropat et al. 2016
Futalognkosaurus dukei	93.5-85.8	Turonian-Santonian	89.65	Upper Cretaceous	Leanza et al. 2003 / Calvo et al. 2007 / Poropat et al. 2016
Neuquensaurus australis	86.3-72.1	Santonian-Campanian	79.2	Upper Cretaceous	PBDB / Powell, 1992
Saltasaurus loricatus	70.6-66	Maastrichtian	68.3	Upper Cretaceous	Quattrocchio et al. 2005 / Poropat et al. 2016
Puertasaurus reuili	70.6-66	Maastrichtian	68.3	Upper Cretaceous	PBDB / Novas et al. 2005
Rapetosaurus krausei	72.1-66	Maastrichtian	69.05	Upper Cretaceous	Rogers et al. 2000 / Rogers et al. 2013 / Poropat et al. 2016
Alamosaurus sanjuanensis	83.5-66	Campanian-Maastrichtian	74.75	Upper Cretaceous	Williamson & Weil, 2008 / Poropat et al. 2016

Not much emphasis has been given in determining a review of ratios among the lengths of necks, trunks and tails of all major clades of sauropods because most sauropod holotypes lack a complete series of vertebrae, making such calculations unfeasible. Despite that, and also the fact that the ratios and measurements differ in every sauropod species, simple observations on the overall basic forms reveal a few generalised patterns. Flagellicaudatan diplodocoids (Diplodocidae and Dicraeosauridae) have tails that can be twice the length of the necks (or trunks), basal titanosauriform macronarians (Brachiosauridae) have necks at least twice that of their tails (or trunks), and all others follow the 'standard' form of having equally lengthened necks and tails, with their trunks having equal lengths to that of their neck or tail or even being shorter than either of the two other body parts (i.e. neck and tail). In this study, 'trunk' is the main body segment that begins from the anterior-most dorsal vertebra and ends in the posterior-most sacral vertebra. Therefore, having an estimated overall length of a given extinct animal and some generalised patterns, we can roughly deduce the lengths of each of its main body segments, i.e. neck, trunk and tail.

2.1.1) Evolution of sauropod vertebral pneumatisation

The modification of the sauropod postcranium by pneumatic diverticula, evidenced as PSP (i.e. Postcranial Skeletal Pneumaticity), has been the only skeletal evidence, thus far, for palaeontologists to detect the presence of pneumatic diverticula in these animals (Britt, 1993 & 1997; Wedel, 2003a, 2009; O'Connor & Claessens, 2005; O'Connor, 2006; Benson et al., 2012; Butler et al., 2012; Yates et al., 2012). This feature has appeared multiple times across their phylogeny (e.g. Upchurch, 1998), in variable expressions, each time governed by biotic factors during the ontogeny of the individual. The expression is not only variable in its forms but also in its locations in the skeleton (e.g. Wedel et al., 2000; Wedel, 2003a,b; Schwarz & Fritsch, 2006; Schwarz et al., 2007a; Wedel & Taylor, 2013). The erratic behaviour of the PSP's presence has been observed in other subclades of Ornithodira like avian and non-avian theropods (O'Connor, 2004, 2009; O'Connor & Claessens, 2005; O'Connor, 2006; Benson et al., 2012), pterosaurs (e.g. Claessens et al., 2009) and, maybe, in ornithischians too. Observations on the variation of PSP in sauropods show that pneumatisation of the cervical and dorsal vertebrae originated in basal sauropodomorphs in the form of shallow (non-invasive) fossae, presacral invasive pneumatisation in eusauropods, invasive pneumatisation of the precaudal vertebrae in mamenchisaurids and most neosauropods, as well as complex and invasive pneumatisation in various regions throughout the entire vertebral column (including the caudal region) and pelvic girdle occurs in diplodocoids, basal titanosauriformes and somphospondylans (Wedel, 2003b; Wedel, 2005; Wedel, 2009; Cerda et al., 2012).

The development and evolution of postcranial skeletal pneumaticity paved the way for sauropods to reach their gigantic sizes, setting a record which no other terrestrial group of animals has ever conquered (Sander et al., 2011). The least expression of PSP is the presence of apneumatic fossae, which may have housed air sacs and/or adipose tissue, cartilage and muscles, as is noted in crocodilians regarding the latter three types of tissue (e.g. Britt, 1993). These fossae have weakly developed margins and are 'blind' i.e. they do not 'lead' further inside the bone. Pneumatic fossae are stronger evidence of PSP and are usually sharp-rimmed and may house multiple subfossae and foramina (e.g. Wedel et al., 2000; Wedel, 2003, 2005), evidence of the deeper penetration of the diverticula inside the cortical and, in many cases, the trabecular bone of the vertebrae (e.g. Upchurch et al., 2004). Further evidence of pneumatisation is the presence of these features accompanied by laminae, i.e. laminated fossa or laminated foramen, as well as any combination among those features in a vertebra (e.g. Wedel et al., 2000; Wedel, 2003, 2005; Apostolaki et al., 2015). The latter observation, along with the presence of internal chambers (i.e. camerae and camellae), occur in the derived neosauropod clades of diplodocoids, macronarians and somphospondylans. If a diagnosis is equivocal, the best course of action is to check if there are other pneumatic features near the ambiguous trait in question (Wedel & Taylor, 2013).

Delving deeper into this analysis, it is important to note the evolutionary progression of pneumaticity on a vertebral level. Studying this attribute in theropods, Benson et al. (2012) discovered two patterns in the vertebral columns, the 'neural arch first' rule and the 'no gaps' rule. The first rule means that pneumatisation by bone resorption in a vertebra begins in the neural arch and progresses towards the centrum and the other parts. The second rule means that pneumatic vertebrae form consistent series without being 'interrupted' in-between by non-pneumatic vertebrae. As will be explained below, neither of these two cases holds true in Sauropodomorpha; in fact, the exact opposite patterns occur. From an evolutionary perspective, findings reveal that after the centrum, the neural arch and the transverse processes are the parts most likely to be pneumatised and also that the first pneumatic occurrences appear in the cervicodorsal region. Wedel and Taylor (2013) also demonstrated that the expression of pneumatic and apneumatic fossae varies among individuals, along their vertebral series and from left to right in a single vertebra.

The parallel existence of a diverticular lung (i.e. with diverticula extending from the lung towards other parts of the body, forming air sacs and/or invading bone material) and air sac system in so many clades has led to the accepted theory that PSP has been a basal trait to Ornithodira (Wedel, 2009; O'Connor & Claessens, 2005; O'Connor, 2006; Benson et al., 2012). PSP has been abundantly documented in non-avian theropod, avian as well as pterosaur axial and appendicular elements (e.g. O'Connor & Claessens, 2005;

O'Connor, 2006; Sereno et al., 2008; O'Connor, 2009; Butler, Barrett & Gower, 2009; Claessens, O'Connor & Unwin, 2009; Benson, Carrano & Brusatte, 2010; Watanabe, Gold, Brusatte et al., 2015). The development of PSP in birds and pterosaurs helped not only in decreasing their overall body density but also in increasing their long bone bending stiffness, especially in the larger pterosaurs since the biomechanical loads they endured during flight were greater than those of birds (Martin & Palmer, 2014). Contrary to that, there are cases of birds where PSP is minimally present and, in many cases, absent, as evidenced in the postcrania of diving birds, resulting in bones that are often devoid of any diverticular signs of bone modification such as resorption and penetration (e.g. O'Connor, 2006; Apostolaki et al., 2015), a condition also found in most basal sauropodomorphs and some vertebral regions of sauropods (see Appendices 1 & 3). The argument behind that is that PSP is the osteological evidence of a diverticular lung system in birds, but such a diverticular system can exist without leaving skeletal traces. Since PSP has been found in several archosaurian lineages, including birds and pterosaurs, it is widely accepted that the diverticular lung may have been present in the ancestor of Ornithodira, even though we do not have direct evidence of PSP in basal ornithodirans to support that.
Furthermore, the 'avian-style lung' respiratory system has been proposed as one of the five main drivers of sauropod gigantism (Sander, 2013) but the role of PSP in relation to size has not been elucidated yet; it is our purpose then, to discover whether or not there is an association between the presence of PSP in sauropods and the variations of size estimates, i.e. mass and length, as a way to confirm or rule out the 'cause-and-effect' link between osteological pneumatisation and size.

This study, among its other goals, attempts to concentrate on recording every account of vertebral and pelvic pneumaticity found in 61 sauropodomorph taxa spanning from the Late Triassic to the Late Cretaceous, thus creating a temporal and morphological 'map' of the expression of PSP. Never before has such a detailed account of pneumaticity been recorded, with the prospect of creating a classification scheme of taxa based on their osteological pneumaticity profile. This tool can be used by any researcher for any archosaurian taxon, sauropod or otherwise.

2.1.2) Aims, objectives and rationale of this project

Chapter 2 aims to test if high degrees of pneumaticity are associated with large body size in sauropods or if the expression of pneumaticity is irrelevant to body size. The objectives are:

i) To test if the relationship between body size and pneumaticity is contingent on the body size metrics (i.e. mass, length).

ii) To test if pneumaticity measured across the vertebral column correlates proportionately (positive), inversely proportionately (negative) or neutrally variable with body size.

It also aims to verify whether pneumaticity varies differently in different families (positive, negative or neutral correlation) and vertebral regions. The alternative scenario would be that all major clades have similar degrees of pneumaticity and that the pneumaticity degree remains stable when comparing the same vertebral regions of different taxa. Thus, we need:

i) To test if there is correlation of pneumaticity with the lengths of vertebral regions and how consistent it is with each region.

ii) To test if and how the degree of pneumaticity varies across taxa using genus as the operational taxonomic unit.

iii) To show if different regions of the vertebral column are pneumatised differently among taxa of the same and of different families.

2.2) Materials and Methods

2.2.1) Pneumatic characters

Several pneumatic phenomena are seen commonly in sauropods (Figures 1-8) and other archosaurs. Below are the basic key pneumaticity traits found mostly in the axial and appendicular elements of sauropods, theropods and pterosaurs but to a relatively lesser extend of expression in birds.

Fossa: a large and wide excavation on the bone, which may be subcircular, oval, or circular, and forms a shallow depression on the bone's surface (Wilson et al., 2011). A pneumatic fossa has smooth and crenulated bone texture, it is larger than a pneumatic foramen and can measure between 2 cm and 10 cm in diameter. Like the pneumatic foramen, the fossa can also be found in pterosaurs, ornithopods, theropods, sauropods (more often in basal sauropodomorphs) and birds, but it is rarely observed in appendicular elements, being more often observed in vertebrae. Unlike pneumatic foramina, fossae are shallow and rarely invade the cancellous tissue of the bone (i.e. blind; Figs. 1, 3, 5, 6, 8). A fossa is usually considered as an ambiguous indication of pneumaticity, since it is less

likely to indicate a place of diverticular invasion and more likely to serve as a muscular attachment site or as a deposition area for adipose tissue. A fossa can be subdivided into many smaller fossae by bony septa and is often bordered by laminae.

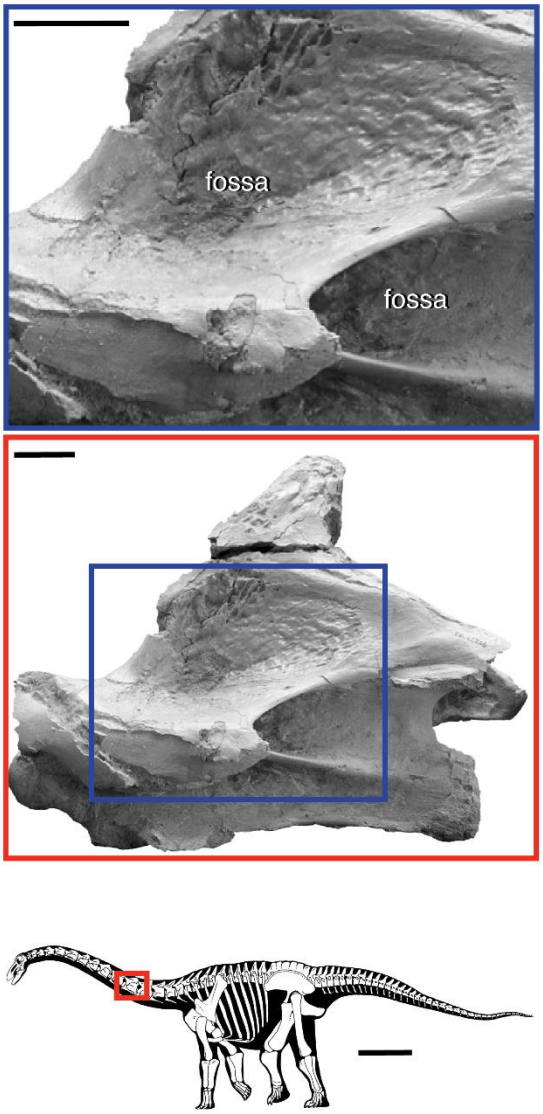

Figure 1. Middle cervical vertebra in left lateral view and illustration of *Rapetosaurus*. Pneumatic fossae in a sauropod vertebra shown in magnification (A). The middle photograph (B) shows the cervical vertebra in its entirety and the fossae which are bordered by laminae of the neural arch (adapted from Curry Rogers & Forster, 2004). A *Rapetosaurus* silhouette is shown in the bottom illustration (C) adapted from Curry Rogers & Forster (2004). Note the smooth and crenulated texture of the bone which is indicative of its pneumatic nature. Scale bars of the cervical vertebra equal 3 cm; scale bar of silhouette equals 1 m. Figure adapted from Wilson et al. (2011, Fig. 1). Image was kindly provided with permission from Jeffrey A. Wilson.

Pneumatic foramen: a perforation on the surface of the bone in the form of an oval or circular hole, having smooth margins and measuring between 0.5 cm and 5 cm in diameter (Figs. 2, 3, 5, 6, 8). It can be found in vertebral and appendicular elements of pterosaurs, theropods, sauropods and birds. A foramen penetrates the cortical bone and often it further penetrates through the cancellous bone. It may also communicate with internal chambers such as camerae, can lie within a fossa or a pleurocoel, can be septated (i.e. many foramina interconnected with bony septa), or a lamina can be part of the boundary of a foramen. A foramen is different from a fossa or a pleurocoel in the facts that its diameter is smaller and its shape is mostly circular. Finally, a foramen can be found in any vertebral part (e.g. centrum, spine, neural arch, etc.).

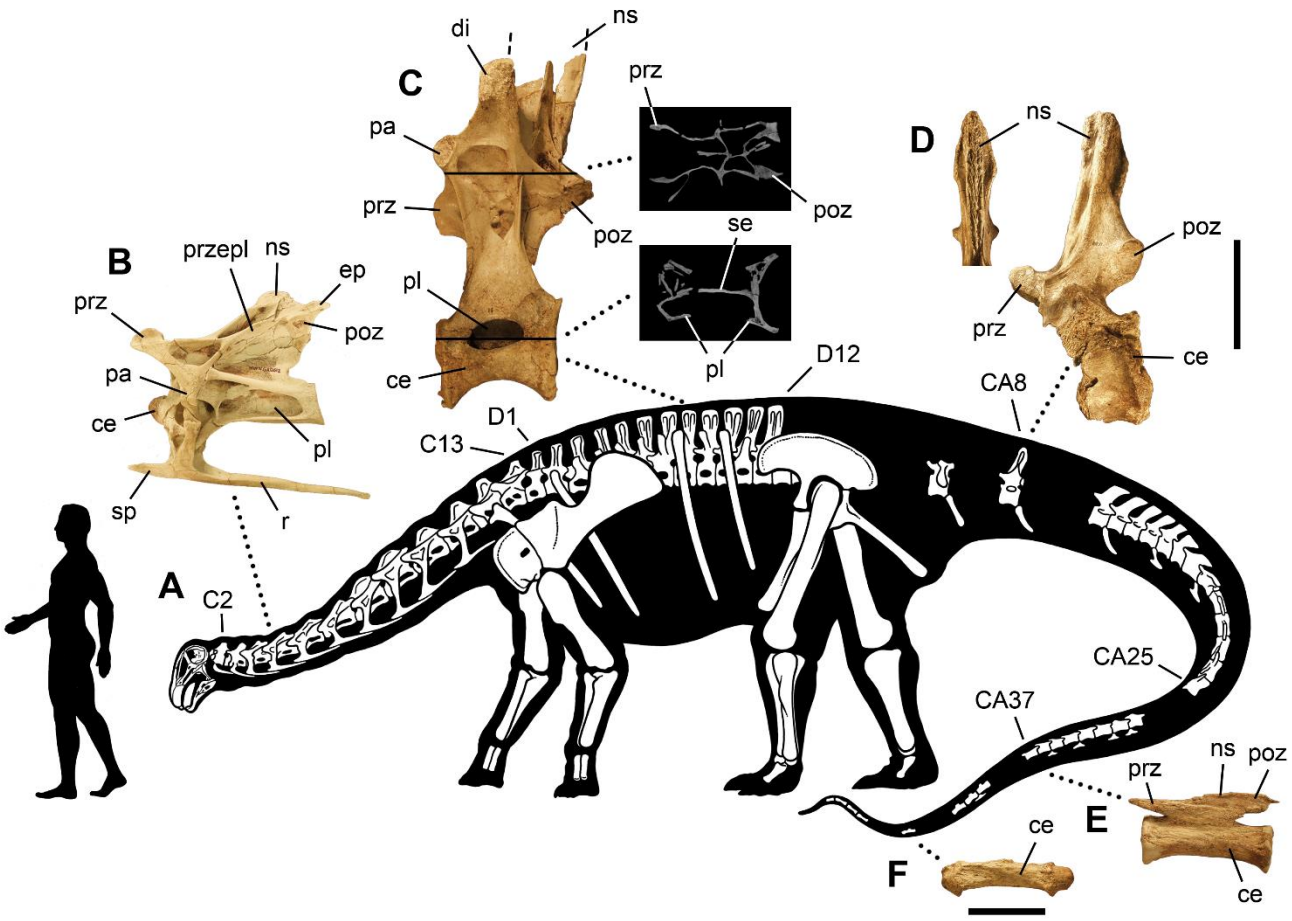

Figure 2. Vertebrae of *Nigersaurus taqueti*. (A) Skeletal reconstruction of *Nigersaurus* based on specimens MNN GAD513, MNN GAD515, MNN GAD516, MNN GAD517 and MNN GAD518. (B) Fifth cervical vertebra in left lateral view; note the pleurocoel excavating a large part of the centrum. (C) Eighth dorsal vertebra in left lateral view with two CT scans of two cross-sections; again, note the large pleurocoel in the centrum

excavating deeply inside the bone. (D) Proximal caudal vertebra (eighth, probably) in left lateral view (whole picture) and anterior view of its neural spine. (E) Mid-posterior caudal vertebra (*ca.*CA37) in left lateral view and (F) distal caudal vertebra (*ca.* CA47) in right lateral view. A large shallow fossa may be evident in the proximal caudal vertebra's centrum while the middle and posterior caudal vertebrae do not possess any pleurocoels or fossae. Human figure measures 1.68 m in height. Upper scale bar equals 10 cm (B-E); lower scale bar equals 5 cm (F). Abbreviations: *C*, cervical vertebra; *CA*, caudal vertebra; *ce*, centrum; *D*, dorsal vertebra; *di*, diapophysis; *ep*, epipophysis; *ns*, neural spine; *pa*, parapophysis; *pl*, pleurocoel; *poz*, postzygapophysis; *prz*, prezygapophysis; *przepl*, prezygapophyseal-epipophyseal lamina; *r*, rib; *se*, septum; *sp*, spine. Figure adapted from Sereno et al. (2007, Fig. 3). Image credit: Sereno et al. 2007 (PLoS One). Image was freely retrieved from PLoS One which acts under CC-BY 4.0 license protocol.

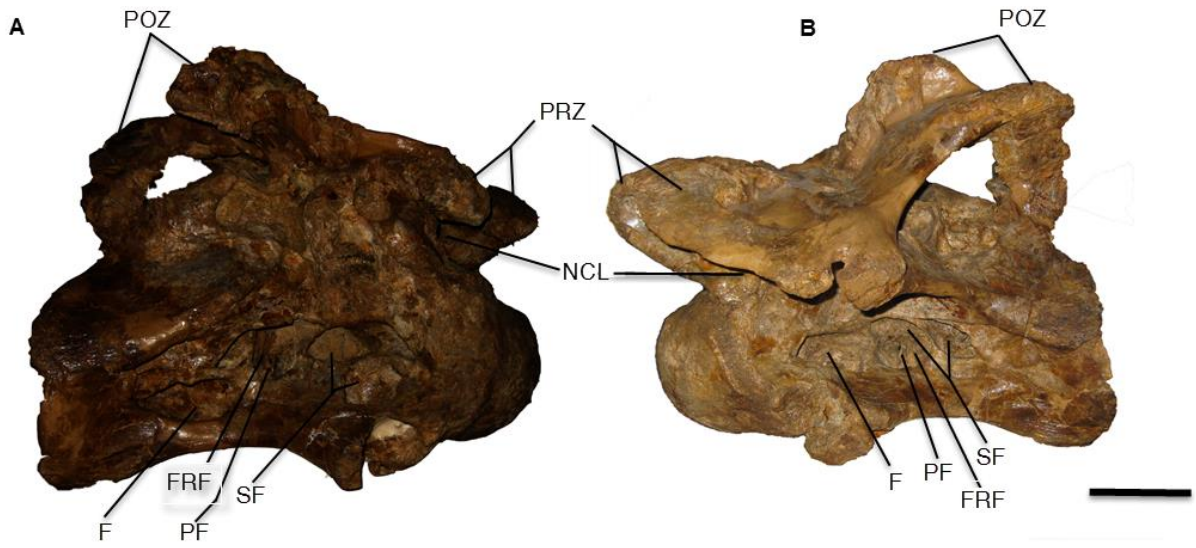

Figure 3. Cervical vertebra of *Janenschia robusta*. (A) Right lateral and (B) left lateral views of a cervical vertebra of *Janenschia* robusta (MB.R.2091.3; Fraas, 1908) showing various pneumatic elements**.** Specimen was documented by Janensch (1929) as well as Bonaparte, Heinrich & Wild (2000). Notice the variation in combination of the elements in the centrum, namely a pneumatic foramen on a fossa, the fossae separated by a septum and the main fossae occupying most of the lateral surface of the centrum on each side, often separated by septa. Scale bar equals 5 cm. Abbreviations: *F*, fossa; *FRF*, foraminous fossa; *NCL*, neural canal, *PF*, pneumatic foramen; *POZ*, postzygapophysis; *PRZ*, prezygapophysis; *SF*, septated fossae. Image credit: Naomi E. Apostolaki.

Pleurocoel: a large and wide cavity with smooth margins, usually oval or subcircular in shape. This term is used to indicate a very large lateral fossa which occupies most of the centrum or neural arch side(s). It is found primarily in the cervical and dorsal vertebrae of sauropods and theropods, most often in the centra, occupying large portions of the bone and excavating deep into it (Figs. 2, 5, 6, 8). A pleurocoel is larger (i.e. wider) and deeper than a fossa, measuring at least 5-6 cm in diameter and at least 2-3 cm in depth in theropod vertebrae and even larger in sauropod vertebrae (at least 10 cm in diameter and 5-6 cm in depth). The 'pleurocoel' is a term adopted by many researchers to describe openings that are larger and deeper than fossae, as well as to indicate their probable pneumatic nature in contrast to the more ambiguously pneumatic nature of fossae (e.g. Wedel et al., 2000a, b; Wedel, 2001; Wedel, 2003b; Sereno et al., 2007, 2008). In fossil vertebrae, the pneumatic nature of pleurocoels is still not definite since these large openings could house reserves of adipose tissue or serve as muscle attachments, but judging from their rounded shape and texture, they probably housed pneumatic diverticula that expanded within the bone during ontogeny, or possibly they could contain any assortment of diverticular, adipose and muscle tissues (Apostolaki, Rayfield & Barrett, 2015). As with pneumatic foramina and fossae, bone tissue undergoes resorption as the diverticular tissue attaches and infiltrates the bone tissue, replacing the bone marrow with air. A pleurocoel may often bear shallow fossae or pneumatic foramina. Some researchers also use the term 'pneumatocoel' to describe a vertebral opening that is more similar to the 'pleurocoel' than to a 'foramen' or they use it as a synonym for the 'pleurocoel' when the large opening is not found in the centrum but on other vertebral parts. In this study, we prefer the term 'pleurocoel' to the term 'pneumatocoel' since we cannot be certain of the diverticular (pneumatic) nature of such openings in sauropod vertebrae.

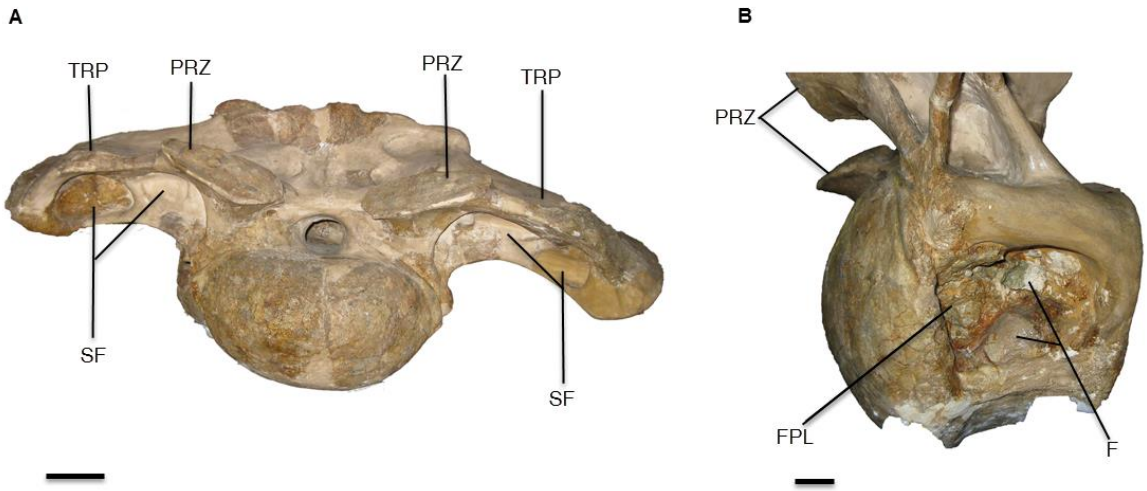

Figure 4. *Tendaguria tanzaniensis* dorsal vertebra. (A) Anterior view of an anterior dorsal vertebra of *Tendaguria tanzaniensis* (MB.R.2092.1; Janensch, 1929) showing large septated fossae on the anterior sides of its transverse processes. This specimen was also documented and described by Bonaparte, Heinrich & Wild (2000). Some researchers may address these fossae as 'coels' due to their larger-than-fossa extensive dimensions and the space they occupy in the vertebra**.** (B) Close up of the left lateral view of the centrum of (A). Notice the pleurocoel which houses fossae, some of them infilled with matrix (green/white/brown areas). Scale bars equal 10cm. Abbreviations: *F*, fossa; *FPL*, fosseous pleurocoel; *PRZ*, prezygapophysis; *SF*, septated fossae; *TRP*, transverse process. Image credit: Naomi E. Apostolaki.

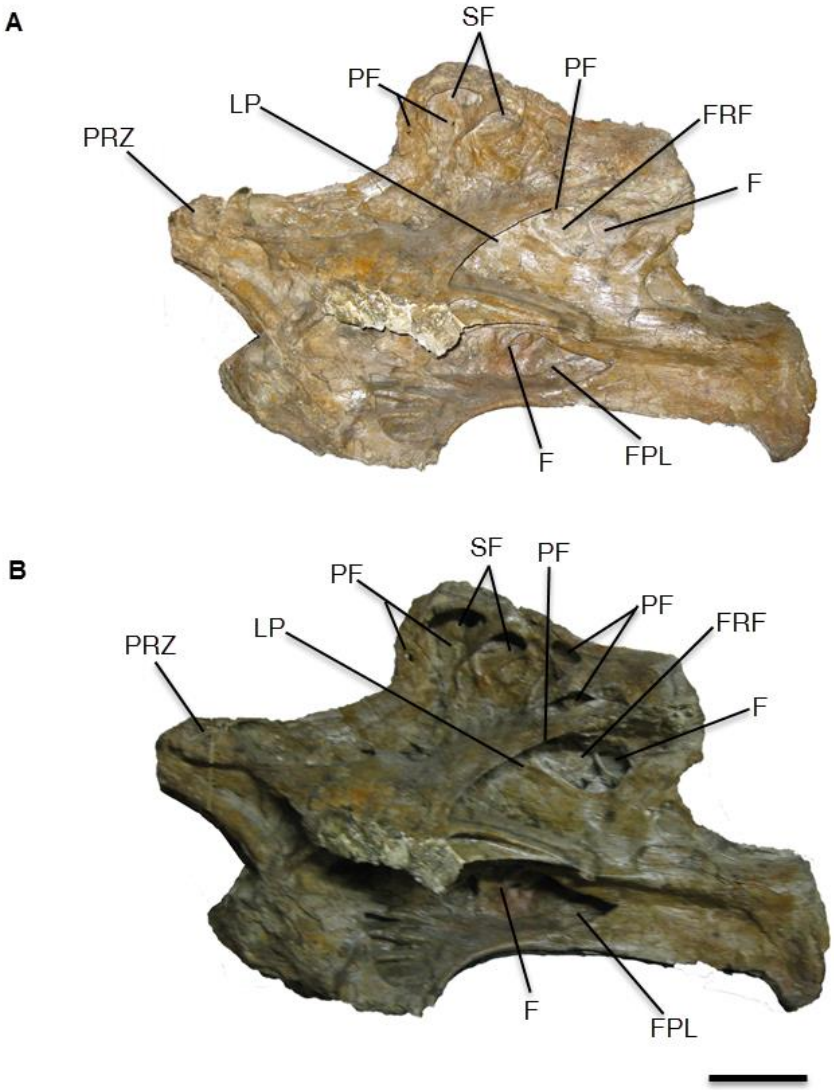

Figure 5. ***Giraffatitan (Brachiosaurus) brancai*** **cervical vertebra.** Illuminated (A) and (B) normal photographs of the 7th cervical vertebra of *Giraffatitan brancai* (MB.R.2180.28; Janensch, 1914) on its left lateral view showing its numerous and complex pneumatic elements. This specimen was also documented by Schwarz & Fritsch (2006). Notice the foramen on the fossa close to the neural spine, the fosseous pleurocoel just below the neurocentral suture and the foramen that is visible just below the lip of the postzygapophyseal-diapophyseal lamina. This pneumatic foramen perforates the light-colored fossa [better visible in (B)] located on the neural arch. The light-colored foraminous fossa and another smaller fossa posterior to it are enclosed within a larger area which can be identified as a laminated pleurocoel (subtriangular shape) which is dorsally bordered by the prezygapophyseal-diapophyseal lamina and covers the areas of neural arch and base of neural spine. Thus, said laminated pleurocoel can also be addressed as a pleurocoel that contains both a foramen and fossae. Scale bar equals 10

cm. Abbreviations: *F*, fossa; *FPL*, fosseous pleurocoel, *FRF*, foraminous fossa; *LP*, laminated pleurocoel; *PF*, pneumatic foramen; *PRZ*, prezygapophysis; *SF*, septated fossae. Image credit: Naomi E. Apostolaki.

Camerae: large internal chambers found in the vertebrae of basal neosauropods, including diplodocoids and macronarians, as well as basal titanosauriform and somphospondylan sauropods (i.e. members of the clade Somphospondyli). These chambers are unambiguous evidence of vertebral pneumaticity and are formed by internal remodelling of the bone during ontogeny. They often communicate with external pneumatic foramina created by the invading diverticula. Their shape is rounded, separated from each other by thick septa (2-10 mm), forming a regular branching pattern (Wedel et al., 2000a, b; Wedel, 2001). They may occupy any or all parts of the vertebra, including centrum, neural arch, and neural spine, and are notably expressed in diplodocoids such as *Apatosaurus* and basal macronarians such as *Camarasaurus*. In some taxa like *Apatosaurus*, the vertebrae possess numerous camerae that propagate further into the bone, forming polycamerate patterns (Figs. 6, 8).

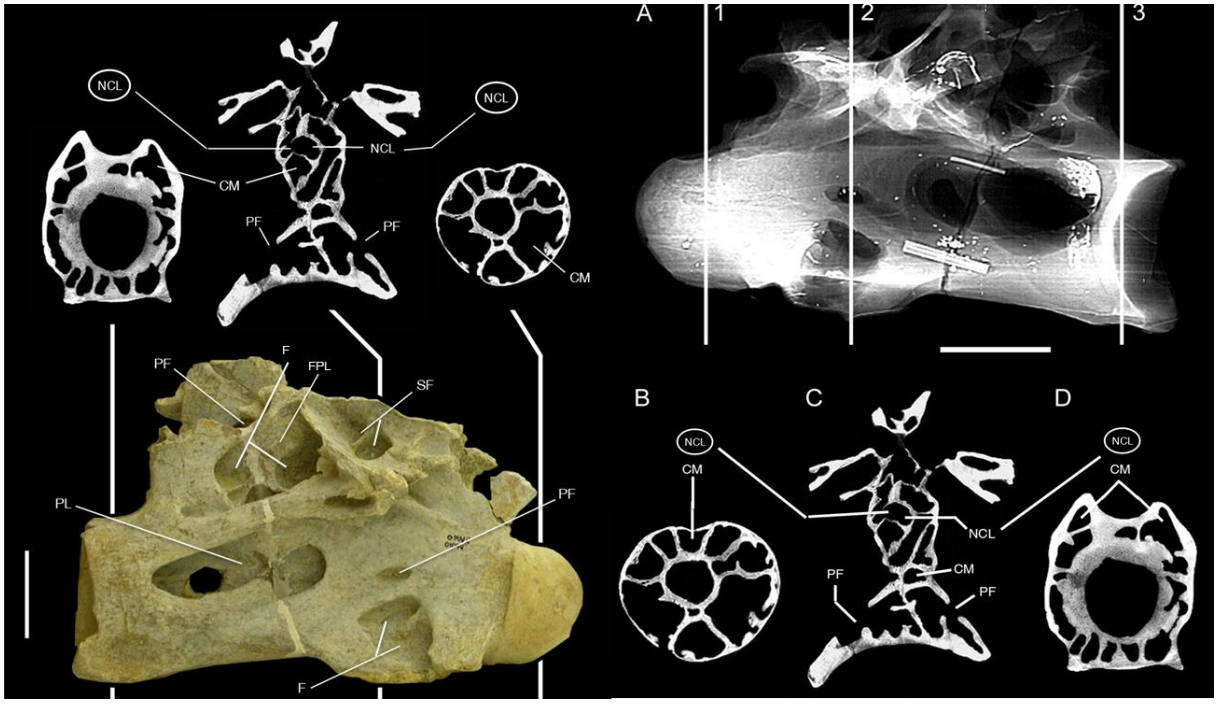

Figure 6. Pneumatic elements in a cervical vertebra of *Apatosaurus*. *Apatosaurus* cervical vertebra (OMNH 01094) in right lateral view, and CT sections from the anterior, middle and posterior parts showing pneumatic foramina, fossae, pleurocoels, subdivided fossae and camerae. (A) The vertebra in left lateral view. (B) Transverse section through

the condyle showing the radially oriented camerae. (C) A mid-section showing all irregularly arranged camerae occupying all vertebral parts. (D) Transverse section through the cotyle showing the radially arranged camerae. 'NCL' enclosed in oval shape indicates approximate position of the neural canal in the anterior and posterior transverse CT sections of the vertebra (B & D). Scale bar equals 10 cm. Abbreviations: *CM,* camera; *F*, fossa; *PF*, pneumatic foramen; *PL*, pleurocoel; *FPL*, fosseous pleurocoel; *NCL,* neural canal; *SF*, subdivided fossae. Photograph and CT sections given with kind permission from Mathew J. Wedel (modification and adaptation by Naomi E. Apostolaki). Figures adapted from Wedel (2001, Fig. 8). Image credit: Mathew J. Wedel.

Camellae: numerous small cavities within the vertebrae of basal titanosauriform and somphospondylous titanosaurian sauropods, resembling a honeycomb-like structure (Figs. 7, 8). These small cavities are not rounded, but instead they are angular and thinly septated, with the osteal walls ranging from less than 1 mm to 3 mm in thickness (Wedel et al., 2000b). Like camerae, camellae are unambiguous indicators of pneumaticity, and represent the highest degrees of ostial aeration. They are presumably the result of further evolution of internal remodelling of the bone by the interactions of osteocytes and the invading diverticula during ontogeny (e.g. Wedel, 2003b). Camellae often lead to external pneumatic foramina, created by the invading diverticula. In somphospondylan vertebrae, they occupy the entirety of the internal space of the bones and form irregular branching patterns, producing 'somphospondylous' vertebrae (i.e. 'sponge-like'; Fig. 7).

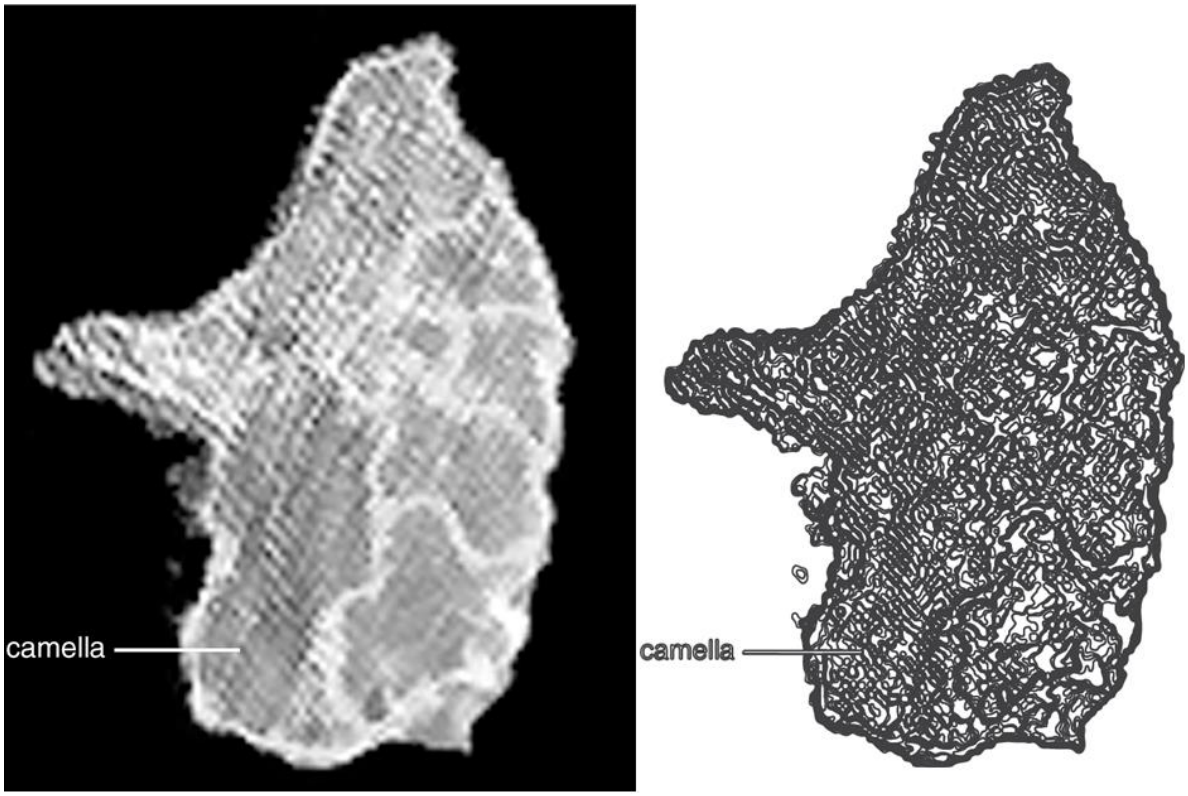

Figure 7. CT section of a *Sauroposeidon* cervical vertebra (OMNH 53062). The tomographic image of a slice of *Sauroposeidon* cervical vertebra (A) and its line drawing to the left (B) showing the camellate structure in the right postzygapophysis, completely occupying the internal structure of the bone. The upper left part is obscured from the x-ray beam by the size and density of the specimen. Figure adapted from Wedel et al. (2000a, Fig. 12H). Line drawing by Naomi E. Apostolaki. Image credit: Mathew J. Wedel. Image (A) was given with kind permission from Mathew J. Wedel.

Semicamellate: the condition in which the internal architecture of a sauropod vertebra is only partially dominated by camellae, while other parts are camerate (Wedel, 2000a, b; Wedel, 2001, 2003, 2005. This condition is found in basal titanosauriforms and somphospondylans, as in the basal titanosauriform *Brachiosaurus* (Fig. 8). The similar term ‘semicamerate’ indicates where the sauropod vertebra is only partially camerate (e.g. only the centrum and the neural arch).

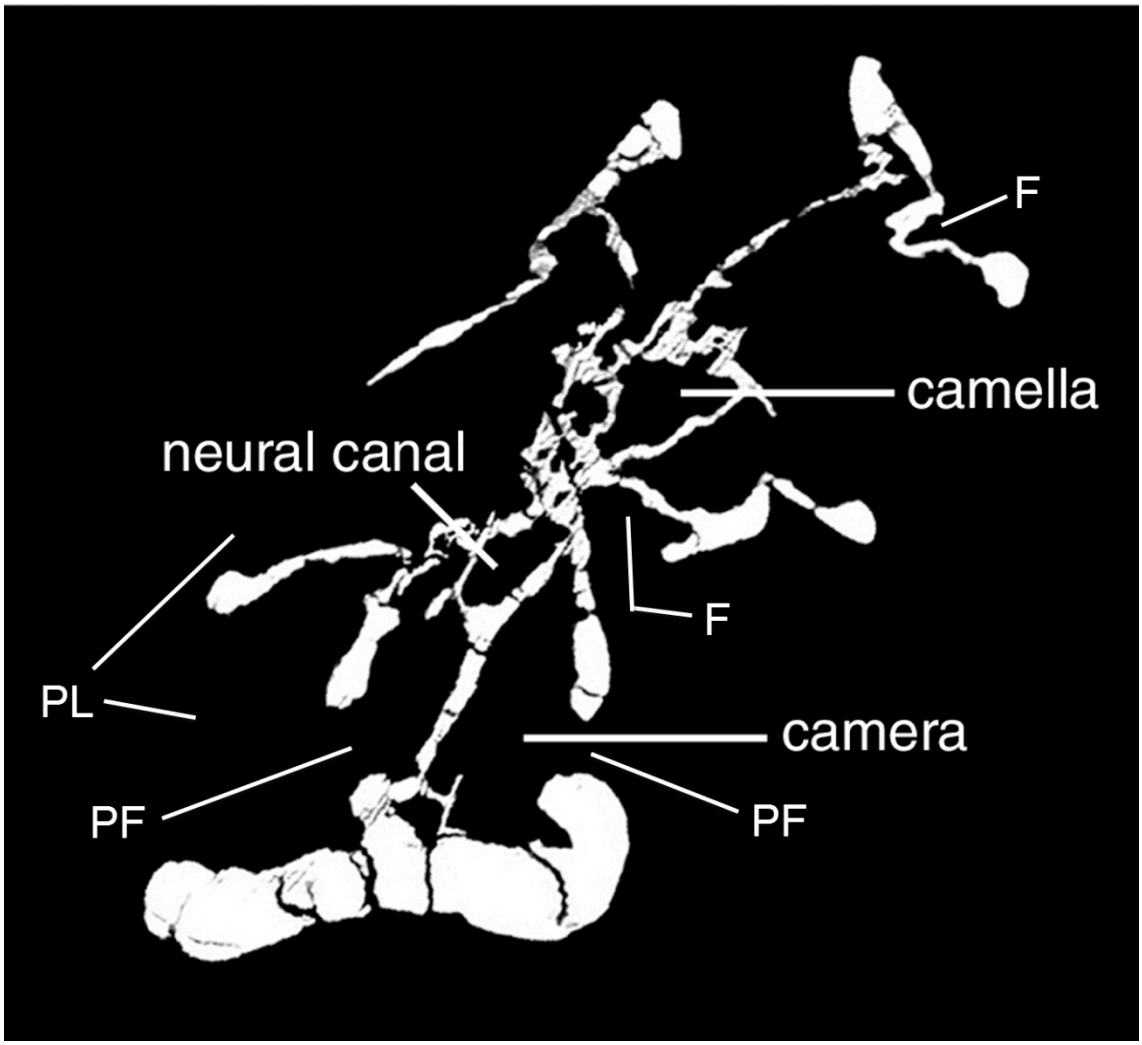

Figure 8. CT section showing the posterior of *Brachiosaurus* cervical vertebra (BYU 12866). The CT scan reveals both camerae and camellae. The lateral open areas of the bone are the pneumatic foramina, pleurocoels and fossae. Camellae occupy the neural spine and the median septum (upper part of neural arch) while most of the vertebra is dominated by large camerae. Also note that the laminae are connected to the median septum by thin bony segments. Abbreviations: *F*, fossa; *PF*, pneumatic foramen; *PL*, pleurocoel. Figure adapted from Wedel et al. (2000a, Fig. 12C). Image credit: Mathew J. Wedel. Image was given with kind permission from Mathew J. Wedel.

These pneumaticity features can be found primarily in sauropods. Many of the features as well as their combined versions, either alone or bordered by laminae, have also been documented in theropods, birds (e.g. Hogg, 1984; O'Connor, 1999; O'Connor, 2006; Sereno et al., 2008; Apostolaki, Rayfield & Barrett, 2015) and pterosaurs (e.g. Butler, Barrett & Gower, 2009; O'Connor, 2009; Claessens, O'Connor & Unwin, 2009; Benson, Carrano & Brusatte, 2010; Watanabe, Gold, Brusatte et al., 2015). In the

literature, many authors do not give adequate emphasis to pneumaticity, perhaps recording laminae and basic pneumatic features, but often only to a basic level and only if these features are outstanding. Most observations can be made with the naked eye, especially if the bone is partially fragmented, but CT scans can resolve uncertainties regarding the extent of pneumatization. Many CT scans are freely available in the literature, while others (such as Figs. 1, 2, 6, 7 & 8) were kindly provided by colleagues.

Table 3. Pneumaticity characters in the vertebral and pelvic elements. List of possible pneumaticity characters that can be accounted for in the vertebral column and pelvis in Sauropodomorpha.

Coding	**Pneumaticity characters**
	Centrum
C1c	pleurocoel
C2c	camera(e)
C3c	foramen(-mina)
C4c	fossa
C5c	foraminous fossa
C6c	camella(e)
C7c	foraminous pleurocoel
C8c	fosseous pleurocoel
C9c	septated foramina
C10c	semicamerated
C11c	semicamellated
C12c	subdivided (septated) fossa(e)
C13c	laminated fossa(e)
C14c	laminated foramen (-mina)
C15c	laminated pleurocoel
	Neural arch
C16na	pleurocoel
C17na	camera(e)
C18na	foramen
C19na	fossa
C20na	foraminous fossa
C21na	camella(e)
C22na	foraminous pleurocoel
C23na	fosseous pleurocoel
C24na	septated foramina
C25na	semicamerated
C26na	semicamellated
C27na	subdivided (septated) fossa(e)
C28na	laminated fossa(e)
C29na	laminated foramen (-mina)
C30na	laminated pleurocoel
	Neural spine
C31ns	pneumatocoel
C32ns	camera(e)
C33ns	foramen
C34ns	fossa
C35ns	foraminous fossa
C36ns	camella(e)
C37ns	foraminous pneumatocoel
C38ns	fosseous pneumatocoel
C39ns	septated foramina
C40ns	semicamerated
C41ns	semicamellated
C42ns	subdivided (septated) fossa(e)
C43ns	laminated fossa(e)
C44ns	laminated foramen (-mina)

C45ns	laminated pneumatocoel
	Prezygapophyses
C46prz	camera(e)
C47prz	foramen
C48prz	fossa
C49prz	foraminous fossa
C50prz	camella(e)
C51prz	infraprezygapophyseal foramina
C52prz	infraprezygapophyseal fossa(e)
C53prz	septated foramina
C54prz	semicamerated
C55prz	semicamellated
C56prz	subdivided fossa
C57prz	laminated(infraprezygapophyseal) fossa(e)
C58prz	laminated foramen (-mina)
	Postzygapophyses
C59poz	camera(e)
C60poz	foramen
C61poz	fossa
C62poz	foraminous fossa
C63poz	camella(e)
C64poz	infrapostzygapophyseal foramina
C65poz	infrapostzygapophyseal fossa(e)
C66poz	septated foramina
C67poz	semicamerated
C68poz	semicamellated
C69poz	subdivided fossa
C70poz	laminated fossa(e)
C71poz	laminated foramen (-mina)
C72poz	infrapostzygapophyseal camera
C73poz	infrapostzygapophyseal camella(e)

	Neural canal
C74nc	pneumatocoel
C75nc	camera(e)
C76nc	foramen
C77nc	fossa
C78nc	fossa + foramen
C79nc	camella(e)
C80nc	foraminous pneumatocoel
C81nc	fosseous pneumatocoel
C82nc	septated foramina
C83nc	semicamerated
C84nc	semicamellated
C85nc	subdivided fossa
C86nc	laminated fossa
C87nc	laminated foramen (-mina)
C88nc	laminated pneumatocoel
	Transverse process
C89tp	pneumatocoel
C90tp	camera(e)
C91tp	foramen
C92tp	fossa
C93tp	foraminous fossa
C94tp	camella(e)
C95tp	foraminous pneumatocoel
C96tp	fosseous pneumatocoel
C97tp	septated foramina
C98tp	semicamerated
C99tp	semicamellated
C100tp	subdivided fossa(e)
C101tp	laminated fossa(e)
C102tp	laminated foramen (-mina)
C103tp	laminated pneumatocoel
	Diapophyses
C104d	camera(e)

C105d	foramen
C106d	fossa (also supradiapophyseal)
C107d	foraminous fossa
C108d	camella(e)
C109d	septated foramina
C110d	semicamerated
C111d	semicamellated
C112d	subdivided fossa
C113d	laminated fossa(e)
C114d	laminated foramen (-mina)
C115d	infradiapophyseal foramen (-mina)
C116d	infradiapophyseal fossa(e) (usually laminated)
C117d	infradiapophyseal camera(e)
	Parapophyses
C118p	camera(e)
C119p	foramen
C120p	fossa
C121p	foraminous fossa
C122p	camella(e)
C123p	septated foramina
C124p	semicamerated
C125p	semicamellated
C126p	subdivided (septated) fossa
C127p	laminated fossa(e)
C128p	laminated foramen (-mina)
C129p	intraparapophyseal foramen (-mina)
C130p	intraparapophyseal fossa(e)
	Costotransverse ring
C131cr	foramen
C132cr	fossa
C133cr	foraminous fossa
C134cr	septated foramina
C135cr	semicamerated
C136cr	semicamellated
C137cr	subdivided fossa
C138cr	laminated fossa(e)
C139cr	laminated foramen(-mina)
	Epipophysis
C140e	camera(e)
C141e	foramen
C142e	fossa
C143e	foraminous fossa
C144e	camella(e)
C145e	septated foramina
C146e	semicamerated
C147e	semicamellated
C148e	subdivided fossa
C149e	laminated fossa(e)
C150e	laminated foramen (-mina)
	Hypapophysis/ haemapophysis
C151h	camera(e)
C152h	foramen
C153h	fossa
C154h	foraminous fossa
C155h	camella(e)
C156h	septated foramina
C157h	semicamerated
C158h	semicamellated
C159h	subdivided fossa
C160h	laminated fossa(e)
C161h	laminated foramen (-mina)
	Condyle
C162con	camera(e)
C163con	foramen
C164con	fossa
C165con	foraminous fossa
C166con	camella(e)

C167con	septated foramina
C168con	semicamerated
C169con	semicamellated
C170con	subdivided (septated) fossa
	Cotyle
C171cot	camera(e)
C172cot	foramen
C173cot	fossa
C174cot	foraminous fossa
C175cot	camella(e)
C176cot	septated foramina
C177cot	semicamerated
C178cot	semicamellated
C179cot	subdivided (septated) fossa
	Ribs
C180r	foramen(-mina)
C181r	fossa(e)
C182r	camellae
	Ilium
D1	camera(e)
D2	foramen
D3	fossa
D4	foraminous fossa
D5	camella(e)
D6	septated foramina
D7	semicamerated
D8	semicamellated
D9	subdivided fossa
	Ischium
D10	camera(e)
D11	foramen
D12	fossa
D13	foraminous fossa
D14	camella(e)
D15	septated foramina
D16	semicamerated
D17	semicamellated
D18	subdivided fossa
	Pubis
D19	camera(e)
D20	foramen
D21	fossa
D22	foraminous fossa
D23	camella(e)
D24	septated foramina
D25	semicamerated
D26	semicamellated
D27	subdivided fossa

The overall volume of pneumaticity in a vertebra can be calculated through CT scanning, but for reasons explained in Chapter 1 this would be costly in time and money, especially because the massive, unwieldy, and delicate sauropod vertebrae would take considerable efforts to transport to and from a suitable, large-body scanner. The purposes of this study demanded the creation of a method that quantifies the extent of the expression of pneumaticity and provides a ranking system which classifies the taxa. The method proposed here, i.e. the Pneumaticity Degree Index (PDI%), can draw information from a single vertebra; the pneumatisation of the vertebra acts as a proxy for the entire vertebral region to which it belongs. The author does not disregard the presence of intervertebral variability with respect to the expression of pneumatisation but due to the scarcity and incompleteness of specimens it would be hard to reveal the complete pneumatisation of a region, let alone an entire column of a sauropod, or even an indicative sample of all major sauropod subfamilies within the allocated time of this study. It would be outside the scope of this study to analytically record, i.e. vertebra by vertebra, and assess the entire pneumaticity of a particular taxon, since the primary goal is to create a method to quantify the degree of pneumatisation and produce a classification scheme that can be applied to any archosaur specimen, whether an isolated bone, a vertebral series (partial or complete), or an entire holotype.

2.2.2) Codification method and scoring of pneumaticity characters

Pneumatic characters were coded from personal observations and on the literature. All aspects of the extent of pneumaticity, such as detected marks, foramina, fossae, laminae, and other structures were recorded. We looked for all pneumatic conditions, namely pleurocoels, foramina, fossae, camerae, camellae, fossae with foramina, laminated pleurocoels laminated foramina, laminated fossae, foraminous pleurocoels, fosseous pleurocoels, septated foramina, subdivided fossae, and the semicamerated and semicamellated conditions. At first, we considered including limb bones and the pectoral girdle, but we found these only exhibited pneumatic foramina, and occasionally fossae, and so we excluded them. Our goal was to collect evidence from bones that possess the largest variety of pneumaticity characters and thus only the axial skeleton and pelvic bones (i.e. ischium, ilium and pubis) are included in our study.

A sauropod vertebra (as well as the vertebrae of most archosaurian taxa) is composed of these compartments: centrum, condyle, cotyle, prezygapophyses, postzygapophyses, diapophyses, parapophyses, transverse processes, neural canal, neural arch, neural spine, and occasionally, epipophyses and hypapophyses. Any of these landmarks may bear fossae, foramina, some of them pleurocoels, any combination of them, as well as laminated versions of these features (Figs. 1-8, Table 3, Table S4 in SI2

and *Excel* file SI3). In documenting pneumaticity features, we created a coding system in which each combination of a vertebral landmark and a pneumaticity feature is assigned as a different character, i.e. ‘C1’ = pleurocoel on the centrum, ‘C2’ = camera in the centrum, and so on (Table S4 in SI2). The sequence for each of the four vertebral regions (cervical, dorsal, sacral and caudal) plus the ribs has 182 characters (see *Excel* file SI3), totalling 182 x 4 = 728 characters for the entire vertebral region, and, including the characters accounting for the three main pelvic bones, we have another 27 characters (755 in total). Each character designation (e.g. C1) is accompanied by a small-lettered abbreviation of the vertebral part it refers to i.e. ‘C1c’ where ‘c’ corresponds to ‘centrum’. Therefore, we have ‘C1c’, ‘C2c’…and so on (Table 3, Table S4 in SI2 and *Excel* file SI3). The characters corresponding to the three pelvic bones are designated as ‘D1, D2,…, D27’. The pneumaticity elements of the ilium span from D1-D9, of the ischium from D10-D18 and of the pubis from D19-D27. The list of all possible pneumaticity characters of the vertebral column and pelvis that can be observed is given in Table 3 and Table S4 (SI2).
A taxon versus character data matrix was compiled (Supplementary information, SI3). Landmarks / compartments that have been associated with any pneumatic trait(s) are noted as '1' if present, '0' if absent and '?' if unknown. The 'unknown' condition may result from absence of fossil material, incomplete description, unpublished data, or unprepared material. We were able to recover more data from cervical and dorsal vertebrae, and less from sacral and caudal vertebrae.

2.2.3) Method of quantification of pneumaticity

To calculate the PDI%, every pneumatic character (from least to most ambiguous with respect to pneumatic invasion) was scored and ranked from one to five, with one indicating the highest level of expression of pneumaticity and five indicating the lowest (1 > 2 > 3 > 4 > 5; Tables 3 & 4). This was not an entirely arbitrary choice of numbers, but rather an educated approximation of how ‘invasive’ these pneumaticity traits are, acting as proxies of pneumatization. Table 3 shows the application of this ranking score method for every part of a vertebra. Pneumaticity characters were recorded for every account of any vertebra representing each of the four regions (or of any pelvic bones) and the ranking scores of the pneumaticity characters were added together and divided by their number to yield the total average pneumaticity ranking for that region. Then, the average pneumatization for that taxon was the total average of the total average scores of all vertebral and pelvic regions together (see a sample of this working in Table 5). For example, in a cervical region we may have recorded e.g. six different pneumatic traits and each trait has a specific score (e.g. foramina – 2, pleurocoel – 2, camerae – 1, fossa – 5, laminated fossa – 4 and foraminous fossa – 2). The total average for that region is 2 + 2 +

1 + 5 + 4 + 2 = 16 / 5 = 3.2. We, then apply the same method to the rest of the regions and we average them to retrieve the total average pneumaticity for that taxon (Table 5 and SI3 for the complete table).

To complete the quantification and yield a percentage, a percentage scale was created ranging from 100% to 1% (scaling from most to least pneumatized condition) classed in one-tenth decimal intervals. In order to derive the percentage of pneumaticity, the percentage scale from 100% to 1% has to be equalised with the pneumatization ranking score numbers of the characters from one to five. (i.e. 1 = 100%–98%, 1.1 = 97%–95%, 1.2 = 94%–92%…5 = 19%–1%), to yield the PDI% for each vertebral and pelvic region (Table 4). Then, in each taxon, the average PDI% from each body section was calculated to obtain the total average PDI% for that taxon. For convenience, when calculating pneumaticity, every numerical point value (i.e. 1, 1.1, 1.2…5) corresponds to two consecutive percentage values (e.g. 59%–58%) so that the values of the numerals match the percentage values across the pneumatization stages (A–E). For simplicity, the rank value of 5 (least pneumatized) was assigned the values from 19%-1% (Table 4), and these were averaged as the value of '10%' to signify the lowest expression of PSP (we do not include zero pneumatization) and because no higher decimals (i.e. 5.1, 5.2, etc.) are needed in this quantification scheme.

In our study, pneumaticity traits (Table 6 and Table S5 in SI2) such as camerae, camellae, semicamerate and semicamellate conditions were assigned a rank of '1' because of their unambiguously pneumatic nature (e.g. Wedel, 2001; Wedel, Cifelli & Sanders, 2001a, b; Wedel, 2005; Schwarz & Fritsch, 2006). Also, we ranked laminated pleurocoels as '1' because they were almost certainly pneumatic. We ranked less certain indicators of pneumaticity as '2', including pneumatic foramina and laminated foramina because in a fossil there is a chance of mistaking a non-pneumatic (i.e. vascular or neural) foramen as pneumatic (i.e. opening of a diverticulum) and we may not be certain that they invade the bone within its cancellous region (e.g. Naish et al., 2013). Laminated foramina and pleurocoels were also given the rank of '1' because when laminae border such traits, their presence strengthens the probability of them being pneumatic (Cerda, Salgado & Powell, 2012; Apostolaki, Rayfield & Barrett, 2015). Pleurocoels, foraminous pleurocoels, fossae with foramina and septated foramina were also given the rank of '2' because of their very high pneumatic nature but not '1' because they might have served as large adipose tissue reserves (e.g. Wedel, 2001; Wedel, 2005, 2006, O'Connor, 2004, 2006, 2009). Fosseous pleurocoels and subdivided (septated) fossae were given the rank of '3' because they do not often lead deep within the bone, but they were not given lower ranking because their complex excavations increase the probability of their having housed diverticula. Fossae were given the rank of '5' because they are shallow and do not invade

the bone like a pleurocoel, but laminated fossae were assigned the rank of ‘4’ because they probably also housed diverticular attachments (apart from adipose tissue) before the diverticula expand and penetrate the bone nearby, thus creating a pneumatic foramen (e.g. Apostolaki, Rayfield & Barrett, 2015). We distinguish fossae from pleurocoels because the latter are, as explained earlier, much deeper and wider than the former, with respect to the vertebral area it occupies. Thus, even if there is not a foramen penetrating the bone from the surface of a pleurocoel, it is very likely to have housed expanded pneumatic diverticula apart from other tissues.

2.2.4) The five states (A, B, C, D, E) of the Pneumaticity Degree Index (PDI%)

The method proposed here for quantifying postcranial skeletal pneumaticity in sauropods may be applied not only to any avian and non-avian dinosaurs, but also to any archosaur since they share the same anatomical landmarks in their vertebral, girdle and appendicular elements. The PDI% comprises five states that document the degree of pneumaticity from highest to lowest, namely ‘A’ (Alpha) > ‘B’ (Beta) > ‘C’ (Gamma) > ‘D’ (Delta) > ‘E’ (Epsilon) (Tables 3–6 and SI3). ‘A’ corresponds to PDI% ranging from 100%–80% of bone pneumatization, ‘B’ is PDI% from 79%–60%, ‘C’ is PDI% from 59%–40%, ‘D’ is PDI% from 39%–20% and ‘E’ is PDI% from 19%–1%. Scoring of pneumatization in any vertebra of a particular vertebral region can act as a proxy score for the entire region, keeping in mind, though, the risk of variability. The more vertebrae available for study in a region, the more accurate the score. The PDI% can be used for a specimen of any ontogenetic stage, but in this study we focused on adult taxa.

Each of the five pneumaticity ranking stages (A, Alpha; B, Beta; C, Gamma; D, Delta and E, Epsilon) are characterised by certain expressions of PSP in terms of both value and morphology of the pneumatised bone (usually a vertebra):

‘Alpha’: There is almost complete pneumatization in the vertebra (1–1.9 or PDI% from 100%–80%), from centrum to spine, including all intermediate compartments. The vertebra is pneumatized either by camellae or by a combination of foramina, fossae, pleurocoels, camerae and camellae (polycamerate-semicamellate-camellate-somphospondylous). Expansion of pneumatization occurs from 'inside towards all compartments', and there may be any combination of pneumatic elements. The vertebra exhibits a fine complex structure of laminated lattices. The condition occurs in cervical (CV), dorsal (DV), sacral (SV) and caudal (CD) vertebrae.

‘Beta’: Extended pneumatization exists (2–2.9 or PDI% from 79%–60%) in centrum, condyle, cotyle, and all zygapophyses, and up to neural arch and spine. Again, any

combination of pneumatic elements (camerate-polycamerate-semicamellate) can be found in all parts of the bone. The vertebral volume is composed of almost equal amounts of air and bone. Pneumatization is more concentrated in the centrum, neural arch, transverse processes, and neural spine. The bone is highly laminated, bearing depressions, septated conditions and subdivisions. This condition occurs in CV, DV, SV, and sometimes CD.

'Gamma': Pneumatization (3–3.9 or PDI% from 59%–40%) is present in centrum, zygapophyses, apophyses, and neural arch, but only in the procamerate condition (foramina, fossae). The vertebra shows moderate expression of external and internal pneumatization traits. The compartments are more 'complete' and less lattice-like. Basic laminations are present and the vertebra possesses less septated and subdivided fossae and pleurocoels. The pneumatic occupation within the vertebra is less expressed than in alpha and beta conditions. This condition occurs in CV, but mostly in DV, SV and CD.

'Delta': Pneumaticity (4–4.9 or PDI% from 39%–20%) is limited to few parts of the vertebra such as centrum, diapophyses, pre- and postzygapophyses and neural spine. There are only foramina and narrow/shallow fossae (acamerate), which are present, but very few in number and level of occupation and invasion of the bone. The vertebra is mostly bone and it exhibits more external pneumaticity than internal. This condition occurs in CV, DV, SV, and mostly in CD.

'Epsilon': Pneumaticity (5 or PDI% = 10%) is very limited. It is only external and limited to very shallow depressions on the centrum or the spine. The vertebra is not internally pneumatized and the compartments are distinct from each other and clear from pneumatic penetration. This condition occurs mostly in basal sauropodomorphs and basal eusauropods and it is generally often observed in the sacral and caudal regions of most sauropods.

Zero degree: PDI% = 0%. Absence of pneumatization.

The classification of a vertebral region into any of these Pneumatisation Degrees follows some simple rules aimed to provide the researcher with a fast and reasonably accurate first-glance estimation of the bone's pneumaticity (depending, of course, on the condition of the bone and how much it is surrounded by matrix):

a) The distinction from one degree to another is based on the hierarchical concept that some pneumatic traits are more useful in demonstrating intraosseous pneumatisation than others. The weakest line of evidence of PSP is the presence of shallow fossae without being laminated. Proceeding 'upwards' in the pneumaticity scale, are the laminated fossae, the foramina, the pleurocoels on the centra and pneumatocoels on other vertebral parts, the existence of foramina and fossae within the pleurocoels, and,

finally, the presence of internal chambers, i.e. camerae and camellae. The latter two may communicate with the vertebra's surface by means of foramina or pleurocoels, a pattern also observed by O'Connor (2006) who, based on that, proposed the term 'Pneumaticity Profile (PP)'. If a vertebra has a well-developed system of laminae, then this feature strengthens the evidence for osseous pneumatisation by air sac diverticula (Wedel et al., 2000, Apostolaki et al., 2015).

b) The estimation should consider not only the nature of the pneumatic elements being expressed but also their presence/occurrence (and if possible level of occupation) on the different vertebral compartments. For example, the evidence might be as little as a centrum possessing, for example, pleurocoelous fossae and no other pneumatic trait. Should this feature be the sole pneumatic label for the entire vertebra or must we also take into consideration the absence of pneumaticity in the other compartments? The decision then rests on whether these pleurocoelous fossae lead into internal chambers that may occupy the entire vertebra from within, or remain only in the centrum. Such a question could only be answered with certainty by the use of CT scanning. Otherwise, if the researcher is certain that such is the case and no other pneumatic trait exists, then the trait denoting the highest degree of pneumaticity present (e.g. pleurocoelous fossa) dominates the overall categorisation of the vertebra.

c) Extreme pneumatisation in a vertebra can result either by possessing internal cavities and chambers, thus leaving the outer parts almost intact, except perhaps the entries of the lung diverticula (foramina, fossae), or by rearranging and 'eliminating' bone material during ontogeny (Wedel, 2005). The latter condition will result in a vertebra that comprises an elaborate lattice-like structure made of laminae which can be seen without CT scanning and it indicates a classification of pneumaticity as 'Alpha' to 'Beta' degrees. Table 4 in Chapter 2 and Table S2 in Appendix 2 neatly summarise the expression of pneumaticity in terms of class and percentage ranges in all examined taxa as well as their body regions of neck, trunk and tail. This quantification of PSP is adaptable and can be used to compare pneumaticity among any archosaurian taxa. Moreover, because this method includes every occurrence of pneumaticity in a single bone, we can acquire a reasonable appreciation of the presence and extent of pneumatization, while considering the intervertebral variability of PSP. The use of such a categorisation scheme (A-E) may not be able to encompass the finer differences between percentages i.e. there may not be any significant anatomical differences between having a 60% ('Beta') and a 59% ('Gamma') pneumatisation degrees, and thus classify them as such. Nevertheless, this scheme can act as a useful general guide to future workers and as a method of 'rough' categorisation of sauropodomorphs, theropods, birds or other archosaurs, with respect to vertebral pneumatisation.

Table 4. Classification of sauropods based on total average pneumaticity ranges. List of all 61 sauropodomorphs examined in this study, sorted by their total average PDI% into the Alpha-Zero classification scheme, measured by the PDI% of each vertebral column (for a summary see Table 7). Abbreviations: PDI% = Pneumaticity Degree Index, BS = Basal Sauropodomorpha, E = Eusauropoda (non-neosauropods), D = Diplodocoidea, M = Macronaria, S = Somphospondyli. Measurements of Mass (Kg) and Length (m) were retrieved from the literature (see Table S1 in SI2).

Class	PDI% total average	Genera	Mass (Kg)	Length (m)	Subfamily
A (Alpha)	**90-100**				
	94	*Saltasaurus l./r.*	4000	12	S
	92	*Brachiosaurus a.*	28264.6	21	M
	90	*Ornithopsis h.*	8000	15	M
	90	*Mamenchisaurus h.*	18169.7	25	E
	90	*Alamosaurus s.*	16000	20	S
A (Alpha)	**80-89**				
	84	*Andesaurus d.*	7000	18	S
B (Beta)	**70-79**				
	79	*Klamelisaurus g.*	5000	15	M
	75	*Euhelopus z.*	4000	11	M
	75	*Camarasaurus g./l./s.*	18413	15.4	M
	73	*Amazonsaurus m.*	5000	12	D
	71	*Tehuelchesaurus b.*	9000	15	M
B (Beta)	**60-69**				
	69	*Barapasaurus t.*	7000	12	E
	69	*Nigersaurus t.*	2000	9	D
	69	*Giraffatitan b.*	47000	24	M
	68	*Malawisaurus d.*	10000	16	S
	67	*Rhoetosaurus b.*	9000	15	E
	67	*Shunosaurus l.*	4793	8.7	E
	66	*Neuquensaurus a.*	1800	7.5	S
	65	*Eucamerotus f.*	8000	15	M
	63	*Futalognkosaurus d.*	50000	30	S

	63	*Amphicoelias a./b.*	18170	25	D
	63	*Apatosaurus l./p./e.*	37500	22	D
	63	*Diplodocus l./c.*	12000	27	D
	60	*Tornieria a.*	20000	25	D
	60	*Phuwiangosaurus s.*	17000	19	S
	60	*Sauroposeidon p.*	50000	30	S
	60	*Omeisaurus t.*	11796	20	E
C (Gamma)	**50-59**				
	59	*Dongyangosaurus s.*	7000	15	S
	59	*Patagosaurus f.*	9435	15	E
	59	*Erketu e.*	5000	15	S
	59	*Europasaurus h.*	690	6.2	M
	59	*Barosaurus l.*	20039.5	26	D
	59	*Amargasaurus c.*	6852.9	10.3	D
	59	*Plateosaurus l./e.*	1073	8,5	BS
	56	*Rapetosaurus k.*	8000	15	S
	55	*Australodocus b.*	4000	17	S
	55	*Cathartesaura a.*	5000	12	D
	53	*Jobaria t.*	16000	24	E
	53	*Dicraeosaurus h./s.*	5700	12	D
	53	*Cetiosaurus b./h.*	15800	16	E
	52	*Huanghetitan r.*	3000	12	S
	51	*Seismosaurus h.*	49275.5	40	D
C (Gamma)	**40-49**				
	49	*Tendaguria t.*	48000	30	M
	49	*Camelotia b.*	2500	10	BS
	49	*Ruehleia b.*	1000	10	BS
	47	*Haplocanthosaurus*	14528.6	14	D
	47	*Eucnemesaurus f.*	500	6	BS
	47	*Thecodontosaurus a.*	40	2,5	BS
	46	*Puertasaurus r.*	50000	30	S
	45	*Suuwassea e.*	5950	15	D
	45	*Janenschia r.*	10000	17	M
	45	*Pleurocoelous n./v.*	12000	15	M

	43	*Antetonitrus i.*	5000	12,2	BS
D (Delta)	**30-39**				
	39	*Seitaad r.*	80	2,8	BS
	39	*Aardonyx c.*	1000	6,5	BS
	37	*Spinophorosaurus n.*	7000	13	E
D (Delta)	**20-29**				
	29	*Vulcanodon k.*	3500	6,5	E
	23	*Tazoudasaurus n.*	5000	9	E
	23	*Kotasaurus y.*	5000	9	E
E (Epsilon)	**1 up to 19 (average: 10)**	None			
	Zero Degree				
	0	*Efraasia m.*	10	1	BS
	0	*Massospondylus c.*	300	4,3	BS

Table 5. Numerical hierarchy of pneumaticity characters. Character ranking is from ‘1’ to ‘5’ with ‘1’ being unambiguously pneumatic and ‘5’ being the least pneumatic, in terms of vertebral ‘invasiveness’ and aeration by pneumatic diverticula.

Hierarchy of pneumatic character significance		
	1=Alpha > 2=Beta > 3=Gamma > 4=Delta > 5=Epsilon	
Coding	**Pneumatic characters**	**Rank**
	Centrum	
C1c	pleurocoel	2
C2c	camera(e)	1
C3c	foramen(-mina)	2
C4c	fossa	5
C5c	foraminous fossa	2
C6c	camella(e)	1
C7c	foraminous pleurocoel	1
C8c	fosseous pleurocoel	3
C9c	septated foramina	2
C10c	semicamerated	1
C11c	semicamellated	1
C12c	subdivided (septated) fossa(e)	3
C13c	laminated fossa(e)	4
C14c	laminated foramen (-mina)	2
C15c	laminated pleurocoel	1
	Neural arch	
C16na	pleurocoel	2
C17na	camera(e)	1
C18na	foramen	2
C19na	fossa	5
C20na	foraminous fossa	2
C21na	camella(e)	1
C22na	foraminous pleurocoel	1
C23na	fosseous pleurocoel	3
C24na	septated foramina	2
C25na	semicamerated	1
C26na	semicamellated	1
C27na	subdivided (septated) fossa(e)	3
C28na	laminated fossa(e)	4
C29na	laminated foramen (-mina)	2
C30na	laminated pleurocoel	1

	Neural spine	
C31ns	pleurocoel	2
C32ns	camera(e)	1
C33ns	foramen	2
C34ns	fossa	5
C35ns	foraminous fossa	2
C36ns	camella(e)	1
C37ns	foraminous pleurocoel	1
C38ns	fosseous pleurocoel	3
C39ns	septated foramina	2
C40ns	semicamerated	1
C41ns	semicamellated	1
C42ns	subdivided (septated) fossa(e)	3
C43ns	laminated fossa(e)	4
C44ns	laminated foramen (-mina)	2
C45ns	laminated pleurocoel	1
	Prezygapophyses	
C46prz	camera(e)	1
C47prz	foramen	2
C48prz	fossa	5
C49prz	foraminous fossa	2
C50prz	camella(e)	1
C51prz	infraprezygapophyseal foramina	3
C52prz	infraprezygapophyseal fossa(e)	4
C53prz	septated foramina	2
C54prz	semicamerated	1
C55prz	semicamellated	1
C56prz	subdivided fossa	4
C57prz	laminated (infraprezygapophyseal) fossa(e)	3
C58prz	laminated foramen (-mina)	2
	Postzygapophyses	

C59poz	camera(e)	1
C60poz	foramen	2
C61poz	fossa	5
C62poz	foraminous fossa	2
C63poz	camella(e)	1
C64poz	infrapostzygapophyseal foramina	1
C65poz	infrapostzygapophyseal fossa(e)	1
C66poz	septated foramina	2
C67poz	semicamerated	1
C68poz	semicamellated	1
C69poz	subdivided fossa	4
C70poz	laminated fossa(e)	3
C71poz	laminated foramen (-mina)	1
C72poz	infrapostzygapophyseal camera	1
C73poz	infrapostzygapophyseal camella(e)	1
	Neural canal	
C74nc	pleurocoel	2
C75nc	camera(e)	1
C76nc	foramen	2
C77nc	fossa	5
C78nc	foraminous fossa	2
C79nc	camella(e)	1
C80nc	foraminous pleurocoel	1
C81nc	fosseous pleurocoel	3
C82nc	septated foramina	2
C83nc	semicamerated	1
C84nc	semicamellated	1
C85nc	subdivided fossa	3
C86nc	laminated fossa	4
C87nc	laminated foramen (-mina)	2
C88nc	laminated pleurocoel	1
	Transverse process	

C89tp	pleurocoel	2
C90tp	camera(e)	1
C91tp	foramen	2
C92tp	fossa	5
C93tp	foraminous fossa	2
C94tp	camella(e)	1
C95tp	foraminous pleurocoel	1
C96tp	fosseous pleurocoel	3
C97tp	septated foramina	2
C98tp	semicamerated	1
C99tp	semicamellated	1
C100tp	subdivided fossa(e)	3
C101tp	laminated fossa(e)	4
C102tp	laminated foramen (-mina)	2
C103tp	laminated pleurocoel	1
	Diapophyses	
C104d	camera(e)	1
C105d	foramen	2
C106d	fossa (also supradiapophyseal)	5
C107d	foraminous fossa	2
C108d	camella(e)	1
C109d	septated foramina	2
C110d	semicamerated	1
C111d	semicamellated	1
C112d	subdivided fossa	3
C113d	laminated fossa(e)	4
C114d	laminated foramen (-mina)	2
C115d	infradiapophyseal foramen (-mina)	2
C116d	infradiapophyseal fossa(e) (usually laminated)	4
C117d	infradiapophyseal camera(e)	1
	Parapophyses	
C118p	camera(e)	1

C119p	foramen	2
C120p	fossa	5
C121p	foraminous fossa	2
C122p	camella(e)	1
C123p	septated foramina	2
C124p	semicamerated	1
C125p	semicamellated	1
C126p	subdivided (septated) fossa	1
C127p	laminated fossa(e)	4
C128p	laminated foramen (-mina)	2
C129p	intraparapophyseal foramen (-mina)	2
C130p	intraparapophyseal fossa(e)	4
	Costotransverse ring	
C131cr	foramen	2
C132cr	fossa	5
C133cr	foraminous fossa	3
C134cr	septated foramina	2
C135cr	semicamerated	1
C136cr	semicamellated	1
C137cr	subdivided fossa	3
C138cr	laminated fossa(e)	4
C139cr	laminated foramen (-mina)	2
	Epipophysis	
C140e	camera(e)	1
C141e	foramen	2
C142e	fossa	5
C143e	foraminous fossa	3
C144e	camella(e)	1
C145e	septated foramina	2
C146e	semicamerated	1
C147e	semicamellated	1
C148e	subdivided fossa	3

C149e	laminated fossa(e)	4
C150e	laminated foramen (-mina)	2
	Hypapophysis/haemapophysis	
C151h	camera(e)	1
C152h	foramen	2
C153h	fossa	5
C154h	foraminous fossa	3
C155h	camella(e)	1
C156h	septated foramina	2
C157h	semicamerated	1
C158h	semicamellated	1
C159h	subdivided fossa	3
C160h	laminated fossa(e)	4
C161h	laminated foramen (-mina)	2
	Condyle	
C162con	camera(e)	1
C163con	foramen	2
C164con	fossa	5
C165con	foraminous fossa	3
C166con	camella(e)	1
C167con	septated foramina	2
C168con	semicamerated	1
C169con	semicamellated	1
C170con	subdivided (septated) fossa	3
	Cotyle	
C171cot	camera(e)	1
C172cot	foramen	2
C173cot	fossa	5
C174cot	foraminous fossa	3
C175cot	camella(e)	1
C176cot	septated foramina	2

C177cot	semicamerated	1
C178cot	semicamellated	1
C179cot	subdivided (septated) fossa	3
	Ribs	
C180r	foramen(-mina)	2
C181r	fossa(e)	5
C182r	camellae	1
	Ilium	
D1	camera(e)	1
D2	foramen	2
D3	fossa	5
D4	foraminous fossa	3
D5	camella(e)	1
D6	septated foramina	2
D7	semicamerated	1
D8	semicamellated	1
D9	subdivided (septated) fossa	3
	Ischium	
D10	camera(e)	1
D11	foramen	2
D12	fossa	5
D13	foraminous fossa	3
D14	camella(e)	1
D15	septated foramina	2
D16	semicamerated	1
D17	semicamellated	1
D18	subdivided (septated) fossa	3
	Pubis	
D19	camera(e)	1

D20	foramen	2
D21	fossa	5
D22	foraminous fossa	3
D23	camella(e)	1
D24	septated foramina	2
D25	semicamerated	1
D26	semicamellated	1
D27	subdivided (septated) fossa	3

Table 6. Equalisation of PDI% with numerals to the tenth decimal. Quantification of PDI percentage from numerical analogous equivalents, based on the character ranking from Table 5. The first four rows indicate the classification scheme 'Alpha – Beta – Gamma – Delta – Epsilon' with their ranges in percentage along with their overall numerical ranking of pneumaticity. For convenience and clarity when calculating pneumaticity, every integer point value (i.e. 1,2,3,4 and 5) has been assigned with two consecutive percentage values. The value of 5 has been paired with 10, being the average value from 19 to 1, since no higher decimal values after 5 (i.e. 5.1, 5.2, etc.) were needed in this method of PSP quantification. Other than these modifications, the intermediate percentage values follow a decreasing pattern by 2.

Alpha (100 - 80)	**Beta (79-60)**	**Gamma (59-40)**	**Delta (39-20)**	**Epsilon (19-1)***
				*simplified to the value of 10 as the average of values 1 and 19
1	2	3	4	5
A	B	C	D	E
Analytical Character Ranking	Analytical Percentage PDI			
1	100	A		
1.1	98	A		
1.2	96	A		
1.3	94	A		
1.4	92	A		

1.5	90	A		
1.6	88	A		
1.7	86	A		
1.8	84	A		
1.9	80	A		
2	79-78	B		
2.1	76	B		
2.2	74	B		
2.3	72	B		
2.4	70	B		
2.5	68	B		
2.6	66	B		
2.7	64	B		
2.8	62	B		
2.9	60	B		
3	59-58	C		
3.1	56	C		
3.2	54	C		
3.3	52	C		
3.4	50	C		
3.5	48	C		
3.6	46	C		
3.7	44	C		
3.8	42	C		
3.9	40	C		
4	39-38	D		
4.1	36	D		
4.2	34	D		
4.3	32	D		
4.4	30	D		
4.5	28	D		
4.6	26	D		
4.7	24	D		
4.8	22	D		
4.9	20	D		

5	10*	E		

2.2.5) Body mass estimates and derivation of the estimate length of the body segments

Over the 130 years of dinosaur palaeontology, many attempts have been made to derive the body mass of the largest beings that have ever walked on this planet. Various techniques of body mass estimates have been implemented, resulting in different numerical approximations, with some being more reasonable than others. During the last 30 years, more accurate methods have been adopted, utilising the principles of engineering and biomechanics. The methods of polynomial volume (e.g. Seebacher, 2001), laser photogrammetry (Gunga et al., 2007) and long bone circumference (e.g. Anderson et al, 1985) have been applied to many sauropod taxa but only where the appropriate anatomical parts of the specimens have been recovered or where the technical resources were available. Therefore, here I choose the body mass estimates of these sauropodomorphs that are derived from these methods, as explained in Chapter 1, adopting the values that are accepted by the general consensus as the most probable according to their approximate sizes (Table 1 in Chapter 1).

The length measurements needed for each body region are estimates according to the best of the author's knowledge, observations and published data from the literature. For the sauropods examined in this study, we do not have information on the length of every vertebra, and so we cannot provide a total body length based on the sum of these lengths. In any case, such a strict total length measurement would exclude additional length from intervertebral cartilages. The lengths of each of the vertebral segments of the columns (i.e. cervical, dorsal, sacral and caudal) of sauropods have not been ever recorded due to insufficient fossil specimens recovered thus far. Therefore, a rough estimation of the length of each segment was derived, based on the total estimated body length of each genus in this study (Table 1 in Chapter 1 and Table 7 below). The body of each sauropodomorph was divided into three parts: neck, trunk and tail. For simplicity, the ‘trunk’ length contains both dorsal and sacral segments of the animal, since, in real life, these two anatomical parts form the main body, whereas the neck and the tail protrude anteriorly and posteriorly with respect to the main body. At first, the total length was divided by three in order to correspond to each of the three body segments. This applies to basal sauropodomorphs, eusauropods and somphospondylans because they have about the same ratio among the lengths of neck, trunk and tail (e.g. Anderson et al., 1985;

Galton, 1986; McIntosh et al., 1997; Sereno et al., 1999; Benton et al., 2000; Calvo et al., 2007; Remes, 2007; also see Table 7 below). In diplodocoid sauropods, tail length is usually twice as long as the trunk, or it is equal to trunk plus neck (e.g. Salgado & Bonaparte, 1991; Christiansen, 1997; McIntosh et al., 1997; Harris & Dodson, 2004; Taylor & Wedel, 2013). Therefore, the total length of the animal is divided by four instead of three because of this analogy. Then, the tail length is calculated by simply multiplying the estimated trunk (or neck) length by two (Table 7). The derivation of the length of the neck had to exclude the skull length, since the pneumaticity of the skull is not included in this study. Again, due to insufficient fossil specimens, few of the sauropodomorph skulls have been recovered and measured. Therefore, an estimated skull length had to be assumed for the sauropodomorphs of this study. For example, the *Plateosaurus* skull is approximately 0.3 m long (Galton, 1986), so this value was subtracted from the estimated total neck length. Similar estimates have been made for the other sauropodomorphs. For instance, the skull length range for the larger sauropods such as macronarians and somphospondylans is between 0.5 and 1 metre (Table 7). For reasons of homogeneity and simplicity, trunk PDI% does not include sacral PDI% due to unavailability of fossil and/or pneumaticity data of sacral elements for many taxa. Dorsal pneumaticity was assumed to be enough since sacral pneumaticity is usually not present or it is unknown, so it would not affect the measurements and results. This procedure is necessary because the lengths of the body segments are not given when the actual fossil specimen is being measured.

Table 7. List of metric details of the 61 examined sauropodomorph taxa. Metric details of PDI% for each vertebral segment, total average PDI%, body mass, body length as well as estimated vertebral segment lengths of the 61 examined taxa.

Genus											
Basal Sauropodomorpha	PDI%_CV	PDI%_DV	PDI%_SV	PDI%_CD	PDI%_Pelvis	PDI% total average	Body Mass (Kg)	Body Length (m)	neck_length (m)	trunk_length (m)	tail_length (m)
Antetonitrus	0	43	NA	NA	NA	43	5000	12.2	2.61	3.05	6.1
Efraasia	0	0	NA	NA	NA	0	700	6.5	1	1.8	3.5
Plateosaurus	53	75	39	0	59	59	1073	8.5	1.2	2	5
Ruehleia	49	49	39	0	0	49	1000	10	1.5	2.7	5.5
Eucnemesaurus	0	47	NA	NA	NA	47	500	6	1.2	1.5	3
Thecodontosaurus	49	39	0	0	0	47	24.6	2.6	0.5	1	1.1
Camelotia	0	49	NA	NA	NA	49	2500	10	2,3	2.5	5
Massospondylus	0	0	0	0	0	0	136.7	4	1	2	1
Aardonyx	0	45	10	NA	NA	39	1000	6.5	1.4	1.62	3.25
Seitaad	NA	39	NA	NA	NA	39	80	2.8	0.5	0.7	1.4
Eusauropoda											
Vulcanodon	79	10	0	10	0	29	3500	6.5	1.4	1.62	3.25
Tazoudasaurus	10	25	NA	NA	NA	23	5000	9.5	2	2.25	4.5
Barapasaurus	49	75	NA	NA	NA	69	7000	12	2.6	3	6
Kotasaurus	23	25	0	0	0	23	5000	9	2	2.25	4.5
Spinophorosaurus	37	39	0	0	0	37	7000	13	2.85	3.25	6.5
Jobaria	65	35	NA	39	0	53	16000	24	7.65	8	8
Rhoetosaurus	67	67	NA	NA	NA	67	9000	15	3.45	3.75	7.5
Cetiosaurus	79	59	0	10	0	53	15800	16	4	4	8
Shunosaurus	67	67	NA	NA	NA	67	4793.5	8.7	3	2.5	3.2
Omeisaurus	60	60	65	59	79	60	11796	20	7.3	6.2	6.5
Patagosaurus	79	71	NA	10	NA	59	9435	15	3.72	4.12	8.24
Klamelisaurus	79	79	NA	NA	NA	79	5000	15	5.5	4.75	4.75
Mamenchisaurus	77	100	NA	NA	NA	90	18169.7	21	9	6	6
Diplodocoidea											
Haplocanthosaurus	35	63	49	NA	NA	47	14528.6	14	4	3	7
Amphicoelias	57	39	NA	79	0	63	18170	25	8.3	8.3	16.6
Apatosaurus	69	55	90	55	0	63	22407.2	21	5.2	5.5	10.3
Suuwassea	47	39	NA	0	NA	45	5950	15	3.45	3.75	7.5
Barosaurus	59	79	NA	NA	0	59	20039.5	26	6.5	6.5	13
Seismosaurus (Diplodocus)	NA	NA	NA	51	0	51	49275.5	40	12	10	18
Diplodocus	69	69	59	47	0	63	19654.6	25.7	6	6	13.7
Tornieria	79	NA	43	69	0	60	20000	25	6	6.25	12.5
Dicraeosaurus	55	49	60	45	0	53	5700	12	4	3	5
Amargasaurus	60	51	NA	0	NA	59	6852.9	10.3	3.13	3.43	6.86
Nigersaurus	53	80	NA	67	NA	69	2000	9	2	2.25	4.5
Amazonsaurus	NA	71	NA	67	100	73	5000	12	2.6	3	6
Cathartesaura	55	NA	NA	51	NA	55	5000	12	2.6	3	6
Macronaria											
Tehuelchesaurus	NA	67	90	NA	NA	71	9000	15	6.9	3.75	4.35
Janenschia	51	NA	NA	10	0	45	10000	17	5.3	5.6	5.6
Camarasaurus	75	90	79	10	0	75	18413	15.4	6	4.27	5.13
Euhelopus	67	75	96	NA	100	75	4000	11	5.5	2.75	2.55
Europasaurus	59	55	59	65	79	59	800	6.2	3.1	1.55	1.55
Brachiosaurus	NA	100	79	10	0	92	28264.6	21	8	7	6
Giraffatitan	73	63	0	55	0	69	38000	24	9	8	7
Ornithopsis	NA	90	NA	NA	NA	90	8000	15	7.5	3.75	3.45
Eucamerotus	NA	65	NA	NA	NA	65	8000	15	7.5	3.75	3.45
Pleurocoelus	10	69	10	NA	NA	45	12000	15	7.5	3.75	3.45
Somphospondyli											
Australodocus	55	NA	NA	NA	NA	55	4000	17	5.6	5.6	5.6
Tendaguria	NA	49	NA	NA	NA	49	48000	30	9.5	10	10
Phuwiangosaurus	60	57	55	49	0	57	17000	19	6	6.3	6.3
Malawisaurus	55	NA	NA	47	NA	63	10000	16	5	5.3	5.3
Sauroposeidon	60	NA	NA	NA	NA	60	40000	27	12	7.5	7.5
Erketu	63	45	NA	NA	NA	59	5000	15	3.45	3.75	7.5
Huanghetitan	NA	NA	10	10	NA	10	32000	22	7	7	8
Andesaurus	NA	90	0	29	0	84	7000	18	5.7	6	6
Dongyangosaurus	NA	45	NA	39	NA	45	7000	15	4.8	5	5
Futalognkosaurus	65	51	NA	67	79	63	45000	30	9.5	10	10
Neuquensaurus	55	67	0	66	0	62	3500	7.5	2.3	2.5	2.5
Saltasaurus	92	90	100	100	NA	94	4000	12	3.8	4	4
Puertasaurus	33	29	NA	NA	NA	31	45000	30	9.5	10	10
Rapetosaurus	57	57	51	39	0	55	8000	15	4.8	5	5
Alamosaurus	79	96	NA	0	100	88	16000	20	6.6	6	7

The Pneumaticity Degree Index (PDI%) is a means of quantifying, sorting and categorising the expression of vertebral pneumatization in a relatively faster and cheaper, though less accurate, method than CT scanning. This quantification scheme can be applied to any archosaur and provides researchers with an initial estimation of PSP of an

unstudied specimen, and without the need for CT scanning. The method requires that specimens are at least 50% free of matrix. This integrated pneumaticity scheme, including the osteological characteristics it encompasses (‘Alpha-Epsilon’), may aid and speed up future research on vertebral pneumaticity.

This chapter concludes with the methods and the tabulated assimilation of data for the requirements of this part of the study Regression analyses and results regarding the correlation of pneumaticity (PDI%) with evolutionary time and body size metrics are demonstrated in detail in Chapter 3 below, finalising with a discussion that assesses the association of pneumaticity with time and body size metrics, not only under the scope of the entire monophyletic group of Sauropodomorpha but also with respect to each of the paraphyletic clades Basal Sauropodomorpha, Eusauropoda, Diplodocoidea, Macronaria and Somphospondyli.

Chapter 3 - Association between PDI% and the metric values of body size

3.1) Introduction - Brief overview of pneumatisation with respect to evolutionary time and metric values of body size

The correlation graphs below (by linear regression in *PAST3*) demonstrate the variation of PDI% of all examined sauropodomorph taxa across evolutionary time (Fig.1), demonstrating the variation of PDI% of each paraphyletic group was depicted (basal Sauropodomorpha, Eusauropoda, Diplodocoidea, Macronaria and Somphospondyli) through time. The time used is the average value of the First Appearance Dates (FADs) and the Last Appearance Dates (LADs) of the taxa, retrieved from the Palaeobiology Database (PBDB) and relevant literature (e.g. Poropat et al., 2016, etc.; see Table 2 for the entire list). Furthermore, the variation of PDI% of each vertebral region of all sauropodomorphs was also depicted against time (Figs. 2-4) as well as the correlations of cervical, dorsal and caudal pneumaticity (in PDI%) against neck, trunk and tail lengths, respectively (Figs.5-7). Finally, the variations of PDI% against body mass and body length of all examined sauropodomorphs were illustrated in Figs. 8-9.

3.2) Results - Variation of sauropodomorph vertebral pneumaticity with respect to evolutionary time, body mass, body length and vertebral segment lengths

3.2.1) Graphical association of pneumaticity (PDI%) and evolutionary time

Temporal progression of pneumaticity graphs were produced in PAST3 (Figs. 1–6; Hammer et al., 2001) showing the variation of total average pneumaticity, expressed as PDI% of each examined sauropodomorph as well as the sauropodomorphs in each subfamily with respect to their average evolutionary time, spanning from the Late Triassic basal sauropodomorphs to the Late Cretaceous somphospondylan titanosaurs. Each taxon was dated based on the average value (midpoint) of the First Appearance Date (FAD) and Last Appearance Date (LAD) retrieved from Table 2.

In each diagram, time progresses from the most recent (left) to the most ancient (right). Total average PDI% values of each taxon can be viewed in Tables 4 and 7 (Chapter 2). The graphs (Figs. 1–6) show how the evolution of pneumaticity follows an increasing trend through evolutionary time, from basal sauropodomorphs to neosauropods, and it becomes stable at moderate and high levels in macronarians and

somphospondylans. Across our sample of basal sauropodomorphs, pneumaticity begins at moderate levels for most taxa and follows a steady path of low and moderate expression, from Late Triassic to Early Jurassic, with the latter epoch showing a decrease and stabilization in the more recent taxa (Fig. 2). As we enter the Jurassic, (non-neosauropod) eusauropod pneumaticity shows an overall increasing trend until it drops again towards the Late Jurassic (Fig. 3). Diplodocoids and macronarians show stable variations of expressions of PDI%, with an increasing trend in the Early Cretaceous, followed by a sudden decrease (Figs. 4–5). Somphospondylan vertebral PDI% shows a steady trend until it increases in the mid-Cretaceous, followed by a sudden decrease and then immediately an increase in the mid-Late Cretaceous (Fig. 6).

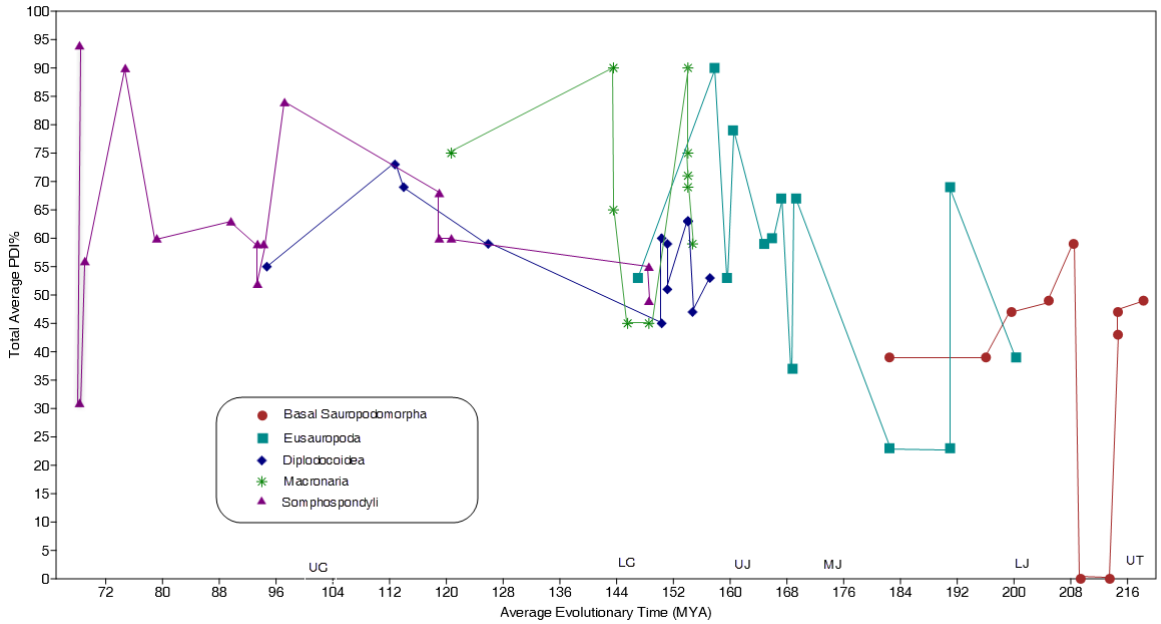

Figure 1. Variation of PDI% of Sauropodomorpha through evolutionary time (MYA). Variation of total average vertebral pneumaticity ('PDI%') of Sauropodomorpha with average evolutionary time, retrieved from Table 2. Notice that the contemporaneous to each other sauropodomorphs show similar expressions of PSP as well as the faintly gradual increase of PDI% as we transcend from the most primitive (right) to the most derived (left) taxa. The numerical values of total average PDI% are retrieved from Table 7 and SI3 and depend on the availability of fossil material. Colour coding: Brown circle = basal Sauropodomorpha, Cyan square = Eusauropoda, Blue diamond = Diplodocoidea, Green star= Macronaria, Purple triangle = Somphospondyli. Abbreviations: *MJ*, Middle Jurassic; *LC*, Lower Cretaceous; *LJ*, Lower Jurassic; *UC*, Upper Cretaceous; *UT*, Upper Triassic.

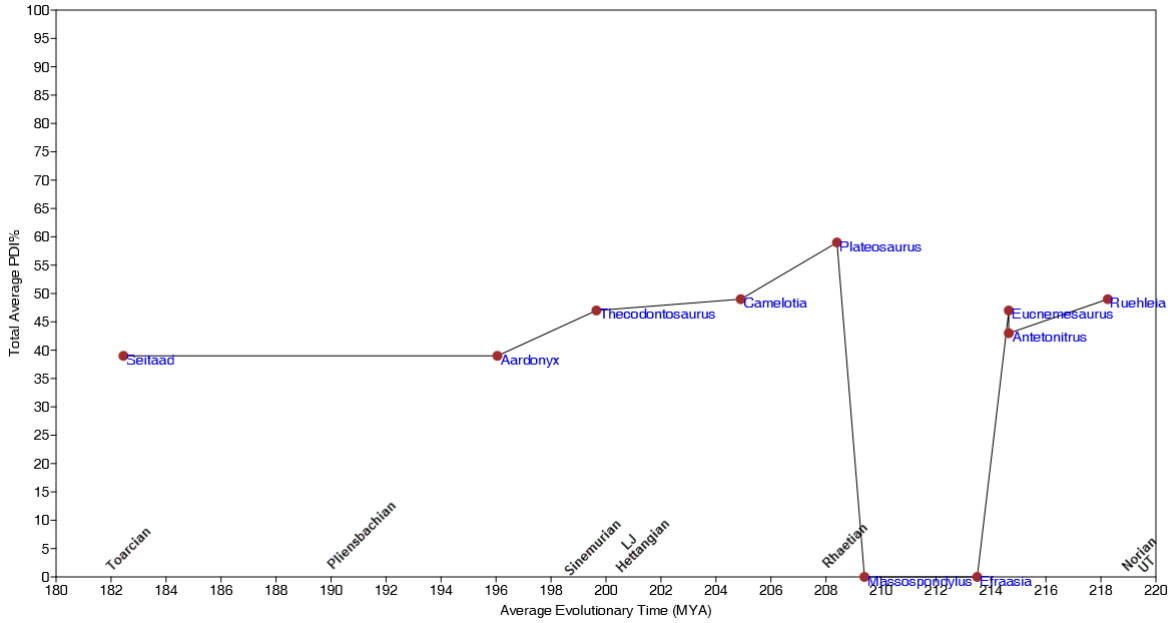

Figure 2. Variation of PDI% of basal Sauropodomorpha through evolutionary time (MYA). The expression of total average vertebral pneumaticity (PDI%) of basal sauropodomorphs through average evolutionary time using the average values of FADs and LADs as retrieved from the literature/PBDB (Table 2). A somewhat variable expression of vertebral pneumaticity can be seen here since the first appearance of the basal sauropodomorphs; some of these taxa express moderate degrees while others zero degrees of pneumaticity throughout the course of time, maintaining a steady trend by the time we reach the Lower-Middle Jurassic. The numerical values of total average PDI% are retrieved from Table 7 and SI3 and depend on the availability of fossil material. Abbreviations: *LJ*, Lower Jurassic; *UT*, Upper Triassic.

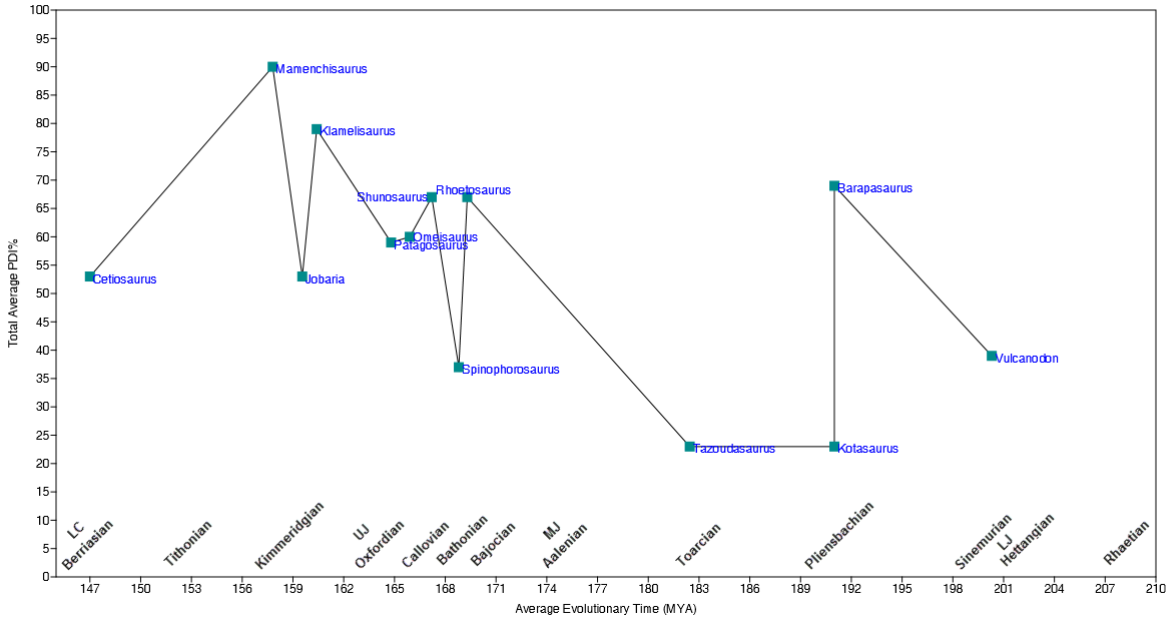

Figure 3. Variation of PDI% of (non-neosauropod) Eusauropoda through evolutionary time (MYA). The expression of total average vertebral pneumaticity (PDI%) of non-neosauropod eusauropods through average evolutionary time using the average value of FADs and LADs as retrieved from the literature/PBDB (Table 2). An overall increasing expression of vertebral pneumaticity can be seen here, after an initial peak in expression, followed by a trough and then steadily increasing as we traverse from the Middle Jurassic to the Late Cretaceous. The numerical values of total average PDI% are retrieved from Table 7 and SI3 and depend on the availability of fossil material. Abbreviations: *LC*, Lower Cretaceous; *LJ*, Lower Jurassic; *MJ*, Middle Jurassic; *UJ*, Upper Jurassic.

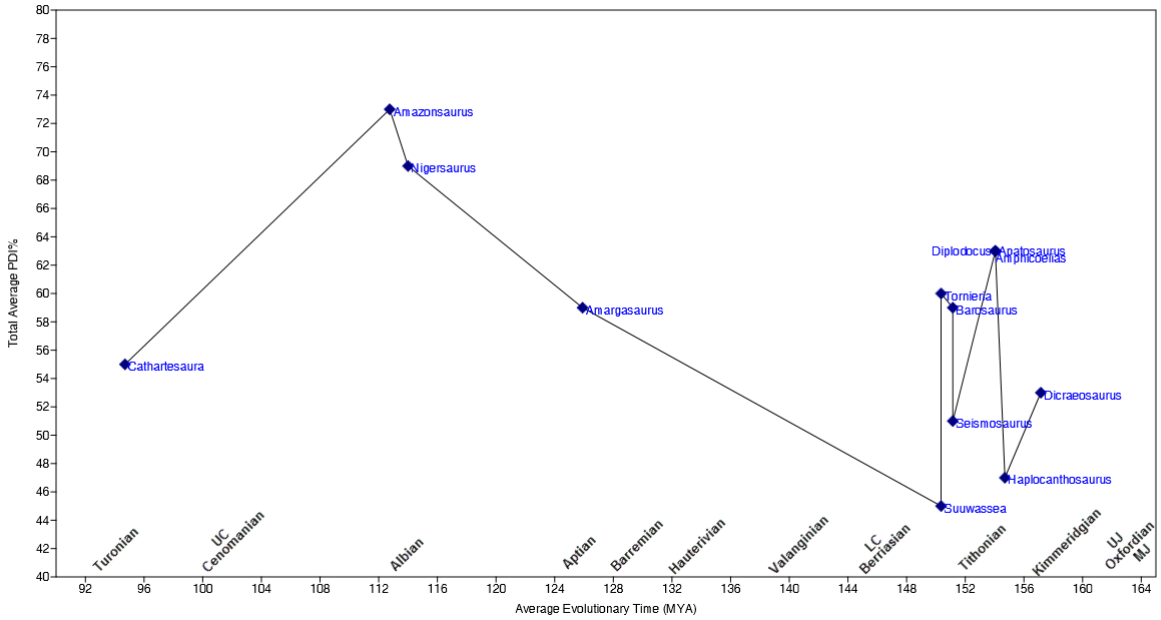

Figure 4. Variation of PDI% of Diplodocoidea through evolutionary time (MYA). The expression of total average vertebral pneumaticity (PDI%) of diplodocoids through average evolutionary time using the average values of FADs and LADs as retrieved from the literature/PBDB (Table 2). The earlier members exhibited variable expressions of vertebral pneumaticity until the Lower Cretaceous where an increasing trend then followed almost up until the Upper Cretaceous. The numerical values of total average PDI% are retrieved from Table 7 and SI3 and depend on the availability of fossil material. Abbreviations: *LC*, Lower Cretaceous; *UC*, Upper Cretaceous; *UJ*, Upper Jurassic.

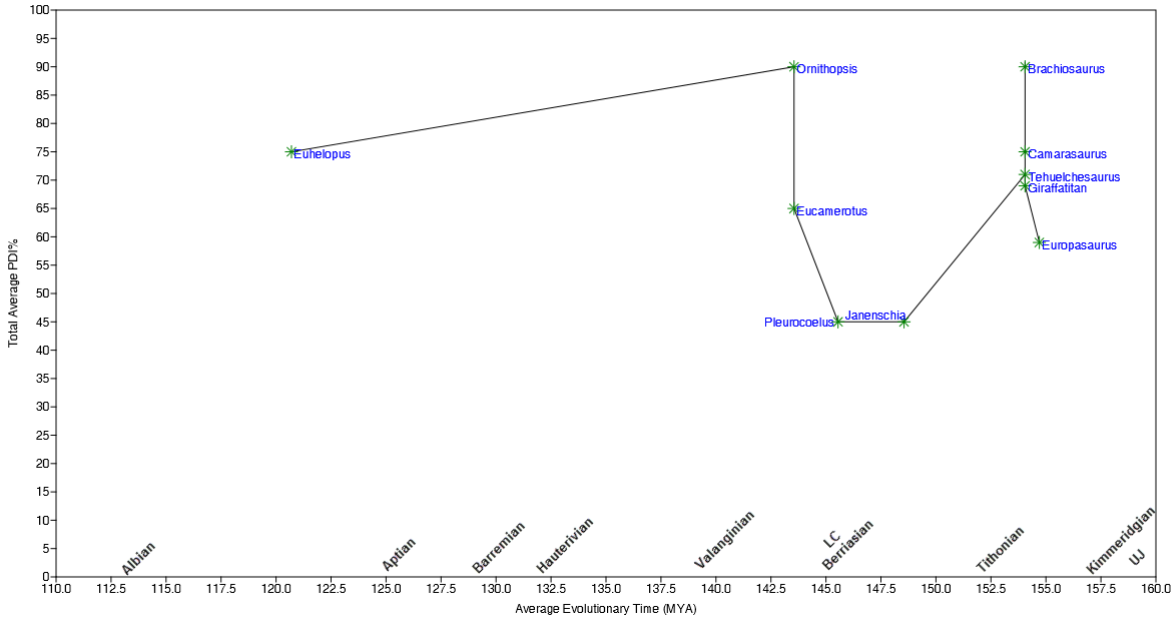

Figure 5. Variation of PDI% of Macronaria through evolutionary time (MYA). The expression of total average vertebral pneumaticity (PDI%) of macronarians (including basal titanosauriformes) through average evolutionary time using the average values of FADs and LADs as retrieved from the literature/PBDB (Table 2). A variable expression of vertebral pneumaticity can be seen here with a suddenly increasing trend appearing in the Lower Cretaceous. The numerical values of total average PDI% are retrieved from Table 7 and SI3 and depend on the availability of fossil material Abbreviations: *LC*, Lower Cretaceous; *UJ*, Upper Jurassic.

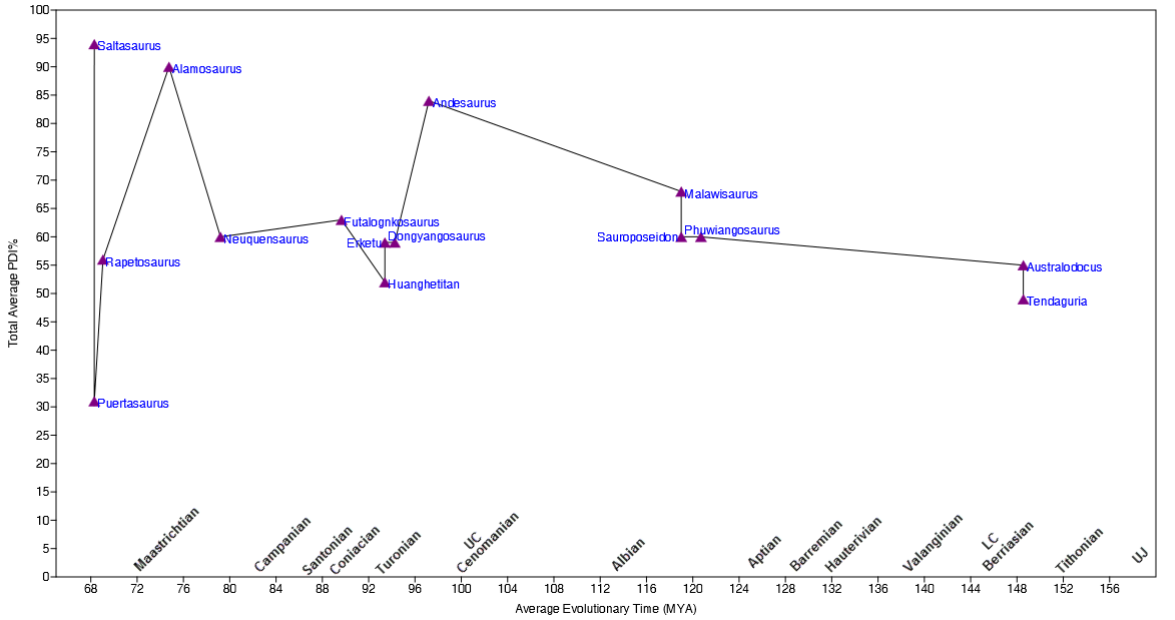

Figure 6. Variation of PDI% of Somphospondyli through evolutionary time (MYA). The expression of total average vertebral pneumaticity (PDI%) of sauropods belonging to the subfamily of Somphospondyli through average evolutionary time using the average values of FADs and LADs as retrieved from the literature/PBDB (Table 2). A steady mid-high expression of vertebral pneumaticity can be seen here with an increasing trend appearing towards the Upper Cretaceous, followed by a sudden decrease and then remaining relatively stable towards the Late Cretaceous, with the most derived members exhibiting variable expressions. The numerical values of total average PDI% are retrieved from Table 7 and SI3 and depend on the availability of fossil material. Abbreviations: *LC*, Lower Cretaceous; *UC*, Upper Cretaceous; *UJ*, Upper Jurassic.

Considering the evolution of pneumaticity of Sauropodomorpha on a vertebral segment level through time, both cervical and dorsal PDI% start at low and moderate levels, increase in Early Jurassic and remain at relatively stable and moderate-high levels until the Mid-Cretaceous (Figs. 7 & 8). Caudal pneumaticity follows an increasing trend which remains stable as we approach the Mid-Cretaceous (Fig. 9). In most cases, for sauropods of equal body lengths but with different overall degrees of pneumaticity, those with more pneumaticity are estimated to be the heavier than the less pneumatic taxa (see 'Table 7' in Chapter 2). Nevertheless, there are taxa with different degrees of pneumaticity and masses that have equal lengths (such as *Barapasaurus* + *Haplocanthosaurus*, *Erketu* + *Ornithopsis*, *Puertasaurus* + *Futalognkosaurus* + *Klamelisaurus* or *Tehuelchesaurus* + *Rhoetosaurus*). Overall (Fig. 10), there is a positive correlation between cervical pneumaticity and neck length across the examined taxa. On a closer view of the sauropodomorph groups, however, there are some noteworthy observations. In basal sauropodomorphs, there is no correlation of cervical PDI% versus neck length, while in eusauropods, neck length is directly correlated to cervical pneumaticity. Diplodocoids, macronarians and somphospondylans with short and long necks exhibit almost equal amounts of moderate to high degrees of cervical pneumatisation, hence there is no correlation. It has to be noted here that, in diplodocoids and macronarians, indiscriminate variability occurs until a length threshold is reached (6 m) after which pneumaticity seems to correlate directly with the increase in neck length. Concerning dorsal PDI% versus trunk length (Fig. 11), there is not a correlation between these two parameters since taxa having relatively long trunks do not necessarily possess more pneumatised dorsal vertebrae than those taxa with shorter trunks. Macronarian and somphospondylan dorsal PDI% shows a direct correlation with trunk length but this is up to a trunk length point; very long trunks (over 6 m) exhibit lower expressions of pneumaticity. In general, this suggests that as dorsal length increases in sauropods, dorsal PDI% tends to decrease.

Finally, tail length and caudal PDI% (Fig. 12) are not correlated to each other since taxa with equal or different tail lengths have variable expressions of caudal pneumaticity. For example, the long tails of diplodocoids (e.g. *Diplodocus* or *Seismosaurus*) show moderate expression of pneumatisation while the relatively short lengths of some somphospondylans (e.g. *Neuquensaurus* and *Saltasaurus*) exhibit very high levels of pneumatisation. Total average PDI% in Sauropodomorpha (Fig. 13) shows no correlation with body mass, as taxa with low or high mass values exhibit variable degrees of pneumatisation. Conversely, there is evident correlation between total average pneumaticity and body length (Fig. 14). For an overview of statistical significance and correlation between pneumaticity and body size data see Table 1 below.

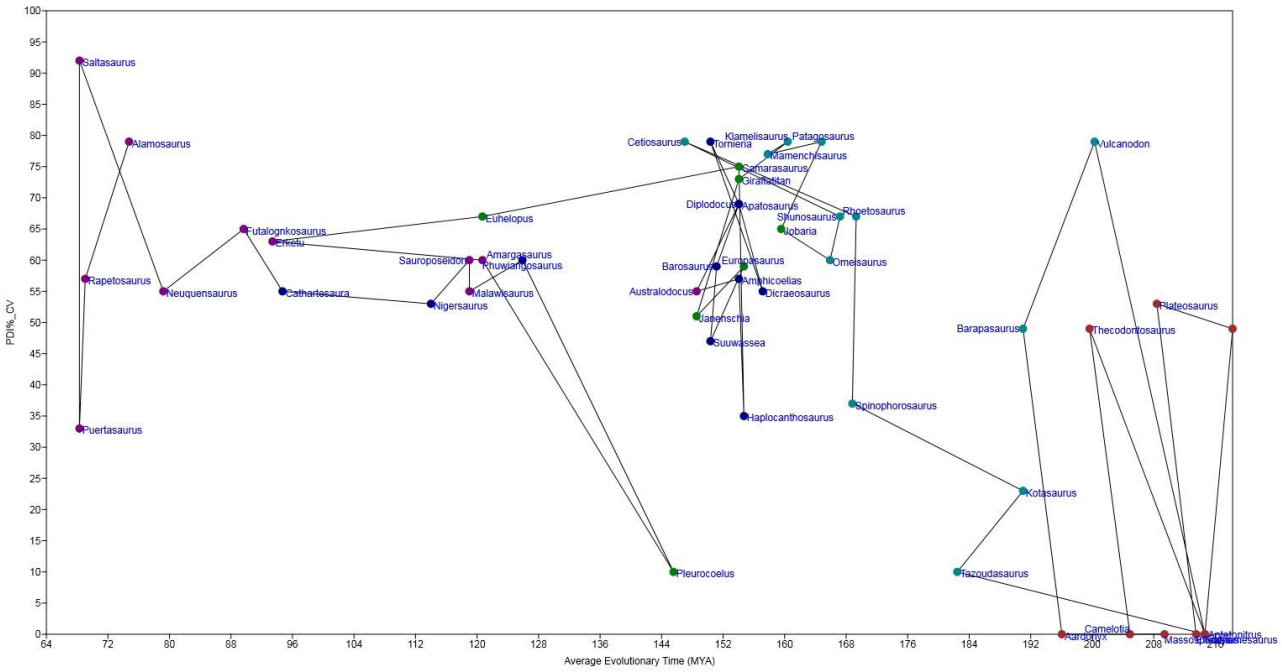

Figure 7. Cervical series PDI% of Sauropodomorpha against evolutionary time (MYA). The expression of cervical pneumaticity (PDI%_CV) of Sauropodomorpha through average evolutionary time using the average values of FADs and LADs as retrieved from the literature/PBDB (Table 2; Chapter 1). The expression of PSP of the cervical vertebrae is stable throughout the evolutionary history of Sauropodomorpha showing a minor decreasing trend as we approach the Late Triassic. Colour coding: Brown = Basal sauropodomorphs, Cyan = Eusauropods, Blue = Diplodocoids, Green = Macronarians, Purple = Somphospondyli.

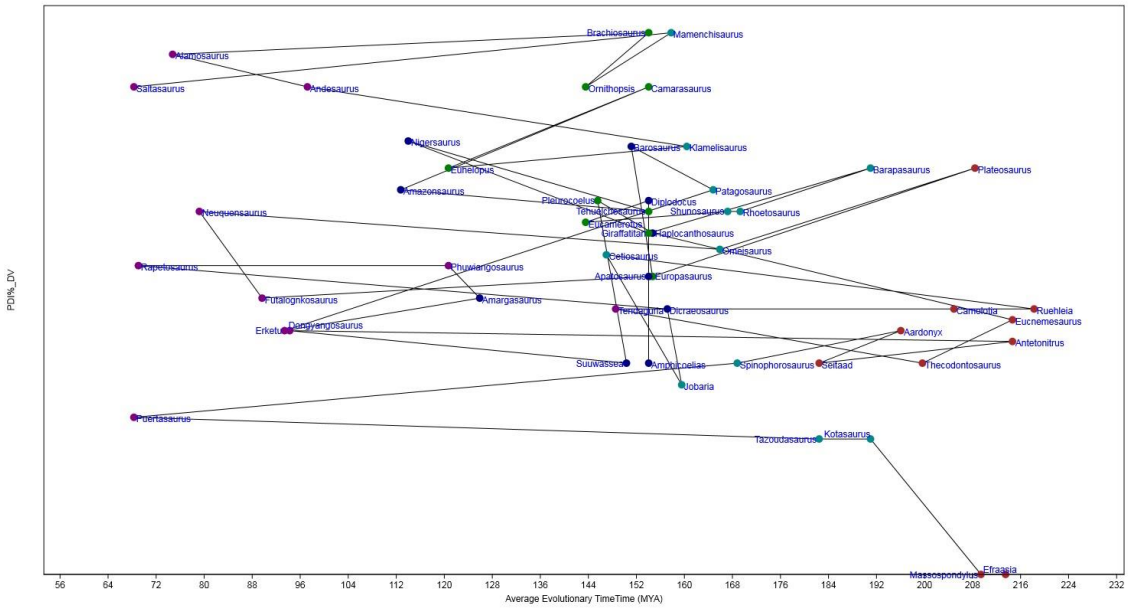

Figure 8. Dorsal series PDI% of Sauropodomorpha against evolutionary time (MYA). The expression of dorsal pneumaticity (PDI%_DV) of Sauropodomorpha through average evolutionary time using the average values of FADs and LADs as retrieved from the literature/PBDB (Table 2; Chapter 1). The expression of PSP in dorsal vertebrae is variable throughout the evolutionary history of sauropodomorphs, with a noticeable decreasing trend in Macronarians. Colour coding: Brown = Basal sauropodomorphs, Cyan = Eusauropods, Blue = Diplodocoids, Green = Macronarians, Purple = Somphospondyli.

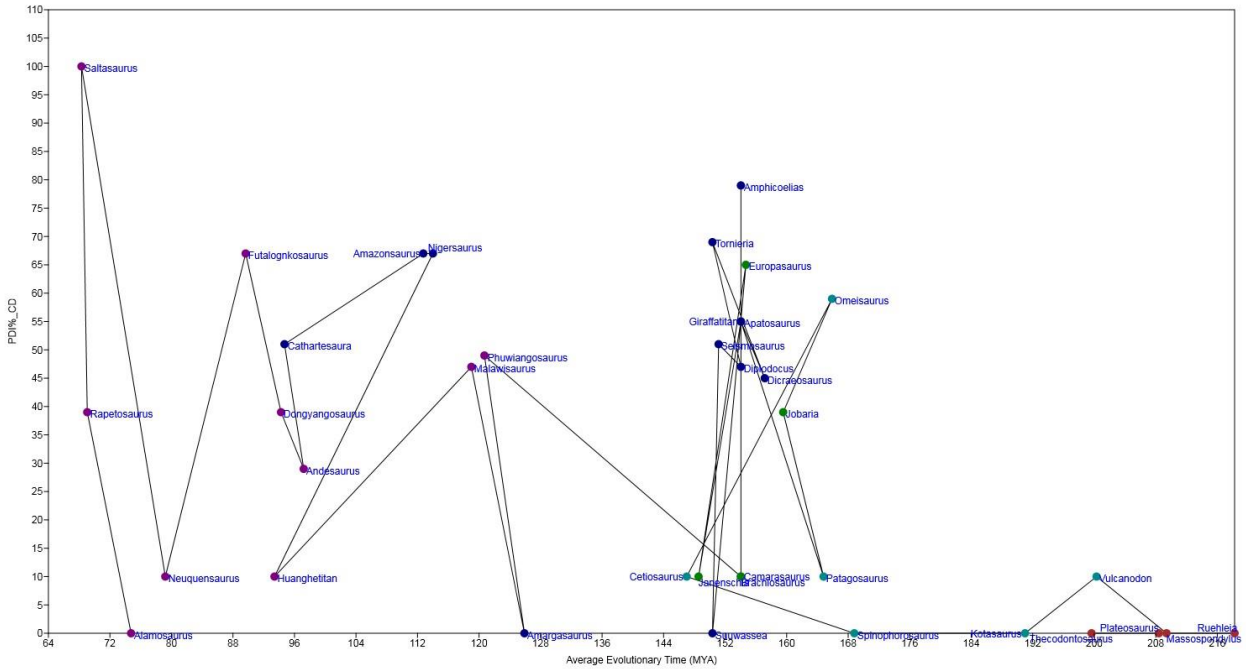

Figure 9. Caudal series PDI% of Sauropodomorpha against evolutionary time (MYA). The expression of caudal pneumaticity (PDI%_CD) of Sauropodomorpha through average evolutionary time using the average values of FADs and LADs as retrieved from the literature/PBDB (Table 2; Chapter 1). The expression of PSP in caudal vertebrae is practically non-existent in Late Triassic basal sauropodomorphs but it shows noticeable increase peaks as we transcend from the Mid-Jurassic to the Mid-Late Cretaceous sauropods. Colour coding: Brown = Basal sauropodomorphs, Cyan = Eusauropods, Blue = Diplodocoids, Green = Macronarians, Purple = Somphospondyli.

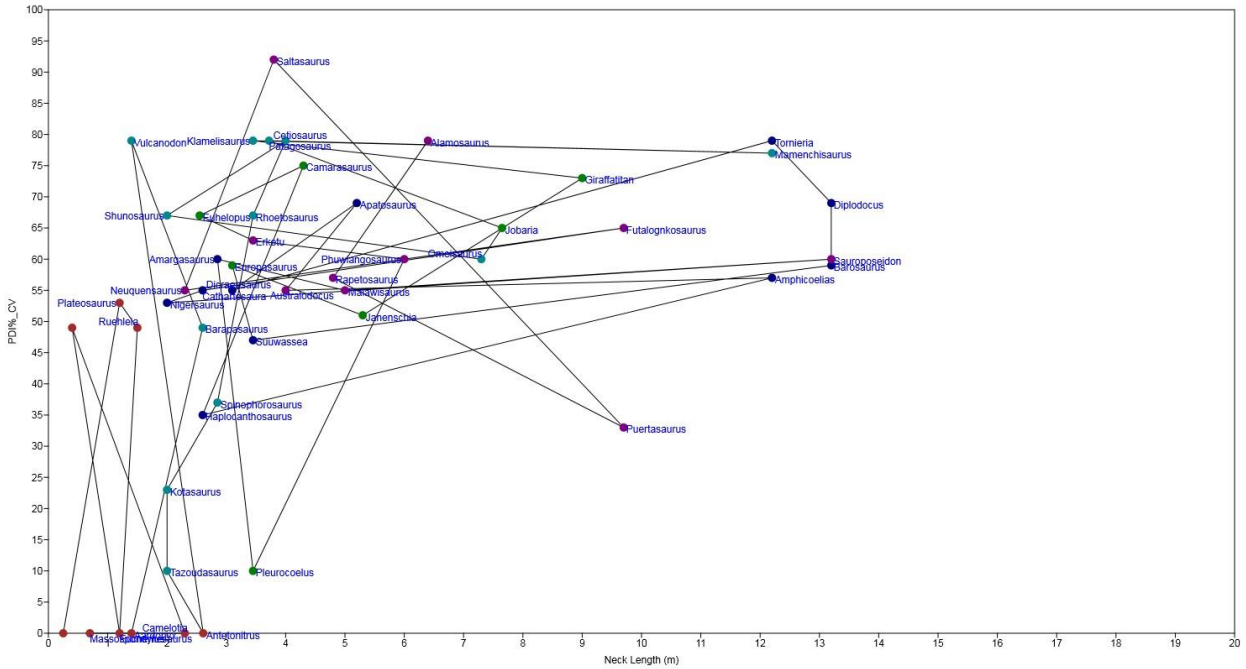

Figure 10. Cervical PDI% of Sauropodomorpha against Neck Length (m). Correlation of cervical pneumaticity (PDI%_CV) with respect to neck length [Neck Length (m)] throughout all examined Sauropodomorpha. The overall trend shows a direct correlation between cervical pneumaticity and neck length for sauropodomorphs, i.e. the longer the neck the more pneumatised it becomes. Colour coding: Brown = Basal sauropodomorphs, Cyan = Eusauropods, Blue = Diplodocoids, Green = Macronarians, Purple = Somphospondyli.

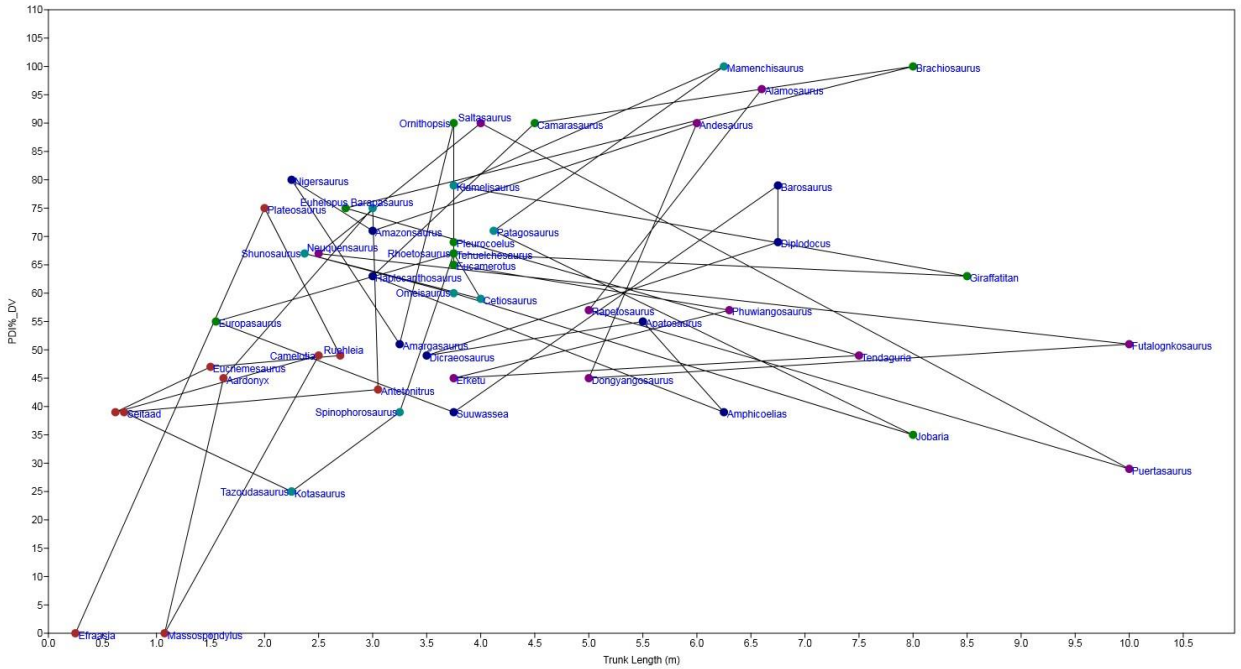

Figure 11. Dorsal PDI% of Sauropodomorpha against Trunk Length (m). Correlation of dorsal pneumaticity (PDI%_DV) with respect to trunk length [Trunk Length (m)] throughout all examined Sauropodomorpha. The overall trend shows no correlation between dorsal pneumaticity and trunk length for sauropodomorphs since taxa with long trunks do not necessarily have high levels of vertebral pneumatisation, especially after a certain value of trunk length. Colour coding: Brown = Basal sauropodomorphs, Cyan = Eusauropods, Blue = Diplodocoids, Green = Macronarians, Purple = Somphospondyli.

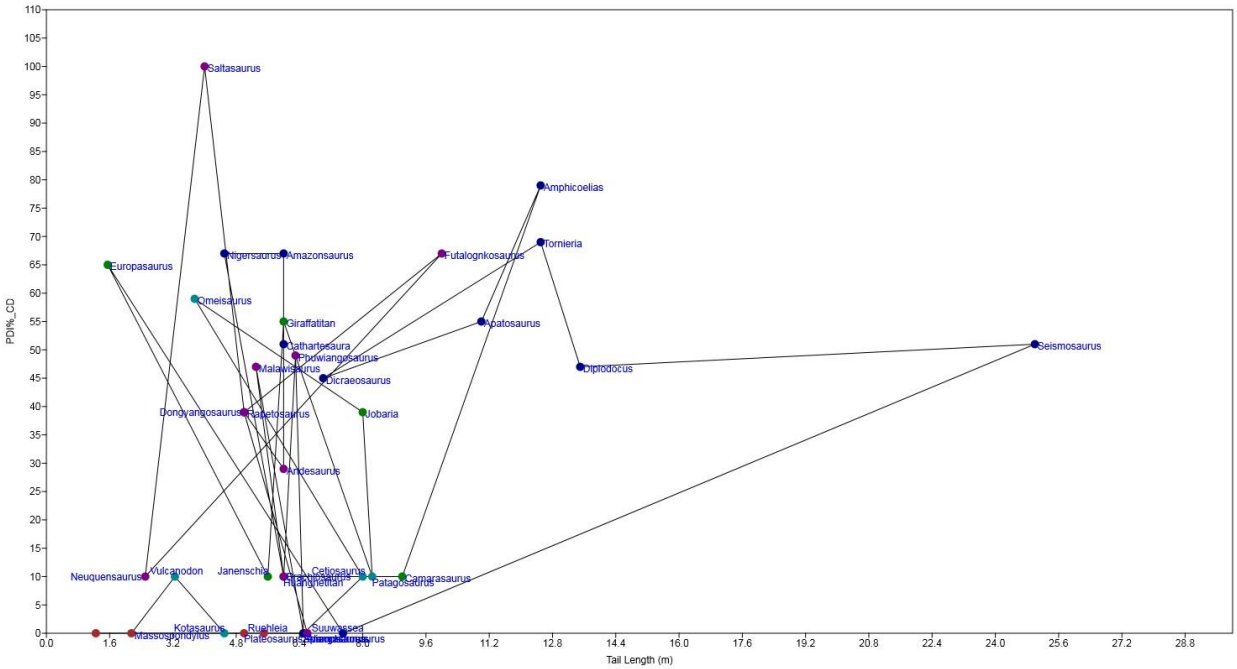

Figure 12. Caudal PDI% of Sauropodomorpha against Tail Length (m). Correlation of caudal pneumaticity (PDI%_CD) with respect to tail length [Tail Length (m)] throughout all examined Sauropodomorpha. The overall trend shows a variable correlation between caudal pneumaticity and tail length for sauropodomorphs. Whether taxa have equal or completely different tail lengths, their expressions of caudal pneumaticity can be equally variable, i.e. caudal pneumaticity is not directly proportional to the tail's length, across the examined sauropodomorph taxa. Colour coding: Brown = Basal sauropodomorphs, Cyan = Eusauropods, Blue = Diplodocoids, Green = Macronarians, Purple = Somphospondyli.

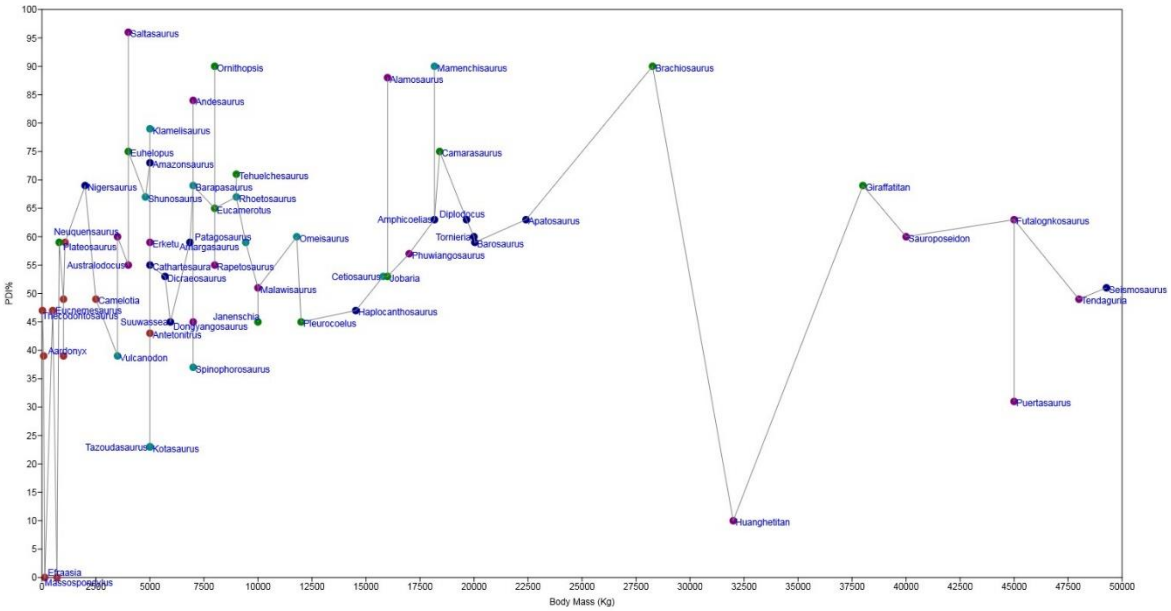

Figure 13. Variation of total average PDI% of Sauropodomorpha against Body Mass (Kg). Correlation of total average pneumaticity (PDI%) with respect to body mass throughout all examined Sauropodomorpha. The overall trend shows no correlation between pneumaticity and body mass for sauropodomorphs. Taxa with high or low values of mass have variably high or low values of PDI%. Thus, pneumaticity is not proportional to body mass, across the examined sauropodomorph taxa. Colour coding: Brown = Basal sauropodomorphs, Cyan = Eusauropods, Blue = Diplodocoids, Green = Macronarians, Purple = Somphospondyli.

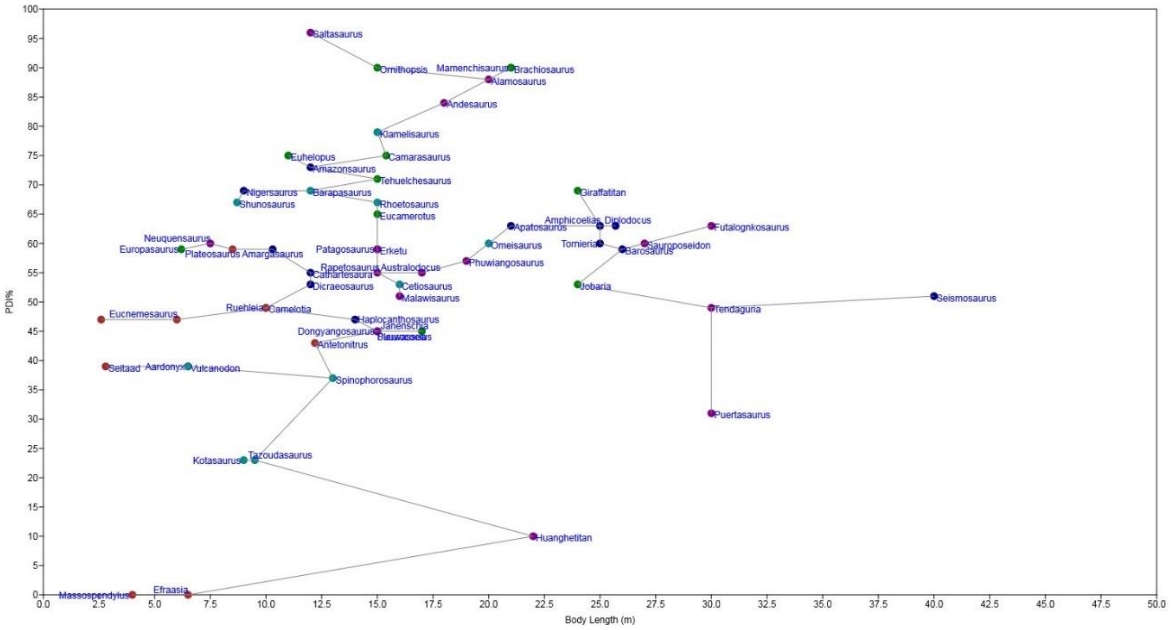

Figure 14. Variation of total average PDI% of Sauropodomorpha against Body Length (m). Correlation of total average pneumaticity (PDI%) with respect to body length throughout all examined Sauropodomorpha. The overall trend shows some correlation between pneumaticity and body length, mostly evident in eusauropods, macronarians and somphospondylans, where as length increases, pneumaticity does too. Colour coding: Brown = Basal sauropodomorphs, Cyan = Eusauropods, Blue = Diplodocoids, Green = Macronarians, Purple = Somphospondyli.

Table 1. Statistical correlations between pneumaticity (PDI%) and body size metrics in Sauropodomorpha. Pearson's correlation results in *p (two-tailed)* and R^2 (coefficient of determination from the Pearson product-moment correlation) show the level of significance between each set of variables. Benjamini-Hochberg False Discovery Rate correction (FDR) is also applied on the *p* values. The initial *p* values range from 0.04 (95%) to 0.8 (99%) indicating that the correlations vary from significant to not significant at $p<0.05$. R^2 values indicate, in general, a weak positive correlation between each set of variables. Tendency of moderate negative correlation between PDI% and body length is expressed in Diplodocoidea and Somphospondyli and sometimes in Macronaria too. Numeric data are taken from Table 7. Non-available pneumaticity data and their corresponding paired values had to be excluded, thus reducing the number of taxa (n), wherever appropriate. Blue indicates statistical significance at $p < 0.05$.

Statistical significance (two-tailed p value) and Pearson's correlations (coefficient of determination R^2) between pneumaticity (PDI%) and body size metrics in Sauropods	
PDI% vs body mass (kg) in all examined sauropodomorphs (n=61)	
p = 0.189197 **FDR p = 0.4300007**	**R = 0.1704** **R^2 = 0.029**
PDI% vs body length (m) in all examined sauropodomorphs (n=61)	
p = 0.017148 **FDR p = 0.17148**	**R = 0.3042** **R^2 = 0.0925**
PDI% vs femur length (m) in all examined sauropodomorphs (n=38)	
p = 0.007228 **FDR p = 0.10842**	**R = 0.4288** **R^2 = 0.1839**
Cervical PDI% vs neck length (m) in all examined sauropodomorphs (n=50)	
p = 0.001662 **FDR p = 0.04986**	**R = 0.4335** **R^2 = 0.1879**
Dorsal PDI% vs trunk length (m) in all examined sauropodomorphs (n=53)	
p = 0.079812 **FDR p = 0.39371**	**R = 0.2428** **R^2 = 0.059**
Caudal PDI% vs tail length (m) in all examined sauropodomorphs (n=37)	
p = 0.100529 **FDR p = 0.39371**	**R = 0.2742** **R^2 = 0.0752**
Cervical PDI% vs neck length (m) in basal Sauropodomorpha (n=9)	
p = 0.303496 **FDR p = 0.569055**	**R = -0.3878** **R^2 = 0.1504**
Cervical PDI% vs neck length (m) in Eusauropoda (n=13)	
p = 0.149086 **FDR p = 0.4300007**	**R = 0.4237** **R^2 = 0.1795**
Cervical PDI% vs neck length (m) in Diplodocoidea (n=11)	
p = 0.200667 **FDR p = 0.4300007**	**R = 0.4181** **R^2 = 0.1748**
Cervical PDI% vs neck length (m) in Macronaria (n=6)	
p = 0.825301 **FDR p = 0.825301**	**R = -0.1174** **R^2 = 0.0138**

Cervical PDI% vs neck length (m) in Somphospondyli (n=11)	
p = 0.533426 FDR p = 0.6286122	R = -0.2119 R^2 = 0.0449
Dorsal PDI% vs trunk length (m) in basal Sauropodomorpha (n=10)	
p = 0.751528 FDR p = 0.7774428	R = 0.1151 R^2 = 0.0132
Dorsal PDI% vs trunk length (m) in Eusauropoda (n=13)	
p = 0.18882 FDR p = 0.4300007	R = 0.3891 R^2 = 0.1514
Dorsal PDI% vs trunk length (m) in Diplodocoidea (n=10)	
p = 0.560353 FDR p = 0.6286122	R = -0.2128 R^2 = 0.0453
Dorsal PDI% vs trunk length (m) in Macronaria (n=9)	
p = 0.368415 FDR p = 0.5885779	R = 0.3415 R^2 = 0.1166
Dorsal PDI% vs trunk length (m) in Somphospondyli (n=11)	
p = 0.17238 FDR p = 0.4300007	R = -0.4438 R^2 = 0.197
Caudal PDI% vs tail length (m) in basal Sauropodomorpha (n=4)	
p = NA FDR p = NA	R = NA R^2 = NA
Caudal PDI% vs tail length (m) in Eusauropoda (n=7)	
p = 0.565751 FDR p = 0.6286122	R = 0.265 R^2 = 0.0702
Caudal PDI% vs tail length (m) in Diplodocoidea (n=11)	
p = 0.372766 FDR p = 0.5885779	R = 0.2984 R^2 = 0.089
Caudal PDI% vs tail length (m) in Macronaria (n=5)	
p = 0.436807 FDR p = 0.6286122	R = -0.4591 R^2 = 0.2108
Caudal PDI% vs tail length (m) in Somphospondyli (n=10)	
p = 0.288421 FDR p = 0.569055	R = -0.3737 R^2 = 0.1397
PDI% vs body length (m) in basal Sauropodomorpha (n=10)	
p = 0.337034 FDR p = 0.5885779	R = 0.3396 R^2 = 0.1153

PDI% vs body length (m) in Eusauropoda (n=13)	
p = 0.055751 **FDR p = 0.39371**	**R = 0.5419** **R^2 = 0.2937**
PDI% vs body length (m) in Diplodocoidea (n=13)	
p = 0.672078 **FDR p = 0.7200836**	**R = -0.1307** **R^2 = 0.0171**
PDI% vs body length (m) in Macronaria (n=10)	
p = 0.530672 **FDR p = 0.6286122**	**R = 0.2257** **R^2 = 0.0509**
PDI% vs body length (m) in Somphospondyli (n=15)	
p = 0.118113 **FDR p = 0.39371**	**R = -0.4215** **R^2 = 0.1777**
PDI% vs body mass (kg) in basal Sauropodomorpha (n=10)	
p = 0.486583 **FDR p = 0.6286122**	**R = 0.2497** **R^2 = 0.0624**
PDI% vs body mass (kg) in Eusauropoda (n=13)	
p = 0.118049 **FDR p = 0.39371**	**R = 0.4552** **R^2 = 0.2072**
PDI% vs body mass (kg) in Diplodocoidea (n=13)	
p = 0.508092 **FDR p = 0.6286122**	**R = -0.2026** **R^2 = 0.041**
PDI% vs body mass (kg) in Macronaria (n=10)	
p = 0.440695 **FDR p = 0.6286122**	**R = 0.2757** **R^2 = 0.076**
PDI% vs body mass (kg) in Somphospondyli (n=15)	
p = 0.077087 **FDR p = 0.39371**	**R = -0.4701** **R^2 = 0.221**

Observations from the literature and museum specimens reveal that the most pneumatised vertebrae are the cervicals and dorsals, even in those sauropods with overall low total pneumatisation (i.e. that belong to gamma, delta and epsilon degrees). Cervicals and dorsals are usually found in ‘Alpha’, ‘Beta’ and ‘Gamma’ degrees, while sacrals, caudals are classified as ‘Delta’ and ‘Epsilon’ degrees (Table S4 in Appendix 2). When considering average categorisation of a subfamily based on the total averages of

pneumatisation of its members, basal sauropodomorphs are classified into ‘Delta’ and ‘Epsilon’ degrees and rarely ‘Gamma’ and this condition occurs in their cervical and dorsal vertebrae. Eusauropods range mostly from ‘Delta’ to ‘Gamma’ degrees with Mamenchisaurids to reach ‘Beta’ and ‘Alpha’ degrees. Neosauropods range from ‘Gamma’ to ‘Alpha’ degrees and they occur in all vertebral groups. Macronarians have moderately to highly pneumatised vertebrae and thus are frequently found to be in ‘Gamma’, ’Beta’ and ‘Alpha’ degrees, while diplodocids, dicraeosaurids and rebbachisaurids to exhibit lower expressions of pneumatisation and are mostly placed in the ‘Beta’ and ‘Gamma’ pneumaticity ranks (Table 7, Chapter 2). It has been often demonstrated (e.g. Wedel et al., 2000; Wedel, 2005; Schwarz & Fritsch, 2006; Schwarz et al., 2007) that the vertebrae of mamenchisaurids (e.g. *Mamenchisaurus*, *Omeisaurus*), macronarians like *Giraffatitan* and somphospondylans like *Sauroposeidon* possess cavernous chambers (camerae) that are interconnected with each other and to the surface (Fig. 15). Pneumatisation in somphospondylan taxa is quite variable, with genera possessing very low, medium or very high pneumatisation levels in their vertebrae, ranging from ‘Gamma’ to ‘Alpha’ degrees (Table 7, Chapter 2). The vertebrae of the taxa that exhibit the highest degrees of pneumaticity are somphospondylous (camellate) i.e. 'sponge-like'. Evidently, the data support an overall increase of pneumatic complexity as the sauropodomorphs evolve from basal to derived forms, with only few exceptions (such as *Mamenchisaurus* and *Apatosaurus*) that show sudden spikes of high pneumaticity along the way.

A sauropod may have vertebral regions belonging to different PDI's and, therefore, cannot be categorised and restricted to only one degree of pneumatisation but instead can be noted as having a range of expressed pneumatisation (for example, *Giraffatitan* cervicals and dorsals have a range of PDI% from ‘Alpha’ to ‘Beta’ and sacrals and caudals from ‘Delta’ to ‘Epsilon’ degrees, respectively); but these variations are accommodated in the calculation of the ‘overall’ pneumaticity. Finally, wherever a vertebral region or a sauropod are found to have a PDI equal to 100%, it does not mean that the entire bone is composed of air; rather, it means that the vertebra (or any other pneumatised bone or series) expresses the most pneumatic traits throughout its composition, for example when the bone is fully camellated as in some somphospondylans (e.g. *Saltasaurus*). For a complete and tabulated presentation of PDI measurements and details see Tables 4 & 7 in Chapter 2 and Tables S2 & S4 in Appendix 2.

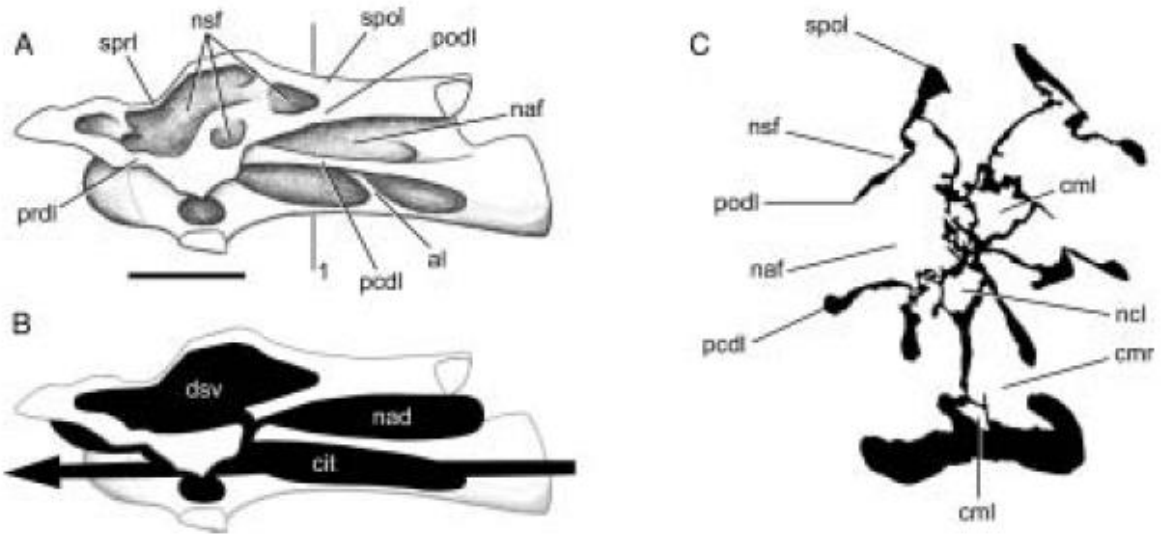

Figure 15. Reconstruction of pneumaticity in a *Giraffatitan* cervical vertebra.
A *Giraffatitan* cervical vertebra (BYU 12866) in left lateral view (A) showing the laminated fossae and pleurocoels that are present in most vertebral parts. (B) Depiction of the pneumatic chambers (black) formed by the assumed pneumatic diverticula that invade and aerate the bone, based on our current knowledge on avian PSP. The intertransverse canal runs parallel through the centrum and the supervertebral diverticulum aerates the neural spine. (C) An image from a CT scanner showing a transverse section of the vertebra and the distribution of its internal pneumatic chambers. For laminae abbreviations see Wilson (1999). Scale bar equals 20 cm. Figure adapted from Wedel (2005).

There appears to be a variable expression of pneumaticity among genera of the same family without a distinct trend. Overall, though, there is a general increase in the expression of pneumaticity from basal to derived sauropodomorph families. Also, as we progress from basal sauropodomorphs to macronarians, pneumaticity seems to shift from the dorsal area to the anterior (cervical) and in some cases (diplodocoids mostly but not in macronarians as much) to the posterior areas (sacral and caudal) and in somphospondylans, pneumaticity extends more and is more pronounced to the sacral and caudal series (Tables S3 and S4 in Appendix 2 and Appendix 3). Cervical pneumaticity begins early in sauropodomorphs and in most families it begins early at moderate-high levels, then decreases and finally remains stable. This pattern is observed in most families from their most primitive to the most derived members. Dorsal pneumaticity, though, seems to be dominant and relatively stable throughout most families. The observations made in this study (Appendix 3) seem to corroborate other researchers' observations (e.g. Wedel & Taylor, 2013), the anterior dorsal area seems to be the initial point of expression

of pneumaticity and from there it progressed variably to either end (anterior-posterior) of the body, varying from taxon to taxon. From the pneumaticity character matrix (Appendix 3) it is evident that the first traces of PSP in basal sauropodomorphs originated in the cervical and dorsal regions of the vertebral column This is also corroborated by the observations made in the ventral region of the dorsal vertebrae of sauropods that indicate that their lungs were attached to them, resembling the avian lung being almost fixed to the ventral side of the dorsal area (e.g. Wedel & Taylor, 2013). Whenever most or all parts of a vertebra belonging to a particular region are available, it appears that the initial point where pneumaticity begins in almost all taxa is the centrum and then the neural arch/transverse process area. This is the opposite phenomenon from the 'neural arch' first rule that holds true in theropods (Benson et al., 2012).

As mentioned above, evolutionary progression of pneumatisation in sauropodomorphs starts from the centrum and continues upwards (internally) to the neural arch, spreading dorsally towards the spine and anteroposteriorly to the zygapophyses (Appendix 3). A vertebra may possess a pneumatised centrum and neural arch but never only a pneumatised neural arch; the opposite can occur i.e. to have its centrum pneumatised. The cervical and dorsal vertebrae of most neosauropods (diplodocoids, macronarians and somphospondylans) appear to have similar expressions of pneumatisation in their centra and neural spines, leading us to assume that diverticular pneumatisation occurred (from an evolutionary aspect) first in these two vertebral areas and then advanced to the others. Basal sauropodomorphs have limited expression of pneumaticity, which is restricted to the cervical and dorsal series in their centra, neural arches, transverse processes, and rarely diapophyses and neural spine. From the eusauropods and, especially, neosauropods onwards, pneumatisation becomes more pronounced and extends to more vertebral parts.

Cervical pneumatisation in basal sauropodomorphs, eusauropods and neosauropods shows a variable and stable trend throughout Sauropodomorpha (Fig. 7). In basal sauropodomorphs, the peak and trough shifts occurred from Rhaetian to Sinemurian stages, throughout the transition from Upper Triassic to Lower Jurassic. Eusauropods exhibit a similar pattern from Pliensbachian-Toarcian (Lower Jurassic) stages, with a peak expression in Callovian and Oxfordian stages. In diplodocoids, the trait's path is characterised by a variable trend throughout the time of this group. Progression of cervical pneumaticity throughout macronarians begins at moderate and continue to high levels in Kimmeridgian and Tithonian stages but then it remains stable and drops in the Early Cretaceous (Aptian). Somphospondylan expression of cervical pneumaticity remains relatively stable throughout until a sudden peak in Santonian and Campanian stages occurs, followed by an equally sudden trough in Maastrichtian stage.

Dorsal pneumaticity in basal sauropodomorphs follows stable trajectory pattern from Norian to Sinemurian. The same trend is observed in eusauropods from Sinemurian until Oxfordian, with an increase of expression in Kimmeridgian stage and in neosauropods we observe the same trend until Tithonian. From Hauterivian stage onwards there is a continuous increase until Aptian stage. Members of macronarian sauropods achieve peak expression in Kimmeridgian while diplodocoidean expression increases from Hauterivian-Aptian onwards. In somphospondylans we see an initial low expression of pneumaticity occurring early in the group (Kimmeridgian-Tithonian) followed by gradually increasing expressions until Maastrichtian (Fig. 8).

Not enough data exist (either because of unavailable material and/or absence of pneumaticity) to document the trends in sacral and pelvic levels of pneumaticity in basal sauropodomorphs, eusauropods and neosauropods (Table 7, Chapter 2). The few available data do not show any patterns. The caudal pneumaticity pattern is almost non-existent in the Late Triassic but there are noticeable increase peaks in expression as we transcend from Early Jurassic to Mid-Late Cretaceous. Diplodocoids begin to demonstrate high caudal PSP from Mid-Late Jurassic up to Early-Mid Cretaceous while macronarians show moderate and low levels of PSP in Mid-Jurassic. The scarce data on sacral and pelvic pneumaticity in macronarians do not allow for any trends to be made clear. Somphospondylan caudal evolution of pneumaticity shows a variable expression of peaks and troughs until the Maastrichtian stage.

Pelvic pneumatisation comprises a group of 27 possible characters (Table 1) that can be found in the ilia, ischia and pubes of sauropodomorph dinosaurs. Not all of these characters were accounted for, as is evidenced in Appendix 3. In fact, the majority of sauropods, provided that fossil material is available, do not show any pneumaticity in their pelvic bones. Pneumatisation in the pelvis is seen only in some of the most derived sauropods that have moderate and high degrees of vertebral pneumatisation. The only exception to this is the presence of foramina and fossae on the ilium as well as foramina on the ischium (pers. obs. of MB.R.4402.1 – 11) of *Plateosaurus* (*longiceps*; PDI = 59%), but these could be artefacts of diagenesis, genetic malformations, muscular attachments and vascular openings, or even due to museum processing and handling of specimens. Only 28 of the 61 examined taxa had pelvic material available and most of them did not bear any pneumatic feature. Apart from the possible presence of pelvic pneumaticity in *Plateosaurus,* six other taxa have pneumatised pelves (Appendix 3). *Omeisaurus* (PDI = 60%) possesses pneumatic foramina on its pubis (He et al., 1988), *Amazonsaurus* (PDI = 73%) has a camerate ilium (Carvalho et al., 2003), *Euhelopus* (PDI = 75%) has a camellate ilium (Wilson & Upchurch, 2009), *Europasaurus* (PDI = 59%) bears foramina on its ilium (pers. obs. of DFMMh - FV 652 series), *Futalognkosaurus* (PDI = 63%) has

foramina on its pubis (Calvo et al., 2007) and *Alamosaurus* (PDI = 90%) has camellate ilium (Woodward & Lehman, 2009).

Approaching this issue from a statistical significance point of view, resulting parameters (*p, FDR p, R,* R^2) from correlation tests of 30 pairs of variables (Table 1) show interesting results. To adjust for the occurrence of false positives i.e. the presence of significant correlation results within our set of 30 tests, the Benjamini-Hochberg False Discovery Rate (B-H FDR) correction was applied to the obtained *p* values (Noble, 2009). Considering that our null hypothesis is that as body mass or body length increase, pneumaticity (expressed in PDI%) should increase too, we do observe an overall positive correlation between each set of variables. Specifically, as body mass increases overall pneumaticity increases too but this positive correlation is weak and the statistical confidence measure (*p* value) is not significant at our significance threshold of $p < 0.05$ and the application of the B-H FDR correction confirms this (Table 1). A similar result was retrieved when testing the correlation between PDI% and body length with the difference that the *p* value is less than 0.05 and, thus, significant. The application of the B-H FDR correction, though, shows that it may not be significant, after all. Same correlation results were found for PDI% and femur length, though the available sample of measurements was nearly half of the total number of examined taxa. When assessing the correlation of pneumaticity and vertebral segment length a weak proportional (positive) correlation is also observed between cervical pneumaticity and neck length in all examined sauropodomorphs and the *p* value is significant not only before but also after the B-H FDR correction has been applied (Table 1). Dorsal and caudal PDI% show weak positive correlation with trunk and tail lengths, respectively, but their *p* values are not significant (Table 1).

From a subfamilial perspective, overall correlations between total average pneumaticity and body mass as well as with body length (Figs 13 & 14), give us a clear view of the association existing among these fundamental morphological parameters. More specifically, heavier and lengthier basal sauropodomorphs tend to be more pneumatic than lighter and shorter ones but this weak positive relationship is not always occurring; rather, a neutral signal seems to be the dominant pattern. Statistically, cervical pneumaticity has a negative, but weak, correlation (inversely proportional) with neck length in basal sauropodomorphs, implying that the longer the neck is, the less pneumaticity it exhibits suggesting that the evolution of longer necks does not depend on increase of vertebral pneumatisation in the cervical vertebrae. This significance of this correlation, though, is not significant at $p < 0.05$. Positive and weak correlations exist between pneumaticity of the cervical series of eusauropods and diplodocoids and their neck lengths. Both are not significant before and after the B-H FDR corrections at $p < 0.05$

(Table 1). In Macronaria and Somphospondyli, though, neck length is inversely proportional (negative) to cervical pneumaticity but the result is not significant at $p < 0.05$ (Fig. 10 & Table 1). Of course, the negative correlations can also be artefacts of the small sample sizes. Dorsal pneumaticity in basal sauropodomorphs, eusauropods and macronarians is positively but weakly correlated with trunk length and the result is not significant at $p < 0.05$ (Table 1). In diplodocoids and somphospondylans, though, the correlation is negative, weak but not significant (Fig. 11 & Table 1). Correlation between caudal pneumaticity with respect to tail length in basal sauropodomorphs could not be computed due to small sample size. In eusauropods and diplodocoids, correlation is positive, weak and not significant while in macronarians and somphospondylans the correlation is negative, weak and not significant at $p < 0.05$ (Fig. 12 & Table 1).

In basal sauropodomorphs and eusauropods, PDI% is positively but weakly correlated with body mass and body length with the results being non-significant., while with length we see a clearer positive association (Figs. 13 & 14, Table 1 and Table 7 in Chapter 2).

In diplodocoidean and somphospondylan taxa (Figs. 8 & 9, Table 1 and Table 7 in Chapter 2) statistical tests reveal that body mass and body length are negatively but weakly correlated to overall vertebral pneumaticity. In macronarian taxa, though, pneumaticity is positively, though weakly, correlated with body mass and body length. In all cases, the results are not statistically significant at $p < 0.05$ (Table 1).

Linear regression graphs reveal that as mass and length increase in diplodocoids, pneumaticity is kept at relatively stable levels but in macronarians it first increases until it reaches a threshold (30 tonnes and 20 metres for each parameter) in which it continues its expression in a declining manner from that point onwards (Figs. 10-14 and Table 7 in Chapter 2). In somphospondylans, pneumaticity is usually negatively correlated (i.e. inversely proportional) with mass, while with respect to length it is positively correlated (i.e. directly proportional) until the threshold of about 18 metres, from which point onwards pneumaticity starts to decline and, therefore, decreases with higher values of length (Figs. 13 & 14 and Table 7 in Chapter 2).

The outcomes of this study indicate weak correlations between PDI% and size metrics, and more so with length rather than with mass, as well as moderate positive correlation with time. Positive association between length of a vertebral region and its level of pneumatisation is frequent implying that longer body regions exhibit higher degrees of pneumaticity. As time progresses, there is a climax where most macronarian, diplodocoid and somphospondylan taxa achieve high degrees of PSP (Late Jurassic – Early Cretaceous) but after that point, pneumatisation seems to be stable and then decreasing. Macroscopically, as we pass from basal to derived forms, the expression of

osteological pneumaticity increases, but intrafamilial levels of expression show variable patterns. In fact, some relatively medium-bodied somphospondylans such as *Alamosaurus* and *Saltasaurus* appear to possess very high degrees of PSP while other, more gigantic forms such as *Puertasaurus*, exhibit low levels of pneumatisation (Table 7 in Chapter 2). It is logical, though, to argue here that in the presence of more available vertebral material from incomplete taxa such as *Puertasaurus* the total average pneumatisation values would be different, probably revealing a different association between PSP and body size. The correlation between total length and pneumaticity was to be expected since body length is a more reliable proxy of body size than an estimated body mass. However, the variable expression of interfamilial pneumaticity contradicts the hypothesis in which we always expected a positive correlation (i.e. that as size increases, pneumaticity should increase), indicating additional, complex causes of size increase which may have affected differently each subfamily. Of course, we cannot rule out the possibility that osteological pneumaticity could be simply an aftereffect of diverticular development of an avian type of respiratory system. Therefore, PSP has a weak positive correlation with mass, correlates positive with overall length and positively with regional (cervical) length. Overall, though, PSP expresses itself almost variably throughout Sauropodomorpha.

3.3) Discussion - Association of body plan, size and expression of vertebral and pelvic pneumaticity

Sauropodomorpha was a highly diverse and successful superfamily of dinosaurs that achieved large body sizes even from the early stages in their evolution (Norian-Rhaetian), with genera such as *Plateosaurus* and *Ruehleia* reaching about 1000 kg in body mass and 6-9 m in body length (Buffetaut et al., 2000; Burness et al., 2001; Buffetaut et al., 2002; Sander et al., 2004). The underlying process behind this evolution of large size is the fact that basal sauropodomorphs had fast growth rates, faster than their dinosauromorph ancestors (Sander et al., 2004). Later on, this trait allowed several sauropod genera to achieve extremely large sizes (≥ 30 tonnes) at least three times in their evolutionary history i.e. within Diplodocoidea, basal Titanosauriformes (Macronaria) and Somphospondyli (Upchurch, 1998; Wilson, 2002).

Methods of mass estimation like, for example, femur diameter, volume by photogrammetry and scaling reconstructions place most sauropods (including the taxa in this study) within the 15 – 50 tonne mass and 10 – 30 m ranges (e.g. Anderson et al., 1985; Seebacher, 2001; Gunga et al., 2008; Benson et al., 2014), while some might have exceeded 50 tonnes (e.g. *Argentinosaurus, Ultrasaurus*) in mass and 30-50 m in length

(e.g. *Seismosaurus*; Gillette, 1991; Wedel et al., 2000; Seebacher, 2001; Benson et al., 2014; Bates, Tschopp et al., 2015). How could such giant sizes have been achieved? According to Sander et al. (2003, 2011) and Sander (2013) the most logical parameter would be a massive increase in metabolic rate during ontogeny. This function, in turn, could have been enabled by the presence of an avian-like respiratory system allowing for increased uptake of oxygen. The avian lung-air sac respiratory system is twice as efficient as the mammalian one, thus reducing the cost of energy when breathing (Perry and Reuter, 1999). Somewhat contrary to these arguments, though, is the discovery of unidirectional air flow in the breathing systems of crocodiles and monitor lizards (Schachner et al., 2013) as well as iguanas (Cieri et al., 2014), reptiles which do not exhibit high metabolic rates. In addition, Benson et al. (2014) demonstrated that evolution towards large sizes was a result of rapid evolutionary rates in association with immediate niche-filling ecological interactions which resulted to the formation of new ecotypes of dinosaurs (and mammals, after the K/Pg boundary).

Numerous studies have provided significant evidence that the avian lung-air sac respiratory system often leaves traces on the skeletons of birds as PSP (e.g. Wedel, 2003; O'Connor, 2004, 2006). The evidence of highly pneumatised vertebrae of sauropods shows that saurischian dinosaurs must also have had an extensive avian-like respiratory system composed of air sacs and diverticula (Wedel et al., 2000; Wedel, 2003; Sereno et al., 2008; Yates et al., 2012). Also, markings and features of the trunk region of the axial skeleton in many sauropods indicate a dorsal attachment of the lungs in that area, a condition found in birds (Perry and Reuter, 1999). But this system of lung and air sac diverticula does not always leave its marks on the postcranium in birds such as grebes, loons and penguins (Hogg, 1980, 1984; O'Connor, 2009; Apostolaki et al., 2015), because of the occurrence of cryptic diverticula (i.e. they do not leave traces on the skeleton) and this may also be true of sauropods (Wedel & Taylor, 2013).

This is where size may have played a key role in conjunction with avian-like respiratory system in sauropods in maintaining high metabolic growth rates which would have resulted in 'gigantothermy' or 'mass endothermy' (Sander et al., 2011) i.e. producing heat due to retention of digestion in large sized taxa as a response to the lack of mastication (Sander, 2013). Recent evidence, though, suggests that the high surface area of the bodies of sauropods would have allowed sufficient cooling, preventing the animal from overheating, thus lowering the body heat to levels like those of mammals (Gillooly et al., 2006; Eagle et al., 2011; Griebeler, 2013; Seymour, 2013). Beyond a neck length of 6-7 m and a body length of at least 15 m, many sauropods show a positive correlation with the extent of pneumatisation. This suggests that osteological pneumatisation became important in sauropods only after a particular size limit where it was required to maintain

rapid growth and high metabolic rates. The other outcome of this study, the neutrally variable expression of pneumaticity, for example, and the evidence of high levels of pneumatisation in small-bodied forms (e.g. *Europasaurus*, *Neuquensaurus*), suggest that pneumatisation may have been an inherited trait from larger ancestors. The reverse, i.e. that some very large forms (e.g. *Tendaguria*, *Puertasaurus*, *Seismosaurus*) possess medium to low amounts of pneumatisation may either indicate different physiological needs or that the diverticular system did not leave many marks of osteological resorption and penetration.

It has been demonstrated that air sac diverticula would have been the primary drivers of neck elongation since the bone marrow inside a normal vertebra would have been replaced by air during the developmental process of pneumatisation, thus reducing its mass (e.g. Wedel, 2003; O'Connor, 2006). The presence of the air sacs though would only have increased neck volume without increasing its mass (Taylor & Wedel, 2013). The long necks of sauropods could only have evolved because of PSP which is correlated to the lung – air sac – diverticula respiratory system and this is supported by the discovery here that after a threshold of neck length (6-7 m), there is, with few exceptions, a positive correlation between the length of the neck and its extent of pneumatisation. This conclusion answers the untested observation by Wedel (2005) that increasing length in sauropod necks was correlated with increasing complexity in pneumaticity.

The basic outcome of this study is that vertebral pneumaticity is, in most taxa, weakly positively correlated to body mass and moderately strong to body length for most sauropodomorph taxa (Figs. 13 & 14 and Table 1). In addition, expression of pneumaticity throughout the most basal to the most derived forms of Sauropodomorpha is variable. This was not expected, as it does not confirm the logical assumption that as sauropods evolved into larger and larger sizes they should also show increasing expressions of osteological pneumatisation. The results, in general, also verify that the elongation of neck in sauropodomorph evolution was possibly achieved with increasing pneumatisation of the cervical series (Taylor & Wedel, 2013). On a subfamilial level, though, only eusauropods and diplodocoids show positive correlation between cervical pneumaticity and neck length. This result contradicts those of basal sauropodomorphs, macronarians and somphospondylans which support the hypothesis that the evolution of the long necks in these three aforementioned subfamilies did not necessarily require higher degrees of vertebral pneumatisation. Perhaps, this occurs due to the fact that the ratio of neck lengths with respect to body lengths in diplodocoids and eusauropods is larger than in basal sauropodomorphs, macronarians and somphospondylans (Taylor & Wedel, 2013). This study has also shed light on the uncertainty surrounding the extent of correlation among parameters of size (mass, length and length of vertebral regions), time and degree

of pneumaticity. These results lead us to assume that PSP played a smaller role in sauropod gigantism than was thought, and sheds more light to the theory that, among the other four factors that resulted in high body mass, as demonstrated by Sander (2013), the presence of the 'avian-style lung-air sac' respiratory system with its pneumatic diverticula was a key factor of size increase, while the level of development of osteological pneumatisation in each taxon contributed to lightening the body mass (Wedel, 2005; Schwartz & Fritsch, 2006). Here it is shown, though, that the latter statement i.e. that high PSP contributed in lightening the skeleton may not be entirely true since PDI% and body mass are not always inversely correlated. Lack of fossil data, on the other hand, prevent us from gaining a complete evaluation of PDI% in the examined 61 taxa. Although this study confirms that the complexity and degree of pneumatisation show a minor increase throughout evolutionary time (e.g. Wedel, 2003, 2005), it appears that at generic and subfamilial levels, the correlation among the examined parameters is non-existent. This contrasts with the observation made by Apostolaki et al. (2015) that larger birds like ostrich and rhea have more complex expression and higher levels of PSP than smaller birds like kiwi and grebe. A final observation is that, overall, taxa from different families may share similar pneumatic features and be placed in the same PSP rank (Table 7 in Chapter 2 and Tables S2, S3 & S4 in Appendix 2) indicating neutrally variable expression of pneumatic features, an observation also made in birds (King, 1957), whales (Cranford et al., 1996), humans (Weiglein, 1999) and sauropods (Wedel, 2003*a,b*).

3.3.1) Comparison of Pneumaticity Degree Index (PDI%) with Pneumatisation Index (PI) and Air-Space Proportion (ASP)

O'Connor's (2004) Pneumatisation Index (PI) is defined it as the number of pneumatic vertebrae units in a region over the total number of vertebrae units of that region. This inspired the creation here of the Pneumatisation Degree Index (PDI%), which is based on the type and summary of pneumaticity features, from the least to most ubiquitous, that in turn are interpreted by their level of invasiveness in the bone. This method of quantifying pneumaticity allows comparisons among taxa, and between portions of the vertebral column, in ways that the PI does not. Wedel (2005) introduced the Air-Space Proportion (ASP) method as a way to assess skeletal pneumaticity in terms of the volume of the air enclosed in a CT cross section of a vertebra. To find the total pneumatisation in a vertebra is done by calculating the means of many cross sections of the bone from CT images, as an approximation of total volume (bone and air). Then the ASP is obtained by dividing the interior area of space over the sum of space (air) area plus the area of the bone material of the vertebra (Wedel, 2005; Fig. 7.5). Wedel's findings

match the segmented and total PDI% deduced in this study i.e. that most sauropod vertebrae (and, therefore, vertebral types such as cervical, dorsal, etc.) are at least 50% pneumatic [Table S4 in Appendix 2 and Wedel (2005); Table 7.5]. Caveats are that ASP measurements can have variable results among slices of a single vertebra, depending on completeness, distortion and mineral infills. This variation, though, can be countered by averaging as documented by Martin & Palmer (2014).

The results in Tables 4 and 7 indicate that some basal sauropods exhibit higher PDI% values than some more derived ones (e.g. *Camarasaurus* and *Sauroposeidon*; *Barosaurus* and *Plateosaurus*; *Giraffatitan* and *Brachiosaurus*). Some of these could be anomalies if they were based only on limited data. For example, if we only have vertebrae from one vertebral region (e.g. *Sauroposeidon*), the total value of the taxon will be that of the only piece of evidence we have, but it may be inaccurate. We suspect that PDI% values for *Barosaurus*, *Brachiosaurus* and *Giraffatitan* might have been higher if we had had more information; for example, for *Barosaurus* material, we did not have any information concerning its sacrals and caudals.

More caveats of the PDI% method are the possibility that pneumatic characters which were not expressed anywhere in the vertebral or pelvic regions may be considered redundant. Another concern is whether the measurements of mass, length and regional length are accurate, especially when specimens are incomplete or distorted due to limitations of size estimation techniques and specimen inadequacy. Furthermore, although the use of a CT scanner is costly, lack of such a technological resource will always yield less than accurate estimates of PSP. Finally, the pneumatic observations of vertebrae and regions of this study did not discriminate among anterior, middle and posterior parts of vertebral regions as this level of detail would be more time-consuming and would narrow down the number of selected taxa for this study.

3.3.2) Implications for understanding sauropod physiology

There has been a new appreciation of the unique character of sauropod physiology and size thanks to recent work (e.g. Sander et al., 2011). Sauropods could reach their huge sizes by a combination of ‘reptilian’ characters (e.g. limited diet and mass homeothermy, no mastication, r-selected by laying many relatively small eggs, limited parental care) and ‘mammalian-avian’ characters (e.g. high basal metabolic rate, high growth rate, avian-style lung and pneumaticity). As mass homeotherms, it is assumed that sauropods maintained default body temperatures somewhat lower than in modern birds and mammals. Pneumaticity is crucial in identifying the presence of a diverticular air sac breathing system and unidirectional air flow through the lungs, as in birds. PSP implies the

presence of an avian lung-air sac system but not vice versa, as in the case of the diving and semi-aquatic birds which exhibit limited, if any, osteological pneumatization.
In addition, the ontogenetic development of pneumaticity of a taxon possessing (or assuming to have possessed) an avian lung respiratory system can be documented by our method, and to an extent infer its diverticular expansion throughout ontogeny. It would be more challenging, though, to infer the metabolic system of such an animal, by merely drawing evidence from the degree of its PSP (via PDI%). Nevertheless, sauropods (and perhaps basal sauropodomorphs) have been assumed to be homeotherms based on a number of dietary and physical factors (Sander et al., 2010), one of them being the highly probable presence of an avian lung respiratory system and all of its implied biological ramifications.

Pneumaticity was an important weight-saving factor along the extended neck of sauropods, which was very long in the largest genera (e.g. Taylor & Wedel, 2013). One hypothesis of the evolutionary drive of neck elongation was to enable them to browse on bushes and tall trees widely without moving their body (Martin, 1987). Another hypothesis was that long necks in sauropods were sexually selected adaptations (Senter, 2006), as may be the case with giraffes, but Taylor et al. (2011) rejected this idea for sauropods. The development of long necks would have been demanding and costly in terms of required energy, especially when such structures constitute about a third of a sauropod's body size.

Reducing the bone mass in the cervical region reduces the cantilever load of the head-neck system, as the necks of sauropods grew longer and longer during both their ontogeny and their evolution (Taylor & Wedel, 2013). Vertebral pneumatization allowed sauropodomorphs to attain large sizes, as an exaptation that persisted throughout their evolution. This is not always the case, however, as shown by the long bones of pterosaurs (Dumont, 2010). In these, although pneumaticity slightly decreases the mass of the bone by replacing the marrow with air during ontogeny, pneumatized long bones are denser and so approximately the same weight as apneumatic bones of similar size.
Expression of dorsal pneumatization early in sauropodomorph evolution may indicate that it might have predated the origin of cervical and sacrocaudal pneumatization, whether from an evolutionary or developmental perspective. However, it is likely that both cervical and dorsal pneumatization evolved synchronously and biomechanical constraints necessitated the further development of dorsal pneumatization since mass reduction in the dorsal series would reduce the load and prevent the animals from being crushed by their own weight.

In terms of evolution, the Late Triassic and Early Jurassic basal sauropodomorphs such as *Plateosaurus* and *Massospondylus* possess moderate or absent PSP. Whenever

present, vertebral pneumaticity exhibits the acamerate condition (Wedel, 2001; Wedel, Cifelli & Sanders, 2003a, b) as in the “Delta” and “Epsilon” degrees of PDI% where the vertebrae possess fossae and, at best, pneumatic foramina. PSP is largely present in the cervical and dorsal series and very rarely, if ever, in the sacral and caudal series. It is worth noting that such a minor expression of PSP, especially the frequently present shallow fossae on the vertebral landmarks, is also a characteristic of the early juvenile members of neosauropods (e.g. *Apatosaurus*, *Camarasaurus*, *Diplodocus*) which are known for possessing high degrees of PSP when they reach adulthood (Table 6 and SI3; Wedel, Cifelli & Sanders, 2003a, b; Melstrom, D’Emic, Chure et al., 2016). Perhaps, ontogeny recapitulates phylogeny since the evolutionary progression of vertebral pneumaticity throughout Sauropodomorpha seem to mirror the ontogenetic development of PSP seen in the more derived members of this superfamily (Zurriaguz & Cerda, 2017).

The variable pattern of pneumaticity in the Late Triassic to Early Jurassic basal sauropodomorphs may indicate either that the avian lung-diverticula system had not yet evolved in these basal archosaurian taxa, or that the diverticula did not invade the postcrania, as in most penguins. Early Jurassic eusauropods exhibit various degrees of moderate vertebral pneumaticity except for a few outliers (e.g. *Omeisaurus*, *Mamenchisaurus*) which exceed the values of the other taxa by at least 15 units in some of their vertebral regions (Tables 4 and 7 in Chapter 2). Considering that many of these eusauropod genera were contemporaneous, we can safely state that vertebral pneumaticity was an integral and constant part of the genetic makeup of eusauropods and neosauropods thereafter.

The Middle Jurassic to Late Cretaceous neosauropods (i.e. Diplodocoidea, Macronaria, basal Titanosauriformes and Somphospondyli) appear to possess increasingly, though intermittently, gradual expressions of PSP (Figs. 1-6 & Table 4 in Chapter 2) until a plateau is reached in the saltasaurines. This could be interpreted as an evolutionarily maximal expression of PSP in Sauropodomorpha, where all possible combinations of osteological pneumaticity had been exhausted and an optimum (i.e. somphospondylous) vertebral condition in terms of osteological aeration design had been achieved in balance with respiration and, perhaps, biomechanical stress distribution due to mass.

3.4) Conclusions

- In general, the most pneumatised parts are the cervical and dorsal vertebrae. There is a general trend of increasing pneumaticity across evolutionary time of Sauropodomorpha which becomes relatively stable and begins to decrease in some

Late Cretaceous titanosaurian somphospondylans (as in *Saltasaurus* and *Alamosaurus*; Powell, 1992; Cerda, Salgado & Powell, 2012; Zurriaguz & Powell, 2015; Zurriaguz & Cerda, 2017). Our findings and values of PDI% are biased due to limited fossil material of some examined taxa.

- Pneumaticity is positively correlated with body length, especially after 15-20m, but not strongly to mass except in cases where taxa are equal or greater than 30 tonnes in body mass.

- From an evolutionary point, in a vertebra, pneumaticity begins from the centrum and extends to the arch and transverse processes, and in the more derived families it begins simultaneously from both the centrum and the neural spine (and, therefore, extends inwards).

- Segment length and PDI% are not always directly proportional. Highest PDI% often appears in medium sized taxa (in terms of length) as well as in the longest ones. Maybe pneumaticity varies intergenericaly rather than intragenericaly in order to best fit the individual's body proportions and it may not reflect a family trend in development. Positive correlation between PDI% and neck length is more frequently observed for necks exceeding 6-7m in length; trunks are also positively correlated with PDI% but at greater range value of lengths i.e. trunks of 5m in length may be as highly pneumatic as those of being 8m, suggesting the greater developmental need for the central body part of an animal to acquire such a weight reduction mechanism, compared to the neck and tail. A neck would need to be as light weight as possible so as to minimise its ‘cantilever-beam’ like stresses when the animal was e.g. browsing. The observed minimal expression of pneumaticity in the tail, its positive correlation between PDI% and tail length in eusauropods and diplodocoids as well as its negative correlation in macronarians and somphospondylans is justified by the fact that a longer tail, as in proportion to body length, would have acted as a counterbalance for the neck and trunk regions and thus it had to be heavy enough to do so.

- There is not any major clade of Sauropodomorpha reaches 100% pneumaticity in all vertebral column segments, although most high values come from Macronaria and Somphospondyli. In very few cases a sauropod expresses a full ‘Alpha’ pneumaticity in all available vertebral segments.

In the method proposed here, sauropods can be categorised based on their expression of pneumaticity into an index (PDI%). In addition to that, the tables provide a

clear overview of the ranges of lengths and masses that accompany the corresponding pneumaticity traits. It should be noted here that only the total mass of a taxon was estimated and compared with total PDI% or with length since masses of individual vertebral regions would be nearly impossible to retrieve.

To summarise, this study also shows that in all examined sauropodomorphs there was no straightforward association of sauropodomorph families and PDI% values. In the necks and trunks we see a clearer but not definite trend; more derived families/genera are more likely to be found in the higher PDI% regions than more basal forms. A general trend is positive correlation then a peak and then a slight decline, but within and among families, different lengths have variable levels of pneumatisation, meaning that large lengths do not necessarily have high pneumatisation levels. Maybe these osteological expressions of pneumaticity depend on animal posture, modes of feeding and weight distribution. Expression of PSP is not always correlated with size and, therefore, may not have been a paramount factor in achieving gigantic sizes, but most probably would have been an artefact of an ‘avian-lung’ system of diverticula which would lighten the skeleton as a result of the bone aeration. Therefore, both the presence of high metabolic growth rates and PSP, both resulting from the avian-like respiratory system, may have acted synergistically in the development of gigantism in sauropods.

Chapter 4 – Expression of pneumaticity in other body size cases; case studies of a dwarf and a normal juvenile sauropod

4.1) Introduction - Sauropod physiology and dwarfism

Understanding the physiology of dinosaurs is a fascinating and contentious topic, perhaps for two reasons; at first because the animals are all extinct and, so, direct observations cannot be made, and, second because they were generally much larger than any comparable living terrestrial animal, so modern analogues are hard to find. In particular, the giant sauropods have been a major focus of study, because of their vast size, tiny heads, and supposed difficulty in eating enough to fuel their bodies. A key theme within such physiological debates has been the search for any association between sauropod size and degree of postcranial skeletal pneumaticity. It is frequently assumed (e.g. Wedel, 2005; Taylor & Wedel, 2013) that high degrees of pneumaticity are associated with large body size in sauropods, i.e. pneumaticity and body size are positively correlated. The theory is widespread due to the supposition that pneumaticity acts as a means of weight reduction, enabling sauropods to attain exceptionally large size. But, as was shown in the previous chapter, this may not be the case since high degrees of pneumaticity can be found in both small and large sauropods (Tables 4 & 7 in Chapter 2 and Table S2 in Appendix 2).

In view of these arguments about giant size and pneumaticity, it is surprising that very few sauropods were apparently dwarfed, i.e. being much smaller as adults than their close relatives. Dwarfism is a result of paedomorphosis, which may be achieved through one of three processes: late developmental timing onset, early developmental timing offset, or growth deceleration (Jianu & Weishampel, 1999). It is an expression of heterochronic shift, which is the evolutionary change in the developmental timing of traits like body size and sexual maturity, from the primitive condition of the ancestors to the derived condition of the descendants (Gould, 1977; Alberch et al., 1979; McKinney, 1988; McKinney & McNamara, 1991). Convincing cases of dwarfism among dinosaurs are *Telmatosaurus*, *Zalmoxes*, and *Magyarosaurus* from the Hateg island formation in Romania (Benton et al., 2006, 2010; Csiki & Benton, 2010) and *Europasaurus* from Hannover, Germany (Sander et al., 2006). The term 'dwarf' refers to sauropods, or animals in general, which retain adult characters in a much smaller than usual body size. *Telmatosaurus* and *Zalmoxes* are ornithischians and do not show any evidence of PSP. *Magyarosaurus* is a sauropod, but at the time of the initial conception of this project its vertebral material was minimal, eroded and embedded in its original matrix. When its dorsal and caudal material became available in NHM and free from matrix, time and

resource limitations prevented the author from examining the specimens and documenting its pneumaticity. Therefore, we cannot explore pneumatisation traits in these taxa, and the only suitable dwarf dinosaurian taxon for detailed study is *Europasaurus*. Evidence that *Magyarosaurus* and *Europasaurus* are dwarf forms comes from histological analyses, linear regression, optimisation and phylogenetic analyses in their long bones (Jianu & Weishampel, 1999; Sander et al., 2006; Stein et al., 2010; Carballido & Sander, 2014). Especially for *Magyarosaurus*, high levels of cortical bone remodelling and small body size of at least an order of magnitude with respect to its South American somphospondylan relatives suggest it is an unambiguous case of dwarfism (Stein et al., 2010).

Observations on animals' size alterations in insular environments, when compared to their mainland relatives, were first made and reported by Nopcsa (1923) who noted that the reptiles living in the Haţeg Island were dwarves in comparison to their continental relatives. Later on, further observations made by Foster (1964) set the grounds for the evolutionary law that we know as 'island rule' (Van Valen, 1973). When species were introduced into an island by, for example, allopatry, and remained there over many generations, the ones that were large in size gradually became smaller and the ones that were small-bodied gradually became larger. We also know this evolutionary phenomenon as 'Foster's rule' (Palombo, 2007; Welch, 2009). This rule has been verified in many phyla such as mammals (Foster, 1964), snakes (Boback & Montgomery, 2003) and aves (Clegg and Owens, 2002). Lizards, though, do not always appear to follow this rule (Case, 1978; Lomolino, 2005; Meiri, 2007). The primary driver for such body size differentiations in animals appears to be the constraint in niche area and resources, which, in time, affects the ecological interrelationships of the inhabitant species. In particular, homeothermic animals (i.e. mammals and birds) seem to be the ones mostly affected by this insular phenomenon (Foster, 1964; Clegg and Owens, 2002; Palombo, 2007; Welch, 2009).

4.1.1) Review of ontogenetic stages in sauropods

Over the past 20 years, discoveries of sauropod specimens in various juvenile stages have led to several descriptions of their ontogenetic development (Carpenter & McIntosh, 1994; Martin, 1994; Wilhite, 2003; Bonnan, 2004; Ikejiri et al., 2005; Tidwell & Wilhite, 2005; Sander et al., 2006; Schwartz et al., 2007; Klein & Sander, 2008; Stein et al., 2010; Carballido et al., 2012; Carballido & Sander, 2014). After examining the histology of long bones and limb girdles of many indicative taxa such as *Apatosaurus*, *Diplodocus*, *Camarasaurus*, *Europasaurus* and *Magyarosaurus*, researchers have established a set of histologic ontogenetic stages (HOS), spanning from early juvenile to adult. The basic characteristics of an adult's bone tissue are cessation of growth,

decreased vascularisation, vascular canals' content replaced with lamellar bone, limited presence or absence of lines of arrested growth (LAGs), change of fibrolamellar to lamellar bone by secondary remodelling and deposition of the outer-most cortical bone (also referred to as EFS, external fundamental system, where the LAGs are very closely spaced together; Chinsamy, 1993; Varricchio, 1993; Curry, 1999; Erickson and Tumanova, 2000; Horner et al., 2000; Chinsamy-Turan, 2005; Erickson, 2005; Stein & Sander, 2008). The bone tissue of an adult that has reached its maximum size shows complete remodelling of the primary cortex by secondary osteons (Stein & Sander, 2008; Table 1, p. 249). Consistent with the life cycles of mammals, reptiles as well as theropod and ornithopod dinosaurs, and sauropods must have also reached sexual maturity long before reaching maximum adult size (Erickson et al., 2007; Lee & Werning, 2008), suggesting a correlation between ontogenetic stage and body size (Klein and Sander, 2008) and affirming that sauropod rates of development were probably comparable to those of mammals or birds.

Hone et al. (2016) redefined the criteria and terms referring to every developmental stage of dinosaurs, from 'nestling' or 'perinate' to 'adult', as an attempt to cast aside doubts around what is defined as a 'juvenile' and what is an 'adult' (Hone et al., 2016; Table 1, p. 2). Fully adult individuals are those that express the "ultimate derived morphology for a taxon, with complete development of autapomorphies and unique character combinations that define that taxon" (Hone et al., 2016; pg. 1). Misapplication of this definition, which happens out of ignorance and lack of more complete growth series of specimens for a given taxon, can result in misidentifying juvenile and adult specimens of the same species as different species, causing major phylogenetic and taxonomic errors (Hone et al., 2016). The morphological parameters examined by Hone et al. (2016) that determine the developmental classification are body size, osteological fusion, osteohistology, bone surface texture, growth curves, reproductive maturity and characteristics of the development of sociosexual dominance. Continuing from the definition of 'adult', those individuals that share features of both juveniles and adults, not possessing though definitive adult characteristics, are classified as subadults (as in e.g. being sexually mature but osteologically immature). A juvenile animal may be considered as an individual not having any of the characteristics that pertain to neither an adult nor subadult like e.g. completely lacking osteological fusion, very few or no LAGs, etc.). Lastly, an embryo or 'perinate' is any specimen confined within an egg or that has the features of an individual prior to hatching, with or without the presence of egg parts because it is sometimes uncertain if the individual has just hatched or is still an embryo (Horner et al., 2000; Hone et al., 2016).

4.1.2) Review of a dwarf-sized sauropod – a case study of *Europasaurus holgeri*

Neosauropoda are mainly characterised by achieving large body sizes, and sometimes even gigantic sizes of about 100 tonnes (Sander et al., 2011). Several of the biggest sauropod genera are found in the clades of basal Titanosauriformes and the Somphospondyli proper (Bonaparte & Coria, 1993; Novas et al., 2005; Calvo et al., 2007; Benson et al., 2014; Lacovara et al., 2014; Bates et al., 2015). Within diplodocoids, the dicraeosaurids and rebbachisaurids are characterised by relatively medium to small body sizes (Rauhut et al., 2005), while the diplodocids produced some of the longest animals that ever walked on Earth. By contrast, exceptionally small sauropods are the island dwarfs such as the macronarian *Europasaurus holgeri* from the Upper Jurassic of Hannover, central Germany (Sander et al., 2006). Another dwarf sauropod is the titanosaurian *Magyarosaurus dacus* from the Upper Cretaceous of Romania (Nopcsa, 1914; Jianu & Weishampel 1999; Le Loeuff, 2005). Insular ecosystems provide excellent isolated niches for evolutionary experiments. The most notable effect of such niches is the tendency for large continental animals to evolve into miniature forms over a few million years. Classic examples of tetrapod dwarfism are the elephants of the Mediterranean (Sicily, Malta and Corfu) and the dwarfed hippos that inhabited Sumatra, both during the Pleistocene (Boekschoten & Sondaar, 1972; Sondaar, 1976; Roth, 1992; Benton et al., 2010). *Europasaurus* is a macronarian notable for its diminutive size, with the largest individual 6.2 m in length and about 800 kg in body mass (Sander et al., 2006). Phylogenetic analyses (Sander et al., 2006) show that it is more derived than *Camarasaurus* and lies next to Brachiosauridae. Debates around *Europasaurus* phylogenetic position revolve around being either a basal macronarian (Carballido et al., 2014) or a basal brachiosaurid (D'Emic et al., 2012; Mannion et al., 2013). At least six individuals have been recorded, spanning all ontogenetic stages, but the specimen descriptions herein correspond to the largest adult individual. The area where *Europasaurus* lived at ~150 million years ago (MYA), the Lower Saxony basin, was an insular area of no more than 200,000 sq. km., an area not large enough to accommodate the niches of gigantic herbivores and carnivores (Ziegler, 1990; Sander et al., 2006). The palaeo-islands were formed by rising of sea levels, forcing phylogenetic and phyletic constraints upon the migrated ancestor of *Europasaurus* (prior to 155 MYA) onto these islands which caused the decrease in size.

4.1.3) Pneumaticity in early ontogeny – a case study of the juvenile sauropod SMA 0009 and other juvenile sauropod cases

The nearly complete postcranial skeleton of a sauropod from Wyoming (USA), with a body length of about 2 m, was determined to be an early juvenile based on the lack of fusion among vertebral elements as well as on long bone histological analyses (Schwarz et al., 2007). The cervical and dorsal vertebrae of SMA 0009 possess large laminated foraminous fossae and pleurocoels, which is unambiguous evidence of pneumatisation (more on its pneumatic traits under 'Results'; Wedel et al., 2000; Wedel, 2003; O'Connor, 2006). At first, Schwarz et al. (2007) mistakenly assigned it to Diplodocidae but later, Carballido et al. (2012) placed it within Brachiosauridae, as a basal titanosauriform. Early juvenile sauropod specimens, especially of more than one stage of development, are rarely found (Carpenter & McIntosh, 1994; Tidwell & Carpenter, 2005; Ikejiri, 2005), hindering our understanding of ontogenetic development of pneumaticity in Sauropodomorpha.

Juveniles and adults of other sauropodomorphs, namely *Massospondylus* (Yates et al., 2011) and *Mussaurus* (Otero & Pol, 2013), show no pneumaticity (except for some very shallow fossae on the dorsal vertebrae), and are thus not useful for comparative study. Juvenile *Camarasaurus* and *Apatosaurus* vertebral specimens bear simple large fossae, a prior condition followed by the formation of camerae in adult individuals, where Wedel (2003) noted it as a gradual continuum of pneumaticity throughout ontogeny, contra Jain & Chatterjee (1979) who claimed that the procamerate to camerate conditions were fundamentally different. Wedel (2003) demonstrated the pattern and mechanism of vertebral pneumatisation, from the simpler and less invading fossae to the camerate, polycamerate and camellate conditions via osteological build-up and diverticular expansion into the bone, both occurring almost simultaneously through ontogeny. The cortical bone would then continue to grow in some cases to form osteal margins and even close the openings of the camerae, while the diverticula would anastomose, completing the pneumatisation process in the adult stage (Wedel, 2003). A juvenile *Barosaurus* (DINO 2921) from Utah (USA), being 1/3 of the size of the adult, possesses fossae, pleurocoels and subdivided (septated) fossae (Melstrom et al., 2016), classifying it with confidence within the 'Beta-Gamma' range of the degree of pneumaticity, which is the same for its adult form. Its vertebral series are variably pneumatised, with gaps of pneumatisation occurring in the dorsal series suggesting, as Melstrom et al. (2016) noted, that the posterior cervical vertebrae were pneumatised first and then the dorsal ones as well as that there must have been two sources of pneumatisation, a cervical air sac and an abdominal air sac. This condition, that the cervical vertebrae might be pneumatised

first followed subsequently by dorsal vertebral pneumatisation, is also observed in SMA 0009 because, as we will examine later, its cervical vertebrae bear more invasive pneumatic elements and, thus, are more pneumatised, than its dorsal vertebrae. The ontogenetic progression of vertebral segmental pneumatisation cannot be clearly determined without live embryo observation, as was performed in the domestic chicken by Hogg (1984) and Wedel (2003, 2009) who discovered that the posterior cervical vertebrae were pneumatised first, followed immediately by the pneumatisation of the anterior dorsal vertebrae during the foetal and neonatal stages of development. The fact that a particular vertebral region may show more prominent pneumatisation, it does not necessitate that this region was the point of pneumatic origin since there could be multiple points of origin and expansion of pneumatic diverticula, but the most prevalent assumption concerning sauropods and theropods is the origin and expansion from the lungs which, in all known vertebrates, reside underneath the anterior dorsal vertebrae (O'Connor, 2009; Wedel, 2003a,b, 2009; Benson et al., 2012; Wedel & Taylor, 2013). In addition, this study seeks to demonstrate which of the sauropods examined by this project could be a probable adult form of SMA 0009, based solely on their pneumaticity profiles. The adult taxa are chosen based on their common geographical location and close phylogenetic relatedness. The purpose of this task is not to show a gradual ontogenetic transition of vertebral pneumaticity from SMA 0009 to adult taxa since this would require sufficient preserved fossil material from individuals spanning throughout all ontogenetic stages, as demonstrated by Hone et al. (2016).

4.1.4) Aims and objectives

This chapter explores pneumaticity in a dwarf sauropod to further shed light on any association between body size and degree of pneumatisation. It also aims to test this relationship in a juvenile sauropod and test if, during ontogeny (i.e. transitioning from juvenile to adult stages), pneumaticity patterns change and the PDI expression increases with age or if pneumaticity patterns form early in life and remain stable throughout ontogeny without variation. The objectives are:

i) To record pneumaticity patterns in the vertebral column of a dwarf sauropod specimen and compare it with related 'normal' sized continental sauropods.

ii) To record and compare the ontogenetic expression and transition of vertebral pneumaticity belonging to the juvenile taxon with the pneumaticity expressed in adult taxa from the subfamily in which this juvenile might belong to.

4.2) Materials and Methods

The terminology of vertebral laminae is according to Wilson's (1999) classification, but we do not use Wilson's (2011) nomenclatural system of the fossae. Instead, we use the author's categorisation of pneumaticity degree, which is a detailed method of recording the presence of pneumatic traits in the vertebral column (see Introduction and Chapter 2). Unless specified otherwise, all traits like 'foramina', 'fossae' and their derivative forms are interpreted as pneumatic.

The study is based on the specimens of *Europasaurus holgeri* (DFFMh – FV series), at different developmental stages, in the Dinosaurier Park collection in Münchehagen (Hannover). Several specimens are partially fragmented while others are nearly complete. Specifically, an axis (706.1), five cervical vertebrae (FV 652.1, FV701.1, FV 291.4, FV 291.5, FV 838.10), four cervical centra (FV 783, FV 403.2, FV 904, FV 1033), two cervical ribs (FV 896.1, FV 890.6), three dorsal centra (FV 402, FV 852.2, FV 019, FV 894), two dorsal vertebrae (FV 1084, FV 652.4), 3 sacral vertebrae (FV 862, FV 890.5, FV 569), a left ilium fragment (FV 863.1), a left pubis (FV 863.2) and four caudal vertebrae (FV 719, FV 781, FV 866, FV 495.3).

Specimens at the DinoPark were examined to establish their pneumaticity along with other pneumatic traits observed from the literature. The purpose was to determine the PDI% for *Europasaurus* and SMA 0009 by using the aforementioned method. Information for *Europasaurus* was retrieved from the specimens in Hannover and the literature (Carballido et al., 2014) and for SMA 0009 from Schwarz et al. (2007) and Carballido et al. (2012). Pneumatic traits in *Europasaurus* specimens were observed and recorded by using simple measurement tools (tape and calliper), flashlight (to light fossae and internal cavities for determining if they are blind or if they excavate deep into the bone) and a camera for photographic data retrieval from the examined specimens.

4.3) Results - Morphological description of pneumaticity

Cervical vertebrae

The cervical vertebrae of *Europasaurus holgeri* are strikingly similar in both morphology and pneumaticity to those belonging to *Giraffatitan brancai* / *Brachiosaurus altithorax* but they are about 5-10 times smaller. The overall stature and shape of a vertebra of *Europasaurus* ranges from being dorsoventrally short and anteroposteriorly long, as is the shape of the cervical vertebrae, to the more equidimensional in dorsal,

sacral and caudal vertebrae. Starting from the axis, all cervical vertebrae are opisthocoelous.

The axis **FV 706.1** (L=75 mm, H=55 mm, W=45 mm) does not possess a preserved centrum but all other parts from the neural arch upwards. It bears a fossa (15 mm wide, 8 mm deep) on the posterior peduncle of the arch and a prespinal (ligamentous) fossa.

The cervical vertebra **FV 652.1** (L=115 mm, H=55 mm, W=85 mm) is most probably the 6th vertebra of the series. It bears all known laminae and on the left side it appears to have a 60 mm wide pleurocoelous fossa on its centrum (Fig.1). The fossa is subdivided into 2 fossae by an oblique septum. The anterior-most fossa [L=30 mm, H=20 mm, and D (depth) =20 mm approx.] has a sub-oval shape and is positioned towards the condyle. The other fossa is parallelogram-shaped, measuring 35 mm in length, and it starts from the middle of the centrum and proceeds posteriorly towards the cotyle. The excavation of this fossa penetrates deeply into the centrum. The margins of the first fossa are formed by the anterior and posterior centroparapophyseal laminae. This fossa penetrates deeply into the condyle, forming two narrow excavations. The two fossae do not communicate with each other and they respectively occupy approximately 20% - 25% and 30% - 35% of the centrum's volume. Neither the condyle nor the cotyle seem to possess any foramina on their surfaces. Absence of foramina or fossae was also noted on the ventral side of the centrum. The prezygapophyses (L=40mm and W=20mm) are well formed and extend anterolaterally well beyond the condyle by 50 mm. Their distal ends have long and broad anterior surfaces. The parapophyses are short (L=10 mm), ending on a flat sub-oval surface and are measured to be 20 mm wide anteroposteriorly on their distal-most surface. They do not bear any foramina but on their distal outer surfaces seem to be shallowly excavated forming one fossa on each parapophysis, measuring about 10 mm in diameter and 4 mm in depth. Each fossa occupies about 40% of the parapophysis volume. Younger *Europasaurus* individuals do not exhibit pneumatic elements, at least on their cervical vertebrae. The transverse process is 50 mm long and 30 mm wide. The diapophysis is 20 mm long and 19 mm wide. Below the transverse process and deep into the left side of the neural arch are two deep circular fossae. The most anterior one is 20 mm in diameter and approximately 25 mm deep. The most posterior fossa is 10 mm in diameter and about 15 mm deep.

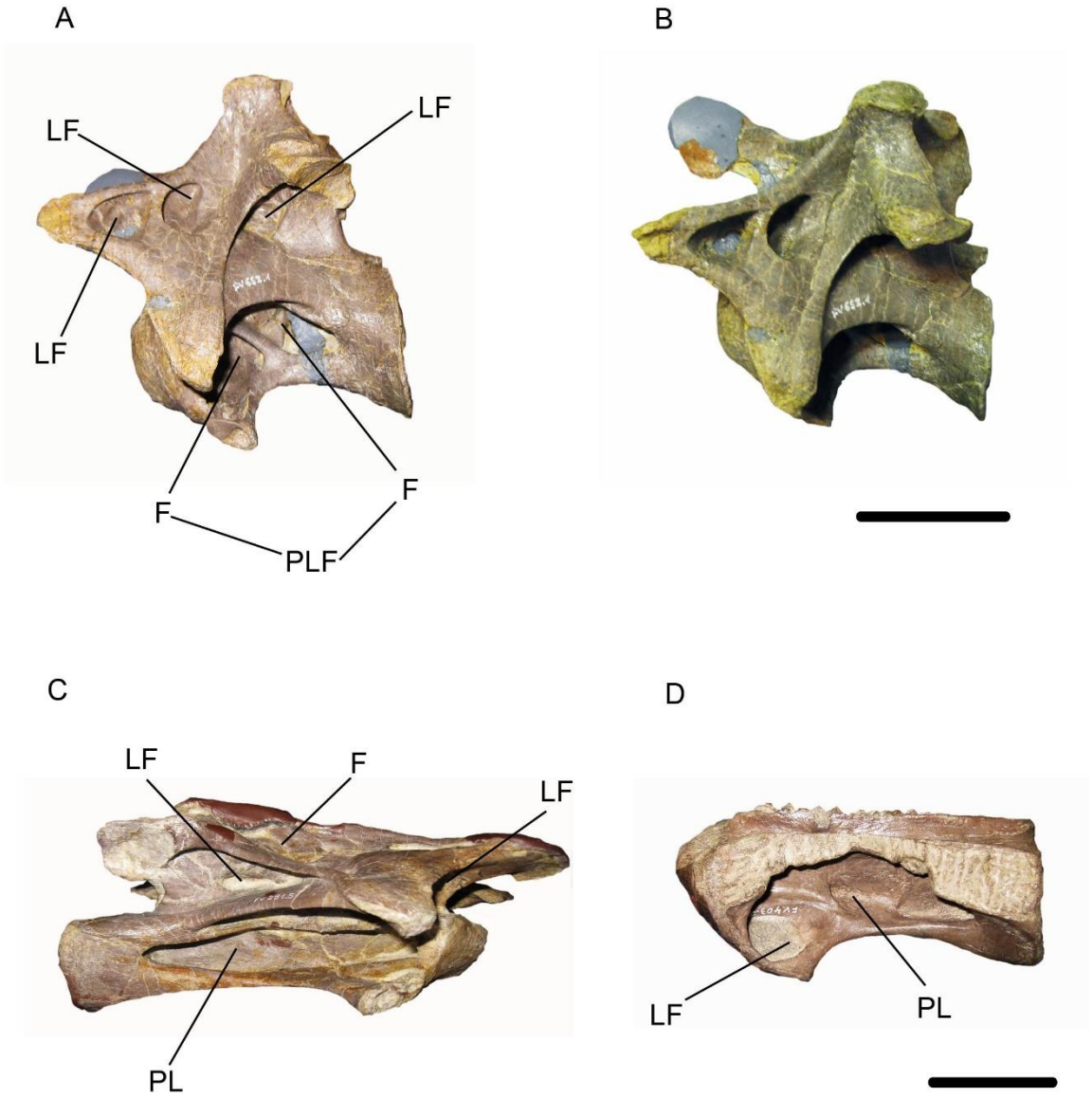

Figure 1. Pneumatic elements in the cervical vertebrae of *Europasaurus*. The 6th anterior cervical vertebra FV 652.1 (A) shown in left lateral view and tilted (B) towards its left side to better view the form and depth of its pneumatic elements. Posterior vertebra FV 291.5 (C) and vertebral centrum FV 403.2 (D) shown in right and left lateral views, respectively. Blue and brown areas indicate plaster replacement of missing parts. For abbreviations see 'Anatomical abbreviations' in Chapter 1. Scale bars measure 5 cm.

Along the left lateral surface between the prezygapophysis and the transverse process are two fossae. The anterior-most fossa is inverted sub-triangular in shape (30 mm length at its base and 25 mm length each side). The posterior-most fossa is sub-oval, measuring 25 mm in maximum width. Maximum depths of both fossae are 15 mm and 10

mm, respectively. The fossae's dorsal margin is the left spinoprezygapophyseal lamina. On the left lateral surface of the neural arch and deep below the postzygapophyseal-spinal surface is a large and deep sub-oval fossa (30 mm in diameter and 35 mm deep). The fossa's dorsal and ventral margins are the postzygodiapophyseal lamina (*podl***)** and another bony lamina-like strut, positioned dorsally to *podl*, connecting the postzygapophysis and the transverse process wing. No foramina are present in this fossa. The fossa occupies 30% of the left postzygapophysis and 50% of the neural arch. Viewing the vertebra anteriorly, the neural canal is relatively small (35 mm in diameter) and it does not bear any foramina or fossae on its inner surface. Its length is 70 mm. The two anterior peduncles are 15 mm deep and 15 mm wide each, sub-oval and each occupy 25% of the anterior surface of the neural arch. On the neural spine there exists a prespinal narrow fossa walled by the two anterior *sprl*. The fossa is 40 mm wide and 10 mm deep. On the distal-most surface of this fossa, the fossa is turned into a bony ridge forming two narrow excavations about 20 mm long and 30 mm deep each.

Viewing the vertebra posteriorly, the area between the spine, both postzygapophyses and neural arch, is very broad and deep, resembling a very large fossa (95 mm long, 50 mm wide and 50 mm deep). It occupies approximately 80% of the vertebra's posterior area. On the right side of the vertebra the prezygapophysis, transverse process and diapophysis are broken and are held together with plaster. Viewed from this side, the centrum bears a large pleurocoel (60 mm approximately from anterior to posterior) which contains three fossae. The anterior-most penetrates deep into the condyle, occupying about 25% of its volume. The middle fossa is shallower than the first one and the posterior-most fossa penetrates the condyle. No foramina seem to be present on any of the fossae. The middle fossa is covered with plaster. The posterior fossa is subtriangular in shape and seems to occupy 15% of the centrum volume; it does not penetrate the cotyle. All three pleurocoelous fossae of the right side occupy about 70% of the centrum total volume. Furthermore, there seems to be one subtriangular fossa on the dorsal area between the right postzygapophysis and the right transverse process. A similar fossa also exists between the right parapophysis and the right transverse process. The postzygapophyses are short (45 mm long) and broad (40 mm wide) on their ventral side, extending dorsolaterally.

The neural arch has one fossa (25 mm long, 10 mm high, 10 mm deep) which occupies about 10%-15% of the arch's volume. On the ventral side of the right transverse process there is one fossa bearing several minor excavations. The fossa is 25 mm long and 25 mm deep. No foramina seem to penetrate the bone. The fossa occupies about 30% of the process. Finally, one large, sub-conical, laminated fossa occupies 20% of the

right postzygapophysis, 60% of the neural arch and it penetrates deeply into the neural spine's base. The fossa bears no foramina and it measures 40 mm long and 20 mm deep.

Vertebra **FV 701.1** (probably the 9th) is ventrally compressed, and the centrum, left prezygapophysis and both parapophyses are damaged by taphonomic pressures. The vertebra is distorted, thus giving very little evidence of unambiguous pneumaticity traits. Nevertheless, there is a blind foramen on the anterodorsal surface of the transverse process and a foramen (3 mm wide) on the posterior side of the process. The foramen is circular and lies along the *podl*. There is an additional narrow foramen (8 mm long) on the ventral side of the left prezygapophysis and a smaller circular one (5 mm wide) on its dorsal surface, almost right above the ventral one. Both sides of the centrum bear one deep pleurocoel each. The right pleurocoel also bears a fossa on its bottom. The left pleurocoel measures 40 mm in length whereas the right one is larger (60 mm in length). The top of the neural spine and right transverse process and diapophysis are covered with plaster due to repair against further fragmentation of the fossil. In addition, both left and right posterior peduncles in the neural arch have each a deep excavation, each walled by a *cpol*. Similarly, the left and right anterior peduncles are shallower and bear each one foramen walled by the anterior *cdpl***.**

Furthermore, vertebra **FV 291.5** (Fig.1C) displays the following pneumatic features: a) a large pleurocoel occupying 90% of the centrum, b) a large pneumatocoel occupying 60% - 70% of the left transverse process, c) a laminated fossa occupying 50% of the neural arch, d) a fossa occupying 50% of the neural spine's base, e) a fossa occupying 50% of the inter-prezygapophyseal area (intraprezygapophyseal), f) a prespinal (probably ligamentous) fossa, g) few shallow fossae on the right transverse process, and h) both condyle and cotyle are pneumatised (50%) by the extended central pleurocoel.

Vertebra **FV 838.10** (L=200 mm, H=120 mm, W=160 mm) is transversely broken in half, where the absence of the centrum reveals the internal formation of the semicamerate pneumatic system located exactly between the neural arch/transverse processes area and the missing centrum. There also appears to be a semicamerate system walled by the transverse processes, the neural arch and the base of the spine. In fact, there seem to be two camerae formed on each side. The camerae range in shape from subtriangular to sub-oval and their width ranges from 10 mm to 15 mm. It can be said with certainty that the semicamerate system invades the transverse process, the neural arch and the base of the spine. The middle and upper part of the spine does not appear to be invaded by the camerae. The shallow fossae on the surface of the transverse processes do not seem to communicate with the internal system of camerae.

The isolated centra **FV 403.2, FV 904** and **FV 1033** (partial centrum) reveal some noteworthy features. **FV 403.2** (150 mm long) possesses some ambiguous foramina,

probably vascular/neural, positioned along the inner dorsal surface (below the level of the neurocentral suture line) of the exposed centrum. These foramina are narrow, ranging from 1 mm to 10 mm in diameter. The centrum also bears a large pleurocoel (85 mm long and 15 mm deep) on its right side, occupying most of it. On the left side of the centrum there is also a pleurocoel that forms a shallow fossa with anteroventral orientation and a shallow laminated fossa on the parapophysis, ventrally walled by the prezygoparapophyseal lamina (Fig.1). **FV 904** is a fragmented centrum with exposed neurocentral fusion. Ambiguous foramina (ranging from 3 mm to 5 mm) exist on the centrum surface, circular in shape, and seem to penetrate the walls of the neural canal. **FV 1033** displays some deep and narrow foramina with sizes like those of **FV 904** and up to 10 mm. They may be vascular/neural, but they could be pneumatic and seem to invade deep in the centrum.

Lastly, cervical centrum **FV 783** shows 3 ambiguous and minuscule (1mm) circular perforations that may have served a vascular, neural, or pneumatic purpose located where the neural arch would attach. These miniscule foramina are expressed on both lateral surfaces of the centrum (1 on the left and 2 on the right). The centrum corpus appears to be dorsoventrally compressed. Furthermore, on the right side, the openings seem to communicate with the pleurocoels located ventrally. An anterior pleurocoelous fossa in the condyle occupies 40% of its volume. The sub-oval condyle measures 25 mm in length, 10 mm in height and 10 mm in depth. A posterior pleurocoel does not invade the cotyle (L=25 mm, H=5 mm, D=5 mm) which is narrow (dorsoventrally compressed) and deep (20 mm). On the left side the anterior pleurocoelous fossa that invades the condyle has a minuscule foramen (0.5 mm wide) on the ventral surface of the bone. In addition, on the ventral side of the condyle there is another 2 mm wide foramen of ambiguous purpose (neural, vascular or pneumatic).

Cervical ribs

Pneumatic traits are minimal to absent on the ribs of sauropodomorph taxa. In this specimen (**FV 896.1**; 170 mm long), though, there is a pneumatic foramen between the regions of capitulum and tuberculum. The foramen is directed anteroventrally (when visualising the rib in its natural position) and it is 3 mm wide. **FV 890.6** is 130 mm long and 20 mm wide from capitulum to tuberculum. It bears two fossae (5 mm wide each) between the capitulum and tuberculum apices which are oriented one above the other. The rib has a bony ridge formed exactly between the two fossae.

Dorsal vertebrae

Dorsal centrum **FV 402** (75 mm long, H=40 mm, W=50 mm) bears small, circular and blind foramina on its inner dorsal surface. Each of them is about 2 mm wide and they are grouped in clusters of three and five. Along the left side there is a long and narrow pleurocoel (40 mm long, 5 mm high, 5 mm deep). On the right side there is also a pleurocoel but its presence may be an artefact of fragmentation. **FV 852.2** (partial centrum – L=60 mm long, H=45 mm, W=30 mm) possesses a pleurocoelous fossa (30 mm long, 18 mm high, 10 mm deep) and the fragmentation reveals a semicamerate centrum.

Vertebra **FV 1084** (L=65 mm, H=285 mm, W=250 mm) is taller and wider than long, placing it among the anterior-most dorsals in the vertebral series. It displays complete lamination and has a deep pleurocoel on each side of the centrum, both occupying a total of 50% of the centrum. Each pleurocoel is 40 mm long, 30 mm high and 20 mm deep. In addition, this vertebra possesses four laminated spinal fossae (two anteriorly and two posteriorly) that run along the spine's height and four laminated fossae on the proximal wings of the transverse processes. As a result of the last feature, a laminated fossa (30 mm wide) is formed on the periphery of the neural arch. Furthermore, the left transverse process possesses a foraminous fossa on its ventral side and the diapophysis bears an ambiguous foramen that could well be characterised as vascular/neural (instead of pneumatic) due to its minuscule size (1 mm) and pore-like appearance. The vertebra in general has a well-developed pneumatic architecture, but it is uncertain whether most foramina are pneumatic or not. Overall, with respect to coverage in pleurocoels, fossae and laminations, the transverse processes are approximately 70% pneumatic, the thinly laminated neural spine that is also about 70% pneumatic (due to pneumatic excavations), a centrum that is 50% pneumatic, a condyle and a cotyle that are 20% pneumatic each (due to the extended pleurocoel), and a neural arch that is about 40% pneumatic. The zygapophyses are not well developed, quite small (postzygapophyses are smaller than the prezygapophyses) and do not bear any pneumatic features whatsoever. Similarly, the neural canal is apneumatic and the parapophyses are vestigial and externally they appear to be apneumatic.

Vertebra **FV 652.4** (L=105 mm, H=185 mm, W=175 mm) has all laminations present and well preserved. The spine is tall with respect to the whole vertebra (80 mm high), having a blunt and flat dorsal surface, well developed system of laminae and laminated pre- and post-spinal fossae. Four laminated fossae exist on the anterior facet of the spine's base (each one supported by each lamina that connects the spine with the other landmarks). Each transverse process bears a deep, longitudinally narrow laminated fossa on its dorsal surface. The left fossa is 45 mm long, 10 mm wide and 15 mm deep. The right fossa is 35 mm long, 10 mm wide and 10 mm deep. There are no pneumatic

foramina present in these fossae, only a few minuscule vascular/neural foramina on the dorsal surface of the processes. The anterior peduncles of the neural arch have one deep fossa each. The fossae are subtriangular, laminated and the anterior one is 20 mm long, 30 mm high and 30 mm deep while the posterior one is 15 mm long, 20 mm high and 15mm deep. There is also a subtriangular laminated fossa on the neural arch measuring 30 mm long, 20 mm high and 15 mm deep. On the anterior side of the vertebra there is a rectangular infraprezygapophyseal fossa measuring an area of 20 mm x 40 mm and its depth reaches 30mm. Fragmented diapophyses showed no evidence of internal pneumatisation. The neural canal (30 mm diameter) does not bear any pneumatic features. Both cotyle and condyle do not have any pneumatic evidence. On the dorsal surface of each transverse process there is a deep, sub-oval fossa (65 mm high, 25 mm wide, 40 mm deep). Both left and right sides of the centrum each have a large, oval and deep pleurocoel (50 mm long, 35 mm high, 20 mm deep) occupying about 45% of the total centrum area. The pleurocoels further develop anteriorly and posteriorly into shallower fossae where each occupies 20% of the condyle and 20% of the cotyle. No pneumatic foramina seem to be present within the pleurocoels or the fossae on the centrum. In addition, both zygapophyses do not bear any pneumatic features. Prezygapophyses are larger and broader than the postzygapophyses, extending anterolaterally from their bases. Postzygapophyses extend medioventrally (point inwards and slightly downwards).

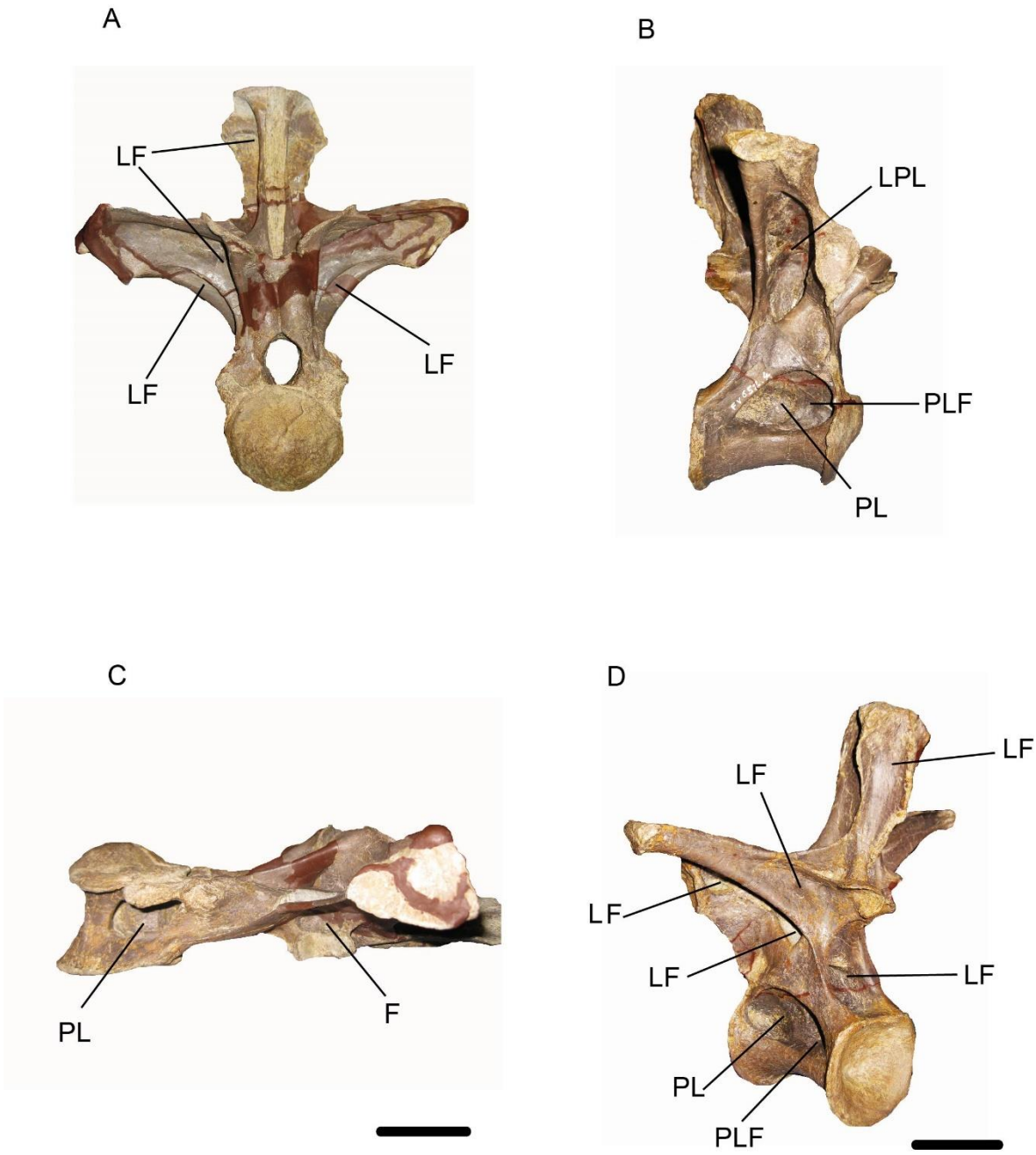

Figure 2. Pneumatic elements in the dorsal vertebrae of *Europasaurus*. Dorsal vertebra FV 1084 (A, C) shown in posterior and left lateral (sitting on its posterior side) views, respectively. Dorsal vertebra FV 652.4 (B, D) shown in right lateral and posterior-left oblique views, respectively. Brown areas indicate plaster replacement of missing parts. For abbreviations see 'Anatomical abbreviations' in Chapter 1. Left scale bar corresponds to plates A and C while the right scale bar corresponds to B and D. Both scale bars measure 5 cm.

Dorsal centrum **FV 019** is the only remnant from a typical dorsal vertebra of its series, having a shallow pleurocoel (25 mm long, 15 mm high, 5 mm deep) on either side of its centrum and on the ventral side of it there are two openings. The openings may be part of the bone's morphology or may be artefacts of fragmentation. The anterior-most opening is 1 mm wide and the posterior-most is 5 mm wide. Several formations of vascular/neural foramina exist on the lateral surface of the broad central (i.e. of the centrum) pleurocoel which none of them exceeds the 1 mm in diameter. When seen from the above, on the mid-shaft surface, there is a foramen (2 mm wide), possibly pneumatic, which appears to penetrate the centrum. On the surface of the cotyle disc (posterior surface of the centrum) there exists a prominent pneumatic foramen (3 mm wide) which is circular in shape and has thick margins. The foramen appears to pass through the cotyle and invade the centrum. Various vascular/neural foramina are present in both condyle and cotyle surfaces. The fractured transverse processes, diapophyses, postzygapophyses and neural arch of the dorsal vertebra **FV 025** revealed few sporadic internal foramina (1- 3 mm wide) on both dorsal and ventral sides of these landmarks. Dorsal centrum **FV 894** has a pleurocoel on its right side and two deep, sub-rounded fossae on its left. The anterior-most fossa is just 10 mm wide covering about 5% of the centrum surface. The posterior-most fossa was twice the size of the former (20 mm wide) and covered about 10% of the surface.

Sacral vertebrae

The upper half remains of the sacral vertebrae (**FV 862**) have fragmented parts of the neural spine, the transverse processes, the diapophyses and the anterior left and right spinodiapophyseal and prezygodiapophyseal laminae. The spine has a distinct post-spinal ligamentous fossa (Fig.3) which bears 4 foramina (probably vascular), each about 2-3 mm wide, arranged in a top-to-bottom sequence. A transverse breakage of the neural arch and the transverse process reveals putative camellate structures inside the bone. On the dorsal surface of the anterior right prezygapophyseal lamina there is a circular foramen located immediately next to it. The foramen is too small to be pneumatic, and thus it may well be vascular/neural.

FV 890.5 (L=140 mm, H=155 mm, W=80 mm) is longitudinally broken in half and its left side is covered with plaster to repair the fragmented parts (Fig.3). The centrum is amphicoelous and the neural spine is very broad (40 mm wide, 70 mm high). There is a narrow depression (30 mm long) on the dorsal (upper) surface of the neural canal (similarly seen in the caudal specimen **FV 866**). On the right dorsal surface of the transverse process is a triangular fossa with sides measuring 20 x 20 x 10 mm and 10 mm deep. Similarly, there is a subtriangular fossa with sides measuring 20 x 20 x 10 mm

and 15 mm deep. Next to the posterior spinal lamina lies a foramen (3 mm wide) that penetrates through the spine, thus invading and aerating the interior of the bone.

FV 569 is a sacral centrum with half of a neural canal (70 mm long, 60 mm wide, 60 mm high). Two foramina (each 5 mm wide and 5 mm deep), a circular and a sub-oval, lie on the bottom surface of the unroofed neural canal (Fig.3). They are separated by a thick bony ridge. Additional deep excavations (fossae) are present on the dorsal base of the transverse processes. There is also a cylindrical shaped fossa located at the bottom left (10 mm deep, 15 mm wide, and 30 mm long) which bears a 5 mm wide foramen. The fossa on the right side of the centrum bears no foramina or any other distinct features. This one is circular to sub-oval in shape and measures 20 mm deep and 20 mm wide.

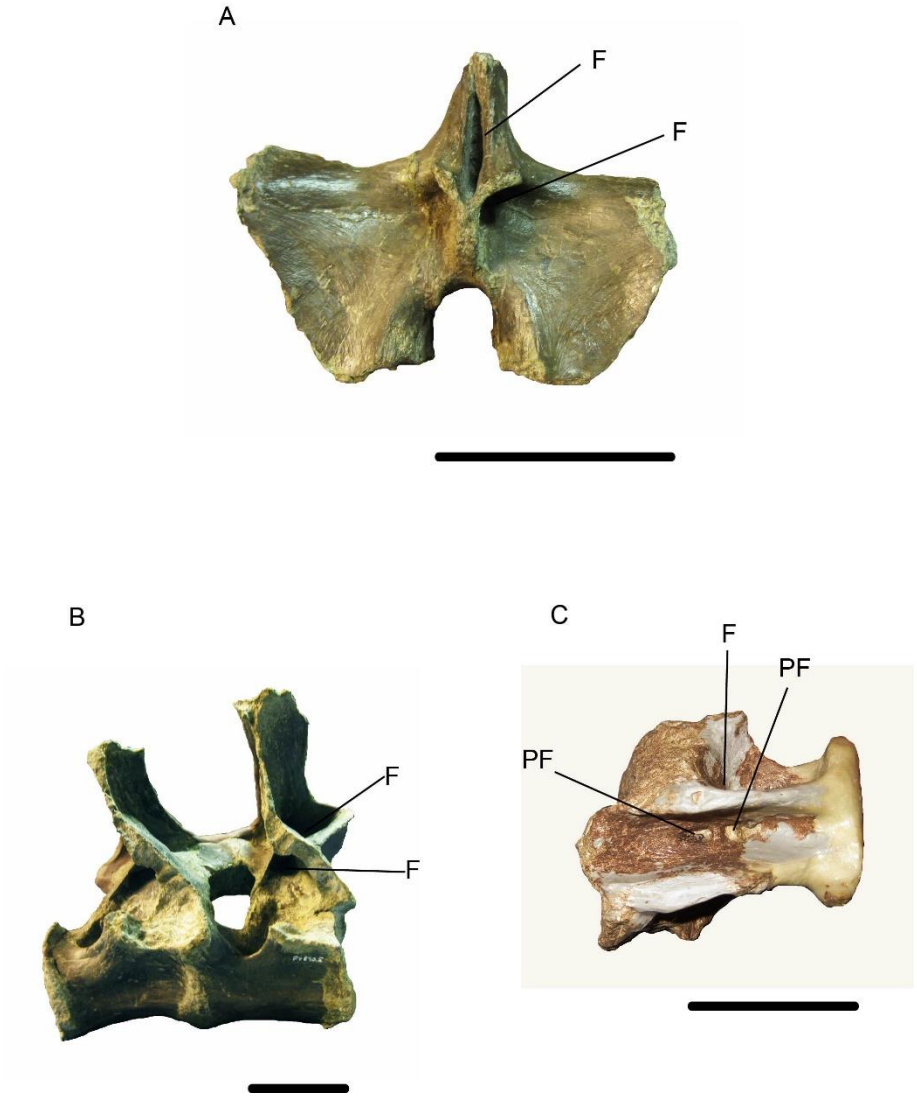

Figure 3. Pneumatic elements in the sacral vertebrae of *Europasaurus*. Transverse processes and spine elements of vertebra FV 862 (A) shown in anterior view. Dorsal

vertebrae FV 890.5 (B) shown in right lateral view, with its transverse processes missing. Sacral centrum FV 569 (C) shown in dorsal view. Brown areas indicate plaster replacement of missing parts. For abbreviations see ‘Anatomical abbreviations’ in Chapter 1. Scale bars measure 5 cm.

Caudal vertebrae

FV 719 (L=35 mm, H=45 mm, W=25 mm) consists of only a centrum with the shaft of its neural canal. No pneumatic features are present (Fig.4). **FV 781** (L=50 mm, H=55 mm, W=30 mm) is broken in parts and has been repaired with plaster. The fragmented centrum reveals no internal pneumatisation. The vertebra is lateromedially compressed.

FV 866 (L=60 mm, H=100 mm, W=70 mm) is a complete opisthocoelous caudal vertebra that, unlike other caudal specimens, possesses many features and perforations that could be identified as being either pneumatic or vascular/neural. The size of this specimen in comparison to the other caudals suggests an anterior-most position in the series, thus perhaps accommodating a posterior expansion of the presumed posterior abdominal air sac diverticula. The posterior surface of the transverse process, the cotyle's margin and dorsal surface as well as the dorsolateral surface of the centrum have all a foramen each. On the neural canal there is a narrow depression following the canal's shaft measuring 10 mm in width, 5 mm in depth and 20 mm in length. Such a feature is quite rare, if not unusual, to find in the vertebral column of sauropods, assuming that it may be an artefact of diagenesis, post mortem compaction or some osteological illness. A final element here is the presence of a prespinal (ligamentous) fossa shaped as a horseshoe (5 mm wide).

FV 495.3 (L=40 mm, H=75 mm, W=130 mm) has a foramen on its centrum dorsal surface and another on the posterior surface of the left transverse process. It also bears multiple foramina, presumably vascular/neural rather than pneumatic, on the right lateral surface of the centrum. Three foramina of about 1 mm each occupy the anterior wall of the neural arch as well as the dorsal surface of the left transverse process.

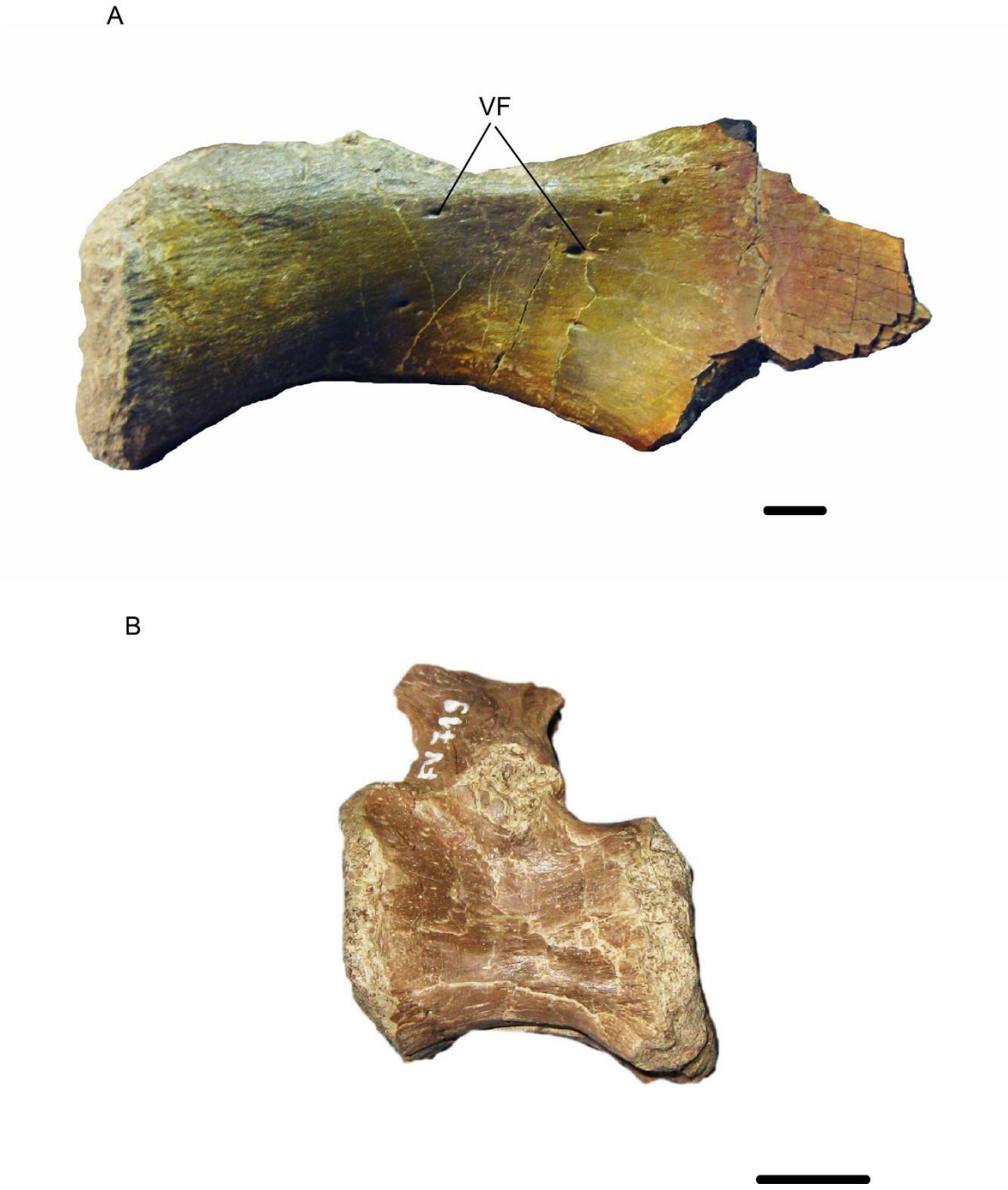

Figure 4. Pelvic element and caudal vertebra of *Europasaurus*. Left ilium FV 863.1 (A) shown in medial view. Dorsal vertebra FV 719 (B) shown in left lateral view. For abbreviations see ‘Anatomical abbreviations’ in Chapter 1. Scale bars measure 1 cm.

Pelvis

A left ilium fragment (**FV 863.1**) displays a cluster of 7-8 foramina in its lateral surface, possibly vascular rather than pneumatic; the foramina width sizes range from 1 mm to 4 mm (Fig.4). A left pubic bone (**FV 863.2**) is complete but it has no indications of pneumatisation.

4.3.1) Evidence of pneumaticity in SMA 0009 and comparison with *Europasaurus* and continental relatives

Further pneumaticity evidence was provided by Carballido & Sander (2014) that corroborated the observations made above. The PDI% of *Europasaurus* was estimated to be at moderate levels (mostly 'Gamma') with a total average of 59% (Table S7 in Chapter 2). From early juvenile to adult, pneumatisation gradually advanced from simple features such as fossae to more complex and invasive elements such as pleurocoels, with evidence of internal (semicamellate) pneumatisation.

According to Carballido et al. (2012), the early juvenile SMA 0009 shares more morphological characters with macronarian sauropods rather than diplodocids (Schwarz-Wings et al., 2007) and the same observation can be affirmed with respect to their pneumaticity characters (Tables 1-9 and Fig.5). The analysis was conducted by measuring the PDI% of each of SMA 0009's vertebral regions as well as the overall PDI%. Its axial and pelvic pneumaticity profiles are compared with those of *Europasaurus*, North American sauropods (*Brachiosaurus*, *Diplodocus*) as well as the African *Giraffatitan*. SMA 0009's cervical vertebrae are more pneumatised than its dorsals (indicating that pneumatisation begins, most likely, in the cervical series), while its sacral and caudal vertebrae have limited pneumaticity and its pelvic bones exhibit none whatsoever. More specifically, for SMA 0009 the following diagnosis was made:

Cervical vertebrae (PDI% = 53). The anterior-most cervical centra have evidence of pleurocoels, laminated fossae and foramina on its diapophyses, infradiapophyseal fossae, subdivided fossae on the centra, fossae on its centra, parapophyses, ribs, foraminous fossae on its centra, laminated infraprezygapophyseal fossae and laminated foramina on its prezygapophyses and infrapostzygapophyseal fossae.

Dorsal vertebrae (PDI% = 43). The dorsals have fossae and foramina on their centra, laminated foramina on their transverse processes, fossae on their ribs, fossae and foramina on their parapophyses, fossae on their neural arches and infradiapophyseal fossae on their diapophyses.

Sacral vertebrae (PDI% = 10). The sacrals present evidence of fossae on their neural arches, postzygapophyses and neural spine.

Caudal vertebrae (PDI% = 10). The only feature is fossae on the cotyles.

Pelvis (PDI% = 0). Pneumaticity is absent.

Examining the potential ontogenetic pathways, starting from the SMA 0009 and leading into *Brachiosaurus* or *Camarasaurus*, pneumatic traits developed from less pneumatisation towards higher and more complicated pneumatisation characters. During ontogeny, low pneumaticity characters were lost, and others evolved to laminated foramina and deep camerae while some non-existent characters in the premature vertebrae gave place to highly pneumatic characters.

Sauropods that share the same pattern of pneumatisation expansion as SMA 0009 are *Klamelisaurus*, *Giraffatitan*, and *Erketu*. By 'pattern of pneumatisation expansion' it is meant the pattern of pneumaticity observed among SMA 0009 and the aforementioned adult taxa, and not a gradual pattern since there are no intermediate juvenile forms of the adult taxa in the fossil record. The early juvenile shares more similar patterns of pneumatisation with *Camarasaurus* than the other adult sauropods, according to current data. This could also be the case with *Brachiosaurus* but its cervicals have not been retrieved and the very few remains are not suitable for examination. *Brachiosaurus* pneumatisation is prominent in its dorsal series, expanding posteriorly to its sacrocaudal series. In addition, SMA 0009 has less total average pneumatisation (49%) than the dwarf adult *Europasaurus* (59%), 41% lower with respect to *Brachiosaurus* total average PDI% (92%), 26% lower than *Camarasaurus* (75%), 20% lower than *Giraffatitan* (69%) and 14% lower than that of *Diplodocus* (63%; Table 7 in Chapter 2 and Tables 8 & 9 in this chapter). Judging from the poor pneumatisation of the juvenile specimens of *Europasaurus* and *Camarasaurus* (Wedel, 2003) it appears that SMA 0009 has more pneumatic cervical and dorsal series, only to be matched by the juvenile *Barosaurus* (Melstrom et al., 2016). Juveniles of *Europasaurus* and *Camarasaurus* taxa, in their very early ontogenetic stages, only bear shallow fossae. Their pneumatic features become increasingly complex as these animals reach maturity but SMA 0009's pneumatic state seems to be similar to the pneumatic state of the late juvenile/subadult stage of *Europasaurus* and *Camarasaurus* (Wedel, 2003; Carballido et al., 2012, 2014) These results place the early juvenile macronarian in approximately the same range of pneumaticity as *Europasaurus* (it has a lower total average PDI% compared to *Europasaurus* but both belong to 'Gamma' degree) and much lower than its adult relatives. From these results we might be able to assume that the adult of SMA 0009 would show a similar expression of pneumaticity as *Camarasaurus*, thus possibly placing this taxon within Camarasauridae. Nevertheless, a possible phylogenetic signal of the degree of pneumaticity has not been established yet, and if it does, it will probably be a shared plesiomorphic state of Sauropodomorpha with little phylogenetic meaning. That

being said, we should defer from assigning a taxon to a particular clade based solely on its pneumaticity status.

Table 1. Tabulation of SMA 0009 pneumaticity characters. Codings are as in Table 5 in Chapter 2.

		SMA 0009		
Cervicals	**Dorsals**	**Sacrals**	**Caudals**	**Pelvis**
C1c	C3c	C19na	C173cot	No characters
C113d	C102tp	C61poz		
C114d	C4c	C34ns		
C116d	C181r			
C12c	C101tp			
C120p	C121p			
C180r	C19na			
C181r	C127p			
C4c	C116d			
C5c	C1c			
C52prz				
C57prz				
C58prz				
C65poz				

Table 2. Tabulation of SMA 0009 pneumaticity character ranking. Ranking numbers correspond to characters presented in Table 1. For coding, go to Table 5 in Chapter 2.

SMA 0009					
PDI Ranking					
Cervicals	**Dorsals**	**Sacrals**	**Caudals**	**Pelvis**	**Total average**
2	2	5	5	0	3.57
4	5	5			Gamma
2	5	5			49%
4	4				
3	2				
5	5				
2	4				
5	4				
5	1				
2					
4					
3					
2					
4					
1					
3.2	3.5	5	5	0	
Gamma	Gamma	Epsilon	Epsilon	Zero	
55%	49%	10%	10%		

Table 3. Pneumaticity characters and PDI% estimation for *Europasaurus*.
PDI% derivation by using the ranking method. Codings are as in Table 5 in Chapter 2.

Pneumaticity characters and PDI% estimation					
Europasaurus					
Cervicals	**Dorsals**	**Sacrals**	**Caudals**	**Pelvis**	**Total average**
C8c	C1c	C35ns	C3c	D2	3.040816327

C164con	C3c	C94tp	C91tp		Gamma
C92tp	C8c	C21na	C172cot		
C19na	C11c	C102tp	C77nc		
C120p	C43ns	C77nc			
C57prz	C10tp	C92tp			
C70poz	C28na	C19na			
C28na	C105d				
C43ns	C93tp				
C89tp	C164con				
C34ns	C173cot				
C173cot	C19na				
C2c	C52prz				
C17na	C172cot				
C90tp	C91tp				
C3c	C4c				
C1c					
C15na					
C105d					
C93tp					
C180r					
3	2	2	2	2	
5	2	1	2		
5	3	1	2		
5	1	2	5		
5	4	5			
3	4	5			
3	4	5			
4	2				
4	2				
2	5				
5	5				
5	5				
1	4				
1	2				
1	2				

2	5				
2					
1					
2					
2					
2					
3	3.25	3	2.75	2	
Gamma	Gamma	Gamma	Beta	Beta	

Table 4. Pneumaticity characters and PDI% estimation for *Brachiosaurus*.

PDI% derivation by using the ranking method. Codings are as in Table 5 in Chapter 2.

Pneumaticity characters and PDI% estimation					
Brachiosaurus					
Cervicals	**Dorsals**	**Sacrals**	**Caudals**	**Pelvis**	**Total average**
NA	C1c	C3c	C4c	0	1.5
	C2c	C33ns			Alpha
	C36ns				
	C6c				
	C11c				
	C21na				
	C45ns				
	C50prz				
	C63poz				
	C166con				
	C175cot				
	2	2	5		
	1	2			
	1				
	1				
	1				
	1				
	1				
	1				
	1				
	1				
	1				
	1.09	2	5	0	
	Alpha	Beta	Epsilon	Zero	

Table 5. Pneumaticity characters and PDI% estimation for *Giraffatitan*.

PDI% derivation by using the ranking method. Codings are as in Table 5 in Chapter 2.

Pneumaticity characters and PDI% estimation					
Giraffatitan					
Cervicals	**Dorsals**	**Sacrals**	**Caudals**	**Pelvis**	**Total Average**
C1c	C1c	0	C3c	0	2.5
C2c	C2c		C4c		Beta
C3c	C3c		C91tp		
C8c	C7c		C101tp		
C15c	C8c				
C17na	C12c				
C19na	C17na				
C28na	C18na				
C34ns	C28na				
C43ns	C31ns				
C57prz	C34ns				
C65poz	C43ns				
C70poz	C52prz				
C89tp	C91tp				
C90tp	C101tp				
C92tp	C164con				
C93tp					
C105d	2		2		
C120p	1		5		
C164con	2		2		
C173cot	1		4		
C180r	3				
C18na	3				
C47prz	1				
C52prz	2				
C48prz	4				
C114d	2				
C118p	5				

C74nc	4				
C21na	4				
C11c	2				
C106d	4				
C63poz	5				
C42ns					
C6c	2.81	0	3.25	0	
C36ns	Beta	Zero	Gamma	Zero	
C32ns					
C119p					
C169con					
C50prz					
C115d					
C103tp					
C111d					
C72poz					
C73poz					
C35ns					
C79nc					
C75nc					
C91tp					
2					
1					
2					
3					
1					
1					
5					
4					
5					
4					
3					
4					
3					
2					

1					
5					
2					
2					
5					
5					
5					
2					
2					
2					
4					
5					
2					
1					
2					
1					
1					
5					
1					
3					
1					
1					
1					
2					
1					
1					
2					
1					
1					
1					
1					
2					
1					
1					
2					

2.34					
Beta					

Table 6. Pneumaticity characters and PDI% estimation for *Camarasaurus*. PDI% derivation by using the ranking method. Codings are as in Table 5 in Chapter 2.

Pneumaticity characters and PDI% estimation					
Camarasaurus					
Cervicals	**Dorsals**	**Sacrals**	**Caudals**	**Pelvis**	**Total average**
C19na	C1c	C1c	C34ns	0	2.215686275
C92tp	C2c				Beta
C1c	C3c			0	
C8cc	C90tp			Zero	
C151h	C91tp				
C2c	C17na	2	5		
C17na	C18na				
C3c		2	5		
C162con		Beta	Epsilon		
C171cot	2				
C118p	1				
C75nc	2				
C6c	1				
C11c	2				
C21na	1				
C32ns	2				
C33ns					
C34ns	1.57				
C35ns	Alpha				
C36ns					
C42ns					
C43ns					
C47prz					
C48prz					
C50prz					

C52prz					
C57prz					
C63poz					
C64poz					
C65poz					
C70poz					
C72poz					
C73poz					
C76nc					
C79nc					
C105d					
C108d					
C113d					
C116d					
C117d					
C120p					
C121p					
C122p					
C166con					
C175cot					
C180r					
5					
5					
2					
3					
1					
1					
1					
1					
1					
1					
1					
1					
1					
2					
5					

2					
1					
3					
4					
2					
5					
1					
4					
3					
1					
3					
4					
3					
1					
1					
2					
1					
2					
1					
4					
4					
1					
5					
2					
1					
1					
1					
2					
2.26					
Beta					

Table 7. Pneumaticity characters and PDI% estimation for *Diplodocus*. PDI% derivation by using the ranking method. Codings are as in Table 5 in Chapter 2.

Pneumaticity characters and PDI% estimation					
Diplodocus					
Cervicals	**Dorsals**	**Sacrals**	**Caudals**	**Pelvis**	**Total average**
C2c	C45ns	C116d	C116d	0	2.857142857
C3c	C30na	C106d	C106d		Beta
C162con	C162con	C19na	C19na		
C171cot	C171cot	C1c	C1c		
C14c	C2c	C2c	C3c		
C114d	C116d	C28na			
C116d	C106d	C29			
C106d	C19na	C34ns			
C19na	C28na	C35ns			
	C29na	C40ns			
		C42ns			
1	1	4	4		
2	1	5	5		
1	1	5	5		
1	1	2	2		
2	1	1	2		
2	4	4			
4	5	2			
5	5	5			
5	4	2			
	2	1			
		3			
2.5	2.5	3	3.6	0	
Beta	Beta	Gamma	Gamma	Zero	

Table 8. Comparative tabulation of pneumaticity and body size metrics. Tabulation of body length, body mass and PDI% (total average) of SMA 0009, *Europasaurus*, *Diplodocus*, *Brachiosaurus*, *Giraffatitan* and *Camarasaurus*.

Taxa	Body length (m)	References	Body mass (Kg)	References	PDI% total average
SMA 0009	2	Schwarz et al. (2007) & Carballido et al. (2012)	250	Schwarz et al. (2007) & Carballido et al. (2012)	49
Diplodocus	25.7	Holland, 1910	19654.6	Seebacher, 2001	63
Brachiosaurus	23	Riggs, 1903	28264.6	Seebacher, 2001	90
Giraffatitan	24	Paul, 1988	38000	Gunga et al., 2008	69
Europasaurus	6,2	Sander et al., 2006	800	Sander et al., 2006	59
Camarasaurus	15	McIntosh et al., 1996	18413	Foster, 2005	75

Table 9. Comparative tabulation of PDI% for different vertebral regions. Analytical tabulation of PDI% for each of the sauropod taxa examined in this chapter, for each vertebral segment, pelvic region as well as total average values.

Taxa	Pneumaticity Degree Index (PDI%)					
	Cervicals (%)	Dorsals (%)	Sacrals (%)	Caudals (%)	Ilium / Ischium / Pubis (%)	Total average
SMA 0009	55	49	10	10	0	49
Diplodocus	69	69	59	47	0	63
Brachiosaurus	NA	100	79	10	0	90
Giraffatitan	73	63	0	55	0	69
Europasaurus	59	55	59	65	79	59
Camarasaurus	75	90	79	10	0	75

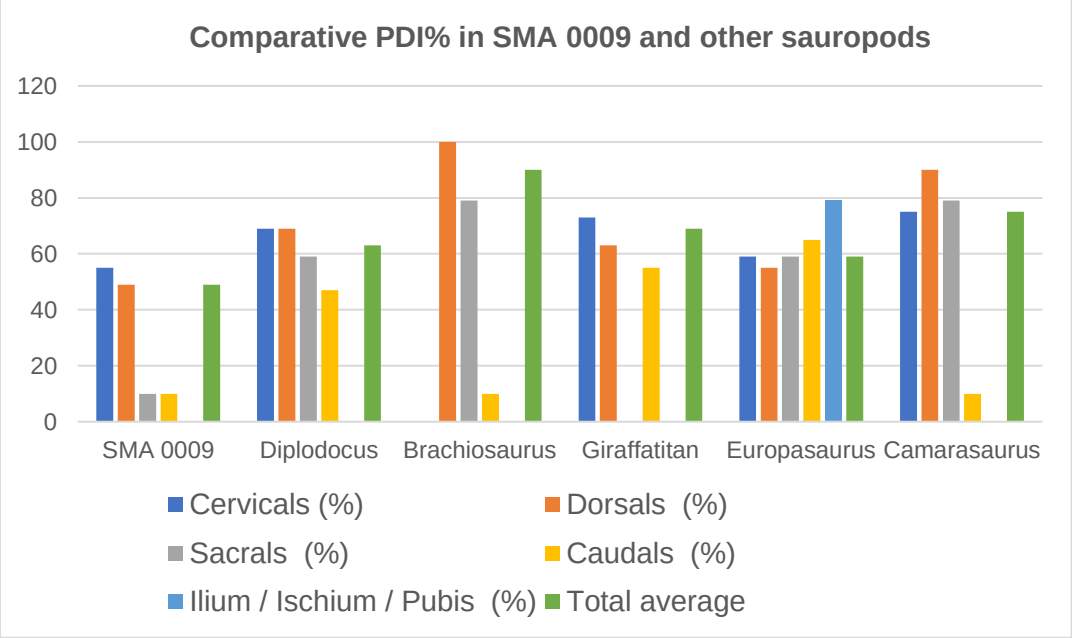

Figure 5. Comparison among the PDI% of SMA 0009, *Europasaurus* and probable adult taxa. Colour-coded comparison of PDI% of each vertebral segment and pelvis as well as the total average among SMA 0009, *Europasaurus*, *Diplodocus, Brachiosaurus, Giraffatitan and Camarasaurus*.

4.4) Discussion - Insular dwarfism due to allopatric speciation and comparison between dwarf and juvenile pneumatisation

It has been assumed that insular species may evolve to an ideal physiology, in terms of body size, if their environment has less constraints and if there is less competition in their ecological interrelationships (Brown et al., 1993; Damuth, 1993; Lomolino, 2005; Palombo, 2007). Brown et al., (1993), Damuth (1993). Meiri et al. (2004) found a large variability of optimal body sizes among insular mammals, which resulted in variable estimates in the amount of maximum energy that they can retrieve from their environment. Abiotic factors such as niche area and local conditions affect body size, even among related species (Raia & Meiri, 2006), since these parameters dictate the amount of food intake and play a key role in the evolution of large-bodied animals (Burness et al., 2001).

Work by Stein et al. (2011) on long bone histology and growth indicated that uninterrupted laminar fibrolamellar bone tissue containing growth marks was present even in the earliest sauropodomorphs like *Thecodontosaurus, Plateosaurus* and *Saturnalia*. The evolution of such bone structure is an indication of high metabolic rates and was, at least partially, responsible for the great sizes of sauropods. It is now believed that this very feature may have also played a key role in the evolution of insular dwarfism for some sauropods. Stein provided evidence that the titanosaur *Magyarosaurus dacus* from the Cretaceous of Romania was not a juvenile of the larger *M. hungaricus* but a rather a histologically mature species with a different ontogenetic trajectory. The histology of *M. dacus* is different from *Europasaurus holgeri* in that it has more intense secondary remodelling which in turn may be explained by peramorphic heterochrony of paedomorphosis combined with increased skeletal pneumatisation. The selective forces of the biological and environmental factors that drive progenetic dwarfing may also account for the absence of large predators and insufficient resources in a niche, thus reducing the optimal conditions of survival for large-bodied sauropods.

Despite the case of gigantism for most sauropods, Foster's rule applies for animals that undergo allopatric speciation when they relocate from a continental environment to an island. Raia & Meiri (2006) proposed that environmental ecological conditions with low death risks promote dwarfism in large herbivores when they are introduced in insular niches. Depending on the trophic level in which an animal may belong to, different evolutionary pathways of body size may develop. Benton et al. (2010) surmised that patterns of body size evolution might be secondarily predicted by the reach of maximum size while ecological interrelationships greatly contribute in the aforementioned patterns.

The SMA 0009 postcranial axial skeleton shows a lower pneumatisation percentage than *Europasaurus*, but both belong to the 'Gamma' degree. It can be safely stated that pneumatisation in the adult version of SMA 0009 would most probably surpass that of adult *Europasaurus*. Wedel (2003), Carballido et al. (2012), Carballido & Sander (2014) and Melstrom et al. (2016) have demonstrated that as sauropods grew throughout ontogeny their PSP, they also grew more complex from blind excavations to deep laminated fossae, foramina and internal chambers due to constant remodeling of the bone and anastomosing of the pneumatic diverticula that perforate the bone. So, within the ontogeny framework, pneumaticity increases with growth, and therefore, with size. On a macroscopic, phylogenetic scale though, this does not seem to be the case; rather it must be seen under a phylogenetic spectrum since every genus can be seen as a separate case of expression of pneumaticity. Skeletal pneumaticity may be a basic characteristic trait of most clades of Archosauria, expressed in pterosaurs, sauropods, theropods and birds, and/or it may be an epigenetic trait, reflecting the development and biomechanics of each taxon since PSP is variably expressed throughout each subclade of the aforementioned superfamilies.

It is surprising that SMA 0009 shows moderate pneumaticity in its cervicals and dorsals at such a young age, verifying that osteological pneumatisation begins at very early stages of growth, perhaps during neonatal development. During ontogeny, pneumaticity patterns change and the PDI% expression increases with age. The development of pneumatisation in early ontogeny appears to be rapid and as the animal grows towards adulthood, pneumatisation development continues at a slower rate. This follows the same mechanism of limb bone development shown by osteological studies [Curry, (1999); Curry-Rogers & Erickson (2005); Klein & Sander (2007, 2008); Klein et al. (2009)] in sauropods. According to the lag states indicated in the limb bones' cortical and fibrolamellar parts, sauropods had fast development during their first years of life up to sexual maturity before reaching maximum size, and from that point onwards, their growth and development continued at slower rates.

4.4.1) Juvenile pneumaticity progression in relation to probable adult forms

This review is an attempt to highlight the most plausible scenario of SMA 0009's adult sauropod form by utilising real morphological (pneumaticity) data from said specimen and other sauropods. The purpose is not to show a gradual ontogenetic transition of pneumaticity from early juvenile to adult sauropod individuals because this task would require more preserved material from individuals that span throughout all stages of ontogeny. Rather, this particular section of this study aims to demonstrate which sauropod may had been a probable

adult for SMA 0009. This task is undertaken only from a pneumaticity point of view and considering taxa that are both from the same geographical location from which the juvenile (i.e. USA) was discovered and that have close phylogenetically affinities (i.e. macronarians; Carballido et al. 2012). Two sauropods match both the North American palaeogeography and phylogenetic relatedness of SMA 0009, *Brachiosaurus* and *Camarasaurus*, An examination of the hypothetical ontogenetic transition of pneumaticity from SMA 0009 (Wyoming, USA) to its possible adult *Brachiosaurus* (Colorado-Utah, USA) showed that:

In dorsals we observe a transition from foramina and fossae in the centra to developing pleurocoelous and semicamerate centra; loss of fossae on ribs; loss of laminated fossa(e) on the transverse processes; loss of foraminous fossae and laminated fossae on parapophyses; fossae on neural arches develop into camellae; infradiapophyseal fossae disappear in the adult form; non-pneumatised neural spines transform into having laminated pneumatocoels on their surfaces; non-pneumatised prezygapophyses, postzygapophyses, condyle and cotyle become camellated.

In sacrals, absence of pneumaticity in the centra in the early juvenile form evolves into foramina; fossae on the neural arches and postzygapophyses, though, disappear in adulthood; fossae on neural spines disappear and give place to foramina on the spines.

In caudals, fossae restricted to the cotyles develop and occupy the entire centra.

In the pelvic region there is no pneumaticity in both SMA 0009 and *Brachiosaurus*.

Another comparative review of the hypothetical ontogenetic development between the pneumaticity expressions of SMA 0009 and *Camarasaurus* (both from Wyoming, USA) showed that:

In cervicals we see a transition from fossae, subdivided fossae, foraminous fossae and pleurocoels on centra onto pleurocoels, pleurocoelous fossae, foramina and camerae in the centra; foramina and fossae on ribs transforming onto foramina; laminated fossae, infradiapophyseal fossae and laminated foramina on diapophyses develop into infradiapophyseal fossae and infradiapophyseal camerae; fossae on parapophyses develop into fossae, foraminous fossae and camellae; laminated and non-laminated infraprezygapophyseal fossae as well as laminated foramina on prezygapophyses transform into foramina, fossae, camellae, simple and laminated infraprezygapophyseal fossae; infrapostzygapophyseal fossae evolve into laminated fossae, infrapostzygapophyseal fossae, infrapostzygapophyseal foramina, infrapostzygapophyseal camerae and camellae; absent pneumatisation in hypapophyses evolves into camerae in hypapophyses; non-pneumatised neural arches become semicamerated; non-pneumatised transverse processes develop bearing laminated fossae, foramina and camellae; non-pneumatised neural canal evolves into having foramina, camellae and camerae; non-pneumatised neural spine develops fossae,

foramina, foraminous fossae, subdivided fossae, laminated fossae and camerae; non-pneumatised condyle and cotyle become semicamellated.

In dorsals, foramina and fossae on the centra give their way into foramina, pleurocoels and camerae; laminated foramina on the transverse processes become non-laminated in the adult *Camarasaurus*; laminated fossae on the transverse processes become absent; fossae on ribs become absent; fossae and foramina on parapophyses become absent; non-pneumatised neural arches develop foramina and become semicamerate.

In sacrals, non-pneumatised centra develop pleurocoels; fossae in neural arches, postzygapophyses and neural spines become absent.

In caudals, fossae on the cotyles disappear and the neural spines obtain fossae, from not having them at all in juvenile form.

In the pelvic region, there is absence of pneumatisation in both SMA 0009 and *Camarasaurus*.

From these comparisons we can deduce that the PDI% of the adult form of SMA 0009 would range between 'Beta' and 'Alpha' degrees and we can also assume that the adult form of SMA 0009 would show similar pneumaticity to *Camarasaurus* but no more can be said until further work establishes the true adult form for SMA 0009.

4.4.2) Final thoughts on the ontogenetic development of pneumaticity and its expression in paedomorphosis

It can be surmised that vertebral pneumatisation advances early in ontogeny, commencing from the cervical region, followed by pneumatisation of the dorsal, sacral and caudal elements (Wedel, 2003; O'Connor, 2006; Melstrom et al., 2016). In most cases, the course of pneumatisation is uninterrupted throughout the column due to the anastomosing diverticula that must have 'met' one another, extending from the cervical and abdominal air sacs towards the 'centre' of the column. Another pathway could be that pneumatisation commences first and extends anteriorly in the cervical region by the cervical air sacs and then, assuming the existence of pulmonary diverticula and anterior thoracic air sacs, the diverticula extend posteriorly to occupy the dorsal regions, followed by the posterior abdominal air sacs which penetrate the sacral and caudal elements. Such patterns have been observed in the chicken by Hogg (1984) and Wedel (2003, 2009). There are cases, though, where sacral pneumatisation is less prominent, if expressed at all, than the caudal pneumatisation and this phenomenon might have occurred due to extramural pneumatisation where pneumatic diverticula do not penetrate the most proximal vertebra but instead extend along the column to attach and invade a more distant region.

This study has also provided a detailed description of pneumatisation in *Europasaurus* and has shown that the level of osteological pneumatisation correlates with size from an ontogenetic, rather than a phylogenetic, point of view. The *Europasaurus* adult specimen maintained a relatively highly pneumatised axial skeleton, comparable to its continental relatives. Its small size might suggest that its postcranial skeleton would have been less pneumatised but that is not the case. Perhaps PSP is a phylogenetically conservative trait in the sense that from eusauropods onwards it has not decreased to zero in any sauropod (as in total average PDI%) but also PSP seems to be affected by physiological changes and be a flexible physiological characteristic, in accordance to their biotic needs. It may serve other functions, or it may be that nanism following insular isolation occurred faster than the organism could adapt. Maybe size is a more malleable trait than osteological re-modification that would result in PSP.

4.5) Conclusions

This chapter aimed to clarify the extent and expression of pneumaticity in a dwarf taxon, thus elucidating whether pneumaticity correlates with size. The focus was also on how the degree of pneumaticity changes with ontogeny, from early juvenile to adult stages of development.

The macronarian early juvenile SMA 0009 was compared to adult continental relatives and especially with taxa discovered in its proximal area in USA (*Brachiosaurus* and *Camarasaurus*), and it was also compared to the African macronarian relative *Giraffatitan* as well as the dwarf basal titanosauriform *Europasaurus*. Comparative discussions on pneumaticity also included observations on juvenile *Camarasaurus*, *Barosaurus* and *Europasaurus*.

Morphological description of SMA 0009 (Carballido et al., 2012) and *Europasaurus* corroborates the presence of fossae, laminated fossae and pleurocoels in all brachiosaurids. There seems to be a relation to *Camarasaurus* and *Brachiosaurus* but without having more specimens covering many ontogenetic stages, we cannot gain a proper and broader perspective of the developmental progression of pneumaticity. SMA 0009 seems to possess pneumaticity patterns similar to those of *Camarasaurus*, verifying Carballido et al.'s (2012) observations that SMA 0009 is most likely a macronarian. Similar observations can be made for *Europasaurus* and *Brachiosaurus*/*Giraffatitan* as the former taxon bears a morphological and pneumatic resemblance with the latter two taxa, corroborating D'Emic's (2012) and Mannion et al.'s (2017) observations, who placed *Europasaurus* within Brachiosauridae.

This study found that *Europasaurus*, despite its relatively small size, possesses moderate-high degrees of pneumaticity, comparable to its large continental macronarian cousins. This discovery, along with the fact that the early juvenile SMA 0009 possesses a moderate degree of pneumaticity, allows us to conclude that pneumaticity originates early in ontogeny and increases in complexity and extent with ontogeny. The adult dwarf sauropod, being about 4m longer than the juvenile, exhibits higher degrees of pneumaticity; it could be argued here that pneumaticity positively correlates with size but there are insufficient dwarf and juvenile sauropod specimens to allow a test.

Concerning the presence of PSP in insular and juvenile sauropods, we might assume that PSP is a malleable trait, showing variable expression throughout Sauropodomorpha but never reaching zero expression from eusauropods onwards, as a total average PDI%. Also, PSP seems to be affected by physiological changes and be a flexible physiological characteristic, in accordance to their biotic needs.

Chapter 5 – Evolution of pneumaticity through phylogeny and time

5.1) Introduction – Phylogenetic interrelationships and evolutionary progression of Sauropodomorph pneumaticity under the scope of accepted phylogenies

Sauropodomorph interrelationships have long been debated. First attempts were made by the famous pioneers of the late 19th and early 20th centuries such as Marsh, Hatcher, Huene and Janensch who set the first steps in sauropod classification. Sauropod systematics began to be explicitly studied in the 1980's, notably by Bonaparte (1986), Powell (1986) and McIntosh (1989) and in the 1990's by e.g. McIntosh (1990), Yu (1990), Upchurch (1993; 1995), Bonaparte and Coria (1993), Russell and Zheng (1993) and Wilson and Sereno (1994). Through these studies, progress on refining and disentangling sauropod phylogeny advanced, with the inclusion of more osteological characters as well as more taxa. The advent of cladistics and continuing discoveries of new specimens have improved understanding. Specimen incompleteness, though, is true for most sauropodomorph species, adding to the "confusion reigning in the systematics and phylogeny of Jurassic sauropods,…" which "has as its origin on the ignorance of the general anatomy of the ancestral forms…" (Bonaparte, 1986, pp. 30). The general consensus is that Sauropodomorpha (Huene, 1932) is the most inclusive clade from basal sauropodomorphs to the end of Somphospondyli, excluding Theropoda. Basal Sauropodomorpha (Huene, 1920) includes all sauropodomorphs from *Saturnalia* but before *Vulcanodon* (McPhee et al., 2014). Eusauropoda (Upchurch, 1995) range from *Shunosaurus* to *Saltasaurus* (Upchurch et al., 2004) and *Vulcanodon* may be placed at the most primitive position (as a Gravisaurian) in that clade due to its very basal features (Upchurch, 1993; 1995). Placed at the base of Eusauropoda is the basal clade of Cetiosauridae (*Cetiosaurus*; Upchurch, 1995) while its derived members are the Mamenchisauridae (Romer, 1956; *Omeisaurus*, *Mamenchisaurus* and *Shunosaurus*).The clade of Sauropoda, therefore, ranges from Eusauropoda (Salgado et al., 1997) to *Saltasaurus* while Neosauropoda (Wilson and Sereno, 1998) range from *Diplodocus* to *Saltasaurus* (Wilson and Sereno, 1998). Diplodocoidea (Upchurch, 1995) consist of Diplodocidae, Dicraeosauridae and Rebbachisauridae (Whitlock, 2011) but not *Camarasaurus*. Brachiosauridae include all basal titanosauriforms, excluding *Camarasaurus* and somphospondylans (Wedel et al., 2000; D'Emic, 2012). According D'Emic (2012), Euhelopodidae contain *Euhelopus* and other titanosauriform euhelopodids such as *Phuwiangosaurus*, *Tangvayosaurus*, *Erketu* etc. which are all included in

Somphospondyli. Finally, Somphospondyli (Wilson and Sereno, 1998) is the least inclusive clade from *Andesaurus* to *Alamosaurus* (D'Emic, 2012).

5.1.1) Approach to phylogenetic comparative methods

It is now increasingly realised that comparative anatomical and functional studies cannot be sufficiently performed without the use of phylogenetic comparative methods (PCMs). These are techniques that map traits (characters) onto a phylogeny, and then estimate rates of trait evolution, timings of major shifts in trait evolutionary rates (unusually fast or slow evolution), and the nature of correlations between pairs of traits (such as pneumaticity and body size). Species comparison in terms of evolutionary relatedness, expressed in the form of phylogenetic trees, can be examined by the use of PCM's (Harvey & Pagel, 1991). With PCM's we can test for the existence of phylogenetic signal (Blomberg et al., 2003) in desired characters as well as to compare evolutionary paths of at least two characters in order to check their correlation. PCM's can utilise morphological data from the fossil record to identify rates of character variation, and, by extension, speciation or extinction. Rather than trying to derive ancestor-descendant relationships among taxa, PCM's can also resolve the phylogenetic relatedness of the taxa under study by using criteria such as parsimony, maximum likelihood, Bayesian methods, etc. Finally, PCM's can be utilised for biodiversity analyses in terms of phenotypic (e.g., physiological, morphological) similarities (synapomorphies) and distinct features (autapomorphies) of the examined taxa.

5.1.2) Aims and objectives

The aim of this study is to test if closely related sauropodomorph taxa are more similar in the degree of pneumaticity than distantly related taxa by examining the distribution of pneumaticity characters in known phylogenies. In addition, under a different set of analyses, it would be interesting to demonstrate if pneumaticity shows phylogenetic signal, i.e. if pneumaticity affects the phylogenetic interrelationships of Sauropodomorpha when incorporated into existing phylogenies. What distinguishes this study from previous ones is the use of an exhaustive set of pneumaticity characters (a set of the most defining features of Sauropodomorpha) in PCMs in an attempt to view sauropodomorph interrelationships under the scope of the distribution and evolution of vertebral pneumaticity. Therefore, the objectives are:

i) To use methods of comparative phylogenetics to inspect the evolution and distribution of discrete and continuous pneumaticity characters in existing phylogenies (via *Mesquite*).

ii) To incorporate pneumaticity discrete characters onto accepted morphological matrices of existing phylogenies in order to inspect intergeneric interrelationships of sauropods so as to test if pneumaticity has a phylogenetic signal [via *PAUP*, *RStudio* (referred to also as *R* from now on) and *TNT*]. In addition, to independently assess the fitness and phylogenetic signal in a small sample of pneumaticity characters, their scores were compared with those of cranial / dental characters, in *TNT*.

5.2) Materials and Methods

5.2.1) Rationale and preparation of phylogenetic techniques

Testing vertebral and pelvic pneumaticity variation among sauropodomorph clades requires examination of a) how the degree of pneumaticity varies across taxa in various accepted phylogenies, using the genus as the operational taxonomic unit, and b) if their interrelationships are affected i.e. if their respective cladograms change, after the incorporation of pneumaticity characters onto existing phylogenies. Analyses involve methods of comparative phylogenetics to inspect the intergeneric interrelationships of sauropods with respect to phylogenetic signal. Pneumaticity characters (discrete) were incorporated into published phylogenies of sauropodomorphs using *Mesquite* (Maddison and Maddison, 2016) as a tree creation tool. In order to have a better visual understanding and depiction of the character evolution in a given tree, I codenamed every character and assigned them to regions (cervical, dorsal, etc.). So, instead of just being 1, 2,...,755 they are also designated as C1c,..,C101tp,.., etc. meaning the 'character 1 in the centrum' or 'character 101 in the transverse process', etc. The list containing the meaning of every character exists in Table 3 (Chapter 2). Thus, in the box of the 'trace character history' of a tree in *Mesquite* we can type any number from 1 to 755, and because there are 4 distinct sets (one for every vertebral region) of the range 1-182 plus the 27 pelvic characters, we can immediately visualise which taxa in a given tree possess e.g. a fossa on the transverse process of the dorsal vertebrae; thus visualising the evolutionary path of a given character in a tree. This method complemented the analyses performed in both parsimony and likelihood reconstruction methods in *Mesquite* (Maddison & Maddison, 2016) as well as the phylogenetic analyses conducted under parsimony in *PAUP* (Swofford, 2002) and *TNT* (Goloboff, Farris & Nixon, 2003).

As aforementioned, reconstruction analyses in *Mesquite* were conducted in parsimony and likelihood, reconstructing (i.e. tracing) the history of characters and mapping them on the tree as well as retrieving their character values. Continuous, i.e. metric data for each of the 61 taxa (PDI% total average, estimated body mass, estimated body length and femur length) are also mapped onto these phylogenies to explore how the evolution of pneumaticity varies with respect to the other three types of data as well as with the expression of a particular discrete pneumaticity character, when the trees with mapped metric characters are compared with the trees with the mapped discrete characters.

Furthermore, selected pneumaticity characters were added into the morphological matrices of the selected published phylogenies and heuristic analyses in parsimony were conducted in *PAUP* (Swofford, 2002), after the existing initial pneumaticity characters of the published morphological character matrices were carefully removed to avoid redundancy in the analyses. The selected pneumaticity characters (nine for section 5.2.3 and eleven for section 5.2.4) were chosen based on their high CI and 'Frequency of state' values, thus having a good fit on the examined hybrid trees described above. These parameters were retrieved from *Mesquite*. Subsequently, the published tree was enforced as a topological constraint in the form of Newick format and a new round of analyses were run, under the same parameters, only this time keeping the trees that were compatible with the enforced constraint tree. This was done in order to determine if and how much the incorporation of the pneumaticity characters would alter the form of the known phylogenies and thus act as an indication of the strength of these characters, i.e. testing how parsimoniously the pneumaticity data fit against the constraint trees. Tree values were also obtained for each case of resulted tree. In addition, a tabulated set of taxa and parameters such as time bins (Table 2 in Chapter 2), metric data (Table 1 in Chapter 1 or Table 7 in Chapter 2) and discrete characters (Appendix 3), in association with a fixed tree of the studied 61 sauropodomorph taxa (traced to a published phylogeny), were processed under various regression and correlation analyses in *R*. Lastly, heuristic analyses under parsimony were run in the phylogenetic software *TNT* (*Tree New Technology; GUI version 1.1 for Windows;* Goloboff, Farris & Nixon, 2008) using the information, parameters and procedure (wherever applicable) as described earlier for the analyses conducted in *PAUP*. All phylogenetic analyses are described in a detailed manner in the sections below.

Such a study required a large amount of postcranial data on vertebral pneumatic characters for every available region of the vertebral column. Information was retrieved for every vertebral anatomical part (i.e. centrum, neural spine, etc.) of the 61 sauropodomorph taxa of this study. The data span through every major subfamily and are

recorded in detail from the literature and personal observations alike. It also required the accumulation of published morphological characters, from accepted phylogenies, in the forms of taxa-character matrices. Finally, it was shown (see Results) how pneumaticity degrees vary across the clades and also illustrated how the phylogenetic affinities of the sauropodomorphs are affected.

5.2.2) Selected phylogenies for conducting phylogenetic analyses in *Mesquite*, *PAUP* and *TNT*

The phylogenetic signal of the pneumaticity characters was firstly tested on the study by McPhee et al. (2014, Fig. 24), which was mainly examining the clade of basal sauropodomorphs. This study was chosen as it is the most complete and recent in this context. A total of 40 taxa clades were chosen for the *Mesquite* analyses (adding eight outgroup taxa only for the analyses in *PAUP* and *TNT* thus processing 48 taxa/groups; the eight added outgroup taxa are: Ornithischia, *Staurikosaurus, Herrerasaurus, Eoraptor, Chindesaurus, Agnosphitys,* Neotherorpoda*, Guaibasaurus*). *Camelotia* was the only taxon inserted from the strict consensus tree in Yates et al. (2009, SI Fig. S2) which in *Mesquite* was manually placed before (i.e. apically, or in a more primitive position on the tree) *Vulcanodon* in the McPhee et al. (2014) phylogeny, thus creating a somewhat hybrid phylogeny [known as McPhee et al. (2014) – Yates et al. (2009) phylogeny].

The process for each of the three tree unifications presented in this section of this study, i.e. merging of two trees into one 'supertree', was performed in *Mesquite* (Maddison & Maddison, 2016) by manually inserting clades of one phylogeny into the other, usually from the one containing the fewer amount of taxa into the one containing the most. Insertion was done while maintaining their phylogenetic relatedness of the sauropodomorphs in accordance with the published literature. The taxa from McPhee et al. (2014) used in *Mesquite* were: *Saturnalia, Chromogisaurus, Pantydraco, Thecodontosaurus, Efraasia, Plateosauravus, Ruehleia, Unaysaurus, Plateosaurus gracilis, P. ingens, P. engelhardti, Riojasaurus, Eucnemesaurus, Massospondylus , Leyesaurus, Adeopapposaurus, Coloradisaurus, Lufengosaurus, Glacialisaurus, Yunnanosaurus, Seitaad, Jingshanosaurus, Anchisaurus, Aardonyx , Melanorosaurus, Blikanasaurus, Lessemsaurus, Antetonitrus, Gonxianosaurus, Vulcanodon, Camelotia, Tazoudasaurus , Shunosaurus, Omeisaurus , Mamenchisaurus, Barapasaurus, Patagosaurus, Isanosaurus, Cetiosaurus* and Neosauropoda*.*

For reasons of simplicity, and unless stated otherwise, the species names in the *Mesquite* analyses were omitted (except from the *Plateosaurus* species), to avoid complications when exporting data from one software to another (e.g. from *Mesquite* to

PAUP). Thus, unless specified otherwise, the taxa of the published trees correspond to this project's taxa when the taxa are presented on the generic level. This study and the related character matrix will be taken as reference and will be used as the composite phylogeny representing basal Sauropodomorpha, as it is the most recent and most complete of its type. Analyses were conducted in the unmodified version of this composite tree, to be used as a reference and imposing as a constraint, and also in its version with the removed original pneumaticity characters, the added pneumaticity characters derived from this study as well as the added question marks in *Camelotia* to equalise its number of characters with the rest of the taxa.

Sander et al. (2011, Fig. 4) presented an integrated sauropod phylogeny, compiled from Wilson (2002), Upchurch et al. (2007), Yates (2007), Allain & Aquesbi (2008), and Remes et al. (2009). This composite phylogeny includes 30 sauropodomorphs plus 1 outgroup (Theropoda). The sauropodomorphs span from basal sauropodomorphs to somphospondylans; thus, it stands as a representative tree, comprising well-known and family-indicative taxa (*Saturnalia, Plateosaurus, Massospondylus, Melanorosaurus, Antetonitrus, Vulcanodon, Spinophorosaurus, Shunosaurus, Barapasaurus, Patagosaurus, Mamenchisaurus, Omeisaurus, Cetiosaurus, Jobaria, Haplocanthosaurus, Limaysaurus, Nigersaurus, Amargasaurus, Dicraeosaurus, Apatosaurus, Barosaurus, Diplodocus, Camarasaurus, Brachiosaurus, Phuwiangosaurus, Malawisaurus, Rapetosaurus, Isisaurus, Opisthocoelicaudia* and *Saltasaurus*).

The genus-level taxa, and therefore, their phylogeny, will be used as they are and without any alterations, additions or omissions. *Saturnalia*, *Melanorosaurus*, *Limaysaurus*, *Isisaurus* and *Opisthocoelicaudia* are well known and representative sauropodomorph taxa but they are not included in the pneumatic dataset, due to temporal constraints of this project, resulting in non-existent pneumatic character designation ('?'). The amount of taxa in the 'Sander et al., 2011' phylogeny that have been scrutinised under the scope of pneumaticity, established in this project, is 25/30 = 83.3%. This phylogeny was only processed in *Mesquite* as an attempt to map the presence of few pneumaticity characters (e.g. 'C1c') as well as metric data (total average PDI%, body mass, body length and femur length).

Furthermore, the phylogenetic trees of D'Emic (2012, Fig. 5) and Whitlock (2011, Fig. 7) were also merged into a composite tree using *Mesquite*. Taxa included in the composite tree from D'Emic are *Shunosaurus, Omeisaurus, Jobaria, Atlasaurus, Diplodocoidea, Camarasaurus, Tehuelchesaurus, Europasaurus, Giraffatitan, Brachiosaurus, Abydosaurus, Cedarosaurus, Venenosaurus, Ligabuesaurus, Sauroposeidon, Tastavinsaurus, Qiaowanlong, Erketu, Euhelopus, Daxiatitan, Tangvayosaurus, Phuwiangosaurus, Chubutisaurus, Andesaurus, Malawisaurus,*

Opisthocoelicaudia, 'Saltasaurini' and *Alamosaurus* and Whitlock's are *Apatosaurus, Supersaurus, Dinheirosaurus, Tornieria, Barosaurus, Diplodocus, Suuwassea, Amargasaurus, Brachytrachelopan, Dicraeosaurus, Histriasaurus, Rebbachisaurus, Cathartesaura, Limaysaurus, Zapalasaurus, Nigersaurus, Amphicoelias, Amazonsaurus, Haplocanthosaurus, Camarasaurus, Australodocus, Brachiosaurus, Jobaria, Losillasaurus* and *Omeisaurus*. Both trees were manually combined in *Mesquite* (Maddison & Maddison, 2016) in accordance with the proper phylogenetic placement of the taxa present in the trees.

Many Eusauropoda (*Shunosaurus, Omeisaurus, Jobaria, Atlasaurus* and *Losillasaurus*) and members of Macronaria, Diplodocoidea and Somphospondyli were left in their phylogenetic positions as in D'Emic's tree. The common taxa present in both phylogenies for this analysis, are: *Shunosaurus, Omeisaurus, Jobaria, Camarasaurus, Tehuelchesaurus, Europasaurus, Giraffatitan, Brachiosaurus, Sauroposeidon, Erketu, Euhelopus, Phuwiangosaurus*, *Andesaurus, Malawisaurus, Alamosaurus*, *Apatosaurus, Tornieria, Barosaurus, Diplodocus, Suuwassea, Amargasaurus, Dicraeosaurus, Cathartesaura, Nigersaurus, Amphicoelias, Amazonsaurus, Haplocanthosaurus, Saltasaurus,* and *Australodocus* (29/48 = 60.4% of taxa belonging to the 'D'Emic-Whitlock' phylogeny share the current author's findings on sauropodomorph pneumatic data).

This composite tree was made in order to have a more complete phylogeny comprising eusauropods, diplodocids and somphospondylans. Several changes were made such as substitution of the clade 'Diplodocoidea' (D'Emic, 2012) with the strict consensus tree of Diplodocoidea (Whitlock, 2011). Unnamed taxa like [e.g. 'Spanish rebbachisaurid' from Whitlock's analysis (2011)] were excluded. The clade *Camarasaurus* was left in the position in D'Emic's strict consensus tree of somphospondylans and the clade '*Saltasaurini'* was replaced with *Saltasaurus* for convenience (for the analyses in *Mesquite* but not for the analyses in *PAUP*). Common clades found in both trees agreed with each other in terms of phylogenetic position and relatedness with their sister clades.

For the analyses in *PAUP*, three taxa were used as outgroups, *Shunosaurus*, *Omeisaurus* and *Jobaria* because Whitlock (2011) uses the latter two and D'Emic (2012) all three of them as outgroup taxa in their studies. The study which used more characters in its character-taxon matrix is that of Whitlock's (2011) having 189 characters whereas D'Emic (2012) used 119. Therefore, the matrices of the taxa in D'Emic's (2012) dataset were supplemented with the appropriate amount of '?' so as to meet the numerical amount of characters found in Whitlock (2011). The character set for the outgroup taxa *Omeisaurus* and *Jobaria* were the one used in Whitlock (2011) whereas for the outgroup taxon *Shunosaurus* the character set were that of D'Emic (2012) and the missing number of character states were supplemented with '?' after the addition of the 11 pneumaticity

characters. The set of taxa used from D'Emic (2012) were all except for *Omeisaurus* and *Jobaria* because for these outgroup taxa the author of this current study used the matrices from Whitlock (2011) due to the larger number of characters. Therefore, for the *PAUP* analyses, the taxa from D'Emic (2012) were: *Shunosaurus, Atlasaurus, Tehuelchesaurus, Europasaurus, Giraffatitan, Abydosaurus, Cedarosaurus, Venenosaurus, Ligabuesaurus, Sauroposeidon, Tastavinsaurus, Qiaowanlong, Erketu, Euhelopus, Daxiatitan, Tangvayosaurus, Phuwiangosaurus, Chubutisaurus, Andesaurus, Malawisaurus, Opisthocoelicaudia, 'Saltasaurini'* and *Alamosaurus* (23 taxa). The taxa from Whitlock (2012) were: *Apatosaurus, Supersaurus, Dinheirosaurus, Tornieria, Barosaurus, Diplodocus, Suuwassea, Amargasaurus, Brachytrachelopan, Dicraeosaurus, Histriasaurus, Rebbachisaurus, Cathartesaura, Limaysaurus, Zapalasaurus, Nigersaurus, Amphicoelias, Amazonsaurus, Haplocanthosaurus, Camarasaurus, Australodocus, Brachiosaurus, Jobaria, Losillasaurus* and *Omeisaurus* (25 taxa). Thus, the resulting phylogeny in *PAUP* consists of 48 taxa. These choices of taxon-character datasets also apply for the analyses in *TNT* conducted later in this project. Analyses were conducted in both the unaltered hybrid phylogeny and the modified hybrid phylogeny, after the appropriate changes applied as explained above.

Carballido and Sander (2014, Fig. 29) produced a strict consensus tree which consists of 70 members of Sauropodomorpha, from basal sauropodomorphs to somphospondylans including the dwarf sauropod *Europasaurus holgeri*. The taxa are *Plateosaurus, Chinshakiangosaurus, Mussaurus, Antetonitrus, Lessemsaurus, Gonxianosaurus, Amygdalodon, Isanosaurus, Vulcanodon, Tazoudasaurus, Shunosaurus, Barapasaurus, Cetiosaurus, Patagosaurus, Omeisaurus, Mamenchisaurus, Turiasaurus, Losillasaurus, Jobaria, Amazonsaurus, Zapalasaurus, Histriasaurus, Comahuesaurus, Rayososaurus, Rebbachisaurus, Cathartesaura, Limaysaurus, Demandasaurus, Nigersaurus, Suuwassea, Amargasaurus, Dicraeosaurus, Brachytrachelopan, Apatosaurus, Diplodocus, Barosaurus, Haplocanthosaurus, Camarasaurus, Bellusaurus, Europasaurus, Galvesaurus, Tehuelchesaurus, Tastavinsaurus, Euhelopus, Brachiosaurus, Giraffatitan, Paluxysaurus, Venenosaurus, Cedarosaurus, Erketu, Chubutisaurus, Tendaguria, Wintonotitan, Ligabuesaurus, Phuwiangosaurus, Andesaurus, Mendozasaurus, Malarguesaurus, Argentinosaurus, Epacthosaurus, Malawisaurus, Nemegtosaurus, Rapetosaurus, Isisaurus, Tapuiasaurus, Trigonosaurus, Alamosaurus, Opisthocoelicaudia, Neuquensaurus,* and *Saltasaurus.* From the research, pneumaticity data have been found in 35 out of these 70 taxa (35/70=50%), namely *Plateosaurus*, *Antetonitrus*, *Vulcanodon*, *Tazoudasaurus*, *Shunosaurus*, *Barapasaurus*, *Cetiosaurus*, *Patagosaurus*, *Omeisaurus*, *Mamenchisaurus*, *Jobaria*, *Amazonsaurus*, *Cathartesaura*, *Nigersaurus*, *Suuwassea*, *Amargasaurus*,

Dicraeosaurus, *Apatosaurus, Diplodocus*, *Barosaurus*, *Haplocanthosaurus*, *Camarasaurus*, *Europasaurus*, *Tehuelchesaurus*, *Euhelopus*, *Brachiosaurus*, *Giraffatitan*, *Erketu*, *Tendaguria*, *Phuwiangosaurus*, *Andesaurus*, *Malawisaurus, Rapetosaurus*, *Alamosaurus*, and *Saltasaurus*. Analyses were conducted initially in the published dataset without any alterations and later on with the modifications of removing the original pneumaticity characters and incorporating the pneumaticity characters derived from this study.

5.2.3) Phylogenetic methods in *Mesquite*

The following analyses required the taxon-character matrix on pneumatic traits, summing a total of 755 (182 x 4 = 728 plus 27 characters of the pelvic region) pneumaticity characters as well as the general morphological taxon-character matrices from the cited phylogenetic analyses. For the purpose of showing a broad aspect of the expression of pneumatization through phylogeny, and for reasons of avoiding redundancy but keeping it concise, I will show in all trees, only the evolution of pneumaticity character 'C1c' (pleurocoel in centrum in cervical vertebrae). Every pneumatically modified tree case will also exhibit the expression of the other nine frequently present pneumaticity characters (as shown in the 'Sauropod Data Matrix' and 'Tree figures' in Appendix 2); specifically, C1c (pleurocoel in centrum) and C8c (pleurocoelous fossa in centrum) for the cervical and dorsal regions, C1c and C33ns (foramen on the neural spine) for the sacral region, C3c (foramen in centrum) and C4c (fossa in centrum) for the caudal region and D2 (foramen in ilium). These character traces are conducted under the parsimony criterion. These pneumaticity characters were chosen because of their frequent expression (among many other characters) in the vertebral column of the sauropodomorphs, as it can be seen in Appendix 3.

Apart from demonstrating the evolution and distribution of pneumaticity in the four phylogenies, both in terms of discrete and continuous data, the additional objective here is to check which of the characters are phylogenetically informative, i.e. if they have signal. This is done in *Mesquite* (Maddison & Maddison, 2016) by ranking and assessing the characters by tabulating their character values, such as the CI (consistency index), RI (retention index), 'Frequency of state', etc. Specifically, the higher the values of CI and 'Frequency of state' the more informative and frequent the characters are, thus allowing their choice of use in the relevant analyses conducted by *Mesquite, PAUP* and *TNT*. Furthermore, metric values of total average PDI%, body mass, body length as well as femur length are mapped in each of the four composite phylogenies (i.e. four versions of each phylogeny) in order to obtain a) a broad understanding of the expression of PSP

throughout Sauropodomorpha and b) a comparative view between PDI% and the other metric values.

5.2.4) Phylogenetic methods in *PAUP*

For the purposes of these analyses in *PAUP* (Swofford, 2002), the taxon-character matrices and character lists of the published phylogenies were obtained and hybrid matrices were manually created in text documents for each case: McPhee et al. (2014)-Yates et al. (2009), D'Emic (2012)-Whitlock (2011) and Carballido & Sander (2014). The uninformative characters were also detected but they were not excluded in the analyses because it was revealed by *PAUP* that nearly half of the added pneumaticity characters of this study were uninformative and the goal was to observe their effect on the phylogenetic relatedness of the taxa. This option is also provided in *Mesquite* (Maddison & Maddison, 2016).

As stated before, eleven of the most frequent and informative pneumatic characters of every vertebral region and pelvis were chosen and coded for each sauropod of the morphological matrix to test how these characters affect the phylogeny, and so giving an indication of their phylogenetic signal. These characters were chosen after carefully reviewing their CI, RI, etc. values among the published phylogenies in *Mesquite* and thus selecting them for their suitability with respect to informativeness and frequency. The 11 chosen pneumaticity characters were few of the characters with the highest values in all examined phylogenies in *Mesquite*. The chosen characters were few in number in order to test if a small sample could alter the existing sauropodomorph interrelationships based on their values and not on their quantity. These were: C1c (pleurocoel in centrum) and C8c (pleurocoelous fossa in centrum) for both the cervical and dorsal regions, C1c and C33ns (foramen on the neural spine) for the sacral region, C3c (foramen in centrum) and C4c (fossa in centrum) for the caudal region and D2 (foramen in ilium), D11 (foramen in ischium) and D20 (foramen in pubis) for the pelvic region. For the sauropodomorphs not studied in this project, these 11 character positions were replaced by '?'. The pneumatic synapomorphies of the sauropod taxa were isolated and tabulated, choosing the most frequently expressed pneumatic characters in state '1' for each vertebral region and pelvic region too. For further clarification, the pneumatic synapomorphies and autapomorphies among the examined sauropodomorphs were also tabulated (Appendix 4), allowing cross-verification with related literature, thus giving a more in-depth point of view of the expression of pneumaticity across sauropodomorph lineages.

The morphological data matrices of the original unaltered trees were used to create composite ones (except from 'Sander et al., 2011' due to the unavailability of the

matrix; the authors composed their matrix from five studies but did not publish their resultant data matrix). In addition, the Newick forms of both original and modified trees (i.e. the master trees with the added pneumatically studied taxa of this project), were obtained as well as the original and pneumatic matrices from which the original morphological characters pertaining to pneumaticity had been removed. The latter action was necessary in order to avoid redundancy in the phylogenetic computations and misleading results.

Therefore, we have three types of matrices for every chosen source tree; the composite pneumatic ones containing only pneumaticity characters for the examined taxa and unknown pneumaticity designations for the character states of the remaining taxa (analysed in *Mesquite*), the original morphological matrices obtained from previous studies and the composite morphological-pneumatic matrices (analysed in *PAUP* and *TNT*) containing the original morphological plus the eleven selected aforementioned pneumatic characters that were added (with the original pneumaticity characters removed), obtained from the sauropodomorph pneumaticity data matrix of Appendix 3.

5.2.5) Phylogenetic methods in *RStudio*

The phylogenetic tree containing only the 61 sauropods (after 'Carballido & Sander, 2014) was manually constructed in *Mesquite* and was then loaded and tip-dated in *R Studio* (see Appendix 2 for the complete command code) by using the FAD and LAD dates (Table 2, Chapter 2) in the S22 Table (Appendix 2). Tip-dating, ancestral state reconstruction, phylogenetic regression and model fitting were performed in order to test for phylogenetic signal of the pneumaticity characters and calculate how strongly the variables of pneumaticity and body size metrics associate with one another. More specifically, I first uploaded the packages 'ape', 'geiger', 'paleotree', 'caper', 'strap', 'phytools' and 'data.table'. In order to tip-date the phylogeny I used the package 'palaeotree' and after assigning the taxa names into the FADs I then ran the tip-date estimate routine by using the code 'timePaleoPhy' which contains the method of 'cal3' time-scaling. To deal with zero branch lengths I used the minimum branch lengths (type='mbl') parameter with a variation time of 1 and I also treated the dates as random observations ('dateTreatment=randObs'). See Appendix 2 for the complete command code in *R* which contains both the code and the explanation of each step. For the ancestral state reconstruction, two pneumaticity characters were chosen, C1c (pleurocoel in centrum) and C8c (pleurocoelous fossae in centrum), both corresponding to the cervical series. Their values for each sauropodomorph were run for the creation of the ancestral state reconstruction (minimum branch lengths again) and the probabilities of each

character state at each node were tabulated (Tables S5 & S6 in Appendix 2). Model fitting utilised the continuous characters of total average PDI%, body mass, body length, femur length, as well as the neck, trunk and tail lengths in order to fit them into the 'brownian motion', 'stasis', 'early burst', 'directional trend' and 'ornstein-uhlenbeck' models and compute the output AICC scores into Akaike weights. The relevant output tables were generated (Tables S7-S21 in Appendix 2).

5.2.6) Phylogenetic methods in *TNT*

Parsimony analyses on the composite phylogenies of 'McPhee et al. (2014) – Yates et al. (2009)', 'D'Emic (2012) – Whitlock (2012)' as well as the phylogeny of Carballido & Sander (2014) in its original length of taxa (70) were run in the *TNT (Windows GUI version 1.1)* software for phylogenetic analyses (Goloboff, Farris & Nixon, 2003, 2008). As in section 5.2.4 concerning the analyses in *PAUP*, the first analysis was conducted in the original dataset matrices for comparative reasons as well as for retrieving the Newick format so as to impose it as a constraint in the pneumatically modified analyses. The pneumatically modified matrices were free from any original pneumaticity features and instead they contained the 11 chosen pneumaticity characters and any necessary added question marks, as explained above. Except from the 'D'Emic-Whitlock' case of pneumatically modified hybrid dataset, the aforementioned characters were positioned first in every set of characters of each pneumaticity-studied sauropodomorph in order for them to be readily chosen within the software and retrieve the required scores (Fit score, CI, RI and HI; the latter index provides us with a sense of how much noise there is in our characters) while conducting the analyses in *TNT*. CI and RI scores were also retrieved for the chosen best-scored tree. *TNT* begins its character counting from zero instead of one, thereby altering the added pneumaticity character numbering (0-10). As a consequence, when we want to retrieve the original character's name, when prompted to detect the e.g. uninformative characters by the given number, we have to subtract 11 positions from the sequence within each matrix of interest in order to locate the correct number and, therefore, character from the original morphological character list of the published phylogeny. The reason for choosing to implement the similar set of analyses in this phylogenetic software is to compare the resulted topologies of the pneumaticity-updated taxa of the aforementioned phylogenies with the original placements of the said taxa from the original published phylogenies. Comparisons were also made on the basis of steps, consistency and retention indices of the resulted trees from each analysis as well as on the consistency and retention indices of the cranial/dental and added pneumaticity characters.

Optimality criteria were set for Wagner-parsimony and for all characters to be unordered ('non-additive') and be treated as having equal weights. This is an acceptable practice for medium-sized datasets such as the ones examined here (>30<1500 taxa and less than 1000 characters per data set) and for employing Wagner-based parsimony analyses. Initially, 'Traditional search' was implemented (because of the medium size of the datasets i.e. >30 taxa and less than 1000 characters in each matrix) performing 10 RAS (Random Addition Sequences), followed by branch-swapping with TBR (Tree Bisection-Reconnection) algorithm, performing 100 replications and keeping 1 tree per replication. Branches with zero branch length were set to collapse. This process is also known as the 'heuristic' method (Goloboff, Farris & Nixon, 2008). Values on the branches indicate the amount of robustness of these clades (i.e. in how many parsimonious trees a particular clade has been recovered). The composite matrices were also resampled by standard 'Bootstrap' method with absolute frequencies and 100 replications. Branches displayed values of clade support. The higher the value, the stronger the phylogenetic signal. Resampling was performed with 'Traditional search' and groups that were found to be of maximum branch length zero (branch length) were set to collapse (rule 3). Strict and Majority rule (50%) consensus trees were also obtained, depending on the nature of the published phylogenies, including all taxa and consensing all trees as given. 'Precision' and 'Accuracy' options were left in their default states (values '3' and '4', respectively). Analyses of 'Traditional search' was then repeated, only this time under the enforcement of the Newick code of each original phylogeny as a positive constraint. The uninformative characters from each examined published matrix were also retrieved and recorded by using the 'info-;' command. Fit scores, CI's, RI's and HI's were also retrieved for 11 dental (cranial) characters from each matrix so as to compare them with those of the 11 added pneumaticity characters. This action was carried out with the purpose of independently comparing the phylogenetic informativeness and fitness of the added pneumaticity characters with those of 11 cranial/dental characters. CIs and RIs of the trees were retrieved by running the macro script 'Stats.run' and all of the scores of all characters for all trees were retrieved by running the macro script 'CharStats.run'. 'Stats.run' and CharStats.run' macro scripts were freely obtained from http://phylo.wikidot.com/tntwiki and https://sites.google.com/site/teosiste/tp/archivos, respectively.

5.3) Results

5.3.1) *McPhee et al. (2014) - Yates et al. (2009)*

Mesquite – discrete and metric characters

Out of the 40 taxa that comprised this composite phylogeny, 18 of them were pneumatically-studied by this project (45% of the total selected taxa): *Thecodontosaurus*, *Efraasia*, *Ruehleia, Plateosaurus* , *Eucnemesaurus* , *Massospondylus* , *Seitaad*, *Aardonyx*, *Antetonitrus*, *Vulcanodon, Camelotia*, *Tazoudasaurus*, *Shunosaurus*, *Omeisaurus*, *Mamenchisaurus*, *Barapasaurus*, *Patagosaurus*, and *Cetiosaurus*. In the *Mesquite* analyses the outgroup taxa need not to be included since the goal was to portray the taxonomic appearance pneumaticity characters and metric values in relevant and studied taxa within their context of phylogenetic relatedness. The species names were removed except from the three *Plateosaurus* species and the pneumaticity character matrix was incorporated in the tree. The pneumaticity character 'C1c' was traced under parsimony as shown below and several tree values such as length, CI and RI were obtained as well as values for each character such as frequency of state, proportion missing, Mk1 likelihood, etc. Character's reconstruction showed a good strength of its signal in this cladogram (TL = 136, CI = 0.70 and RI = 0.31 in Fig.1).

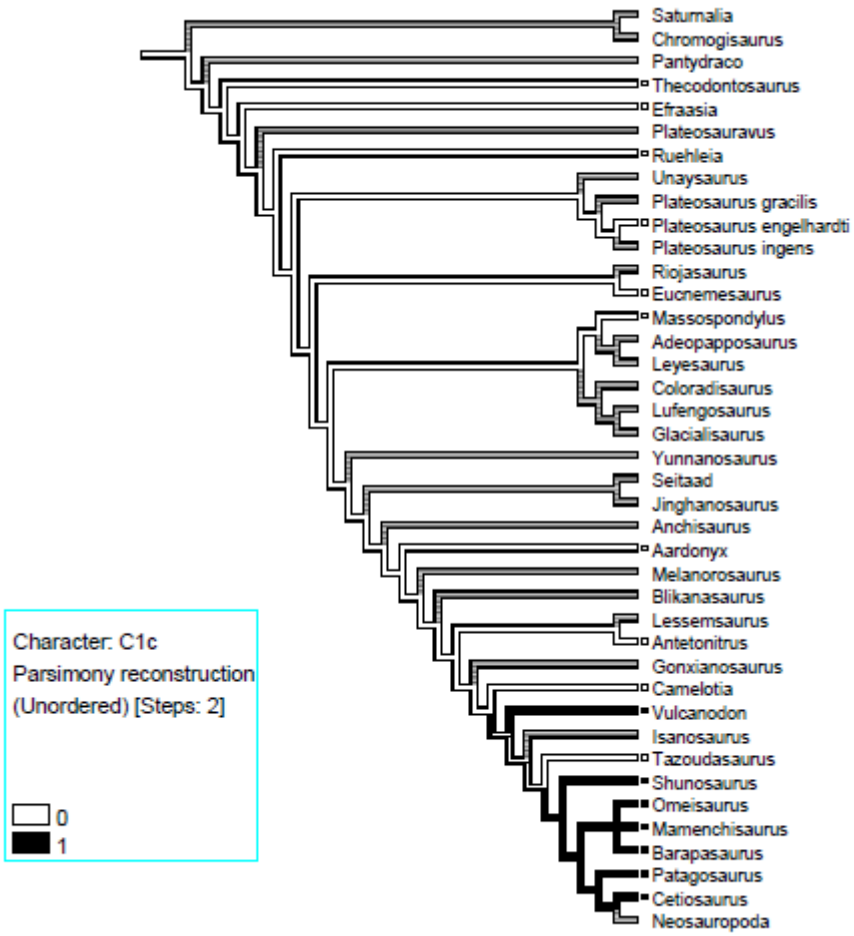

Figure 1. Parsimony reconstruction of character 'C1c' (cervical) in 40 sauropodomorph taxa from the 'McPhee-Yates' composite phylogeny. Values for

tree: TL = 136, CI = 0.70, RI = 0.31. Grey branches indicate ‘unknown’ data. *Camelotia* is inserted from the Yates et al. (2009) phylogeny.

Mesquite – continuous characters

Metric data characters of PDI% (total average), mass, length and femur length were mapped on the original ‘McPhee-Yates’ composite phylogeny of the examined taxa showing the evolution of PDI% across the 40 sauropodomorph taxa. Comparison of this trait with the other traits was made easily observable (see Figs.2-5).

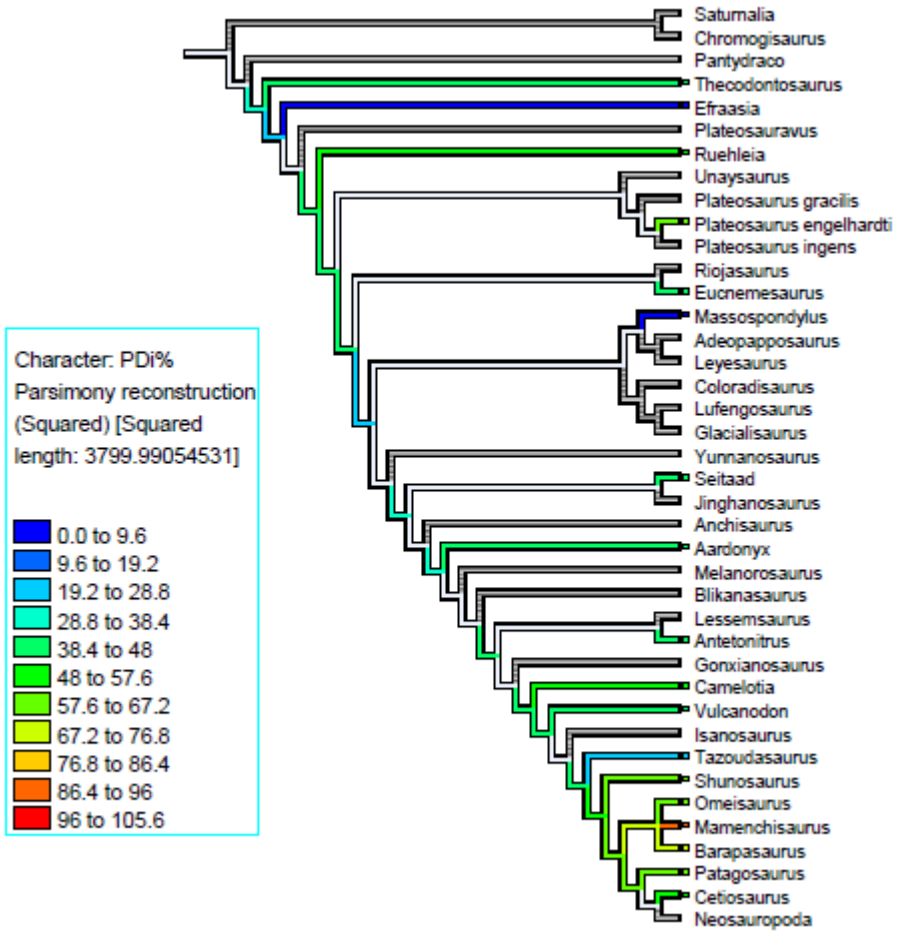

Figure 2. Distribution of total average PDI% in the 'McPhee-Yates' phylogeny. Cladogram of 40 of the studied taxa in the phylogenetic adaptation of the original 'McPhee-Yates' composite tree demonstrating the distribution of total average PDI% across the phylogeny. The evolution of PDI% is almost gradual with the noticeable sudden increase in *Mamenchisaurus.*

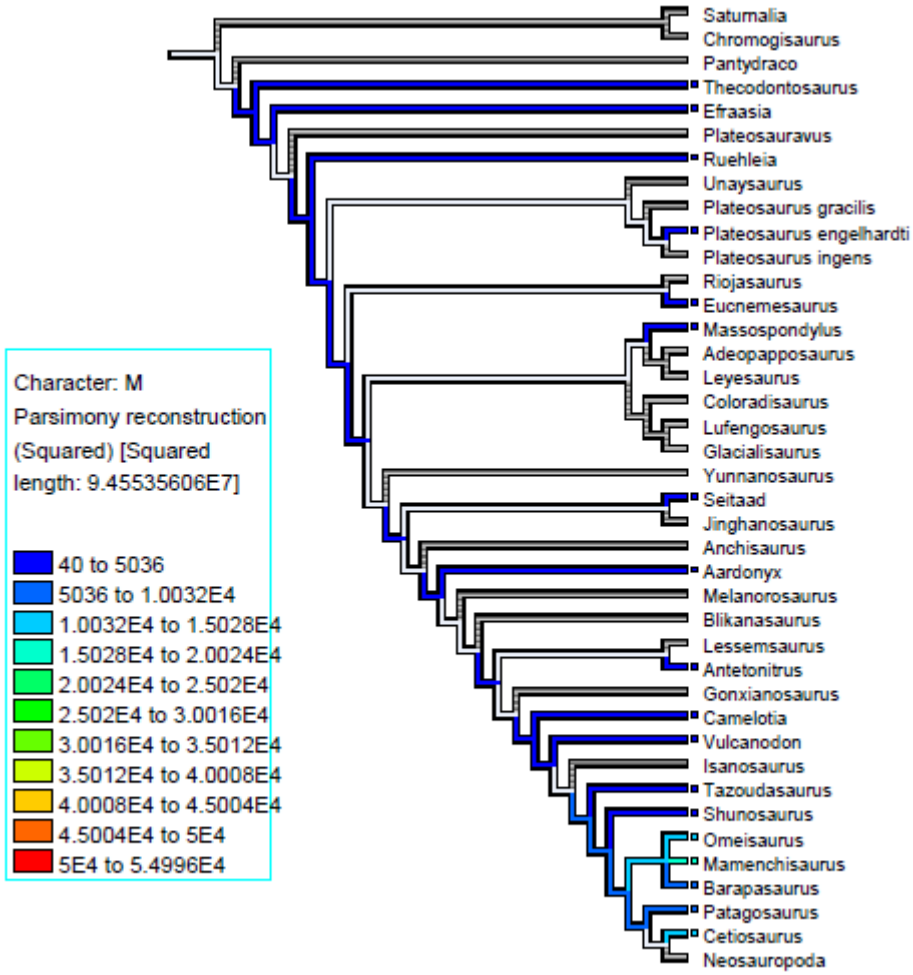

Figure 3. Body mass distribution in the 'McPhee-Yates' phylogeny. Cladogram of 40 of the studied taxa in the phylogenetic adaptation of the original 'McPhee-Yates' composite tree demonstrating the distribution of body mass (M, in kilogrammes) across the phylogeny.

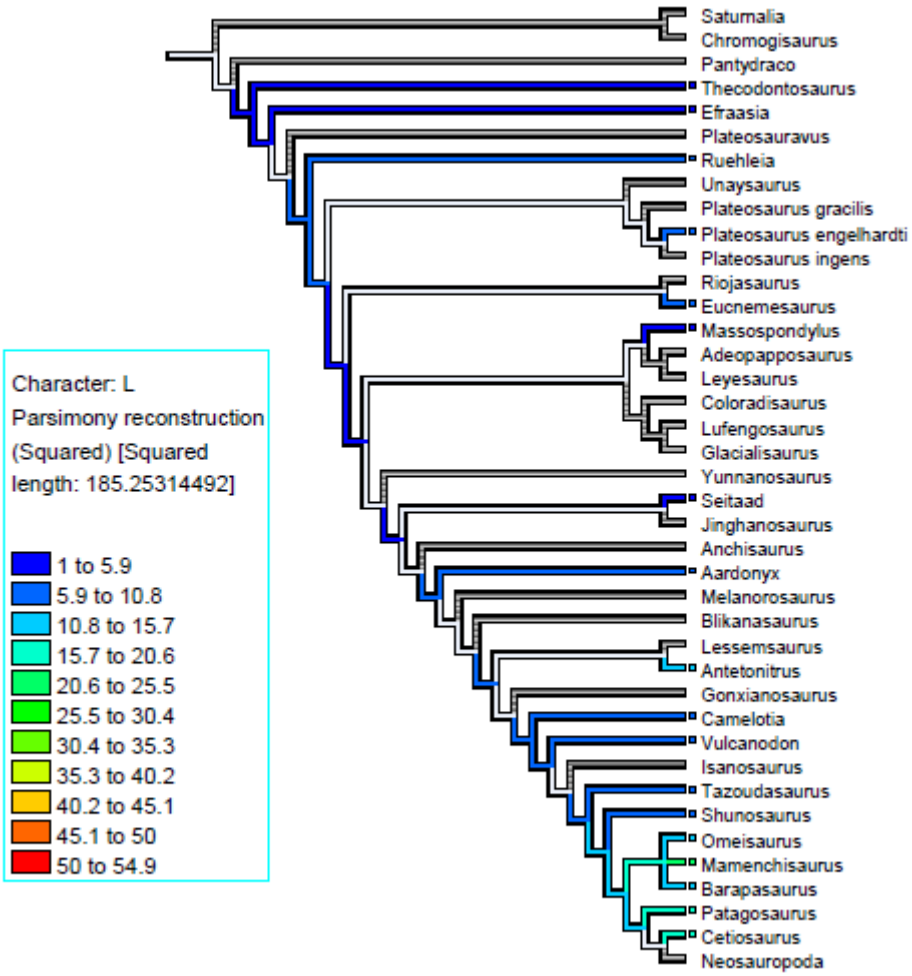

Figure 4. Body length distribution in the 'McPhee-Yates' phylogeny. Cladogram of 40 of the studied taxa in the phylogenetic adaptation of the original 'McPhee-Yates' composite tree demonstrating the distribution of body length (L, in metres) across the phylogeny.

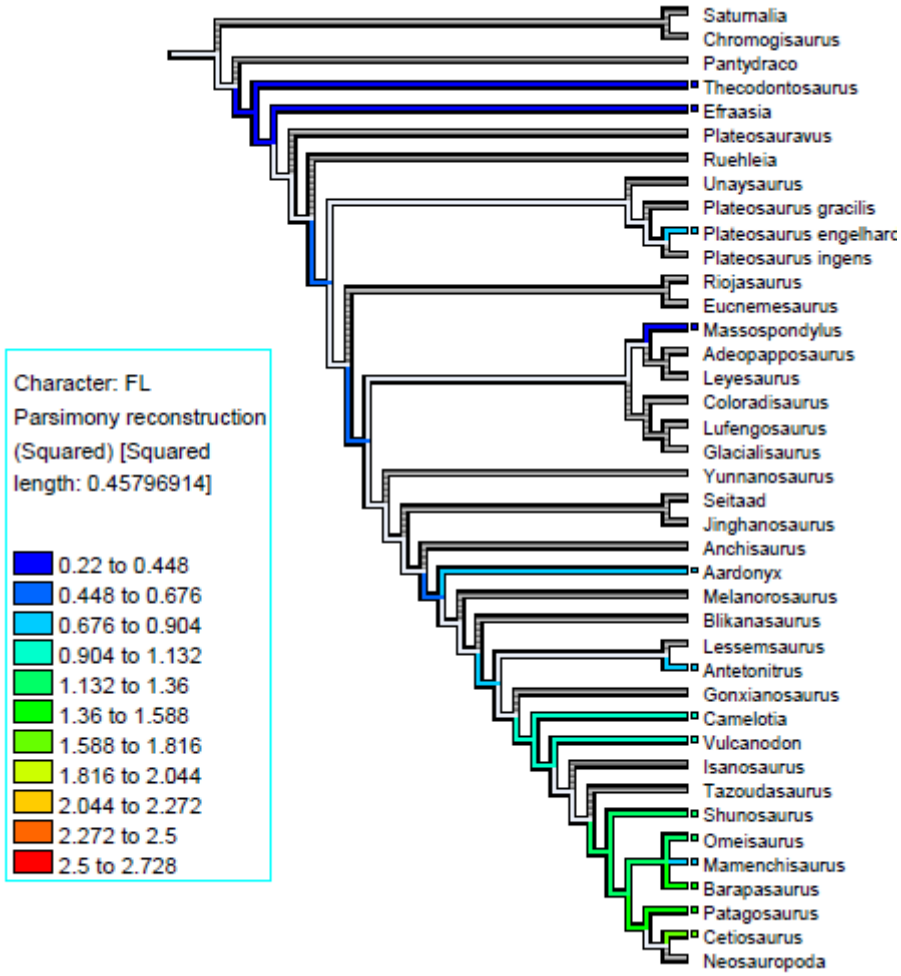

Figure 5. Femur length distribution in the 'McPhee-Yates' phylogeny. Cladogram of 40 of the studied taxa in the phylogenetic adaptation of the original 'McPhee-Yates' composite tree demonstrating the distribution of femur length (FL, in metres) across the phylogeny. Grey branches signify 'unknown' data.

The characteristic of possessing central pleurocoels in the cervical vertebrae (character 'C1c' in Fig.1) appears firstly in the Hettangian (Lower Jurassic) with the basal eusauropod *Vulcanodon* but not its sister taxa. It later re-appears in the Sinemurian and Pliensbachian with the eusauropods (*Barapasaurus* but not its sister taxon *Tazoudasaurus*) and it continues almost intermittently until the most derived somphospondylans of the Maastrichtian. In between, many close and sister clades express this trait, thus agreeing with their phylogenetic interrelationships. As in dorsal vertebrae too, it is a character mostly expressed in Neosauropoda (from the Kimmeridgian-Tithonian onwards), as are the characters 'C8c' (pleurocoelous fossae in centrum) in cervicals and dorsals alike.

‘C8c’ in the dorsals appears in fewer taxa and from the Bajocian stage, namely in *Rhoetosaurus* but not its sister taxon *Spinophorosaurus* (Aalenian-Callovian), the sister clades *Apatosaurus* and *Suuwassea* (Kimmeridgian-Tithonian), as well as in the rebbachisaurid from the Aptian and Albian stages *Amazonsaurus* (see list of ‘Tree figures’ in Appendix 2). In sacral vertebrae, ‘C1c’ appears in the Upper Jurassic and Lower Cretaceous neosauropods *Tehuelchesaurus* (Kimmeridgian-Tithonian) and *Haplocanthosaurus* (Kimmeridgian-Tithonian), and after a 5-taxon hiatus it reappears in *Diplodocus*, *Camarasaurus* and *Euhelopus* (see list of ‘Tree figures’ in Appendix 2).

The presence of foramina in the neural spine (‘C33ns’) of the sacrals is a character found in only two members of Kimmeridgian-Tithonian Flagellicaudata, *Diplodocus* and *Dicraeosaurus* (‘Tree figures’ in Appendix 2). Foramina in the centra (‘C3c’) of the caudal vertebrae is a more frequently expressed trait than the fossae in the aforementioned landmark; nevertheless, both foramina and fossae appear in various members of Eusauropoda (e.g. *Shunosaurus*) during the Middle and Upper Jurassic (Bathonian-Oxfordian), as well as in Early (Kimmeridgian-Tithonian) and Late (Hauterivian-Aptian) Diplodocoidea (e.g. *Apatosaurus* and *Nigersaurus*, respectively). In this tree, character ‘D2’ indicating the foramen on the ilium, is only present in *Plateosaurus* (Norian-Rhaetian) which is quite intriguing for such a trait to be found in a basal sauropodomorph rather than a more derived and more pneumatic sauropodomorph, where pneumatisation traits are expressed at a higher percentage in the postcranium (see ‘Tree figures’ in Appendix 2 and Fig. 2 for PDI% coverage concerning this phylogeny).

At a first glance there seems to be little or no correlation to the taxa in which these traits appear. Few common occurrences appear as in the case where *Diplodocus* possesses pleurocoels in its centrum and foramina in its spine on its sacral vertebrae. Pleurocoels and foramina appear more often in the cervical and dorsal regions and are present in most taxa from Neosauropods onwards. Morphological synapomorphies of these taxa and their representative clades can be viewed in the SI of Yates et al. (2009).

Evolution and correlation between PDI% and body mass, body length and femur length

Quantification of PDI% in total average percentage has enabled the immediate visualisation of its evolution and gradient in a phylogeny. *Plateosaurus* (*engelhardti*) is the most pneumatic and one of the largest basal sauropodomorphs (Table 7 in Chapter 2). Its femur length is greater than *Aardonyx*, only to be surpassed by the facultative quadrupedal *Antetonitrus* and few large eusauropods (e.g. *Mamenchisaurus*, *Omeisaurus*, *Patagosaurus*, etc.) where body sizes rapidly increase throughout the transition from basal sauropodomorphs to eusauropods, a phenomenon that is frequently reflected in

their increased average pneumatisation. The transition is not entirely linear and gradual, resulting in occasional sudden peaks followed by short 'downslopes', or troughs, in pneumaticity. It must be noted though that larger body size, whether it is expressed in terms of mass or length, is not always positively correlated with an increase in the degree of pneumatisation, as we see here with the case of *Antetonitrus*. Being contemporaneous but geographically distant to *Plateosaurus*, *Antetonitrus* physiology is different. *Antetonitrus* is about five times heavier, has a larger femur length and its total length is almost five meters longer than *Plateosaurus* but its total average PDI% is 16 units less (Table 7 in Chapter 2).

PAUP – discrete characters

The 'McPhee-Yates' composite phylogenetic matrix consists of 372 morphological characters and 48 taxa, 18 of which are pneumatically-studied through this project. The set of characters and related matrix that McPhee et al. (2014) and Yates et al. (2009) used and based their research was retrieved from Yates (2007). This set of characters will be used for the current analyses in *PAUP*. McPhee et al. (2014) and Yates (2007) morphological sets were comprised of 361 characters [polymorphic characters included but kept unordered as opposed to McPhee et al. (2014) who kept only these characters ordered] but after the modifications by the author i.e. adding the 11 pneumaticity characters, the character matrix ended up with 372 characters. The eleven pneumaticity characters were added in the following 18 taxa in the 'McPhee-Yates' morphological matrix: *Aardonyx (000000?????), Antetonitrus (0000???????), Barapasaurus (10100000000), Cetiosaurus (10100001000), Efraasia (0000???????), Eucnemesaurus (0000???????), Mamenchisaurus (1110???????), Massospondylus (00000000000), Omeisaurus (11110011001), Patagosaurus (1010??01???), Plateosaurus (engelhardti) (00000000000), Ruehleia (00000000000), Seitaad (??00???????), Shunosaurus (1111???????), Tazoudasaurus (0000???????), Thecodontosaurus (0000??00???), Camelotia (0000???????)* and *Vulcanodon (10??0001000)*. Within PAUP eight (122, 129, 147, 148, 152, 158, 161 and 162; see Appendix 'List of removed vertebral pneumaticity characters from the original matrices') original morphological pneumaticity characters from the Yates (2007) were manually removed in order to avoid redundancy in the results.

As we can see above, the choice of strictly 'present' characters that would always be of state '1' was avoided because the aim is to assess a fair evaluation of the same selection of pneumaticity characters ("most informative" and not "always informative").

The number of character states per taxon was modified so that every taxon (pneumatically-studied and not) will have 372 character states (prior to the deletion of the

eight original pneumaticity characters) to account for those taxa without the pneumaticity characters derived through this study by supplementing the missing ones with '?' until the desired number was reached. Then, every taxon in the pneumatically composite phylogeny had 372-8 original pneumaticity characters = 364 characters in total.

Prior to the analyses of the composite pneumatic datasets, though, a parsimony analysis of the 'McPhee-Yates' composite tree under TBR, without having any of the 11 pneumaticity characters added and without the extra '?' [except from the eight question marks added in *Camelotia* to reach the number '361' of McPhee et al. (2014) dataset] leaving its characters as originally set (361) yielded a most parsimonious 50% majority-rule consensus tree of 1170 steps with CI: 0.351 and RI: 0.653 [Fig. 6; McPhee et al's. (2014) best trees were 1206 steps and in a subsequent analysis their shortest tree was 1194 steps]. Perhaps the fewer steps resulted due to the insertion of *Camelotia* and because the polymorphic characters were kept unordered instead of ordered. Time limitations did not allow the author to manually find and alter these characters into being ordered for all relevant taxa. This simple analysis was done in order to retrieve the Newick code so as to impose it as a constraint later.

Heuristic analyses under parsimony were conducted in the composite pneumatic matrix (now containing the 11 pneumaticity characters), excluding the eight original pneumaticity characters and the 50% majority-rule consensus tree was obtained. Out of the 372 characters, *PAUP* found 26 of them to be uninformative [(3, 9, 35, 48, 51, 56, 70, 77, 79, 80, 127, 140, 182, 206, 221, 241, 271, 287, 303, 319, 366, 367, 368, 370, 371, 372); see Appendix 2 'List of uninformative characters from the composite pneumatic examined matrices'].The analyses were conducted retaining the uninformative characters (found by *PAUP*) because some of the 11 added pneumaticity characters were found to be uninformative; thus, deleting them from the start would render this set of analyses futile. Then, the original author(s)' tree was imposed (the merged tree from 'McPhee et al., 2014' and Yates et al., 2009' in the form of Newick code) as a constraint onto the composite morphological-pneumatic matrix. Then, the same round of analyses were conducted with the constraint tree imposed, obtaining the 50% majority-rule consensus trees, thus, aiming to observe whether the phylogenetic interrelationships of sauropods are being altered or not, when pneumaticity characters are added and trace any differences in the tree topologies to these characters.

For the parsimony optimality criterion in the heuristic search, all characters included are considered to have equal weight, starting trees were obtained by stepwise addition with one tree to be held at each step. TBR (Tree-Bisection Reconnection) was implemented as the branch-swapping algorithm with a limit of 8 moves. Except from setting the polymorphic characters unordered, all other parameters were kept as in McPhee et al. (2014) did in their analyses. These

parameters were chosen because the chosen phylogeny was the one with nearly all the taxa while the Yates et al. (2009) phylogeny accounts only for the taxon *Camelotia*. Analyses of the modified taxon-character matrix while keeping the uninformative characters, adding the 11 pneumaticity characters, supplementing with '?' wherever necessary to reach the 372 characters limit, excluding the eight initial pneumaticity characters (372-8=364) and without any topological constraints in effect, yielded 10 most parsimonious trees (indicatively, below is shown the best parsimonious tree in Fig.7). The best tree score was 1154, with CI = 0.354 and RI = 0.636. Same values were also yielded for the 50% Majority rule consensus tree (Fig. 8). Interesting to note is the moderate HI (Homoplasy Index) = 0.646, the very low RC (Rescaled Consistency Index) = 0.225 and the low tree length score which is less than that of McPhee et al. (2014).

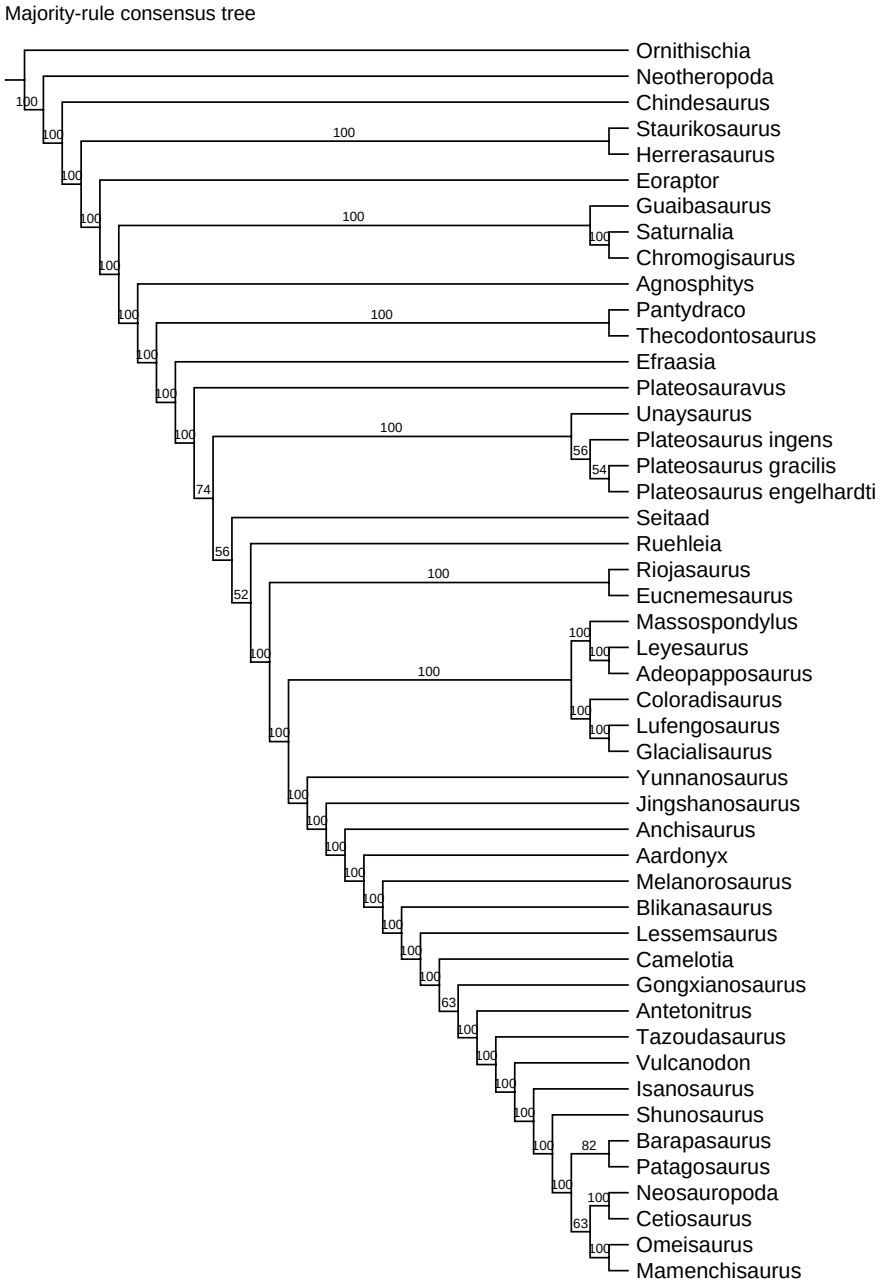

Figure 6. 'McPhee-Yates' composite 50% Majority rule consensus parsimonious tree. Tree derived from the original composite 'McPhee-Yates' phylogeny with 48 taxa and 361 original morphological characters under heuristic search in parsimony criterion and without any added pneumaticity characters or question marks (1170 steps with CI: 0.351 and RI: 0.653). Assigned outgroups: Ornithischia, *Staurikosaurus*, *Herrerasaurus*, *Eoraptor*, *Chindesaurus*, *Agnosphitys*, Neotheropoda and *Guaibasaurus*. Polymorphic characters were kept unordered.

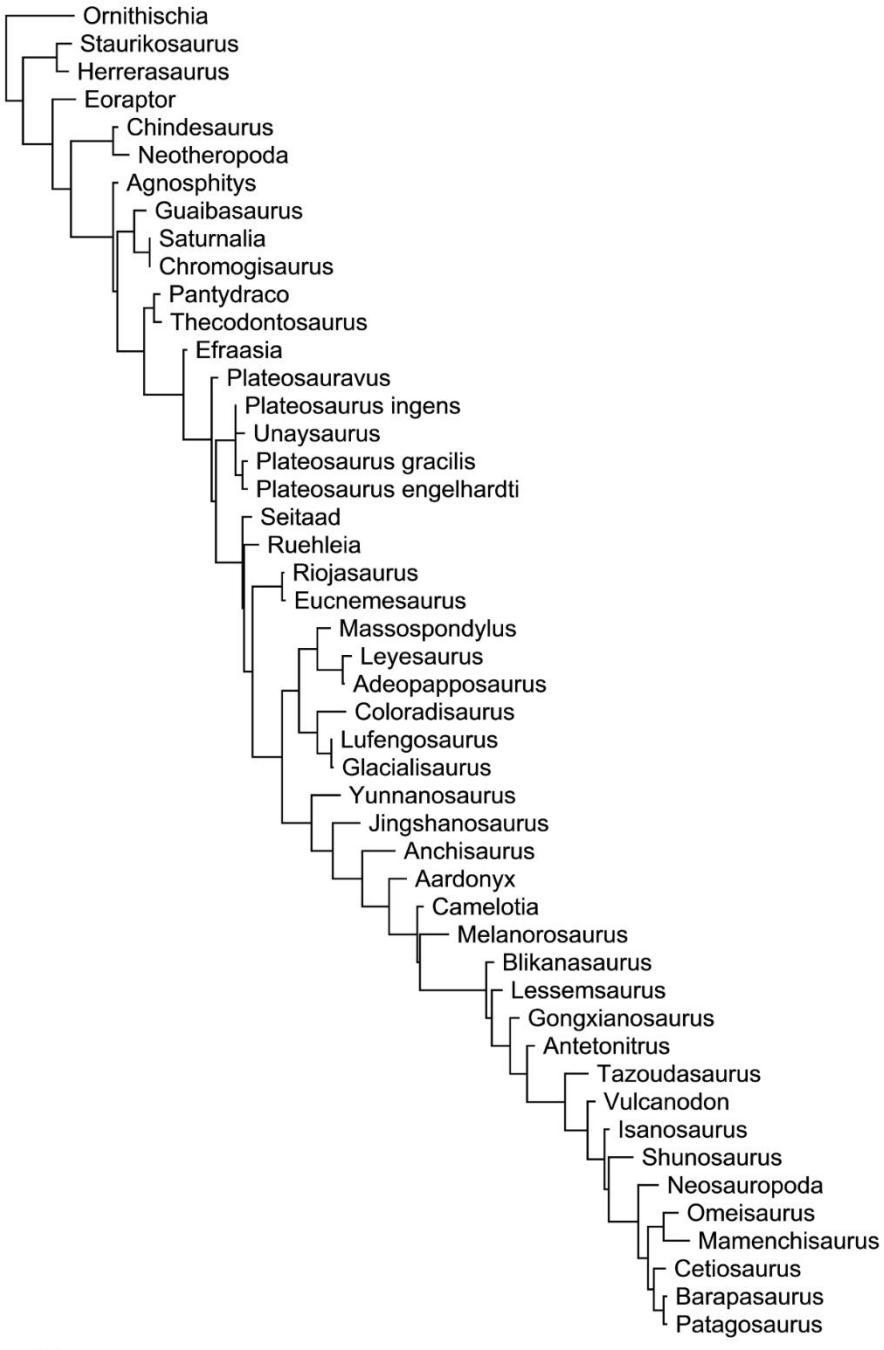

Figure 7. 'McPhee-Yates' most parsimonious composite pneumatic tree. Tree derived from the composite pneumatic 'McPhee-Yates' phylogeny of 48 taxa and 364 characters (372-8 original pneumatic) under heuristic search with TBR in parsimony criterion (1154, with CI = 0.354 and RI = 0.636). Assigned outgroups: Ornithischia, *Staurikosaurus*, *Herrerasaurus*, *Eoraptor*, *Chindesaurus*, *Agnosphitys*, Neotheropoda and *Guaibasaurus*. Uninformative characters were included.

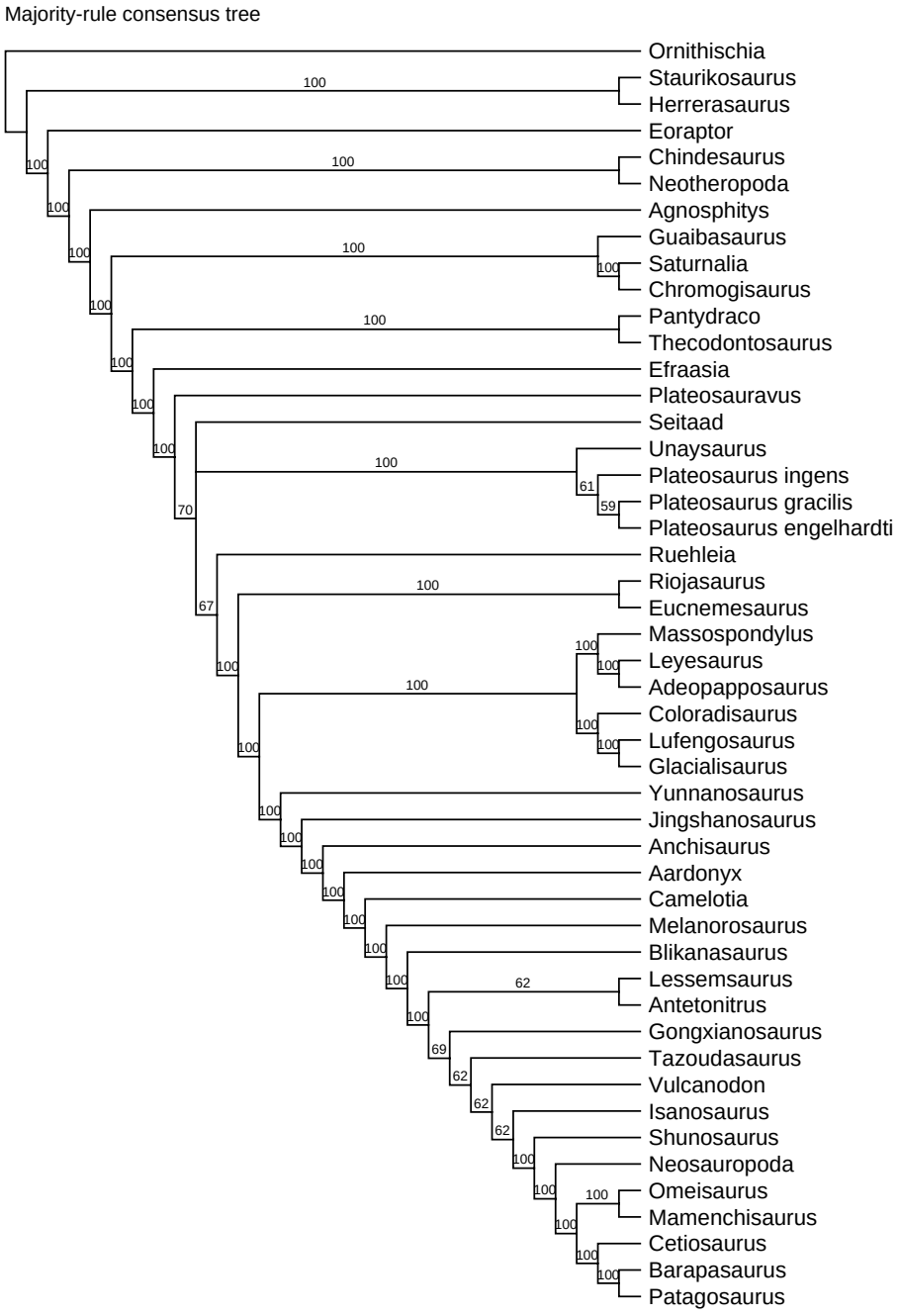

Figure 8. 50% Majority rule 'McPhee-Yates' tree. 50% Majority-rule tree of the pneumatic composite 'McPhee-Yates' most parsimonious trees of 48 taxa and 364 characters (372-8 original pneumatic) under heuristic search with TBR in parsimony criterion (Tree length = 1154 steps, with CI = 0.354 and RI = 0.636). Assigned outgroups: Ornithischia, *Staurikosaurus*, *Herrerasaurus*, *Eoraptor*, *Chindesaurus*, *Agnosphitys*, Neotheropoda and *Guaibasaurus*. Uninformative characters were included.

Furthermore, an analysis was conducted keeping the uninformative characters, under the same parameters, and imposing the constraint of the original composite 'McPhee-Yates' phylogeny onto the pneumaticity modified composite version yielded a tree of scores of 1157 steps, CI: 0.354, RI: 0.634, RC: 0.224 and HI: 0.646 (Fig. 9).

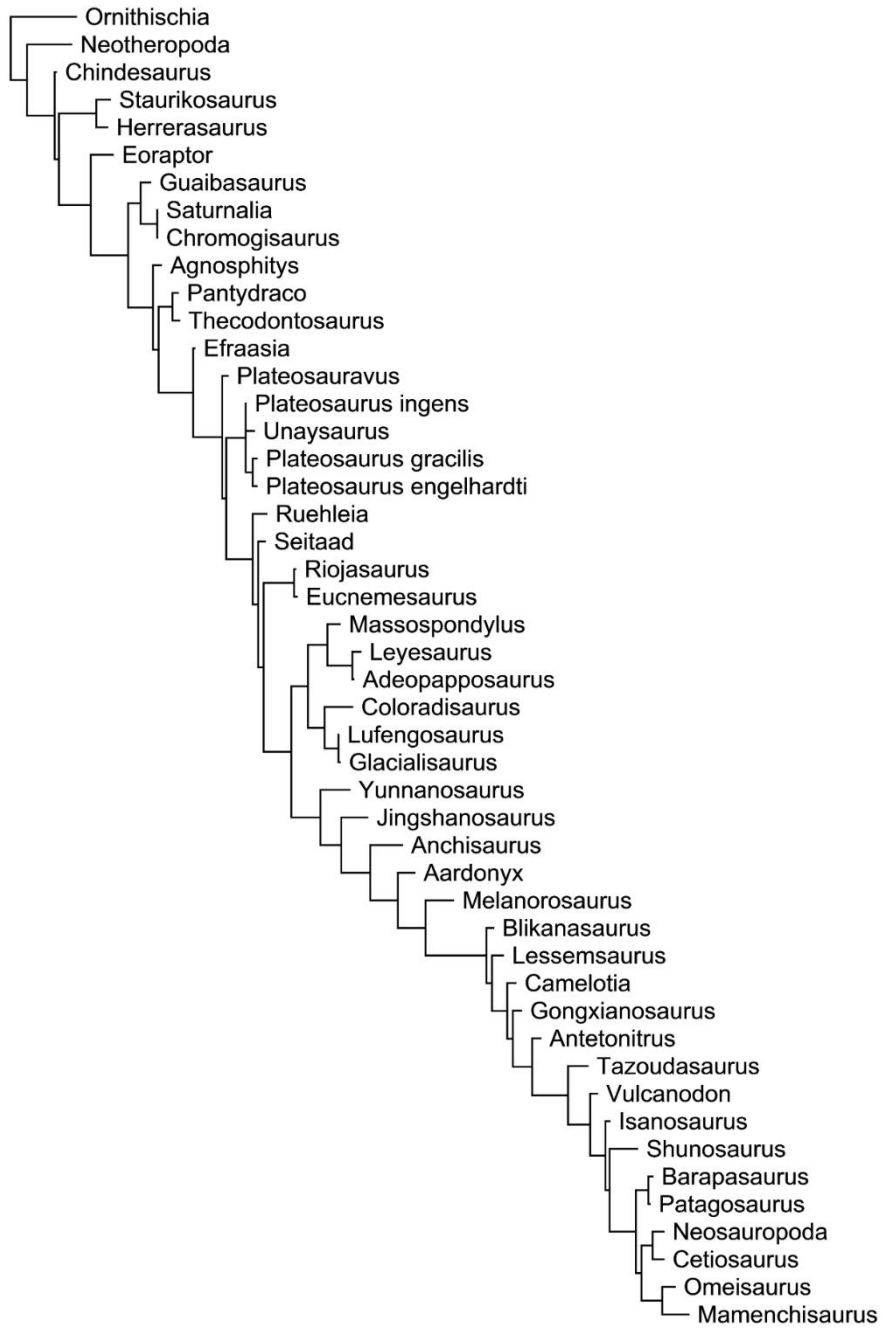

Figure 9. Constrained 'McPhee-Yates' parsimonious tree. Tree derived from the modified composite 'McPhee-Yates' phylogeny (48 taxa and 372-8 original pneumatic characters = 364) by heuristic search under parsimony with the 26 uninformative characters included and with enforced topological constraint of the original composite phylogeny. Assigned outgroups: Ornithischia, *Staurikosaurus*, *Herrerasaurus*, *Eoraptor*,

Chindesaurus, *Agnosphitys*, Neotheropoda and *Guaibasaurus*. Tree scored at 1157 steps, CI: 0.354 and RI: 0.634.

The original McPhee et al. (2014) phylogeny (Fig.24, pp. 192) was analysed in *TNT* 1.1 (Goloboff, Farris & Nixon, 2008) using heuristic search and parsimony criteria with TBR swapping and had a tree length of 1194 steps. The Yates et al. (2009) original phylogeny (Figure S5 in Yates et al., 2009 SI) has 1119 steps while the composite tree (Fig.1) in *Mesquite* (40 taxa) with the pneumaticity characters incorporated had a length of 526 steps. Consistency and Retention Indices were not given in the published cladistic analyses but analyses in *Mesquite* for the composite phylogeny yielded a CI = 0.43 and an RI = 0.14 whereas the *PAUP* parsimonious heuristic analyses (48 taxa, 364 characters; Fig. 7) resulted in best score of 1154 steps and outputted a CI = 0.354 and an RI = 0.636. Before proceeding further, it can be stated at this point that, on the basis of tree length, the addition of pneumaticity characters mapped on the composite phylogeny while keeping the uninformative characters (i.e. including all 11 added pneumaticity characters) results in a better tree score than both the original tree of McPhee et al. (2014) and of the composite 'McPhee-Yates' tree analysis (1170 steps, CI: 0.351 and RI: 0.653) but a slightly larger score than the 1119 step long phylogeny of Yates et al. (2009). Interesting to note is that the constrained parsimonious tree with the 26 uninformative characters included (Fig. 9) yielded slightly larger tree scores (1157 steps) than the consensus tree of Fig. 8. The presence of the eleven extra pneumaticity characters and the combinatory nature of the phylogeny with regard to its morphological characters, produced a tree with much fewer steps and slightly different taxonomic interrelationships.

In general, the trees generated in *PAUP* (Figs. 7-9) yielded a similar tree to the original tree published by McPhee et al. (2014). Apart from being 36 steps smaller and only regarding the pneumatically-studied ingroup taxa, the *PAUP* tree of Fig. 6 differs from the original published tree in the facts that the limitedly pneumatic basal sauropodomorph *Seitaad* (PDI%=39) was paired as a sister clade with the more pneumatic basal sauropodomorph *Ruehleia* (PDI%=49) instead of *Jingshanosaurus*. The non-pneumatic basal sauropodomorph *Massospondylus* (PDI%=0) was recovered as a sister clade to the pair of sister taxa *Leyesaurus* and *Adeopapposaurus*. The moderately-low pneumatic *Antetonitrus* (PDI%=43) was not paired with *Lessemsaurus* but the moderately-high pneumatic eusauropod *Barapasaurus* (PDI%=69) was paired with the moderately pneumatic eusauropod *Patagosaurus* (PDI%=59) and the moderately-high pneumatic eusauropod *Omeisaurus* (PDI%=60) with the highly pneumatic eusauropod *Mamenchisaurus* (PDI%=90). As mentioned before, such alterations were probably because the polymorphic characters were kept unordered as well as perhaps due to the

insertion of *Camelotia*. Beginning from the most primitive towards the most derived positions in a tree (i.e. from top to bottom), the parsimonious composite pneumatic tree with the original pneumatic characters excluded (Fig. 7) differed from the original tree in that the moderately-low basal sauropodomorph *Thecodontosaurus* (PDI%=47) was paired as a sister clade with *Pantydraco* and *Seitaad* was not paired with *Jingshanosaurus*. The moderately-low basal sauropodomorph *Camelotia* (PDI%=49) was recovered to be paraphyletic to *Melanorosaurus* and *Blikanasaurus* and was instead placed in a more derived position than the latter two taxa. *Antetonitrus* was not recovered to be not paired with *Lessemsaurus* but instead it was paraphyletic to the minimally pneumatic eusauropod *Tazoudasaurus* (PDI%=23). *Isanosaurus* formed a dichotomy with the moderately-high pneumatic eusauropod *Shunosaurus* (PDI%=67), *Omeisaurus* was paired with *Mamenchisaurus*, *Barapasaurus* was paired with *Patagosaurus* while the moderately pneumatic eusauropod *Cetiosaurus* (PDI%=53) was recovered in a paraphyletic position with respect to the previous two pairs. The consensus tree (Fig. 8) differed only from the previous tree in the fact that *Antetonitrus* was paired as a sister clade to *Lessemsaurus* which agrees with the original tree. In addition, *Isanosaurus* did not form a dichotomy with *Shunosaurus* but instead the former taxon was positioned more primitively to the latter, as in the original published phylogeny. The insertion of the 11 added pneumaticity characters affected the phylogenetic interrelationships of the pneumatically-studied taxa, pairing the taxa with the closest pneumaticity statuses together. The constrained tree which contained the uninformative characters (Fig. 9) was almost identical to the tree of Figure 7 but not to Figure 8. Regarding the ingroup taxa, in the constrained tree, *Camelotia* found to be placed in a more derived position than in the non-constrained tree of Figure 7, i.e. just two paraphyletic positions more primitive with respect to *Antetonitrus* rather than four. In addition, in the constrained tree, *Cetiosaurus* was paired with Neosauropoda whereas in the non-constrained tree *Cetiosaurus* was recovered to be immediately paraphyletic to the sister taxa *Barapasaurus* and *Patagosaurus* which were placed in the most derived positions in the tree. Furthermore, *Melanorosaurus*, *Blikanasaurus* and *Lessemsaurus* were placed in more primitive positions with respect to *Camelotia* in the constrained tree whereas the opposite occurs in the majority rule consensus tree (Fig. 8). In this tree, *Cetiosaurus* was not recovered to be paired with Neosauropoda (as it happened in the constrained tree) but it formed a paraphyly to the most derived pair of the sister taxa *Barapasaurus* and *Patagosaurus*. In both trees, *Omeisaurus* and *Mamenchisaurus* were paired and placed in more derived positions than Neosauropoda but *Shunosaurus* was not; it was placed in a more primitive location in the tree. A noteworthy observation is that the pair of *Omeisaurus* and *Mamenchisaurus* was placed in the most derived location in the constrained tree whereas this position in the consensus tree was occupied by the

Barapasaurus-Patagosaurus pair. The latter pair, in the constrained tree, was placed in a more primitive position than the Neosauropoda clade whereas in the consensus tree, this pair was placed in a more derived (and last) position with respect to the Neosauropoda clade. The original tree of McPhee et al. (2014) differs from the constrained tree here in that *Pantydraco* was not paired with *Thecodontosaurus*, *Seitaad* was paired with *Jingshanosaurus*, *Antetonitrus* was paired with *Lessemsaurus* and *Omeisaurus* formed a trichotomy with *Mamenchisaurus* and *Barapasaurus*. Last but not least, Neosauropoda and *Cetiosaurus* formed the most derived pair of sister taxa, with *Patagosaurus* being immediately paraphyletic to the pair.

The low values of Consistency and Retention indices denote a moderate, if not poor, fit between the morphological data and the recovered topologies. It is evident, though, that the resulted sauropodomorph interrelationships in the pneumatic composite phylogenies reflect their morphological similarity with respect to pneumaticity, as was showed, described and discussed in Chapters 1-3 as well as in the earlier '*Mesquite'* section of this chapter. Taxa with similar values of pneumaticity were recovered to be paired together as sister taxa (e.g. *Omeisaurus-Mamenchisaurus* and *Patagosaurus-Barapasaurus*) than their depiction in the non-pneumatically modified phylogeny of Figure 6. The other pneumatically studied taxa that were recovered in a close phylogenetic relationship with each other (e.g. *Seitaad* and *Ruehleia*) in the non-modified phylogeny, they did not seem to be affected by the addition of the 11 pneumaticity characters of this study and retained in these pneumatic phylogenies their phylogenetic placements they had with each other in the original phylogenies. In conclusion, the insertion of the 11 added pneumaticity characters affected their interrelationships moderately but in an expected positive manner and, in some cases, in accordance to their pneumatic affinities.

5.3.2) *Sander et al. (2011)*

Mesquite – discrete characters

This phylogeny will be used as it is without any alterations, additions or omissions. *Saturnalia*, *Melanorosaurus*, *Limaysaurus*, *Isisaurus* and *Opisthocoelicaudia* are well known and representative sauropodomorph taxa but they are not included in the pneumatic dataset, due to temporal constraints of this project, resulting in non-existent pneumatic character designation ('?'). Pneumaticity characters were assigned for this phylogenetic tree in *Mesquite* and, as in the previous case, only to those taxa for which there were pneumaticity data obtained from this study. The percentage of taxonomic congruence with regard to existing pneumatic data in this phylogeny is 25/30 = 83.3%. The pneumaticity characters were incorporated and several character traces were carried

out (here for traced character ‘C1c’) in parsimony and likelihood, obtaining values as mentioned above for the previous case.

Analyses in this phylogeny showed a poor fit of the mapped pneumaticity characters. The distribution and evolution of the pneumaticity characters across these taxa became evident and the values of Tree length, CI and RI were computated. The character’s reconstruction (‘C1c’) showed low signal strength (TL = 491, CI = 0.48 and RI = 0.12 in Fig.10). Consistency and Retention indices for character ‘C1c’ are 0.2 and 0.5, respectively. Trees with other traced pneumaticity characters can be viewed in Appendix 2 (‘Tree figures’).

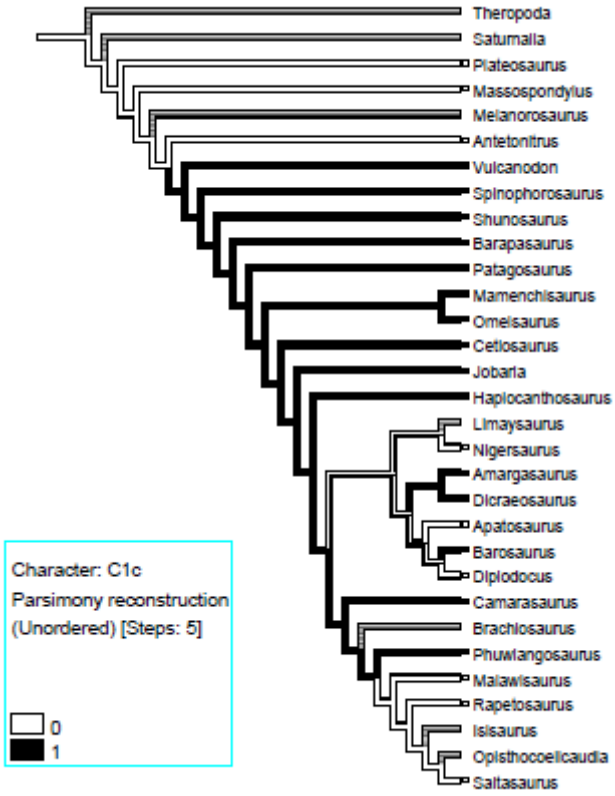

Figure 10. Parsimony reconstruction of character ‘C1c’ (cervical) in 31 taxa in the ‘Sander et al., 2011’ phylogeny. Reconstruction of pneumaticity character ‘C1c’ (cervical) in 31 taxa under parsimony in the published phylogeny of ‘Sander et al. (2011)’. Grey branches indicate ‘unknown’ data. Values for tree: TL = 491, CI = 0.48 and RI = 0.12.

Mesquite – continuous characters

Metric data characters of PDI% (total average), mass, length and femur length were mapped on the original ‘Sander et al. (2011)’ phylogeny of the examined taxa showing the evolution of PDI% across the 31 sauropodomorph taxa. Comparison of the traits with each other was made easily observable (see Figs.11-14).

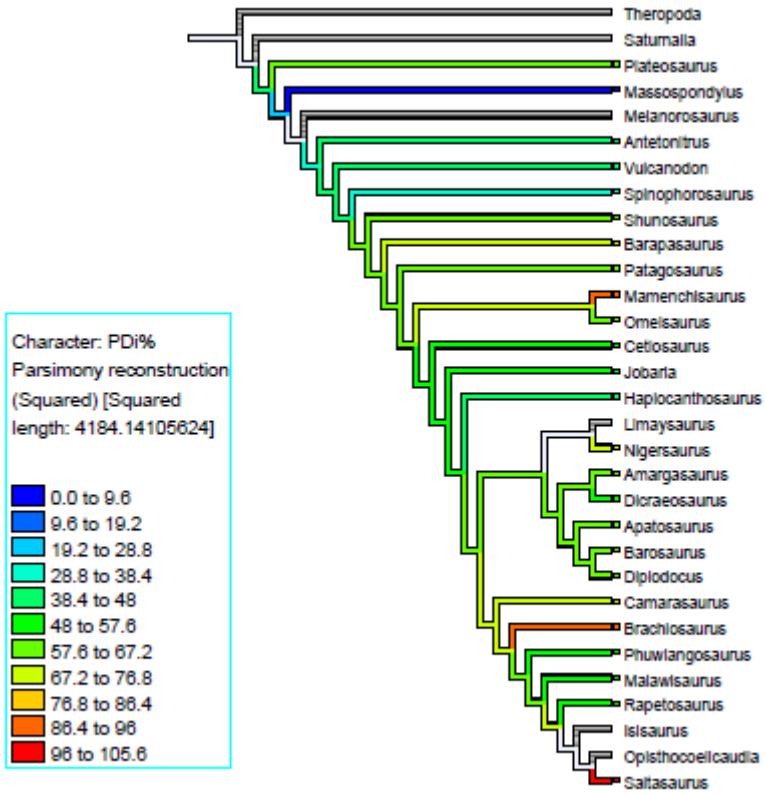

Figure 11. Distribution of total average PDI% in the 'Sander et al., 2011' phylogeny. Cladogram of 31 sauropodomorph taxa of the original 'Sander et al. (2011)' phylogeny, demonstrating the distribution of total average PDI% across the phylogeny. The evolution of PDI% is nearly gradual with the noticeable sudden increases, evident in *Mamenchisaurus, Brachiosaurus* and *Saltasaurus.* Grey branches indicate 'unknown' data.

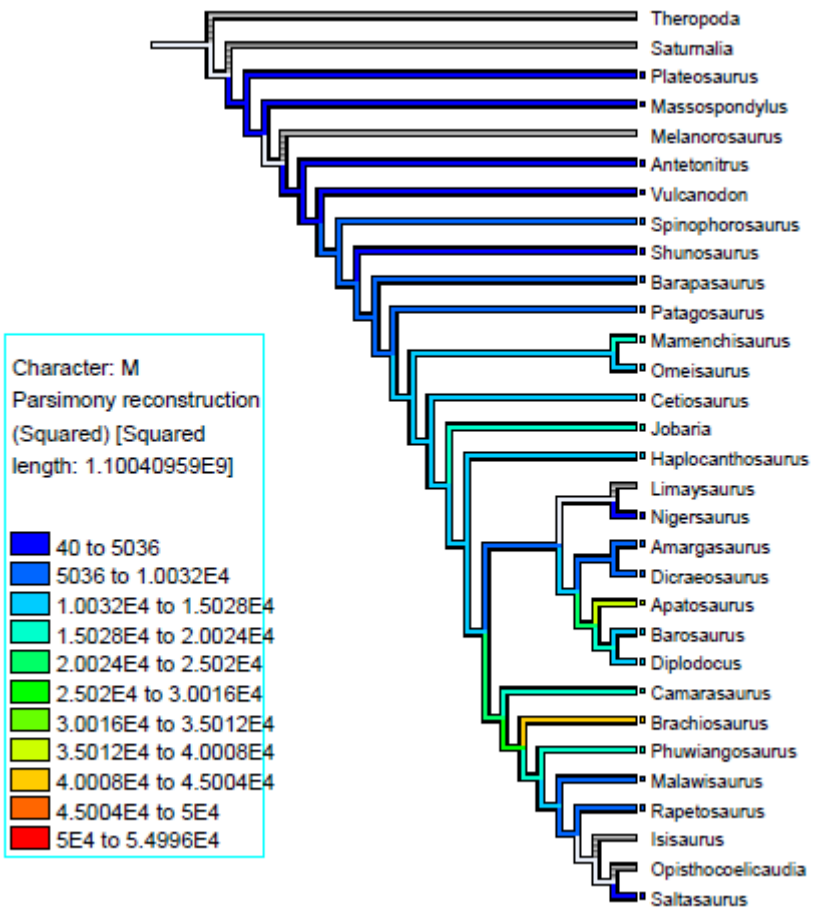

Figure 12. Body mass distribution in the 'Sander et al., 2011' phylogeny. Cladogram of 31 sauropodomorph taxa of the original 'Sander et al. (2011)' phylogeny, demonstrating the distribution of body mass (M, in kilogrammes) across the phylogeny. Grey branches indicate 'unknown' data.

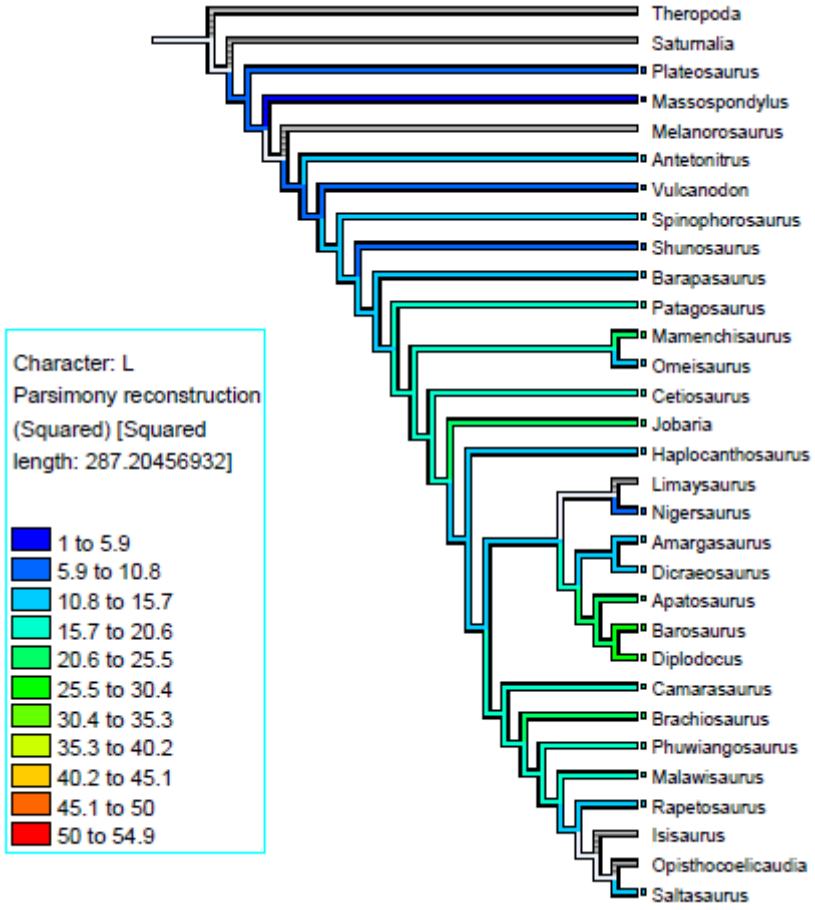

Figure 13. Body length distribution in the 'Sander et al., 2011' phylogeny. Cladogram of 31 sauropodomorph taxa of the original 'Sander et al. (2011)' phylogeny, demonstrating the distribution of body length (L, in metres) across the phylogeny. Grey branches indicate 'unknown' data.

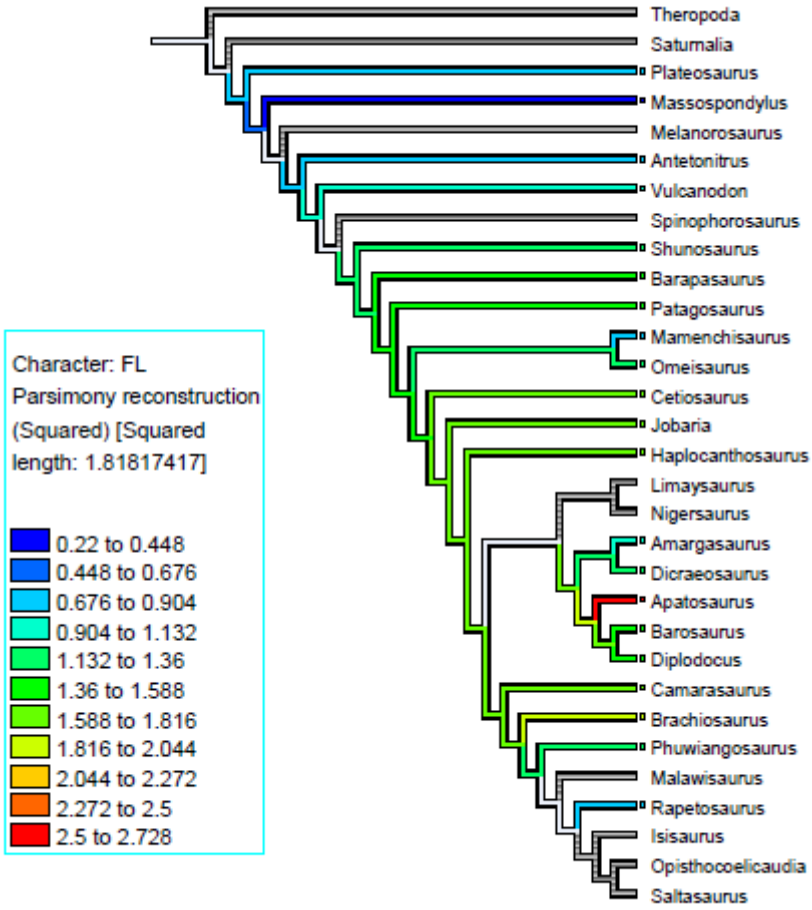

Figure 14. Femur length distribution in the 'Sander et al., 2011' phylogeny. Cladogram of 31 sauropodomorph taxa of the original 'Sander et al. (2011)' phylogeny, demonstrating the distribution of femur length (FL, in metres) across the phylogeny. Grey branches indicate 'unknown' data.

The central pleurocoel in the cervical vertebrae is present in 15 out of 31 sauropod taxa (Fig.10 in section 5.3.2), appearing almost continuously from *Vulcanodon* and towards the most derived positions in the tree, finishing in the Barremian-Aptian basal somphospondylan *Phuwiangosaurus*. *Phuwiangosaurus* is larger (Table 7 in Chapter 2) than the ones that are positioned in more derived positions from it in this phylogeny, thus it is justified to have such a weight-lighting feature. 'C1c' in cervicals also appears in both members of most sister clades except in the '*Barosaurus-Diplodocus'* clade where it is only present in *Barosaurus* (Table S1 in Appendix 2). Both taxa have almost the same size but *Barosaurus* possesses a longer neck than *Diplodocus* (Table 7 in Chapter 2) which may explain the need to develop such a prominent weight-reducing pneumatic trait. Nevertheless, the totality and invasiveness of other pneumaticity characters present in the

cervicals of *Diplodocus* amount to a higher PDI% in its cervicals than in those of *Barosaurus* (Appendix 3). Fossae within pleurocoels ('C8c') in cervical centra is a derived pneumaticity trait found only in the most highly pneumatised eusauropods, such as the sister clades *Mamenchisaurus* from Oxfordian-Tithonian and *Omeisaurus* from Bathonian-Oxfordian but also in the moderately pneumatic *Jobaria* (Aalenian-Berriasian). Then, 'C8c' appears in most members of Diplodocoidea and the Early macronarian *Camarasaurus* before making its last appearance in the Maastrichtian-aged, mid-sized and moderately pneumatic *Rapetosaurus* (see 'Tree figures' in Appendix 2 and Table 7 in Chapter 2). Pleurocoels in the dorsal vertebrae are expressed in all but the earliest eusauropods and in conjunction with the fact that cervical pleurocoels are found in its earliest members (i.e. *Vulcanodon*) it is possible that the latter feature predated, from an evolutionary perspective, the former i.e. dorsal pleurocoels. Such an assumption may shed further light on the observations and assumptions made by many workers on studies about sauropod, theropod and bird pneumaticity (e.g. Upchurch, 1995, Wedel et al., 2000; Wedel, 2003*a*, *b*; Benson et al., 2012; Wedel and Taylor, 2013).

It is observed that vertebral pneumaticity of the dorsal series became a frequent and rather common osteological trait in most early eusauropods but also in the more derived neosauropods (either by inheritance, gene flow or both) before the developmental path of deep cervical pneumatisation was laid. Perhaps this is the case because the main body trunk in these animals is naturally their heaviest part and also where the centre of mass is, so it was an evolutionary priority to lighten the main body before proceeding to the pneumatisation of increasingly long necks and tails (see Taylor and Wedel, 2013; Wedel and Taylor, 2013), throughout sauropod evolution. Contrary to this trait's frequency, character 'C8c' in the dorsals does not appear in more than four taxa in this phylogeny, classifying it as a rare characteristic, variably inherited in taxa from almost every subfamily ('Tree figures' in Appendix 2). In addition, the fact that dorsal pneumaticity is more prominent in the cervical or sacrocaudal series does not necessitate its pre-existence either on evolutionary or ontogenetic levels. Rather, it may have appeared after cervical pneumaticity did but it developed more than the cervical pneumatisation for, perhaps, biomechanical reasons or simply because of inheritance through speciation.

Pneumatisation in the sacral series is present in few middle- and high-weight derived taxa which are known to possess four or five fused vertebrae (Upchurch, 1995; Wedel, 2003; see 'Tree figures' in Appendix 2 and Table 7 in Chapter 2). Pneumatisation in the caudal series is limitedly expressed, found only in *Omeisaurus, Nigersaurus*, *Apatosaurus* and *Diplodocus* – the latter two being few of the heaviest and longest representatives of their subfamily in this phylogeny ('Tree figures' and Table 7 in Chapter 2). Basal titanosauriformes (i.e. macronarians) do not express invasive caudal

pneumatisation as observed in their fossils, since their tails were comparatively shorter and bulkier than the diplodocids' tails. Superficial pneumatisation, though, was more commonly developed in the early and middle eusauropods as well as reappearing in the macronarian *Brachiosaurus*. Quantification of total vertebral pneumatisation (Fig.11) in the Sander et al. (2011) phylogeny demonstrates and verifies that the most bone-invasive and, therefore, unambiguously pneumatic traits discussed above are found in the mostly pneumatised taxa (*Mamenchisaurus, Omeisaurus, Nigersaurus, Camarasaurus, Brachiosaurus* and *Saltasaurus*), thus spanning in time from Middle Jurassic to Upper Cretaceous.

Evolution and correlation between PDI% and body mass, body length and femur length

The taxonomic progression of body mass and body length in this phylogeny begins with a couple of repeated 'high value-low value' sets that also correspond to 'high value-low value' of pneumatisation in these taxa (*Plateosaurus* – high value, *Massospondylus* – lower value; *Antetonitrus* – high value – *Vulcanodon* – lower value; see Fig.1 in Chapter 3 or Table 7 in Chapter 2). It forms an 'uphill-downhill' type of pattern until it continues from *Spinophorosaurus* on a gradual increase which culminates in *Mamenchisaurus*. The mapped metric data have similar patterns in this phylogeny, with some being shorter than others, until the value of pneumaticity reaches the maximum in somphospondylans. In Diplodocoidea, *Amargasaurus* is heavier and more pneumatic than *Dicraeosaurus* but it has shorter total body length and femur length. *Apatosaurus* is heavier and more pneumatic than *Amargasaurus* and *Barosaurus* and has larger femur length than *Barosaurus* and *Diplodocus*, though its body length is not as long as its flagellicaudatan relatives. From there, pneumaticity increases until it climaxes in the macronarian titanosauriform *Brachiosaurus* and then drops again as we enter into the Somphospondyli clade. Finally, *Phuwiangosaurus* is heavier and longer than *Saltasaurus* and *Rapetosaurus* but its pneumaticity level is higher than that of *Rapetosaurus* but much less than that of *Saltasaurus*. Much of *Rapetosaurus* material is known from juvenile specimens but for the purposes of this study, pneumaticity data were obtained from the most mature individuals. Given their phylogenetic position in this tree, *Saturnalia* may possess no or very low expression of pneumaticity, *Melanorosaurus* very low levels and *Limaysaurus* low or medium expression of pneumaticity. *Isisaurus* and *Opisthocoelicaudia* may reflect gradual increase of pneumaticity between *Rapetosaurus* and *Saltasaurus* or exhibit a completely variable expression. The 'peak-trough' patterns in the graphs and trees of this project showing taxa and vertebral areas with more and less pneumaticity may also reflect the amount of missing fossil data. This study did not include taxon,

vertebral area or specimen completeness in its comparisons and calculations since it was not within its scope; nevertheless, it is evident from Table 7 (Chapter 2) and SI3 that results presented here are biased by specimen incompleteness and, surely, having more complete skeletal material would result in a clearer understanding of vertebral pneumaticity and its variability in sauropod evolution. A further comparison and interpretation of the missing vertebral material among the examined sauropodomorphs as well as its implications on the overall perspective of vertebral pneumaticity can be the basis of a future related study.

5.3.3) *D'Emic (2012) - Whitlock (2011)*

Mesquite - discrete characters

Using *Mesquite* (Maddison & Maddison, 2016), the pneumaticity character matrix was merged with the 'D'Emic-Whitlock' composite cladogram, applying the pneumaticity characters and carrying out parsimony as well as maximum likelihood analyses. As before, every phylogeny was kept at a genus level and the characters were codenamed as explained in the Methods section above (5.2.1). Subsequently, tracing of character 'C1c' and obtaining tree and character values alike were further conducted.

In this composite phylogeny, the pneumaticity characters show a weak fit with values of TL = 615, CI = 0.43 and RI = 0.16. In Fig.15 below we see the reconstructed 'C1c' character on this composite phylogeny consisting of 48 sauropodomorph taxa. Trees with the other traced pneumaticity characters can be viewed in Appendix 2.

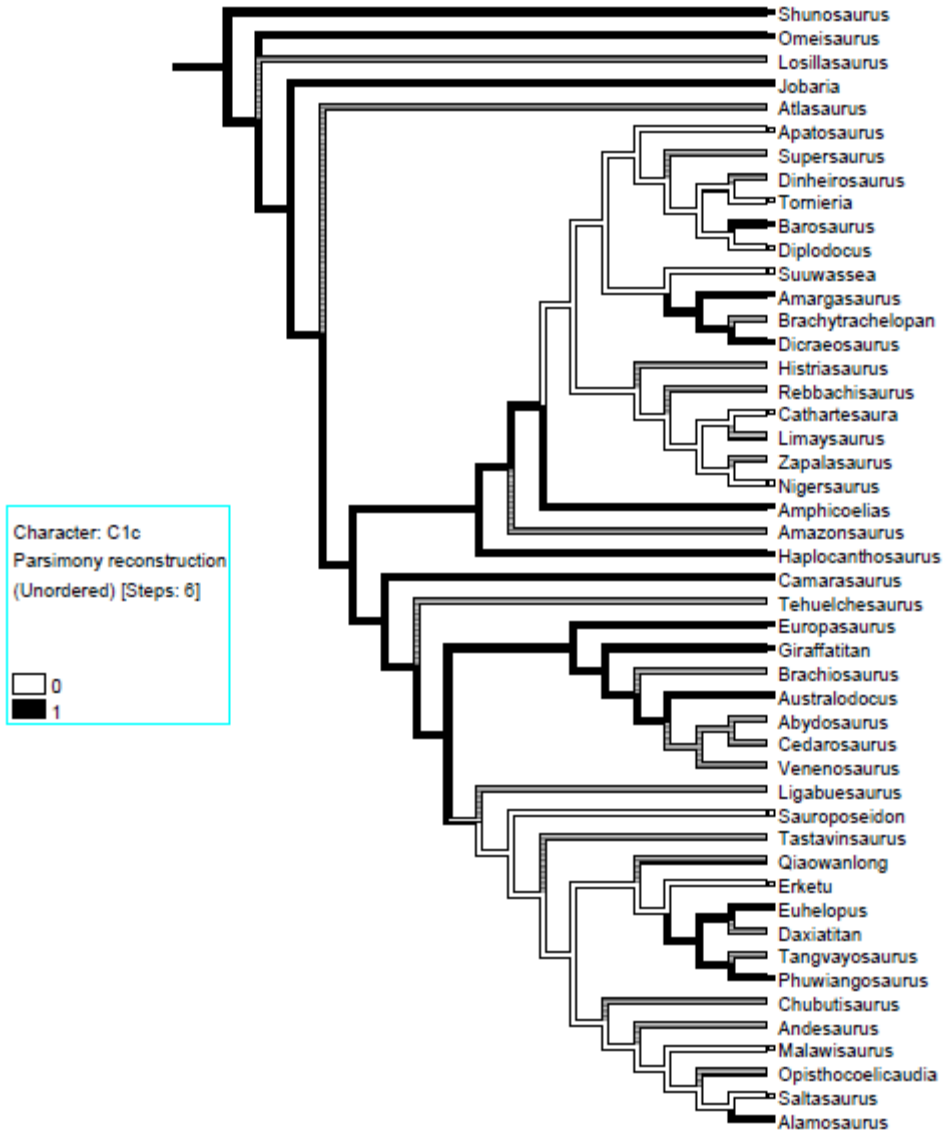

Figure 15. Parsimony reconstruction of character 'C1c' (cervical) in 48 taxa in the 'D'Emic-Whitlock' composite phylogeny. Reconstruction of pneumaticity character 'C1c' (cervical) in the composite phylogeny 'D'Emic-Whitlock' consisting of 48 sauropodomorph taxa under parsimony. Grey branches indicate 'unknown' data. Tree values: TL = 615, CI = 0.43 and RI = 0.16.

Mesquite – continuous characters

Continuous data characters of PDI% (total average), mass, length and femur length were mapped on the composite 'D'Emic (2012) – Whitlock (2011)' phylogeny showing the evolution of PDI% across the 48 sauropodomorph taxa. Comparison of the traits with each other was made easily observable (see Figs.16-19).

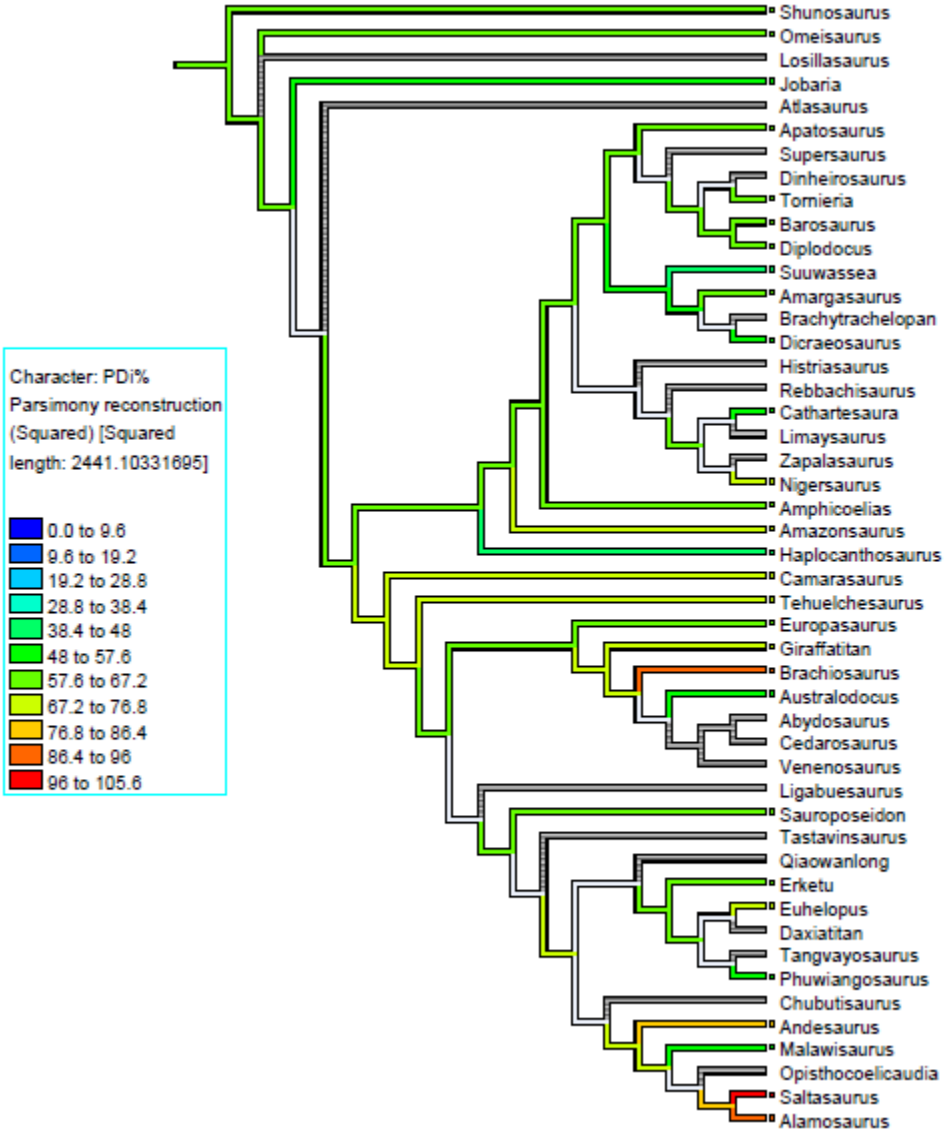

Figure 16. Distribution of total average PDI% in the 'D'Emic-Whitlock' composite phylogeny. Evolution of PDI% in 48 sauropodomorph taxa of the composite 'D'Emic (2012) -Whitlock (2011)' phylogeny, demonstrating the distribution of total average pneumatisation across the phylogeny. The evolution of PDI% is nearly gradual with noticeable sudden increases, evident in *Apatosaurus, Brachiosaurus, Giraffatitan, Sauroposeidon, Euhelopus, Saltasaurus* and *Alamosaurus.* Grey branches indicate 'unknown' data.

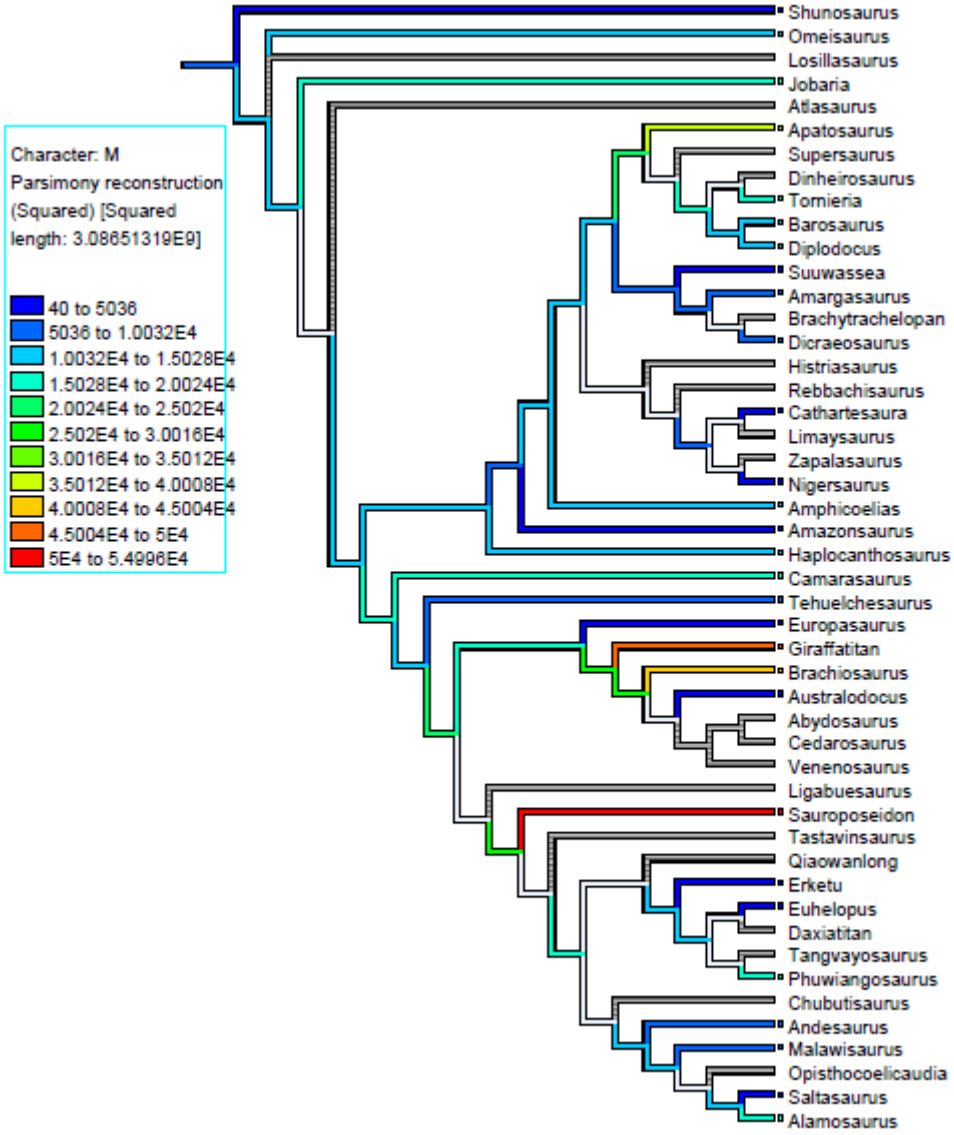

Figure 17. Body mass distribution in the 'D'Emic-Whitlock' composite phylogeny. Cladogram of 48 sauropodomorph taxa of the original 'D'Emic (2012) – Whitlock (2011)' phylogeny, demonstrating the distribution of body mass (M, in kilogrammes) across the phylogeny. Grey branches indicate 'unknown' data.

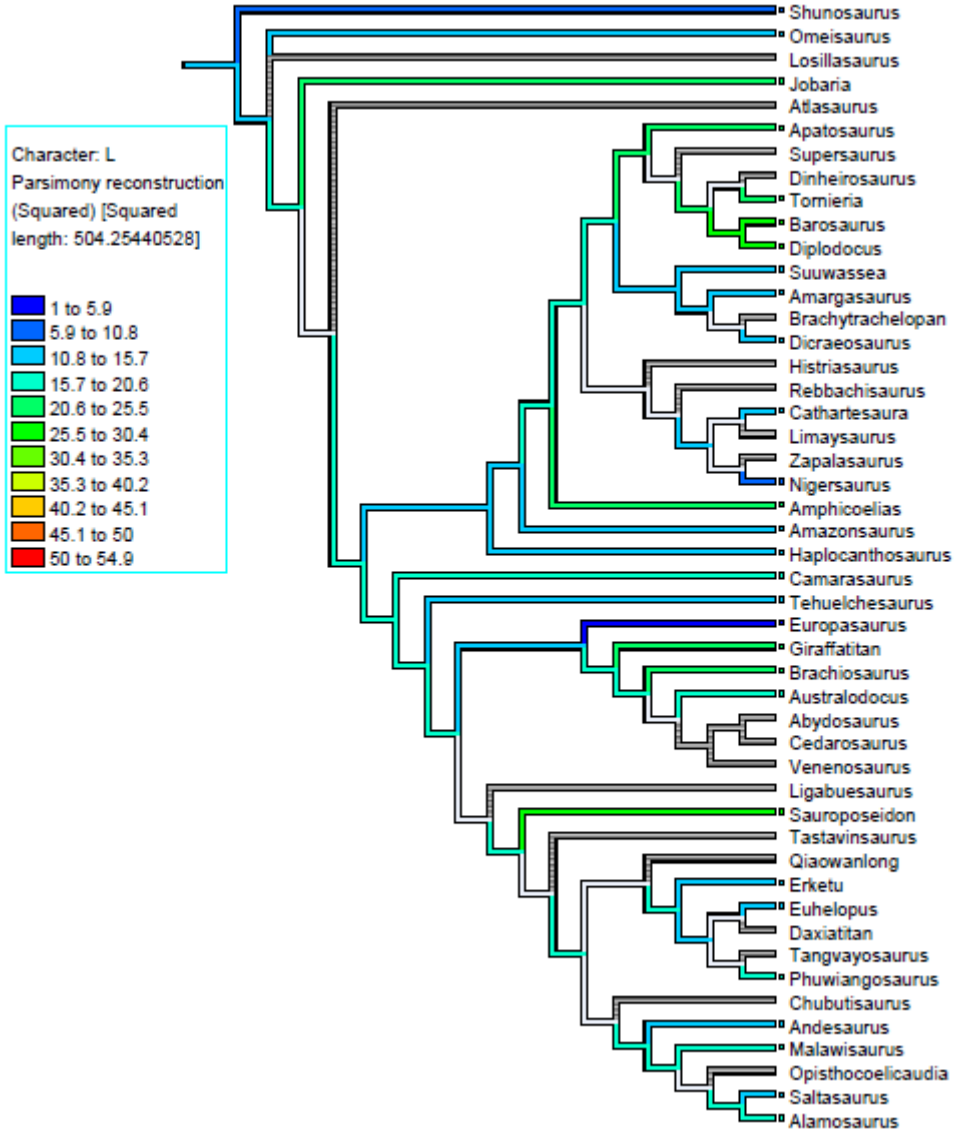

Figure 18. Body length distribution in the 'D'Emic-Whitlock' composite phylogeny. Cladogram of 48 sauropodomorph taxa of the original 'D'Emic (2012) – Whitlock (2011)' phylogeny, demonstrating the distribution of body length (L, in metres) across the phylogeny. Grey branches indicate 'unknown' data.

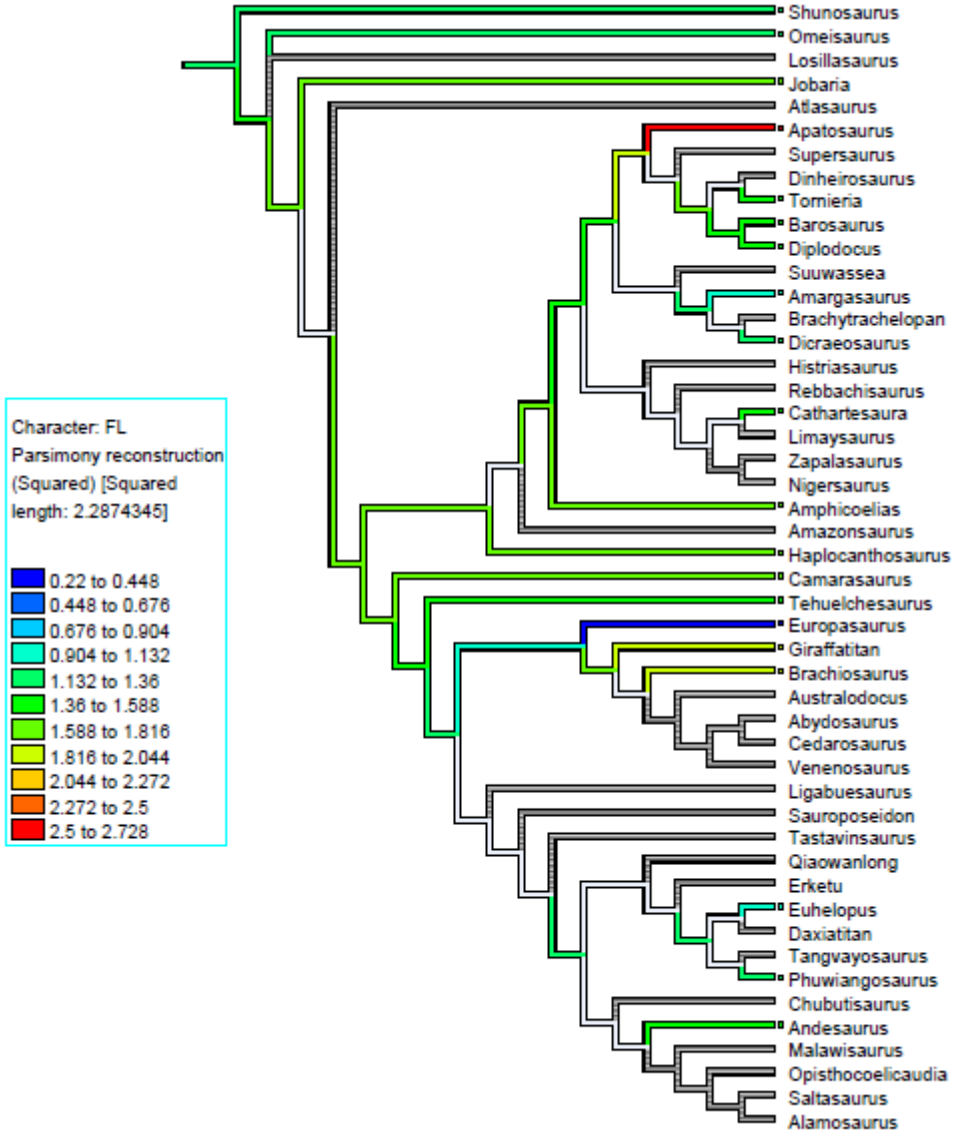

Figure 19. Femur length distribution in the 'D'Emic-Whitlock' composite phylogeny. Cladogram of 48 sauropodomorph taxa of the original 'D'Emic (2012) – Whitlock (2011)' phylogeny, demonstrating the distribution of femur length (FL, in metres) across the phylogeny. Grey branches indicate 'unknown' data.

Tracing of 'C1c' in this composite and larger phylogeny (Fig.15) reveals more taxa having developed pleurocoelous cervical centra, though this occurs in only 15 out of 48 taxa (less than 50%; see 'Tree figures' in Appendix 2). In this case, as well as the previous ones, it can be suggested that taxa for which we do not have sufficient osteological data, but are phylogenetically positioned between taxa possessing a particular trait, that they may also possess that trait; otherwise, we have an evolutionary hiatus where a trait stops being expressed and then reappears throughout an evolutionary lineage (Upchurch, 1995; Wedel, 2003), assuming that these taxa are not

contemporaneous to one another but that each taxon is the result of a speciation event of its predecessor. Many of these taxa, though, were contemporaneous to each other, implying that PSP was inherited to them at variable levels of expression from their last common ancestor. A phylogeny cannot inform us with certainty if such a relationship exists among the presented taxa but it shows us their 'closeness' to each other, based on the most parsimonious correlation of their shared and non-shared morphological characters. In many cases, the trait may have existed in a common ancestor of a clade but it then became expressed in only half, or less, of the descendants.

Such appears to be the case, for example, in the node splitting the subclade '*Europasaurus* to *Venenosaurus'* from the subclade '*Ligabuesaurus* to *Phuwiangosaurus'* (see 'Tree figures' in Appendix 2). 'C1c' is present discontinuously throughout the phylogeny but 'C8c' ceases to appear after *Sauroposeidon* in Aptian-Albian stages, and unless *Tastavinsaurus*, *Qiaowanlong*, *Daxiatitan*, *Tangvayosaurus*, *Chubutisaurus* and *Opisthocoelicaudia* possess it, the trait does not appear at all in the remaining Titanosauriformes (see 'Tree figures' in Appendix 2). However, as noted in previous cases too, most eusauropods, diplodocids and basal titanosauriform macronarians do have 'C8c' in their cervicals (see 'Tree figures' in Appendix 2). In accordance to previous observations, it is again evident that dorsal, rather than cervical, pneumatisation is present in more sauropod taxa (see 'Tree figures' in Appendix 2).

Having the opportunity to examine more taxa in this phylogeny, we can see here that sacral pneumatisation is rare among sauropods, with foramina in the neural spine to be present in only four taxa, two of which being closer to each other (*Diplodocus* and *Dicraeosaurus*) than to the other two (the basal titanosauriform *Brachiosaurus* and the somphospondylan *Phuwiangosaurus*). Foramina in the caudal centra have been expressed in more taxa than fossae have been on the same landmark (see 'Tree figures' in Appendix 2). Considering the ambiguous nature of the fossae (e.g. Wedel et al., 2000, 2003 *a, b*; Wilson et al., 2011) whether serving as bone reduction, adipose tissue deposition or both, it is evident that vertebral perforation (and possibly invasion of air sac diverticula) and subsequently less bone mass was a more prominent evolutionary path towards weight reduction than having depressions on the vertebrae. Nevertheless, we must consider the different taxonomic expression of these traits. Most of these taxa express both foramina and fossae in their caudals but the Upper Cretaceous (Cenomanian) *Andesaurus* has only fossae. This depends on the physiological needs and demands of the body plan of the animal as well as on chances of inheritance.

Finally, the foramen in the ilium (D2) appears to be present only in the dwarf macronarian sauropod *Europasaurus*. As noted by Wedel, Cifelli and Sanders (2000b), somphospondylans possess higher levels of skeletal pneumaticity than other

sauropodomorph clades. Examples are *Sauroposeidon* and *Saltasaurus* (e.g. Wedel et al., 2000; D'Emic, 2012) which have somphospondylous vertebrae. In neosauropods, vertebral fossae are highly variable with respect to their occurrence and the pattern of their subdivision (Wilson et al., 2011). Another feature observed in neosauropods is having large fossae in the centroprezygapophyseal areas of the presacral vertebrae, as in *Camarasaurus* (Osborn and Mook, 1921). For a detailed discussion on sauropod, and especially titanosauriform and somphospondylan) synapomorphies see D'Emic (2012).

Evolution and correlation between PDI% and body mass, body length and femur length

The 'D'Emic-Whitlock' phylogeny exhibits similar patterns to those found in the previous one ('Sander et al., 2011') but with more taxa placed in between the taxa seen in the 'Sander et al., 2011' tree; see Figs.17-20). *Haplocanthosaurus* is placed in a derived position in Diplodocoidea, setting a lower pneumatisation value (matched by its comparatively smaller size) towards the end of this group. The evolutionary expression of pneumaticity then increases with *Camarasaurus* and the basal Titanosauriformes *Giraffatitan* and *Brachiosaurus*. Taking the opportunity to examine more taxa displayed in this phylogeny, we could make inferences on the pneumatisation values of the 'grey' unknown taxa. *Losillasaurus* may have had a value as high as *Omeisaurus* or, judging by the newly observed unusual pattern, it could be as low as the taxon that follows it i.e. *Jobaria*. *Supersaurus* and *Dinheirosaurus*, bracketed by *Apatosaurus* and *Tornieria*, probably had pneumaticity values somewhere in between them so as to form a 'downslope' pattern or, due to their large sizes (estimated to be even greater than *Apatosaurus*) might have high levels of pneumatisation, maybe at least as much as *Apatosaurus*. *Supersaurus* and *Dinheirosaurus* could have acquired different degrees of PDI% as part of their set autapomorphic characters. Due to their position, it is likely that *Histriasaurus* and *Rebbachisaurus* had moderate expressions since they are bracketed by almost equally pneumatic taxa. *Limaysaurus* and *Zapalasaurus* may had intermediate or gradually increasing values to the moderately and highly pneumatic taxa they are bracketed by (i.e. *Cathartesaura* and *Nigersaurus*), an assumption strengthened by their sister taxa correlation as we see in Fig.16. The macronarians *Abydosaurus*, *Cedarosaurus*, *Venenosaurus* and *Ligabuesaurus* may show a gradual increase until we see the highly pneumatic *Sauroposeidon* while *Tastavinsaurus* and *Qiaowanlong* may show either variable or decreasing levels of pneumaticity. The Titanosauriformes *Daxiatitan* and *Tangvayosaurus* may show a decrease since the taxon that precedes them (i.e. more basal than them), *Euhelopus*, is very pneumatic while the taxon that follows them (i.e. placed in a more derived position than them), *Phuwiangosaurus*, is less

pneumatic. As for *Opisthocoelicaudia*, its pneumaticity degree may have intermediate or any of the two values of the taxa that bracket it since there is a considerable pneumaticity difference between the bracketing taxa. The other metric measures of these sauropodomorph taxa show an irregular 'downhill – uphill' pattern with very few expected notable peaks in Brachiosaurinae and Diplodocinae but without matching the pattern of pneumaticity; rather, most of the taxa located between sudden size increases, as seen through the phylogenies, do not have large deviations from one another.

PAUP – discrete characters

At first, heuristic analyses were performed in the unaltered composite phylogeny composed of D'Emic (2012) and Whitlock (2011) datasets i.e. retaining their initial set of morphological characters. For this analysis, 189-119 = 70 question marks had to be added to each taxon's character set in D'Emic's dataset in order to equalise with Whitlock's number of 189 characters. This modification and procedure was done separately from the procedure described below for the composite pneumatic phylogenetic analysis for the purpose of retrieving comparative results with respect to the original published phylogenies as well as for obtaining the Newick code of the composite tree to impose it later as a constraint. Optimality criterion was set to parsimony applying TBR under DELTRAN optimisation in an attempt to replicate the method which both authors used in their analyses. As aforementioned, the selected outgroup taxa were *Shunosaurus*, *Omeisaurus* and *Jobaria* to account for both D'Emic's and Whitlock's studies. All characters were unordered and the uninformative characters were included. Score of best tree found to be 447 (Tree length = 447, CI = 0.459, RI = 0.758, RC = 0.348 and HI = 0.541; Fig. 20).

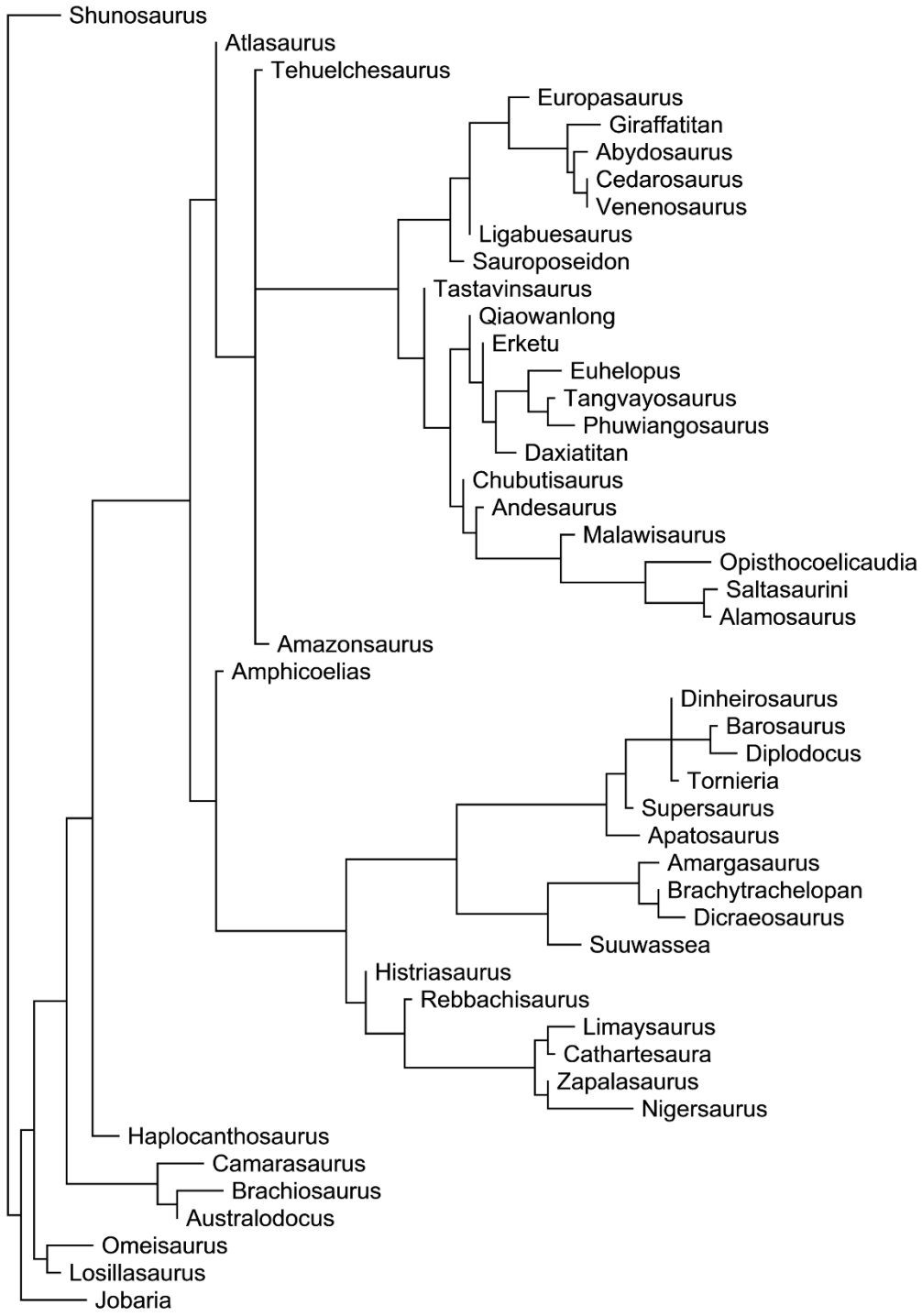

Figure 20. D'Emic (2012) – Whitlock (2011) composite unaltered tree. Composite phylogeny with the modification of having 70 question marks added to D'Emic's character set so as both datasets to have equal number of characters. The phylogeny consists of 48 taxa and 189 characters. Assigned outgroups: *Omeisaurus*, *Shunosaurus* and *Jobaria*. Heuristic analysis was conducted using parsimony with TBR under DELTRAN optimisation. Uninformative characters were included. Tree length: 447 steps, CI = 0.459, RI = 0.758, RC = 0.348 and HI = 0.541.

The analyses of Whitlock's study (2011; Figure 7) yielded a parsimonious tree of 273 steps with a CI: 0.740 and RI: 0.844. The analyses of D'Emic's study (2012; Figure 5) yielded a parsimonious tree of 197 steps with a CI: 0.64 and RI: 0.80. These values indicate good and moderate fits, respectively, between the authors' morphological data and recovered phylogenies. The larger number of steps in the composite unaltered tree of Figure 20 can be attributed to the combination of two trees into one while the moderate values of the indices denote a moderately low fit between the composite data and the resulted hybrid phylogeny.

Herein, the recovered positions and interrelationships of, primarily, the pneumatically-studied taxa are briefly described in the published phylogenies of Whitlock (2011; Figure 7) and D'Emic (2012; Figure 5). In Whitlock's phylogeny, working from the most basal to the most derived positions, the outgroup and moderately-high pneumatic taxon *Omeisaurus* (PDI%=60) was recovered in a dichotomy with *Losillasaurus* in the most-basal position of the tree, while the other outgroup and moderately pneumatic, *Jobaria* (PDI%=53), was recovered to be paraphyletic to this dichotomous pair. Stepping into the Neosauropoda and, in particular, the Macronaria node, the highly pneumatic *Brachiosaurus* (PDI%=92) was positioned as a sister taxon to the moderately pneumatic *Australodocus* (PDI%=55) and the greatly pneumatic *Camarasaurus* (PDI%=75) was recovered to be a paraphyletic taxon to this pair. The node of basal Diplodocoidea recovered moderately pneumatic *Haplocanthosaurus* (PDI%=47) to be more basal than the moderately-high pneumatic *Amazonsaurus* (PDI%=73) which, in turn, is basal to the moderately pneumatic *Amphicoelias* (PDI%=63). Continuing on, the moderately pneumatic *Nigersaurus* (PDI%=69) was recovered to be a sister taxon to the Spanish rebbachisaurid (which is excluded in the current analyses). The moderately pneumatic *Cathartesaura* (PDI%=55) was recovered as a sister taxon to *Limaysaurus* in the Limaysaurinae node while the moderately pneumatic *Dicraeosaurus* (PDI%=63) was recovered as a sister taxon to *Brachytrachelopan* and the moderately-low pneumatic *Suuwassea* (PDI%=43) was positioned paraphyletically to the pair. Finally, the moderately pneumatic sauropods *Diplodocus* (PDI%=63) and *Barosaurus* (PDI%=59) were sister taxa and paraphyletic to the dichotomous pair of *Tornieria* (PDI%=60) and *Dinheirosaurus*. The last most derived taxa were *Supersaurus* and the moderately pneumatic *Apatosaurus* (PDI%=63).

In D'Emic's phylogeny, going from the most basal to the most derived taxa, the moderately-high pneumatic eusauropod Shunosaurus (outgroup) was recovered basalmost, followed by *Omeisaurus* and *Jobaria* outgroup taxa. *Camarasaurus* was recovered to be basal to the moderately-high macronarian *Tehuelchesaurus* (PDI%=71) followed by the moderately pneumatic titanosauriform *Europasaurus* (PDI%=59).

Furthermore, the trichotomy of the three brachiosaurids (*Abydosaurus*, *Cedarosaurus* and *Venenosaurus*) was recovered in a more derived positions than *Brachiosaurus* which was recovered to be more derived than the moderately-high pneumatic *Giraffatitan* (PDI%=69) and the moderately pneumatic somphospondylan *Sauroposeidon* (PDI%=60) was recovered to lie between the more basal *Ligabuesaurus* and more derived *Tastavinsaurus*. Euhelopodidae comprised of Qiaowanlong followed by the more derived and moderately pneumatic sauropod *Erketu* (PDI%=59), followed by a dichotomy of the moderately-high *Euhelopus* (PDI%=75) and *Daxiatitan*. The final two Euhelopodidae are the sister taxa *Tangvayosaurus* and the moderately pneumatic *Phuwiangosaurus* (PDI%=60). Delving into the last few and most derived taxa of Titanosauria, Lithostrotia, Saltasauridae and Saltasaurinae, *Chubutisaurus* was recovered basal to the highly pneumatic *Andesaurus* (PDI%=84), followed by the moderately-high pneumatic *Malawisaurus* (PDI%=68) which was basal to *Opisthocoelicaudia*, 'Saltasaurini' and the highly pneumatic and most derived sauropod *Alamosaurus* (PDI%=90).

In the unaltered composite phylogeny (Fig. 20), starting from the most basal positions and proceeding to the most derived ones, *Shunosaurus* was recovered as a basalmost clade followed by *Jobaria*. Contrary to Whitlock's phylogeny where *Omeisaurus* and *Losillasaurus* formed a dichotomous pair, here they formed a pair of sister taxa, paraphyletic to *Jobaria*. The resulted outgroup recoveries must have occurred as an effect of the addition of the question marks and the use of D'Emic's dataset for *Shunosaurus*. As expected, the interrelationships of the rest of Whitlock's and D'Emic's taxa were recovered here without any deviations. Simply, one half of the hybrid phylogeny was Whitlock's phylogeny and the other half was D'Emic's phylogeny The moderate value of consistency and homoplasy indices, as well as the very low value of rescaled consistency and high retention indices denote a moderate fit between the data and the resulted hybrid phylogeny (Fig. 20).

Focusing on the composite pneumatic D'Emic-Whitlock' hybrid tree, the taxa from the two original trees have different numbers of characters and a similar approach had to be taken to compensate for the lack of character states in the taxa. D'Emic's taxa had 119 characters while Whitlock's had 189. The taxa and their corresponding characters from both phylogenies were merged together, following the same procedure as in the 'McPhee-Yates' phylogeny. 15 original pneumaticity characters [(76, 77, 81, 82, 83, 85, 88, 89, 95, 103, 106, 111, 122, 133, and 134); see Appendix 2 'List of removed vertebral pneumaticity characters from the original matrices'] were removed from Whitlock's (2011) dataset and five [(17, 18, 21, 56 and 63); see Appendix 2 'List of removed vertebral pneumaticity characters from the original matrices'] from D'Emic's (2012) dataset (retrieved from the Supplementary Material files of these articles). This was applied in all taxa, pneumatically-

studied and not. This was done prior to the insertion of the 11 pneumaticity characters in the studied taxa of this project so as to avoid redundancy and, thus, misleading results. The datasets were carefully examined and no incongruencies with respect to the nature of the characters between D'Emic's (2012) and Whitlock's (2011) datasets were found. With the subtraction of the 15 original pneumaticity characters, Whitlock's character list was left with 189-15 = 174 characters. Adding the 11 pneumaticity characters in the studied taxa or, respectively, the 11 question marks in the non-studied ones, the total number of characters was 185. After the removal of the five original pneumaticity characters, D'Emic's dataset was left with 119-5 = 114 characters. The taxa where the 11 pneumaticity characters needed to be added were: *Shunosaurus (1111???????), Omeisaurus (11110011001), Jobaria (1100??00000), Haplocanthosaurus (101010?????), Amphicoelias (1110??10000), Amazonsaurus (??11??100??), Apatosaurus (01110010000), Barosaurus (111????????), Diplodocus (00101110000), Tornieria (00????0000?), Amargasaurus (1010??00???), Dicraeosaurus (1110010000?), Suuwassea (0101??00???), Cathartesaura (00????00???), Nigersaurus (0100??10???), Australodocus (11??????????*, *Camarasaurus (11101000000), Tehuelchesaurus (??1010?????), Europasaurus (11110010170), Giraffatitan (11110011000), Brachiosaurus (??100101000), Sauroposeidon (01??????????), Erketu (0000???????), Euhelopus (101010??000), Phuwiangosaurus (10101100000), Andesaurus (??100?01?00), Malawisaurus (00????00???), Alamosaurus (1010??00000),* and *'Saltasaurini' (*given the pneumaticity characters of *Saltasaurus - 00000000???)* – (29 common taxa among the two phylogenies and the taxa studied in this project).

The total number of taxa in this composite phylogeny was 48, out of which 29 were the ones that this project has pneumatically studied. These 29 taxa were assigned the 11 pneumaticity characters from this study. Adding the 60 question marks in D'Emic's dataset and then the 11 pneumaticity characters in the pneumatically-studied taxa the total number of 185 characters was reached. This was done in order to reach the number '185' so that all taxa have the same number of characters and also for the added 11 pneumaticity characters to occupy the same positions in both taxon-character matrices i.e. D'Emic's and Whitlock's (positions 174-185). These modifications made possible not only the process of these datasets by *PAUP* but it also made easier the tracking of the added pneumaticity characters. Concerning the unstudied taxa, 71 question marks had to be added to the 114 morphological characters with the aim to equalise with Whitlock's final number of 185 characters in total. The author acknowledges the fact that the addition of question marks in D'Emic's dataset to fill in the respective positions (126-173) of Whitlock's characters of taxa may not be the most favourable condition in a phylogenetic process since the paucity of data cannot give a true appreciation of the sauropods

interrelationships. The ideal condition would be for both datasets to have the same number of characters.

PAUP found 17 uninformative characters in the composite pneumatic hybrid dataset (118, 136, 138, 144, 145, 159, 161, 162, 166, 167, 169, 170, 173, 183, 184 and 185; see 'List of uninformative characters from the composite pneumatic examined matrices' in Appendix 2). All characters except from the last three can be attributed to either 'D'Emic's assigned question mark or Whitlock's character. Since some of the added pneumatic characters (183, 184 and 185) were found to be uninformative and the aim is to see their effect on the sauropod interrelationships, all uninformative characters were retained in the analyses. Employing the aforementioned parameters of parsimony, DELTRAN optimisation and TBR swapping method, the most parsimonious result of the composite pneumatic hybrid 'D'Emic-Whitlock' dataset yielded a tree of 461 steps, CI: 0.434, RI: 0.732, RC: 0.318 and HI: 0.566 (Fig. 21). A strict consensus tree can be seen in Figure 22. The composite non-modified 'D'Emic-Whitlock' tree (Fig. 20) was then loaded and imposed as a constraint on the composite pneumatic hybrid tree and the most parsimonious tree can be seen in Figure 23 and a strict consensus phylogeny in Figure 24.

In the composite pneumatic 'D'Emic-Whitlock' tree (Fig. 21) the outgroup taxa were recovered almost as in Figure 20 with the slight alteration that *Shunosaurus* was the basalmost taxon while *Omeisaurus* and *Jobaria* were recovered paraphyletic not only to each other but also to *Shunosaurus*. Paraphyletic to this group of taxa was recovered the pair of sister taxa *Camarasaurus* and *Brachiosaurus*. *Haplocanthosaurus* was recovered basal to *Atlasaurus* and *Tehuelchesaurus*. *Giraffatitan* was recovered as a sister taxon to *Amazonsaurus* as a monophyletic group with *Europasaurus* positioned paraphyletically not only with respect to them but also to *Abydosaurus*, *Cedarosaurus* and *Venenosaurus* which form another clade, sister to *Giraffatitan* and *Amazonsaurus*. The remaining somphospondylans retained their positions as in D'Emic's phylogeny with the exception that *Phuwiangosaurus* was paired as a sister taxon to *Daxiatitan* instead of Tangvayosaurus which was positioned as a separate monophyly to this group, in a more derived position with respect to *Qiaowanlong*. Paraphyletic to the aforementioned relationships is another large clade consisting of the diplodocoidean subclades. Histriasaurus was recovered a basal taxon to this clade which splits into two main subclades, one containing the flagellicaudatan diplodocid and the dicraeosaurids and the other subclade the rebbacchisaurids. *Tornieria* did not form a dichotomy with *Dinheirosaurus*; instead, *Dinheirosaurus* was recovered to be paraphyletic to *Amphicoelias*. Proceeding further to more derived taxa, *Apatosaurus* is basal to *Barosaurus* which was recovered as a sister taxon to *Australodocus* and *Diplodocus*

positioned as a sister taxon to this pair. *Tornieria* and *Supersaurus* retained their relative positions as paraphyletic to each other. *Brachytrachelopan* and *Dicraeosaurus* retained their position as sister taxa with *Amargasaurus* being immediately paraphyletic and *Suuwassea* one step further paraphyletic to that pair. *Zapalasaurus* and *Nigersaurus* were recovered as sister taxa and *Rebbachisaurus* a paraphyletic to them. *Limaysaurus* and *Cathartesaura* retained their position as sister taxa in a monophyletic subclade.
In the strict consensus tree (Fig. 22), the recovered interrelationships of the sauropod taxa have some similarities with respect to the original published phylogenies as opposed to the previously examined tree of Figure 21. *Shunosaurus* was recovered as the most basal clade, followed by the pair of *Omeisaurus* and *Losillasaurus*. *Jobaria*, *Atlasaurus* and *Tehuelchesaurus* were recovered with almost the same interrelationships as we see in Whitlock's phylogeny. *Europasaurus* and *Giraffatitan*, though, were recovered as a dichotomy and not in the expected sequence i.e. the latter being more derived than the former. Then, the trichotomy of the three brachiosaurids proceeded them, followed by *Amazonsaurus*. The taxa from *Europasaurus* to *Amazonsaurus* formed a clade of monophyletically related taxa separate from the rest of the taxa in this tree. *Ligabuesaurus* was recovered one position more basal to Sauroposeidon, as in D'Emic's phylogeny, followed by the remaining somphospondylans. A separate clade contained the remaining of Whitlock's diplodocoids. Their interrelationships were recovered quite differently, though. *Dinheirosaurus* was recovered in a dichotomy with *Apatosaurus* instead with *Tornieria*. Suuwassea was recovered to be basal to *Histriasaurus* instead of the opposite as seen in Whitlock's tree and *Rebbachisaurus*, *Limaysaurus*, *Cathartesaura*, *Zapalasaurus* and *Nigersaurus* formed a polytomy instead of being positioned in a deriving progression sequence, starting from *Nigersaurus* (more basal) up to *Rebbachisaurus* (more derived). Furthermore, D'Emic's Euhelopodidae were recovered more derived than the previous clades, with the difference here that *Euhelopus* was recovered more basal to *Daxiatitan* by the former taxon being placed paraphyletically one step more basal to the latter, instead of being in a dichotomy as in Whitlock's phylogeny. In addition, *Daxiatitan* was recovered as a sister taxon to *Phuwiangosaurus*. The diplodocids *Haplocanthosaurus* and *Amphicoelias* were recovered here in a dichotomy as moderately derived taxa and the bottom positions of this tree were occupied by the macronarian *Camarasaurus* being paraphyletic to the pair of sister taxa *Brachiosaurus* and *Australodocus*, as in Whitlock's phylogeny.

The resulted composite pneumatic tree in Figure 23 with the imposed constrained from the original unaltered composite hybrid tree (Fig. 20) was different than the previously described topologies. The outgroup taxa *Shunosaurus* and *Omeisaurus* were recovered in a dichotomy in the basalmost position of the tree. *Losillasaurus* was

recovered in a derived paraphyletic position with respect to the former taxa and the outgroup *Jobaria* in an even more derived position. Continuing progressively to the more derived members of this phylogeny, *Jobaria* was basal to *Atlasaurus* which, in turn, was basal to Tehuelchesaurus as in D'Emic's phylogeny. *Amphicoelias* was recovered to be more derived than *Jobaria* and then, from the node where *Amphicoelias* was placed, the tree was split into two major clades. One clade recovered D'Emic's macronarians, titanosauriforms and somphospondylans and the other one recovered Whitlock's diplodocids. In the first clade, the only deviations from the original phylogeny were the fact that *Daxiatitan* was not paired in a dichotomy with *Euhelopus* but instead was paraphyletic and one step more basal to *Euhelopus*. The other clade is split into two subclades. *Dinheirosaurus* was not recovered in a dichotomy with Tornieria but instead more basal to it. *Barosaurus* and *Diplodocus* were recovered as a pair of sister taxa (as in the original Whitlock's phylogeny) but *Histriasaurus* was recovered basal to *Rebbachisaurus* instead of the opposite. All other diplodocids maintained the interrelationships as were recovered in Whitlock's phylogeny. Lastly, *Camarasaurus* was recovered basal to *Brachiosaurus* which was recovered to pair with *Australodocus* as seen in Whitlock's phylogeny.

Finally, the strict consensus constrained tree of Figure 24 bears many similarities with both the previously described tree and the original phylogeny. *Shunosaurus* and Omeisaurus were paired in a dichotomy, with *Jobaria* positioned one derived step further and paraphyletic to them. The *Atlasaurus* was again recovered more basal to Tehuelchesaurus followed by *Europasaurus* being more basal to *Giraffatitan*. The tree brachiosaurids, *Abydosaurus*, *Cedarosaurus* and *Venenosaurus* were not recovered in a trichotomy, as in D'Emic's phylogeny, but instead *Abydosaurus* and *Cedarosaurus* were recovered as a pair of sister taxa with *Venenosaurus* to be immediately paraphyletic to them. The rest of the taxa maintained their interrelationships as they were in the original phylogenies with the exceptions that *Euhelopus* and *Tornieria* were not recovered in dichotomous pairs with *Daxiatitan* and *Dinheirosaurus*, respectively.

In all resulted examined topologies, the recovered interrelationships of the sauropod taxa can be attributed to the fact that, wherever there were common taxa between the two main original phylogenies, the author chose to use those taxa having the most assigned morphological characters i.e. from Whitlock's dataset. Another factor was probably the fact that all characters were treated as unordered as well as that all uninformative characters were included. Another factor of the altered relationships was the addition of the question marks, a necessary action to equalise the number of character states in D'Emic's shorter dataset with those in Whitlock's dataset for the purpose of merging them together in a 'supertree'. Moderate values of consistency, retention, rescaled consistency and homoplasy indices denote moderate fit between the combined

datasets and the resulted phylogenies. The deletion of the original pneumatic characters and the insertion of the pneumatic characters derived from this study caused minor changes in the composite pneumatic hybrid trees. Overall though, most taxa maintained their original interrelationships from the published phylogenies.

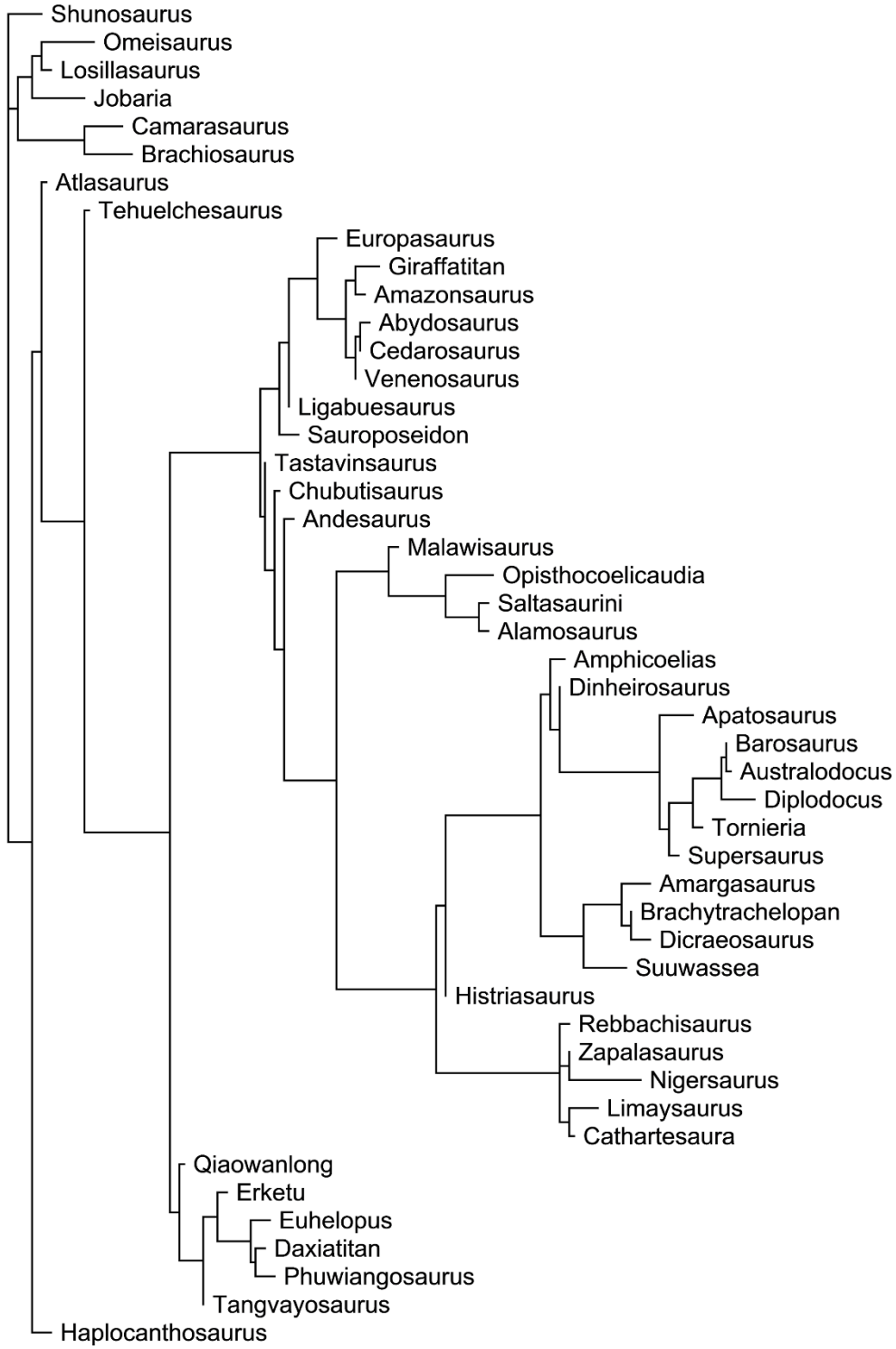

Figure 21. Composite pneumatic ‘D’Emic-Whitlock’ tree. Phylogeny consisting of 48 taxa and 185 characters. Assigned outgroups: *Omeisaurus*, *Shunosaurus* and *Jobaria*. Heuristic analysis using parsimony with TBR algorithm under DELTRAN optimisation yielded a tree of 461 steps, CI: 0.434, RI: 0.732, RC: 0.318 and HI: 0.566.

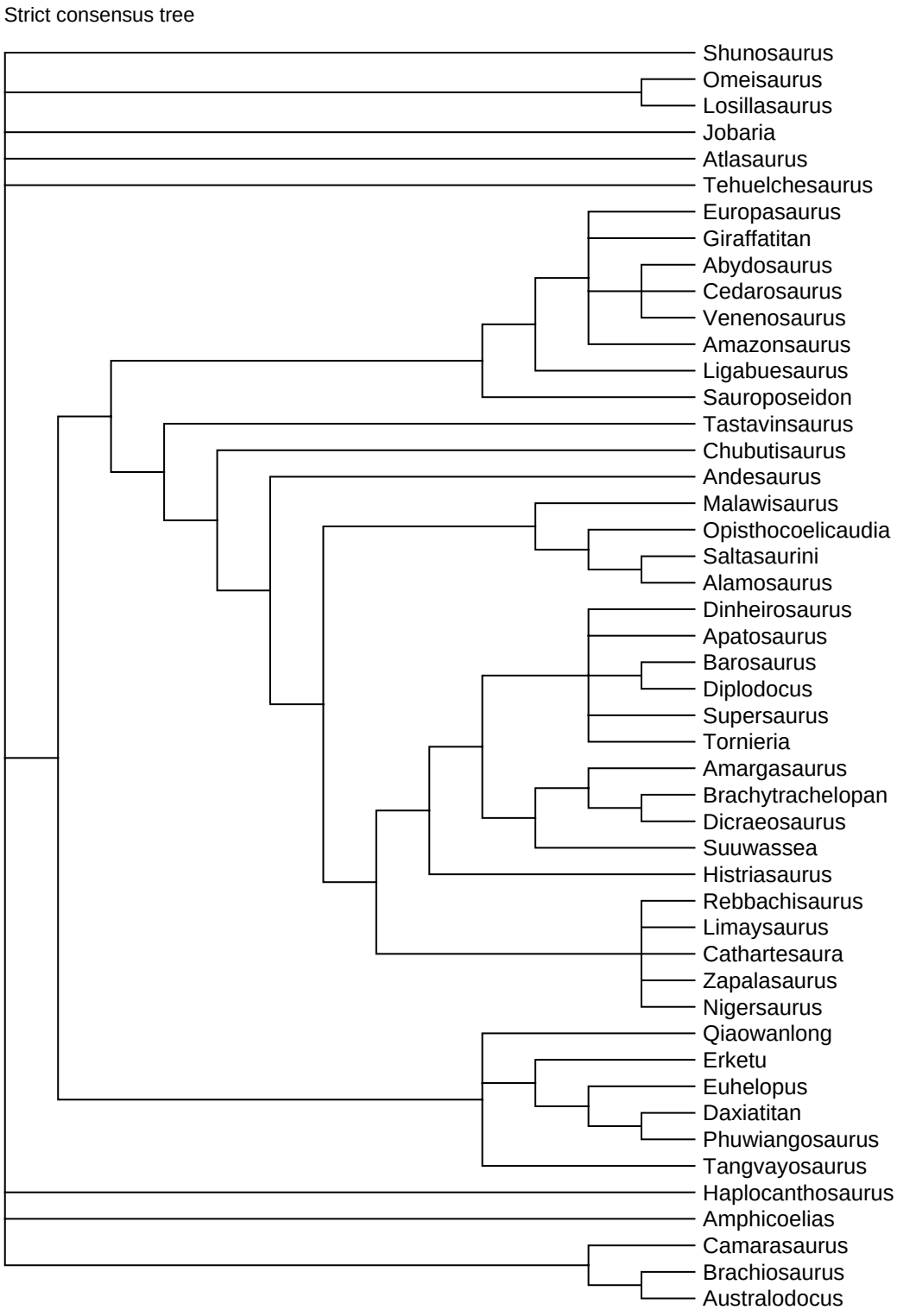

Figure 22. Strict consensus of the composite pneumatic 'D'Emic-Whitlock' trees. Strict consensus tree consisting of 48 taxa and 185 characters computed from the most parsimonious trees. Assigned outgroups: *Omeisaurus*, *Shunosaurus* and *Jobaria*.

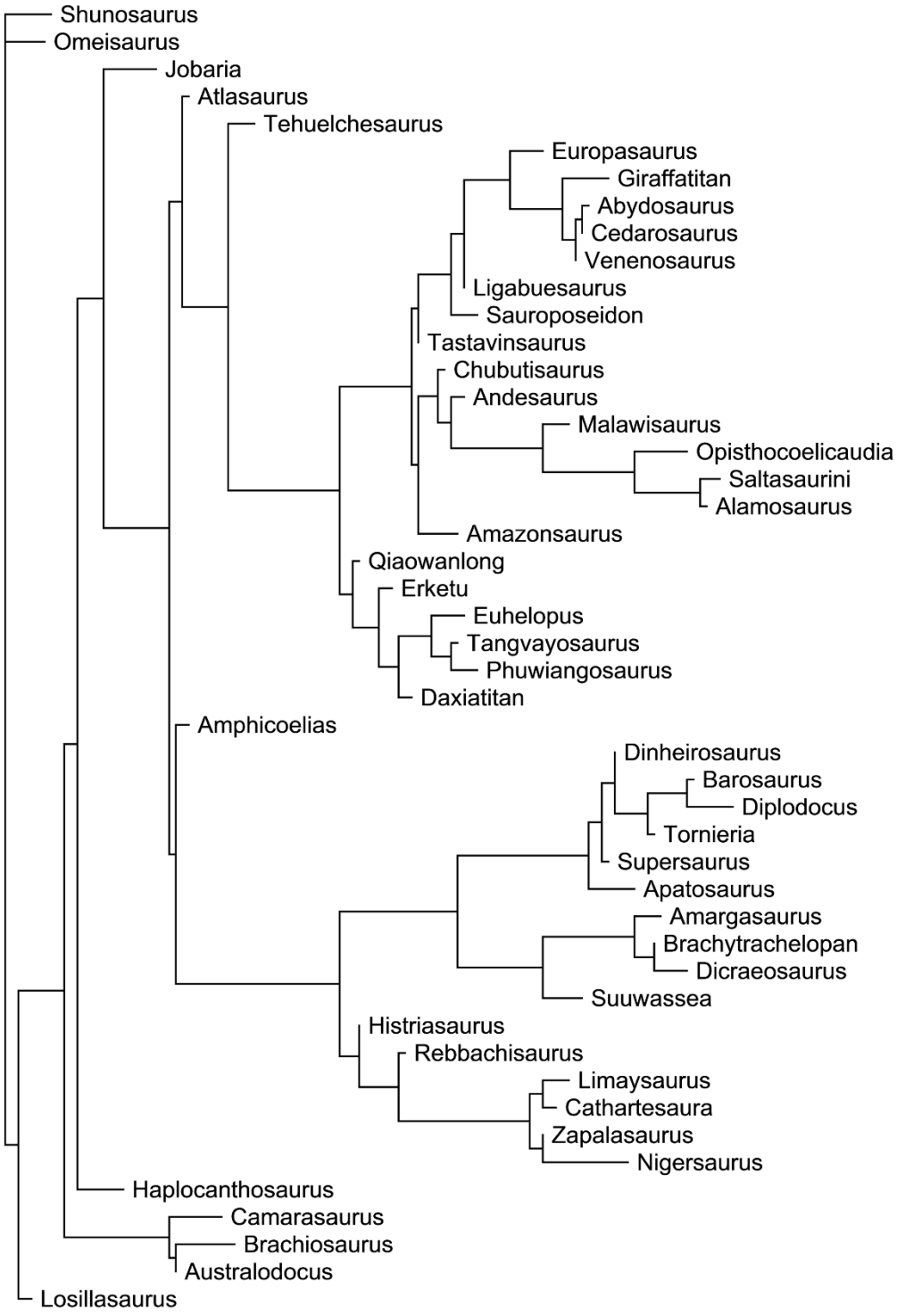

Figure 23. Constrained composite pneumatic 'D'Emic-Whitlock' tree. Heuristic analysis under parsimony, TBR and DELTRAN of the composite pneumatic tree consisting of 48 taxa and 185 characters with imposed constraint of the original unaltered composite 'D'Emic-Whitlock' phylogeny. Assigned outgroups: *Omeisaurus*, *Shunosaurus* and *Jobaria*. Tree length: 471 steps, CI: 0.425, RI: 0.722, RC: 0.306 and HI: 0.575.

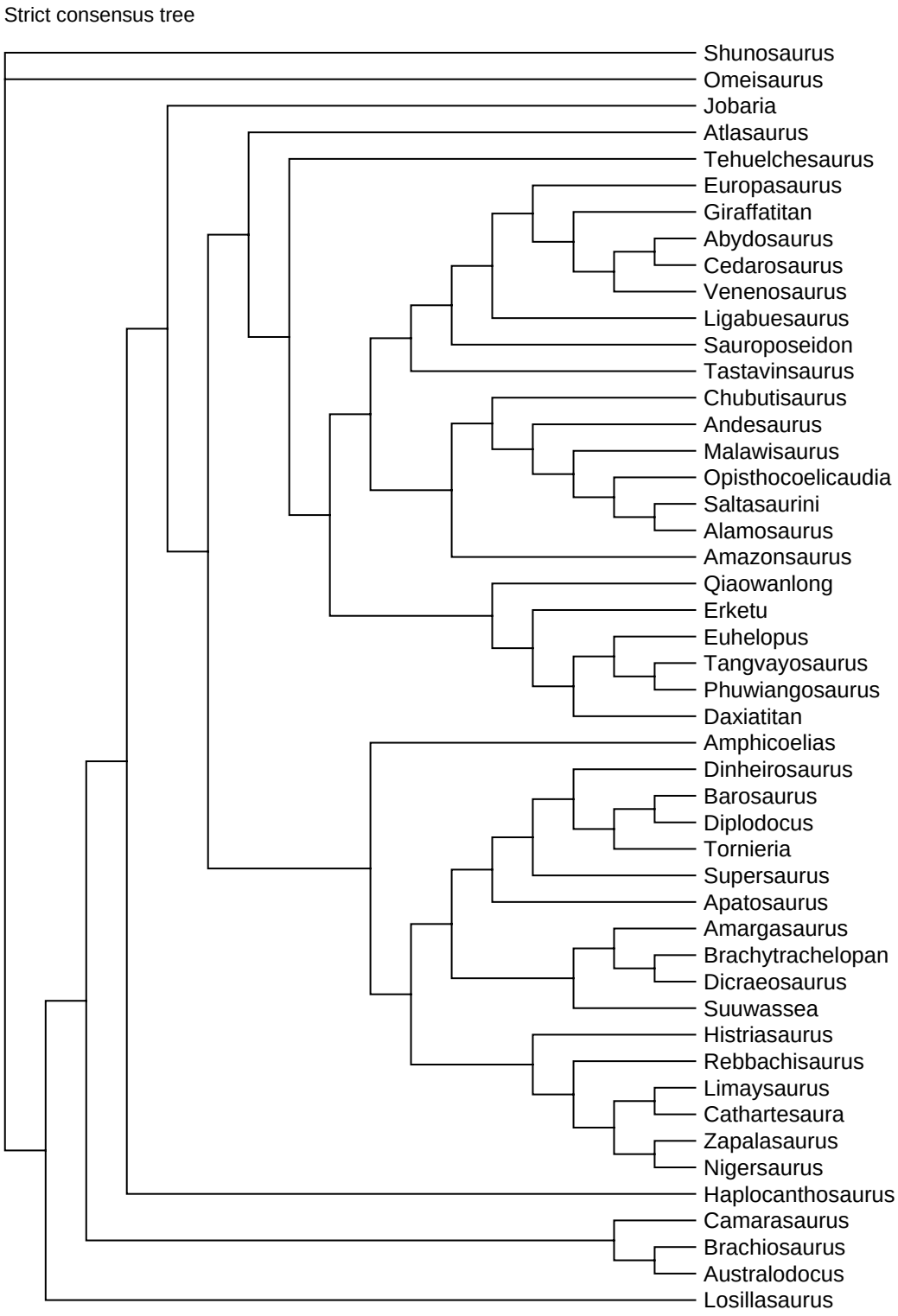

Figure 24. Constrained strict consensus 'D'Emic-Whitlock' tree. Strict consensus tree consisting of 48 taxa and 185 characters, obtained from the constrained parsimonious 'D'Emic-Whitlock trees. Assigned outgroups: *Omeisaurus*, *Shunosaurus* and *Jobaria*.

5.3.4) *Carballido & Sander (2014)*

Mesquite – discrete characters

The pneumatisation characters were firstly mapped on the normal phylogeny of this study, comprised of 70 taxa, which was then subsequently manipulated by adding the remaining taxa, resulting to 95 terminal taxa in total – arranged to best match their mostly accepted interrelationships. For basal Sauropodomorpha, interrelationships are based on the 'McPhee-Yates' tree. *Efraasia* and *Thecodontosaurus* are placed in more basal positions than *Plateosaurus* while, further down the tree towards the derived positions, *Camelotia* is more derived than *Antetonitrus* and *Lessemsaurus* and more primitive than *Vulcanodon*. *Kotasaurus* is more derived than *Barapasaurus* as the next most primitive eusauropod in this group, based on Yadagiri (2001) and Gillette (2003). *Spinophorosaurus* is positioned in a more basal place than *Shunosaurus*, after Sander et al. (2011). *Rhoetosaurus* is placed between *Barapasaurus* and *Shunosaurus* after Nair and Salisbury (2012). *Amphicoelias* is placed in a more derived position than *Nigersaurus* and is placed in a more basal position than *Amazonsaurus,* following Sander et al. (2011). *Australodocus* is positioned in a more derived place after the *Brachiosaurus-Giraffatitan* clade and basal to the group comprised of *Palyxusaurus*, *Abydosaurus*, *Cedarosaurus* and *Venenosaurus*, according to D'Emic (2012). Also, *Suuwassea*, based on the same study, is positioned before *Amargasaurus* (also in D'Emic, 2012). *Seismosaurus* is closer to *Diplodocus* than to *Apatosaurus*, according to Gillette (1991) and Tschopp et al., 2015, and thus is placed between them. The somphospondylan *Puertasaurus* is placed after *Argentinosaurus* based on more derived autapomorphic characters and later stratigraphic age (Novas et al., 2005). *Tornieria* is the sister taxon to *Diplodocus* + *Barosaurus* group (Remes, 2006). *Klamelisaurus* was considered to lie within Brachiosauridae and closer to *Camarasaurus* (placed in a more derived position than *Camarasaurus* and a more basal one than that of *Brachiosaurus-Giraffatitan*) following Zhao & Downs (1993) but recent evidence (Upchurch et al. 2004, 2011) has shown that *Klamelisaurus* is, in fact, a mamenchisaurid (eusauropod). *Ornithopsis* and *Eucamerotus* (Blows, 1995) are basal titanosauriformes (Mannion, 2010; Upchurch et al. 2011; Mannion et al., 2013) and are placed in a more basal position than that of *Brachiosaurus*. *Pleurocoelus* exact position is uncertain but Gallup (1989), Salgado et al. (1997) and Wedel et al. (2010) have placed it within the macronarian clade. *Huanghetitan* (Junchang et al., 2007) is a somphospondylan placed in a more derived position than *Malawisaurus* and *Rapetosaurus*. *Sauroposeidon,* as a somphospondylan, is placed in the somphospondylan group (Mannion et al., 2017), in a more derived position with respect to the *Brachiosaurus-Giraffatitan* clades, based on Mannion & Calvo (2011), D'Emic (2012),

Mannion et al. (2013) and Mannion et al. (2017). Bonaparte (2000) states a close relationship between Camarasauridae and *Janenschia* (here, is placed in a more derived position than *Camarasaurus* and in a more basal one than that of *Brachiosaurus*). Recent cladograms from studies of Mannion et al. (2013) and Upchurch et al. (2015) support the position of *Janenschia* being a basal macronarian. According to Junchang et al (2008), *Dongyangosaurus* is a somphospondylan from the Late Cretaceous; here it is placed within Somphospondyli [based on Mannion et al. (2013) and Poropat et al. (2015), (2016) who used updated versions of this matrix], after *Huanghetitan* (Lu et al., 2008). *Futalognokosaurus* is sister taxon to *Mendozasaurus* (Calvo et al., 2007). *Neuquensaurus* is placed in a more derived position than that of *Saltasaurus*, based on Salgado et al. (2005).

Analyses of the pneumaticity characters on the normal phylogeny revealed them to have a fit below average (Fig. 25). Nevertheless, and as it is shown in previous cases, the evolution of a character (‘C1c’) throughout the sauropodomorph phylogeny can be viewed across a wide spectrum of taxa. Tree values using the entire set of pneumaticity characters resulted a TL = 684, CI = 0.39 and RI = 0.11. Trees with more reconstructions of pneumaticity characters can be found in Appendix 2.

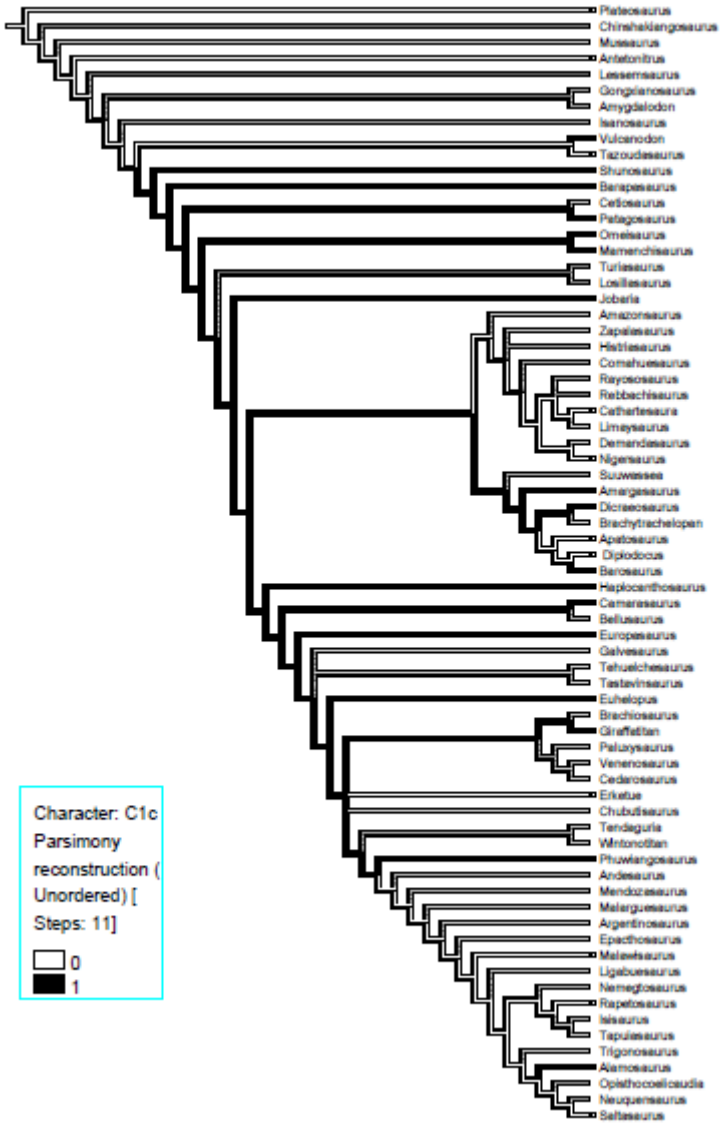

Figure 25. Parsimony reconstruction of character ‘C1c’ (cervical) in 70 taxa in the ‘Carballido & Sander’ phylogeny. Evolution of character ‘C1c’ (cervical) in the normal phylogeny of ‘Carballido & Sander (2014)’ across 70 taxa under parsimony. Grey branches indicate ‘unknown’ data. Tree values from matrix for this tree: TL = 684, CI = 0.39 and RI = 0.11.

In this phylogeny, not many taxa share ‘C1c’ (Fig.26) in their cervical series. Few of the most pneumatic taxa (Appendix 3) possess this trait but ‘C8c’ taxon expression is higher than ‘C1c’ for this series. In the dorsal series we see again a wider distribution of pneumatisation in nearly all taxa with some brief gaps in the phylogeny. Pleurocoelous fossae in the dorsal centra is a less frequent feature in this phylogeny than having pleurocoelous centra, as we have observed in previous cases (see also ‘Tree figures’ in Appendix 2). Very few eusauropods, and then few taxa from each subfamily, variably express the character ‘C8c’ in their dorsal series. These sauropods have different body

masses and lengths and thus the only similar features they may possess are their morphological subfamilial synapomorphies. Pleurocoels in the sacral centra (Appendix 3) is a feature shared among two diplodocoids (*Haplocanthosaurus, Diplodocus*), three macronarians (*Tehuelchesaurus*, *Camarasaurus*, *Euhelopus*) and one somphospondylan (*Phuwiangosaurus*). Pneumaticity in the sacral neural spines is only developed in very few diplodocids and titanosauriformes as is the case with the occurrence of caudal foramina in the centra. Fossae in the caudal centra are mostly developed in Early neosauropods and less in titanosauriformes. The character 'D2' seems to be shared only by *Plateosaurus* and *Europasaurus*. Perhaps the reason for this lies in the fact that they were both small for sauropod standards and similarly sized in terms of mass and length, even though *Plateosaurus* was a facultative and not an obligatory graviportal quadrupedal animal like *Europasaurus*. It is easy to assume that despite both having relatively small size, the most massive part of their body and centre of mass would be close to their pelvic system; therefore, such a trait may have been useful in weight reduction. This trait is expected to be found in more derived sauropods and not in a basal sauropodomorph where the only pneumatic (though ambiguous) characteristics are fossae. It may be either a rare morphological oddity or a diagenetic artefact.

Resulting in a longer tree length, lower CI and slightly higher RI, analyses on the extended composite phylogeny revealed an even poorer fitness of the pneumaticity characters than in the normal phylogeny (Fig.26a). Figs.26b – 26i can be viewed in Appendix 2.

Figure 26a. Parsimony reconstruction of character 'C1c' (cervical) in 95 taxa in the 'Carballido & Sander' composite phylogeny. Evolution of character 'C1c' (cervical) in the composite extended phylogeny of 'Carballido & Sander (2014)' across 95 taxa under parsimony. Grey branches indicate 'unknown' data. Tree values from matrix for this tree: TL = 916, CI = 0.32, and RI = 0.12.

Mesquite - continuous characters

Metric characters of PDI% total average, body mass, body length and femur length were mapped across both normal and composite extended phylogenies resulting in 2 pairs of 4 trees depicting metric distributions. Evolution of PDI% along the 70 and 95 taxa phylogenies can be easily traced and comparisons with the other metric data are evident (Figs.27-34).

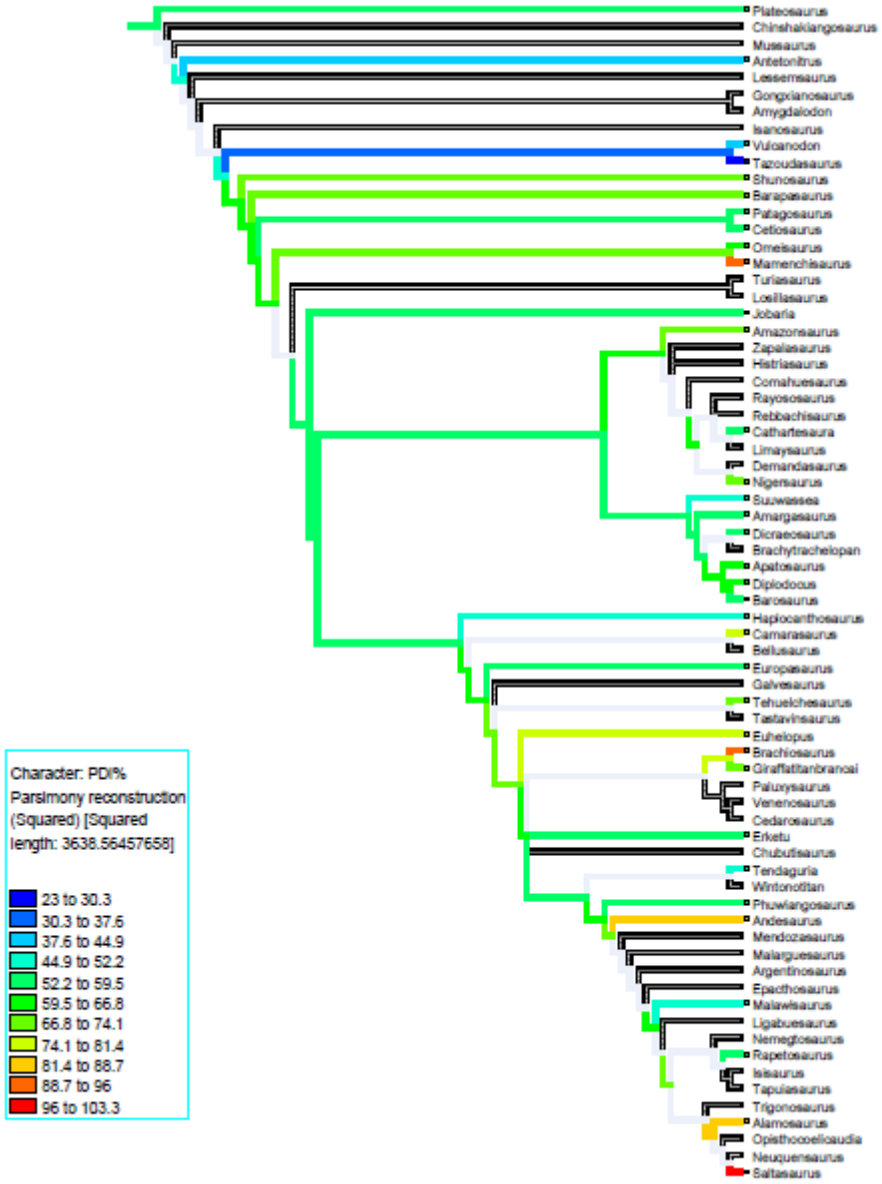

Figure 27. Distribution of total average PDI% in the 'Carballido & Sander' composite phylogeny. Evolution of PDI% in 70 sauropodomorph taxa of the normal 'Carballido & Sander (2014)' phylogeny, demonstrating the distribution of total average pneumatisation across the phylogeny. The evolution of PDI% is nearly gradual with the noticeable sudden increases, evident in *Mamenchisaurus, Brachiosaurus, Alamosaurus* and *Saltasaurus.* Grey branches indicate 'unknown' data.

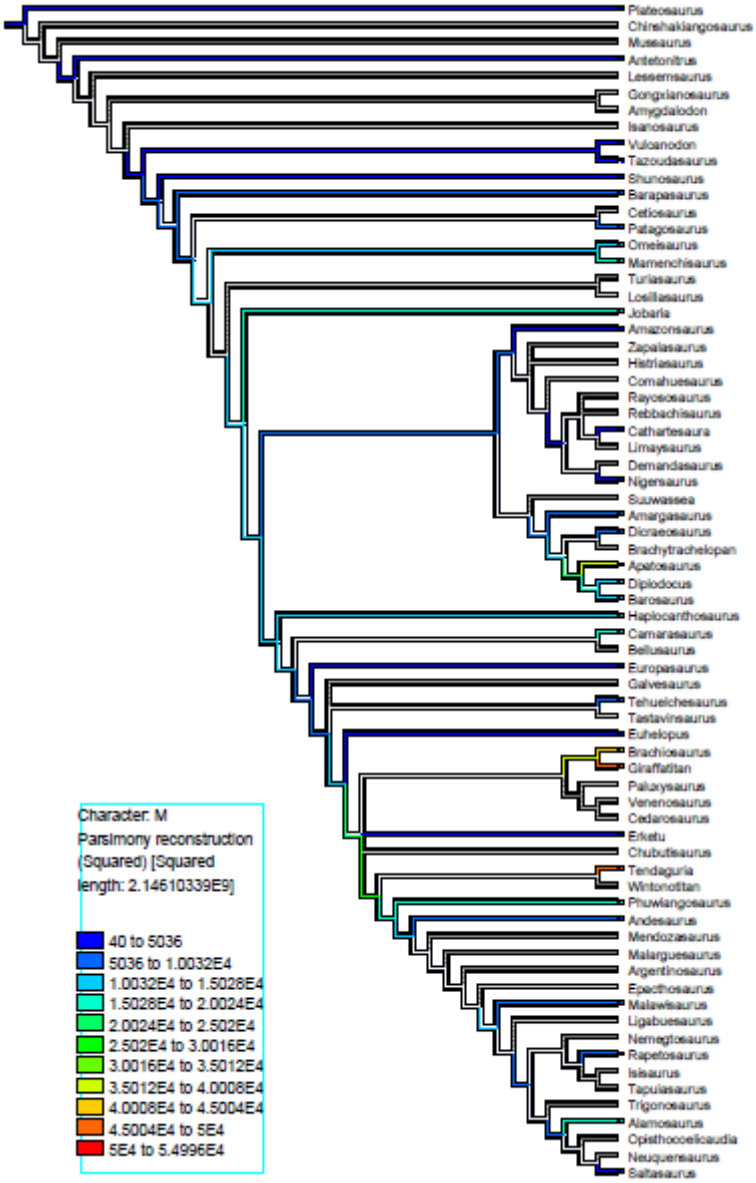

Figure 28. Body mass distribution in the 'Carballido & Sander' composite phylogeny. Distribution of body mass (M, in kilogrammes) across 70 sauropodomorph taxa of the normal 'Carballido & Sander (2014)' phylogeny. Grey branches indicate 'unknown' data.

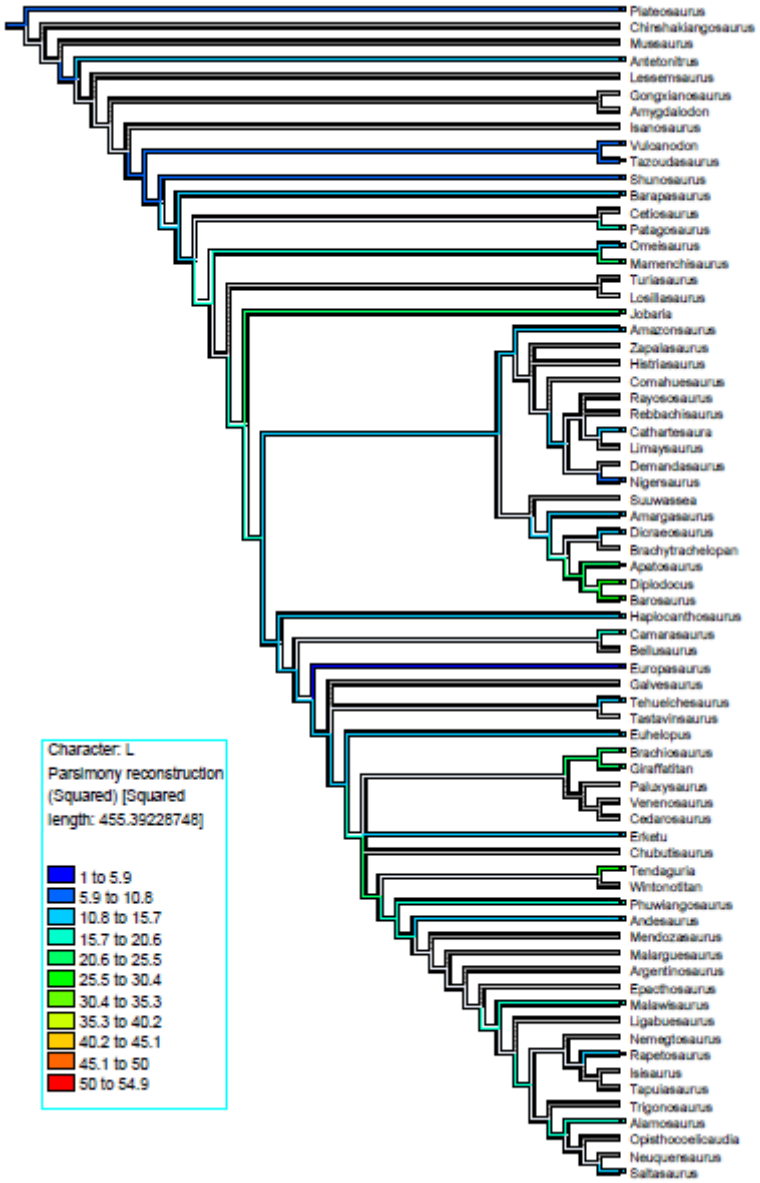

Figure 29. Body length distribution in the 'Carballido & Sander' composite phylogeny. Distribution of body length (L, in metres) across 70 sauropodomorph taxa of the normal 'Carballido & Sander (2014)' phylogeny. Grey branches indicate 'unknown' data.

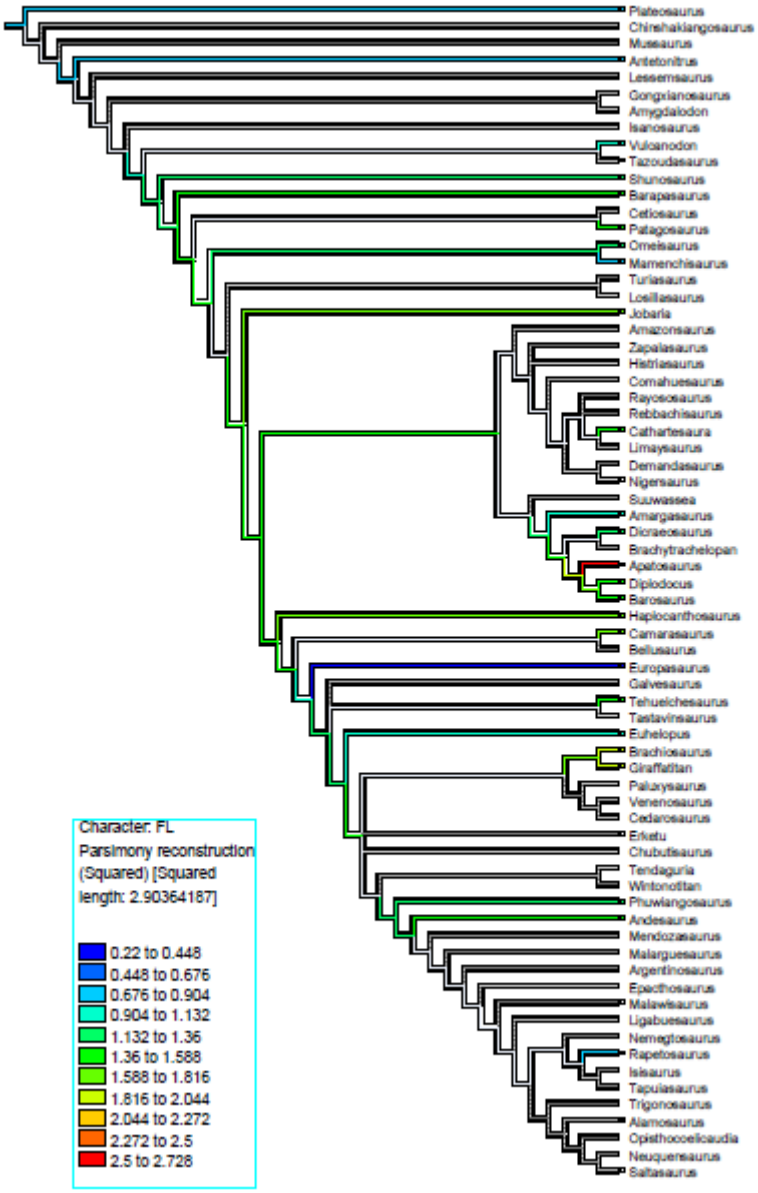

Figure 30. Femur length distribution in the 'Carballido & Sander' composite phylogeny. Distribution of femur length (FL, in metres) across 70 sauropodomorph taxa of the normal 'Carballido & Sander (2014)' phylogeny. Grey branches indicate 'unknown' data.

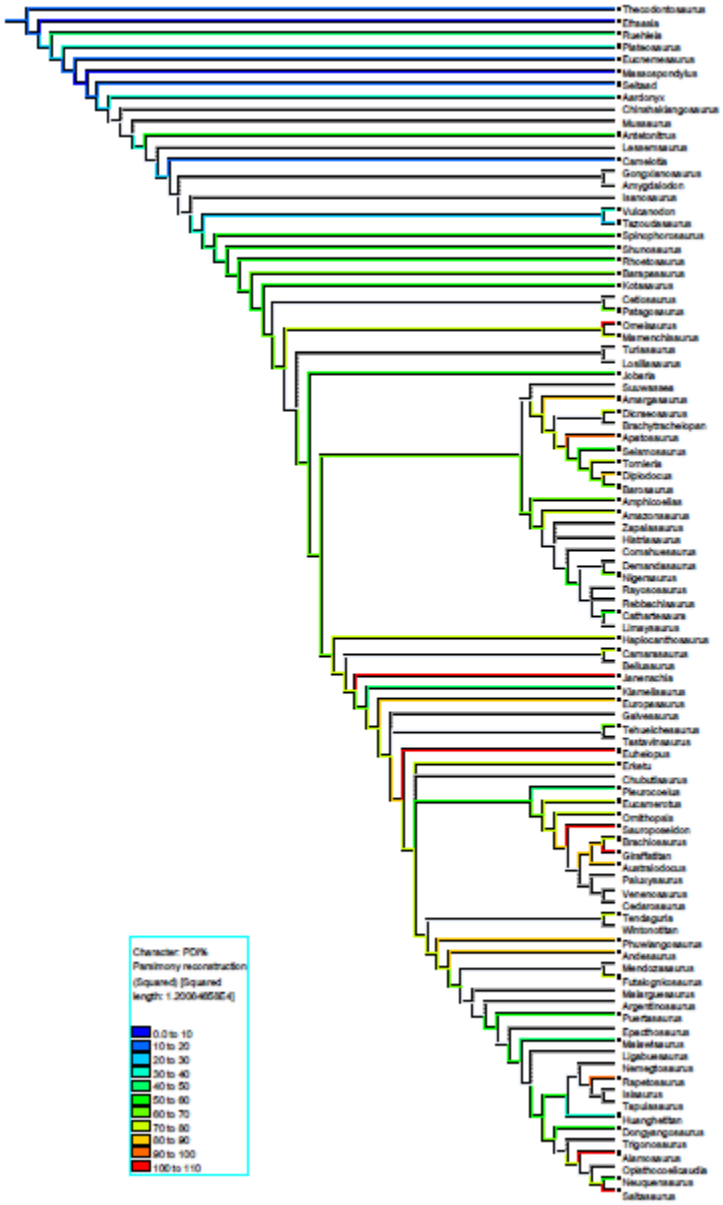

Figure 31. Distribution of total average PDI% in the 'Carballido & Sander' extended composite phylogeny. Evolution of PDI% in 95 sauropodomorph taxa of the extended composite 'Carballido & Sander (2014)' phylogeny, demonstrating the distribution of total average pneumatisation across this broad phylogeny. The evolution of PDI% is nearly gradual with the noticeable sudden increases, evident in *Omeisaurus, Apatosaurus, Janenschia, Euhelopus, Sauroposeidon, Giraffatitan, Rapetosaurus, Alamosaurus* and *Saltasaurus.* Grey branches indicate 'unknown' data.

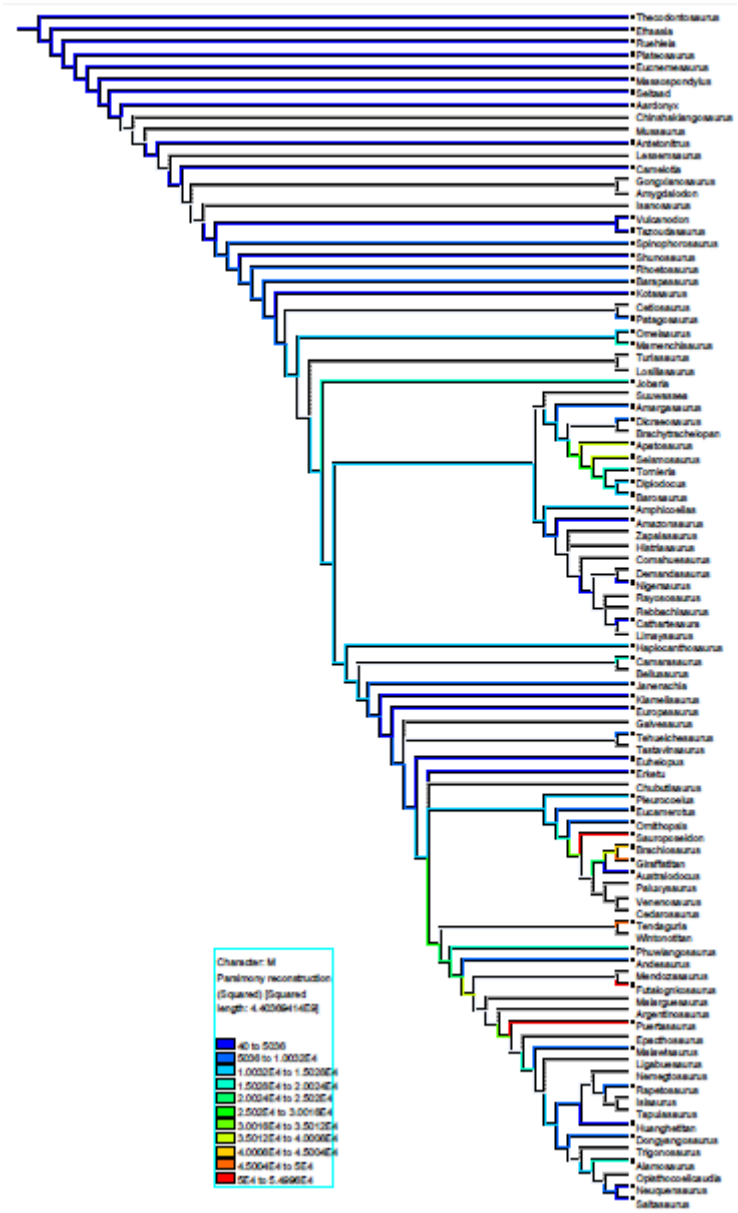

Figure 32. Body mass distribution in the 'Carballido & Sander' extended composite phylogeny. Distribution of body mass (M, in kilogrammes) across 95 sauropodomorph taxa of the extended composite 'Carballido & Sander (2014)' phylogeny. Grey branches indicate 'unknown' data.

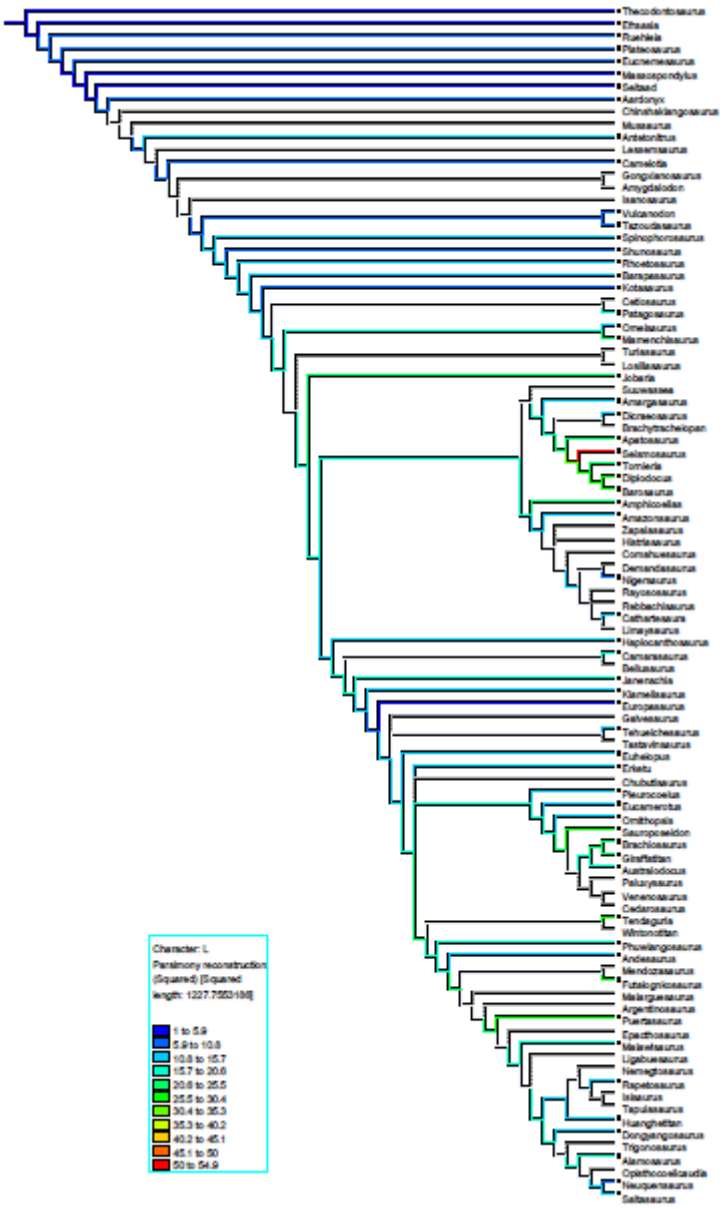

Figure 33. Body length distribution in the 'Carballido & Sander' extended composite phylogeny. Distribution of body length (L, in metres) across 95 sauropodomorph taxa of the extended composite 'Carballido & Sander (2014)' phylogeny. Grey branches indicate 'unknown' data.

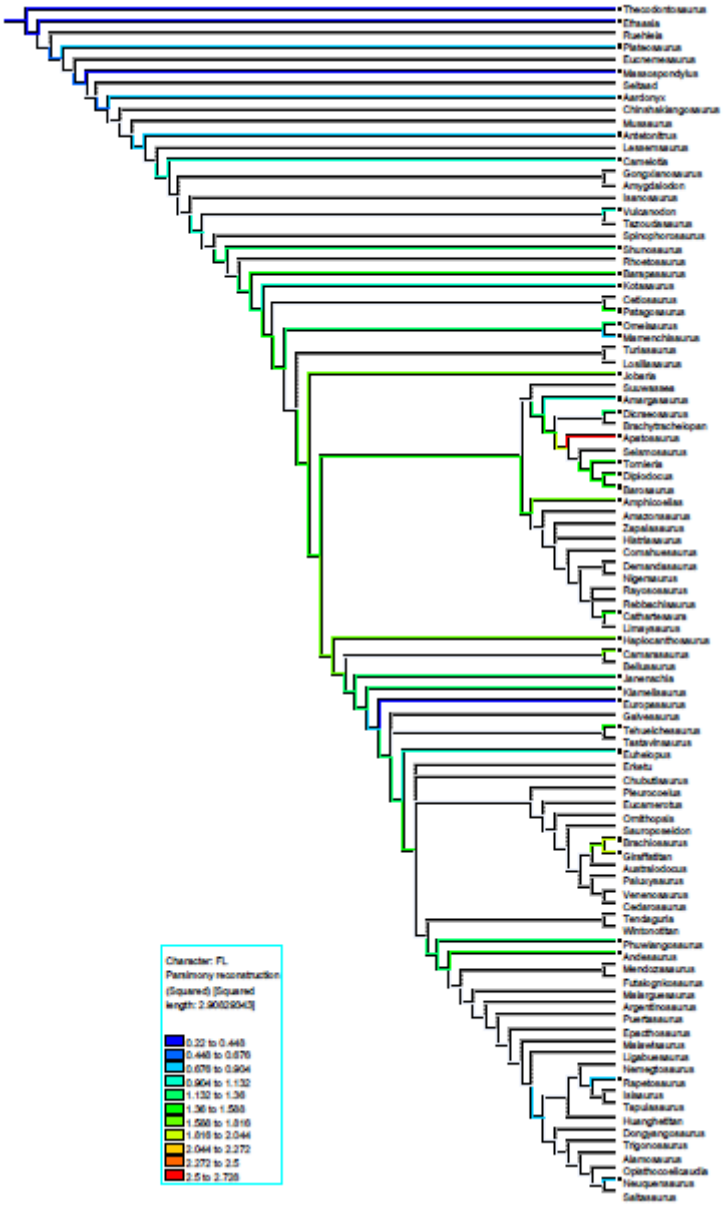

Figure 34. Femur length distribution in the 'Carballido & Sander' extended composite phylogeny. Distribution of femur length (FL, in metres) across 95 sauropodomorph taxa of the extended composite 'Carballido & Sander (2014)' phylogeny. Grey branches indicate 'unknown' data.

The same patterns and observations described above apply for the 95-taxa composite phylogeny (Figs.27a – 27i in Appendix 2) as well as for the phylogeny consisting only of the 61 taxa (Figs.42a – 42i in Appendix 2) examined in this study. Overall, pneumaticity increases in a nearly gradual manner with few peaks of high expression in few taxa from almost every subfamily and it also originates from the dorsal series, expanding mostly to the cervical and less towards the sacral and caudal series.

The recorded observations of this current project corroborate the observations and interrelationships of Sauropodomorpha extrapolated by previous researches with regard to their vertebral morphologies. *Jobaria* and all Neosauropoda (Bonaparte, 1986) have divided pleurocoels in cervical vertebrae (Upchurch, 1995), as well as pre-spinal and post-spinal laminae present on anterior caudal neural spines (Wilson, 2002). This study has also revealed that Neosauropoda also share characters: 'C1c', 'C4c', 'C8c', 'C19na', 'C2c', 'C101tp', 'C3c', 'C120p', 'C33ns', 'C28na', 'C12c', 'C13c', 'C43ns', 'C164con' and 'C91tp' in their cervicals; 'C1c', 'C8c', 'C43ns', 'C101tp', 'C2c', 'C19na', 'C28na', 'C91tp', 'C113d' and 'C116d' in their dorsals; 'C1c', 'C28na', 'C33ns', 'C92tp', 'C2c', 'C19na' and 'C4c' in their sacrals; 'C1c', 'C3c', 'C4c', 'C19na' and 'C43ns' in their caudals; and, finally, 'D2' and 'D5' in their pelvic bones (for character explanation and detailed lists of pneumatic synapomorphies per taxa group see Table 3 in Chapter 2 and Appendix 4).

Evolution and correlation between PDI% and body mass, body length and femur length

The number of the unknown taxa in this phylogeny is higher than in previous phylogenies, thus obscuring the evolution of pneumatisation through phylogeny and evolutionary time making it more difficult to draw any sensible patterns. The 'increase – decrease' patterns of pneumatisation are more irregular and sudden. Similar but smoother patterns are evident in the other mapped metric data on this phylogeny. Similar streams of assumptions can be made of the taxa with unknown metric data, as in the previous case of phylogeny, about their probable levels of pneumatisation, based on the levels of their bracketing or sister taxa. Overall, there seems to be no general pattern, neither a gradual increase from basal sauropodomorphs to somphospondylans but in most major subfamilies (i.e., basal Sauropodomorpha, Eusauropoda, Diplodocoidea, Macronaria and Somphospondyli) there is a noticeable general pattern in each subfamily, best described as starting (in evolutionary terms) with low-value taxa and finishing with high-value taxa. Perhaps this is the pattern; in every major speciation event which results in a new subfamily group, there is a gradual increase in vertebral pneumatisation within the context of that group, an increase usually matched by increase in size.

PAUP – discrete characters

The last morphological matrix for this set of analyses is that of Carballido & Sander (2014). The total number of the original phylogenetic matrix consists of 70 taxa and 341 morphological characters. 12 characters that refer to pneumaticity were removed [(114, 115, 120, 124, 135, 139, 144, 145, 147, 179, 186 and 194); see Appendix 2 'List of

removed vertebral pneumaticity characters from the original matrices] from all taxa in order to avoid redundancy in the analyses. The 11 pneumaticity characters were added to the 35 pneumatically-studied taxa (having 341 initial characters minus 12 = 329; 329 plus 11 = 340. 11 question marks, '?', were also added to the non-studied taxa to equalise the number of characters per taxon for all taxa in the dataset. The 35 taxa with the added 11 pneumaticity characters were: *Plateosaurus (00000000000), Antetonitrus (0000???????), Vulcanodon (10??0001000), Tazoudasaurus (0000???????), Shunosaurus (1111???????), Barapasaurus (10100000000), Cetiosaurus (10100001000), Patagosaurus (1010??01???), Omeisaurus (11110011001), Mamenchisaurus (1110???????), Jobaria (1100??00000), Haplocanthosaurus (101010?????), Camarasaurus (11101000000), Europasaurus (111100101?0), Tehuelchesaurus (??1010?????), Euhelopus (101010??000), Brachiosaurus (??100101000), Giraffatitan (11110011000), Erketu (0000???????), Tendaguria (??11???????), Phuwiangosaurus (10101100000), Andesaurus (??100?01?00), Malawisaurus (00????00???), Rapetosaurus (01010000000), Alamosaurus (1010??00000), Neuquensaurus (00110000?0?), Saltasaurus (00000000???), Amazonsaurus (??11??100??), Cathartesaura (00????00???), Nigersaurus (0100??10???), Suuwassea (0101??00???), Amargasaurus (1010??00???), Dicraeosaurus (1110010000?), Apatosaurus (01110010000), Diplodocus (00101110000)* and *Barosaurus (111????????)*. 17 uninformative characters were identified by *PAUP* [(62, 80, 92, 93, 98, 104, 169, 173, 188, 209, 215, 238, 266, 300, 338 and 340); see Appendix 2 'List of uninformative characters from the composite pneumatic examined matrices']. They were kept included in the analyses since the last three of them belong to the set of the 11 added pneumaticity characters.

All analyses were conducted with heuristic search in parsimony using TBR swapping algorithm and under the same parameters as Carballido & Sander (2014) did when they conducted their analyses in *TNT*. The published tree (Carballido & Sander, 2014; Figure 29) is 998 steps long with CI: 0.406 and RI: 0.725. An initial set of analyses were first performed using the dataset as it was published by Carballido & Sander (2014) so as not only to retrieve the Newick format of the resultant tree in order to impose it as a constraint later but also for comparative reasons. The authors did not specify an outgroup taxon or list of taxa that served as outgroups. In the authors resultant tree (Carballido & Sander, 2014; Figure 29) four taxa (*Plateosaurus*, *Chinshakiangosaurus*, *Mussaurus* and *Antetonitrus*) were recovered prior to the node of Sauropoda, so I conducted preliminary experimental analyses with and without treating them as outgroups. In addition, the authors did not specify if they applied their analyses employing ACCTRAN or DELTRAN optimisation, so I experimentally ran the aforementioned analyses (with and without

outgroups) in both optimisation techniques. The resultant phylogenies (most parsimonious and strict consensus) were almost identical in both form and scores, whether retaining the outgroups or not, in either ACCTRAN or DELTRAN. The analyses I performed on the same dataset under the same parameters without assigning the outgroups (in either optimisations) yielded a tree of 1049 steps, CI: 0.438, RI: 0.725, RC: 0.317 and HI: 0.614. The analysis that included the outgroups yielded a tree of 1050 steps, CI: 0.437, RI: 0.724, RC: 0.317, HI: 0.614 (Fig. 35). As in previous analyses that involved *PAUP*, the first run of analyses was carried out with no topological constraints in effect. The resultant tree (Fig. 35) was 1050 steps long, with CI: 0.437, RI: 0.724, RC: 0.317 and HI: 0.614. The strict consensus tree (Fig. 36) yielded a remarkably similar tree to that of Figure 29 (Carballido & Sander, 2014). The pneumatically modified version yielded a most parsimonious tree of 1028 steps, with CI: 0.433, RI: 0.705, RC: 0.305 and HI: 0.615 Fig. 37). The computed strict consensus (Fig. 38) tree recovered several polytomies not existing in the published phylogeny. Then, the phylogeny of the unaltered phylogeny (Fig. 35) was imposed on the pneumatically modified tree as a constraint and the same set of computational parameters were applied. The result was a most parsimonious tree of 1031 steps, CI: 0.432, RI: 0.703, RC: 0.303 and HI: 0.615 (Fig. 39). Finally, the strict consensus was computed from the constrained parsimonious trees and the resultant phylogeny did not recover any polytomies (Fig. 40). The moderately larger tree lengths and values of indices of the resultant trees than the ones produced by the published phylogeny show similarity among the resultant trees produced here and the tree shown in Figure 29 (Carballido & Sander, 2014) and indicate a moderate fit between the datasets and the produced phylogenies.

Figure 35. Most parsimonious tree of the unaltered 'Carballido & Sander (2014). Heuristic search in parsimony using TBR algorithm of the published dataset containing 70 taxa and 341 characters. Assigned outgroups were the taxa *Plateosaurus, Chinshakiangosaurus, Mussaurus* and *Antetonitrus*. Tree length: 1050 steps, CI: 0.437, RI: 0.724, RC: 0.317 and HI: 0.614.

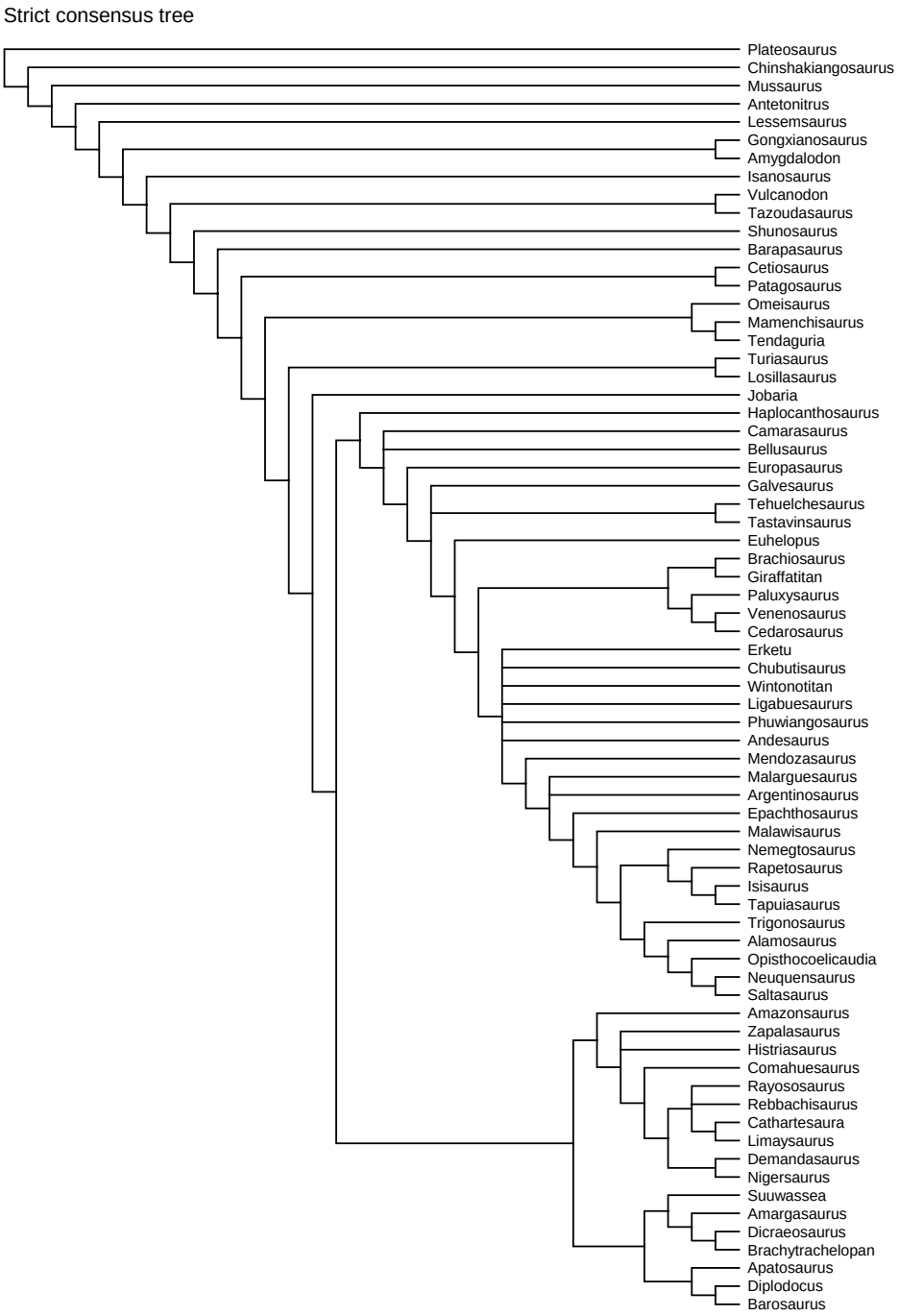

Figure 36. Strict consensus tree - unaltered 'Carballido & Sander (2014)'. Computed strict consensus from the non-modified 'Carballido & Sander (2014)' most parsimonious trees. Assigned outgroups were the taxa *Plateosaurus, Chinshakiangosaurus, Mussaurus* and *Antetonitrus*. A polytomy was recovered among few somphospondylan taxa.

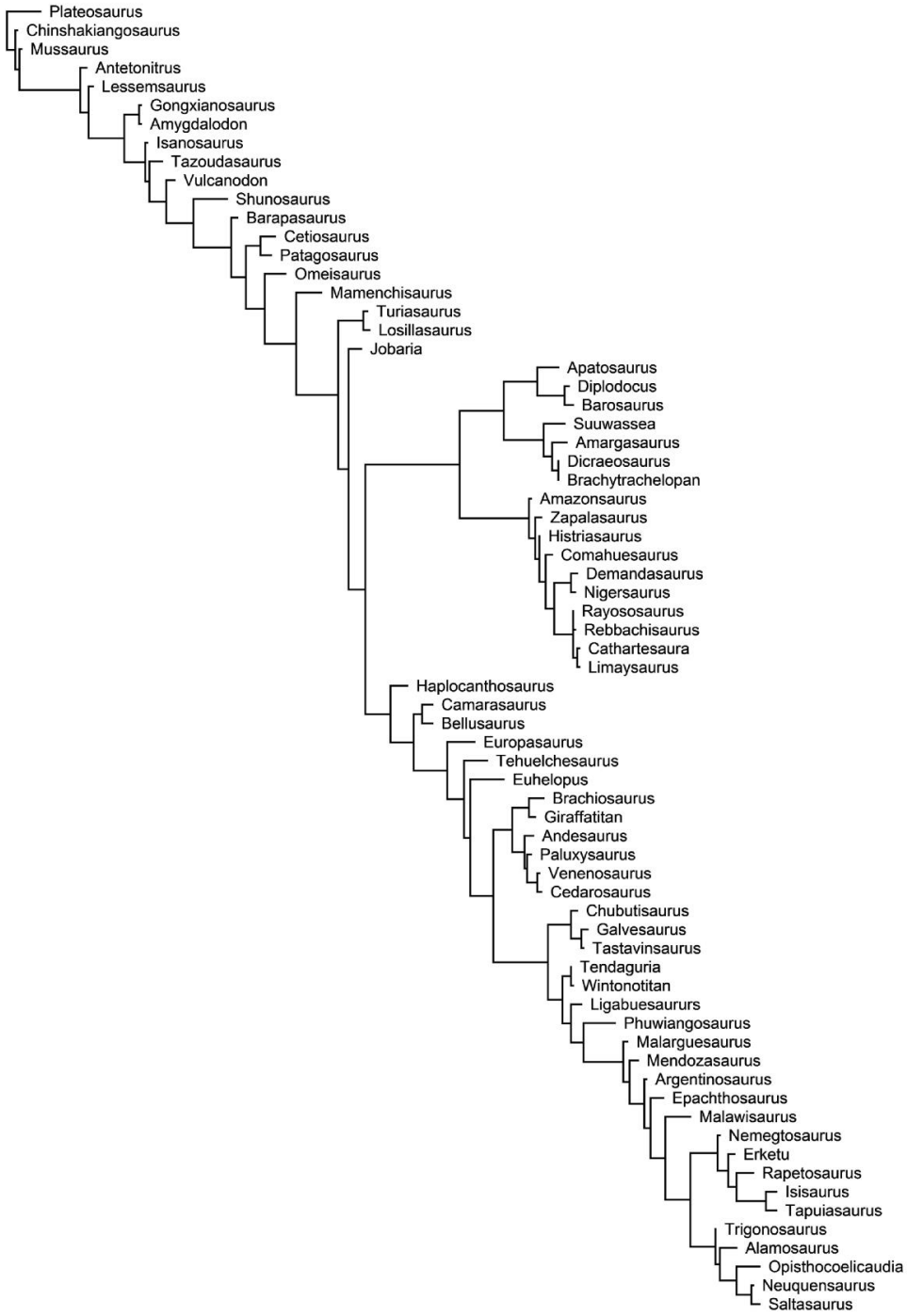

Figure 37. Most parsimonious tree of the pneumatically modified 'Carballido & Sander (2014). Heuristic search in parsimony using TBR algorithm of the published dataset containing 70 taxa and 340 characters. Original pneumaticity characters were removed and replaced with the eleven ones derived from this study. Assigned outgroups were the taxa *Plateosaurus, Chinshakiangosaurus, Mussaurus* and *Antetonitrus*. Tree length: 1028 steps, CI: 0.433, RI: 0.705, RC: 0.305 and HI: 0.615.

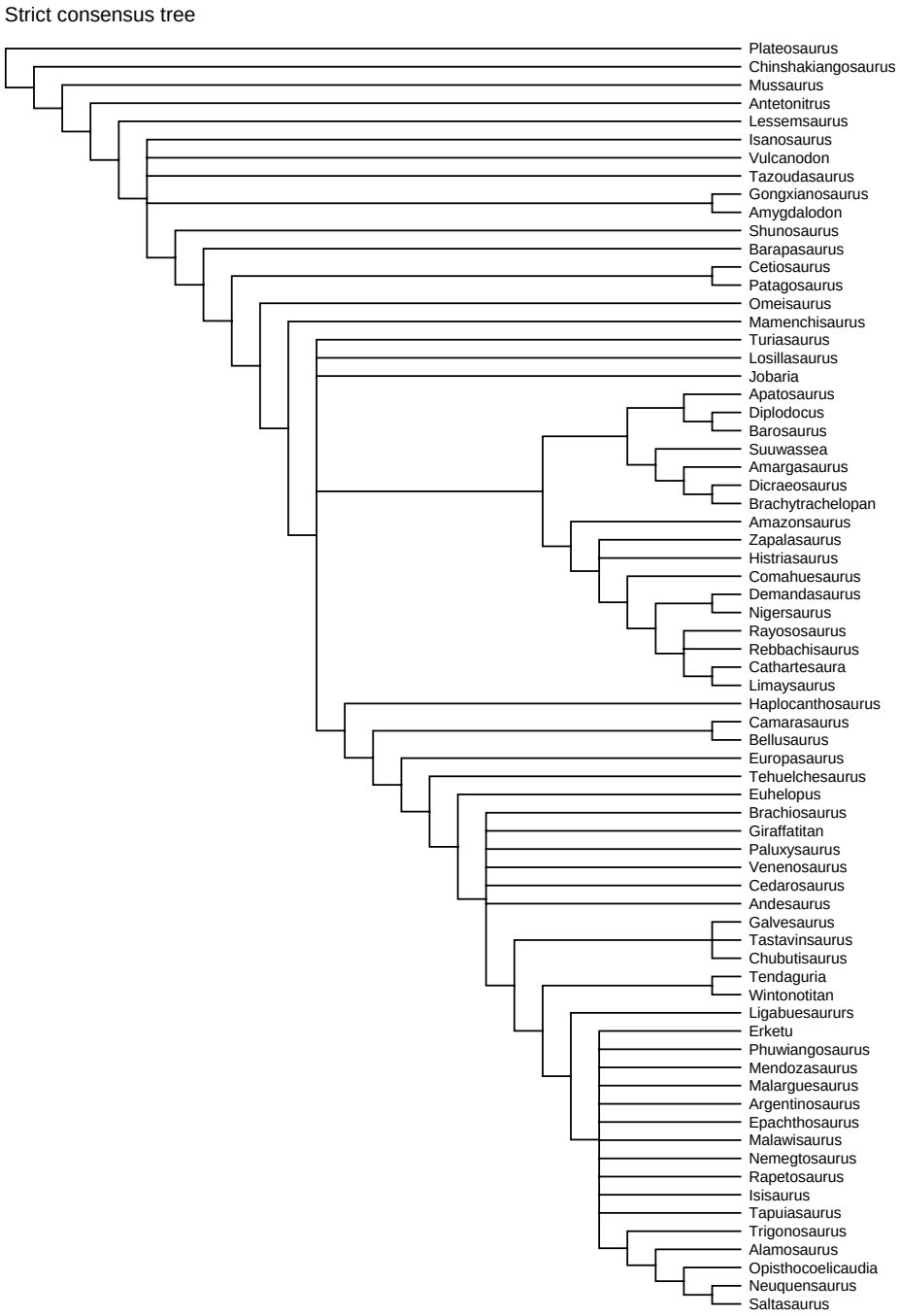

Figure 38. Strict consensus tree - pneumatically modified 'Carballido & Sander (2014). Computed strict consensus from the pneumatically modified most parsimonious trees. Assigned outgroups were the taxa *Plateosaurus, Chinshakiangosaurus, Mussaurus* and *Antetonitrus*. Polytomies were formed in basal titanosauriformes and somphospondylans.

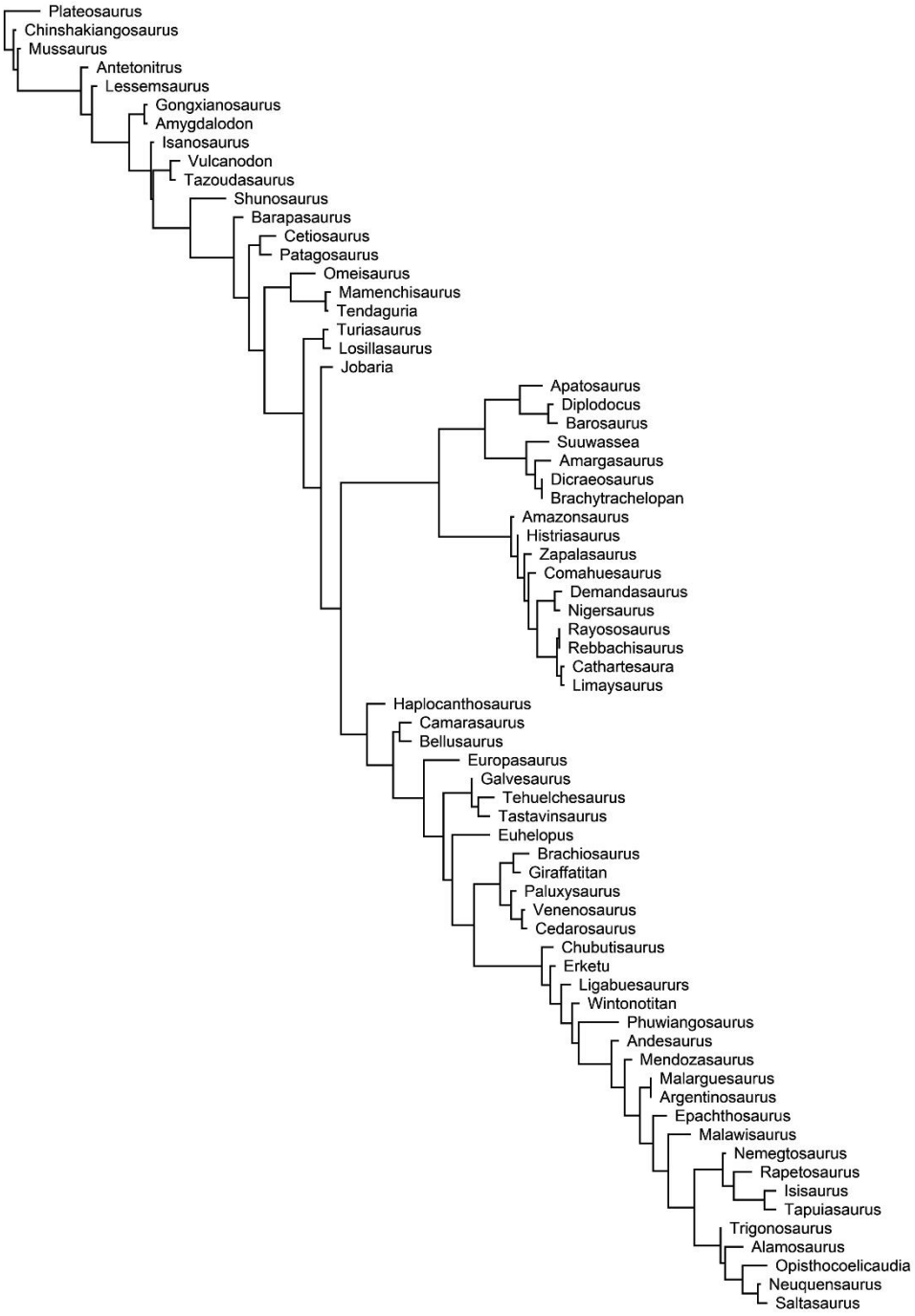

Figure 39. Constrained most parsimonious tree of the pneumatically modified 'Carballido & Sander (2014). Heuristic search in parsimony using TBR algorithm of the published dataset containing 70 taxa and 340 characters. Original pneumaticity characters were removed and replaced with the eleven ones derived from this study. Constrained of the unaltered phylogeny (Fig. 35) was imposed. Assigned outgroups were the taxa *Plateosaurus, Chinshakiangosaurus, Mussaurus* and *Antetonitrus*. Tree length: 1031 steps, CI: 0.432, RI: 0.703, RC: 0.303 and HI: 0.615.

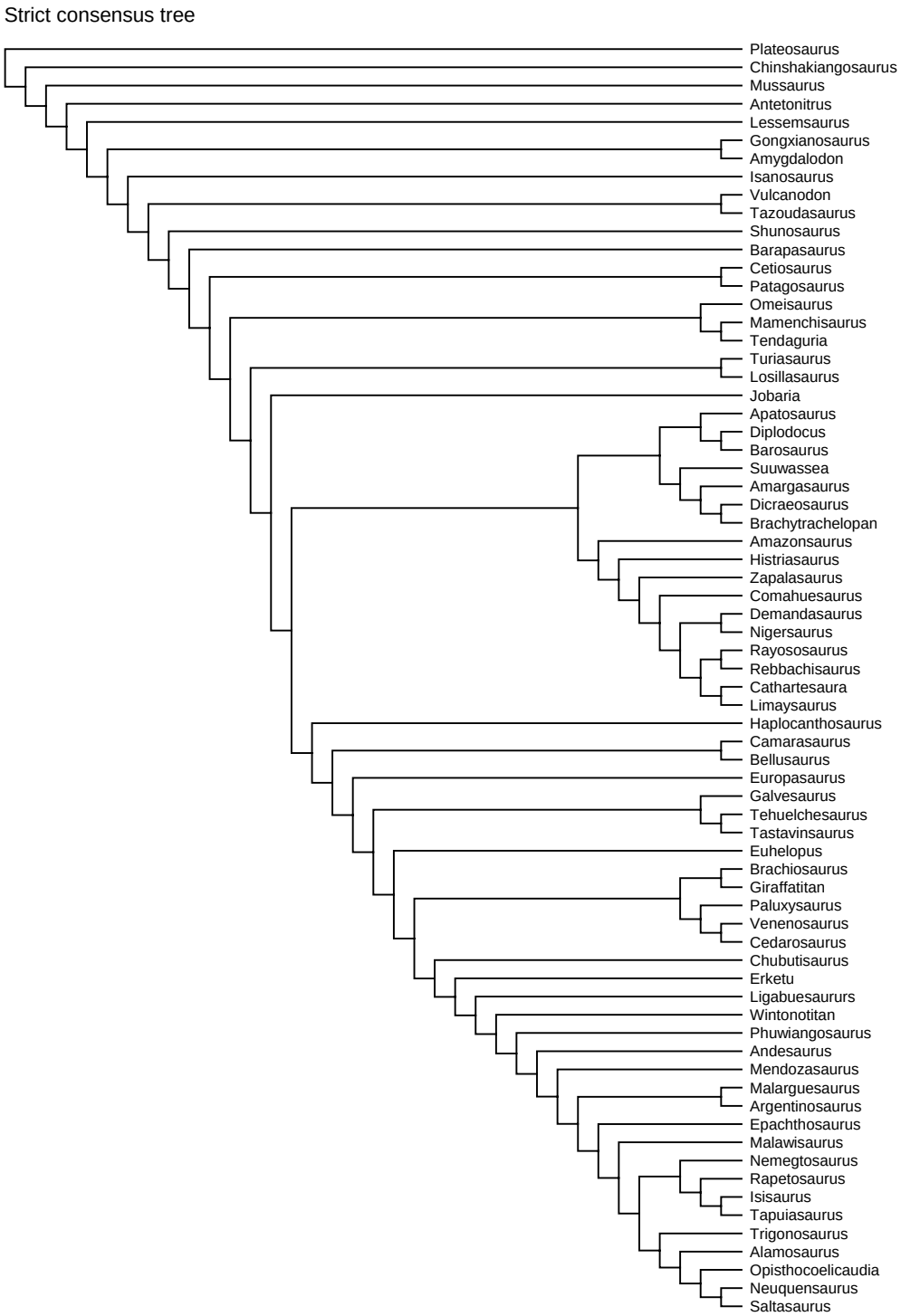

Figure 40. Constrained strict consensus tree - pneumatically modified ‘Carballido & Sander (2014). Computed constrained strict consensus from the pneumatically modified most parsimonious trees that resulted with the imposed constraint of the unaltered phylogeny. The tree is resolved without any polytomies. Assigned outgroups were the taxa *Plateosaurus, Chinshakiangosaurus, Mussaurus* and *Antetonitrus*.

The analysis of the unaltered dataset of Carballido & Sander (2014) yielded a tree (Fig. 35) which is longer than the published phylogeny by 52 steps (Carballido & Sander, 2014; Fig. 29) The resultant tree bears similarities to the published one except from few different topologies. Namely, *Omeisaurus* is not paired with *Mamenchisaurus* but instead it is monophyletically related to *Mamenchisaurus* and *Tendaguria* which are recovered as sister taxa instead of *Tendaguria* being a sister taxon to *Wintonotitan* and despite the fact that the former is a highly pneumatised eusauropod (PDI% = 90) and the latter is a moderately-low pneumatic (PDI% = 49) somphospondylan. In addition, *Camarasaurus* was recovered to be paraphyletic to basal titanosauriforms instead of being paired as a sister taxon to *Bellusaurus* and *Chubutisaurus* was recovered one position more basal to *Erketu* instead of these two taxa being in a dichotomy.

The strict consensus tree (Fig. 36) is very similar to the published phylogeny but they differed in few points. Specifically, *Camarasaurus* was recovered in a dichotomy with *Bellusaurus* instead of being sister taxa. *Erketu*, *Chubutisaurus*, *Wintonotitan*, *Ligabuesaurus*, *Phuwiangosaurus* and *Andesaurus* were recovered in a polytomy instead of being paraphyletic to one another (as a sequence of more basal to more derived taxa). Finally, in the published phylogeny, among these somphospondylan taxa, only *Erketu* and *Chubutisaurus* were in a dichotomy.

The pneumatically modified resultant tree (Fig. 37) is 30 steps longer than the phylogeny shown in Figure 29 (Carballido & Sander, 2014) and it differed from it in several topological recoveries. *Vulcanodon* was recovered to be more derived than *Tazoudasaurus* instead of these two taxa being a pair of sister taxa and *Omeisaurus* basal to *Mamenchisaurus* instead of being sister taxa with each other. Furthermore, *Tehuelchesaurus* was not recovered as a sister taxon to *Tastavinsaurus* but instead more basal to it; *Tastavinsaurus* was recovered as a sister taxon to *Galvesaurus*. *Erketu* was recovered to be more derived than *Chubutisaurus* instead of forming a dichotomy with each other and *Nemegtosaurus* more basal to *Erketu* than being more derived. *Malarguesaurus* was not recovered in a dichotomy with *Argentinosaurus* but instead more basal to it and more basal to *Mendozasaurus* rather than *Mendozasaurus* being more basal to *Malarguesaurus*. Finally, *Tendaguria* was recovered at a more basal position with respect to *Erketu* rather than the reverse, as is the case in the published phylogeny.

The strict consensus tree (Fig. 38) recovered a polytomy among *Isanosaurus*, *Vulcanodon* and *Tazoudasaurus* instead of the latter two taxa being a pair of sister taxa, Omeisaurus was recovered basal to *Mamenchisaurus*, rather than being a pair of sister taxa and *Turiasaurus*, *Losillasaurus* and *Jobaria* formed a trichotomy instead of the former two taxa being a pair of sister taxa. *Tehuelchesaurus* was not recovered to be paired with *Tastavinsaurus* but instead more basal to it. The basal titanosauriforms *Brachiosaurus*,

Giraffatitan, *Paluxysaurus*, *Venenosaurus*, *Cedarosaurus* and the somphospondylan *Andesaurus* were recovered in a polytomy instead of *Brachiosaurus* and *Giraffatitan* as well as *Venenosaurus* and Cedarosaurus two being pairs of sister taxa. In more derived positions, *Galvesaurus*, *Tastavinsaurus* and *Chubutisaurus* forming a trichotomy and *Ligabuesaurus* was recovered to be basal to a polytomy of somphospondylans. Finally, *Erketu* should be in a dichotomy with *Chubutisaurus* but instead it forms a large polytomy with *Phuwiangosaurus*, *Mendozasaurus*, *Malarguesaurus*, *Argentinosaurus*, *Epacthosaurus*, *Malawisaurus*, *Nemegtosaurus*, *Rapetosaurus*, *Isisaurus* and *Tapuiasaurus*.

Moving on to the constrained resultant tree (Fig. 39), *Omeisaurus* is not paired with *Mamenchisaurus* but, as in Figure 35 above, the latter taxon is paired with *Tendaguria*. *Zapalasaurus* and *Histriasaurus* do not form a dichotomy as in the published phylogeny, instead the latter taxon was recovered to be basal to the former. Every other sauropod interrelationship matches with those of the published phylogeny.

Finally, in the strict consensus tree (Fig. 40) *Mamenchisaurus* was recovered, as before, to be a sister taxon to *Tendaguria* and Histriasaurus to be basal to Zapalasaurus instead of these two taxa forming a dichotomy with each other. All other sauropod interrelationships are identical to the ones shown in the published phylogeny.

5.3.5) Character mapping on the 61 studied taxa

Mesquite – discrete and continuous characters

Here, the tree of the 61 taxa is firstly presented with the character ‘C1c’ mapped using parsimony (Fig.41a). Figs.41b-41i can be viewed in Appendix 2. In addition, the four metric characters (PDI% total average, body mass, body length and femur length – Figs.43-46) are also mapped on this tree. The pneumaticity characters do not have a strong fit on this tree, as indicated by the low CI (0,33) of the entire matrix (see ‘Tree figures’ in Appendix 2) for more trees with mapped pneumaticity characters.

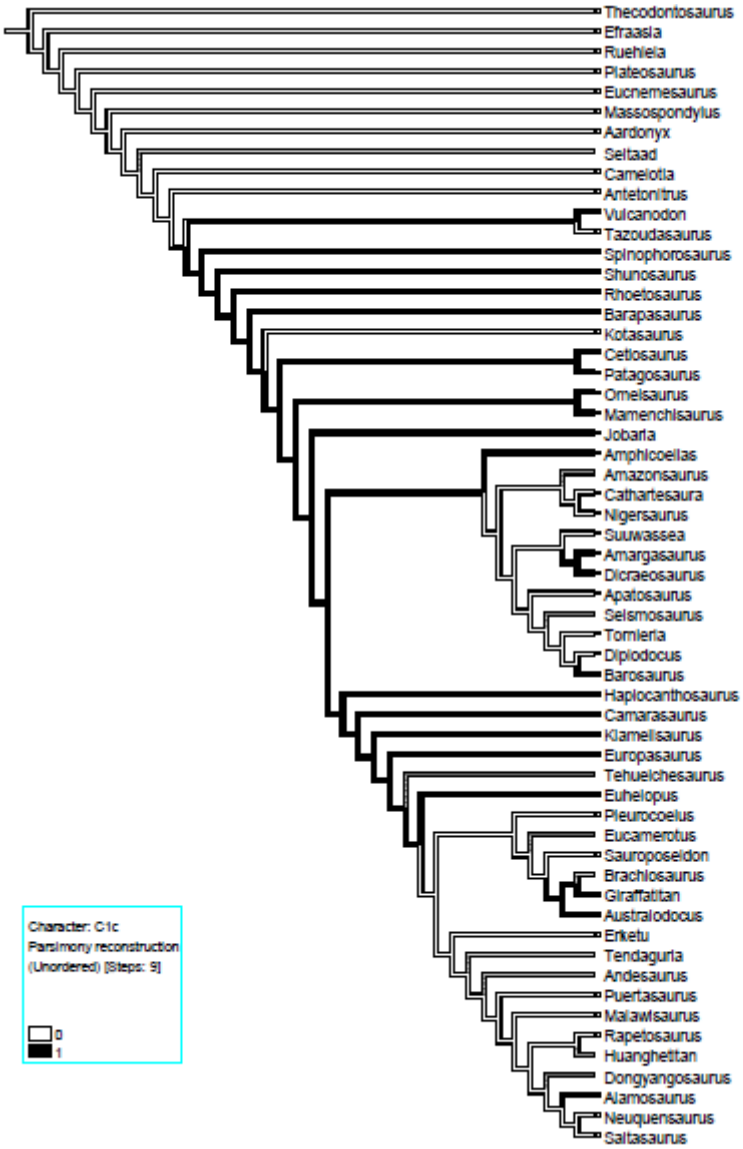

Figure 41a. Parsimony reconstruction of character ‘C1c’ (cervical) in 61 taxa in the ‘Carballido & Sander’ phylogeny. Reconstruction of character ‘C1c’ (cervical) on the 61 pneumatically studied taxa, placed in a phylogeny based on ‘Carballido & Sander (2014)’. Tree values for this tree derived from the entire pneumaticity matrix: TL = 838, CI = 0.33, RI = 0.13. Grey branches indicate ‘unknown’ data.

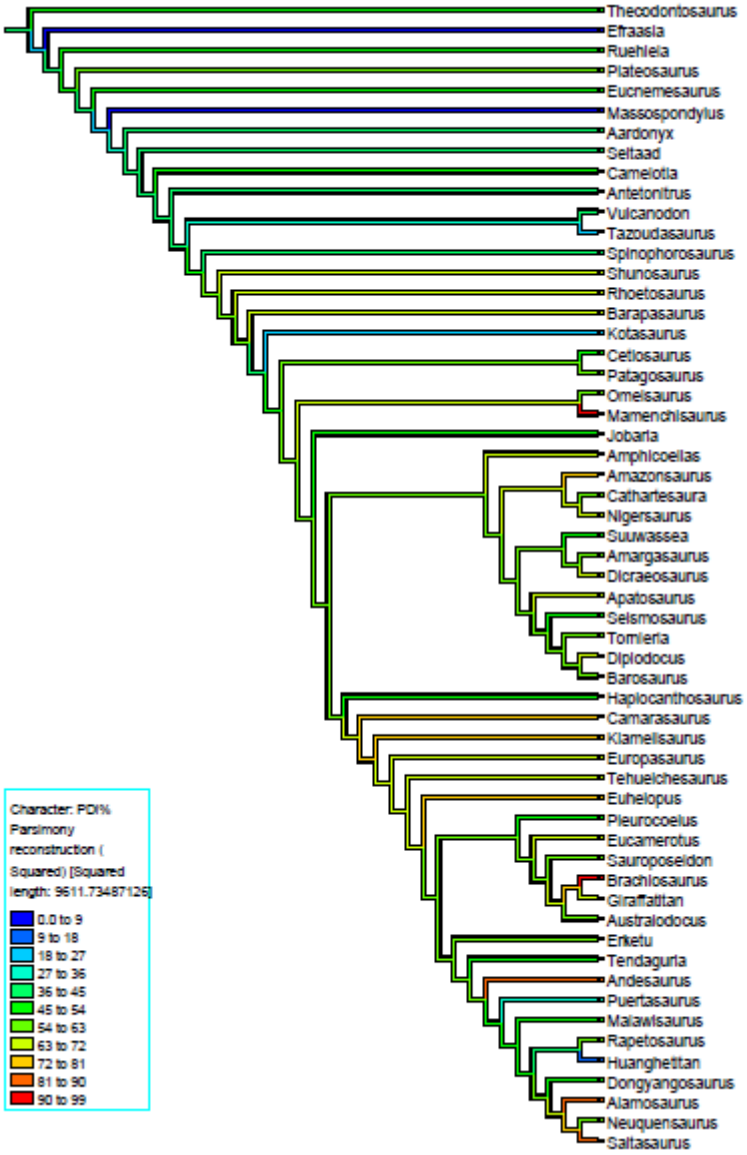

Figure 42. Distribution of total average PDI% in the 'Carballido & Sander' 61 taxa composite phylogeny. Evolution of PDI% in 61 sauropodomorph taxa based on the 'Carballido & Sander (2014)' phylogeny, demonstrating the distribution of total average pneumatisation across this broad phylogeny. The evolution of PDI% is nearly gradual with the noticeable sudden increases, evident in *Mamenchisaurus, Amazonsaurus, Camarasaurus, Brachiosaurus, Andesaurus, Alamosaurus* and *Saltasaurus.* Grey branches indicate 'unknown' data.

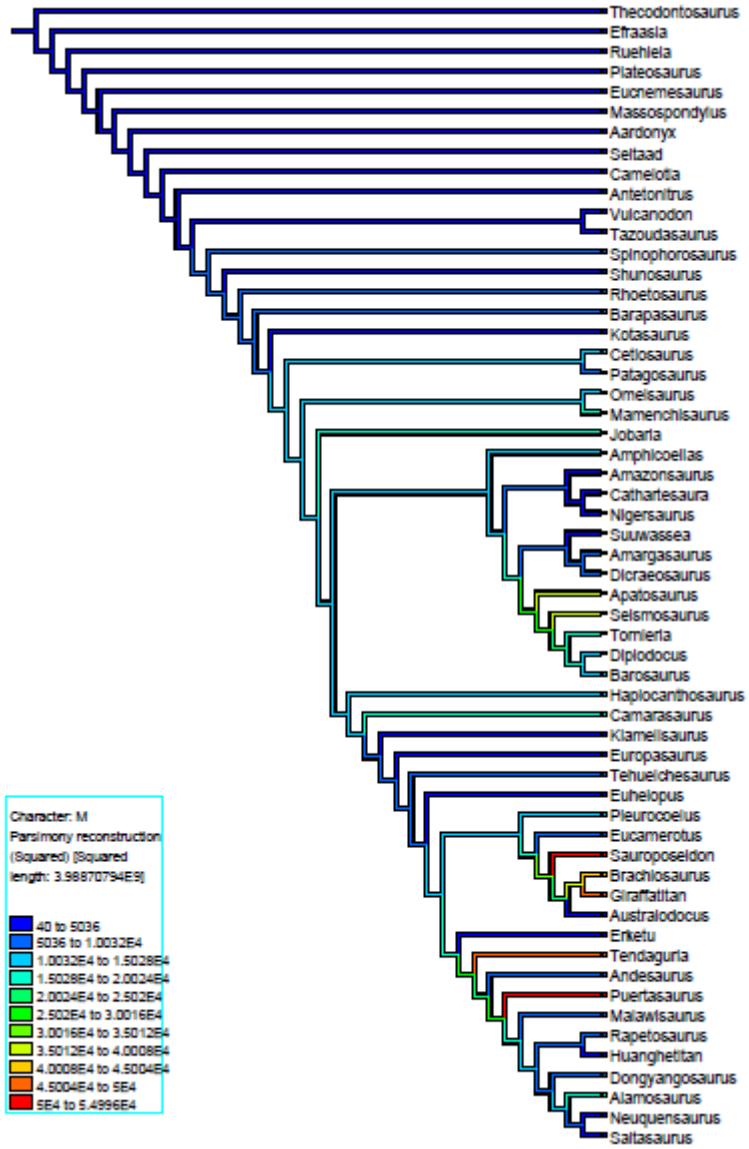

Figure 43. Body mass distribution in the 'Carballido & Sander' 61 taxa composite phylogeny. Distribution of body mass (M, in kilogrammes) across 61 sauropodomorph taxa based on the 'Carballido & Sander (2014)' phylogeny. Grey branches indicate 'unknown' data.

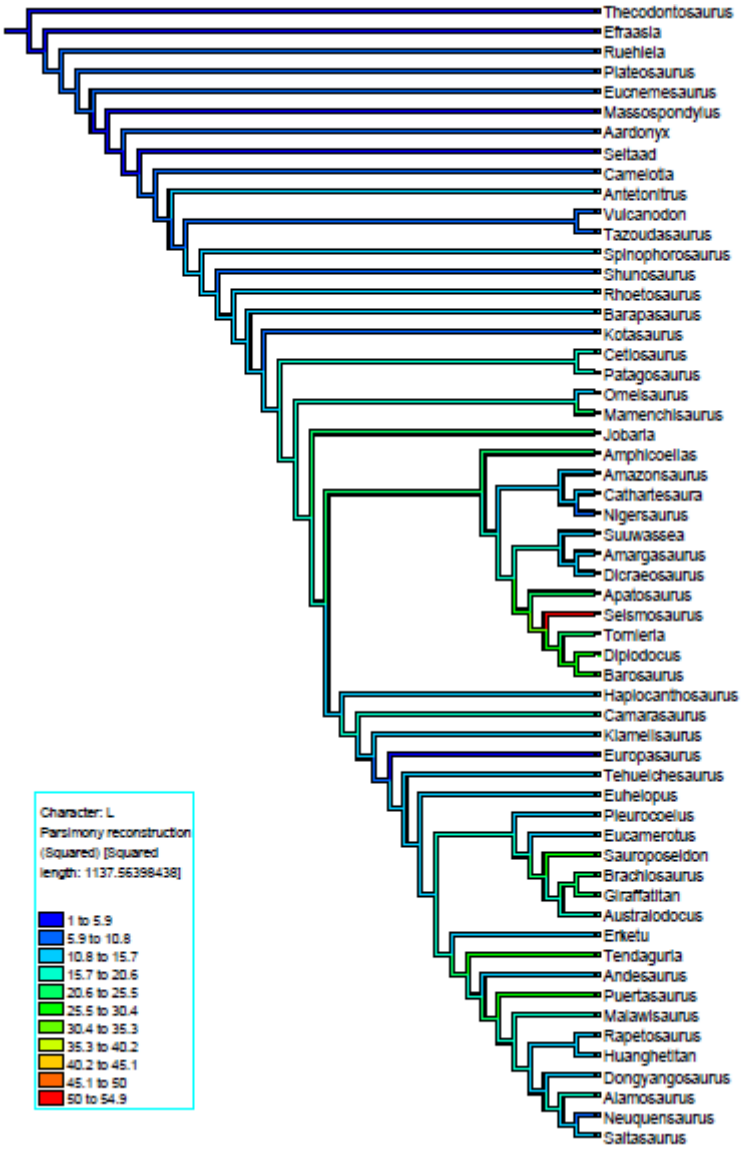

Figure 44. Body length distribution in the 'Carballido & Sander' 61 taxa composite phylogeny. Distribution of body length (L, in metres) across 61 sauropodomorph taxa based on the 'Carballido & Sander (2014)' phylogeny. Grey branches indicate 'unknown' data.

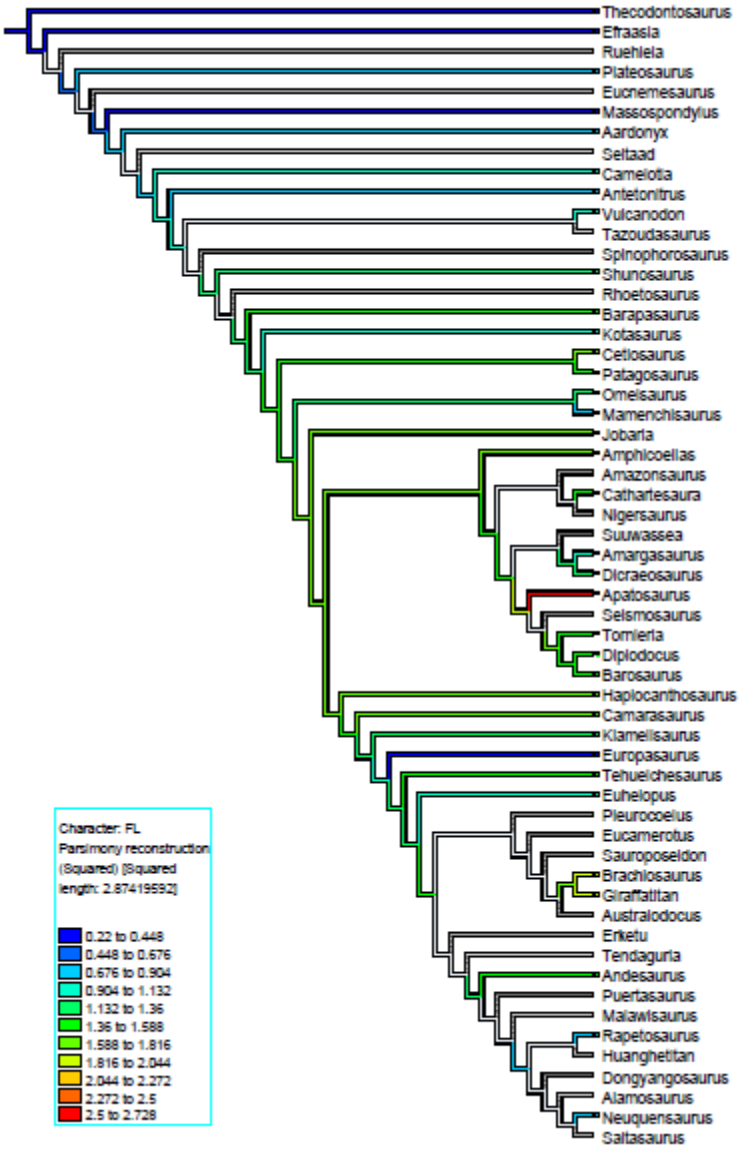

Figure 45. Femur length distribution in the 'Carballido & Sander' 61 taxa composite phylogeny. Distribution of femur length (L, in metres) across 61 sauropodomorph taxa based on the 'Carballido & Sander (2014)' phylogeny. Grey branches indicate 'unknown' data.

In the cervical vertebrae, pleurocoel in the centrum ('C1c'; CI = 0.11, RI = 0.61, Mk1 rate = 0.14, Char. Likelihood = 27.53 and Frequency of state = 0.52) has a weak fit to the tree but it appears in a third of the taxa (21/61). It is firstly expressed in *Vulcanodon* and not in its sister taxon *Tazoudasaurus* (the former has higher overall degree of pneumatisation as shown in Table 7 in Chapter 2), only to later continue throughout the basal neosauropods. Limited expression occurs in the diplodocid lineage and it recovers in most members of the basal titanosauriforms. The only taxon to be seen afterwards,

within Somphospondyli, is *Alamosaurus* even though it is less pneumatic than *Saltasaurus* (Fig.41a).

Pleurocoelous fossae in the centrum ('C8c'; CI = 0.09, RI = 0.41, Mk1 rate = 0.19, Char. Likelihood = 29.52 and Frequency of state = 0.62) is an even rarer trait than 'C1c' and less likely to be expressed in Sauropoda. This character appears in 18 of the taxa and it is firstly documented in the basal eusauropods *Shunosaurus* and *Rhoetosaurus*. This is followed by a short taxonomic hiatus until it re-emerges in Omeisaurus and throughout most diplodocoids. It is interesting to note that, as was also shown in the case of the previous character, *Barosaurus* possesses such a trait (and a pleurocoel in the centrum too) while the more pneumatised *Diplodocus* lacks it. Despite that, *Diplodocus* higher degree of pneumaticity is characterised by the presence of more numerous and invasive traits as displayed in Table 7 (Chapter 2). The same condition occurs between *Amargasaurus* and *Dicraeosaurus*. 'C8c' occurs in few basal Titanosauriformes and, finally, only in *Rapetosaurus* (Fig.41b in Appendix 2).

'C1c' in the dorsal vertebrae does not have a good fit in this tree (CI = 0.125, RI = 0.58, Mk1 rate = 0.11, Char. Likelihood = 26.42 and Frequency of state = 0.34), though a better one than when present in the cervicals. It appears in more taxa (32/61) than in their cervicals, starting from basal eusauropods and throughout most neosauropods with few taxonomic gaps until we see the character present even in the most derived somphospondylans. 'C8c', though, is only expressed by few taxa of each sauropod subfamily (Figs.42c and 42d in Appendix 2). Its fit to the tree is poorer (CI = 0.08, RI = 0.0, Mk1 rate = 0.22, Char. Likelihood = 32.30 and Frequency of state = 0.76) than when present in the cervical series and weaker than 'C1c'.

Pleurocoels in the centra of the sacral vertebrae is a rare trait to be found in the sauropod family but, nonetheless, present in taxa that possess very pneumatic sacral series (see Table S4 in Appendix 2). These few taxa (here, 5; see Fig.41e) are members of the Diplodocoidea, Macronaria and Somphospondyli clades and, until further evidence is to be discovered, the only known members possessing this trait. 'C1c' consistency and retention indices are both 0.25, its Mk1 rate is 0.11, its likelihood is 13.50 and its Frequency of state is 0.76. Moving on to a different vertebral landmark, the neural spine, we see (Fig.41f in Appendix 2) that the condition of having pneumatic foramina ('C33ns'; CI = 0.33, RI = 0.0, Mk1 rate = 0.08, Char. Likelihood = 10.73 and Frequency of state = 0.83) is present in only 3 taxa, two of which are diplodocids and one basal titanosauriform. No other common feature seems to connect these taxa except for any macronarian synapomorphies they may share with each other (e.g. Upchurch, 1995; Wedel et al., 2000; Wedel 2003; Wedel and Taylor, 2013).

Foramina in the centrum of the caudal series (character 'C3c' CI = 0.12, RI = 0.0, Mk1 rate = 0.22, Char. Likelihood = 20.72 and Frequency of state = 0.77) could be characterised as a semi-derived trait appearing in a basal neosauropod, some basal and derived diplodocids and a couple of basal titanosauriforms (Fig. 41g). To have foramina in the centrum is the most expected pneumatic trait and quite unambiguous with respect to its ontogenetic development as a result of pneumatic diverticular penetration to the bone (e.g. Wedel et al., 2000; Wedel, 2005; Schwartz & Fritsch, 2006; O'Connor & Claessens, 2005). Contrary to that, fossae (here, 'C4c' in caudals; CI = 0.16, RI = 0.16, Mk1 rate = 0.13, Char. Likelihood = 18.57 and Frequency of state = 0.77) are ambiguous indications of pneumatic diverticula, as it has been discussed (e.g. Wedel et al., 2000; Wedel, 2003; Wilson, 1999, 2002; Wilson et al., 2011), and, because the condition of having fossae is a superficial and more frequent characteristic of a vertebra, is classified as a basal trait (e.g. Wilson & Sereno; 1998; Wedel et al., 2000). In most sauropodomorph taxa, the caudal series is rarely pneumatised and only some of the most pneumatised and larger taxa, from every subfamily (except basal sauropodomorphs) possess this trait.

Finally, the condition of having foramen in the ilium ('D2'; CI = 0.5, RI = 0.0, Mk1 rate = 0.05, Char. Likelihood = 8.56 and Frequency of state = 0.88) is very rare; despite that it is found in *Plateosaurus* and *Europasaurus*, although, in the case of the former it could be an isolated event since no other basal sauropodomorph possess this trait.

The adaptations of the metric data in the phylogeny reveal a nearly gradual increase of total average pneumaticity degree throughout Sauropodomorpha, with occasional pneumatic 'nadirs' occurring more often than not. We have not discovered every vertebral section of most sauropodomorphs yet, in order to correct for inconsistencies between pneumaticity degree and size. For the most part, mass is stable on moderate levels, slowly increasing as we progress from basal to derived taxa. Pneumaticity increases are often congruent with mass increases except in cases like *Eucamerotus* which has moderate size and mass but is more pneumatised than its larger macronarian relatives like *Giraffatitan* or *Sauroposeidon* (Figs.43 and 44). As we saw in Chapter 2, length is more correlated to pneumaticity than mass. Femur length follows a gradual increase which climaxes in diplodocids and basal titanosauriforms and then it decreases in somphospondylans (Fig.45) but we need more femur specimens from this group in order to verify such an observation.

5.3.6) Results from analyses in *RStudio* - phylogenetic regression, ancestral state reconstruction and model fitting

These analyses required the use of the following packages: *ape* (Paradis, Claude and Stimmer, 2004), *geiger* (Harmon et al., 2008), *paleotree* (Bapst, 2012), *caper* (Orme et al., 2013)*, strap* (Bell & Lloyd, 2014), *phytools* (Revell, 2012), and *data*.*table* (Dowle et al., 2015). The phylogenetic tree containing only the 61 sauropods (after 'Carballido & Sander, 2014) which was constructed in *Mesquite* was loaded and tip-dated in *RStudio* (R Core Team, 2016; see Appendix 2 for complete command code). The dates required for assigning branch lengths were in the form of "FAD" (First Appearance Date) and "LAD" (Last Appearance Date) from the dataset "Sauropod_data_table.csv" (Table 2 in Chapter 2 and Table S22 in Appendix 2). The parameters involved were the FAD and LAD of each taxon, total average PDI%, body mass, body length, neck length, femur length, neck PDI%, trunk PDI%, sacral PDI% and tail PDI%.

Phylogenetic regression was conducted using phylogenetic generalised least squares analyses ('pgls' programme in *R*) comparing each time a pair of continuous variables (see Appendix R code). The pairs were: a) "Length" vs "PDI total", b) "Mass" vs "PDI total", c) "Length" vs "PDI CV", d) "Mass" vs "PDI CV", e) "Length" vs "PDI DV", f) "Mass" vs "PDI DV", g) "Length" vs "PDI SV", h) "Mass" vs "PDI SV", i) "Length" vs "PDI CD", j) "Mass" vs "PDI CD, k) "Neck length" vs "PDI CV", l) "trunkl" vs PDI DV", m) "Tail length" vs "PDI CD", n) "Femur length" vs "PDI total" and o) "Estimated First Appearance Date (FAD)" vs "PDI total" (Appendix 2). The final set of analyses required to fit the dataset into models of evolution in order to compute the AIC scores from the Akaike weights. Specifically, the models used were Brownian, Stasis, Early Burst, Directional Trend and Ornstein-Uhlenbeck (Table 1).

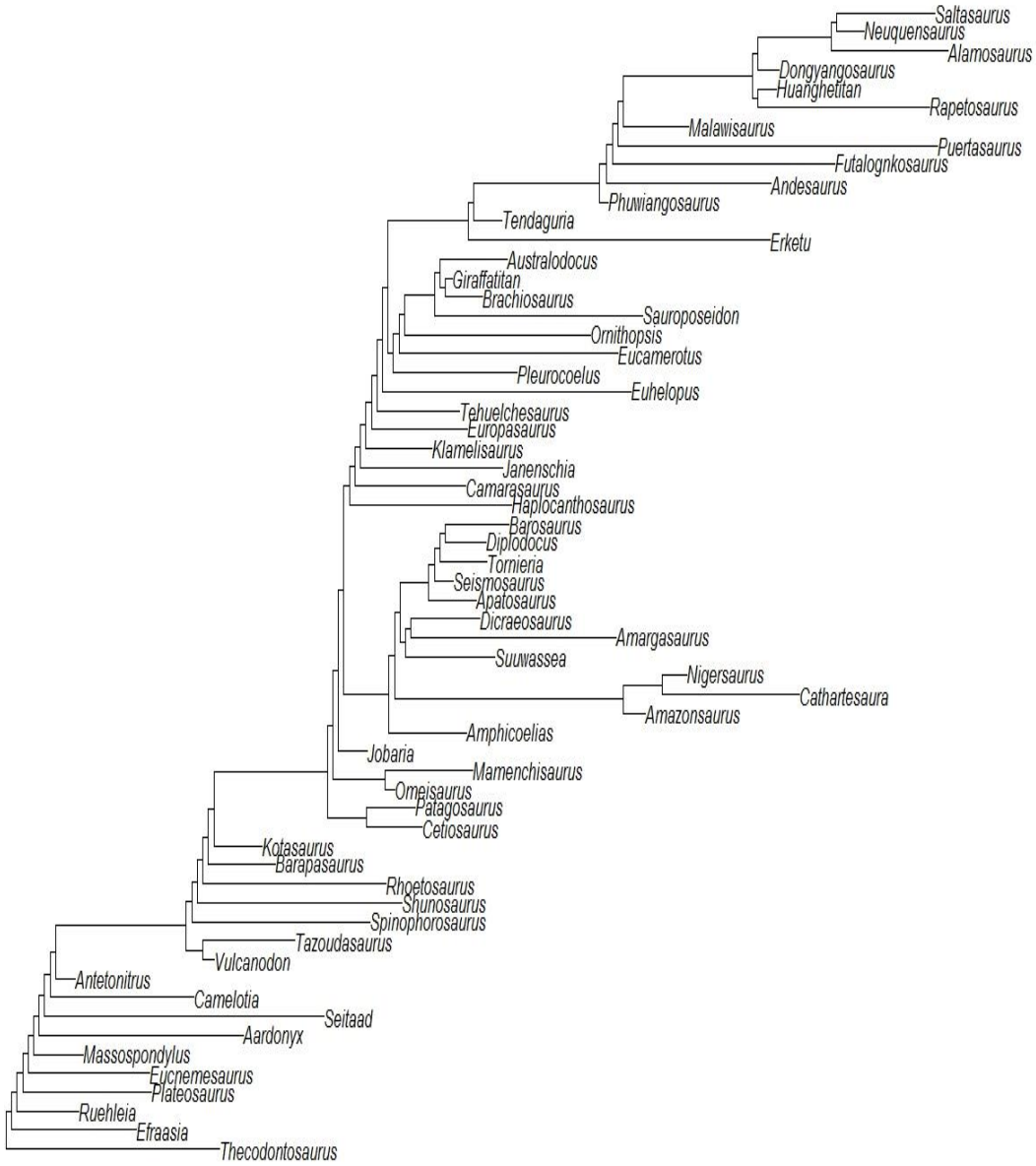

Figure 46. Time bin constrained ‘Carballido & Sander’ 61 taxa tree. Time-calibrated phylogeny of the 61 studied sauropodomorph taxa with branch lengths using FADs and LADs from the taxa corresponding time bins (Table 2, Chapter 2). The phylogenetic tree used is after the ‘Carballido & Sander (2014)’ normal phylogeny. Basal-most taxa begin from the bottom of the tree. Time calibration was performed with the command ‘TimePaleoPhy’ and method ‘cal3’ (R code in Appendix 2).

Ancestral state reconstructions were computed for both pneumaticity characters 'C1c_CV' and 'C8c_CV'. The scaled likelihood of 'C1c_CV' for state '?' = 0.02, for state '0' = 0.95 and for state '1' = 0.02. For 'C8c_CV' the values are: '?' = 0.33, '0' = 0.33 and '1' = 0.33. Under the same phylogenetic framework ('Carballido and Sander, 2014') but with enforced first and last appearance dates of the 61 taxa (Fig. 46), the probability of the character 'C1c' of the cervical vertebrae in the nodes of this phylogeny to be unknown is less than either being absent or present (Table S5 in Appendix 2). The probability of being absent is highly variable throughout the nodes while its probability to be present peaks rapidly from the 11th node and remains relatively high throughout until it begins to drop gradually, reaching a very low value at the last 3 nodes. The probabilities of the character 'C8c', for the same vertebral series, to be unknown, absent or present are equal to each other and with an almost stable value (0.33) throughout the nodes (Table S6 in Appendix 2). The results here demonstrate that this character has a very weak fit in the tree (CI = 0,09) and a 62% frequency of being expressed. The expression of central pleurocoels ('C1c') in the cervical series has 52% frequency to be present and pleurocoelous fossae in the centra ('C8c') of the same series has a 62% frequency of being expressed as present. These results corroborate the findings presented in section 5.3.1., justifying their multiple nodal appearances seen in Figures 41a and 41b.

5.3.7) Phylogenetic correction of continuous data

Correlation analyses among the size metrics [mass, length, neck length (i.e. length of the cervical series), trunk length (i.e. length of the dorsosacral series), femur length, PDI% total average, as well as separate PDI% values of the cervical, dorsal, sacral and caudal series)] that were carried out in *R* (R Core Team, 2016) yielded interesting results. In general, mass seems to be less correlated with the degree of pneumaticity, in contrast to body length's higher correlation to pneumaticity (Tables S7 & S8 in Appendix 2). This is supported by the facts that the *Estimate* value of 'PDI total' (explanatory variable) with respect to body length is 0.11 and that the probability of observing the slope by chance is low (*p-value* = 0.1085), therefore, the slope is unlikely to exist due to chance. In addition, the *Adjusted R-squared* shows that 11.45% of the variation in body length varies with PDI% total (Table S7 in Appendix 2). Conversely, the *Estimate* for 'PDI total' when correlated with mass is very high (37.87), the *Adjusted R-squared* indicates negative correlation of about 4.1% between pneumaticity and mass. The probability of observing the slope is quite high (*p-value* = 0.53), therefore, the slope is very likely to exist by chance (i.e. not significant; Table S12 in Appendix 2). These extrapolations can also be deduced by the Table S8 (Appendix 2).

At this point, it is important to address the lambda value i.e. the maximum likelihood estimate of the response variable (here, 'mass' and 'length'). In Table S7 (Appendix 2), the maximum likelihood estimate of lambda is 0.66. The *p-value* for the likelihood ratio test at the lower bound is not much smaller than the one on the upper bound, showing there is not a significant difference between the maximum likelihood estimate and zero, indicating that body length has a moderately strong phylogenetic signal. Interestingly, the lambda for mass is 0.94 (larger than that of length's lambda value; Table S8 in Appendix 2) and we see a much lower *p-value* of the lower bound in comparison to the one at the upper bound indicating a moderate phylogenetic signal in body mass.

Pneumaticity of the cervical series is less correlated to total length (*Adjusted R-squared* = 0.2018; Table S9) than to body mass (*Adjusted R-squared* = 0.2319; Table S10) but the probability of the slope to exist by chance is lower (i.e. very significant) when cervical pneumaticity is correlated to body mass (*p-value* = 0.03) than to body length (*p-value* = 0.04; Tables S9 and S10 in Appendix 2). Body mass and body length have both a strong correlation to cervical pneumaticity. For both mass and length, the upper bound *p-value* of lambda is much greater than the one in the lower bound. Nevertheless, in both cases, the general *p-values* are small (<0.05) indicating that the variables' slopes are not likely to have occurred by chance. Correlation of pneumaticity in the dorsal series with mass and length, shows an 11% correlation occurring between length and dorsal pneumaticity while mass has negative correlation of -5% (Tables S11 and S12 in Appendix 2). General *p-values* in both tables (0.10 for length and 0.62 for mass with respect to dorsal pneumaticity) show moderate and low significance, respectively, indicating small likelihood of both slopes to not have occurred by chance.

Pneumaticity in the sacral series is weakly but positively correlated with total length *(Adjusted R-squared* =3.5%) and negatively correlated with mass (*Adjusted R-squared* = -6.7%). Length and mass *p-values* are large (0.23 and 0.82, respectively) but the definitive factor is the nearly identical *p-value* of the lower bound of lambda of length when compared to the *p-value* of the upper bound indicating a non-existent signal for length (Tables S13 and S14 in Appendix 2). Caudal pneumaticity is highly correlated with both mass and length (*Adjusted R-squared* values of 42% and 39%, respectively; Tables S13 and S14 in Appendix 2), strongly supported by very low *p-values* (0.003 for mass and 0.005 for length with respect to caudal pneumaticity). The *Estimate Coefficient* value for mass with respect to caudal pneumaticity is very large (248.81) while for length is quite low (0.17) indicating that length has better correlation to caudal pneumaticity than mass does. The *p-value* on the upper bound of lambda for both length and mass with respect to caudal pneumaticity is larger (1 for both) than its lower bound (0.03 and 0.14,

respectively) indicating no difference between maximum likelihood estimate and zero, which shows minimal phylogenetic signal of body length and mass with respect to caudal pneumaticity (Tables S15 & S16 in Appendix 2).

Correlation between the length of the neck and its pneumaticity degree (Table S17 in Appendix 2) is higher (*Adjusted R-squared* = 20% correlation) than the length of the trunk and the pneumaticity degree of the dorsal series (Table S18 in Appendix 2; *Adjusted R-squared* = 7.7% correlation). Neck length has a stronger phylogenetic signal than trunk length supported by the fact that the slope of the former is more unlikely to have occurred by chance (*p-value* = 0.04) than in the latter (*p-value* = 0.15). Correlation between tail length and its pneumaticity degree is very small but negative (*Adjusted R-squared* = -0.9%). Minimal correlation is also demonstrated by the moderately high value of *p* = 0.37). The lower bound *p-value* is larger than that of the upper bound indicating minimal phylogenetic signal of tail length with respect to caudal pneumaticity (Table S19). Femoral length shows little correlation with total average PDI% (*Adjusted R-squared* = 5%, *p-value* = 0.19) but it has a phylogenetic signal (*Estimate Coefficient* of femur length with respect to total average pneumaticity is 0.008); not very strong, though, because the lower bound *p-value* of maximum likelihood is larger than that of the lower bound (Table S20). Finally, the correlation of total average pneumaticity (PDI%) with evolutionary time with regard to the first appearance date of each taxon is moderately significant (*Adjusted R-squared* = 1.9%, *p-value* = 0.05). The *p-value* of the lower bound is significantly smaller than that of the upper bound indicating the slope could not have occurred by chance, thus showing a strong phylogenetic signal of pneumaticity with respect to evolutionary time (Table S21). The value of *kappa* in Tables S7-S21 (Appendix 2) is 1, suggesting a gradual model of evolution (Brownian) of pneumaticity (in PDI% total average) for this phylogeny.

5.3.8) *Brownian Motion*, *Stasis*, *Early Burst*, *Trend* & *Ornstein – Uhlenbeck* model fitting

Akaike Information Criterion (AIC) is a measure of the fit of the model to the data (Crawley, 2007; Table 1). Analysis was run in *R* in the modified 'Carballido & Sander, 2014' phylogeny, having only the 61 taxa from which pneumatic data were obtained (see Table 1 below). The parameters analysed were the FAD and LAD of each taxon, total average PDI%, body mass, body length, neck length, femur length, neck PDI%, trunk PDI%, sacral PDI% and tail PDI%. Lower values of the models fitted in AIC indicate better fit i.e. when comparing two models, the smaller the AIC value (which is smaller lack of fit), the better the fit of the data to the model (Crawley, 2007). Analysis of the data demonstrated the Ornstein-Uhlenbeck (OU) and Stasis models best fit the data for this

phylogeny, and specifically for having pleurocoels and pleurocoelous fossae in cervical centra (C1c-CV and C8c-CV). Their values of *delta* being less than 1 suggest these models of evolutionary change to have arose early in the phylogenetic history of Sauropodomorpha and that remained stable after a point onwards in their evolutionary history, with an indication of decrease as we approach the present (i.e. slowdown in evolutionary rate). This fact is also supported by the observations made in Chapters 2&3 concerning the course of these two characters but also of total average pneumaticity throughout sauropodomorphs, i.e. that PDI% follows a gradual increasing trend until it reaches a climax in macronarians and then it minimally decreases along the course of somphospondylans, denoted by the limited appearance of these as well as other invasive pneumaticity features (Appendix 3).

Table 1. Model fitting scores and weights. Results of model fitting in the 61 sauropodomorph data. Results refer to the modified 'Carballido & Sander, 2014' phylogeny with the 61 pneumaticity taxa. Calculation performed with programmes 'pgls' and 'AIC' in *R* using the R code and the data from Table S22 (Appendix 2).

Akaike scores

BM	Stasis	Early Burst	Trend	OU
547.6945	540.0422	549.9090	548.9591	539.1375

Akaike weights

	fit	delta	w
BM	547.6945	8.5570330	0.008341612
Stasis	540.0422	0.9047245	0.382760999
Early Burst	549.9090	10.7715641	0.002756580
Trend	548.9591	9.8216764	0.004432372
OU	539.1375	0.0000000	0.601708436

5.3.9) Results from analyses in *TNT*

Phylogenetic analyses conducted in *TNT* (Goloboff, Farris & Nixon, 2008) were performed in the character-taxon composite matrices of *McPhee et al. (2014) – Yates et al. (2009), D'Emic (2012) – Whitlock (2011)* and *Carballido & Sander (2014)*. The *Sander et al. (2009)* case did not provide a character-taxon matrix in order to be able to perform analyses on it, as explained in the 'Materials and Methods' section of this chapter. All analyses were performed in parsimony and the uninformative characters were kept included, for reasons explained in earlier parts of this project.

McPhee et al. (2014) – Yates et al. (2009)

TNT only accepts one outgroup, unlike PAUP which can accept multiple outgroup taxa. So, the Ornithischia clade was chosen as the outgroup since it is the most distantly related clade with respect to Sauropodomorpha when compared to the other previously assigned outgroup taxa (i.e. Ornithischia, *Staurikosaurus*, *Herrerasaurus*, *Eoraptor*, *Chindesaurus*, *Agnosphitys*, Neotheropoda and *Guaibasaurus*). Traditional search was conducted under parsimony optimality criterion (all characters were included and set to be non-additive i.e. unordered and active) using TBR swapping algorithm in the original composite dataset which yielded a majority-rule consensus tree (from 23 most parsimonious trees) with the best score length of 1088 steps (Fig.47), CI: 0.377 and RI: 0.659. The length score of this tree and its consistency and retention index values are smaller than that of the original published tree (1206 steps) in McPhee et al. (2014; Fig.24) as well as that of the majority-rule consensus tree in Fig.6 (1170 steps), suggesting a better fit between the dataset and the resulted phylogeny when the analysis is conducted under *TNT*. Compared to the tree in Figure 6, this tree differs in the fact that *Seitaad* was recovered in a more basal position than *Ruehleia*.

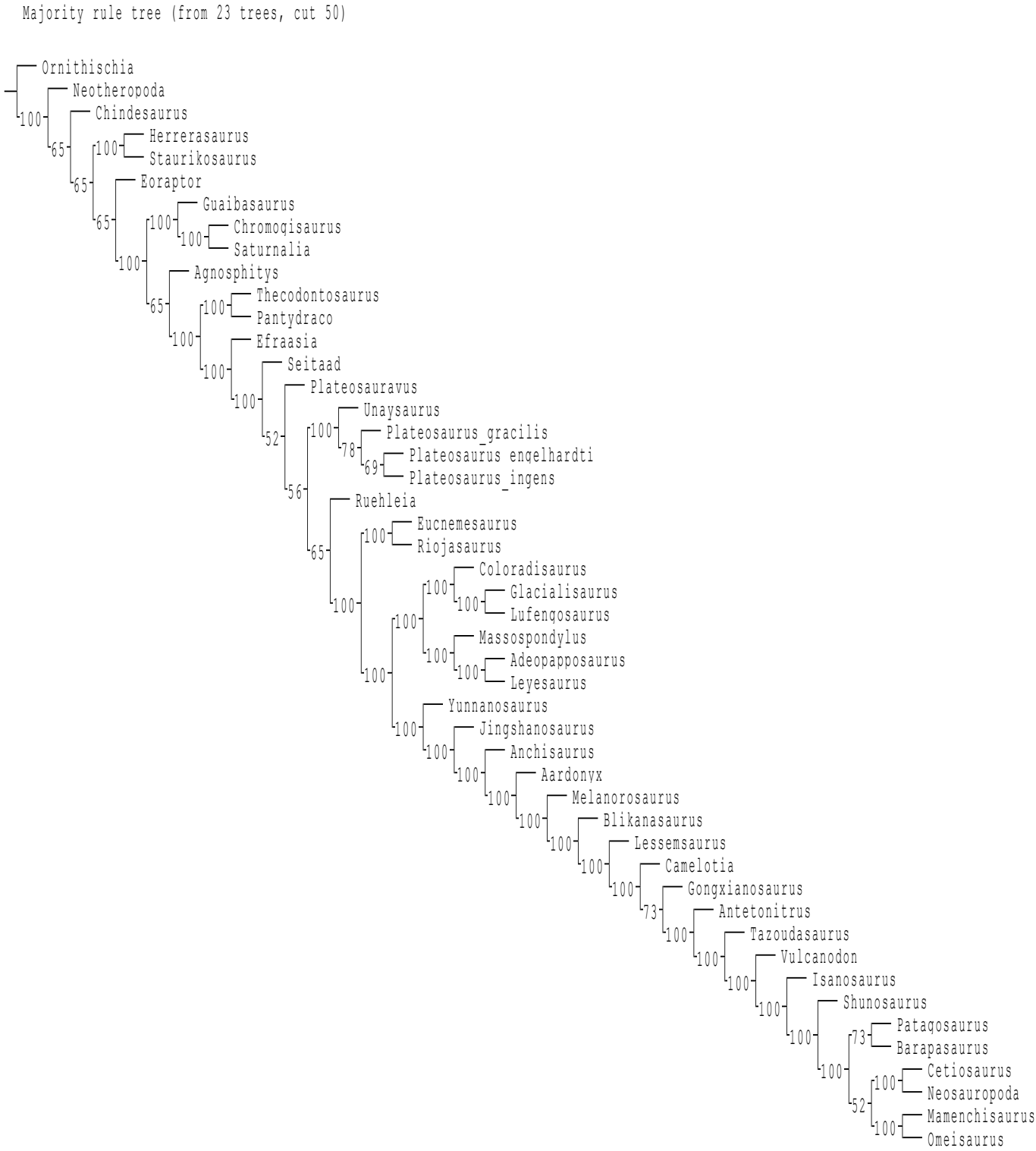

Figure 47. Composite majority-rule consensus tree of the original 'McPhee-Yates' phylogeny. Traditional search (parsimony) of the original 'McPhee-Yates' dataset of 48 taxa and 361 characters using TBR algorithm yielded a tree of 1088 steps, CI: 0.377 and RI: 0.659. Assigned outgroup: Ornithischia. Numbers indicate robustness of clades (number of parsimonious trees the particular clade has been recovered; the higher the value, the higher level of robustness).

The pneumatically modified composite ‘McPhee-Yates’ dataset of 48 taxa and 364 characters yielded 18 best trees of 1073 steps, CI: 0.380 and RI: 0.662 (Fig.48).

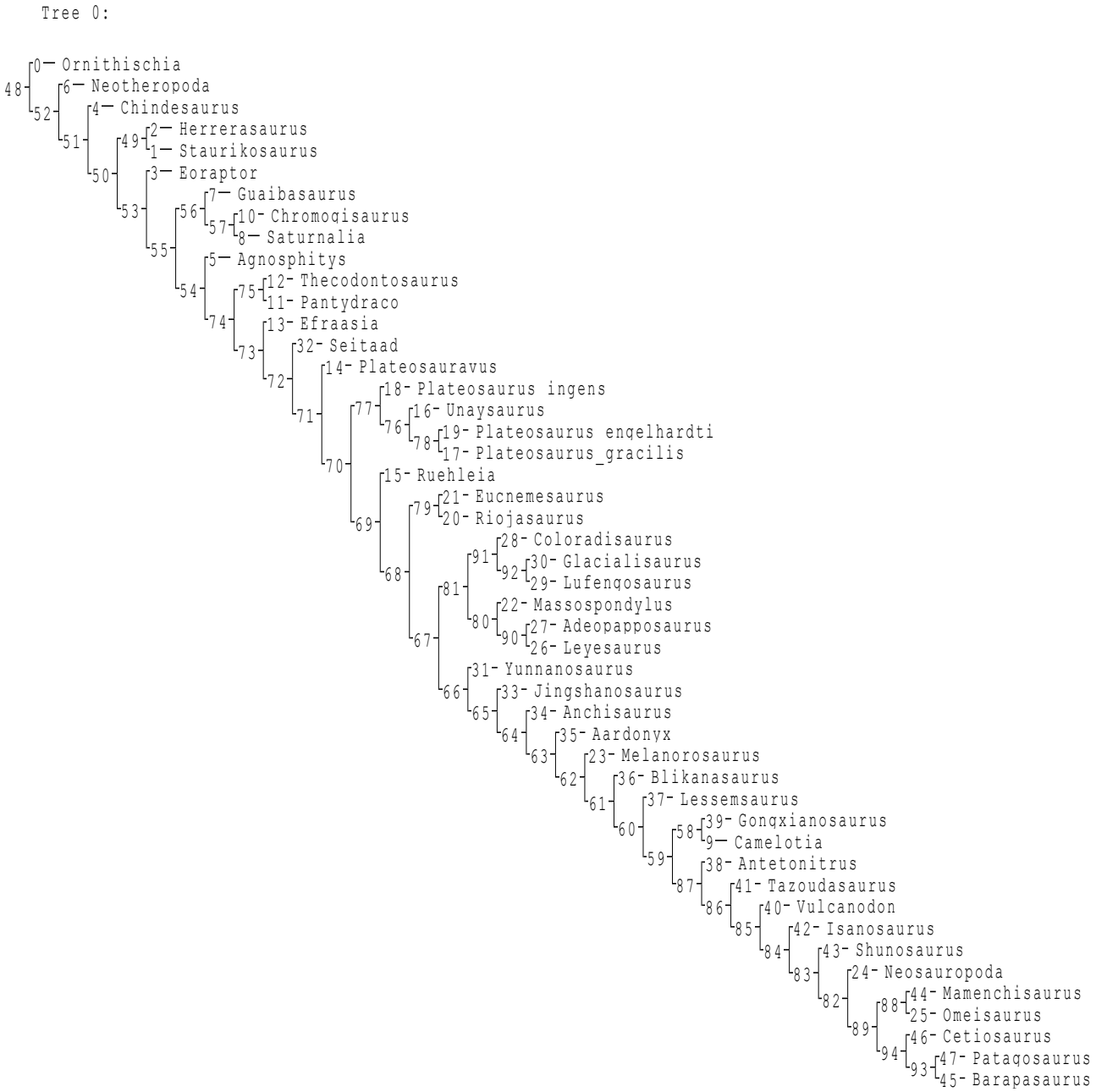

Figure 48. Most parsimonious tree of the pneumatic composite ‘McPhee-Yates’ phylogeny. Traditional search (parsimony) of the original ‘McPhee-Yates’ dataset of 48 taxa and 364 characters using TBR algorithm yielded 18 best trees of 1073 steps, CI: 0.380 and RI: 0.662. Assigned outgroup: Ornithischia. Numbers indicate robustness of clades (number of parsimonious trees the particular clade has been recovered; the higher the value, the higher level of robustness).

Compared to Figure 7 (tree length = 1154 steps, with CI = 0.354 and RI = 0.636) and the published tree of McPhee et al. (2014; Fig.24), this tree in Figure 48 had a shorter length and similar consistency and retention indices implying a better fit between the data and the resulted phylogeny when the analysis ran in *TNT*. This phylogeny bears resemblance with both the published phylogeny and the one in Figure 7. Here, *Efraasia* was recovered just one paraphyletic step more basal to *Seitaad*, rather than three (Fig.7) and *Seitaad* more basal to *Plateosaurus engelhardti* rather than more derived. Also, *Camelotia* was recovered as sister taxon to *Gongxianosaurus* rather than being more basal to it. Such differences may have occurred due the obligatory choice of one outgroup instead of many, as it was allowed in *PAUP* and possibly due to the different software although the author conducted the analysis under the same parameters, wherever applicable.

The 11 added pneumaticity characters' scores were retrieved and compared with those of 11 dental characters:

Characters:	353	354	355	356	357	358	359	360	361	362	363
Fit Scores:	1	2	1	2	0	0	1	2	0	0	1
CI =	1	0.50	1	0.50	1	1	1	0.50	1	1	1
RI =	1	0.50	1	0	1	1	1	0.66	1	1	1
HI =	0	0.25	0	0.25	0	0	0	0.25	0	0	0

Comparison with 11 dental characters' scores:

118 [107. Number of premaxillary teeth: four (0) or more than four (1) (Galton 1990)].

Fit Score: 1 CI = 1 RI = 1 HI = 0

119 [108. Number of dentary teeth (in adults): less than 18 (0) or 18 or more (1) (modified from Wilson and Sereno 1998)].

Fit Score: 1 CI = 1 RI = 1 HI = 0

120 [109. Arrangement of teeth within the jaws: linearly placed, crowns not overlapping (0) or imbricated with distal side of tooth overlapping mesial side of the succeeding tooth (1)].

Fit Score: 2 CI = 1 RI = 1 HI = 0

121 [110. Orientation of the maxillary tooth crowns: erect (0) or procumbent (1) (modified from Gauthier 1986)].

Fit Score: 3 CI = 0.33 RI = 0 HI = 0.40

122 [111. Orientation of the dentary tooth crowns: erect (0) or procumbent (1) (modified from Gauthier 1986)].

Fit Score: 2 CI = 0.50 RI = 0 HI = 0.25

123 [112. Teeth with basally constricted crowns: absent (0) or present (1) (Gauthier 1986)].
Fit Score: 5 CI = 0.20 RI = 0.50 HI = 0.57
124 [113. Tooth–tooth occlusal wear facets: absent (0) or present (1) (Wilson and Sereno 1998)].
Fit Score: 4 CI = 0.25 RI = 0.57 HI = 0.50
125 [114. Mesial and distal serrations of the teeth: fine and set at right angles to the margin of the tooth (0) or coarse and angled upwards at an angle of 45 degrees to the margin of the tooth (1) (Benton et al. 2000)].
Fit Score: 1 CI = 1 RI = 1 HI = 0
126 [115. Distribution of serrations on the maxillary and dentary teeth: present on both the mesial and distal carinae (0), absent on the posterior carinae (1), or absent on both carinae (2) (Wilson 2002). Unordered].
Fit Score: 2 CI = 1 RI = 1 HI = 0
127 [116. Long axis of the tooth crowns distally recurved: present (0) or absent (1) (Gauthier 1986)].
Fit Score: 2 CI = 0.50 RI = 0.50 HI = 0.25
128 [117. Texture of the enamel surface: entirely smooth (0), finely wrinkled in some patches (1), or extensively and coarsely wrinkled (2) (modified from Wilson and Sereno 1998)].
Fit Score: 7 CI = 0.28 RI = 0.66 HI = 0.62
129 [118. Lingual concavities of the teeth: absent (0) or present (1) (Upchurch 1995)].
Fit Score: 11 CI = 0.09 RI = 0.23 HI = 0.76

The 11 added pneumaticity characters carried a stronger phylogenetic signal than the 11 dental characters since the majority of the former revealed to possess greater CI and lower HI values than those of the latter. By contrast, the fitness of the added pneumaticity characters was, in general, marginally lower than the fitness of the dental characters implying, nevertheless, moderate and low fitness scores of the pneumaticity characters in this phylogeny. The majority-rule (50%) consensus tree of the most parsimonious ‘McPhee-Yates’ phylogeny is shown below in Figure 49.

Figure 49. Majority-rule consensus tree of the most parsimonious 'McPhee-Yates' trees. 50% majority rule consensus 'McPhee-Yates' tree from the most parsimonious trees of 48 taxa and 364 characters (tree length = 1073 steps, CI = 0.380 and RI = 0.662). Assigned outgroup: Ornithischia. Numbers indicate robustness of clades (number of parsimonious trees the particular clade has been recovered; the higher the value, the higher level of robustness).

Compared to the tree shown in Figure 8 (tree length: 1154 steps, with CI = 0.354 and RI = 0.636) this tree in Figure 49 was shorter but its indices were slightly larger. In this phylogeny, *Seitaad* was recovered one step more basal than its position in Figure 8. *Camelotia* was

recovered to be paired as a sister taxon to *Melanorosaurus* rather than being one paraphyletic step more basal to it. All other recovered topologies match those of Figure 8.

The original composite 'McPhee-Yates' phylogeny was then imposed as a constraint onto the pneumatically modified phylogeny for monophyly (i.e. positive) and traditional heuristic search with TBR algorithm was conducted yielding a tree of 1090 steps, CI: 0.376 and RI: 0.658 (Fig.50) and the estimated consensus can be seen in Figure 51 (1090 steps, CI: 0.337, RI: 0.594).

Figure 50. Constrained most parsimonious pneumatically modified 'McPhee-Yates' tree. Constrained 'McPhee-Yates' most parsimonious tree of 48 taxa and 364 characters. The original phylogeny of the composite 'McPhee-Yates' parsimonious tree. Numbers indicate robustness of clades. Assigned outgroup: Ornithischia. Tree length: 1090 steps, CI: 0.376 and RI: 0.658.

The constrained tree shown in Figure 50 has fewer steps and smaller CI and RI values than the tree shown in Figure 9 (1157 steps, CI: 0.354 and RI: 0.634). *TNT* reveals a better fit between the dataset and resulted phylogeny. The former tree also has some topological differences with respect to the latter. *Agnosphitys* was recovered basal to *Guaibasaurus* instead of the reverse situation, as it was seen in Figure 9. In addition, *Melanorosaurus* and *Camelotia* were recovered as a pair of sister taxa instead of the former taxon being basal to the latter. Another different point here is that *Antetonitrus* was recovered as sister taxon with *Lessemsaurus* instead of the latter taxon being basal to the former. A worth noticing common feature between Figure 50 and Figure 9 is that the pair of sister taxa *Patagosaurus* and *Barapasaurus* was recovered as a sister pair to the pair of *Cetiosaurus* and Neosauropoda.

D'Emic (2012) – Whitlock (2011)

For this set of parsimony analyses in *TNT*, *Shunosaurus* was chosen as the outgroup since it is the most distantly related clade with respect to Sauropoda when compared to the other previously assigned outgroup taxa (i.e. *Omeisaurus* and *Jobaria*). Traditional heuristic search was conducted in the original (pneumatically unaltered) composite phylogeny made of Whitlock (2011) and D'Emic (2012) phylogenies under parsimony optimality criterion and TBR swapping algorithm in the original composite dataset (48 taxa, 189 characters). Uninformative characters were kept included, and all characters were set to be non-additive and active. The resultant tree is shown below in Figure 51 (tree length = 447 steps**,** CI: 0.459 and RI: 0.758) has the same length as the one in Figure 20 and, as a result, it is longer than any of the two published phylogenies and seven steps longer than the two of them combined together, just as we saw in the *PAUP* analyses (Whitlock, 2011; tree in Fig.7 is 273 steps long and has a CI: 0.740 and RI: 0.844 and the tree shown in Figure 5 (D'Emic, 2012) is 197 steps long with a CI: 0.64 and RI: 0.80. The values of consistency and retention indices of the tree in Figure 51 are much lower than the published trees which denotes a poorer fit between the data and the resulted hybrid phylogeny.

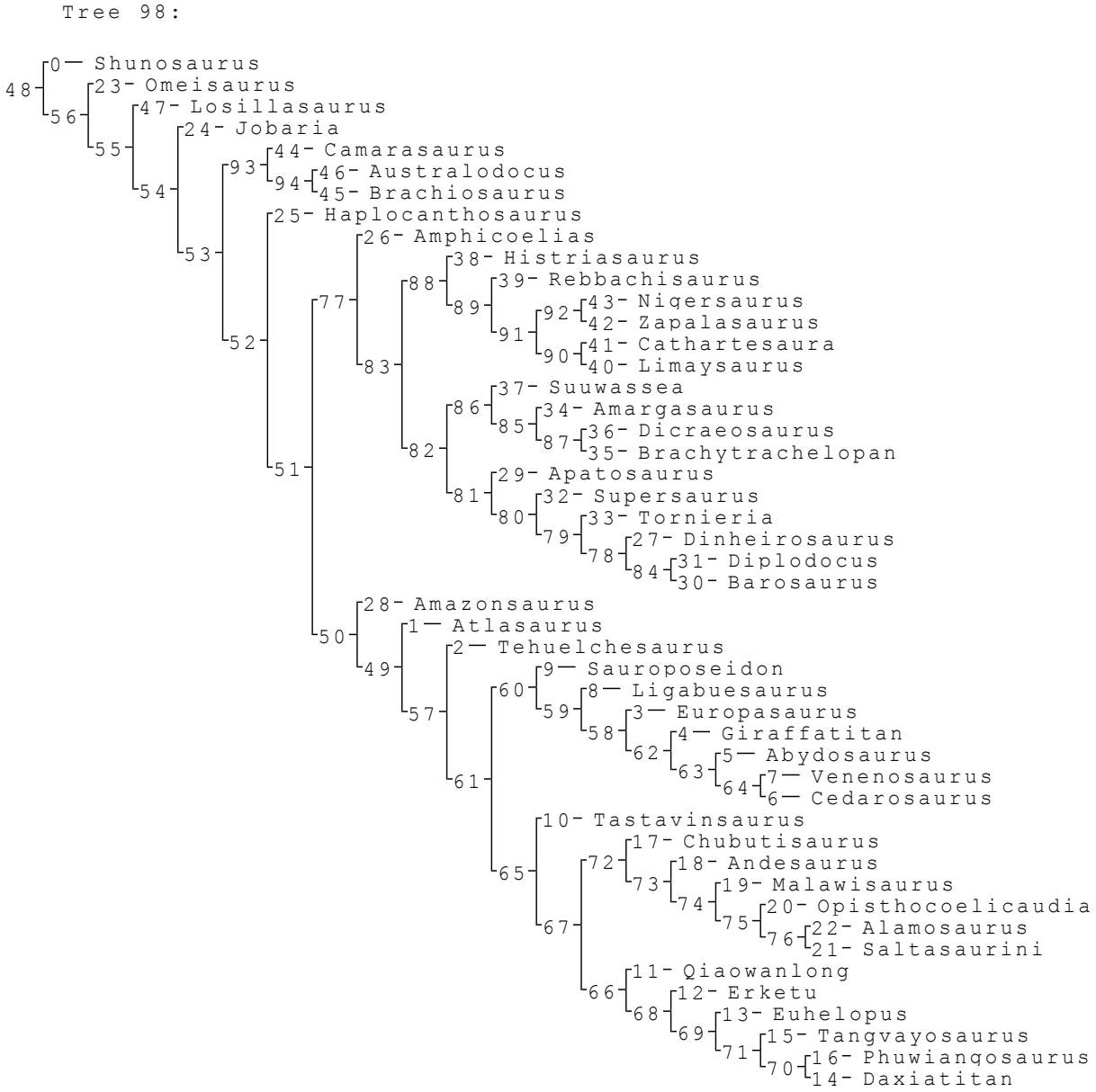

Figure 51. Original composite unaltered 'D'Emic-Whitlock' tree. Original composite parsimonious tree comprised of both D'Emic's (2012) and Whitlock's (2011) datasets under TBR of 48 taxa and 189 characters. Assigned outgroup: *Shunosaurus*. Tree length: 447 steps**,** CI: 0.459 and RI: 0.758.

Compared to the tree in Figure 20 and the published trees, this tree is a combination of the two published trees and looks less like the one in Figure 20. The difference of the tree above is that *Omeisaurus* was recovered to be basal to *Losillasaurus* instead of either forming a dichotomous pair or a pair of sister taxa as seen in Whitlock's tree (2011; Fig.7) or the tree in the tree in Figure 20. In addition, *Tornieria* was recovered basal to *Dinheirosaurus* rather than in a dichotomy as was seen in both the

published tree and the tree in Figure 20. *Amazonsaurus* was recovered here to be basal to *Atlasaurus* while the opposite occurs in Figure 20. Also, *Phuwiangosaurus* was recovered as a sister taxon with *Daxiatitan* instead of being with *Tangvayosaurus* (Fig. 20 and in D'Emic, 2012; Fig.5). All other recovered topologies were identical to those in Figure 20.

The pneumatic composite dataset consisting of 48 taxa and 185 characters was analysed under the same parameters followed in the previous analyses and yielded 21 most parsimonious trees of tree length = 459 steps, CI: 0.436 and RI: 0.734 (Figure 52).

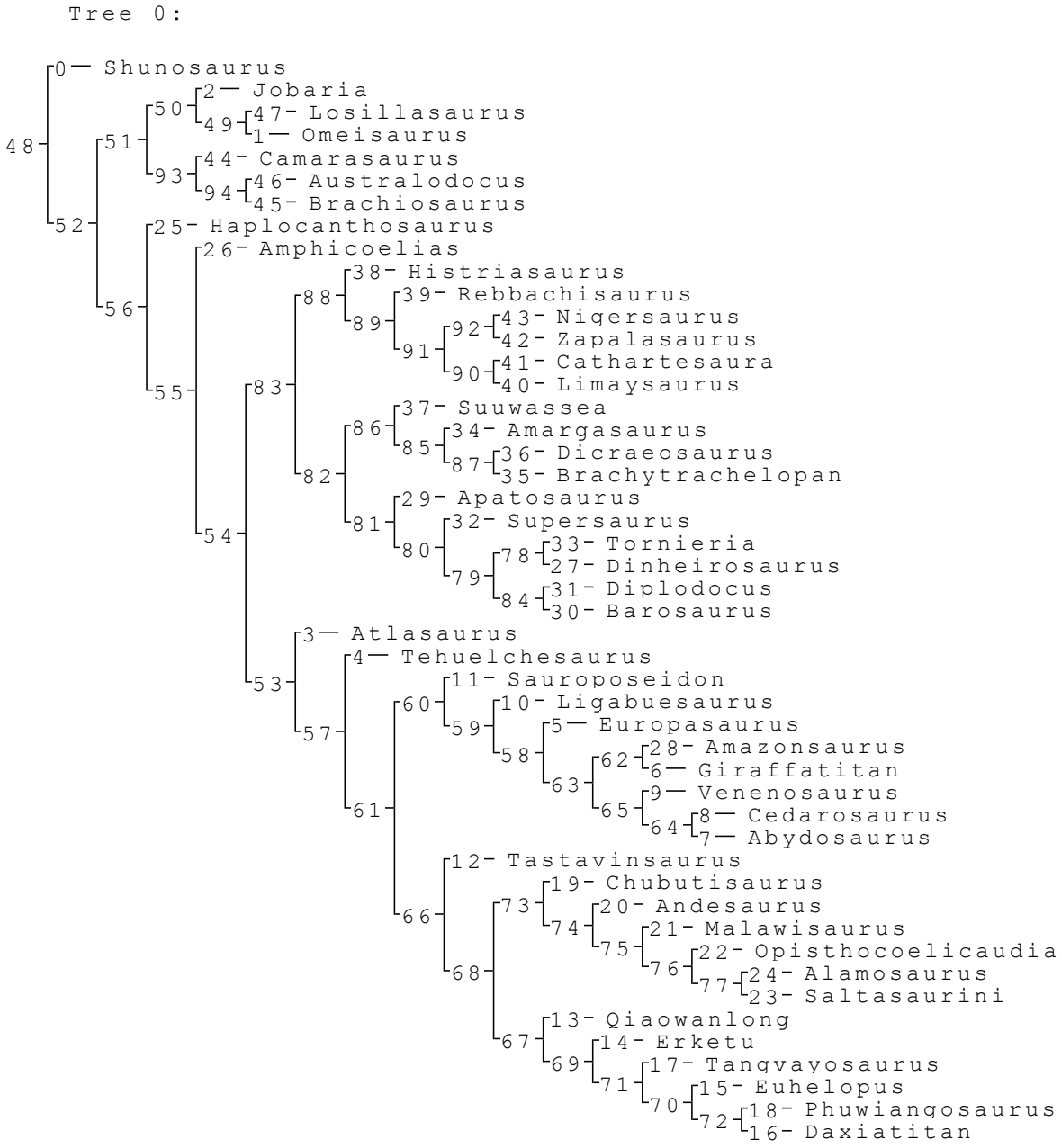

Figure 52. Pneumatic composite 'D'Emic-Whitlock' tree. Pneumatic composite parsimonious tree under TBR of 48 taxa and 185 characters. Assigned outgroup: *Shunosaurus*. Tree length**:** 459 steps, CI: 0.436 and RI: 0.734.

This tree is shorter than its equivalent shown in Figure 21 (461 steps, CI: 0.434 and RI: 0.732). Differences between them are that *Omeisaurus* was not paired with *Losillasaurus* but instead it was recovered basal to it. Camarasaurus was recovered as in Whitlock's phylogeny of being paraphyletic to the pair of sister taxa *Brachiosaurus* and *Australodocus*. Different from Figure 21 also in the act that in that tree *Camarasaurus* was recovered as a sister taxon to *Brachiosaurus*. Also, here in Figure 52 *Diplodocus* was recovered as sister taxon with *Barosaurus* (as in Whitlock's tree) whereas in Figure 21 *Barosaurus* was recovered as a sister taxon to *Australodocus*. *Amazonsaurus* was recovered basal to *Giraffatitan* instead of them being sister taxa as shown in Figure 21. One final difference is that in Figure 51 *Tangvayosaurus* was recovered in a more derived position than *Erketu* and *Euhelopus* (as in Whitlock's tree) while the opposite occurred in the tree shown in Figure 21. Unlike Whitlock' tree, *Tangvayosaurus* was not recovered as a sister taxon with *Phuwiangosaurus* but instead more basal to it.

The fit scores and indices of the 11 added pneumaticity characters (here numbered 174-184 because TNT starts counting from zero instead of one) were retrieved and compared with those of 11 cranial/dental characters.

The 11 added pneumaticity characters' scores:

Characters:	174	175	176	177	178	179	180	181	182	183	184
Fit Scores:	6	6	5	5	5	4	6	4	1	0	1
CI =	0.20	0.16	0.20	0.25	0.25	0.25.	0.20	0.25	1	1	1
RI =	0.55	0.50	0	0.50	0.40	0.40	0.42	0	1	1	1
HI =	0.57	0.62	0.57	0.50	0.50	0.50	0.57	0.50	0	0	0

Comparison with 11 cranial/dental characters' scores:

16 [5. Parietal, distance separating supratemporal fenestrae: less than (0) or twice (1) the long axis of supratemporal fenestra. (Wilson, 2002)]

Fit Score: 2 CI = 0.50 RI = 0.66 HI = 0.25

17 [6. Supraoccipital, height: twice (0) subequal to or less than (1) height of foramen magnum. (Wilson, 2002)]

Fit Score: 2 CI = 0.50 RI = 0.66 HI = 0.25

18 [7. Basal tubera, width relative to occipital condyle: less than 1.4 (0); greater than 1.6 (1). (Modified from Mannion, 2011)]

Fit Score: 2 CI = 0.50 RI = 0.83 HI = 0.25

19 [8. Paroccipital process, ventral non-articular process: absent (0); present (1). (Wilson, 2002)]

Fit Score: 2 CI = 0.50 RI = 0.50 HI = 0.25

20 [9. Quadradojugal, anterior ramus, ventral triangular projection: absent (0); present (1).

Fit Score: 2 CI = 0.50 RI = 0.75 HI = 0.25

21 [10. Dentary, posteroventral process, shape: single (0); divided (1). (Modified from Chure et al., 2010)]

Fit Score: 3 CI = 0.50 RI = 0.75 HI = 0.25

22 [11. Surangular depth: less than twice (0) or more than two and a half times (1) maximum depth of the angular (Wilson, 2002)]

Fit Score: 3 CI = 0.33 RI = 0.75 HI = 0.25

23 [12. Dentary teeth, number: greater than 20 (0); 17 or fewer (1). (Wilson, 2002)]

Fit Score: 4 CI = 0.33 RI = 0.60 HI = 0.40

24 [13. Tooth crowns, orientation: aligned anterolingually, tooth crowns overlap (0); aligned along jaw axis, crowns do not overlap (1). (Modified from Wilson, 2002)]

Fit Score: 3 CI = 0.50 RI = 0.87 HI = 0.25

25 [14. Marginal tooth denticles: present on anterior and posterior edges of tooth (0); only present in posterior-most few teeth (1); absent on both anterior and posterior edges (2). (Modified from Wilson, 2002)]

Fit Score: 3 CI = 0.33 RI = 0.77 HI = 0.40

26 [15. Maxillary teeth, shape: straight along axis (0); twisted axially through an arc of 30-45° (1). (Modified from Chure et al., 2010)]

Fit Score: 4 CI = 0.25 RI = 0.50 HI = 0.50

The 11 pneumaticity characters have better fitness scores in the ‘D’Emic-Whitlock’ composite pneumatically modified phylogeny than the 11 cranial / dental ones but the pneumaticity characters had lower phylogenetic signal than the dental characters due to lower CI and higher HI values.

The strict consensus tree in Figure 53 differs considerably from the one shown in Figure 22. It recovered many polytomies. One involving three eusauropods and one diplodocid (*Losillasaurus*, *Haplocanthosaurus*, *Jobaria* and *Omeisaurus*) and another polytomy comprised of 17 neosauropods (*Amazonsaurus*, *Amphicoelias*, *Andesaurus*, *Chubutisaurus*, *Phuwiangosaurus*, *Tangvayosaurus*, *Daxiatitan*, *Euhelopus*, *Erketu*, *Qiaowanlong*, *Tastavinsaurus*, *Sauroposeidon*, *Ligabuesaurus*, *Giraffatitan*,

Europasaurus, *Tehuelchesaurus* and *Atlasaurus*). *Tornieria* and *Dinheirosaurus* were recovered as sister taxa. All other topologies match those of Figure 52.

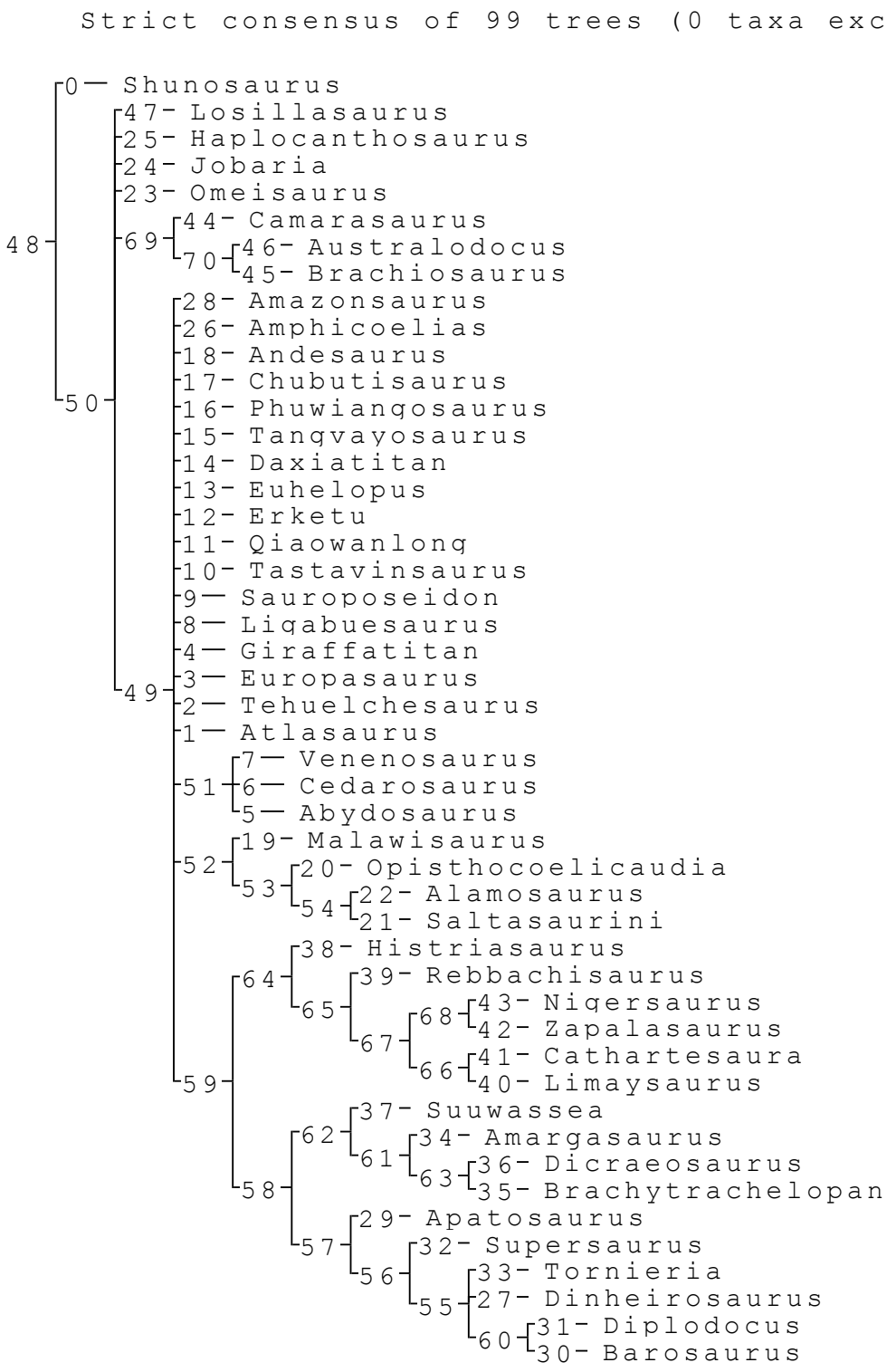

Figure 53. Strict consensus pneumatic composite 'D'Emic-Whitlock' tree. Strict consensus pneumatic composite from 21 most parsimonious trees of 48 taxa and 185 characters. Assigned outgroup: *Shunosaurus*. Note the two polytomies, one of three

eusauropods and one diplodocid and the other of 17 neosauropods (diplodocoids, basal titanosauriforms, and somphospondylans).

The imposition of the original hybrid ‘D’Emic-Whitlock’ phylogeny onto the pneumatically modified dataset yielded one constrained most parsimonious tree of 459 steps, CI: 0.436 and RI: 0.734.

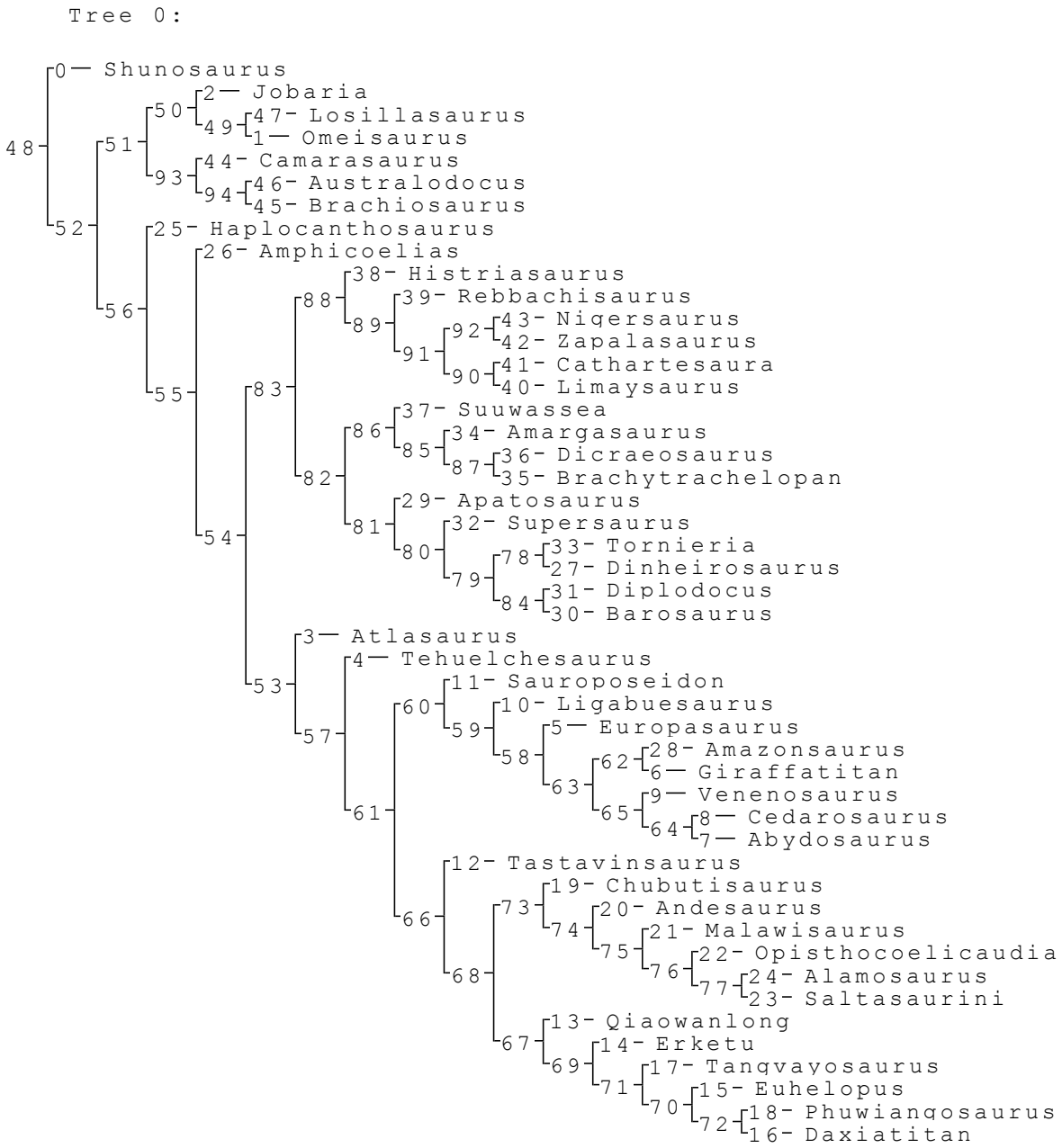

Figure 54. Constrained pneumatic composite ‘D’Emic-Whitlock’ tree. Constrained pneumatic composite parsimonious tree under TBR of 48 taxa and 185 characters. The phylogeny of the original composite ‘D’Emic-Whitlock’ was imposed onto the

pneumatically modified dataset. Assigned outgroup: *Shunosaurus*. Tree length**:** 459 steps, CI: 0.436 and RI: 0.734.

This tree and the one shown in Figure 55 not only differ from the ones in Figures 23 and 24 in several recovered topologies but, in fact they are identical to the pneumatic composite tree of Figure 52. Given the facts that the original composite phylogeny was imposed as a constraint onto the pneumatically modified dataset and that the topological recovery of the clades match to a good extent with those of the published phylogenies, it can be said that adding the pneumaticity characters derived form this study onto the hybrid dataset did not result into considerably altered interrelationships of sauropods.

Figure 55. Estimated consensus of the constrained pneumatic composite 'D'Emic-Whitlock' tree. Estimated consensus of the constrained pneumatic parsimonious tree. Assigned outgroup: *Shunosaurus*.

Carballido & Sander (2014)

For this set of parsimony analyses in *TNT*, *Plateosaurus* was chosen as the outgroup since it is the most distantly recovered and related clade with respect to Sauropoda when compared to the other previously assigned outgroup taxa (i.e. *Chinshakiangosaurus*, *Mussaurus* and *Antetonitrus*) as was revealed by the published phylogeny by Carballido & Sander (2014; Figure 29)**.** All uninformative characters were kept included and all characters were set to be active. Following the authors' parameters, the traditional heuristic search of the original dataset yielded two most parsimonious trees of tree length = 987 steps**,** CI: 0.410 and RI: 0.725. This tree, though shorter in steps than the one shown in Figure 35, is almost identical in both length and values of consistency and retention indices to the published phylogeny (tree length = 988 steps**,** CI: 0.406 and RI: 0.725). Compared to the tree shown in Figure 35 and to the published phylogeny, the tree shown below in Figure 56 bears few differences. *Gongxianosaurus* was recovered basal to *Isanosaurus* and *Amygdalodon*, instead of being a sister taxon to *Amygdalodon*. *Omeisaurus* was successfully recovered as a sister taxon to *Mamenchisaurus* as shown in the published phylogeny and unlike the tree in Figure 35 where *Mamenchisaurus* was paired as a sister taxon to *Tendaguria*. Additionally, in agreement with the published phylogeny but not with the tree in Figure 35, *Camarasaurus* was recovered as a sister taxon to *Bellusaurus* and *Tendaguria* as a sister taxon to *Wintonotitan*. Unlike both the published phylogeny and the one in Figure 35, *Paluxysaurus* was recovered as a sister taxon to *Cedarosaurus*, instead of *Venenosaurus* and *Cedarosaurus* being sister taxa. Finally, *Malarguesaurus* was recovered as a sister taxon to *Argentinosaurus* instead of these two being in a dichotomous pair as in the published phylogeny. The strict consensus tree of the two most parsimonious trees shown in Figure 57 is quite similar to the published phylogeny and shorter in steps. Most recovered topologies match those recovered in the published phylogeny the exceptions that *Zapalasaurus* was recovered basal to *Histriasaurus* instead of these two taxa forming a dichotomous pair. Similarly, *Rayososaurus* was recovered basal to *Rebbachisaurus* instead of these two forming a dichotomy. Unlike the published phylogeny but in agreement with the tree in Figure 36, *Camarasaurus* was recovered in a dichotomy with *Bellusaurus*. In addition, unlike either of the other two trees, *Chubutisaurus*, *Erketu* and *Venenosaurus* were recovered in a trichotomy. Finally, *Paluxysaurus* and *Cedarosaurus* were recovered as sister taxa

instead of *Cedarosaurus* being a sister taxon to *Venenosaurus* as shown in the other two phylogenies.

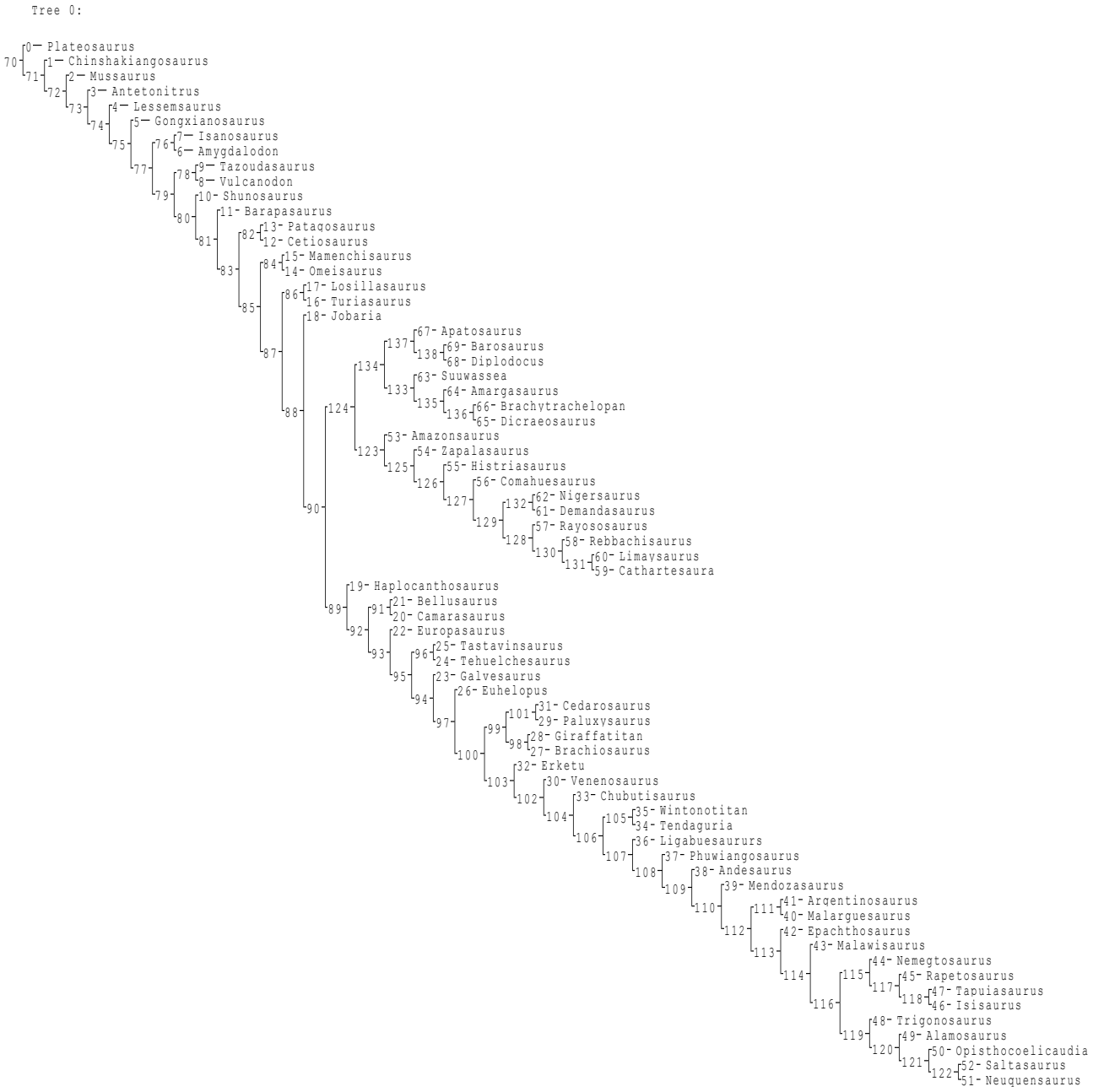

Figure 56. Original 'Carballido-Sander' phylogeny. Traditional heuristic search using TBR swapping algorithm of the original dataset of 70 taxa and 341 characters yielded two most parsimonious trees of tree length: 987 steps, CI: 0.410 and RI: 0.725. Assigned outgroup: *Plateosaurus*.

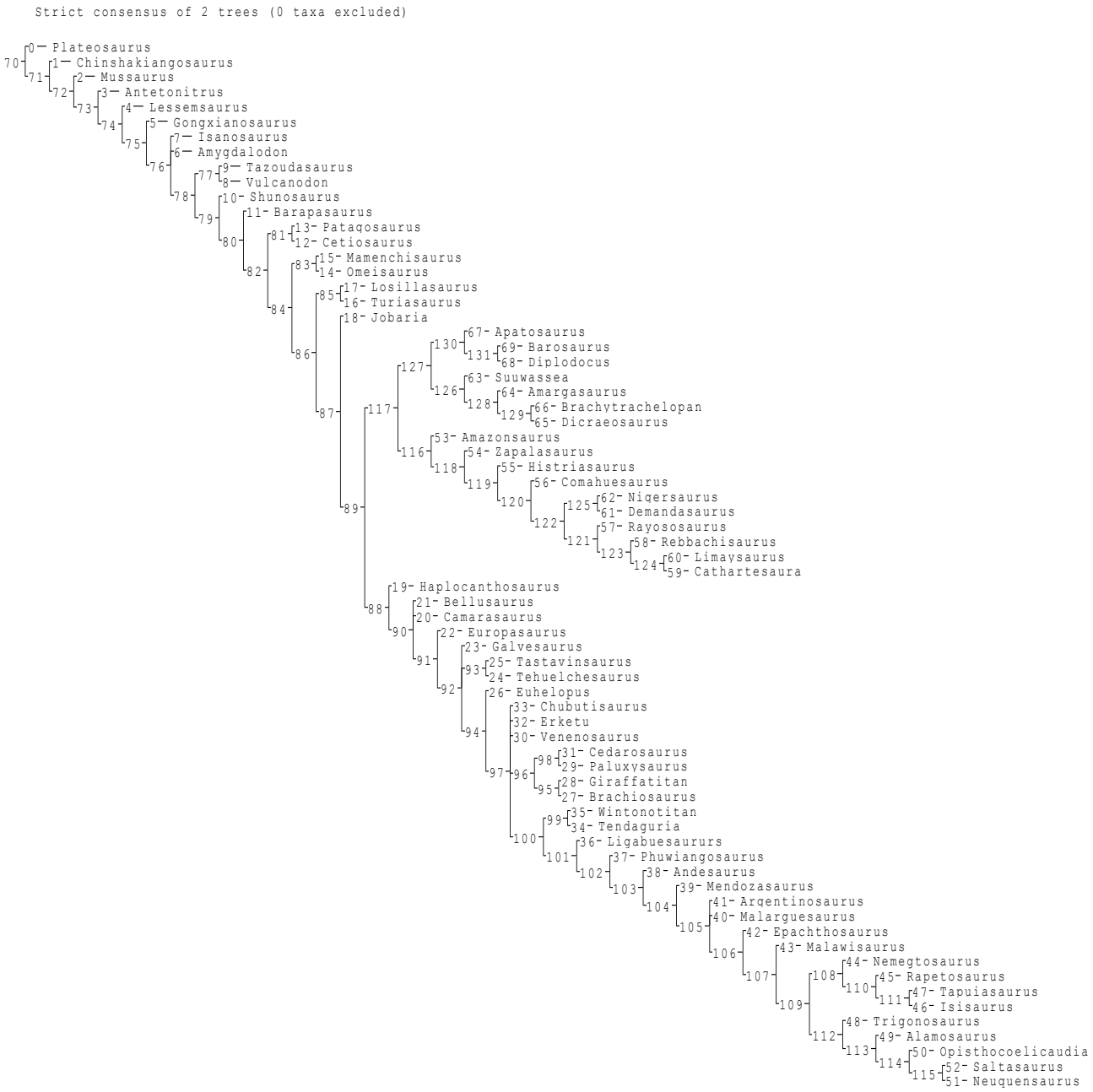

Figure 57. Strict consensus original 'Carballido-Sander' tree. Strict consensus of the two most parsimonious trees of the original dataset comprised of 70 taxa and 341 characters. Assigned outgroup: *Plateosaurus*.

Traditional heuristic search with TBR swapping algorithm in the pneumatically modified dataset yielded nine most parsimonious trees of 971 steps, CI: 0.408 and RI: 0.705 (Figure 58). This tree is shorter than both the published phylogeny and the one shown in Figure 37. The indices imply a moderate fit between the data and the resulted phylogeny. In contrast to the published phylogeny and the tree shown in Figure 37, the tree in Figure 58 differs in following points: *Gongxianosaurus* was not recovered as sister taxon to *Amygdalodon* but rather basal to it.

Similarly, *Omeisaurus* was recovered basal to *Mamenchisaurus* instead of being sister taxa with each other and *Losillasaurus* basal to *Turiasaurus* instead of being sister taxa with each other. Furthermore, *Zapalasaurus* was recovered basal to *Histriasaurus*, as it was also seen in Figure 37, instead of forming a dichotomy, as it was evident in the published phylogeny. *Rayososaurus* and *Rebbachisaurus* were recovered as sister taxa instead of forming a dichotomy. *Tehuelchesaurus* was recovered basal to *Tastavinsaurus* by five clades instead of being sister taxa (shown in the published phylogeny). Unlike both other phylogenies, *Cedarosaurus* was recovered as a sister taxon to *Paluxysaurus*, *Venenosaurus* to *Giraffatitan* and *Chubutisaurus* to *Tastavinsaurus*. *Wintonotitan* was successfully recovered as a sister taxon to *Tendaguria*. In contrast to the published phylogeny, though, *Andesaurus* was recovered basal to *Phuwiangosaurus* and *Malarguesaurus* to *Argentinosaurus*, as it was also seen in Figure 37. Finally, unlike either phylogenies, *Erketu* was recovered as the most derived taxon and sister to *Tapuiasaurus* instead of forming a dichotomy with *Chubutisaurus* and being more basal to some titanosauriform and somphospondylan taxa (e.g. *Tendaguria*, *Chubutisaurus*, *Rapetosaurus*, *Isisaurus*, etc.) as it was evident in the published phylogeny.

The strict consensus tree of the nine most parsimonious trees in Figure 59 bore little resemblance to neither the published phylogeny nor the tree in Figure 38. At first, Omeisaurus was recovered basal to Mamenchisaurus, instead of being sister taxa to each other and, secondly, it recovered two unresolved polytomies; one containing four eusauropod and one basal sauropodomorph taxa (*Tazoudasaurus*, *Vulcanodon*, *Isanosaurus*, *Amygdalodon* and *Gongxianosaurus*) and another containing 29 neosauropod taxa, including diplodocoids, basal titanosauriforms and somphospondylans. The remaining recovered topologies match those depicted on the published phylogeny and considering the index values it can be said that there is a moderate fit between the data and the resulted phylogeny.

Figure 58. Pneumatic 'Carballido-Sander' parsimonious phylogeny. Traditional heuristic search using TBR swapping algorithm of the pneumatically modified dataset of 70 taxa and 340 characters. The result yielded nine most parsimonious trees of tree length: 971 steps, CI: 0.408 and RI: 0.705. Assigned outgroup: *Plateosaurus*.

The scores and index values of the 11 added pneumaticity characters (329-339) were retrieved and compared with those of 11 dental characters:

Characters:	329	330	331	332	333	334	335	336	337	338	339
Fit Scores:	7	9	9	10	5	4	6	4	1	0	1
CI =	0.14	0.11	0.16	0.10	0.20	0.25	0.16	0.25	1	1	1
RI =	0.50	0.33	0.37	0	0.20	0	0.16	0.50	1	1	1
HI =	0.66	0.72	0.62	0.75	0.57	0.50	0.62	0.50	0	0	0

Comparison with 11 cranial / dental characters' scores:

107 [(96) Dentary teeth, number: greater than 20 (0); 10-17 (1); 9 or fewer (2). (modified from Wilson, 2002:ch.73)]

Fit Score: 5 CI = 0.60 RI = 0.84 HI = 0.40

108 [(97) Replacement teeth per alveolus, number: two or fewer (0); more than four (1). (Wilson, 2002:ch. 74)]

Fit Score: 6 CI = 0.66 RI = 0.66 HI = 0.40

109 [(98) Lateral plate: absent (0); present (1). (Upchurch et al., 2004:ch. 9)]

Fit Score: 2 CI = 0.50 RI = 0.66 HI = 0.25

110 [(99) Teeth, orientation: perpendicular (0); or oriented anteriorly relative to jaw margin (1). (Wilson, 2002:ch. 75)]

Fit Score: 6 CI = 1 RI = 1 HI = 0

111 [(100) Tooth crowns, orientation: aligned along jaw axis, crowns do not overlap (0); aligned slightly anterolingually, tooth crowns overlap (1). (Wilson, 2002:ch. 69)]

Fit Score: 6 CI = 0.16 RI = 0.70 HI = 0.62

112 [(101) Crown-to-crown occlusion: absent (0); present (1). (Wilson, 2002:ch. 67)]

Fit Score: 5 CI = 0.20 RI = 0.63 HI = 0.57

113 [(102) Occlusal pattern: interlocking, V-shaped facets (0); high-angled planar facets (1); low-angled planar facets (2). (Wilson, 2002:ch. 68)]

Fit Score: 8 CI = 0.37 RI = 0.75 HI = 0.62

114 [(103) Tooth crowns, cross-sectional shape at mid-crown: elliptical (0); D-shaped (1); cylindrical (2). (Wilson, 2002:ch. 70)]

Fit Score: 2 CI = 0.50 RI = 0 HI = 0.25

115 [(104) Enamel surface texture: smooth (0); wrinkled (1). (Wilson, 2002:ch.71)]

Fit Score: 4 CI = 0.25 RI = 0.66 HI = 0.50

116 [(105) Thickness of enamel asymmetric labiolingually: absent (0); present (1). (Whitlock, 2011:ch. 74)]

Fit Score: 3 CI = 0.33 RI = 0.66 HI = 0.40

117 [(106) Marginal tooth denticles: present (0); absent on posterior edge (1); absent on both anterior and posterior edges (2). (Wilson, 2002:ch. 72)]
Fit Score: 4 CI = 0.25 RI = 0 HI = 0.50

The 11 added pneumaticity characters revealed to have high fitness scores in the 'Carballido & Sander (2014)' pneumatic phylogeny but compared to the 11 cranial/dental characters they had relatively low CI and RI values and high HI values. These values indicate that the added pneumaticity characters had moderately low phylogenetic signal and high levels of homoplasy. The 11 dental characters, however, had higher CI and RI values, moderately high HI values but they also yielded high fitness scores.

The imposition of the trees derived from analysing the original dataset of Carballido & Sander (2014) as enforced constraints onto the pneumatically modified dataset yielded one parsimonious tree of length = 975 steps, CI: 0.406 and RI: 0.702 (Figure 60). The resulted tree has smaller length value from either the published tree or the one shown in Figure 39, similar consistency and retention values index values with the published tree and smaller index values than the tree in Figure 39. The constrained pneumatic tree (Figure 60) differed from the published phylogeny and the tree depicted in Figure 39 in several topological points. *Isanosaurus* was recovered as a sister taxon to *Gongxianosaurus* instead of the latter taxon being sister to *Amygdalodon*, *Vulcanodon* was recovered in a derived position with respect to *Tazoudasaurus* instead of being sister taxa to each other and *Tendaguria* was recovered as a sister taxon to *Mamenchisaurus* instead of the former taxon being sister taxon to *Wintonotitan* and the latter taxon sister to *Omeisaurus*. This altered topology also positioned *Omeisaurus* basally to *Tendaguria* and *Mamenchisaurus* and it can also be seen in Figure 38. Contrary to the published phylogeny and the one depicted in Figure 39, *Zapalasaurus* was recovered basal to *Histriasaurus*, *Cedarosaurus* was recovered as a sister taxon to *Paluxysaurus* and *Venenosaurus* as a sister taxon to *Giraffatitan*. *Rayososaurus* was recovered basal to *Rebbachisaurus* instead of forming a dichotomy with each other and *Chubutisaurus* was not recovered in a dichotomy with *Erketu* but instead basal to it. *Phuwiangosaurus* was recovered as a sister taxon to *Erketu* instead of the latter being basal to the former, and *Andesaurus* to *Wintonotitan* instead of the latter being more basal to the former. Finally, *Malarguesaurus* was recovered basal to *Argentinosaurus* instead of forming a dichotomy with each other. All other remaining topologies match those shown in the published phylogeny. The estimated constrained consensus shown in Figure 61 was identical to the previous tree (Fig.60).

It is noticeable that the pneumatically modified parsimonious tree as well as its constrained version are fully resolved i.e. they lack polytomies, while the strict consensus tree of the original dataset is almost fully resolved and the strict consensus of the pneumatically modified version is largely unresolved, bearing two large polytomies.

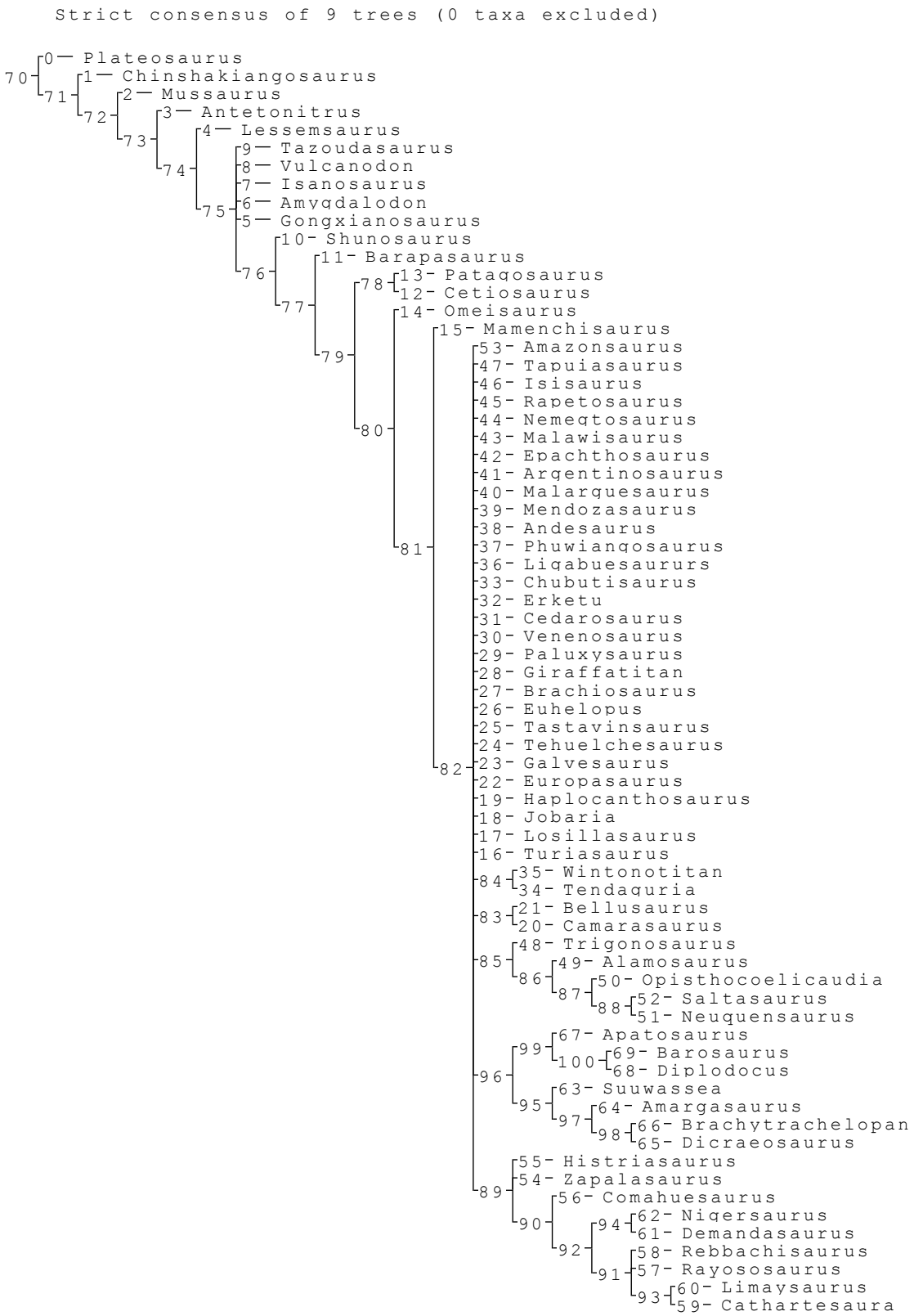

Figure 59. Strict consensus of pneumatic 'Carballido-Sander' parsimonious trees. Strict consensus tree of the nine most parsimonious trees of 70 taxa and 340 characters. Assigned outgroup: *Plateosaurus*.

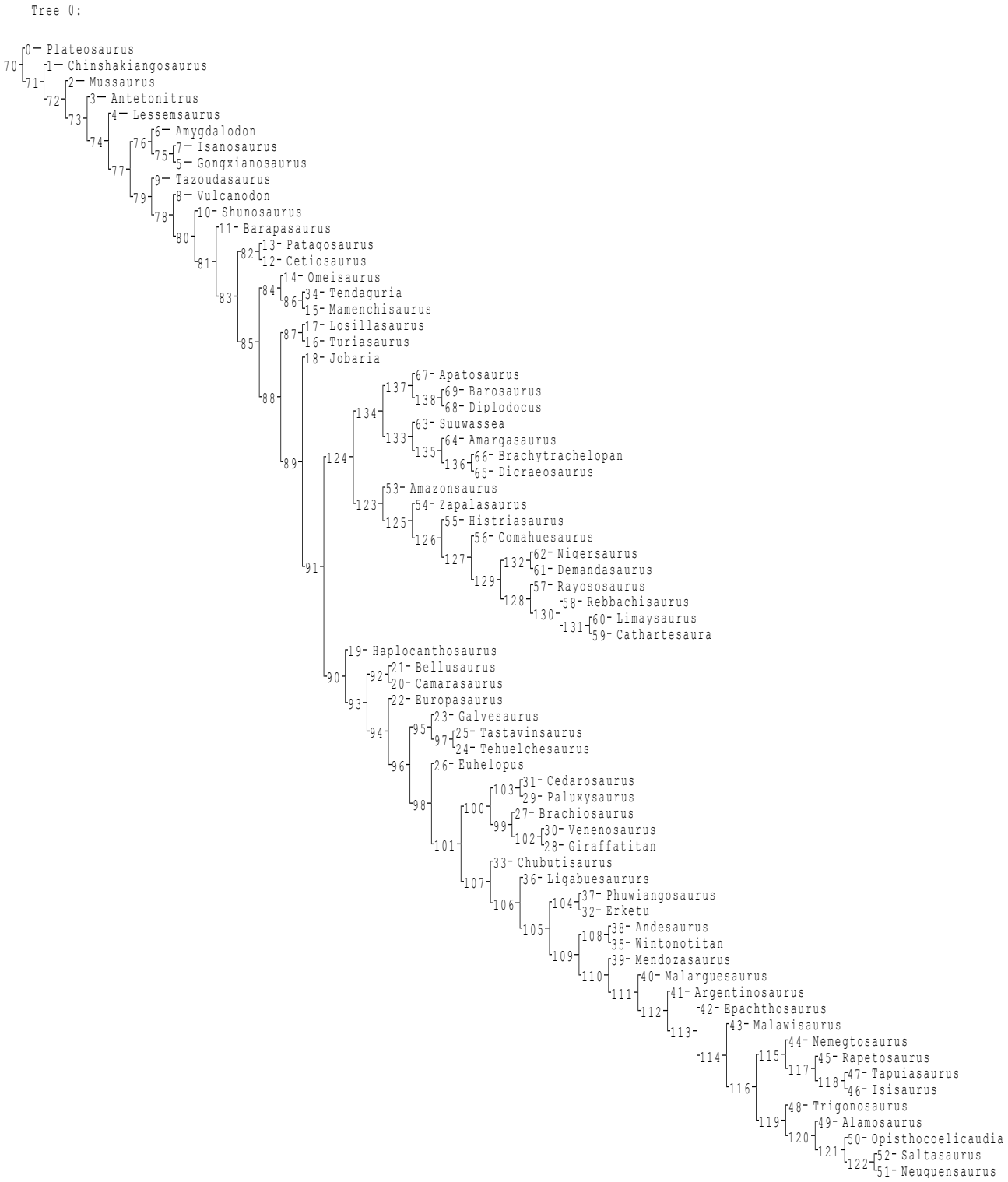

Figure 60. Constrained pneumatic 'Carballido-Sander' parsimonious phylogeny. The original phylogeny resulted from the unmodified published dataset of Carballido & Sander (2014) was imposed as a constraint on the pneumatically dataset of 70 taxa and 340 characters. The result yielded one parsimonious tree of length = 975 steps, CI: 0.406 and RI: 0.702. Assigned outgroup: *Plateosaurus*.

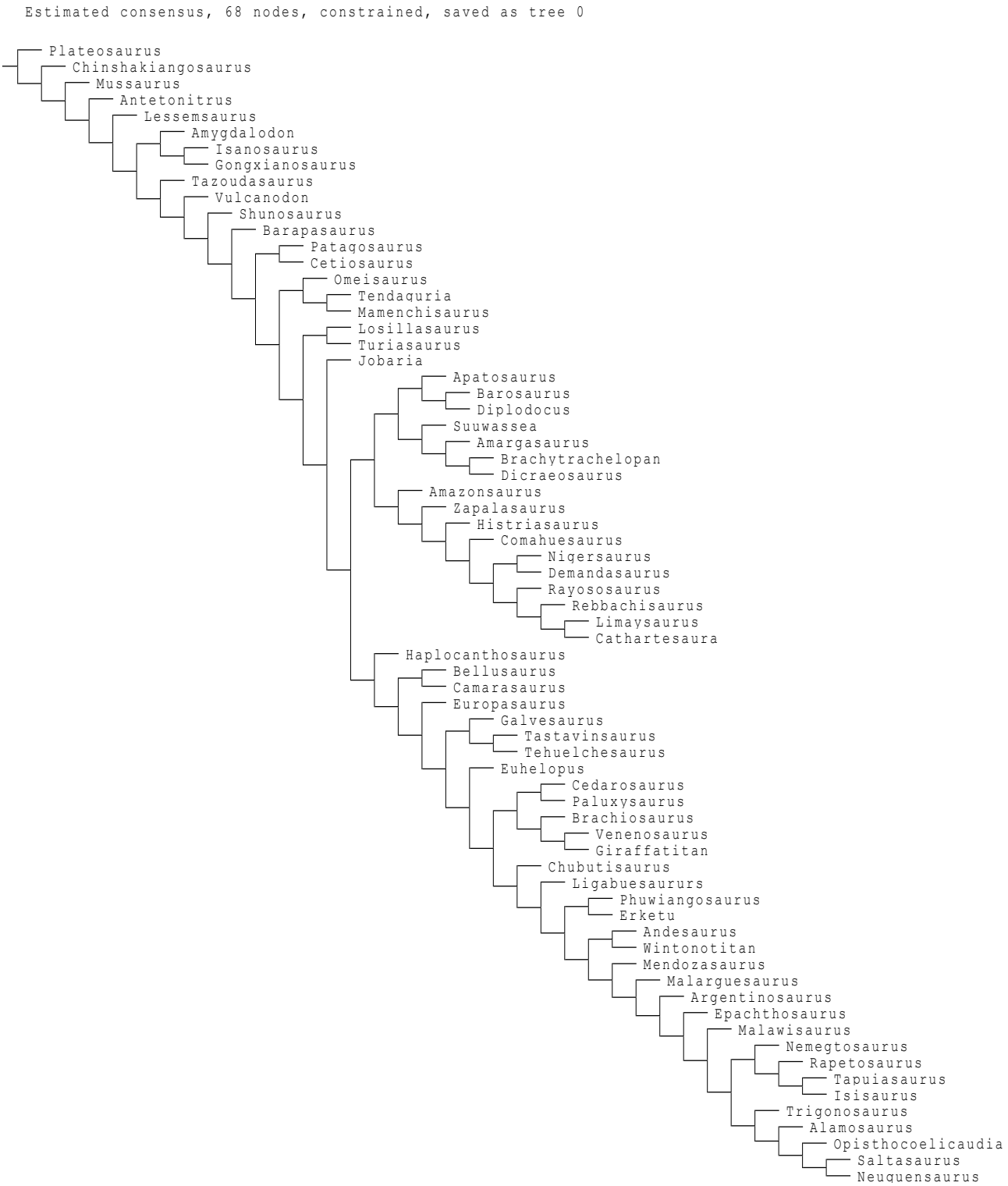

Figure 61. Constrained estimated consensus of pneumatic 'Carballido-Sander' parsimonious trees. Constrained estimated consensus tree of the constrained parsimonious tree of 70 taxa and 340 characters. Assigned outgroup: *Plateosaurus*.

5.4) Discussion - Evolution of sauropodomorph pneumaticity - observations and corroborations of sauropod vertebral pneumatisation from previous studies

The vertebral column of sauropodomorphs is a highly informative body section (Bonaparte, 1999) not least because of its pneumaticity, the great variety of which is a subject of continuous discussion (e.g. Wedel et al., 2000; Taylor and Wedel, 2009; Sander et al., 2011; Carballido and Sander, 2014). Observations from past studies corroborate with the findings of this project, though previous authors did not record in detail the pneumaticity features of most taxa, as was one of the main aims of this project. The following sets of examined sauropodomorph taxa are roughly grouped with respect to their relative subfamily. These observations can then be compared with the results of this study and possibly draw new inferences regarding their interrelationships. According to Yates et al. (2009) the pneumatic features of derived neosauropods do not appear in basal sauropodomorphs and basal sauropodomorphs, as they (e.g. *Aardonyx*) lack features such as infradiapophyseal fossae in their vertebrae. This feature is present in primitive saurischians but it is not expressed in most basal sauropodomorphs (Yates et al., 2009). Laminated pneumatic subdivided fossae are present in the infradiapophyseal fossae in the neural arch of the dorsal vertebrae of basal sauropodomorphs from the Hettangian-Pliensbachian stages onwards, like *Antetonitrus* (McPhee et al., 2014). It is evident that less developed pneumatic features are present in the dorsal vertebrae of basal sauropods like in *Eucnemesaurus* (Norian-Rhaetian) and *Aardonyx* (Hettangian-Sinemurian) but also present in the dorsal vertebrae of the more derived Pliensbachian-Toarcian eusauropod *Tazoudasaurus* (McPhee et al., 2014). Lastly, in the dorsal region of *Aardonyx* and caudal region of *Antetonitrus*, there is a deep fossa on the dorsal side of the transverse processes (McPhee et al., 2014). *Isanosaurus*, *Vulcanodon*, *Kotasaurus* and Eusauropoda (from Norian to Toarcian age) have dorsal centra with deep fossae on their lateral surfaces that approach the midline (Yates & Kitching, 2003; also verified for *Kotasaurus* by Yadagiri, 2001). Eusauropoda have dorsal excavations on their cervical parapophyses and excavations on the anterior face of the dorsal neural arches (Yates & Kitching, 2003). *Barapasaurus*, *Omeisaurus* and Neosauropoda (from Sinemurian to Tithonian ages) share excavations of the anterior face of the dorsal neural arches (for *Barapasaurus,* also verified by Carballido et al., 2012), and also *Omeisaurus* and Neosauropoda possess invasive, sharp-rimmed pleurocoels on the lateral surface of their dorsal centra and dorsal excavations on their cervical parapophyses (Yates & Kitching, 2003). *Vulcanodon* was reported to have a ventral hollow on its middle caudal centra (Raath, 1972; Cooper, 1984). *Barapasaurus* (Jain et al., 1975) neural arches of the dorsal

vertebrae bear infradiapophyseal pneumatopores that lead into the neural canal (Jain & Chatterjee, 1979; Bandyopadyay et al., 2010). *Patagosaurus* (Bonaparte, 1979) cervical vertebrae bear centroprezygapophyseal laminae and infra-prezygapophyseal pneumatocoels (Wilson, 2002). Like *Barapasaurus*, its middle and posterior dorsal neural arches have an infradiapophyseal pneumatopore opening into the neural canal (Jain & Chatterjee, 1979; Bonaparte, 1986; Bandyopadyay et al., 2010). *Mamenchisaurus* (Young, 1954) has spongy presacral vertebrae and the *Apatosaurus* (Marsh, 1877a) atlantal neural arch is pierced by a pneumatic foramen.

Moreover, Diplodocoidea (Upchurch, 1995) share spinoprezygapophyseal laminae in dorsal vertebrae that are fused to form a single pre-spinal lamina and short cervical ribs with non-overlapping posterior centra (Berman & McIntosh, 1978). Janensch (1929a) states that Dicraeosauridae (Huene, 1927) share dorsal vertebrae without pleurocoels but, contrary to that, it was later found by Bonaparte, Heinrich and Wild (2000) that *Dicraeosaurus sattleri* does possess pleurocoels in its dorsal centra. In addition, their anterior caudal centra have irregularly placed foramina on the ventral surface (Harris, 2007). *Jobaria* (Sereno et al., 1999) has a pronounced coel between centropostzygapophyseal and intrapostzygapophyseal laminae on its cervical neural arches (Sereno et al., 1999). The basal Titanosauriform *Euhelopus* (Wiman, 1929) has subdivided pneumatocoels in the neural spines of its presacral vertebrae, which lie above the prezygapophyseal–postzygapophyseal laminae (Wilson & Sereno, 1998; Wilson & Upchurch, 2009). *Malawisaurus* (Jacobs et al., 1993) has a large pneumatocoel between anterior centroparapophyseal lamina and posterior centrodiapophyseal lamina in the neural arches of its posterior dorsals (Wilson, 2002), highly pneumatised diapophyses and its cervical vertebrae possess undivided pleurocoels (Wilson, 2002). Also, *Malawisaurus* has pneumatised dorsal and caudal neural spines (Jacobs et al., 1993; Wilson, 2002). Furthermore, Titanosauriformes from Upper Jurassic to Lower Cretaceous (Oxfordian-Kimmeridgian to Albian; Salgado et al., 1997) share semicamellate cervical and dorsal vertebrae (Wilson, 2002). *Giraffatitan, Brachiosaurus*, *Abydosaurus*, *Cedarosaurus* and *Venenosaurus* possess shallow fossae on the lateral surfaces of their caudal vertebrae (Wilson, 2002; Wedel, 2003). Somphospondyli (Wilson & Sereno, 1998) have fully camellate presacral vertebrae (Wilson, 2002; Wedel, 2003). Somphospondyli from Upper Jurassic to Upper Cretaceous (Kimmeridgian to Campanian; Bonaparte & Coria, 1993) have undivided cervical pleurocoels and the Maastrichtian Saltasaurinae (Powell, 1992) have spongy texture (camellate) in their caudal vertebrae (Powell, 1986). *Tangvayosaurus* + *Phuwiangosaurus* do not have camellae in their cervical and dorsal vertebrae; their internal pneumaticity is expressed by possessing camerate centra (Wedel et al., 2000, Wilson, 2002) but Suteethorn et al. (2009) also demonstrates that *Phuwiangosaurus*

possesses numerous pneumatic elements such as pleurocoels, fossae, foramina and laminated versions of these elements throughout its vertebral column. Finally, moving on to Lithostrotian somphospondylans (Maastrichtian; Upchurch et al., 2004), the anterior and middle caudal vertebrae of *Alamosaurus* (Gilmore, 1922) have several foramina opening at the base of their transverse processes and its cervical vertebrae have undivided pleurocoels (Woodward & Lehman, 2009; D'Emic, 2012). The first caudal vertebra of *Alamosaurus* bears a fossa on its condyle, occupying only the ventral side of the centrum (D'Emic et al., 2011). *Saltasaurus* (Bonaparte & Powell, 1980) anterior caudal neural arches have postspinal fossae (Wilson, 2002) but also Wedel (2003) discovered that it possesses fully camellate vertebrae throughout its column.

It is generally agreed that postcranial pneumatisation in sauropods, and perhaps, basal sauropodomorphs, stands as evidence for utilising an air sac pulmonary system similar to that of birds (Perry, 2001; Wedel, 2003*a*, *b*, 2005, 2009; O'Connor & Claessens, 2005; Schwarz & Fritsch, 2006; Schwarz et al., 2007*a*; O'Connor, 2009 and Sander et al., 2011). Reasons for this have been widely discussed but the main arguments revolve on matters of metabolism and weight reduction enabling many taxa (e.g. *Seismosaurus, Giraffatitan, Futalognkosaurus*) to achieve sizes much greater than any other terrestrial group of animals that has ever lived (Table 1 in Chapter 1; Wedel, 2003*a, b*; Sander et al., 2011; Wedel and Taylor, 2014). The often hollowed nature of the cervical and dorsal vertebrae of most non-basal sauropodomorph sauropods results in light-weight supportive constructions, a function that has been biomechanically addressed and quantified in terms of stress endurance and mass reduction (Wedel, 2003*a*, *b*, 2005, 2009; Schwarz & Fritsch, 2006; Schwarz et al., 2007*a*). Considering these lines of evidence, it can, therefore, be suggested that an avian-like pulmonary system and its related development of pneumaticity has appeared, evolved and remained a key trait of sauropodomorphs throughout their evolution, exhibiting variable expression on an intergeneric level.

5.4.1) Sauropodomorph body size and pneumaticity

Sauropodomorpha possessed the most variable array of sizes, with differences spanning up to three orders of magnitude; from the 'dwarf'-sized *Magyarosaurus* and *Europasaurus* in reaching few hundred kilograms in mass up to the gigantic-sized *Sauroposeidon* and *Puertasaurus* weighing about 40 tonnes by average estimation. Within the first 10 million years of evolution, basal sauropodomorphs progressed from being well below 100kg, such as *Eoraptor*, *Pantydraco* and *Thecodontosaurus* to the tonne-scaled *Plateosaurus*, *Ruehleia* and *Camelotia* (Buffetaut et al., 2002; Sander et al., 2004, 2011). In their studies on sauropod body size evolution, Hone et al. (2005) and

Carrano (2005, 2006) showed a rapid increase in size, starting from the Late Triassic, which continued throughout the Jurassic and slowed down in the Cretaceous resulting in many small and gigantic sized macronarian and somphospondylan sauropods in the last period of the Mesozoic era. This most probably happened due to geographic fragmentation that occurred as a result of tectonic plate separation of Pangea that began in the mid-Jurassic and continued until the end of the Mesozoic era (Sander et al., 2011).

There is a general consensus that an avian-like respiratory system, able to supplement constantly all tissues with more oxygen than a mammalian style lung would be able to, in association with the cavernous light-weight construction of the pneumatised postcranial axial skeleton has enabled sauropods to attain gigantic sizes many times throughout their evolution. The lower specific density of the (mostly vertebral) bone structure due to pneumaticity reduced the overall weight of these animals by 10% - 30%, an observation verified via computer tomography (Wedel, 2000*a*, 2003*b*, 2005, 2009; Schwarz & Fritsch, 2006; Schwarz et al., 2007*a*) and histological studies (Woodward & Lehman, 2009). Sander et al. (2011) mention that the large terrestrial and herbivorous mammal *Paraceratherium* possessed large pneumatic openings in its presacral vertebrae, such as the pleurocoels found on sauropod vertebrae, but it is unknown whether they were filled with tissue or not.

Numerous studies have demonstrated the pneumatic nature of the axial skeleton of sauropods (e.g. Henderson, 2004; Wedel, 2005, 2007, 2009; Schwarz, Frey & Meyer, 2007). The findings of this study corroborate the observations from other workers i.e. that pneumatisation expands and increases during sauropodomorph evolution but it has also verified that pneumatisation originates from the proximal cervical and anterior-to-mid dorsal vertebrae and develops towards the posterior dorsal, sacral and caudal vertebrae (e.g. Wedel and Taylor, 2013; Taylor and Wedel, 2013).

Discrepancies between body mass, body length and degree of total average pneumatisation may occur either when using less accurate mass estimate techniques (e.g. scale model, femur to humerus ratio, femur length to width ratio, etc.- see Table 1 in Chapter 1) or when using more accurate methods like convex hull, polynomial volume or laser photogrammetry. Measurements that generate a fairly logical mass estimate for one animal with respect to its length and pneumaticity may produce a rather irrational result for another animal, even if that animal has a similar length and/or pneumaticity to the previous one. Furthermore, less accurate methods like e.g. scale modelling may produce reasonable estimates.

From our observations so far, it seems that the majority of the taxa belonging to Somphospondyli proper (i.e. from *Andesaurus* to *Saltasaurus*) may not express as many pneumaticity traits as the clades that precede them but the somphospondylans do

possess pneumatic elements that are considered to be unambiguously pneumatic (for example, the presence of camellae). This may also be an artefact of limited skeletal material and more discoveries should elucidate the degree of expression of pneumaticity in both intra- and intergeneric levels. In most cases, sauropods with equal length but less overall pneumaticity are lighter in mass but this is not a standard pattern. Similarly, taxa with different degrees of pneumaticity and masses have equal lengths; this can be due to technical inaccuracies or rounded estimates of size calculation attempts (mass and size estimates are discussed in Chapter 2). It is verified that some of the largest representatives of each subfamily, especially among the diplodocids and basal titanosauriforms, express the largest degrees of vertebral pneumatisation, though within each subfamily considerable variations in expression occur. The fact that there is a non-linear but gradual increase in pneumaticity within each subfamily, as if the expression of pneumaticity 'resets' with every new subfamily and increasing throughout its lineage, may suggest that each subfamily is phylogenetically distant from one another. In every major speciation event, i.e. from one subfamily to the next, vertebral pneumatisation almost zeroes-out, starting with low expression and culminating in high expression; it never reaches zero, though. This provides us with some interesting assumptions when considering that some of these major subfamilies temporally and geographically overlapped for a considerable amount of time (e.g. Diplodocoidea and Titanosauriformes). Examining pneumatisation to great detail, it leads us to assume that the expression of pneumaticity was not as simple as an overall gradually increasing event (e.g. Upchurch et al., 2004, Wedel, 2005) but rather a trait that appeared independently multiple times within Sauropodomorpha, a phenomenon that also occurred in Theropoda as demonstrated by Benson et al. (2012).

This study reveals that the expression of pneumaticity does not always concur with the expected mass or length when comparing similarly sized taxa, suggesting other biotic, and possibly abiotic, parameters to have played role in the expression of pneumatisation such as genetic mutations, changes in oxygen levels, variations in gravity, changes in niche partitioning per species as well as amount and type of resources available; or, as our phylogenetic results show, the variable expression of this trait may have been irrelevant to any such factors and its presence may be due to chance events of inheritance, genetic drift or random mutations in the developmental pathway (Sander et al., 2011).

5.4.2) Phylogenetic signal of pneumaticity characters - interpretation of pneumaticity character fit in the studied phylogenies and its implications on the development of pneumaticity throughout Sauropodomorpha

The phylogenetic signal of pneumaticity characters has never been considered by previous works examining the phylogenetic relatedness of sauropods. This is partly because the proportion of pneumaticity characters is quite low in comparison to the overall assembly of morphological characters of every taxon or subfamily. This is not meant to imply that this study produced more pneumaticity characters out of thin air; rather, it is realised how large and variable such a dataset can be when focus is given solely on this part of animal anatomy. It is evident that, any author may perform none, few or several changes in terms of character development in such a set of morphological characters, depending on the quantity and quality of newly acquired data with respect to this case. As a result, every worker or team of workers may agree to omit, change or add characters in the set, thus affecting, more often than not, more than one taxon in a given phylogeny.

The decisions taken in order to prepare the data for the analyses to be carried out in this study reflect the diversity of both hypotheses that needed to be examined and also the methods undertaken as well as the different types of results that needed to be derived. One of the main initial mandates of this work's hypothesis was to test if the pneumaticity characters have phylogenetic signal, to what extend and how could this be demonstrated in accepted phylogenies. The results of this study showed mostly poor or moderate signal and rarely a good fit, as seen by the resultant values of Consistency, Retention and Homoplasy indices of the trees derived from *Mesquite*, *PAUP* and *TNT* analyses. The effect of the application of those characters into phylogenies was minimal to moderate, maintaining the taxa into their taxonomic subgroups as known, with only the most unstable taxa to be changing positions. The added pneumaticity characters in the character matrices demonstrated moderate and weak signal, depending on the phylogeny examined in each case. When these characters where compared to dental characters, the majority of the results showed that the pneumaticity characters were weaker in terms of scores (signal) and fitness. In addition, as was demonstrated by the results from the analyses conducted n *PAUP* and *TNT* and in comparison with the published phylogenies [McPhee et al. (2014), Yates et al. (2009), Whitlock (2011), D'Emic (2012) and Carballido & Sander (2014)], the phylogenetic positions of the pneumaticity-studied sauropodomorphs not only changed within the resulted trees but their clade support was weak too. Moreover, even though the selection of the added pneumaticity characters was based on their high CI, RI and Frequency of state which were derived in *Mesquite*, their

incorporation in the published character matrices ('McPhee-Yates', 'D'Emic-Whitlock' and 'Carballido & Sander') decreased the tree lengths and scores (e.g. CI and RI) of the trees, when compared to the published phylogenies. These results may be a consequence of the hybridisation and merging of some of the examined phylogenies, the incorporation of the pneumaticity characters in these matrices but also probably due to the different algorithmic processes and parameters employed by the different phylogenetic programmes. The number of the inserted pneumaticity characters may have been small enough not to cause any significant topological changes in the phylogenies but adequate enough to shift taxonomic subgroups into different locations with respect to the original phylogenies from which they derived. The fact that only a small number of pneumaticity characters were informative (about 1/3 of the totality of pneumaticity characters according to *Mesquite*; but 8 out of the 11 added pneumaticity characters were informative, according to *PAUP* and *TNT*) and that these ranged in terms of phylogenetic signal from low to moderate, leads us to conclude that the expression of postcranial skeletal pneumaticity may not have played a major role in sauropod evolution; it is more likely a result of convergent evolution, rather than inheritance, because the latter would result in a steadily increasing and consistent appearance throughout the entire sauropodomorph lineage. The results of this study showed variable intrafamilial expression of vertebral pneumaticity and, from eusauropods onwards, never ceasing to exist (i.e. total PSP does not reach zero expression). This is also supported by the fact that pneumatisation was found to be less correlated to mass and more correlated to length, as was evidenced by the results retrieved from the correlation and phylogenetic least square analyses conducted in *R*. On a subfamilial level, though, expression due to inheritance seems to be more likely, evidenced by the nearly gradual increase from the most basal to the most derived member. Accumulation of chance mutations of vertebral pneumaticity traits, with considerable variations in expression of PSP, may have progressed from ancestor to descendant, increasing its pneumatisation in every speciation event but reduced expression is observed in the basalmost forms of every newly emerged subfamily i.e. the basal forms of each subfamily (basal sauropodomorphs, eusauropods, diplodocoids, macronarians and somphospondylans) exhibit lower pneumatisation levels than their more derived members (e.g. Table 7 in Chapter 2).

The few most frequent pneumaticity characters had, at best, a consistency index between 0.5 and 1 but that comprised a very small part of the entire dataset (about 1/3). The chosen pneumaticity characters that were used for the analyses were selected based on their CI, RI Frequency scores derived by *Mesquite*. However, as it was demonstrated by the analyses in *PAUP*, *R* and *TNT* their scores as well as the scores of the resulted trees, in which they were added, were not always identical in each set of phylogenetic

analyses. A deeper investigation, in terms of determining which pneumaticity characters would best fit the trees, would require the incorporation and testing of the entire pneumaticity dataset (755 characters) in each published character matrix (and thus phylogeny) and implementing analyses in each of the phylogenetic programmes used in this study. Such a study would be a separate task on its own since it would require a significant amount of time in order to be carried out thoroughly. Naturally, a complete phylogenetic analysis based solely on all retrieved pneumaticity characters would be meaningless due to it being highly homoplastic and, therefore, uninformative. In the analyses carried out in *PAUP* and *TNT*, I incorporated synapomorphic pneumaticity characters and not autapomorphic as the latter ones would be uninformative under parsimony (Lewis, 2001). Under parsimony, the expression of the same character(s) in the taxa (as we saw, for example, with 'C1c') is attributed to inheritance whereas likelihood allows for the explanation of convergent or parallel evolution (Lewis, 2001). An outcome that has not escaped our attention is the high score of homoplasy index of the characters in *PAUP* whose causal factor can be the existence of adaptive convergence among the taxa (Lewis, 2001). A final observation is that when the added pneumaticity characters were compared with the dental ones, in 2 out of 3 times ('D'Emic-Whitlock' and 'Carballido-Sander' but not 'McPhee-Yates') their CI and RI were only marginally lower (and, consequently, the HI values were higher), verifying that there is not much phylogenetic significance (or signal) in pneumaticity characters. Upon the conducted analyses, changes in sauropodomorph phylogenetic position in the examined phylogenies occurred mostly in eusauropods and diplodocoids. As it was shown in the results from *PAUP* and *TNT*, the interrelationships of the taxa within each respective group shifted in relation to each other, so that some sauropods established as primitive occupied more derived positions and vice versa. Furthermore, some results in *PAUP* and TNT (especially the constrained trees) showed. The Majority and Strict consensus trees, though, reflected a more realistic, and closer to the published phylogenies, picture with regard to the sauropodomorph interrelationships.

5.4.3) What do the results on model fitting tell us about the evolution of pneumaticity from a phylogenetic trend perspective?

Akaike's Information Criterion OU model modifies Brownian motion (BM) by having a particular direction to random trait evolution by applying selective adaptive optima (Butler & King, 2004) of increased pneumatisation such as those seen not only at the onset of every sauropod subfamily (except basal sauropodomorphs) but also in specific taxa with unexpectedly high expression of PSP e.g. *Omeisaurus* and *Mamenchisaurus*

(for eusauropods), *Apatosaurus* for diplodocoideans, *Giraffatitan* and *Brachiosaurus* for macronarians as well as *Saltasaurus* and *Alamosaurus* for somphospondylans (see also results in *Mesquite*). The adaptive optimum of PDI% is adapting towards stabilisation at high degrees of pneumatisation in somphospondylans i.e. from Early and Mid-Cretaceous onwards. Middle and Late Cretaceous somphospondylans possess highly pneumatised postcrania, while more basal forms did not. This application of selective optima is done by including parameters such as the *delta* shown here (see Table 1). The lower the value of the parameter the closer our data fit the Brownian motion, thus the OU model results, here, describe BM. The Early Burst model would be the second best candidate to fit the data and this can be observed in the fact that PSP developed further from eusauropods onwards, after a limited presence of PSP throughout the basal sauropodomorphs. Nevertheless, for the EB model to have been the best, PSP should have exhibited high expressions form the very onset of basal sauropodomorphs, which is not the case. Congruent to this argument are the 'w' values of the weight of each model on the data fit, with the higher values being those of OU and Stasis. Brownian motion assumes that a given phylogeny explains the variation in the values of the taxa under a gradual model of evolution. This model likely fits the data but it is unlikely that Stasis, or Trend would fit the data; their very low 'weight' values corroborate this outcome. Their *delta* values are greater than 1 suggesting that if these models fit the data they would indicate a late evolutionary change. The fit of the OU-BM model suggests an early speeded development of pneumaticity characters 'C1c' (pleurocoel in cervical centrum) and 'C8c' (pleurocoelous fossa in cervical centrum) starting from mid-Eusauropoda, increasing throughout Neosauropoda and become stabilised at some points in Somphospondyli, thus verifying the empirical observations presented in this study. The overall set of data accumulated in this study allows us to argue that PSP appeared early and developed fast in sauropodomorphs (e.g. Appendix 3), while maintaining variable expression throughout their evolutionary path. In conclusion, the analyses performed thus far as well as the resultant OU-BM models suggest that adaptive optima occurred not only in derived basal sauropodomorphs and eusauropods but also in the evolutionary onset of every other subfamily of sauropodomorphs that followed i.e. diplodocoids, macronarians and somphospondylans.

5.5) Conclusions

Based on the analysis of 755 pneumaticity characters across four published phylogenetic trees of different subclades of sauropodomorphs, some key results were obtained:

- The metric of total body length has a stronger phylogenetic signal than mass and correlates positively with the total average pneumaticity of a taxon. Also, total average pneumaticity correlates much less with mass (than with length) and, often, this correlation is negative.

- In every major speciation event which results in a new subfamily group, there is a gradual increase in vertebral pneumatisation within the context of that group, an increase usually matched by an increase in size. Pneumaticity characters possess little phylogenetic signal, as indicated by the low values of consistency and retention indices shown by *Mesquite, PAUP* and *TNT* as well as by the little effect they caused in the tree analyses in *PAUP* and *TNT*. In addition, only about a third of the characters are phylogenetically informative as it was shown by *Mesquite*.

- From a macroscopic point of view, metric data in the phylogeny reveal a nearly gradual increase of total average pneumaticity throughout Sauropodomorpha, with occasional low expressions. From a subfamilial perspective, though, pneumatisation starts with low expression and culminates with high expression; exception to this observation are the macronarians where pneumatisation remains relatively stable at medium-high levels throughout the clade.

- Dorsal pneumatisation is prevalent in more sauropodomorph clades than cervical, sacral or caudal pneumatisation and its expression is higher than the other regional expressions of pneumatisation. Pneumaticity in the sacral and caudal regions is sparse and limited, expressed only in the most pneumatic members of Eusauropoda, Diplodocoidea, Macronaria and Somphospondyli. This might imply that dorsal pneumatisation evolved prior to the evolution of cervical and sacrocaudal pneumatisation or that it evolved synchronously with cervical pneumatisation and then it developed more and more frequently in every subfamilial group. This may have plausible ramifications from a developmental point of view. This was probably done to alleviate the main and primary body

stresses occurring in the area around the centre of mass which is located in the trunk (and secondarily as a response to the stresses occurring in the long necks and tails of the animals) as a mechanism to reduce muscle energy required to power them.

- Unambiguous traits and high degrees of pneumaticity are expressed variably throughout the phylogenies and are observed in various taxa from almost every subfamily, excluding basal sauropodomorphs which are limited to the expression of fossae.

- Closely related taxa and sister taxa within a subfamily do not always share the same pneumatic synapomorphies. Rather, a highly pneumatised basal eusauropod (e.g. *Mamenchisaurus*) may be equally or more pneumatic than a derived diplodocid (e.g. *Diplodocus*) or a brachiosaurid. Conversely, there may be derived taxa with high body mass (e.g. the basal titanosauriform *Janenschia* or the somphospondylan *Puertasaurus*) that do not possess highly pneumatised vertebrae.

- The totality of pneumaticity characters mapped on the composite phylogeny results in a better fit than the original trees. The Ornstein-Uhlenbeck (OU) model of Brownian motion fits the data best, indicating an early speeded development of pneumaticity starting from mid-Eusauropoda, increasing throughout Neosauropoda and becoming stabilised in Somphospondyli. Pneumaticity evolved once in Sauropodomorpha, starting from its basalmost forms (e.g. *Plateosaurus*) and it maintained a variable expression throughout every subfamily of Sauropoda. The overall set of data accumulated in this study and the conducted analyses allow us to conclude that PSP appeared early and developed fast in sauropodomorphs (from the derived basal sauropodomorphs onwards), while maintaining a variable expression throughout their evolutionary path. The analyses performed thus far as well as the resultant OU-BM models suggest that adaptive optima of high levels of pneumatisation occurred not only in eusauropods but also in the evolutionary onset of every other subfamily of sauropodomorphs that followed i.e. diplodocoids, macronarians and somphospondylans.

The expression and development of pneumaticity seems to be a result of parallel evolution in a macroscopic view since contemporaneous (and not) taxa from different subfamilies share the same characters and similar pneumaticity degrees. On a more

focused subfamilial scale, skeletal pneumatisation seems to be the result of accumulated mutation, inheritance or gene flow. In general, pneumatisation increases over evolutionary time as speciation progresses from basal to derived forms. Thus, its level of expression may not be associated purely with size factors but instead be a result of many other biotic parameters. Skeletal pneumatisation may have been beneficiary to the locomotion of the large animals since it would aid in a decrease in muscular effort to power their large bones and it would also be cost-effective in the sense of energy reduction in order to minimise the body heat production. Other biotic factors could be that the expression of PSP is subject to random mutations or even the accumulated result of gene flow across speciation events.

Chapter 6 – Thesis Conclusions

6.1) Project's rationale and significance

Vertebral pneumaticity in sauropodomorphs is a key morphological characteristic, and we want to know whether it was associated with body size, its evolution and its phylogenetic significance. A detailed account of pneumaticity, on a vertebral and vertebral region levels, allowed for the demonstration of its development in Sauropodomorpha across phylogeny and time. This was based on a data matrix consisting of 755 pneumaticity characters mapped across four published phylogenetic trees of sauropodomorphs. Comparison between pneumaticity and body size was accomplished by the creation of the Pneumaticity Degree Index (PDI %), a metric to quantify the expression of osteological pneumaticity and categorise sauropodomorphs, based on the nature and extent of their pneumatic characteristics. This study addressed the intergeneric and subfamilial phylogenetic relationships from a pneumaticity point of view and it also focused on the pneumatic similarities and differences among dwarf, juvenile and normal gigantic adult taxa. The prediction of an analogous expression and evolution of pneumaticity with sauropod size and/or evolution was shown to be false and, as results showed, pneumaticity does not correlate with size.

Specifically, this study aimed to test if the expression of pneumaticity measured across the vertebral column, both as total average as well as per vertebral segment, correlates proportionately (positive), inversely proportionately (negative) or neutrally with total body mass, total body length, femur length (used as a proxy of size) and vertebral segment length. The project also aimed to verify if pneumaticity varies differently in different families (positive, negative or neutrally variable correlation) and whether or not pneumaticity characters affect the phylogenetic interrelationships of sauropodomorphs when inserted in accepted phylogenies. In addition, the study also sought to demonstrate if pneumaticity characters have phylogenetic signal and to compare them with other morphological characters, such as cranial / dental ones. In summary, this study, among its other goals, attempted to record all aspects of vertebral and pelvic pneumaticity in 61 sauropodomorph taxa spanning from the Late Triassic to the Late Cretaceous, achieving the creation of a classification scheme based on the expression of pneumaticity as well as demonstrating a temporal and phylogenetic visualisation of the evolution of pneumaticity.

6.2) Concluding statements about the correlation of the expression of osteological pneumaticity and body size

The results of this study can be summarised as follows:

- In general, the most pneumatised parts are the cervical and dorsal vertebrae. There is a relatively stable general trend of the expression of pneumaticity throughout the geological evolutionary time of Sauropodomorpha.

- Pneumaticity is mostly correlated to length and less correlated to mass, except in cases where taxa are equal to or greater than 30 tons; exceptions may occur (e.g. *Seismosaurus*, *Puertasaurus*) but this may be an observational artefact due to limited fossil material. Body length has a stronger phylogenetic signal than mass and correlates positively with pneumaticity degree while body mass correlates less with PDI% (see Appendix 2 Tables S7-S16). Resultant parameters (such as *p-value, Estimate, Adjusted R-squared*) corresponding to the correlations among pneumaticity (total average or in the vertebral segments, expressed in PDI%), body mass (Kg), body length (m), neck length (m), trunk length (m) and tail length (m) had low values and, consequently, reflected noise. The *p values* for these metrics were not significant at the level of significance of $p = 0.05$ and there is no evidence for any signal between PDI% and body mass or body length since only a very small percent of mass or length correlated with pneumaticity.

- In a vertebra, pneumaticity begins from the centrum and extends to the arch and transverse processes, and in the more derived families it begins simultaneously from both the centrum and the neural spine (and, therefore, extends inwards).

- Segment length and PDI% are not directly proportional. Highest PDI% often appears more often in medium sized taxa (in terms of length). Pneumaticity varies intergenericaly in order to best fit the individual's body proportions since interfamilial expression of PSP is variable.

- No family of sauropods reaches 100% pneumaticity in all vertebral column segments, although some of the highest values are observed in Macronaria and Somphospondyli. In very few cases a sauropod expresses a full ‘Alpha’ pneumaticity in all available vertebral segments. Positive correlation between PDI% and neck length is more frequently observed for necks exceeding 6-7m in length; trunks are

also positively correlated with PDI% but at greater range value of lengths i.e. trunks of 5m in length may be as highly pneumatic as those of being 8m, suggesting the greater developmental need for the central body part of an animal to acquire such a weight reduction mechanism, compared to the neck and tail. A neck would need to be as light weight as possible so as to minimise its 'cantilever-beam' like stresses when the animal was e.g. browsing. The observed minimal expression of pneumaticity in the tail (and thus its frequently inversed correlation with PDI%) is justified by the fact that the tail probably had acted as a counterbalance for the neck and trunk regions, thus it had to be heavy enough.

- Among all examined sauropodomorphs there was no association of sauropodomorph families and distinct PDI% value ranges i.e. in any subfamily, taxa may express various levels of PSP. In the necks and trunks we see a clearer but not definite trend; more derived families/genera are more likely to be found in the higher PDI% regions than more basal forms such as basal sauropodomorphs and eusauropods. Gradual increase of PSP throughout Sauropodomorpha is a general trend, there is no evidence supporting that taxa in every subfamily exhibit increasing expression of PSP as we transcend from basal to derived forms. Within and among families, different vertebral lengths have variable levels of pneumatisation, except when neck and trunk lengths exceed certain values of length (six and eight metres, respectively).

- Dorsal pneumatisation is present in more sauropodomorph clades than cervical, sacral and caudal expressions of pneumatisation and its expression is higher than them. Pneumaticity in the sacral and caudal regions is sparse and limited, expressed only in the most pneumatised members of Eusauropoda, Diplodocoidea and Somphospondyli. It is likely that both cervical and dorsal pneumatisation evolved synchronously and biomechanical constraints necessitated the further development of dorsal pneumatisation; an adaptation that persisted throughout the evolutionary path of sauropodomorphs.

- Unambiguous traits and high degrees of pneumaticity are expressed variably throughout the phylogenies and are observed in various taxa from almost every subfamily, excluding basal sauropodomorphs which are limited to the expression of fossae.

- Closely related taxa and sister taxa within a subfamily do not always share the same pneumatic synapomorphies. Rather, a highly pneumatised basal eusauropod (e.g.

Mamenchisaurus) may be equally or more pneumatic than a derived diplodocid (e.g. *Diplodocus*) or a brachiosaurid. Conversely, there may be derived taxa (e.g. the basal macronarian *Janenschia* or the somphospondylan *Puertasaurus*) that do not possess highly pneumatised vertebrae.

- The early juvenile SMA 0009 seems to possess pneumaticity patterns similar to those of *Camarasaurus*, verifying Carballido et al.'s (2012) observations that SMA 0009 is most likely a macronarian. Similar observations can be made for the dwarf *Europasaurus* and *Brachiosaurus*/*Giraffatitan* as the former taxon bears a pneumatic resemblance with the latter two taxa, disagreeing on that aspect with Carballido and Sander's (2014) observations who support its placement within basal macronarians, and agreeing with D'Emic (2012) and Mannion et al. (2013) who have argued that *Europasaurus* is as a brachiosaurid.

- This study found that *Europasaurus*, despite its relatively small size, possesses moderate-high degrees of pneumaticity, comparable to its large continental macronarian cousins. This discovery, along with the fact that the early juvenile SMA 0009 possesses a moderate degree of pneumaticity, allows us to conclude that pneumaticity increases in complexity and extent with ontogeny, but it is irrelevant to the body size, although the adult dwarf sauropod, being about 4 m longer than the juvenile, exhibits higher degrees of pneumaticity; however, not sufficient comparisons were made (as, for example, with *Camarasaurus* juvenile specimens) in order to make a safe argument about the nature of ontogenetic development of pneumaticity. Comparison was only made on a hypothetical level and these lines of evidence do not construe a solid conclusion but can only form speculation regarding which adult sauropod would be a probable adult form of SMA 0009 and only under the spectrum of vertebral pneumatisation. The study of *Barosaurus* juvenile and adult specimens suggest PSP is formed in early ontogeny and gradually increased as the animal was reaching adulthood.

- In every paraphyletic subfamily each group has members of variable degrees of pneumatisation with no evidence to support that the more primitive members had the lowest amounts of pneumaticity and the more derived members the highest expression of pneumaticity.

- Pneumaticity characters possess little phylogenetic signal, as indicated by the low values of consistency and retention indices shown by *Mesquite*, *PAUP* and *TNT* as well as by the little effect they caused in the tree analyses in *PAUP* and *TNT*. This observation was also corroborated when the fit scores, consistency, retention and homoplasy indices of the pneumaticity characters were compared to those of cranial / dental ones. Pneumaticity characters were found to have lower index values than the cranial / dental ones but marginally higher fitness scores. In addition, only about a third of the characters were shown to be phylogenetically informative (as was shown by *Mesquite*).

- From a monophyletic point of view, metric data in the phylogeny reveal an almost sudden increase of total average pneumaticity after the clade of basal sauropodomorphs and from eusauropods onwards. Sauropods maintain a range of total average PDI% from 30% to about 80%, with few outliers exceeding the upper value (e.g. *Mamenchisaurus*, *Alamosaurus*).

- The Ornstein-Uhlenbeck (OU) model of Brownian motion fits the data best, indicating a burst of development of pneumaticity starting from mid-Eusauropoda, increasing and soon remaining at variable but stable levels up to Somphospondyli. Pneumaticity evolved at least once in eusauropods and, subsequently, in every subfamily of Sauropoda. The analyses performed thus far as well as the resultant OU-BM models suggest that adaptive optima of high levels of pneumatisation occurred in specific taxa with unexpectedly high expression of PSP e.g. *Omeisaurus* and *Mamenchisaurus* (for eusauropods), *Apatosaurus* for diplodocoideans, *Giraffatitan* and *Brachiosaurus* for macronarians as well as *Saltasaurus* and *Alamosaurus* for somphospondylans.

The expression and development of pneumaticity seems to be a result of parallel evolution in a macroscopic view since taxa from different subfamilies share the same characters and similar pneumaticity degrees. On a more focused, subfamilial, scale skeletal pneumatisation seems to be the result of accumulated inheritance, mutation or gene flow. In general, PSP increases over time as speciation progresses quite fast from basal sauropodomorphs to eusauropods. Osteological expression of pneumaticity is most probably the result of biomechanical and genetic factors such as weight distribution on each taxon's body parts. Expression of PSP is positively correlated with mass when the 30 tonne threshold is reached but because we also observed low PDI% values for taxa estimated to exceed this threshold, PSP may not have been a paramount factor in

achieving gigantic sizes; most probably it would have been an artefact of an ‘avian-lung’ system of diverticula which would lighten the skeleton as a result of bone aeration. In the case of insular dwarfism, PSP seems to be a phylogenetically conservative trait that is retained during evolution due to allopatric speciation and is not affected by the reduction of body size. Maybe size is a more malleable trait than osteological re-modification that would result in PSP. This leads us to conclude that intrinsic factors such as high metabolic growth rates and, to a lesser extent, the presence of PSP may have acted synergistically in the gigantic development of sauropods, except when faced against limited resources due to insular isolation, in which case, body size is the trait that will be affected first.

6.3) Future work

Sauropods achieved the largest body size of any terrestrial group that has ever existed, and acquired the highest expressions of skeletal remodification in terms of pneumatisation (e.g. Wedel et al., 2000; Wedel, 2003). This study could lay the basis of a biomechanical approach to test the structural importance and limits of osteological pneumatisation. The idea would be based on the hypothesis that pneumatised sauropod vertebrae can absorb multiaxial high stresses because of their complex pneumatic design that entails lattice-like laminae structures, caverns and internal chambers (from simple spaces up to honey-comb structures). The hypothesis is to test whether the application of such a pneumatisation design in common or composite materials and engineering construction units could improve biomechanical performance. The results of such a study would not only have impact on our understanding of this characteristic in the extant relatives of sauropods that also exhibit pneumatised postcrania, but might also lay the grounds for novel engineering and material approaches through the scope of biomimetics.

References

Alberch P, Gould SJ, Oster GF, Wake DB. Size and shape in ontogeny and phylogeny. Paleobiology. 1979; pp.296-317.

Alexander RM. All-time giants: the largest animals and their problems. Palaeontology. 1998; 41(6):1231-45.

Allain R, Aquesbi N, Dejax JC, Meyer A, Monbaron M, Montenat C, Rechir P, Rochdy M, Russell DA and Taquet P. A basal sauropod dinosaur from the Early Jurassic of Morocco. Comptes Rendus Palevol. 2004; **3(3)**: 199-208

Allain R, Aquesbi N. Anatomy and phylogenetic relationships of *Tazoudasaurus naimi* (Dinosauria, Sauropoda) from the late Early Jurassic of Morocco. Geodiversitas. 2008; 30(2):345-424.

Anderson JF, Hall-Martin A, Russell DA. Long-bone circumference and weight in mammals, birds and dinosaurs. Journal of Zoology (London). 1985; 207(1):53-61.

Apostolaki NE, Rayfield EJ, Barrett PM. Osteological and soft-tissue evidence for pneumatisation in the cervical column of the ostrich (*Struthio camelus*) and observations on the vertebral columns of non-volant, semi-volant and semi-aquatic birds. PLoS ONE. 2015; 10(12): e0143834. doi: 10.371/journal.pone.0143834.

Bakker RT. Dinosaur heresy-dinosaur renaissance. Am. Assoc. Adv. Sci. Selected Symp. 1980; 28: 351-462.

Bapst DW. paleotree: an R package for paleontological and phylogenetic analyses of evolution. Methods Ecol. Evol. 2012; 3: 803-807. doi: 10.1111/j.2041-210X.2012.00223.x

Bates KT, Manning PL, Hodgetts D & Sellers WI. Estimating mass properties of dinosaurs using laser imaging and 3D computer modelling. PLoS One. 2009; *4*(2), e4532.

Bates KT, Falkingham PL, Macaulay S, Brassey C, & Maidment SC. Downsizing a giant: re-evaluating Dreadnoughtus body mass. Biology letters. 2015; 11(6), 20150215.

Bell MA, Lloyd GT. strap: Stratigraphic Tree Analysis for Palaeontology. R package version 1.4. 2014. https://CRAN.R-project.org/package=strap

Benson RBJ, Carrano MT, Brusatte SL. A new clade of archaic large-bodied predatory dinosaurs (Theropoda: Allosauroidea) that survived to the latest Mesozoic. *Naturwissenschaften*. 2010; 97(1): 71.

Benson RBJ, Butler RJ, Carrano MT, O'Connor PM. Air-filled postcranial bones in theropod dinosaurs: physiological implications and the 'reptile'–bird transition. Biological Reviews. 2012; 87: 168–193. doi: 10.1111/j.1469-185X.2011.00190.x.

Benson RB, Campione NE, Carrano MT, Mannion PD, Sullivan C, Upchurch P, & Evans DC. Rates of dinosaur body mass evolution indicate 170 million years of sustained ecological innovation on the avian stem lineage. PLoS Biology. 2014; 12(5), e1001853.

Benson RBJ, Campione NE, Carrano MT, Mannion PD, Sullivan C, Upchurch P, Evans DC (2014) Data from: Rates of dinosaur body mass evolution indicate 170 million years of sustained ecological innovation on the avian stem lineage. Dryad Digital Repository. http://dx.doi.org/10.5061/dryad.gr1qp

Benton MJ, Juul L, Storrs GW, Galton PM. Anatomy and systematics of the prosauropod dinosaur *Thecodontosaurus antiquus* from the upper Triassic of southwest England. *Journal of Vertebrate Paleontology*. 2000; 20(1):77-108.

Benton MJ, Minter NJ, Posmosanu E. Dwarfing in ornithopod dinosaurs from the Early Cretaceous of Romania. Mesozoic and Cenozoic vertebrates and paleoenvironments; tributes to the career of Prof Dan Grigorescu, Ars Docendi, Bucharest. 2006:79-87.

Benton MJ, Csiki Z, Grigorescu D, Redelstorff R, Sander PM, Stein K, Weishampel DB. Dinosaurs and the island rule: The dwarfed dinosaurs from Haţeg Island. Palaeogeography, Palaeoclimatology, Palaeoecology. 2010; 293(3):438-54.

Berman DS, McIntosh JS. Skull and relationships of the Upper Jurassic sauropod *Apatosaurus* (Reptilia, Saurischia). Bulletin of Carnegie Museum of Natural History. 1978; 8: 1–35.

Blomberg SP, Garland T, Ives AR. Testing for phylogenetic signal in comparative data: behavioral traits are more labile. Evolution. 2003; 57(4):717-45.

Blows WT. The early Cretaceous brachiosaurid dinosaurs *Ornithopsis* and *Eucamerotus* from the Isle of Wight, England. Palaeontology. 1995; 38(1):187-98.

Boback SM. Body size evolution in snakes: evidence from island populations. Copeia. 2003; 2003(1):81-94.

Boekschoten GJ, Sondaar PY. On the fossil Mammalia of Cyprus, Proceedings of the Koninklijke Nederlandse Akademie van Wetenschappen. 1972; 75(4): 306-338.

Bonaparte JF. Dinosaurs: a Jurassic assemblage from Patagonia. Science. 1979; 205(4413):1377-9.

Bonaparte JF, Powell JE. A continental assemblage of tetrapods from the Upper Cretaceous beds of El Brete, northwestern Argentina (Sauropoda-Coelurosauria-Carnosauria-Aves). Mémoires de la Société Géologique de France, Nouvelle Série. 1980; **139**:19-28.

Bonaparte JF. The dinosaurs (Carnosaurs, Allosaurids, Sauropods, Cetiosaurids) of the Middle Jurassic of Cerro Cóndor (Chubut, Argentina). In Annales de Paléontologie (Vert.-Invert.). 1986; 72 (4): 325-386.

Bonaparte JF. The early radiation and phylogenetic relationships of the Jurassic sauropod dinosaurs, based on vertebral anatomy. The beginning of the age of dinosaurs. 1986:247-58.

Bonaparte JF, Coria RA. Un nuevo y gigantesco saurópodo titanosaurio de la Formación Río Limay (Albiano-Cenomaniano) de la Provincia del Neuquén, Argentina. Ameghiniana. 1993; 30(3):271-82.

Bonaparte JF. An armoured sauropod from the Aptian of northern Patagonia, Argentina. National Science Museum Monographs. 1999; 15:1-2.

Bonaparte JF, Heinrich WD, Wild R. Review of *Janenschia* Wild, with the description of a new sauropod from the Tendaguru beds of Tanzania and a discussion on the systematic value of procoelous caudal vertebrae in the Sauropoda. Palaeontographica Abteilung A. 2000; 256(1-3): 25-76.

Bonnan MF. Morphometric analysis of humerus and femur shape in Morrison sauropods: implications for functional morphology and paleobiology. Paleobiology. 2004; 30: 444–470.

Bonner JT. Why Size Matters. Princeton University Press, Princeton; 2006.

Brassey CA, Maidment SCR, Barrett PM. Body mass estimates of an exceptionally complete Stegosaurus (Ornithischia: Thyreophora): comparing volumetric and linear bivariate mass estimation methods. Biol. Lett. 2015; 11: 20140984. http://dx.doi.org/10.1098/rsbl.2014.0984

Britt BB. Pneumatic postcranial bones in dinosaurs and other archosaurs. PhD thesis, University of Calgary, Canada. 1993.

Britt BB. Postcranial pneumaticity. Encyclopedia of dinosaurs; 1997: pp.590-593.

Brown JH, Marquet PA, Taper ML. Evolution of body size: consequences of an energetic definition of fitness. American Naturalist. 1993:573-84.

Buffetaut E, Suteethorn V, Cuny G, Tong H, Le Loeuff J, Khansubha S, Jongautchariyakul S. The earliest known sauropod dinosaur. Nature. 2000; 407(6800):72-4.

Buffetaut E, Suteethorn V, Le Loeuff J, Cuny G, Tong H, Khansubha S. The first giant dinosaurs: a large sauropod from the Late Triassic of Thailand. Comptes Rendus Palevol. 2002; 1(2):103-9.

Burness GP, Diamond J, Flannery T. Dinosaurs, dragons, and dwarfs: the evolution of maximal body size. Proceedings of the National Academy of Sciences. 2001; 98(25):14518-23.

Butler MA, King AA. Phylogenetic comparative analysis: a modeling approach for adaptive evolution. Am Nat. 2004; 164: 683-695.

Butler RJ, Barrett PM, Gower DJ. Postcranial skeletal pneumaticity and air-sacs in the earliest pterosaurs. *Biology Letters*. 2009; *5*(4): 557-560.

Butler RJ, Barrett PM, Gower DJ. Reassessment of the evidence for postcranial skeletal pneumaticity in Triassic archosaurs, and the early evolution of the avian respiratory system. PLoS ONE. 2012; 7(3): e34094. doi:10.1371/journal.pone.0034094

Calvo JO, Bonaparte JF. *Andesaurus delgadoi gen. et sp. nov.* (Saurischia-Sauropoda), dinosaurio Titanosauridae de la Formacion Rio Limay (Albiano-Cenomaniano), Neuquén, Argentina [*Andesaurus delgadoi gen. et sp. nov.* (Saurischia-Sauropoda), a titanosaurid dinosaur from Rio Limay Formation (Albian-Cenomanian), Neuquén, Argentina]. Ameghiniana. 1991; 28(3-4):303-310.

Calvo JO, Porfiri JD, González-Riga BJ, Kellner AW. A new Cretaceous terrestrial ecosystem from Gondwana with the description of a new sauropod dinosaur. Anais da Academia Brasileira de Ciências. 2007; 79(3):529-41.

Campione NE & Evans DC. A universal scaling relationship between body mass and proximal limb bone dimensions in quadrupedal terrestrial tetrapods. Bmc Biology. 2012; *10*(1): 60.

Campione NE, Evans DC, Brown CM, Carrano MT. Body mass estimation in non-avian bipeds using a theoretical conversion to quadruped stylopodial proportions. Methods in Ecology and Evolution. 2014; *5*(9), 913-923.

Carballido JL, Marpmann JS, Schwarz-Wings DA, Pabst B. New information on a juvenile sauropod specimen from the Morrison Formation and the reassessment of its systematic position. Palaeontology. 2012; 55(3):567-82.

Carballido JL, Sander PM. Postcranial axial skeleton of *Europasaurus holgeri*, (Dinosauria, Sauropoda) from the Upper Jurassic of Germany: implications for ontogeny and phylogenetic relationships of basal Macronaria. Journal of Systematic Palaeontology. 2014; 12(3): 335-387. doi: 10.1080/14772019.2013.764935

Carvalho IdS, Avilla LdS, Salgado L. *Amazonsaurus maranhensis* gen. et sp. nov. (Sauropoda, Diplodocoidea) from the Lower Cretaceous (Aptian-Albian) of Brazil. *Cretaceous Research*. 2003; 24:697-713.

Carpenter KE, McIntosh JS. Upper Jurassic sauropod babies from the Morrison Formation. Dinosaur eggs and babies. 1994; 265:278.

Carpenter K, Tidwell V. Reassessment of the Early Cretaceous sauropod *Astrodon johnsoni* Leidy 1865 (Titanosauriformes). Thunder-lizards. Indiana University Press, Bloomington and Indianapolis. 2005: 78-114.

Carrano MT. Body-Size Evolution in the Dinosauria. Amniote Paleobiology: Perspectives on the Evolution of Mammals, Birds, and Reptiles: a Volume Honoring James Allen Hopson. 2006; 225.

Carrier DR, Farmer CG. The integration of ventilation and locomotion in archosaurs. Am. Zool. 40:87–100. 2000. doi:10.1668/0003-1569(2000)040[0087:TIOVAL]2.0.CO;2.

Case TJ. A general explanation for insular body size trends in terrestrial vertebrates. Ecology. 1978; 59:1-18

Cerda IA, Salgado L, Powell JE. Extreme postcranial pneumaticity in sauropod dinosaurs from South America. Palaontologische Zeitschrift, 2012; 86(4): 441–449.

Chinsamy A. Bone histology and growth trajectory of the prosauropod dinosaur *Massospondylus carinatus* (Owen). Modern Geology. 1993; 18:319–329.

Chinsamy-Turan A. The microstructure of dinosaur bone: deciphering biology with fine-scale techniques. John Wiley & Sons; 2005.

Christian A, Preuschoft H. Deducing the body posture of extinct large vertebrates from the shape of the vertebral column. Palaeontology. 1996; 39: 801–812.

Christiansen P. Locomotion in sauropod dinosaurs. Gaia. 1997; 14:45–75.

Christiansen P. Mass allometry of the appendicular skeleton in terrestrial mammals. Journal of Morphology. 2002; 251(2):195-209.

Cieri RL, Craven BA, Schachner ER, and Farmer CG. New insight into the evolution of the vertebrate respiratory system and the discovery of unidirectional airflow in iguana lungs. PNAS. 2014; 111(48): 17218–17223.

Claessens LP, O'Connor PM, Unwin DM. Respiratory evolution facilitated the origin of pterosaur flight and aerial gigantism. PloS one. 2009; 4(2):e4497.

Clegg SM, Owens PF. The island rule in birds: medium body size and its ecological explanation. Proceedings of the Royal Society of London B: Biological Sciences. 2002; 269(1498):1359-65.

Clutton-Brock TH, Harvey PH. The functional significance of variation in body size among mammals. Advances in the study of mammalian behaviour (Special Publication of the American Society for Mammalogy 7). Shippenburg State College, Shippenburg. 1983: pp.632-663.

Colbert EC. The weights of dinosaurs. American Museum Novitates. 1962; 2076: 1-16.

Colbert EH. The Triassic dinosaur *Coelophysis*. Museum of Northern Arizona Bulletin. 1989; 5:71-174.

Cooper MR. A reassessment of *Vulcanodon karibaensis* Raath (Dinosauria: Saurischia) and the origin of the Sauropoda. Paleontologia africana. 1984: 25: 203-231.

Cope ED. On a gigantic saurian from the Dakota Epoch of Colorado. Paleontological Bulletin. 1877; 25:5-10.

Cranford TW, Amundin M, Norris KS. Functional morphology and homology in the odontocete nasal complex: implications for sound generation. Journal of Morphology. 1996; 228: 223-285.

Crawley MJ. The R Book. John Wiley & Sons Ltd. 2007. England. ISBN-13: 978-0-470-51 024-7.

Csiki Z, Benton MJ. An island of dwarfs—Reconstructing the Late Cretaceous Haţeg palaeoecosystem. Palaeogeography, Palaeoclimatology, Palaeoecology. 2010; 293(3):265-70.

Cúneo R, Ramezani J, Scasso R, Pol D, Escapa I, Zavattieri AM & Bowring SA. High-precision U–Pb geochronology and a new chronostratigraphy for the Cañadón Asfalto Basin, Chubut, central Patagonia: Implications for terrestrial faunal and floral evolution in Jurassic. Gondwana Research. 2013; 24(3), 1267-1275.

Curry KA. Ontogenetic histology of *Apatosaurus* (Dinosauria: Sauropoda): new insights on growth rates and longevity. Journal of Vertebrate Paleontology. 1999; 19(4):654-65.

Curry-Rogers KA & Forster CA. The last of the dinosaur titans: a new sauropod from Madagascar. *Nature*. 2001; 412(6846), 530-534.

Curry-Rogers KA, & Forster CA. The skull of *Rapetosaurus krausei* (Sauropoda: Titanosauria) from the Late Cretaceous of Madagascar. Journal of vertebrate Paleontology. 2004; 24(1): 121-144.

Curry-Rogers KA. Titanosauria: a phylogenetic overview. The Sauropods: Evolution and Paleobiology. University of California Press, Berkeley, California. 2005; pp. 50-103.

Curry-Rogers KC & Ericsson GM. Sauropod histology. In *The Sauropods, Evolution and Paleobiology* (pp. 303-326). 2005. University of California Press Berkeley.

Damuth J. Cope's rule, the island rule and the scaling of mammalian population density. 1993. Available from: www.nature.com.

David BW. paleotree: an R package for paleontological and phylogenetic analyses of evolution. Methods in Ecology and Evolution. 2012; 3: 803-807 . doi: 10.1111/j.2041-210X.2012.00223.x

D'Emic M. The early evolution of titanosauriform sauropod dinosaurs. Zoological Journal of the Linnaean Society. 2012; 166: 624–671.

Dodson P. Sauropod paleoecology. In The Dinosauria (ed. D. B. Weishampel, P. Dodson & H. Osmolska). 1990; pp. 402–407. Berkeley, CA: University of California Press. doi: 10.1111/j.2041-210X.2012.00223.x

Dong Z, Zhou S, Zhang H. Dinosaurs from the Jurassic of Sichuan. *Palaeontologica Sinica, New Series C, Whole Number*. 1983. 162(23):1-136.

Dowle M, Srinivasan A, Short T, Lianoglou S with contributions from Saporta R. and Antonyan E. data table: Extension of data.frame. R package version 1.9.6. 2015. https://CRAN.R-project.org/package=data.table

Dumont ER. Bone density and the lightweight skeletons of birds. *Proceedings of the Royal Society B*. 2010. doi:10.1098/rspb.2010.0117.

Eagle RA, Tutken T, Martin TS, Tripati AK, Fricke HC, et al. Dinosaur body temperatures determined from isotopic (13C-18O) ordering in fossil biominerals. Science. 2011; 333: 443–445

Erickson GM, Rogers KC, Varricchio DJ, Norell MA, Xu X. Growth patterns in brooding dinosaurs reveals the timing of sexual maturity in non-avian dinosaurs and genesis of the avian condition. Biology Letters. 2007; 3(5):558-61.

Erickson GM, Tumanova TA. Growth curve of *Psittacosaurus mongoliensis* Osborn (Ceratopsia: Psittacosauridae) inferred from long bone histology. Zoological Journal of the Linnean Society. 2000; 130(4):551-66.

Erickson GM. Assessing dinosaur growth patterns: a microscopic revolution. Trends in Ecology & Evolution. 2005; 20(12):677-84.

Fraas E. Ostafrikanische Dinosaurier [East African dinosaurs]. *Palaeontographica* 1908; 55:105–144.

Foster BJ. Evolution of mammals on islands. Nature. 1964; 202:234–235.

Foster JR. 2005. New juvenile sauropod material from western Colorado, and the record of juvenile sauropods from the Upper Jurassic Morrison Formation. In K. Carpenter and V. Tidwell (eds.), Thunder-Lizards: The Sauropodomorph Dinosaurs. Indiana University Press, Bloomington. 2005; 141-153.

Galiano H and Albersdörfer R. A new basal diplodocoid species, *Amphicoelias brontodiplodocus* from the Morrison Formation, Big Horn Basin, Wyoming, with taxonomic re-evaluation of *Diplodocus*, *Apatosaurus*, *Barosaurus* and other genera. Dinosauria International (Ten Sleep, WY) Report for September 2010. 2010; 1-41.

Gallina PA, Apesteguía S. *Cathartesaura anaerobica* gen. et sp. nov., a new rebbachisaurid (Dinosauria, Sauropoda) from the Huincul Formation (Upper Cretaceous), Río Negro, Argentina. *Revista del Museo Argentino de Ciencias Naturales, nuevo serie*. 2005; 7(2):153-166.

Gallup MR. Functional morphology of the hindfoot of the Texas sauropod *Pleurocoelus* sp. indet.: in Farlow, J.O., ed., Paleobiology of the Dinosaurs: Geological Society of America Special Paper. 1989; 238: 71–74.

Galton PM, Yates AM, Kermack D. *Pantydraco* n. gen. for *Thecodontosaurus caducus* Yates, 2003, a basal sauropodomorph dinosaur from the Upper Triassic or Lower Jurassic of South Wales, UK. Neues Jahrbuch für Geologie und Paläontologie-Abhandlungen. 2007; 243(1):119-25.

Galton PM. Notes on the Melanorosauridae, a family of large prosauropod dinosaurs (Saurischia: Sauropodomorpha). Geobios. 1985; 18(5):671-6.

Galton PM. On the anatomy and relationships of *Efraasia diagnostica* (Huene) n. gen., a prosauropod dinosaur (Reptilia: Saurischia) from the Upper Triassic of Germany. Paläontologische Zeitschrift .1973; 47(3): 229-255.

Galton PM. Prosauropod dinosaur *Plateosaurus* (= *Gresslyosaurus*) (Saurischia: Sauropodomorpha) from the Upper Triassic of Switzerland. Geologica et Palaeontologica. 1986; 20: 167-183.

Galton PM. The prosauropod dinosaur *Plateosaurus* Meyer, 1837 (Saurischia: Sauropodomorpha; Upper Triassic). II. Notes on the referred species. Revue Paléobiologie, Genève. 2001; 20(2):435-502.

Gillette DD. *Seismosaurus halli*, gen. et sp. nov., a new sauropod dinosaur from the Morrison Formation (Upper Jurassic/Lower Cretaceous) of New Mexico, USA. Journal of Vertebrate Paleontology. 1991; 11(4):417-33.

Gillette DD. *Seismosaurus: the earth shaker*. Columbia University Press, 1994.

Gillette DD. The geographic and phylogenetic position of sauropod dinosaurs from the Kota formation (Early Jurassic) of India. Journal of Asian Earth Sciences. 2003; 21(6):683-9.

Gillooly JF, Allen AP, Charnov EL. Dinosaur fossils predict body temperatures. PLoS Biology. 2006; 4:1467–1469.

Gilmore CW. A new sauropod dinosaur from the Ojo Alamo Formation of New Mexico. Smithsonian Miscellaneous Collections. 1922; 72(34):1–9.

Goloboff P, Farris J, & Nixon K. TNT: Tree Analysis using New Technology.2003. Program and documentation, available from the authors, and at www.zmuc.dk/public/phylogeny.

Goloboff P, Farris J, & Nixon K. TNT, a free program for phylogenetic analysis. "Cladistics, The International Journal of the Willi Hennig Society": Cladistics. 2008; 24:774-786.

Gomani EM, Jacobs LL, Winkler DA. Comparison of the African titanosaurian, Malawisaurus, with a North American Early Cretaceous sauropod. National Science Museum Monographs. 1999; (15): 223-233.

González Riga BJ and Ortiz David L. A New Titanosaur (Dinosauria, Sauropoda) from the Upper Cretaceous (Cerro Lisandro Formation) of Mendoza Province, Argentina. Ameghiniana. 2014; 51(1 3-25.

González Riga BJ, Lamanna MC, Ortiz David LD, Calvo JO, and Coria JP. A gigantic new dinosaur from Argentina and the evolution of the sauropod hind foot. Scientific Reports, 2016*;* 6: 19165:1-15.

Gorscak E, O'Connor PM, Stevens NJ, & Roberts EM. The basal titanosaurian *Rukwatitan bisepultus* (Dinosauria, Sauropoda) from the middle Cretaceous Galula Formation, Rukwa Rift Basin, southwestern Tanzania. Journal of Vertebrate Paleontology. 2014; 34(5), 1133-1154.

Gould SJ. Ontogeny and phylogeny. Harvard University Press; 1977.

Griebeler EM. Body temperatures in Sauropodomorpha: the hypothesis of inertial homeothermy revisited. PLoS ONE. 2013; 8.

Grigorescu D. Nonmarine cretaceous formations of Romania. Aspects of Nonmarine Cretaceous Geology. China Ocean Press, Beijing. 1992:142-64.

Gunga HC, Suthau T, Bellmann A, Friedrich A, Schwanebeck T, Stoinski S, Trippel T, Kirsch K, Hellwich O. Body mass estimations for *Plateosaurus engelhardti* using laser scanning and 3D reconstruction methods. Naturwissenschaften. 2007; 94(8):623-30.

Gunga HC, Suthau T, Bellmann A, Stoinski S, Friedrich A, Trippel T, Kirsch K, Hellwich O. A new body mass estimation of *Brachiosaurus brancai* Janensch, 1914 mounted and exhibited at the Museum of Natural History (Berlin, Germany). Fossil Record. 2008; 11(1):33-8.

Gutzwiller SC, Su A, O'Connor PM. Postcranial pneumaticity and bone structure in two clades of neognath birds. The Anatomical Record. 2013; 296(6):867-76.

Hammer Ø, Harper DAT, Ryan PD. PAST: Paleontological Statistics Software Package for Education and Data Analysis. Palaeontologia Electronica. 2001; 4(1): pp. 9

Harris JD. The appendicular skeleton of *Suuwassea emilieae* (Sauropoda: Flagellicaudata) from the Upper Jurassic Morrison Formation of Montana (USA). Geobios. 2007; 40(4):501-22.

Hatcher JB. Diplodocus (Marsh): its osteology, taxonomy, and probable habits, with a restoration of the skeleton. Carnegie institute; 1901.

Haughton SH. On some reptilian remains from the Dinosaur Beds of Nyasaland. Transa ctions of the Royal Society of South Africa. 1928;16(1):67-75.

Harvey PH, Pagel MD. The comparative method in evolutionary biology. Oxford: Oxford university press; 1991.

Hazlehurst GA, Rayner JM. Flight characteristics of Triassic and Jurassic Pterosauria: an appraisal based on wing shape. Paleobiology. 1992; 18(04):447-63.

Heinrich RE, Ruff CB, Weishampel DB. Femoral ontogeny and locomotor biomechanics of *Dryosaurus lettowvorbecki* (Dinosauria, Iguanodontia). Zoological Journal of the Linnean Society. 1993; 108: 179–196.

Henderson DM. Estimating the masses and centers of mass of extinct animals by 3-D mathematical slicing. Paleobiology. 1999; pp.88-106.

Henderson DM. Tipsy punters: sauropod dinosaur pneumaticity, buoyancy and aquatic habits. Proceedings of the Royal Society of London B: Biological Sciences. 2004; 271(Suppl 4):S180-3.

Henderson DM. Burly gaits: centers of mass, stability, and the trackways of sauropod dinosaurs. Journal of Vertebrate Paleontology. 2006; 26(4):907-21.

He X, Li K, Cai K, Gao Y. *Omeisaurus tianfuensis*—a new species of *Omeisaurus* from Dashanpu, Zigong, Sichuan. *Journal of Chengdu College of Geology*. 1984; (suppl. 2): 13–32.

Hogg DA. A comparative evaluation of methods for identification of pneumatization in the avian skeleton. *International Journal of Avian Science.* 1980**;** 122**:** 359–363.

Hogg DA. The development of pneumatization in the postcranial skeleton of the domestic fowl. *Journal of Anatomy*. 1984; 139**:** 105–113.

Holland WJ. A review of some recent criticism of the restorations of sauropod dinosaurs existing in the museums of the United States, with special reference to that of *Diplodocus carnegiei* in the Carnegie Museum. American Naturalist. 1990; 44:259–283.

Holtz Jr TR. Dinosaurs: the most complete, up-to-date encyclopedia for dinosaur lovers o f all ages. Random House Childrens Books; 2007.

Hone DW, Farke AA, Wedel MJ. Ontogeny and the fossil record: what, if anything, is an adult dinosaur?. Biology letters. 2016; 12(2):20150947.

Horner JR, De Ricqlès A, Padian K. Long bone histology of the hadrosaurid dinosaur *Maiasaura peeblesorum*: growth dynamics and physiology based on an ontogenetic series of skeletal elements. Journal of Vertebrate Paleontology. 2000; 20(1):115-29.

Huene F von. Bemerkingen zur Systemauk und Stammesgeschichte einiger Reptilien Zeitschrift fuer Induktive Abstammungs – und Vererbungslehre. 1920; 24:162-166.

Huene FV. Short review of the present knowledge of the Sauropoda. Memoirs of the Queensland Museum. 1927; 9(1):121-6.

Hunt G, Roy K. Climate change, body size evolution, and Cope's Rule in deep-sea ostracodes. Proceedings of the National Academy of Sciences. 2006; 103(5):1347-52.

Hunter J. An account of certain receptacles of air, in birds, which communicate with the lungs, and are lodged both among the fleshy parts and in the hollow bones of those animals. By John Hunter, FRS. Philosophical Transactions. 1774; 64:205-213.

Ibiricu LM, Casal GA, Lamanna MC, Martínez RD, Harris JD and Lacovara KJ. The southernmost records of Rebbachisauridae (Sauropoda: Diplodocoidea), from early Late Cretaceous deposits in central Patagonia. Cretaceous Research*.* 2012*;* 34: 220-232.

Ikejiri T, Tidwell V, Trexler DL. New adult specimens of *Camarasaurus lentus* highlight ontogenetic variation within the species. Thunder-lizards: the Sauropodomorph dinosaurs. Indiana University Press, Bloomington. 2005:154-79.

Ikejiri T. Distribution and biochronology of *Camarasaurus* (Dinosauria, Sauropoda) from the Jurassic Morrison Formation of the Rocky Mountain Region. In New Mexico Geological Society, 56th Field Conference Guidebook, Geology of the Chama Basin; 2005. pp. 367-379.

Jaekel O. Über die Wirbeltierfunde in der oberen Trias von Halberstadt. *Paläontologische Zeitschrift*. 1914; 1: 155–215.

Jacobs LL, Winkler DA, Downs WR, Gomani EM. New material of an Early Cretaceous titanosaurid sauropod dinosaur from Malawi. Palaeontology, London. 1993; 36(3):523-534.

Jain SL, Kutty TS, Chowdhury Roy T and Chatterjee S. The sauropod dinosaur from the Lower Jurassic Kota Formation of India. Proceedings of the Royal Society of London A. 1975; 188: 221-228.

Jain SL, Chatterjee S. Some characteristics of *Barapasaurus tagorei,* a sauropod dinosaur from the Lower Jurassic of Deccan, India. Proceedings of the IV International Gondwana Symposium, Calcutta. 1979; 1: 204-216.

Janensch W. Übersicht über die Wirbeltierfauna der Tendaguru-Schichten [Overview of the vertebrate fauna of the Tendaguru beds]. *Archiv für Biontologie.* 1914; 3: 81–110.

Janensch W. Material und Formengehalt der Sauropoden in der Ausbeute der Tendaguru-expedition. Palaeontographica-Supplementbände. 1929; 1:1-34.

Janensch W. Pneumatizitat bei wirlbeln von sauropoden und anderen saurischiern. Palaeontographica. 1947; 3: 1-25.

Janensch W. Die wirbelsäule von *Brachiosaurus brancai*. Palaeontographica-Supplementbände. 1950; pp.27-93.

Jianu CM, Weishampel DB. The smallest of the largest: a new look at possible dwarfing in sauropod dinosaurs. Geologie en Mijnbouw. 1999; v 78(3-4):335-43.

Junchang L, Azuma Y, Rongjun C, Wenjie Z, Xingsheng J. A new titanosauriform sauropod from the Early Late Cretaceous of Dongyang, Zhejiang province. Acta Geologica Sinica. 2008; 82(2): 225-235.

Junchang L, Li X, Xingliao Z, Weiyong H, Yanhua W, Songhai J, Qiang J. A new gigantic sauropod dinosaur with the deepest known body cavity from the Cretaceous of Asia. Acta Geologica Sinica (English edition). 2007; 81(2):167-76.

Kilbourne BM, & Makovicky PJ. Limb bone allometry during postnatal ontogeny in non-avian dinosaurs. Journal of Anatomy. 2010; 217(2), 135-152.

King AS. The aerated bones of *Gallus domesticus*. Cells Tissues Organs. 1957; 31(2):220-230.

Klein N, Sander PM. Bone histology and growth of the prosauropod dinosaur *Plateosaurus engelhardti* von Meyer, 1837 from the Norian bone beds of Trossingen (Germany) and Frick (Switzerland). Special Papers in Palaeontology. 2007; 77:169.

Klein N, Sander M. Ontogenetic stages in the long bone histology of sauropod dinosaurs. Paleobiology. 2008; 34(02):247-63.

Klein N, Sander M, Suteethorn V. Bone histology and its implications for the life history and growth of the Early Cretaceous titanosaur *Phuwiangosaurus sirindhornae*. Geological Society, London, Special Publications. 2009; 315(1):217-28.

Kowallis BJ, Christiansen EH, Deino AL, Peterson F, Turnern CE, Kunk MJ & Obradovich JD. The age of the Morrison Formation. Modern Geology. 1998; 22: 235-260.

Ksepka DT, Norell MA. *Erketu ellisoni*, a long-necked sauropod from Bor Guvé (Dornogov Aimag, Mongolia). American Museum Novitates. 2006; 3508:1-16.

Lacovara KJ, Lamanna MC, Ibiricu LM, Poole, JC, Schroeter ER, Ullmann P V, ... & Egerton VM. A gigantic, exceptionally complete titanosaurian sauropod dinosaur from southern Patagonia, Argentina. Scientific Reports. 2014; *4*, srep06196.

Lambertz M, Bertozzo F, Sander PM. Bone histological correlates for air sacs and their implications for understanding the origin of the dinosaurian respiratory system. *Biology letters.* 2018; 4(1), 20170514.

Le Loeuff J. Romanian Late Cretaceous dinosaurs: big dwarfs or small giants?. Historical Biology. 2005; 17(1-4):15-7.

Lee AH, Werning S. Sexual maturity in growing dinosaurs does not fit reptilian growth models. Proceedings of the National Academy of Sciences. 2008; 105(2):582-7.

Lewis PO. A likelihood approach to estimating phylogeny from discrete morphological character data. Systematic biology. 2001; 50(6):913-25.

Lida X, Yong YE, Chunkang SHU, Guangzhao PENG, & Hailu YOU. Structure, orientation and finite element analysis of the tail club of Mamenchisaurus hochuanensis. *Acta Geologica Sinica (English edition)*. 2009; 83(6): 1031-1040.

Lomolino MV. Body size evolution in insular vertebrates: generality of the island rule. Journal of Biogeography. 2005; 32(10):1683-99.

Longman, 1926, a gravisaurian sauropodomorph dinosaur from the Middle Jurassic of Queensland, Australia. Journal of Vertebrate Paleontology. 2012; 32(2):369-94.

Lovelace D, Wahl WR, Hartman SA. Evidence for costal pneumaticity in a diplodocid dinosaur (*Supersaurus vivianae*). Journal of Vertebrate Paleontology. 2003; 23: 73A-73A.

Lovelace DM, Hartman, S. A., & Wahl, W. R. Morphology of a specimen of *Supersaurus* (Dinosauria, Sauropoda) from the Morrison Formation of Wyoming, and a re-evaluation of diplodocid phylogeny. *Arquivos do Museu Nacional, Rio de Janeiro.* 2007; 65**:** 527–544.

Lü J, Xu L, Zhang X, Hu W, Wu Y, Jia S, Ji Q. A new gigantic sauropod dinosaur with the deepest known body cavity from the Cretaceous of Asia. Acta Geologica Sinica. 2007; 81 (2):167-176.

Lu J, Azuma Y, Chen R, Zheng W, Jin X. A new titanosauriform sauropod from the Early Late Cretaceous of Dongyang, Zhejiang Province. Acta Geologica Sinica. 2008; 82(2):225 -235.

Lucas SG, Spielmann JA, Rinehart LF, Heckert AB, Herne MC, Hunt AP., ... & Sullivan R M. Taxonomic status of *Seismosaurus hallorum*, a Late Jurassic sauropod dinosaur from New Mexico. New Mexico Museum of Natural History and Science Bulletin. 2006; 36: 149-162.

Luke JH, Weir JT, Brock CD, Glor RE, Challenger W. GEIGER: investigating evolutio nary radiations. Bioinformatics. 2008; 24:129-131.

Lull RS. The Reptilia of the Arundel Formation. Maryland Geological Survey. 1911; 171-211.

Lydekker R. Contributions to a knowledge of the fossil vertebrates of Argentina. I. — The dinosaurs of Patagonia. *Anales del Museo de La Plata. Paleontología Argentina*. 1893; 2**:** 1–16.

Maddison WP. Maddison DR. Mesquite: a modular system for evolutionary analysis. 2016. Version 3.10 http://mesquiteproject.org

Makarieva AM, Gorshkov VG, Li BL. Gigantism, temperature and metabolic rate in terrestrial poikilotherms. Proceedings of the Royal Society of London B: Biological Sciences. 2005; 272(1578):2325-8.

Mannion PD & Barrett PM. Additions to the sauropod dinosaur fauna of the Cenomanian (early Late Cretaceous) Kem Kem beds of Morocco: Palaeobiogeographical implications

of the mid-Cretaceous African sauropod fossil record. Cretaceous Research. 2013; 45: 49-59.

Mannion PD, Upchurch P, Barnes RN and Mateus O. Osteology of the Late Jurassic Portuguese sauropod dinosaur *Lusotitan atalaiensis* (Macronaria) and the evolutionary history of basal titanosauriforms. Zoological Journal of the Linnean Society*.* 2013*;* 168:98-206.

Mannion PD, Allain R, and Moine O. The earliest known titanosauriform sauropod dinosaur and the evolution of Brachiosauridae. *PeerJ*. 2017; 5: e3217, 1–82.

Marpmann JS, Carballido JL, Sander PM & Knötschke N. Cranial anatomy of the Late Jurassic dwarf sauropod *Europasaurus holgeri* (Dinosauria, Camarasauromorpha): ontogenetic changes and size dimorphism. Journal of Systematic Palaeontology. 2015; *13*(3): 221-263.

Marsh OC. Notice of a new and gigantic dinosaur. American Journal of Science. 1877a; 14:87-88.

Marsh OC. Principal characters of American Jurassic dinosaurs. Part I. *American Journal of Science and Arts*. 1878; 16: 411–416.

Marsh OC. Notice of a new genus of Sauropoda and other new dinosaurs from the Potomac Formation. American Journal of Science. 1888; 135: 89-94.

Martin V, Buffetaut E, Suteethorn V. A new genus of sauropod dinosaur from the Sao Khua Formation (Late Jurassic or Early Cretaceous) of northeastern Thailand. Compte Rendus de l'Academie des Sciences, Paris, série IIa. 1994; 319:1085-1092.

Martin V. Baby sauropods from the Sao Khua Formation (Lower Cretaceous) in Northeastern Thailand. Gaia. 1994; 10: 147–153.

Martin EG, Palmer, C. Air Space Proportion in Pterosaur Limb Bones Using Computed Tomography and Its Implications for Previous Estimates of Pneumaticity. 2014; PLoS ONE 9(5): e97159. doi:10.1371/journal.pone.0097159

Martínez RN, Alcober OA. A basal sauropodomorph (Dinosauria: Saurischia) from the Ischigualasto Formation (Triassic, Carnian) and the early evolution of Sauropodomorpha. 2009; PLoS One 4(2): e4397.

Martínez RN, Sereno PC, Alcober OA, Colombi CE, Renne PR, Montañez IP, Currie BS. A basal dinosaur from the dawn of the dinosaur era in southwestern Pangaea. 2011; Science 331: 206–210.

Mazzetta GV, Christiansen P, Fariña RA. Giants and bizarres: body size of some southern South American Cretaceous dinosaurs. Historical Biology. 2004; 16(2-4):71-83.

McIntosh JS. The sauropod dinosaurs: a brief survey. The Age of Dinosaurs. Short Courses in Paleontology. 1989; 2:85-99.

McIntosh JS. Sauropoda. The Dinosauria. University of California Press, Berkeley. 1990; 1:345-401.

McIntosh JS, Miller WE, Stadtman KL, Gillette DD. The osteology of *Camarasaurus lewisi* (Jensen, 1988). Brigham Young University Geology Studies. 1996; 41:73-95.

McIntosh JS, Brett-Surman MK, and Farlow JO. Sauropods; pp. 264–290 *in* J. O. Farlow and M. K. Brett-Surman (eds.). 1997. The Complete Dinosaur. Indiana University Press, Indianapolis.

McKinney ML, McNamara KJ. Heterochrony. In Heterochrony. Springer US.1991. pp.1-12.

McKinney ML. Heterochrony in evolution. In Heterochrony in Evolution. Springer US.1988. pp. 327-340.

McPhee BW, Yates AM, Choiniere JN, Abdala F. The complete anatomy and phylogenetic relationships of *Antetonitrus ingenipes* (Sauropodiformes, Dinosauria): implications for the origins of Sauropoda. Zoological Journal of the Linnean Society. 2014; 171: 151-205.

Meiri S, Dayan T, Simberloff D. Body size of insular carnivores: little support for the island rule. The American Naturalist. 2004; 163(3):469-79.

Meiri S. Size evolution in island lizards. Global Ecology and Biogeography. 2007; 16(6):702-8.

Melstrom KM, D'emic MD, Chure D, Wilson JA. A juvenile sauropod dinosaur from the Late Jurassic of Utah, USA, presents further evidence of an avian style air-sac system. Journal of Vertebrate Paleontology. 2016 Mar 17:e1111898.

Meyer Hv. Mittheilungen, an Professor Bronn gerichtet. Neues Jahrbuch für Mineralogie, Geognosie, Geologie und Petrefaktenkunde. 1837; 314–317.

Mocho P, Royo–Torres R, Ortega F. Phylogenetic reassessment of *Lourinhasaurus alenquerensis*, a basal Macronaria (Sauropoda) from the Upper Jurassic of Portugal. Zoological Journal of the Linnean Society. 2014. 170**:** 875–916.

Motta MJ, Aranciaga Rolando AM, Rozadilla S, Agnolin FL, Chimento NR, Brissón Egli F, and Novas FE. New theropod fauna from the Upper Cretaceous (Huincul Formation) of Northwestern Patagonia, Argentina. In A. Khosla & S. G. Lucas (ed.), Cretaceous Period: Biotic Diversity and Biogeography. New Mexico Museum of Natural History and Science Bulletin. 2016; 71: 231-253.

Motani R. Estimating body mass from silhouettes: testing the assumption of elliptical body cross-sections. Paleobiology. 2001; 27(4):735-50.

Morris J. A Catalogue of British Fossils. 1843. British Museum, London: pp. 222.

Müller B. The air-sacs of the pigeon. Smith Miscellaneous Collections. 1908; 50:365–414.

Nair JP, Salisbury SW. New anatomical information on Rhoetosaurus brownei Longman, 1926, a gravisaurian sauropodomorph dinosaur from the Middle Jurassic of Queensland, Australia. Journal of Vertebrate Paleontology. 2012; 32(2):369-94.

Nesbitt SJ, Smith ND, Irmis RB, Turner AH, Downs A, Norell MA. A complete skeleton of a Late Triassic saurischian and the early evolution of dinosaurs. Science. 2009; 326(5959):1530-3.

Noble WS. How does multiple testing correction work? Nature Biotechnology. 2009; 27(12): 1135-1137.

Norman DB. On the anatomy of *Iguanodon atherfieldensis* (Ornithischia: Ornithopoda). Bulletin-Institut royal des sciences naturelles de Belgique. Sciences de la terre. 1986; 56:281-372.

Norman DB, Barrett PM. Ornithischian dinosaurs from the Lower Cretaceous (Berriasian) of England. Special Papers in Palaeontology. 2002; 68, 161–189.

Noto CR, Grossman A. Broad-Scale Patterns of Late Jurassic Dinosaur Paleoecology. PLoS ONE. 2010; 5(9): e12553. doi:10.1371/journal.pone.0012553

Novas FE, Salgado L, Calvo J, Agnolin F. Giant titanosaur (Dinosauria, Sauropoda) from the Late Cretaceous of Patagonia. Revista del Museo Argentino de Ciencias Naturales Nueva Serie. 2005; 7(1):31-36.

Novas FE, Salgado L, Calvo JO, Agnolín FL. Giant titanosaur (Dinosauria, Sauropoda) from the Late Cretaceous of Patagonia. Revista del Museo Argentino de Ciencias Naturales, nuevo serie. 2005; 7(1):37-41.

O'Connor PM. Pulmonary pneumaticity in the postcranial skeleton of extant aves: a case study examining Anseriformes. Journal of Morphology. 2004; 261:141–161.

O'Connor PM, Claessens LPAM. Basic avian pulmonary design and flow through ventilation in non-avian theropod dinosaurs. Nature. 2005; 436(7038):253–256. doi:10.1038/nature03716.

O'Connor PM. Postcranial pneumaticity: an evaluation of soft-tissue influences on the postcranial skeleton and the reconstruction of pulmonary anatomy in archosaurs. Journal of Morphology. 2006; 267:1199–1226.

O' Connor PM. Evolution of archosaurian body plans: skeletal adaptations of an air sac-based breathing apparatus in birds and other archosaurs. Journal of Experimental Zoology. 2009; 311:629–646.

Orme D, Freckleton R, Thomas G, Petzoldt T, Fritz S, Nick I, Pearse W. caper: Compar ative Analyses of Phylogenetics and Evolution in R. 2013. R package version 0.5.2.htt ps://CRAN.R-project.org/package=caper

Osborn HF, Mook CC. *Camarasaurus*, *Amphicoelias* and other sauropods of Cope. Memoirs of the American Museum of Natural History. 1921; 3: 247-387.

Otero A, Pol D. Postcranial anatomy and phylogenetic relationships of *Mussaurus patagonicus* (Dinosauria, Sauropodomorpha). Journal of Vertebrate Paleontology. 2013;33(5):1138-68.

Ouyang H & Ye Y. The First Mamenchisaurian Skeleton with Complete Skull, *Mamenchisaurus youngi*. Sichuan Publishing House of Science and Technology, Chengdu. 2002 111 pp. (in Chinese, with English summary).

Palombo MR. How can endemic proboscideans help us understand the “island rule”? A case study of Mediterranean islands. Quaternary International. 2007; 169:105-24.

Paradis E, Claude J. Strimmer K. APE: analyses of phylogenetics and evolution in R lang uage. Bioinformatics. 2004; 20: 289-290.

Paul GS. The brachiosaur giants of the Morrison and Tendaguru with a description of a new subgenus, *Giraffatitan*, and a comparison of the world's largest dinosaurs. Hunteria. 1988; 2(3):1-14.

Paul G. *Chasmosaurus*, *Homocephale*, *Monoclonius*, *Pentaceratops*, *Bactrosaurus*, *Massospondylus*, *Omeisaurus*, *Stegosaurus*, pp. 58–215 *in* P. Dodson (ed.), Encyclopedia of Dinosaurs. 1990. Beekman House, New York.

Paul GS. The science and art of restoring the life appearance of dinosaurs and their relatives: a rigorous how-to guide. Dinosaurs past and present. 1987; 2:4-9.
Peczkis J. Implications of body-mass estimates for dinosaurs. Journal of Vertebrate Paleontology. 1995; 14(4):520-33.

Paul GS. Dinosaur models: the good, the bad, and using them to estimate the mass of dinosaurs. DinoFest International Proceedings. Philadelphia: The Academy of Natural Sciences. 1997; pp.129-154.

Peczkis J. Implications of body-mass estimates for dinosaurs. Journal of Vertebrate Paleontology. 1995; 14(4):520-33.

Perry SF, Reuter C. Hypothetical lung structure of Brachiosaurus (Dinosauria: Sauropoda) based on functional constraints. Fossil Record. 1999; 2(1):75-79.

Perry SF. Functional morphology of the reptilian and avian respiratory systems and its implications for theropod dinosaurs. New Perspectives on the Origin and Early Evolution of Birds (J. Gauthier and LF Gall, Eds.). Peabody Museum of Natural History, Yale University, New Haven, Connecticut. 2001; pp.429-41.

Perry SF, Christian A, Breuer T, Pajor N, Codd JR. Implications of an avian-style respiratory system for gigantism in sauropod dinosaurs. Journal of Experimental Zoology Part A: Ecological Genetics and Physiology. 2009; 311(8):600-10.

Peters RH, Wassenberg K. The effect of body size on animal abundance. Oecologia. 1983; 60(1):89-96.

Poropat SF, Upchurch P, Mannion PD, Hocknull SA, Kear BP, Sloan T., ... & Elliott DA. Revision of the sauropod dinosaur *Diamantinasaurus matildae* Hocknull et al. 2009 from the mid-Cretaceous of Australia: implications for Gondwanan titanosauriform dispersal. Gondwana Research. 2015; 27(3), 995-1033.

Poropat SF, Mannion, PD, Upchurch P, Hocknull SA, Kear BP, Kundrát, M., ... & Elliott DA. New Australian sauropods shed light on Cretaceous dinosaur palaeobiogeography. Scientific reports. 2016; 6.

Powell JE. Revision de los Titanosauridos de America del Sur. Doctoral dissertation. Universidad Nacional de Tucumin, Tucumin. 1986. pp.340

Powell JE. Osteologia de Saltasaurus loricatus (Sauropoda - Titanosauridae) del Cretácico Superior del noroeste Argentino [Osteology of Saltasaurus loricatus (Sauropoda - Titanosauridae) from the Upper Cretaceous of northwest Argentina]. *In J. L. Sanz & A. D . Buscalioni (eds.), Los Dinosaurios y Su Entorno Biotico: Actas del Segundo Curso de Paleontologia in Cuenca. Institutio Juan de Valdes, Cuenca, Argentina*. 1992; 165-230.

R Core Team. R: A language and environment for statistical computing. 2016. R Found ation for Statistical Computing, Vienna, Austria. URL https://www.R-project.org/.

Raath MA. Fossil vertebrate studies in Rhodesia: a new dinosaur (Reptilia: Saurischia) from near the Triassic-Jurassic boundary. 1972; Arnoldia. 5(31):1-37.

Raath MA, McIntosh JS. Sauropod dinosaurs from the Central Zambezi Valley, Zimbabwe, and the age of the Kadzi Formation. South African Journal of Geology. 1987; 90(2):107-19.

Raia P, Meiri S. The island rule in large mammals: paleontology meets ecology. Evolution. 2006; 60(8):1731-42.

Rauhut OW, Remes K, Fechner R, Cladera G, Puerta P. Discovery of a short-necked sauropod dinosaur from the Late Jurassic period of Patagonia. Nature. 2005; 435(7042):670-2.

Rayfield EJ, Norman DB, Horner CC, Horner, JR, Smith, PM, Thomason JJ, & Upchurch P. Cranial design and function in a large theropod dinosaur. Nature. 2001; 409(6823): 1033-1037.

Rayfield EJ. Aspects of comparative cranial mechanics in the theropod dinosaurs *Coelophysis*, *Allosaurus* and *Tyrannosaurus*. Zoological Journal of the Linnean Society. 2005 144(3): 309-316.

Remes K. Revision of the Tendaguru sauropod dinosaur Tornieria africana (Fraas) and its relevance for sauropod paleobiogeography. Journal of vertebrate Paleontology. 2006; 26(3):651-69.

Remes K. A second Gondwanan diplodocid dinosaur from the Upper Jurassic Tendaguru Beds of Tanzania, East Africa. Palaeontology. 2007; 50(3):653-667.

Remes K, Ortega F, Fierro I, Joger U, Kosma R, Ferrer JM, Ide OA, Maga A. A new basal sauropod dinosaur from the Middle Jurassic of Niger and the early evolution of Sauropoda. PLoS One. 2009; 4(9):e6924:1-13.

Revell LJ. phytools: An R package for phylogenetic comparative biology (and other things). Methods in Ecology and Evolution. 2012; 3: 217-223.

Rich TH, Vickers-Rich P, Gimenez O, Cúneo R, Puerta P, Vacca R. A new sauropod dinosaur from Chubut province, Argentina. Proceedings of the Second Gondwanan Dinosaur Symposium, National Science Museum Monographs. 1999; 15:61-84.

Riggs ES. *Brachiosaurus altithorax*, the largest known dinosaur. American Journal of Science, series 4. 1903; 15:299-306.

Rogers KC, Ericsson GM. Sauropod histology. In The Sauropods, Evolution and Paleobiology. University of California Press Berkeley; 2005. pp. 303-326. doi:10.1111/j.2041-210X.2011.00169.x

Rogers KC. Titanosauria: A Phylogenetic Overview. In The Sauropods: Evolution and Paleobiology. Berkeley, California; 2005.

Romer AS. Osteology of the reptiles. University of Chicago Press. Chicago, 1956; pp. 772.

Romer AS. Vertebrate Paleontology. Second Edition. University of Chicago Press. Chicago, 1966; pp. 468.

Roth VL. Inferences from allometry and fossils: dwarfing of elephants on islands. Oxford surveys in evolutionary biology. 1992; 8:259-259.

Russell DA, Zheng Z. A large mamenchisaurid from the Junggar Basin, Xinjiang, People's Republic of China. Canadian Journal of Earth Sciences. 1993; 30(10):2082-95.

Salgado L. and Bonaparte JF. Un nuevo sauropodo Dicraeosauridae, *Amargasaurus cazaui* gen. et sp. nov., de la formacion La Amarga, Neocomiano de la provincia del Neuquen, Argentina. Ameghiniana. 1991; 28:333–346.

Salgado L, Calvo JO, Coria RA. Relaciones filogeneticas de *Pleurocoelus* Marsh (Sauropoda). Jornadas Argentinas de Paleontologia de Vertebrados, Resumenes. 1995; 11.

Salgado L, Coria RA, Calvo JO. Evolution of titanosaurid sauropods: Phytogenetic analysis based on the postcranial evidence. Ameghiniana. 1997; 34(1):3-2.

Salgado L, Apesteguía S, Heredia SE. A new specimen of *Neuquensaurus australis*, a Late Cretaceous saltasaurine titanosaur from north Patagonia. J Vert Paleontol. 2005; 25(3):623-34.

Sander PM, Klein N, Buffetaut E, Cuny G, Suteethorn V, Le Loeuff J. Adaptive radiation in sauropod dinosaurs: bone histology indicates rapid evolution of giant body size through acceleration. Organisms Diversity & Evolution. 2004; 4(3):165-73.

Sander PM, Mateus O, Laven T, Knötschke N. Bone histology indicates insular dwarfism in a new Late Jurassic sauropod dinosaur. Nature. 2006; 441(7094):739-41.

Sander PM, Christian A, Clauss M, Fechner R, Gee CT, Griebeler EM, Gunga HC, Hummel J, Mallison H, Perry SF, Preuschoft H. Biology of the sauropod dinosaurs: the evolution of gigantism. Biological Reviews. 2011; 86(1):117-55.

Sander PM. An Evolutionary Cascade Model for Sauropod Dinosaur Gigantism-Overview, Update and Tests. PloS ONE. 2013; 8(10):e78573.

Sanz JL, Powell JE, Le Loeuff JE, Martínez RU, Pereda Suberbiola X. Sauropod remains from the Upper Cretaceous of Laño (northcentral Spain). Titanosaur phylogenetic relationships. Estudios del Museo de Ciencias Naturales de Alava. 1999; 14(1):235-55.

Schachner ER, Cieri RL, Butler JP, Farmer CG. Unidirectional pulmonary airflow patterns in the savannah monitor lizard. Nature. 2013; 506: 367-370. doi: 10.1038/nature12871.

Schmidt-Nielsen K. Scaling: why is animal size so important?. Cambridge University Press; 1984.

Schwarz D, Fritsch G. Pneumatic structures in the cervical vertebrae of the Late Jurassic Tendaguru sauropods *Brachiosaurus brancai* and *Dicraeosaurus*. Eclogae Geologicae Helvetiae. 2006; 99:65–78.

Schwarz D, Frey E, Meyer CA. Pneumaticity and soft-tissue reconstructions in the neck of diplodocid and dicraeosaurid sauropods. Acta Palaeontologica Polonica. 2007; 52:167–188.

Seebacher F. A new method to calculate allometric length-mass relationships of dinosaurs. J Vert Paleontol. 2001; 21(1):51-60.

Seeley HG. On *Ornithopsis*, a gigantic animal of the pterodactyle kind from the Wealden. Annals of the Magazine of Natural History (Series 4). 1870a; 5:279-283.

Sekiya T. Re-examination of *Chuanjiesaurus anaensis* (Dinosauria: Sauropoda) from the Middle Jurassic Chuanjie Formation, Lufeng County, Yunnan Province, southwest China. Memoir of the Fukui Prefectural Dinosaur Museum. 2011; 10: 1-54.

Sellers WI, Hepworth-Bell J, Falkingham PL, Bates KT, Brassey CA, Egerton VM and Manning PL. Minimum convex hull mass estimations of complete mounted skeletons. Biology Letters. 2012; 8, 842–845. doi:10.1098/rsbl.2012.0263

Sereno PC, Beck AL, Dutheil DB, Larsson HC, Lyon GH, Moussa B, Sadleir RW, Sidor CA, Varricchio DJ, Wilson GP, Wilson JA. Cretaceous sauropods from the Sahara and the uneven rate of skeletal evolution among dinosaurs. Science. 1999; 286(5443):1342-7.

Sereno PC, Wilson JA., Witmer LM Whitlock JA, Maga A, Ide O, Rowe TA. Structural extremes in a Cretaceous dinosaur. 2007; PLoS ONE. 2(11): e1230.

Sereno PC, Martinez RN, Wilson JA, Varricchio DJ, Alcober OA, Larsson HCE. Evidence for avian intrathoracic air sacs in a new predatory dinosaur from Argentina. PLoS ONE. 2008; 3:e3303. doi:10.1371/journal.pone.0003303

Sertich JJW and Loewen MA. A new basal sauropodomorph dinosaur from the Lower Jurassic Navajo Sandstone of southern Utah. PLoS One. 2010; 5(3):e9789

Seymour RS. Maximal aerobic and anaerobic power generation in large crocodiles versus mammals: implications for dinosaur gigantothermy. PLoS One. 8.7 (2013): e69361.

Sondaar PY. The island sweepstakes. Why did pygmy elephants, dwarf deer and large mice populate the Mediterranean? Natural History. 1976; 95 (9): 50–57.

Sookias RB, Benson RB, Butler RJ. Biology, not environment, drives major patterns in maximum tetrapod body size through time. *Biology letters*. 2012; 8(4): 674-677.

Stein K, Csiki Z, Rogers KC, Weishampel DB, Redelstorff R, Carballido JL, Sander PM. Small body size and extreme cortical bone remodeling indicate phyletic dwarfism in *Magyarosaurus dacus* (Sauropoda: Titanosauria). Proceedings of the National Academy of Sciences. 2010; 107(20):9258-63.

Sternfeld R. Zur Nomenklatur der Gattung Gigantosaurus Fraas [On the nomenclature of the genus Gigantosaurus Fraas]. *Sitzungsberichte der Gesellschaft Naturforschender Freunde zu Berlin*. 1911; 8:398.

Suteethorn S, Le Loeuff J, Buffetaut E, Suteethorn V, Talubmook C, Chonglakmani C. A new skeleton of *Phuwiangosaurus sirindhornae* (Dinosauria, Sauropoda) from NE Thailand. Geological Society, London, Special Publications. 2009; 315(1):189-215.

Swofford DL. PAUP*. Phylogenetic Analysis Using Parsimony (*and Other Methods). 2002. Versions 4.0a147 & 4.0a149. Sinauer Associates, Sunderland, Massachusetts.

Taylor MP, Wedel MJ. Why sauropods had long necks; and why giraffes have short necks. PeerJ. 2013;1:e36.

Tidwell V, Carpenter K. Thunder-Lizards: the sauropodomorph dinosaurs. Indiana University Press; 2005.

Tidwell VI, Wilhite DR. Ontogenetic variation and isometric growth in the forelimb of the Early Cretaceous sauropod Venenosaurus. Thunder Lizards: the Sauropodomorph Dinosaurs. 2005:187-98.

Tschopp E, Mateus O & Benson RB. A specimen-level phylogenetic analysis and taxonomic revision of Diplodocidae (Dinosauria, Sauropoda). PeerJ. 2015; *3*, e857.

Upchurch P. The anatomy, phylogeny and systematics of sauropod dinosaurs. Doctoral dissertation. 1993.

Upchurch P. The evolutionary history of sauropod dinosaurs. Philosophical Transactions of the Royal Society of London B: Biological Sciences. 1995; 349(1330):365-90.

Upchurch. The phylogenetic relationships of sauropod dinosaurs. Zoological Journal of the Linnean Society. 1998; 124(1): 43–103.

Upchurch P, Barrett PM, Dodson P. Sauropoda. In Weishampel DB, Dodson P, Osmolska H. (eds.). The Dinosauria. 2nd edition. University of California Press, Berkeley. 2004. pp. 259-322.

Upchurch P, Barrett PM, Xijin Z, Xing X. A re-evaluation of *Chinshakiangosaurus chunghoensis* Ye vide Dong 1992 (Dinosauria, Sauropodomorpha): implications for cranial evolution in basal sauropod dinosaurs. Geological Magazine. 2007; 144(02):247-62.

Upchurch P, Mannion PD, and Taylor MP. The Anatomy and Phylogenetic Relationships of “Pelorosaurus “becklesii (Neosauropoda, Macronaria) from the Early Cretaceous of England. PLoS One. 2015; 10.6: e0125819.

Van Valen L. A new evolutionary law. Evolutionary theory. 1973;1:1-30.

Van Hoepen ECN. 1920. Contributions to the knowledge of the reptiles of the Karroo Formation. 6. Further dinosaurian material in the Transvaal Museum. *Annals of the Transvaal Museum* **7(2)**:93-141

Varricchio DJ. Bone microstructure of the Upper Cretaceous theropod dinosaur *Troodon formosus*. Journal of Vertebrate Paleontology. 1993; 13(1):99-104.

von Huene FR. Die Fossile Reptil-ordnung Saurischia: Ihre Entwicklung und Geschichte. Gebrüder Borntraeger. 1932.

Watanabe A, Gold MEL, Brusatte SL, Benson RB, Choiniere J, Davidson A, Norell MA. Vertebral Pneumaticity in the Ornithomimosaur *Archaeornithomimus* (Dinosauria: Theropoda) revealed by computed tomography imaging and reappraisal of axial pneumaticity in ornithomimosauria. 2015; PloS One. 10(12): e0145168.

Wedel MJ, Cifelli RL, Sanders RK. *Sauroposeidon proteles*, a new sauropod from the Early Cretaceous of Oklahoma. Journal of Vertebrate Paleontology. 2000*a*; 20(1):109-14.

Wedel MJ, Cifelli RL, Sanders RK. Osteology, paleobiology, and relationships of the sauropod dinosaur *Sauroposeidon*. Acta Palaeontologica Polonica. 2000*b*; 45(4).

Wedel MJ. The evolution of vertebral pneumaticity in the Sauropoda. 2001. MS. Thesis. University of Oklahoma.

Wedel MJ. Vertebral pneumaticity, air sacs, and the physiology of sauropod dinosaurs. Paleobiology. 2003a; 29:243–255.

Wedel MJ. The evolution of vertebral pneumaticity in sauropod dinosaurs. Journal of Vertebrate Paleontology. 2003b; 23(2):344–357, DOI: 10.1671/0272-4634(2003)023[0344:TEOVPI]2.0.CO;2

Wedel MJ. Postcranial skeletal pneumaticity in sauropods and its implications for mass estimates. In: Curry-Rogers KA, Wilson JA, editors. Berkeley: University of California Press; 2005. pp. 201–228.

Wedel MJ. What pneumaticity tells us about 'prosauropods', and vice versa. Special Papers of Paleontology. 2007; 77:207–222.

Wedel MJ. Evidence for bird-like air sacs in saurischian dinosaurs. Journal of Experimental Zoology. 2009; 311A. DOI: 10.1002/jez.513.

Wedel MJ, Taylor MP. Caudal pneumaticity and pneumatic hiatuses in the sauropod dinosaurs *Giraffatitan* and *Apatosaurus*. PLoS ONE. 2013; 8(10): e78213. doi:10.1371/journal.pone.0078213

Weiglein AH. Development of the paranasal sinuses in humans. In: Koppe, T., Nagai, H., and Alt, K.W., (eds.). The Paranasal Sinuses of Higher Primates. 1999. Quintessence, Chicago, IL. pp. 35–50.

Weishampel DB, Grigorescu D, Norman DB. The dinosaurs of Transylvania. National Geographic Research & Exploration. 1991; 7(2):196-215.

Welch JJ. Testing the island rule: primates as a case study. Proceedings of the Royal Society of London B: Biological Sciences. 2009; 276(1657):675-82.

Whitlock, JA. A phylogenetic analysis of Diplodocoidea. Zoological journal of the Linnaean Society. 2011; 161: 872-915.

Wilhite DR. Biomechanical reconstruction of the appendicular skeleton in three North American Jurassic sauropods. Ph.D. Dissertation, Louisiana State University. 2003. Available at: http://etd02.lnx390.lsu.edu/docs/available/etd-0408103-003549/.

Wild R. *Janenschia n. g. robusta* (E. Fraas 1908) pro *Tornieria robusta* (E. Fraas 1908) (Reptilia, Saurischia, Sauropodomorpha) [*Janenschia n. g. robusta* (E. Fraas 1908) for *Tornieria robusta* (E. Fraas 1908) (Reptilia, Saurischia, Sauropodomorpha)]. Stuttgarter Beiträge zur Naturkunde, Serie B (Geologie und Paläontologie). 1991; 173:1-4.

Williamson TE & Weil A. Stratigraphic distribution of sauropods in the Upper Cretaceous of the San Juan Basin, New Mexico, with comments on North America's Cretaceous 'sauropod hiatus'. *Journal of Vertebrate Paleontology*. 2008; *28*(4): 1218-1223.

Wilson JA, Sereno PC. Early evolution and higher-level phylogeny of sauropod dinosaurs. Journal of Vertebrate Paleontology. 1998; 18(S2):1-79.

Wilson JA. A nomenclature for vertebral laminae in sauropods and other saurischian dinosaurs. Journal of Vertebrate Paleontology. 1999; 19: 639–653.

Wilson JA. Sauropod dinosaur phylogeny: critique and cladistic analysis. Zoological Journal of the Linnean Society. 2002; 136**:**217–276.

Wilson JA, Upchurch P. Redescription and reassessment of the phylogenetic affinities of *Euhelopus zdanskyi* (Dinosauria: Sauropoda) from the Early Cretaceous of China. Journal of Systematic Palaeontology. 2009; 7(2):199-239.

Wilson JA, D'Emic MD, Ikejiri T, Moacdieh DM, Whitlock JA. A nomenclature for vertebral fossae in sauropods and other saurischian dinosaurs. PLoS ONE. 2011; 6(2): e17114 (doi:10.1371/journal.pone.0017114).

Wilson JA, Allain R. Osteology of *Rebbachisaurus garasbae* Lavocat, 1954, a diplodocoid (Dinosauria, Sauropoda) from the early Late Cretaceous–aged Kem Kem beds of southeastern Morocco. Journal of Vertebrate Paleontology. 2015; 35: e1000701, 1–33.

Wiman C. Die Kreide-Dinosaurier aus Shantung. Palaeontologia Sinica (series C). 1929; 6:1–67.

Whitlock JA. A phylogenetic analysis of Diplodocoidea (Saurischia: Sauropoda). Zoological Journal of the Linnean Society. 2011; 161(4): 872-915.

Witmer LM. The craniofacial air sac system of Mesozoic birds (Aves). Zoological Journal of the Linnean Society. 1990; 100:327–378.

Woodward HN, Lehman TM. Bone histology and microanatomy of *Alamosaurus sanjuanensis* (Sauropoda: Titanosauria) from the Maastrichtian of Big Bend National Park, Texas. Journal of Vertebrate Paleontology. 2009; 29(3):807-21.

Wright JL. Ichnological evidence for the use of the forelimb in iguanodontid locomotion. Cretaceous Fossil Vertebrates. 1999; pp. 209–219.

Xing L, Miyashita T, Zhang J, Li D, Te Y, Sekiya T, Wang F and Currie PJ. A new sauropod dinosaur from the Late Jurassic of China and the diversity, distribution, and relationships of mamenchisaurids. Journal of Vertebrate Paleontology*.* 2015*;* 35**(**1**)**: e889701:1-17.

Yadagiri P. A new sauropod Kotasaurus yamanpalliensis from Lower Jurassic Kota Formation of India. Records of the Geological Survey of India. 1988; **11**:102-127

Yadagiri P. The osteology of *Kotasaurus yamanpalliensis*, a sauropod dinosaur from the Early Jurassic Kota Formation of India. Journal of Vertebrate Paleontology. 2001; 21(2):242-52.

Yates AM, Kitching JW. The earliest known sauropod dinosaur and the first steps towards sauropod locomotion. Proceedings of the Royal Society of London B: Biological Sciences. 2003; 270(1525):1753-8.

Yates AM. The first complete skull of the Triassic dinosaur *Melanorosaurus* Haughton (Sauropodomorpha: Anchisauria). Evolution and palaeobiology of early sauropodomorph dinosaurs. 2007; 77:9-55.

Yates AM, Bonnan MF, Neveling J, Chinsamy A, Blackbeard MG. Prosauropod pneumaticity. A new transitional sauropodomorph dinosaur from the Early Jurassic of South Africa and the evolution of sauropod feeding and quadrupedalism. Proceedings of the Royal Society B. 2009; 279: 787-794. doi: 10.1098/rspb.2009.1440

Yates AM, Bonnan MF, Neveling J, Chinsamy A, Blackbeard MG. A new transitional sauropodomorph dinosaur from the Early Jurassic of South Africa and the evolution of sauropod feeding and quadrupedalism. Proceedings of The Royal Society B. 2010; 277(1682):787-794

Yates AM, Bonnan MF, Neveling J. A new basal sauropodomorph dinosaur from the Early Jurassic of South Africa. Journal of Vertebrate Paleontology. 2011; 31(3):610-25.

Yates AM, Wedel MJ, Bonnan MF. The early evolution of postcranial skeletal pneumaticity in sauropodomorph dinosaurs. Acta Palaeontologica Polonica. 2012; 57(1):85–100. doi: http://dx.doi.org/10.4202/app.2010.0075

You H, Li D, Zhou L, Ji Q. *Huanghetitan liujiaxiaensis*, a new sauropod dinosaur from the Lower Cretaceous Hekou Group of Lanzhou Basin, Gansu Province, China. Geological Review. 2006; 52(5):668-674.

Young CC. On a new sauropod from Yiping, Szechuan, China. Scientologia. Sinica. 1954; 3(4): 481-504.

Yu C. Sauropod phylogeny: a preliminary cladistic analysis. Journal of Vertebrate Paleontology. 1990; 10.

Zhang Y, Li K, Zeng Q, Downs TBW. A new species of sauropod from the Late Jurassic of the Sichuan Basin (*Mamenchisaurus jingyanensis* sp. nov.). Journal of the Chengdu University of Technology. 1998**;** 25**:** 61–68.Zhao XJ, Downs TB. A new Middle Jurassic sauropod subfamily (Klamelisaurinae subfam. nov.) from Xinjiang Autonomous Region, China. Vertebra PalAsiatica. 1993; 31:132-8.

Ziegler PA. Geological atlas of western and central Europe. Geological Society of London; 1990.

Zurriaguz V & Powell J. New contributions to the presacral osteology of *Saltasaurus loricatus* (Sauropoda, Titanosauria) from the Upper Cretaceous of northern Argentina. Cretaceous Research. 2015; 54: 283-300.

Zurriaguz VL, Cerda IA. Caudal pneumaticity in derived titanosaurs (Dinosauria: Sauropoda). Cretaceous Research. 2017; 73: 14-24.

Appendix 1

Supplementary references to the PhD thesis

Literature sources of the retrieved pneumaticity data

List of characters found in Sauropodomorph vertebrae and pelvises

Source: Schwarz, D. and Fritsch, Guido. Pneumatic structures in the cervical vertebrae of the Late Jurassic Tendaguru sauropods *Brachiosaurus brancai* and *Dicraeosaurus.* Eclogae geol. Helv. 99 (2006) 65–78. DOI 10.1007/s00015-006-1177-x
Specimen: *Giraffatitan (Brachiosaurus) brancai* (HMN SI 70 - SI 71)

General observations: semicamellate cervical vertebrae, odontoid process of axis non pneumatized.

Characters: Fig. 1, 66pp

4th cervical vertebra (Polycamerate-Semicamellate) (HMN SI 70)**;** 55cm length, 40cm height; 15cm width : approx. volume = 330cm^3

A

C34 - spinal fossae (2), lateral and posterior;

C18 - foramina in neural arch (2)

C65 - infrapostzygapophyseal fossa (1)

C48 - prezygapophyseal fossa (1)

C47 - prezygapophyseal foramen (2)

C52 - infraprezygapophyseal fossa (1)

C114 - infradiapophyseal fossa (1)

C8 - fosseous pleurocoel (2), anterior and middle, centrum

C118 - parapophyseal fossa (1)

C3 - foramina (2) in centrum

B

C74 - foramen (1) in neural canal

C18 **-** foramina (2) in peduncle (neural arch), anterior

C18 **-** foramina (2) in peduncle (neural arch), posterior

Fig.4, 69pp

I

C2 - camerae (2) in centrum

C21 - camellae (3) in neural arch

J

C11 - semicamellate (4) in centrum

C106 - camellae (2) in diapophyses

C63 - camellae (4) in postzygapophyses

7th cervical vertebra (SI 71)

C

C42 - spinal fossae (2), lateral (subdivided), posterior

C18 **-** foramina (2) in peduncle (neural arch), posterior

C74 **-** foramen (1) in neural canal

D

C65 - infrapostzygapophyseal fossa (1)

C117 **-** parapophyseal fossa (1)

C8 **-** fosseous pleurocoel in centrum (2)

C34 **-** (inter)spinal fossa (1)

E

C74 **-** foramen (1) in neural canal

C18 **-** foramina (2) in peduncle (neural arch), posterior

C47 **-** prezygapophyseal foramen (2)

F

C18 **-** foramina (2) in peduncle (neural arch), anterior

C18 **-** foramina (2) in peduncle (neural arch), posterior

C34 **-** spinal fossa (1), posterior

C74 **-** foramen (1) in neural canal

Fig. 2, 67pp

Axis (SI 71)

D

C17 - camerae (2) in neural arch

C21 **-** camella (1) in neural arch

C6 - camellae (2) in centrum

C2 **-** camerae (3) in centrum

G

C106 **-** camellae (2) in diapophysis

C21 **-** camellae (5) in neural arch

C36 - camellae (3) in neural spine

C32 - camera (1) in neural spine

H

C17 **-** camera (1) in neural arch

I

C3 - foramen (1) in centrum

C2 - camera (1) in centrum

C1 - pleurocoel (1) in centrum

J

C34 - spinal fossa (1), posterior

C6 - camellae (13) in centrum

Figs. 1A, D; 2–4, 4E, F, pp 71 - 72

C120 - (inter) parapophyseal (1) camella

C119 - parapophyseal fossa (1) with foramen

C164 - camellae in condyle

C169 - camerae (4) in cotyle

C50 - camellae (4) in prezygapophyses

C115 - infradiapophyseal camera (Figs. 3F; 4H)

C103 - foramen (1) in diapophysis

C57 - prezygodiapophyseal lamina with fossa

C70 - postzygodiapophyseal lamina with fossa

C111 - laminated fossa relating to diapophyses

C72 - infrapostzygapophyseal camera

C73 - infrapostzygapophyseal camellae

C43 - laminated (latero)spinal fossa

C35 - fossa with foramina in spine

C79 - camellae (3) in neural canal

C75 - camera in neural canal

C180 - foramen (1) on cervical rib

C91 - foramen in transverse process

Specimen: *Dicraeosaurus hansemanni*

General characteristics: From the 3rd cervical vertebra onwards, all neural spines are deeply bifurcate; The pneumatic structures found in the cervical vertebrae of *Dicraeosaurus* are simple and restricted to the external surface of the vertebrae (Janensch 1929a, 1947), and represent according to the scheme of Wedel et al. (2000b) the procamerate condition. Location: 'E' from Tendaguru.

Characters: Fig. 1G, H; pp66,74

8th Cervical vertebra E14 (Procamerate)

C8 - fosseous pleurocoel (divided) in centrum

C52 - infraprezygapophyseal fossa

C119 - foramen on parapophysis

C162 - camera in the condyle

C5 - fossa with foramen on dorsal inner surface of centrum (from the 5th cervical onwards)

Axis

C116 - infradiapophyseal fossa

C52 - infraprezygapophyseal fossa

C65 - infrapostzygapophyseal fossa

(**axis and 3d cervical)**

C34 - (latero and post)spinal fossa

(between 3d and 7th cervical)

C19 - fossa on neural arch (at base of spine)

Dicraeosaurus sp. **4th cervical vertebra (HMN E14), Fig. 5A**

(condyle not pneumatic -> 0 for C162-C170)

C8 - fosseous pleurocoel in centrum **(Fig. 5C, D)**

C116 - infradiapophyseal fossa

C65 - infrapostzygapophyseal fossa **(Fig. 5E, F)**

(**C31-C44 -> 0 -** bifurcate spines are massive bone)

same features for both 12th cervical and D. *hansemanni* and D. sp.

12th cervical (D. *hansemanni* ; E27); Fig. 5H

centrodiapophyseal lamina

postzygodiapophyseal lamina

(HMN E14 has apneumatic neural canal; E27 has excavation in n.c. - Fig. 5K)

C77 - fossa in neural canal (E27)

C19 - fossae (2) in neural arch (peduncular fossae)

C34 - (latero)spinal fossa (E27)

C91 - foramen in transverse process

C33 - (inter)spinal foramina (1 on each part of the bif. spine)

C115 - infradiapophyseal foramen **(Fig. 6C)**

C64 - infrapostzygapophyseal foramen **(Fig. 6C)**

(parapophyses not pneumatised 0-> C118 - C130)

Source: LU Junchang, XU Li, ZHANG Xingliao, HU Weiyong, WU Yanhua, JIA Songhai and JI Qiang. 2007. A New Gigantic Sauropod Dinosaur with the Deepest Known Body Cavity from the Cretaceous of Asia**.** *Acta Geologica Sinica* **81**(2), pp**.** 167-176.

Specimen: *Huanghetitan ruyangensis* **(41HIII-0001)**

Characters: Sacral vertebrae; pp. 168 (Acamerate)

C1 -> 0 - No pleurocoels on centra

C4 -> 0 - No fossae on centra

pp. 171

C92 - concavity (fossa) anterodorsally to the transverse process

C34 - postspinal fossa

Caudal vertebrae; pp. 171 (Amphiplatyan vertebrae unlike diplodocids, and *Titanosaurus*, but some similarities with *Opisthocoelicaudia*)

absent spinopostzygapophyseal lamina

weakly present and later absent spinoprezygapophyseal lamina

present prespinal lamina

C34 - postspinal fossa

C1 -> 0 No pleurocoels on centra

shallow and wide groove on ventral surface of centrum - possible presence of hypapophysis (?)

Thoracic ribs; pp. 173

C180 -> 0 - No pneumatic foramina on ribs

Source: Lu Junchang, Yoichi Azuma, Chen Rongjun**,** Zheng Wenjie and Jin Xingsheng. 2008. A New Titanosauriform Sauropod from the Early Late Cretaceous of Dongyang, Zhejiang Province**.** Acta Geologica Sinica **Vol.** 82 NO**. 2 pp.** 225-235.

Specimen: *Dongyangosaurus sinensis gen. et sp. nov.* **(DYM 04888)**

Characters: Dorsal vertebrae; (**Procamerate -** short and bifurcate neural spines)

pp. 225

C48 - fossa on ventral surface of prezygapophyses

pp. 226

C57 - (centro)prezygapophyseal laminated fossa

C52 - intraprezygapophyseal laminated fossa

C70 - postzygapophyseal laminated concavity (fossa?)

pp. 227

C1 - pleurocoel on most centra

C43 - laminated spinal fossa

C19 - fossa on neural arch

C181 - fossa posteriorly to tuberculum

pp. 230

C61 - postzygapophyseal fossae (2)

Anterior Caudal vertebrae; pp. 226-7 (Acamerate)

C61 - fossa on lateral surface of postzygapophysis

C70 - postzygapophyseal laminated fossa

C28 - laminated fossa on base of neural arch

pp. 230

C61 **-** postzygapophyseal fossae (2)

Source: Ismar de Souza Carvalho, Leonardo dos Santos Avilla, Leonardo Salgado. 2003. *Amazonsaurus maranhensis* gen. et sp. nov. (Sauropoda, Diplodocoidea) from the Lower Cretaceous (Aptian–Albian) of Brazil. Cretaceous Research Vol. 24 pp. 697–713.

Specimen: *Amazonsaurus maranhensis* gen. et sp. nov. (Two dorsal neural spines (MN 4558-V; UFRJ-DG 58-R/9); two dorsal centra (MN 4559-V; MN s/n(-V); neural spine of anterior caudal vertebra (UFRJ-DG 58-R/7); one mid caudal vertebra (MN 4555-V); one mid-posterior caudal vertebra (MN 4560- V); one posterior caudal vertebra (MN 4556-V); one posterior caudal vertebra (UFRJ-DG 58- R/10); an ilium (UFRJ-DG 58-R/1); a partial pubis (MN s/n(-V))

Characters: Dorsal vertebrae; pp. 700-701 (Semicamerate)

C1 - pleurocoel in centra

C8 - fosseous pleurocoel in centra

C10 - semicamerated centra

pp. 702

C44 - laminated foramen (1) laterally on spine

C43 - laminated fossae on spine

Caudal vertebrae (Procamerate)

pp. 703

C44 - laminated foramina (3) anteriorly on spine

pp. 705

C43 - prespinal laminated fossa

pp. 707

C3 - foramina (2) on the centrum

Ilium

D1 - pneumatic cavity inside ilium - camerated

Source: Pablo A. Gallina and Sebastian Apesteguia. 2005. *Cathartesaura anaerobica* gen. et. sp. nov., a new rebbachisaurid (Dinosauria, Sauropoda) from the Huincul Formation (Upper Cretaceous), Rio Negro, Argentina. Rev. Mus. Argentino Cienc. Nat., n.s. Vol. 7 No. 2 pp.153-166.

Specimen: *Cathartesaura anaerobica gen. et. sp. nov.* **(MPCA - 232)**

Characters: Caudal vertebrae; (Acamerate)

pp. 153

C92 - fossa below transverse process framed by bony bar

pp. 154

C101 - laminated fossa of transverse process

pp. 156

No pneumatic cavities on centrum

C19 - (2) fossae in neural arch

pp. 157

C18 - foramina (2) on neural arch

(**C76 ? -** possible foramen inside neural canal)

Cervical vertebrae; Fig. 2A,B; pp. 155 (Procamerate)

C3 - (2) independent and successive foramina in centrum

C2 - foramina connected internally with camerae

(C2 and C3 exist also in *Limaysaurus* and *Diplodocus*)

C15 - laminated (pcdl) pleurocoel

C9 - septated foramina

C28 - laminated fossae (2) in neural arch (podl, cpol, & pcdl; prdl & acdl)

pp. 156

Not preserved ansa costotransversaria (**C131 - C139 -> ?**)

Source: Mathew J. Wedel, Richard L. Cifelli, and R. Kent Sanders. 2000. Osteology, paleobiology, and relationships of the sauropod dinosaur *Sauroposeidon*. *Acta Palaeontologica Polonica* **45** (4), pp. 343-388.

pp. 334

All Eusauropoda (from 29-35 and 37-50) have **C1** - pleurocoel in centrum in cervical and dorsal vertebrae.

Specimen: *Shunosaurus lii* (**IVPP V.9065**)

Characters: Cervical & Dorsal vertebrae (Acamerate-Procamerate)

C1 - central pleurocoel (1)

C8 - fosseous pleurocoel (2)

C12 - subdivided fossae (2)

pp.346; Fig. 2

Specimen: *Haplocanthosaurus priscus* (**CM 897-7**)

Characters: Dorsal vertebra (Procamerate-Camerate)

C4 - fossae (2) on centrum (10% each of vol. of entire vert.)

C17 - camerated neural arch (1) (5%)

C19 - fossae (2) on neural arch (10% each)

C32 - camerated neural spine (1) (35%)

pp. 361; Fig. 11

Cervical vertebrae (Procamerate)

C34 - fossae (2) in neural spine (40% & 40% of spine)

C19 - fossae (2) in neural arch (20% & 30% of arch)

C92 - fossa (1) in transverse process (100%)

C4 - fossa (1) on centrum (70%)

pp. 362

C164 - deep fossa on condyle

C170 - subdivided septated fossae in condyle

C173 -> 0 - deep fossa on cotyle is absent

C179 -> 0 - subdivided septated fossae in cotyle are absent

Specimen: *Camarasaurus* sp. (**OMNH 01313**)

Characters: Dorsal vertebra (Camerate)

C3 - foramina on centrum (2)

C2 - camerae in centrum (2)

C91 - foramen below transverse process

C90 - camerae (2) in transverse processes

C18 - foramen in neural arch

C17 - camera in neural arch

pp. 361; Fig. 11

Cervical vertebrae (Camerate)

B1

C19 - fossae (2) on neural arch (50% & 20%)

C92 - fossa (1) on transverse process (100%)

C1 - pleurocoel on centrum (40%)

C8 - fosseous pleurocoel (2) on centrum (40% both)

C151 - camerate hypapophysis (50%)

B2

C2 - camerae (6) in centrum (5% each)

C17 - camerae (2) in neural arch (5% & 10%)

C151 **-** camerae (2) in hypapophysis (30% & 20%)

C8 - fosseous pleurocoel on centrum (2) (40% both)

B3 - same as B2 but interconnected

pp. 362

C3 - foramina on centrum

C162 - camerae (50% at least) in condyle

C171 - camerae (50% at least) in cotyle

C118 - camerae (more than 50%) in parapophyses

C75 - camerae (70% - 80%) in neural canal

Specimen: *Apatosaurus* sp. **(OMNH 01380) Cervical vertebrae**

-camerae in condyles/cotyles arise from quaternary generations of central camerae

C1 - pleurocoel (1) on centrum

C4 - fossa (1) on centrum

C2 - camerae (10 - 27 approx.) in centrum (5% - 1% each when internal camerate evolutions reach the 27 approx.)

C17 - camerae (2) in neural arch (50% each)

C90 - camera (1) in transverse process (100%)

C162 - small camerae in condyles

C171 - small camerae in cotyles

Specimen: *Saltasaurus loricatus* (**PVL 4017-137**)

Characters: Dorsal vertebra (Somphospondylous)

C6 - camellated centrum (70%-80%)

C108 - camellated diapophyses (70%-80%)

Specimen: *Sauroposeidon proteles* (**OMNH 53062**, articulated cervical vertebrae 5-8, with cervical ribs preserved in place) **Cervical vertebrae (camerate - camellate)**

Characters: pp. 352 & Fig. 7 (pp. 353)

C4 - fossae in centrum

C34 - fossae in spines (2)

C2 - lateral camerae (2) on centrum

C32 - camera in neural spine

C12 - subdivided fossae

C13 - laminated fossae on centrum

C164 - fossae on condyles

C5 - fossae with foramina on centrum just posterior to diapophyses

C14 - laminated foramina on centrum

pp. 354

C8 - fosseous pleurocoel (2) on centrum

C33 - foramina (2) - one pre- and one post-spinal

C173 - fossa on cotyles

pp. 357

C43 - laminated fossae on spine

pp. 362

C6 - camellae in centrum

C36 - camellae in neural spine

pp. 360

Specimen: *Diplodocus* sp.

Cervical & Dorsal vertebrae (Polycamerate)

-camerae in condyles/cotyles arise from quaternary generations of central camerae

C162 - small camerae in condyles

C171 - small camerae in cotyles

pp. 362

C2 - large camerae which further bifurcate into secondary and tertiary camerae in centrum

Specimens: *Barapasaurus & Shunosaurus*

(In general, vertebrae are **Acamerate**, especially in centra)

C2 -> 0

Specimen: *Brachiosaurus* ; **Fig. 12, B-D; (BYU 12866) Cervical & Dorsal vertebrae (semicamellate)**

C166 - camellae (numerous - 70%) in condyles

C175 - camellae (numerous - 50%) in cotyles

C50 - camellae in prezygapophyses

C63 - camellae in postzygapophyses

C6 - camellae in centrum

C21 - camellae (3) in median septum (neural arch)

C36 - camellae in neural spine

C2 - camerae in centrum

pp. 364

Specimen: *Mamenchisaurus hochuanensis / sinocanadorum*

Cervical vertebrae (semicamellate)

C6 - camellae (somphospondylous - 40% - 50%) in centrum

- lack of lateral camerae; camellae developed independently in this group

Specimen: *Gondwanatitan faustoi*

Cervical vertebra (semicamellate)

C2 - camerae in centrum

pp. 366, Fig. 14

Specimen: *Pleurocoelous nanus* **(USNM 5678, 4968, 4946; UMNH VP900)**

Cervical (juvenile) - **C4 -** fossa in centrum;

Dorsal (juvenile) - C1 - pleurocoel in centrum; **C12 -** subdivided fossae

Sacral (juvenile) - C4 - fossae in centrum

Specimen: *Apatosaurus* sp. **(OMNH 1251, 1217)**

Cervical - C1 - pleurocoel in centrum

Specimen: *Camarasaurus* sp. **(CM 578)**

Cervical - C8 - fosseous pleurocoel in centrum

Sacral - C1 - pleurocoel in centrum

Specimen: *Eucamerotus foxi* **(BMNH R2524)**

Dorsal - C1 - pleurocoel in centrum

pp. 373

Diplodocidae (taxa 66 - 74 - **Cervical vertebrae - C2 -** camerae in centrum

Source: Ostrom, J. H. and McIntosh, J. S. (1966). *Marsh's dinosaurs. The collections from Como Bluff*. Yale University Press, New Haven and London.

Specimen: *Apatosaurus excelsus,* **8th Cervical vertebra** (50cm tall**,** 30cm long, 30cm wide - neural spine is missing) **YPM 1980 (holotype), plates 12 &13, pp. 88-89**

Characters: C8 - fosseous pleurocoel (1) on centrum (10cm long - centrum is about 20cm long - 40% occupied by pl. fossa)

C70 - laminated fossa (1) below postzygapophysis (fossa size 15cm x 10cm x 10cm) - centropostzygapophyseal fossa surrounded by anterior podl, cdpl, and posterior cpol. Occupies all of poz (100%) and about 10% of bone.

C120 - fosseous pleurocoel (1) on centroparapophyseal area (fossa size 10cm long - occupies about 35% of parapophysis (30cm long) and 5% of centrum)

C57 - laminated fossae (2) anterior to prezygapophyses (1on each prz - 10cm long occupying 60% of the front prz surface)

C52 - infraprezygapophyseal fossae (2) anterior to prz (1for each prz - 40% of ant. prz. surface.

pp. 90-91

C102 - laminated foramina (4) on posterior peduncle (post. transverse processes - 2 foramina for each side - larger 80%, smaller 20% of peduncle surface size)

C132 - fossae (shallow) on costotransverse ring

3d Dorsal vertebra, YPM 1980, plates 17 & 18, pp. 98-101

Characters: C43 - lateral laminated fossa (1) on lateral base of spine (fossa size 7cm - spine is 15cm tall; 2 postspinal fossae).

C70 - laminated fossa (1) on postzygapophysis (1on each poz - fossa size 9cm - occupies 90% of poz surface)

C106 - fossa (1) on diapophysis (fossa size 3cm - di size 9cm - occupies about 30% of di surface)

C28 - laminated fossae (1) on neural arch (10cm ; 100% of area)

C57 - laminated fossa (1) prezygapophysis (10cm; 100% of area)

C101 - laminated fossae (2) on lateral peduncles (1 on each lateral side of transverse process posterior surface; 5cm; 50%) and 1 laminated fossa (10cm) on each posterior surface of t.p. occupying 10% of its surface area

C8 - fosseous pleurocoel on centrum (3 - 2 lateral and 1ventrolateral; each one occupies 20% of centrum surface they probably communicate internally - possible cameration)

C120 - fossae (2) on parapophysis (fossae size 3cm and 4cm resp. - pa size 10cm; 30% & 40% resp.)

C2 - camerated centrum

C93 - foraminous fossae (2) on posterior of transverse processes (1 for each; 10cm fossa with 4cm foramen on each t.p.; each f.f. occupies about 50% of the t.p. area)

C19 - fossa (1) on neural arch (occupies 100% of n.a.; fossa 10cm; n.a. 10cm tall, 5cm wide)

Specimen: *Apatosaurus ajax*, **5th (last) Sacral vertebra, YPM 1860 holotype, pp. 124-125, plate 30**

Characters: C11 - semicamellate centrum

C97 - numerous septated foramina on transverse processes dorsal side

Specimen: *Apatosaurus excelsus,* **3d Caudal vertebra, YPM 1980 holotype, pp. 130-131, plate 33;**

Characters: C3 - foramen (for sure 1) on centrum (about 2cm)

C34 - prespinal fossa

4th Caudal vertebra, pp. 132-133, plate 34

C34 - postspinal fossa

C19 - fossa (1) on each of posterior sides of neural arch areas

C136 - semicamellate costotransverse ring

Specimen: *Camarasaurus grandis,* **2nd Caudal vertebra, YPM 1901, pp. 138-139, plate 37**

Characters: no foramina, fossae or any other external pneumatic element visible except a spinal (pre- and post-) fossa - C34

Source: Upchurch, P. and Martin, J. 2010. The anatomy and taxonomy of *Cetiosaurus* (Saurischia, Sauropoda) from the Middle Jurassic of England. *Journal of Vertebrate Palaeontology* **23**:1, pp. 208-231.

Specimen: *Cetiosaurus* (**OUMNH J13644/2**)

Characters: Caudal vertebrae

pp. 212, Fig. 3 (A,C,E,F)

C1 - C179 ---> 0 - absence of pleurocoels or any other pneumatic elements except: **C4 -** fossa along dorsal surface of centrum and **C164 -** lateral fossa (shallow) on condyle

Sacral vertebrae

C1 - C15 ---> 0 no pits or pleurocoels (unlike *Haplocanthosaurus, Brachiosaurus, Camarasaurus, and diplodocids*)

pp. 214

Dorsal vertebrae

C1 - pleurocoels (2) on centrum (also in *Haplocanthosaurus*)

C76 - foramen in neural canal (also in *Barapasaurus , Patagosaurus*)

C91 - foramen on transverse process (also in *Barapasaurus, Patagosaurus)*

{From discussion with Paul Upchurch: Neuquensaurus dorsal in CT scan revealed that a foramen on centrum is expanded inside into a polycamerate structure which then progresses into camellae.} ***-> C3 (foramen on centrum),C2 (camerae in centrum),C6 (camellae in centrum).***

C43 - laminated spinal fossae (4; one on each side and between spinoprezygapophyseal and spinopostzygapophyseal laminae)

Cervical vertebrae (J13660)

C1 - pleurocoels on centrum (2; separated by oblique septum; same case as in *Patagosaurus* - **Wilson, 2002 -> infraprezygapophyseal 'coels' (fossae) -> C52**

Source: Remes Kristian. 2007. A second Gondwanan diplodocid dinosaur from the upper Jurassic Tendaguru beds of Tanzania, east Africa. *Palaeontology*, Vol. 50, Part 3, pp. 653–667

Specimen: *Australodocus bohetti*

Characters: pg. 653, Abstract, two mid-Cervical vertebrae, MB.R.2455 [G 70] and MB.R.2454 [G 69]

C1 - pleurocoel on centrum (weakly developed)

C57 - laminated fossa ventral to prezygapophysis

pg. 658

C8 - fosseous pleurocoel on centrum (divided by broad shelf)

C5 - pn. foramen in fossa in centrum

pg. 659-660

C85 + C86- subdivided and laminated fossa near neural canal

pg. 661

C43 - laminated fossa on the anterior of the base of the neural spine

(laminated **p cdpl** foramina on centrum **C14** and diapophyses **C114** in *Apatosaurus* and *Diplodocus*)

pg. 663

C119 - pneumatic foramina on parapophyses

Specimen: *Barosaurus*

pg. 662 Cervical vertebrae

C43 - laminated fossa in spine

Specimen: *Suuwassea*

pg. 661, Cervical vertebrae

C43 - (1) laminated deep concavity (fossa) on base of spine (but identified as an elastic ligament fossa by Tsuihiji in 2004)

Source: Harris, J.D. and Dodson, P. 2004. A new diplodocoid sauropod dinosaur from the Upper Jurassic Morrison Formation of Montana, USA. *Acta Palaeontologica Polonica* 49 (2): 197–210.

Specimen: *Suuwassea emilieae* **(ANS 21122)**

Characters: pg. 201, Axis and Cervical vertebrae 3,5,6,7

C8 - fosseous pleurocoel (some weakly divided and some undivided) on both sides of centrum (right side fossa is divided into two)

C28 - laminated fossae on neural arch

C113 - laminated fossae on diapophyses (The spinoprezygapophyseal, pre−, and postzygadiapophyseal laminae surround distinct, triangular fossae on the lateral sides of the bases of the spinoprezygapophyseal laminae)

C116 - infradiapophyseal fossa

C34 - deep postspinal fossa

C20 - foraminous fossae on arch

C13 - laminated fosse on centrum

C5 - foraminous fossae on centrum

C120 - fossae on parapophyses

C52 - infraprezygapophyseal fossae

C57 - laminated fossae between prezygapophyses

C101 - laminated fossae (2) exactly before and after transverse processes (The transverse processes overhang tetrahedral infradiapophyseal and infraprediapophyseal fossae that are separated by short, thick cranial centrodiapophyseal laminae that stem from the caudodorsal margins of the fosseous pleurocoel)

Dorsal vertebrae (2nd - 4th); pg 202

C8 - pleurocelous fossae on centrum

C101 - laminated (prdl) fossae (posteriorly) on transverse processes

C34 - fossa laterally on spine (as in *Apatosaurus*)

non-pneumatic ribs

Caudal vertebrae; pg. 202

all semi-destroyed; lack fosseous pleurocoel (C8 = 0)

Personal observations from the specimens of *Thecodontosaurus antiquus* cervicals 7 (26621), and 9 (26629); generally acamerate and procamerate

Characters: C106 - fossa triangular in shape positioned exactly below diapophyses (one at each side) but does not aerate neural arch.

C33 & C91 - foramen that lies both at base of spine and at the most proximal

Dorsal 10 and dorsal 23968;

Characters: C43 - laminated postspinal fossa

proximal Caudal B023/26592 - non-pneumatised at all

Source: Sereno, P. C., et al. 2007. Structural Extremes in a Cretaceous Dinosaur. *PLoS ONE* **2**(11): e1230. doi:10.1371/journal.pone.0001230

Specimen: *Nigersaurus taqueti* **(MNN GAD513, GAD 515-518)**

Characters: pg. 4

Cervical vertebrae

C15 - laminated pleurocoel on centrum
C8 - fosseous pleurocoel on centrum
C3 - foramina (3) on centrum
C163 - foramen on condyle
C181 - fossa behind base of rib
C164 - fossa on condyle
C132 - fossae on costotransverse ring
C12 - septated fossa on centrum
C16 - pleurocoel on neural arch
C19 - fossa on neural arch

Dorsal vertebrae

C18 - foramina (4) on neural arch
C28 - laminated fossa on neural arch
C15 - laminated pleurocoel on centrum
C2 - camera on centrum
C34 - paired fossae on base of spine
C105 - foramen on diapophysis
C60 - foramen on postzygapophysis

C17 - camerae (3) in neural arch
C175 - camellae in cotyle
C75 - camera in neural canal
C46 - camera in prezygapophysis

Caudal vertebrae

C43 - shallow laminated fossae (2) on spine
C3 - foramina (2) on centrum
C18 - foramina (2-3) on neural arch

no pneumaticity info for Pelvic girdle (?) neither its Sacrals (?)

Source: Novas, F.E, Salgado, L., Calvo, J., and Agnolin, F. 2005. Giant titanosaur (Dinosauria, Sauropoda) from the Late Cretaceous of Patagonia. *Rev. Mus. Argentino Cienc. Nat.,* n.s.**7**(1), pp. 37-41.

Specimen: *Puertasaurus reuili* **(MPM 10002 - Cervical 9, Dorsal 2, and two mid-caudals)**

Characters: Cervical 9

pg 38 & Fig. 1

C34 - fosse (2) on spine (pre- and post-)
C28 - laminated fossa on neural arch
C13 - laminated fossa on centrum
(cervical is poorly pneumatised and lacks pleurocoels **- C1--> 0**)

Dorsal 2

pg 39 & Fig. 2

C4 - fossa on centrum
C34 - fosse (2) on spine (pre- and post-) - wider and deeper than more derived titanosaurs such as *Saltasaurus, Opisthocoelicaudia.*
C100 - subdivided fossae(2-3) on anterior of transverse processes
C19 - fossae (2) on anterior of neural arch (anterior peduncles)

Sacrals, Caudals & Pelvic bones

no information available

Source: Carballido, J. L., Rauhut, O. W. M., Pol, D. and Salgado, L. 2011. Osteology and phylogenetic relationships of *Tehuelchesaurus benitezii* (Dinosauria, Sauropoda) from the Upper Jurassic of Patagonia. *Zoological Journal of the Linnean Society.* **163**, pp. 605–662.

Specimen: *Tehuelchesaurus benitezii* (**MPEF-PV 1125;** 10 articulated presacral vertebrae plus an eroded element, 4 sacral vertebrae, parts of the sacricostal yoke, several ribs, right scapulacoracoid, right humerus, left radius and ulna, fragment of right ilium, right pubis and

fragment of left pubis, left ischium and shaft of right ischium, both femora, and skin impressions.)

Characters: Dorsal vertebrae

pg 605 - Abstract

C1 - pleurocoels on centra (and 1st **Sacral** centrum)
C2 - camerae in centra (and 1st **Sacral** centrum)
C113 - laminated fossae on diapophyses
C116 - infradiapophyseal fossa
C28 - laminated fossae on neural arches

pg 609

C19 - fossa in neural arch (also in *Barapasaurus, Cetiosaurus,* and *Patagosaurus*)

C18 - foramen in neural arch (also in *Barapasaurus* and *Patagosaurus*)

C17 - camera in neural arch (also in *Barapasaurus* and *Patagosaurus*)

pg 610

C162 - camerae on condyle on dorsal 1

vertebrae are not camellated contra *Brachiosaurus* and Titanosauriformes

Source: *Europasaurus* specimens from DinoPark in Münchehagen, Hannover.

Specimen: *Europasaurus holgeri* (**DFFMh/FV XXX)**

General Observations: *Europasaurus holgeri* is a dwarf sauropod (4-7 meters long) classified as a basal Macronarian. It shows extensive pneumatisation throughout its postcranial skeleton, especially on its vertebral column. Despite the vertebrae small size, they are very similar to the ones from *Giraffatitan / Brachiosaurus* in both general morphology and expression of pneumaticity. Neurocentral suture is visible - evidence of retaining juvenile features when adult, or progenetic paedomorphosis. Younger individuals exhibit simpler pneumatisation features such as simple fossae, gradually becoming more complex and invading as we transcend from early juvenile to adult.

Characters: Cervical vertebrae (FV 652.1)

C8 - fosseous pleurocoel on centrum (septated and laminated, whose margins are ant. and post. **cprl**; 2 on each side of the centrum each set being separated by oblique septum - the anteriormost set of fossae on each side occupies

approx. 20% - 25% and the posteriormost set about 30% - 35% of the centrum volume)

C164 - fossae in condyle (pneumatised by the pleurocoel - the anteriormost central fossa that develops into 2 smaller fossae in the condyle - occupying about 50% of it.)

C92 - fossae (2) below each transverse process and (2) more on their sides

C19 - fossae (2) on each lateral side of neural arch

C120 - fossa (shallow) on each parapophysis

C57 - laminated fossae (2) on medial surface of prezygapophyses (50% occupation)

C70 - laminated (podl & postzygo-transversal lamina) fossa below postzygapophysis (one on each side)

C28 - laminated (podl & postzygo-transversal lamina) fossa in neural arch

C43 - laminated (sprl) prespinal fossa

C89 - pleurocoel on transverse process

C34 - fossa on base of spine

C173 - fossa in cotyle (pneumatised by the pleurocoel)

C2 - camerae in centrum (2)

C17 - camerae in neural arch (2)

C90 - camerae in transverse process (2)

The fossae do not communicate with the camerae. No foramina whatsoever.

C3 ? - ambiguous foramina on internal dorsal part of a half-broken centrum near the neurocentral suture region; possibly neural / vascular /pneumatic.

C1 - pleurocoel on centrum (one on each side)

C15 - laminated (cdpl & left lateral spinocentral lamina) pleurocoel

C105 - foramen on (left) diapophysis

C93 - fossa & foramen on transverse process

Cervical rib

C180 - foramen between capitulum & tuberculum heads

Dorsal vertebrae (FV 652.4, FV 019, FV 896.1, FV 1084)

C1 - pleurocoels (2) on centrum

C3 - foramina on centrum

C8 - fosseous pleurocoel on centrum

C11 - semicamellated centrum

C43 - laminated spinal fossae (4)

C101 - laminated fossae on transverse process

C28 - laminated (podl & postzygo-transversal lamina) fossa in neural arch

C105 - foramen on diapophysis

C93 - fossa & foramen on transverse process

C164 - fossa in condyle (pneumatised by the pleurocoel)

C173 - fossa in cotyle (pneumatised by the pleurocoel)

C19 - fossae (2) on each side (anterior and posterior) of neural arch

C52 - infraprezygapophyseal fossa

fragmented diapophyses show internal pneumatisation

C172 - foramen on cotyle

C91 - foramina on transverse processes

C4 - fossae (2) on left side of centrum

Sacral vertebrae (FV 862, FV 890.5, FV 569)

C35 - postspinal fossa with foramina (4)

C94 - camellated transverse processes

C21 - camellated neural arches

C102 - laminated foramen on dorsal surface of right anterior prezygodiapophyseal lamina, i.e. on transverse process

C77 - fossa on neural canal

C92 - fossa on transverse process

C19 - fossa on neural arch

Caudal vertebrae (FV 719, FV 866, FV 495.3)

C3 - foramen on centrum

C91 - foramina on transverse process

C172 - foramen on cotyle

C77 - fossa on neural canal

Pubis (FV 863.2)

no pneumatic features

Ilium (FV 863.1)

D2 - foramina

Ischium (not preserved)

Source: Yihong Zhang, Kui Li, and Qinghua Zeng. 1998. A new species of sauropod from the Late Jurassic of the Sichuan Basin (*Mamenchisaurus jingyanensis* sp. nov.). *Journal of the Chengdu University of Technology.* **25**:1. pp. 61-68
Translated By Will Downs
Bilby Research Center
Northern Arizona University
January, 2001

Specimen: *Mamenchisaurus jingyanensis* sp. nov. (CV00734 / JV002 / CV00219)

Characters: Cervical vertebrae

C1 - well developed pleurocoels on centra

Lack of ventral keel (absent hypapophyses)
Fig.3
C3 - foramina (6-7) on centrum
C7 - foraminous pleurocoel on centrum
C8 - fosseous pleurocoel on centrum
C93 - fossa & foramen on transverse process

C164 - fossae on condyle
C2 - camerae in centrum

Dorsal vertebrae
C1 - Not well developed pleurocoels on centra but existent
Sacral vertebrae
?
Caudal vertebrae
?

Source: Xijing Zhao. 1993. A new Middle Jurassic sauropod subfamily (Klamelisaurinae subfam. nov.) from Xinjiang Autonomous Region, China. *Vertebrata PalAsiatica* **31**:2 pp. 132-138.
Translated By Will Downs
Bilby Research Center
Northern Arizona University
2000

Specimen: *Klamelisaurus gobiensis* gen. et sp. nov. (**IVVP # V9492**)

Characters: Cervical vertebrae
C1 - pleurocoels on centra

Dorsal vertebrae
C1 - pleurocoels on centra

Sacral vertebrae
?
Caudal vertebrae
?

Source: He Xinlu, Li Kui and Cai Kaiji. 1988. The Middle Jurassic dinosaur fauna from Dashanpu, Zigong, Sichuan. Sauropod Dinosaurs (2), *Omeisaurus tianfuensis*. *Sichuan Publishing House of Science and Technology*, **4** pp. 143.

Specimen: *Omeisaurus tianfuensis*

Characters: Cervical vertebrae including **Atlas (T5703)** and **Axis (T5701)**

pgs. 28, 29, 30, 31, 32 - Figs. 18, 19, 20, 21, 22
C1 - pleurocoels on centrum
C8 - fosseous pleurocoel on centrum
C164 - fossa on condyle of Atlas and other cervicals
C173 - fossa on cotyle of Atlas and other cervicals

C34 - prespinal fossae / fossa on neural spine
C22 - foraminous pleurocoel on neural arch
C17 - camerated neural arch
C15 - laminated pleurocoels on centrum
C12 - subdivided (septated)fossa on centrum
C92 - fossae below and above transverse processes
C65 - infrapostzygapophyseal fossa
C72 - infrapostzygapophyseal camera
C163 - foramina on condyle
C18 - foramen on neural arch
C13 - laminated fossae on centrum
pg. 34 Fig. 23
C43 - laminated fossa on spine
C47 - foramina on prezygapophysis
C28 - laminated fossa on neural arch
C33 - foramen on spine

Also by Yates and Kitching, 2003 -> fossae on parapophyses -> C120

Dorsal vertebrae (T5701)
Fig. 25 & 28
C60 - foramina on postzygapophysis
C70 - laminated fossa on postzygapophysis
C43 - laminated fossae on spine
C22 - foraminous pleurocoel on neural arch
C28 - laminated fossae on neural arch
C91 - foramina on transverse process
C92 - fossae on transverse processes
C1 - pleurocoels on centrum
C8 - fosseous pleurocoel on centrum
C34 - fossae on neural spine
C26 - semicamellated neural arch

pg. 133

C65 - infrapostzygapophyseal fossa

Sacral vertebrae (T5704)

pg. 45 Fig. 31

C43 - laminated fossae on spine
C28 - laminated fossae on neural arch
C26 - semicamellated neural arch

C163 - foramen on condyle

Caudal vertebrae (T5701, T5704)

pg. 47 Fig. 34

C3 - foramen on centrum
C4 - fossa on centrum
C163 - foramen on condyle
C43 - laminated fossae on spine
C28 - laminated fossae on neural arch

pg. 51 Fig. 39
C152 - foramina on caudal hypapophyses (chevrons)
C156 - septated foramina on caudal hypapophyses

Ilium (T5701)
no features

Ischium (T5701)
no features

Pubis (T5701)

D20 - foramen

Source: Paul C. Sereno, Allison L. Beck, Didier B. Dutheil, Hans C. E. Larsson, Gabrielle H. Lyon, Bourahima Moussa, Rudyard W. Sadleir, Christian A. Sidor, David J. Varricchio, Gregory P. Wilson, Jeffrey A. Wilson. 1999. Cretaceous Sauropods from the Sahara and the Uneven Rate of Skeletal Evolution Among Dinosaurs. *Science* **286**, 1342. DOI: 10.1126/science.286.5443.1342

Specimen: *Jobaria tiguidensis*

Characters: Cervical vertebrae
pg. 1343

C1 - pleurocoels on centrum
C8 - fosseous pleurocoel on centrum
C12 - subdivided fossae on centum

pg. 1344, 1345 & Fig. 3
C15 - laminated pleurocoel

pgs. 1345 - 1346
C28 - laminated fossa in neural arch
C65 - infrapostzygapophyseal fossa
C44 - laminated fossa on spine

Dorsal vertebrae
C28 - fossa on neural arch
C132 - fossa between parapophyses and diapophyses i.e. costotransverse ring area
C43 - laminated prespinal (spine) fossa
C86 - laminated fossa on neural canal

Sacral vertebrae
features not recorded

Caudal vertebrae
C43 - laminated prespinal (spine) fossa

Source: Sertich, J.J.W. and Loewen, M.A. 2010. A New Basal Sauropodomorph Dinosaur from the Lower Jurassic Navajo Sandstone of Southern Utah. *PLoS ONE* **5**:3:e9789. doi:10.1371/journal.pone.0009789

Specimen: *Seitaad ruessi* gen. et sp. nov. (**UMNH VP 18040**)
Only dorsal vertebrae are preserved and are eroded and sheared. Most spines are missing. No pneumatic features exist on the incomplete pectoral and pelvic girdles.

Characters: Dorsal vertebrae

C113 - laminated (infradiapophyseal) fossa
C116 - infradiapophyseal fossa

Source: Adam M. Yates and James W. Kitching. 2003. The earliest known sauropod dinosaur and the first steps towards sauropod locomotion. *Proc. R. Soc. Lond. B* **270**, pp. 1753-1758. doi: 10.1098/rspb.2003.2417

Specimen: *Antetonitrus ingenipes* (**BP/1/4952**)

Characters: From the current paper only pneumatic data from dorsal vertebrae were able to be recovered.
Fig.3 pp. 1756

Dorsal vertebrae

C19 - fossae on neural arch
C28 - laminated fossae on neural arch
C43 - laminated fossa (pre- and post-) on spine
C101 - laminated fossa on transverse process
C138 - laminated fossa on costotransverse ring

Source: Yates, A. M., Wedel, M. J., and Bonnan, M. F. 2011. The early evolution of postcranial skeletal pneumaticity in sauropodomorph dinosaurs. *Acta Palaeontologica Polonica* **5X**(X), pp. xxx-xxx. doi: 10.4202/app.2010.0075

Specimen: *Plateosaurus engelhardti* (**AMNH 6810**)

Characters: Cervical vertebrae

pg. 8

C27 - subdivided fossa on neural arch **(posterior cervical, dorsolateral surface Fig. 4B)**

from **SMNS F65 -> C116 -** infradiapophyseal
and **C112 -** subdivided fossae (shallow) on diapophyses and within infradiapophyseal fossa ('subfossae' but not 'fosseous pleurocoel' because these cannot exist on a diapophysis)

Dorsal vertebrae

pg.9

SMNS 12950 -> C105 foramina on diapophyses and **C116 -** infradiapophyseal fossa

C114 - laminated foramen on diapophysis (Janensch, 1947: 21-22)

C107 - fossa (the infradiapophyseal) with foramen on diapophysis

Specimen: *Eucnemesaurus fortis* (**BP/1/6107 Fig. 5A1-A3, TM 119 Fig. 5B**)

Characters: Cervical vertebrae

no pneumatic features on cervicals

Dorsal vertebrae (only posterior - anterior & middle lack PSP)
pg.1 (Abstract)

C116 - infradiapophyseal fossa

C112 - subdivided fossae (shallow) on diapophyses and within infradiapophyseal fossa ('subfossae' but not 'fosseous pleurocoel' because these cannot exist on a diapophysis)

pg.9

C113 - laminated fossa on diapophysis (laminated middle infradiapophyseal fossa; on both middle and posterior infradiapophyseal fossae

Specimen: *Aardonyx celestae* (**BP/1/6644, BP/1/6513, 6615, 6662, 6681; Fig. 6, BP/1/6287, 6323, 6591, 6642, 6666; BP/1/6261, 6324, 6613, BP/1/6566; Fig. 7, BP/1/5379, 6309; Fig. 8A; BP/1/6241; Fig. 8B**)

Characters: Cervical vertebrae

pg.10 and 21

no pneumatisation on neural arches nor centra (from C1 - C30 = 0); the most of the rest vertebral parts are missing/fragmented

Dorsal vertebrae (only posterior - anterior & middle lack PSP)

pp.1 (Abstract)

C116 - infradiapophyseal fossa

C112 - subdivided fossae (regular depth) on diapophyses and within infradiapophyseal fossa ('subfossae' but not 'fosseous pleurocoel' because these cannot exist on a diapophysis)

pg.10 (**BP/1/ 6566**)

C116 **-** infradiapophyseal fossa (anterior and posterior)

C113 - laminated fossa on diapophysis (laminated anterior infradiapophyseal fossa)

pg.11

C28 - laminated fossa on neural arch (lie inside the posterior infradiapophyseal fossa bound ventrally by the **pcdl - Fig. 7**)

[**BP/1/ 6666**, probably the 14th dorsal neural arch) lacks subfossae in its PIDF, whereas they are present in a dorsosacral neural arch (**BP/1/ 5379: Fig. 8A**). The latter specimen is incomplete, having been split coronally behind the enlarged sacral rib attachment and through the sacral homologue of the PIDF (**Fig. 8A1-3**)]

Sacral vertebrae (**Fig.8 BP/1/5379, BP/1/6241**)

pg.11

C4 - fossa on centrum (all sacral centra recovered)

Specimen: *Antetonitrus ingenipes* (**Fig.9 BP/1/4952**)

Characters: Cervical vertebrae

no pneumatic features on cervical centrum (the sole specimen)

Dorsal vertebrae (only posterior - anterior & middle lack PSP)

pp.1 (Abstract)

C116 - infradiapophyseal fossa

C112 - subdivided fossae (deep, asymmetrical) on diapophyses and within infradiapophyseal fossa ('subfossae' but not fosseous pleurocoel because these cannot exist on a diapophysis)

pg.12

C19 - fossae on neural arch (on both sides)

C27 - subdivided fossa on neural arch

Haplocanthosaurus **(Wedel 2009: fig. 8a-d)**
Sacral vertebrae

C1 - pleurocoel on centrum (sacrals 1-4; not 5th)
C4 - fossa on centrum (sacrals 1-4; not 5th)

pg.16

Camelotia borealis

Dorsal vertebra (posterior - NHM R.2873b, Yates, 2007)

C116 - infradiapophyseal fossa (posterior)

C112 - subdivided fossae on diapophyses and within infradiapophyseal fossa

pg.16-17

Tazoudasaurus naimi

Dorsal vertebrae (posterior - Allain and Aquesbi 2008: fig. 14 c, d)

C116 - infradiapophyseal fossa (posterior)

C106 - fossa in diapophysis (in PIDF)

C19 - fossae on neural arch

C4 - fossae (deep) on centrum

but not the middle dorsal (example of pneumatic hiatus)

Cervical vertebrae

C4 - fossae (deep) on centrum

pg.19

Apatosaurus sp. **(OMNH 01380)**

Dorsal vertebrae (posterior)

C116 - infradiapophyseal fossa (posterior)

C106 - fossa in diapophysis (in PIDF)

C19 - fossae on neural arch

C21 - camellae in neural arch

Erketu ellisoni **(Ksepka and Norell 2006: fig. 7d)**

Dorsal vertebrae (posterior)

C116 - infradiapophyseal fossa (posterior)

C106 - fossa in diapophysis (in PIDF)

C19 - fossae on neural arch

C21 - camellae in neural arch

pg.25

Diplodocus sp.

Cervical, Dorsal, Sacral and proximal Caudal

C116 - infradiapophyseal fossa (posterior)

C106 - fossa in diapophysis (in PIDF)

C19 - fossae on neural arch

Specimen: *Thecodontosaurus antiquus* (**BRSUG 26629, 28124, 28133, 26621, 28131, 23969, 26645, 26589, 28122**)

Characters: no pneumatic features

Specimen: *Efraasia minor* (**SMNS 12354, 12684**)

Characters: no pneumatic features

Specimen: *Massospondylus carinatus* (**BP/1/4934, 5143, 5241**)

Characters: no pneumatic features

Source: Woodward, H. N. and Lehman, T. M. 2009. Bone histology and microanatomy of *Alamosaurus sanjuanensis* (Sauropoda: Titanosauria) from the Maastrichtian of big bend National park, Texas. *Journal of Vertebrate Paleontology* **29(**3), pp. 807–821.

Specimen: *Alamosaurus sanjuanensis* (**TMM 43598**)

Characters: Cervical vertebra (1 posterior, TMM 43598-6; Fig. 5A, 6A)

pg.809

C6 - camellae in centrum

pg.811

C21 - camellae in neural arch

C94 - camellae in transverse processes
Also, **D'Emic (2012) -> foramina on transverse process -> C91**

C36 - camellae in neural spine

pg.818
C1 - pleurocoel in centrum

also *Brachiosaurus, Euhelopus, Magyarosaurus, Ampelosaurus, Astrodon, Venenosaurus* **have: C180 -** foramina on ribs

Dorsal vertebrae (2, TMM 43598-2; Fig. 5B, TMM 43598-5; Fig. 5C, pg.819; 65% air filled, ribs 52% air filled)

pg.807 (Abstract)

C6 - camellae in centrum

C180 - foramina on ribs **(TMM 41541-1)**

pg.809

C1 - pleurocoel in centrum

C166 - camellae in condyle

pg.811

C21 - camellae in neural arch

C94 - camellae in transverse processes

C36 - camellae in neural spine

Sacral vertebrae not found ('?')

Caudal vertebrae (2, TMM 45865-1; Fig. 6C, TMM 43598-1, TMM 43599-1)

pg.807 (Abstract)

C6, C21, C36, C50, C63, C79, C94, C108, C122, C144, C155, C166, C175, = 0 -> no camellae in the caudal vertebrae

Ilium (TMM field no. TL 05-8)

pg.813

D5 - camellae

pg.819

Saltasaurus loricatus (**PVL 4017-137**)

Dorsal vertebra (Somphospondylous)

C21 - camellae in neural arch

C94 - camellae in transverse processes

C36 - camellae in neural spine

Source: Jacobs, L. L. et al. 1993. New material of an early Cretaceous Titanosaurid sauropod dinosaur from Malawi. *Palaeontology* **36** (3), pp. 523-534.

Specimen: *Malawisaurus dixeyi* comb. nov. (**MAL**)

Characters: Cervical vertebrae (MAL 89-78)

pg.525 & 526 Fig. 1-E

no pleurocoels -> C1 = 0 but Wilson (2002) -> pleurocoels on centrum -> C1

C86 - laminated fossa on neural canal (external)

C13 - laminated fossa on centrum

Dorsal vertebrae (MAL 89-137)

no reference on their pneumaticity ('?') but Wilson (2002) -> laminated (pneumato)coel on neural arch -> C30

Sacral vertebrae not recovered

Caudal vertebrae (MAL 89-79, MAL -1)

pg.528 Fig. 2

C19 - fossa on neural arch

C33 - foramina on spine

C43 - laminated fossae on spine

Ischium (MAL - 42)

no reference on pneumaticity ('?')

Source: Rogers, K. C. 2009. The postcranial osteology of *Rapetosaurus krausei* (Sauropoda: Titanosauria) from the Late Cretaceous of Madagascar. *Journal of Vertebrate Paleontology*, **29**(4), pp. 1046-1086.

Specimen: *Rapetosaurus krausei* **(FMNH PR 2209)**

Characters: Cervical vertebrae (some partially fragmented but contain all compartments/landmarks and laminae)

pg.1048

C43 - laminated fossae on spine (lateral, pre- and postspinal for anterior cervicals); **pg.1062 -** also in *Alamosaurus, Neuquensaurus* and *Saltasaurus* but absent in *Mendozasaurus* and *Ligabuesaurus*

C34 - fossae on spine (without laminae on middle cervicals - also on **Fig. 10 pg. 1053**)

C12 - subdivided fossa on centrum (also in *Isisaurus, Malawisaurus and Saltasaurus* but not in *Alamosaurus* and *Neuquensaurus*; **C12 = 0**)

pg.1050

Fig.5 (11th cervical)

C8 - fosseous pleurocoel on centrum

C13 - laminated fossa on centrum

C116 - infradiapophyseal fossa

C28 - laminated fossae on neural arch

Fig.6 [Atlas (SMM P2007.3.1)]

C60 - foramen on postzygapophysis

C6 - camellated centra

C5 - fossa with foramina on centra (also in *Isisaurus, Malawisaurus and Saltasaurus,* **pg.1061**)

pg.1051

Fig.7

C3 - foramen on centrum

C101 - laminated fossa on (below and posterior) transverse process

pg.1052

Fig.9 (9th cervical)

C20 - fossa with foramen on neural arch

pg.1053

C4 - fossae on centra

pg.1053 Fig.13 (17th cervical)

C91 - foramina (clusters) on transverse processes

C105 - foramina (clusters) on diapophysis

pg.1056 (16th & 17th cervicals)

C52 - infraprezygapophyseal fossa

C57 - laminated fossae on prezygapophyses

pg.1058

C65 - infrapostzygapophyseal fossa

C70 - laminated fossae between postzygapophyses

pg.1064

C180 - foramina on rib

C181 - fossae on rib

Dorsal vertebrae

pg.1048

C65 - infra (or intra-) postzygapophyseal fossa

C70 - laminated fossa on postzygapophyses (intra)

C43 - laminated fossae on spine (pre- and post-); not present in *Opisthocoelicaudia* (**C43 = 0**)

C19 - fossae on neural arch (in *Isisaurus* **C19 = 0**)

C28 - laminated fossae on neural arch (indicated by the presence of spinodiapophyseal lamina present)

pg.1057 Fig.16 (3d dorsal)

C8 - fosseous pleurocoel on centrum

C29 - laminated foramen on neural arch

C101 - laminated fossa on (below and posterior) transverse process

pg. 1058 Fig. 17 (4th dorsal)

C43 - laminated fossa on spine

C30 - laminated pleurocoel on neural arch

Fig.18 (5th dorsal)

C45 - laminated pleurocoel on side of base of spine

(for dorsals 6th-10th same as above; pgs.1059-1060 & 1065 Figs. 19-22)

also...

C33 - foramen on spine

C44 - laminated foramen on spine

pg.1062

C4 - fossae on centra

pg.1064

C180 - foramina on rib

C181 - fossae on rib

pg. 1065-1066

C127 - laminated fossae on parapophyses

pg.1067

C57 - laminated fossae on prezygapophyses (also in *Saltasaurus* but not in *Rocasaurus* and *Argentinosaurus* because the infraprezygapophyseal lamina is absent)

Sacral vertebrae

pg.1048

C4 - fossae on centra

pg. 1061 Fig.23 (2nd sacral)

C3 - foramina on centrum

C100 - subdivided fossae on transverse processes

C101 - laminated fossae on transverse processes

C44 - laminated foramina on spine

C43 - laminated fossae on spine (pre- and post-)

pg.1063

C180 - foramen on rib

pg.1068

C27 - subdivided fossa in neural arch (2nd sacral)

C19 - fossae on neural arch

C52 - infraprezygapophyseal fossae (by tprl)

C28 - laminated fossae on neural arch

Caudal vertebrae

pg.1048

C43 - laminated fossae on spine (pre- and post-)

no other pneumatic elements on caudals as well as the pelvic girdle

Source: Salgado, L., Apesteguía, S. & Heredia, S. E. 2005. A new specimen of *Neuquensaurus australis*, a Late Cretaceous saltasaurine titanosaur from north Patagonia. *Journal of Vertebrate Paleontology*, **25**:3, pp. 623-634.

Specimen: *Neuquensaurus australis* (**MCS-5**)

Characters: **Cervical vertebra (one posterior only, 12th or 13th, MCS-5/17, diapophyses are fragmented and missing)**

pg.625-626 (also from Fig.2)

C15 - laminated pleurocoel on centrum

C43 - laminated fossae on spine (sprl)

C101 - laminated fossa on transverse processes (prdl, podl, pcdl)

C28 - laminated fossa on neural arch (pcdl)

Dorsal vertebrae (six mid and posterior dorsal vertebrae MCS-5/18-23

{From discussion with Paul Upchurch: Neuquensaurus dorsal in CT scan revealed that a foramen on centrum is expanded inside into a polycamerate structure which then progresses into camellae.}

C2 - camerae in centrum

C3 - foramen on centrum

C6 - camellae in centrum

pg.625

[Anteriormost dorsal vertebrae lacking centroprezygapophyseal (cprl) and centropostzygapophyseal (cpol) laminae]

C1 - pleurocoels on centra

pg.626 & Fig.3 on pg.628

C8 - fosseous pleurocoel in centra

C10 - semicamerated centra

C28 - laminated fossae on neural arch

C43 - laminated fossae on spine (sprl)

C113 - laminated fossa on diapophysis

C102 - laminated foramina on transverse processes

C57 - laminated fossae on prezygapophyses

C127 - laminated fossae on parapophyses

C153 - fossa on hypapophyses (between them)

Sacral vertebrae (seven, MCS-5/16)

no pneumatic elements

Caudal vertebrae (fifteen, MCS-5/1-15, also observed from MLP-Ly) pg.625

C153 - fossa on hypapophyses (between them)

Also: one left ischium (MCS-5/24), both femora (the left one, MCS-5/27 and the right one, MCS-5/28), a right femur (MCS-9), and a left humerus (MCS-8) - no pneumatic features

Source: Calvo, J. O. et al. 2007. Anatomy of *Futalognkosaurus dukei* Calvo, Porfiri, González Riga & Kellner, 2007 (Dinosauria, Titanosauridae) from the Neuquén group (late cretaceous), Patagonia, Argentina. *Arquivos do Museu Nacional*, Rio de Janeiro, **65** (4) pp.511-526.

Specimen: *Futalognkosaurus dukei* **(MUCPv-323)**

Characters: Cervical vertebrae

pg.514

C130 - infraparapophyseal fossa

pg.515 & 516

C1 = 0 -> no pleurocoels on axis centrum or any other vertebra

C28 - laminated fossa on neural arch (**Figs. 5 & 6**)

pg.516 & Figs.7 & 8

C57 - laminated fossa on prezygapophyses

C37 - foraminous pleurocoel on spine

C44 - laminated foramina on spine

C45 - laminated pleurocoel on spine

pg.517

C28 - laminated fossa on neural arch (**podl**)

C130 - infraparapophyseal fossa

Figs.9 & 10

C101 - laminated fossa on transverse process
C43 - laminated fossae on spine (also **pg.518** - same features in *Isisaurus & Mendozasaurus*)

pg.518

C112 - subdivided (septated) fossa on diapophysis

Figs. 11 & 12

C30 - laminated pleurocoel on neural arch

Dorsal vertebrae

pg.519

C1 - pleurocoels on centra

C43 - laminated fossae on spine

pg.520

C57 - laminated fossa on prezygapophyses

C113 - laminated fossa on diapophyses

C28 - laminated fossa on neural arch

from dorsal no.5 to end there is a ventral ridge (hypapophysis) but without any pneumatic element observed

Sacral vertebrae

no pneumatic info observed due to incomplete preparation - only size measurements taken (?)

Caudal vertebra

pg.514

C43 - laminated fossae on spine (pre- and postspinal laminae)

pg.521 & Fig.16 & pg.522 Fig.17

C57 - laminated fossa on prezygapophyses

C41 - semicamerated spine

Pubis

D20 - pneumatic foramen on pubis

Source: Blows, W. T. 1995. The early Cretaceous brachiosaurid dinosaurs *Ornithopsis* and *Eucamerotus* from the Isle of Wight, England. *Palaeontology* **38**(1), pp. 187-197.

Specimen: *Ornithopsis hulkei* (lectotype, posterior dorsal vertebra **BMNH 28632**)

Characters: Dorsal vertebra (centrum only)

pg.188 & pg.189 Fig.1A

C1 - pleurocoel on centrum

pg.189

C2 - camerae in centrum

Specimen: *Eucamerotus foxi* (**Dorsal Vertebrae BMNH R2522, BMNH R91**)

Characters: C43 - laminated fossa on spine

C91 - foramina on transverse process

C103 - laminated pleurocoel on transverse process

pg.190

C1 - pleurocoels on centra

C4 - fossa on centrum

C19 - fossae on neural arch

pg.191 - Plate 1

C43 - laminated fossae on spine

C44 - laminated foramina on spine

C105 - foramen on diapophysis

C28 - laminated fossae on neural arch

C16 - pleurocoel on neural arch

C101 - laminated fossa on transverse process

C18 - foramina on neural arch

C30 - laminated pleurocoels on neural arch

C77 - fossae on neural canal (lateral-posterior & inside)

C32 - camera in spine

C85 - subdivided fossa on neural canal

C45 - laminated pleurocoel on spine

C70 - laminated fossa on (partially) postzygapophysis

C71 - laminated foramen on postzygapophysis

C8 - fosseous pleurocoel in centrum

C13 - laminated fossae on centrum

pg.192 (especially for R89 & R90)

C5 - foramina within fosse in centrum

C12 - subdivided fossae in centrum

Source: Wedel, M. J. 2003. The evolution of vertebral pneumaticity in sauropod dinosaurs. *Journal of Vertebrate Palaeontology* **23**(2), pp. 344-357.

Specimen: both *Brachiosaurus* from N. America & E. Africa

Characters: (pg. 349) Cervicals & Dorsals

C1 - pleurocoels

C2 - camerae
C3 - foramina

It is not specified By Wedel whether these features are found only in centra or also in most other vertebral parts. I will assume it is the centra since they are the most prominent to bear such distinguishable pneumatic features.

Specimen: *Saltasaurus*

Characters: (pg. 351) Cervicals, Dorsals, Sacrals & proximal Caudals

-> fully camellate (C6, C21, C36, C50, C63, C94, C108, C122, C166 & C175 = '1')

Also, Wilson (2002) -> Caudal vertebrae: fossae on neural spine -> C34

Source: Ksepka, D. T & Norell, M. A. 2006. *Erketu ellisoni*, a long-necked sauropod from Bor Guve´ (Dornogov Aimag, Mongolia)

Specimen: *Erketu ellisoni* **(IGM 100/1803)**

Characters: Cervical vertebrae (Fig.4 pg.5, Fig.5 pg.8, Fig.6 pg. 9, Fig.7 pg.10)

pg.4

C4 - fossa on spine

C120 - fossa on parapophyses

C122 - camellae in parapophyses

C160 - laminated fossa on hypapophysis

C166 - camellae in condyle

pg.6

C5 - fossa with foramina on centrum

C6 - camellae in centrum

C13 - laminated fossae

pg.7

C16 - pneumatocoel on neural arch

C28 - laminated fossae on neural arch

C34 - fossae (lateral, pre- and post-) on spine

C42 - subdivided fossa on spine

C76 - foramen on neural canal

C105 - foramen on diapophysis

C108 - camellae in diapophyses

C131 - foramen on costotransverse ring

C132 - fossa in costotransverse ring

Source: Berlin Museum fur Naturkunde - Tendaguru Collection

Specimen: *Tornieria africana*

Characters: Cervical vertebra (MB.R.3816)

Poorly preserved. Spine, transverse processes, diapophyses and half neural arch are missing (C31 - C45 = ?, C89 - C103 = ?, C104 - C117 = ?). Also incomplete are poz and prz (C46 - C58 = ?, C59 - C73 = ?).

C3 - foramina on centrum

Caudal vertebrae (MB.R.2958)

Broken transverse processes (C89 - C103 = ?). Spine incomplete.

C1 - pleurocoels on centrum
C8 - fosseous pleurocoel on centrum
C86 - laminated fossa on neural canal
C43 - laminated prespinal fossae

MB.R.2957 has spine, poz, prz, tr.pr. half broken.

C23 - fosseous pleurocoel on neural arch
C15 - laminated pleurocoel on centrum
C27 - septated fossae on neural arch

C28 - laminated fossae on neural arch
C1 - pleurocoel on centrum
C89 - pneumatocoel below transverse process
C91 - foramen on transverse process base
C17 - camera in neural arch
C13 - laminated fossae on centrum

C43 **-** laminated fossae on spine
C45 - laminated pneumatocoels on spine
C103 - laminated pneumatocoels on transverse process
C42 - subdivided fossae on spine

Ilium (MB.R.2713) & Ischium (MB.R.2733) are not pneumatic
Pubis not present (=?)

Specimen: *'Barosaurus africanus'* (i.e. *Tornieria africana)*

Characters: Caudal vertebra (MB.R.2956.1/d474)

C15 - laminated pleurocoel on centrum
C12 - subdivided fossae on centrum
C5 - foramina in fossae in centrum
C43 - laminated fossae on spine
C42 - subdivided fossae on spine
C101 - laminated fossae on transverse process
C103 - laminated pneumatocoel on transverse process
C8 - fosseous pleurocoel on centrum
C173 - fossa on cotyle

(MB.R.4021)

C7 - foraminous pleurocoel on centrum
C45 - laminated pneumatocoels on spine

Sacral vertebrae (indeterminate - possibly *Tornieria africana*)

Centrum seems to bear no pneumatic elements

C101 - laminated fossae on transverse process
C19 - fossae on neural arch
C52 - infraprezygapophyseal fossa
C43 - laminated fossae on spine
C45 - laminated pneumatocoels on spine
C127 - laminated fossae on parapophyses
C92 - fossae on transverse processes (ant and post surfaces/peduncles)

Additional source: Bonaparte, J.F., Heinrich, W.-D., and Wild, R. 2000. Review of *Janenschia* WILD, with the description of a new sauropod from the Tendaguru beds of Tanzania and a

discussion on the systematic value of procoelous caudal vertebrae in the Sauropoda. *Palaeontographica* **256**(1-3), pp.25-76.

Specimen: *Tendaguria tanzaniensis*

Characters: Dorsal vertebrae (MB.R.2092.1, MB.R.2092.2)

pg. 46-53

C1 - pleurocoels on centrum
C8 - fosseous pleurocoel on centrum
C12 - subdivided fossae on centrum
C19 - fossa on neural arch
C106 - fossae ventrally and posteriorly on diapophyses
C27 - subdivided fossa on neural arch
C17 - camera in neural arch
C2 - camera in centrum
C92 - fossae on transverse processes
C101 - laminated fossae on transverse process
C43 - laminated fossae on spine
C34 - fossae on spine
C103 - laminated pneumatocoel on transverse process (ventrally)
C28 - laminated fossa on neural arch
C142 - fossa on epipophyses
C61 - fossae on (below) postzygapophyses
C77 - fossae on neural canal

Hypapophyses do not exist (151 - 161 = ?)

Specimen: *Janenschia robusta*

Characters: Cervical vertebra (MB.R. 2091.31(g45))

C1 - pleurocoel on centrum
C8 - fosseous pleurocoel on centrum
C12 - subdivided fossae on centrum
C120 - fossae in parapophyses
C126 - septated fossa in parapophysis
C5 - foramina in fossae in centrum
C28 - laminated fossae on neural arch
C101 - laminated fossae on transverse process
C23 - fosseous pleurocoel in neural arch
C19 - fossae on neural arch
C13 - laminated fossa on centrum
C43 - laminated fossae on spine
C2 - camera in centrum
C106 - fossae ventrally on diapophysis
C105 - foramen on diapophysis
C92 - fossa on transverse process

C27 - septated fossae on neural arch
C32 - camera in spine
C113 - laminated fossa on diapophysis
C116 - infradiapophyseal fossa in diapophyses
C34 - fossae on spine (ventrally)

Caudal vertebra (MB.R.2094, Oa12)

C34 - fossa on spine

pg.61 - 64

(MB.R.2091.1-30 (G1 - G30))

C92 - fossae on transverse process
C19 - fossae on neural arch
C61 - fossa on (anterior) postzygapophyses
C48 - fossae below prezygapophyses
C4 - fossa on centrum

Specimen: *Dicraeosaurus sattleri*

Characters: Dorsal vertebrae (MB.R.3677-80)

C1 - pleurocoel on centrum
C13 - laminated fossa on centrum
C16 - pneumatocoel on neural arch
C19 - fossae on neural arch
C23 - fosseous pleurocoel on neural arch
C27 - subdivided fossae on neural arch
C28 - laminated fossae on neural arch
C92 - fossae on transverse processes
C100 - subdivided fossae on transverse processes
C101 - laminated fossae on transverse processes
C127 - laminated fossa on parapophysis
C34 - fossae on spine
C35 - fossa with foramen on spine
C42 - septated fossae on spine
C52 - infraprezygapophyseal fossa
C43 - laminated fossae on spine
C91 - foramina on transverse processes
C48 - fossa on prezygapophyses
C57 - laminated fossae on prezygapophyses

Caudal vertebrae (MB.R.3681-87 (M53, M55, M36, M13, M14, M15 M16)

C92 - fossae on transverse processes
C101 - laminated fossae on transverse processes

C19 - fossae on neural arch

C43 - laminated fossae on spine

C57 - laminated fossae on prezygapophyses

C70 - laminated fossae on postzygapophyses

C33 - foramina on spine

Also **by Harris, 2007 -> foramina on centrum -> C3**

Sacral vertebrae (MB.R.3688 (M30))

C23 - fosseous pleurocoel on neural arch

C28 - laminated fossae on neural arch

C30 - laminated pneumatocoel on neural arch

C33 - foramina on spine

C43 - laminated fossae on spine

C20 - fossa with foramina on neural arch

C92 - fossa on transverse process

C93 - fossa with foramina on transverse process

C64 - infrapostzygapophyseal foramen

C101 - laminated fossae on transverse process

C105 - foramina on diapophyses

Ilium (MB.R.2711, MB.R.2714 - M3)

not pneumatic

Ischium (MB.R.2731 - O10, MB.R.2732 - M7)

not pneumatic

Pubis (?)

Specimen: *Giraffatitan brancai 'Brachiosaurus'*

Characters: Dorsal vertebrae (MB.R.2189.87, MB.R.3824)

Diapophyses and postzygapophyses are fragmented and missing (C104 - C117 = ?, C59 - C73 = ?)

Vertebrae are lattice-like structured - highly pneumatic

C1 - pleurocoels on centrum
C2 - camerae in centrum

C7 - foraminous pleurocoel on centrum

C8 - fosseous pleurocoel on centrum

C12 - subdivided fossae

C18 - foramina on neural arch

C91 - foramina on transverse process

C28 - laminated fossae on neural arch

C101 - laminated fossa on transverse process

C43 - laminated fossae on spine

C17 - camerae in neural arch

C34 - fossae on spine

C31 - pneumatocoels on spine

C52 - infraprezygapophyseal fossa

C164 - fossa on condyle

Caudal vertebrae (MB.R.2921, series 1-18, A17 - A34)

C4 - fossa on centrum

C101 - laminated fossa on transverse process

C91 - foramen on transverse process

Ilium (MB.R.2712 - Aa13)

not pneumatic

Specimen: *Ruehleia bedheimensis (Plateosaurus plieningeri)*

Characters: Cervical vertebrae (only MB.R.4718.20 & MB.R.4718.55 have reg. numbers out of 9 vertebrae)

Costotransverse ring not present (C131 - C139 = ?)

C34 - fossae on spine

C164 - fossa on condyle

C92 - fossa on transverse process

C18 - foramen on neural arch

C101 - laminated fossae on transverse process

C28 - laminated fossae on neural arch

C100 - subdivided fossae on transverse process

C20 - fossae with foramina on neural arch

C93 - fossae with foramina on transverse process

Dorsal vertebrae (MB.R.4718.42, .43, .41, .46, .72, .70)

C28 - laminated fossae on neural arch

C101 - laminated fossae on transverse process

C93 - fossae with foramina on transverse process

C100 - subdivided fossae on transverse process

C57 - laminated fossa on prezygapophyses

C92 - fossa on transverse process

C76 - foramina on neural canal (blind though)

C180 - foramina on ribs

Sacral vertebrae (MB.R.4718.27)

spines are missing (only bases exist), transverse processes, prz and poz partly damaged

C43 - laminated fossae on spine

C101 - laminated fossae on transverse process

Caudal vertebrae (MB.R.4718.38, .32)

severely fragmented - no pneumatic elements

Ilium (MB.R.4719.4, MB.R.4737)

no pneumatic elements

Ischium (MB.R.4744)

Pubis (MB.R.4771)

no pneumatic elements

Specimen: *Plateosaurus longiceps*

Characters: Sacrum with 2 sacral vertebrae with ilia, incomplete ischia and incomplete pubes (MB.R.4402.24 - KKL P0954)

D3 - fossa on ilium

D11 - foramina on ischium

D2 - foramen on iliac peduncle

C100 - subdivided fossae on transverse process

C92 - fossa on transverse process

C34 - fossa on spine

C42 - subdivided fossa on spine

Bone is lighter than expected but massive; inside seems to be partially hollow (minor fragmentations allow a partial inside look)

Pubes (MB.R.4398.119.1/2)

no pneumatic elements

Dorsal ribs (MB.R.4398.84, .77)

no pneumatic elements

Dorsal vertebra MB.R.4402.12

C60 - foramina on postzygapophysis

C91 - foramina on transverse process

C33 - foramina on spine

Foramina and fossae may not be pneumatic at all but they have to be recorded

Caudal vertebrae (MB.R.4398)

no pneumatic elements

Also, personal observations from specimens in Museum fur Naturkunde, Berlin:

D2 - foramina on the ilium

D3 - fossae on the ilium

D11 - foramina on the ischium

Source: *Amphicoelias "brontodiplodocus".* A New Sauropod, from The Morrison Formation, Big Horn Basin, Wyoming, with Taxonomic Reevaluation of *Diplodocus, Apatosaurus, Barosaurus* and Other Genera. Galiano, H. and Albersdörfer, R. Dinosauria International, LLC. Wyoming, USA, 2010.

Specimen: *Amphicoelias altus, "brontodiplodocus", emiliae* (basal diplodocid) **(DQ-TY, AMNH5764)**

Characters: Cervical vertebrae

pg.12, Fig.10

C1 - pleurocoels on centra

C3 - foramina on centrum

C5 - fossa with foramen on centra

C18 - foramen on neural arch

C8 - fosseous pleurocoel on centra

C28 - laminated fossae on neural arch

C33 - foramen on spine

C34 - fossa on spine

C43 - laminated fossae on spine

C48 - fossae on prezygapophyses

C57 - laminated fossae on prezygapophyses

C101 - laminated fossae on transverse processes

Dorsal vertebrae

no pneumatic elements on ribs

C1 - pleurocoels on centra

C3 - foramina on centrum

C18 - foramina on neural arch

C101 - laminated fossae on transverse processes

C43 - laminated fossae on spine

C28 - laminated fossae on neural arch

Sacral vertebrae

no description was made (?)

Caudal vertebrae (DQ-BS 403 & 447A, AMNH 223)

pg.6

C1 - pleurocoel on centrum

pg.34, Fig. 29

C3 - foramen on centrum

C18 - foramen on neural arch

C24 - septated foramina on neural arch

C33 - foramen on spine

C39 - septated foramina on spine

C44 - laminated foramina on spine

C91 - foramen on transverse process

Ilium (DQ-BS)

pg.9, Fig7G

no pneumatic elements

Ischium (DQ-BS)

pg.9, Fig7G

no pneumatic elements

Pubis (DQ-BS)

pg.9, Fig7G

no pneumatic elements

Source: Gillette, D. David. 1991. *Seismosaurus halli*, gen. et sp. nov., a new sauropod dinosaur from the Morrison formation (Upper Jurassic/Lower Cretaceous) of New Mexico, USA. *Journal of Vertebrate Paleontology*, **11**(4), pp.417-433.

Specimen: *Seismosaurus halli* **(NMMNH 3690)**

Characters: Cervical vertebrae

unknown

Dorsal vertebrae

unknown (undescribed)

Sacral vertebrae

pg.424

unknown (undescribed)

Caudal vertebrae

pg.418

C1 - pleurocoel on centrum

pg.424

C4 - fossa on centrum

pg.426, Figs 5 & 6

C12 - septated fossa on centrum

C27 - septated fossa on neural arch

C92 - fossa on transverse process

C34 - fossa on spine

pg.427, Figs 7 & 8

C45 - laminated pneumatocoel on spine

C33 - foramina on spine

C19 - fossa on neural arch

pg.430, Fig 11

C152 - foramen on chevron (hypapophysis/haemapophysis)

C153 - fossa on chevron (hypapophysis/haemapophysis)

Ilium

unknown (undescribed)

Ischium

pg.422, Fig 3

no pneumatic elements

Pubis

pg.420, Fig 2

no pneumatic elements

Source: Mannion, D. Philip & Calvo, O. Jorge. 2011. Anatomy of the basal titanosaur (Dinosauria, Sauropoda) *Andesaurus delgadoi* from the mid-Cretaceous (Albian–early Cenomanian) Río Limay Formation, Neuquén Province, Argentina: implications for titanosaur systematics. *Zoological Journal of the Linnean Society*, **163**, pp.155–181.

Specimen: *Andesaurus delgadoi* **(MUCPv 132)**

Characters: Cervical vertebrae

Unknown

Dorsal vertebrae

pg.155 & pg.158 Fig.2 & pg.160

C1 - pleurocoel on centrum

C5 - fossa with foramen on centrum

C7 - foraminous pleurocoel on centrum

C20 - fossa with foramen on neural arch

C45 - laminated pneumatocoel on spine (also in *Brachiosaurus, Dongyangosaurus, Neuquensaurus, Diplodocus, and Apatosaurus*)

C113 - laminated fossa on diapophysis (**PCDL**)

C120 - fossa on parapophysis (postparapophyseal)

pg.159

C30 - laminated pneumatocoel on neural arch (also in *Diplodocus*)

pg.167 (also in *Mamenchisaurus*)

C6 - camellate centrum

C21 - camellate neural arch

C36 - camellate spine

C50 - camellate prezygapophysis

C63 - camellate postzygapophysis

C79 - camellate neural canal

C94 - camellate transverse process

C108 - camellate diapophysis

C122 - camellate parapophysis

C166 - camellate condyle

C175 - camellate cotyle

Dorsal ribs

pg.160

non-pneumatic

Sacral vertebrae

pg.160

mostly destroyed-only anterior part of centrum-not pneumatic; rest compartments unknown (?)

Caudal vertebrae

pg.161, pg.162, pg.163, Figs 3, 4, 5 & pg.165, Fig. 7

C4 - fossa on centrum

C43 - laminated fossa on spine

pg.155

C4 **-** fossa on centrum

Ilium

Unknown

Ischium

pg.170

no pneumatic elements

Pubis

pg. 169

no pneumatic elements

Source: Yadagiri, P. 2001. The osteology of *Kotasaurus yamanpalliensis*, a sauropod dinosaur from the Early Jurassic Kota formation of India. *Journal of Vertebrate Paleontology,* **21**(2): pp.242-252

Specimen: *Kotasaurus yamanpalliensis* **(21/SR/PAL)**

Characters: Cervical vertebrae (1 - 12/S1Y/76)

pg. 245 Fig. 4

C4 - fossa on centrum

C19 - fossa on neural arch

C34 - fossa on spine

C48 - fossa on prezygapophysis

C52 - infraprezygapophyseal fossa

C92 - fossa on transverse process

Dorsal vertebrae (13 - 25/S1Y/76)

pg. 245 Fig. 4

C19 - fossa on neural arch

C92 - fossa on transverse process

pg.246

C4 - fossa on centrum

C28 - laminated fossa on neural arch

pg.250 - 251 for *Barapasaurus tagorei*

C76 - foramen on neural canal (dorsally)

C17 - camera in neural arch

C16 - pneumatocoel on neural arch

Sacral vertebrae (26/S1Y/76)

pg. 245 Fig. 4 & pg.246

no pneumatic elements

Caudal vertebrae (29-81/S1Y/76)

pg. 245 Fig. 4 & pg.246

no pneumatic elements

Haemapophyses (Chevrons 82-89/S1Y/76)

pg.247

no pneumatic elements

Ilium (108/S1Y/76)

pg.248, Fig 5 & pg.249

no pneumatic elements

Ischium (109/S1Y/76)

pg.248, Fig 5

no pneumatic elements

Pubis (110/S1Y/76)

pg.248, Fig 5

no pneumatic elements

Source: Remes, K. et al. 2009. A New Basal Sauropod Dinosaur from the Middle Jurassic of Niger and the Early Evolution of Sauropoda. *PLoS ONE* **4**(9): e6924. doi:10.1371/journal.pone.0006924

Specimen: *Spinophorosaurus nigerensis* gen. et sp. nov.**(GCP-CV-4229 & NMB-1698-R)**

(foramen on femur, lateral to the fourth trochanter**)**

Characters: Cervical vertebrae

pg.3

C28 - laminated fossa on neural arch

C1 - pleurocoel on centrum

pg.4

C120 - fossa on parapophysis

pg.6, Fig. 3

C13 - laminated fossa on centrum

C153 - fossa on hypapophysis

C34 - fossa on spine

Dorsal vertebrae

pg.4

C1 - pleurocoel on centrum

C4 - fossa on centrum

C19 - fossa on neural arch

Ribs

no pneumatic elements

Sacral vertebrae

Unknown (undescribed - possibly zero)

Caudal vertebrae

no pneumatic elements

Ilium

no pneumatic elements

Ischium

no pneumatic elements

Pubis

no pneumatic elements

Source: S. Suteethorn, J. Le Loeuff, E. Buffetaut, V. Suteethorn, C. Talubmook and C. Chonglakmani. 2009. A new skeleton of *Phuwiangosaurus sirindhornae* (Dinosauria, Sauropoda) from NE Thailand. *Geological Society, London, Special Publications* **315**, pp. 189-215. doi: 10.1144/SP315.14

Specimen: *Phuwiangosaurus sirindhornae* (**Holotype: SM PW1-0001 to SM PW1-0022; Paratype: SM K11-0001 to SM K11-0167)**

Characters: Cervical vertebrae

Pg.203

C34 – fossa on spine

C1 – pleurocoels on centrum

C130 – intraparapophyseal fossa

Ventral keel not present in cervicals (hypapophysis = ?)

Pg. 204 Fig.12

C91 – foramina on transverse process

C30 – laminated pneumatocoel on neural arch

C16 – pneumatocoel on neural arch

C34 **–** fossa on spine

C17 – camerae in neural arch

C106 – fossa on diapophysis

C113 – laminated fossa on diapophysis

C18 – foramina on neural arch

C33 – foramen on spine

C47 – foramina on prezygapophysis

C173 – fossa on cotyle

C31 – pneumatocoel on spine

C103 – laminated pneumatocoel on transverse process

C15 - laminated pneumatocoel on centum

C19 - fossa on neural arch

Pg.205

C127 - laminated fossa on parapophysis (lamina on capitulum depression)

C138 - laminated fossa on costotransverse ring

C181 - fossa on rib

Pg.211 - 212 Figs 18-19

C29 - laminated foramen on neural arch

C28 - laminated fossae on neural arch

Dorsal vertebrae

Pg.195

C1 – pleurocoel on centrum

Pg.205

Ventral keel is present

C1 **–** pleurocoel on centrum

C43 - laminated fossae on spine

C101 - laminated fosse on transverse process

Pg.206 Fig.13

C106 – fossa on diapophysis

C28 - laminated fossa on neural arch

C113 - laminated fossa on diapophysis

C127 - laminated fossa on parapophysis

C86 - laminated fossa on neural canal

C87 - laminated foramen on neural canal

C78 - fossa with foramen on neural canal

C76 - foramen on neural canal

C29 - laminated foramina on neural arch

C44 - laminated foramina on spine

C97 - septated foramina on transverse process

C91 - foramen on transverse process

C102 - laminated foramen on transverse process

C103 - laminated pneumatocoel on transverse process

C27 - septated fossae on neural arch

C30 - laminated pneumatocoel on neural arch

C61 - fossa on postzygapophysis

C70 - laminated fossa on postzygapophysis

Pg.207

C132 - fossa on costotransverse ring

C181 - fossa on rib

C120 - fossa on parapophysis

Sacral vertebrae

Pg.207

C120 - fossa on parapophysis

Pg.208 Fig.14

C43 - laminated fossae on spine

C45 - laminated pneumatocoel on spine

C101 - laminated fosse on transverse process

C33 - foramina on spine

C1 - pleurocoel on centrum

C16 - pneumatocoel on neural arch

C19 - fossa on neural arch

C92 - fossa on transverse process

C4 - fossa on centrum

C131 - foramina on costotransverse ring (sacrocostal yoke)

C180 - foramina or ribs

Caudal vertebrae

Pg.210 Fig.16

C33 - foramina on spine

C19 - fossa on neural arch

Ilium (SM K11-0147 & SM PW1-0011)

Pg.212

no pneumatic elements

Ischium (SM K11-0149 and SM K11-0150 & SM PW1-0014 and SM PW1-0015)

Pg.213

no pneumatic elements

Pubis (SM K11-0148 & SM PW1-0013)

Pg. 213

no pneumatic elements

Source: Wilson, J. A. & Upchurch, P. 2009. Redescription and reassessment of the phylogenetic affinities of *Euhelopus zdanskyi* (Dinosauria: Sauropoda) from the Early Cretaceous of China. *Journal of Systematic Palaeontology* **7** (2): pp. 199–239. doi:10.1017/S1477201908002691

Specimen: *Euhelopus zdanskyi* **(PMU 233)**

Has epipophyses; has epipophyseal-prezygapophyseal lamina (eprl)

Characters: Cervical vertebrae

Pg.199

C30 - laminated pneumatocoels on neural arch

Pg.205

for specimen (IVPP 10601)

C6 - camellae in centrum

C21 - camellae in neural arch

C1 - pleurocoel on centrum

C38 - fosseous pleurocoel on spine

C7 - foraminous pleurocoel on centrum

Pg.211 Fig7 (PMU 233)

C4 - fossa on centrum

C61 - fossa on postzygapophysis

C142 - fossa on epipophysis

C42 - septated fossae on spine

Pg.212

C15 - laminated pleurocoel on centrum

C43 - laminated fossae on spine

C69 - septated fossae on postzygapophysis

C70 - laminated fossa on postzygapophysis

Pg.214

C65 - infrapostzygapophyseal fossa

Pg.215

C45 - laminated pneumatocoel on spine

C182 - camellate ribs

Dorsal vertebrae

Pg.203 Fig.3

C1 - pleurocoel on centrum

C45 - laminated pneumatocoel on spine

C27 - septated fossae on neural arch

C103 - laminated pneumatocoel on transverse process

C39 - septated foramina on spine

C22 - foraminous pleurocoel on neural arch

C23 - fosseous pleurocoel on neural arch

C30 - laminated pneumatocoels on neural arch

Pg.217

C6 - camellae in centrum

C21 - camellae in neural arch

Pg.219 & Figs 17, 18

C42 - septated fossae on spine

C159 - septated fossa on hypapophysis

C28 - laminated fossae on neural arch

Pg.220 & Fig.19

C101 - laminated fossae on transverse processes

C103 **-** laminated pneumatocoel on transverse processes

C113 - laminated fossae on diapophyses

Pg.221 Fig.21

C180 - foramen on rib

Sacral vertebrae

Pg.222 & Fig.23

C1 - pleurocoel on centrum

C6 - camellae in centrum

C21 - camellae in neural arch

C36 - camellae in spine

Caudal vertebrae

Unknown (?)

Ilium

Pg.199

(pneumatic ilium)

Pg.223 & Fig. 24

D5 - camellae (also in *Epacthosaurus, Lirainosaurus, Sonidosaurus*)

Ischium

Pg.223

no pneumatic elements

Pubis

Pg.223

no pneumatic elements

Source: Cooper, M. R. 1984. A reassessment of *Vulcanodon karibaensis* Raath (Dinosauria: Saurischia) and the origin of the Sauropoda. *Paleontología africana* **25**, pp. 203-231.

Specimen: *Vulcanodon karibaensis* **(QG24)**

Characters: Cervical vertebrae

Pg.204

Unknown (?)

Pg. 211 for QG-1406

Neural spine absent -> C31 - C45 = ? ; poz absent -> C59 - C73 = ?

C1 - pleurocoel on centrum

Pg.213

cervical ribs -> Unknown (?)

Dorsal vertebrae

Pg.204

Unknown (?); but in Yates and Kitching (2003) -> fossae in centrum -> C4

Fossae on parapophyses -> C120

Fossae on neural arches -> C19

Pg.213

dorsal ribs -> Unknown (?)

Sacral vertebrae

no pneumatic elements

Caudal vertebrae

Pg.204 & Pg.205

(they lack pleurocoels, so C1 at least is zero, but have 'incipient cavitation', so fossa on centrum is presumably present, 1)

C4 - fossa on centrum (also in *Barapasaurus* cervical centra)

(no pneumatic elements for *Barapasaurus* in sacral vertebrae and pelvic girdle)

(pleurocoels on dorsal centra of *Camarasaurus* -> **C1 = 1)**

Pg.213

all lack neural spines (C31-C45 = ?)

caudal ribs -> no pneumatic elements

Pg.213-214, Fig.15

(ventral groove ventral to centrum)

C153 - fossa in hypapophysis

Ilium

Pg.213

no pneumatic elements

Ischium

Pg.214

no pneumatic elements

Pubis

Pg.213-214

no pneumatic elements

List of characters found in juvenile Sauropodomorph vertebrae

Source: Daniela Schwarz , Takehito Ikejiri , Brent H. Breithaupt , P. Martin Sander & Nicole Klein (2007) A nearly complete skeleton of an early juvenile diplodocid (Dinosauria: Sauropoda) from the Lower Morrison Formation (Late Jurassic) of north central Wyoming and its implications for early ontogeny and pneumaticity in sauropods, Historical Biology: An International Journal of Paleobiology, 19:3, 225-253, DOI: 10.1080/08912960601118651

Specimen: Juvenile, possibly macronarian, sauropod, formerly assigned as a diplodocid – SMA 0009. Features are similar to *Giraffatitan*, *Camarasaurus*, and *Omeisaurus* and less similar to *Barapasaurus*.

General observations: Complete juvenile sauropod (SMA 0009) with an estimated total length of about 2 m.

Characters: **Pg. 231 – Cervical vertebrae**

C12 - Subdivided fossae on centrum

C5 - Fossae with foramina on centrum

C113 - Laminated fossa on the diapophysis

Pg. 232

C116 - Infradiapophyseal fossa

C65 - Infrapostzygapophyseal fossa

C58 - Laminated prezygapophyseal foramen

C114 - Laminated foramen on diapophysis

Fig. 5E – Dorsal vertebrae

C3 - Foramen on centrum

C102 - Laminated foramen on transverse process

Pg. 234 – Cervical vertebrae

C181 - Fossa on cervical rib

C180 - Foramen on cervical rib

Pg. 235 – Dorsal vertebrae

C4 - Fossa on centrum

C121 - Fossa with foramen on parapophysis
C101 - Laminated fossae on transverse process

C181 - Fossa on dorsal rib

Pg. 236 – Sacral vertebrae

C19 - Fossa on neural arch

C61 - Fossa on postzygapophysis

C34 - Fossae on neural spine

Caudal vertebrae

C173 - Fossa on cotyle

Ilium/ischium/pubis

No pneumatic elements

Source: New information on a juvenile sauropod specimen from the Morrison formation and the reassessment of its systematic position. 2012. Jose l. Carballido, Jean S. Marpmann, Daniela Schwarz-Wings and Ben Pabst. Palaeontology 55(3): pp. 567-582.

Specimen: SMA 0009.

General observations: Complete juvenile sauropod (SMA 0009) with an estimated total length of about 2 m.

Characters: Pg. 569-Fig. 3A. Anterior-most **Cervical vertebrae**

Also pg. 571-**C1** - Pleurocoels (2) on centrum

3B. C52 - infraprezygapophyseal fossae (2)

3C. **C1-** Pleurocoel on centrum

3D. **C52 -** infraprezygapophyseal fossae (2) – (also in *Omeisaurus*)

Pg. 570-Fig. 4. Anterior-most **Dorsal vertebrae**

C116 - Infradiapophyseal fossa (laminated)

Pg. 571

Posterior **Cervical vertebrae**

C4 - Fossa(e) on centrum

C120 - Fossa on parapophysis

C57- Laminated infraprezygapophyseal fossae

Pg. 572 – Dorsal vertebrae

C19 - Fossae on neural arches

Pg. 573 – Dorsal verebrae

C116 - Laminated infradiapophyseal fossae

C127 - Laminated fossa on parapophysis

Sacral vertebrae

No further pneumatic elements observed

Caudal vertebrae

No further pneumatic elements observed

Ilium/ischium/pubis

No pneumatic elements

<u>Comparative analysis of SMA 0009 (Wyoming, USA) and *Brachiosaurus* (Colorado- Utah, USA)</u>

<u>Dorsals</u> - Transition from:

Foramina and fossae on centrum into pleurocoel, camerate, semicamellate and camellate centrum.

Fossa on ribs -> absent pn.

laminated fossa(e) on transverse process -> absent pn.
foraminous fossae and laminated fossae on parapophyses -> absent pn.

fossa on neural arch -> camellae in neural arch

infradiapophyseal fossa -> absent pn.

absent pn. in neural spine -> laminated pneumatocoel on neural spine

absent pn. in prezygapophyses, postzygapophyses, condyle and cotyle -> camellated prz, poz, condyle, and cotyle.

<u>Sacrals</u> – Transition from:

absent pn. in centrum -> foramina on centrum

Fossae on neural arch and poz -> absent pn.

Fossae on neural spine -> foramen on neural spine

<u>Caudals</u> – Transition from:

Fossa on cotyle -> fossa on centrum

<u>Pelvis</u> – absent pn. In both SMA 0009 and Brachiosaurus

<u>Comparative analysis of SMA 0009 (Wyoming, USA) and *Camarasaurus* (Wyoming, USA)</u>

<u>Cervicals</u> - Transition from:

Fossae, subdivided fossae, foraminous fossae and pleurocoel on centrum -> pleurocoel, fosseous pleurocoel, foramina and camerae in centrum

Foramen and fossa on ribs -> foramina on ribs

Laminated fossae, infradiapophyseal fossae and laminated foramina on diapophyses -> infradiapophyseal fossae and infradiapophyseal camerae

Fossa on parapophyses -> fossae, foraminous fossae and camellae in parapophyses

Laminated and simple infraprezygapophyseal fossae as well as laminated foramina on prezygapophyses -> foramina, fossae, camellae, simple and laminated infraprezygapophyseal fossae in prezygapophyses

Infrapostzygapophyseal fossae -> laminated fossae, infrapostzygapophyseal fossae, infrapostzygapophyseal foramina, infrapostzygapophyseal camerae and camellae

Absent pn. in hypapophyses -> camerae in hypapophyses

Absent pn. in neural arch -> camerae and camellae in neural arch

Absent pn. in transverse process -> laminated fossae, foramina and camellae in transverse process

Absent pn. in neural canal -> foramina, camellae and camerae in neural canal

Absent pn. in neural spine -> fossae, foramina, foraminous fossae, subdivided fossae, laminated fossae, camerae and camellae in neural spine

Absent pn. in condyle -> camellated condyle

Absent pn. in cotyle -> camellated cotyle

Dorsals - Transition from:

Foramina and fossae on centrum -> foramina, pleurocoels and camerae in centrum

Laminated foramen on transverse process -> foramen on transverse process

Laminated fossa on transverse process -> absent laminated fossa in transverse process

Fossa on ribs -> absent pn. on ribs

Fossa and foramen on parapophyses -> absent pn. in parapophyses

Absent pn. on neural arch -> foramina and camerae in neural arch

Sacrals - Transition from:

absent pn. In centrum -> pleurocoel in centrum

fossae in neural arch, postzygapophyses and neural spine -> absent pn. In neural arch, poz and neural spine

Caudals - Transition from:

Fossa on cotyle -> fossa on neural spine

Pelvis - absent pn. In both SMA 0009 and Camarasaurus

Appendix 2

Supplementary tables, figures and character lists of the PhD thesis

Tables

Table S1. Sauropod Data Matrix (sample).

Sauropodomorph taxa		Cervicals	Centrum									
Genus	species		C1	C2	C3	C4	C5	C6	C7	C8	C9	C10
Basal Sauropodomorpha												
Efraasia	*minor*		0	0	0	0	0	0	0	0	0	0
Plateosaurus	*longiceps*		0	0	0	0	0	0	0	0	0	0
Ruehleia	*bedheimensis*		0	0	0	0	0	0	0	0	0	0
Eucnemesaurus	*fortis*		0	0	0	0	0	0	0	0	0	0
Thecodontosaurus	*antiquus*		0	0	0	1	0	0	0	0	0	0
Camelotia	*borealis*		0	0	0	0	0	0	0	0	0	0
Massospondylus	*carinatus*		0	0	0	0	0	0	0	0	0	0
Aardonyx	*celestae*		0	0	0	0	0	0	0	0	0	0
Seitaad	*ruessi*		?	?	?	?	?	?	?	?	?	?
Antetonitrus	*ingenipes*		0	0	0	0	0	0	0	0	0	0
Eusauropoda												
Vulcanodon	*karibaensis*		1	0	0	0	0	0	0	0	0	0
Tazoudasaurus	*naimi*		0	0	0	1	0	0	0	0	0	0
Barapasaurus	*tagorei*		1	0	0	1	0	0	0	0	0	0
Kotasaurus	*yamanpalliensis*		0	0	0	1	0	0	0	0	0	0
Spinophorosaurus	*nigerensis*		1	0	0	0	0	0	0	0	0	0
Rhoetosaurus	*brownei*		1	0	0	0	0	0	0	1	0	0
	brevis/humerocristatus/mogrebiensis/oxonie											
Cetiosaurus	*nsis*		1	0	0	0	0	0	0	0	0	0
Jobaria	*tiguidensis*		1	0	0	0	0	0	0	1	0	0
Shunosaurus	*lii*		1	0	0	0	0	0	0	1	0	0
Omeisaurus	*tianfuensis*		1	0	0	0	0	0	0	1	0	0
Patagosaurus	*fariasi*		1	0	0	0	0	0	0	0	0	0
Klamelisaurus	*gobiensis*		1	0	0	0	0	0	0	0	0	0
Mamenchisaurus	*jingyanensis*		1	1	1	0	0	0	1	1	0	0
Diplodocoidea												
Haplocanthosaurus	*priscus/delfsi*		1	0	0	1	0	0	0	0	0	0
Amphicoelias	*altus/brontodiplodocus*		1	0	1	0	1	0	0	1	0	0
Apatosaurus	*parvus/louisae/excelsus/ajax*		0	1	0	0	0	0	0	1	0	0
Suuwassea	*emilieae*		0	0	0	0	1	0	0	1	0	0
Barosaurus	*lentus*		1	0	0	0	1	0	0	1	0	0
Seismosaurus	*hallorum*		?	?	?	?	?	?	?	?	?	?
Diplodocus	*carnegii/longus*		0	1	1	0	0	0	0	0	0	0
Tornieria	*africana*		0	0	1	0	0	0	0	0	0	0
Dicraeosaurus	*sattleri*		1	0	0	0	1	0	0	1	0	0
Amargasaurus	*cazaui*		1	0	0	0	1	0	0	0	1	0
Nigersaurus	*taqueti*		0	0	1	0	0	0	0	1	0	0
Amazonsaurus	*maranhensis*		?	?	?	?	?	?	?	?	?	?
Cathartesaura	*anaerobica*		0	1	1	0	0	0	0	0	1	0
Macronaria												
Tehuelchesaurus	*benitezii*		?	?	?	?	?	?	?	?	?	?
Janenschia	*robusta*		1	1	0	0	1	0	0	1	0	0
Camarasaurus	*grandis/lentus/lewisi/supremus*		1	1	1	0	0	1	0	1	0	0
Euhelopus	*zdanskyi*		1	0	0	1	0	1	1	0	0	0
Europasaurus	*holgeri*		1	1	1	0	0	0	0	1	0	0
Brachiosaurus	*altithorax/nougaredi*		?	?	?	?	?	?	?	?	?	?
Giraffatitan	*brancai*		1	1	1	0	0	1	0	1	0	0
Ornithopsis	*hulkei*		?	?	?	?	?	?	?	?	?	?
Eucamerotus	*foxi*		?	?	?	?	?	?	?	?	?	?
Pleurocoelus	*nanus/valdensis*		0	0	0	1	0	0	0	0	0	0
Titanosauria												
Australodocus	*bohetii*		1	0	0	0	1	0	0	1	0	0
Phuwiangosaurus	*sirindhornae*		1	0	0	0	0	0	0	0	0	0
Sauroposeidon	*proteles*		0	1	0	1	1	1	0	1	0	0
Erketu	*ellisoni*		0	0	0	1	1	1	0	0	0	0
Tendaguria	*tanzaniensis*		?	?	?	?	?	?	?	?	?	?
Huanghetitan	*liujiaxiaensis*		?	?	?	?	?	?	?	?	?	?
Malawisaurus	*dixeyi*		0	0	0	0	1	0	0	0	0	0
Andesaurus	*delgadoi*		?	?	?	?	?	?	?	?	?	?
Dongyangosaurus	*sinensis*		?	?	?	?	?	?	?	?	?	?
Futalognkosaurus	*dukei*		0	0	0	0	0	0	0	0	0	0
Neuquensaurus	*australis*		0	0	0	0	0	0	0	0	0	0
Saltasaurus	*loricatus/robustus*		0	0	0	0	1	1	0	0	0	0
Puertasaurus	*reuili*		0	0	0	0	0	0	0	0	0	0
Rapetosaurus	*krausei*		0	0	1	1	1	1	0	1	0	0
Alamosaurus	*sanjuanensis*		1	0	0	0	1	0	0	0	0	0

Table S2. Table of sauropod classification into PDI% ranks of Cervical (CV), Dorsal (DV), and Caudal (CD) vertebral regions along with their region estimated lengths. Abbreviations: BS, Basal Sauropodomorpha; E, Eusauropoda; D, Diplodocoidea; M, Macronaria; T, Titanosauria.

Class	PDI% CV	Genera	neck_length (m)	Family
A	90-100	*Saltasaurus*	3,8	T
	80-89	None		
B	70-79	*Vulcanodon*	1,4	E
		Cetiosaurus	4	E
		Patagosaurus	3,72	E
		Mamenchisaurus	9	E
		Tornieria	6	D
		Klamelisaurus	5,5	E
		Camarasaurus	6	M
		Giraffatitan	9	M
		Alamosaurus	6,6	T
	60-69	*Rhoetosaurus*	3,45	E
		Shunosaurus	3	E
		Omeisaurus	7,3	E
		Apatosaurus	5,2	D
		Diplodocus	6	D
		Amargasaurus	3,13	D
		Euhelopus	5,5	M
		Erketu	3,45	T
		Sauroposeidon	12	T
		Phuwiangosaurus	6	T
		Futalognkosaurus	9,5	T
C	50-59	*Plateosaurus*	1,2	BS
		Amphicoelias	8,3	D
		Australodocus	4	T
		Barosaurus	6,5	D
		Dicraeosaurus	4	D
		Nigersaurus	2	D
		Cathartesaura	2,6	D
		Europasaurus	3,1	M
		Janenschia	5,3	M
		Malawisaurus	5	T

		Neuquensaurus	2,3	T
		Rapetosaurus	4,8	T
	40-49	*Ruehleia*	1,5	BS
		Thecodontosaurus	0,5	BS
		Barapasaurus	2,6	E
		Suuwassea	3,45	D
D	30-39	*Spinophorosaurus*	2,85	E
		Haplocanthosaurus	4	D
		Puertasaurus	9,5	T
	20-29	*Kotasaurus*	2	E
E	10	*Tazoudasaurus*	2	E
		Pleurocoelus	7,5	M
Zero PDI		*Efraasia*	1	BS
		Eucnemesaurus	1,2	BS
		Camelotia	2,3	BS
		Massospondylus	1	BS
		Aardonyx	1,4	BS
		Antetonitrus	2,61	BS
Unknown PDI CV		*Seitaad*		BS
		Tehuelchesaurus		M
		Seismosaurus		D
		Amazonsaurus		D
		Tendaguria		T
		Brachiosaurus		M
		Ornithopsis		M
		Eucamerotus		M
		Huanghetitan		T
		Andesaurus		T
		Dongyangosaurus		T

Class	PDI% DV	Genera	trunk_length (m)	Family
A	90-100	*Mamenchisaurus*	6	E
		Camarasaurus	4,27	M
		Brachiosaurus	7	M
		Ornithopsis	3,75	M
		Andesaurus	6	T
		Saltasaurus	4	T
		Alamosaurus	6	T
	80-89	*Nigersaurus*	2,25	D
B	70-79	*Plateosaurus*	2	BS
		Barapasaurus	3	E
		Patagosaurus	4,12	E
		Barosaurus	6,5	D
		Amazonsaurus	3	D
		Klamelisaurus	4,75	E
		Euhelopus	2,75	M
	60-69	*Rhoetosaurus*	3,75	E
		Shunosaurus	2,5	E
		Omeisaurus	6,2	E
		Tehuelchesaurus	3,75	M
		Haplocanthosaurus	3	D
		Diplodocus	6	D
		Giraffatitan	8	M
		Eucamerotus	3,75	M
		Pleurocoelus	3,75	M
		Neuquensaurus	2,5	T
C	50-59	*Cetiosaurus*	4	E
		Apatosaurus	5,5	D
		Amargasaurus	3,43	D
		Europasaurus	1,55	M
		Phuwiangosaurus	6,3	T
		Futalognkosaurus	10	T
		Rapetosaurus	5	T
	40-49	*Ruehleia*	2,7	BS
		Eucnemesaurus	1,5	BS
		Camelotia	2,5	BS
		Aardonyx	1,62	BS
		Dicraeosaurus	3	D
		Tendaguria	10	T
		Erketu	3,75	T

		Dongyangosaurus	5	T
D	30-39	*Thecodontosaurus*	1	BS
		Seitaad	0,7	BS
		Spinophorosaurus	3,25	E
		Jobaria	8	M
		Amphicoelias	8,3	D
		Suuwassea	3,75	D
	20-29	*Tazoudasaurus*	2,25	E
		Kotasaurus	2,25	E
		Puertasaurus	10	T
E	10	None		
	Zero PDI	*Efraasia*	1,8	P
		Massospondylus	2	P
	Unknown PDI DV	*Vulcanodon*		E
		Cathartesaura		D
		Huanghetitan		T
		Australodocus		T
		Malawisaurus		T
		Janenschia		M
		Tornieria		D
		Sauroposeidon		T
		Seismosaurus		D

Class	PDI% CD	Genera	tail_length (m)	Family
A	90-100	*Saltasaurus*	4	T
	80-89	None		
B	70-79	*Amphicoelias*	16,6	D
	60-69	*Tornieria*	12,5	D
		Nigersaurus	4,5	D
		Amazonsaurus	6	D
		Europasaurus	1,55	M
		Futalognkosaurus	10	T
C	50-59	*Omeisaurus*	6,5	E
		Apatosaurus	10,3	D
		Seismosaurus	18	D
		Cathartesaura	6	D
		Giraffatitan	7	M
	40-49	*Diplodocus*	13,7	D
		Dicraeosaurus	5	D
		Phuwiangosaurus	6,3	T
		Malawisaurus	5,3	T
D	30-39	*Jobaria*	8	M
		Dongyangosaurus	5	T
		Rapetosaurus	5	T
	20-29	*Andesaurus*	6	T
E	10	*Vulcanodon*	3,25	E
		Cetiosaurus	8	E
		Patagosaurus	8,24	E
		Camarasaurus	9	M
		Brachiosaurus	6	M
		Huanghetitan	6	T
		Janenschia	5,6	M
		Neuquensaurus	2,5	T
	Zero PDI	*Plateosaurus*	5	BS
		Ruehleia	5,5	BS

	Thecodontosaurus	1,1	BS
	Massospondylus	1	BS
	Kotasaurus	4,5	E
	Spinophorosaurus	6,5	E
	Suuwassea	7,5	D
	Amargasaurus	6,86	D
	Alamosaurus	7	T

Unknown PDI CD	*Efraasia*	BS
	Eucnemesaurus	BS
	Camelotia	BS
	Aardonyx	BS
	Seitaad	BS
	Antetonitrus	BS
	Tazoudasaurus	E
	Barapasaurus	E
	Rhoetosaurus	E
	Shunosaurus	E
	Mamenchisaurus	E
	Tehuelchesaurus	M
	Haplocanthosaurus	D
	Australodocus	T
	Barosaurus	D
	Euhelopus	M
	Tendaguria	T
	Erketu	T
	Ornithopsis	M
	Eucamerotus	M
	Pleurocoelus	M
	Sauroposeidon	T
	Puertasaurus	T

Table S3. Table of numerical PDI derivation of the sauropod taxa (small sample).

		Efraasia						Plateosaurus			
Cervicals	Dorsals	Sacrals	Caudals	Pelvis	average total	Cervicals	Dorsals	Sacrals	Caudals	Pelvis	average total
0	0	NA	NA	NA	0 Zero	c27	c33	c34	0	d2	3 Gamma
						c112	c60	c42		d3	
						c116	c91	c92		d11	
							c105	c100			
							c116				
							c114				
							c107				
						3	2	5		2	
						3	2	3		5	
						4	2	5		2	
							2	3			
0 Zero	0 Zero					3,333333 Gamma	4	4 Delta	0 Zero	3 Gamma	
							2				
							2				
							2,285714 Beta				

		Ruehleia						Eucnemesaurus			
Cervicals	Dorsals	Sacrals	Caudals	Pelvis	average total	Cervicals	Dorsals	Sacrals	Caudals	Pelvis	average total
c18	c28	c43	0	0	3,57 Gamma	0	c112	NA	NA	NA	3,6 Gamma
c20	c57	c101					c113				
c28	c76						c116				
c34	c92										
c92	c93										
c93	c100										
c100	c101										
c101	c181										
c164											
2	4	4					3				
2	3	4					4				
4	2						4				
5	5										
5	2										
2	3										
3	4										
4	5										
5											
3,5 Gamma	3,5 Gamma	4 Delta	0 Zero	0 Zero		0 Zero	3,6 Gamma				

Table S4. Table of sauropodomorph regional pneumaticity.

Sauropodomorph taxa	Pneumaticity Degree index				
Genus	PDi Cervicals (%)	PDi Dorsals (%)	PDi Sacrals (%)	PDi Caudals (%)	PDi Ilium / Ischium / Pubis (%)
Basal Sauropodomorpha					
Efraasia	Zero degree (0)	Zero degree (0)	Unknown (?)	Unknown (?)	Unknown (?)
Plateosaurus	Gamma (40-59)	Beta (60 - 79)	Delta (20 - 39)	Zero (0)	Gamma (40-59)
Ruehleia	Gamma (40-59)	Gamma (40-59)	Delta (20 - 39)	Zero Degree (0)	Zero Degree (0)
Eucnemesaurus	Zero degree (0)	Gamma (40-59)	Unknown (?)	Unknown (?)	Unknown (?)
Thecodontosaurus	Gamma (40-59)	Delta (20 - 39)	Unknown (?)	Zero Degree (0)	Unknown (?)
Camelotia	Zero degree (0)	Gamma (40-59)	Unknown (?)	Unknown (?)	Unknown (?)
Massospondylus	Zero degree (0)	Zero degree (0)	Zero degree (0)	Zero Degree (0)	Zero Degree (0)
Antetonitrus	Zero degree (0)	Gamma (40-59)	Unknown (?)	Unknown (?)	Unknown (?)
Aardonyx	Zero degree (0)	Gamma (40-59)	Epsilon (1 - 19)	Unknown (?)	Unknown (?)
Seitaad	Unknown (?)	Delta (20 - 39)	Unknown (?)	Unknown (?)	Unknown (?)
Eusauropoda					
Tazoudasaurus	Epsilon (1 - 19)	Delta (20 - 39)	Unknown (?)	Unknown (?)	Unknown (?)
Vulcanodon	Beta (60 - 79)	Unknown (?)	Zero Degree (0)	Epsilon (1 - 19)	Zero Degree (0)
Barapasaurus	Gamma (40-59)	Beta (60 - 79)	Zero Degree (0)	Zero Degree (0)	Zero Degree (0)
Kotasaurus	Delta (20 - 39)	Delta (20 - 39)	Zero Degree (0)	Zero Degree (0)	Zero Degree (0)
Spinophorosaurus	Delta (30 - 50)	Delta (30 - 50)	Zero Degree (0)	Zero Degree (0)	Zero Degree (0)
Jobaria	Beta (60 - 79)	Delta (20 - 39)	Unknown (?)	Delta (20 - 39)	Zero Degree (0)
Rhoetosaurus	Beta (60 - 79)	Beta (60 - 79)	Unknown (?)	Unknown (?)	Unknown (?)
Cetiosaurus	Beta (60 - 79)	Gamma (40-59)	Zero Degree (0)	Epsilon (1- 19)	Zero Degree (0)
Shunosaurus	Beta (60 - 79)	Beta (60 - 79)	Unknown (?)	Unknown (?)	Unknown (?)
Omeisaurus	Beta (60 - 79)	Beta (60 - 79)	Beta (60 - 79)	Gamma (40-59)	Beta (60 - 79)
Patagosaurus	Beta (60 - 79)	Beta (60 - 79)	Unknown (?)	Epsilon (0 - 30)	Unknown (?)
Mamenchisaurus	Beta (60 - 79)	Alpha (80 - 100)	Unknown (?)	Unknown (?)	Unknown (?)
Klamelisaurus	Beta (60 - 79)	Beta (60 - 79)	Unknown (?)	Unknown (?)	Unknown (?)
Diplodocoidea					
Haplocanthosaurus	Delta (20 - 39)	Beta (60 - 79)	Gamma (40-59)	Unknown (?)	Unknown (?)
Amphicoelias	Gamma (40-59)	Gamma (40-59)	Unknown (?)	Beta (60 - 79)	Zero Degree (0)
Apatosaurus	Beta (60 - 79)	Gamma (40-59)	Alpha (80 - 100)	Gamma (40-59)	Zero Degree (0)
Suuwassea	Gamma (40-59)	Delta (20 - 39)	Unknown (?)	Zero Degree (0)	Unknown (?)
Barosaurus	Gamma (40-59)	Beta (60 - 79)	Unknown (?)	Unknown (?)	Zero Degree (0)
Seismosaurus	Unknown (?)	Unknown (?)	Unknown (?)	Gamma (40-59)	Zero Degree (0)
Diplodocus	Beta (60 - 79)	Beta (60 - 79)	Gamma (40-59)	Gamma (40-59)	Zero Degree (0)
Tornieria	Beta (60 - 79)	Unknown (?)	Gamma (40-59)	Beta (60 - 79)	Zero Degree (0)
Dicraeosaurus	Gamma (40-59)	Gamma (40-59)	Beta (60 - 79)	Gamma (40-59)	Zero Degree (0)/Zero Degree (0)/Unknown (?)
Amargasaurus	Beta (60 - 79)	Gamma (40-59)	Unknown (?)	Zero Degree (0)	Unknown (?)
Nigersaurus	Beta (60 - 79)	Alpha (80 - 100)	Unknown (?)	Gamma (40-59)	Unknown (?)
Amazonsaurus	Unknown (?)	Beta (60 - 79)	Unknown (?)	Beta (60 - 79)	Alpha (80 - 100)
Cathartesaura	Gamma (40-59)	Unknown (?)	Unknown (?)	Gamma (40-59)	Unknown (?)
Macronaria					
Janenschia	Gamma (40-59)	Unknown (?)	Unknown (?)	Epsilon (1 - 19)	Zero Degree (0)
Tehuelchesaurus	Unknown (?)	Beta (60 - 79)	Alpha (80 - 100)	Unknown (?)	Unknown (?)
Camarasaurus	Beta (60 - 79)	Alpha (80 - 100)	Beta (60 - 79)	Epsilon (1 - 19)	Zero Degree (0)
Euhelopus	Beta (60 - 79)	Beta (60 - 79)	Alpha (80 - 100)	Unknown (?)	Alpha (80 - 100)/Zero (0)/Zero (0)
Europasaurus	Gamma (40-59)	Gamma (40-59)	Gamma (40-59)	Beta (60 - 79)	Beta(60-79)/Unknown (?)/Zero Degree (0)
Brachiosaurus	Unknown (?)	Alpha (80 - 100)	Beta (60 - 79)	Epsilon (1 - 19)	Zero Degree (0)
Giraffatitan	Beta (60 - 79)	Beta (60 - 79)	Zero Degree (0)	Gamma (40-59)	Zero Degree (0)
Ornithopsis	Unknown (?)	Alpha (80 - 100)	Unknown (?)	Unknown (?)	Unknown (?)
Eucamerotus	Unknown (?)	Beta (60 - 79)	Unknown (?)	Unknown (?)	Unknown (?)
Pleurocoelus	Epsilon (1 - 19)	Beta (60 - 79)	Epsilon (1 - 19)	Unknown (?)	Unknown (?)
Titanosauria					
Australodocus	Gamma (40-59)	Unknown (?)	Unknown (?)	Unknown (?)	Unknown (?)
Sauroposeidon	Beta (60 - 79)	Unknown (?)	Unknown (?)	Unknown (?)	Unknown (?)
Tendaguria	Unknown (?)	Gamma (40-59)	Unknown (?)	Unknown (?)	Unknown (?)
Erketu	Beta (60 - 79)	Gamma (40-59)	Unknown (?)	Unknown (?)	Unknown (?)
Huanghetitan	Unknown (?)	Unknown (?)	Epsilon (1 - 19)	Epsilon (1 - 19)	Unknown (?)
Phuwiangosaurus	Beta (60 - 79)	Gamma (40-59)	Gamma (40-59)	Gamma (40-59)	Zero Degree (0)
Malawisaurus	Delta (20 - 39)	Unknown (?)	Unknown (?)	Epsilon (1 - 19)	Unknown (?)
Andesaurus	Unknown (?)	Alpha (80 - 100)	Zero Degree (0)	Delta (20 - 39)	Zero Degree (0) Zero Degree (0)/Unknown (?)
Dongyangosaurus	Unknown (?)	Gamma (40-59)	Unknown (?)	Delta (20 - 39)	Unknown (?)
Futalognkosaurus	Beta (60 - 79)	Gamma (40-59)	Unknown (?)	Beta (60 - 79)	Beta (60 - 79)
Neuquensaurus	Gamma (40-59)	Beta (60 - 79)	Zero Degree (0)	Epsilon (1 - 19)	Unknown (?)/Unknown (?)/Zero Degree (0)
Saltasaurus	Alpha (80 - 100)	Alpha (80 - 100)	Alpha (80 - 100)	Alpha (80 - 100)	Unknown (?)
Puertasaurus	Delta (20 - 39)	Delta (20 - 39)	Unknown (?)	Unknown (?)	Unknown (?)
Rapetosaurus	Gamma (40-59)	Gamma (40-59)	Gamma (40-59)	Delta (20 - 39)	Zero Degree (0)
Alamosaurus	Beta (60 - 79)	Alpha (80 - 100)	Unknown (?)	Zero Degree (0)	Alpha (80 - 100)
Where:					
Alpha >	Beta >	Gamma >	Delta >	Epsilon >	Zero Degree

Table S5. Probabilities of 'C1c_CV'. Probabilities of pneumaticity character 'C1c_CV' f or each character state ('?', '0', '1') in each of the 60 nodes of the dated phylogeny (referri ng to the modified 'Carballido & Sander, 2014' phylogeny with the 61 pneumaticity taxa). Calculation performed in *RStudio* using the R code and the data from Table S17 below.

	?	0	1
[1,]	0.0213119492	0.9573961859	0.021291865
[2,]	0.0089438868	0.9821338972	0.008922216
[3,]	0.0046005489	0.9908236180	0.004575833
[4,]	0.0031081157	0.9938151483	0.003076736
[5,]	0.0025150928	0.9950141818	0.002470725
[6,]	0.0044613686	0.9911748875	0.004363744
[7,]	0.0066795519	0.9868172235	0.006503225
[8,]	0.0104743089	0.9793685177	0.010157173
[9,]	0.0151874616	0.9701426599	0.014669879
[10,]	0.0140722037	0.9671687730	0.018759023
[11,]	0.0270407918	0.1107773889	0.862181819
[12,]	0.0219590750	0.0839596741	0.894081251
[13,]	0.0274042587	0.1009901155	0.871605626
[14,]	0.0285749055	0.0950988707	0.876326224
[15,]	0.0290732275	0.0849886827	0.885938090
[16,]	0.0307696513	0.0789960536	0.890234295
[17,]	0.0122815233	0.0141158743	0.973602602
[18,]	0.0003644362	0.0005277994	0.999107764
[19,]	0.0004417929	0.0004983720	0.999059835
[20,]	0.0003755391	0.0008478494	0.998776611
[21,]	0.0053267441	0.0054943665	0.989178889
[22,]	0.0013763179	0.0039489974	0.994674685

[23,] 0.0083295967 0.0262752411 0.965395162
[24,] 0.1703538952 0.3078984946 0.521747610
[25,] 0.1287233623 0.3728848729 0.498391765
[26,] 0.0058881876 0.0062387350 0.987873077
[27,] 0.0049220743 0.0051496565 0.989928269
[28,] 0.0884409893 0.4470824790 0.464476532
[29,] 0.0443673100 0.4656777543 0.489954936
[30,] 0.0400670288 0.3877926976 0.572140274
[31,] 0.0904792000 0.4960174595 0.413503341
[32,] 0.0253862557 0.5949846448 0.379629099
[33,] 0.0127274002 0.5696190967 0.417653503
[34,] 0.0038788486 0.0879908495 0.908130302
[35,] 0.0121957776 0.0367533430 0.951050879
[36,] 0.0158187897 0.0363057847 0.947875426
[37,] 0.0125624968 0.0359645040 0.951472999
[38,] 0.0092516872 0.0202186577 0.970529655
[39,] 0.0128349624 0.0197416900 0.967423348
[40,] 0.0258950218 0.0267579799 0.947346998
[41,] 0.0587097336 0.0461514794 0.895138787
[42,] 0.1846110781 0.1218910601 0.693497862
[43,] 0.3140216104 0.1356502364 0.550328153
[44,] 0.4106655045 0.1492199350 0.440114560
[45,] 0.4765219297 0.1645303125 0.358947758
[46,] 0.5702050350 0.1867260742 0.243068891
[47,] 0.6697671247 0.1950713465 0.135161529
[48,] 0.8850176064 0.0674567349 0.047525659
[49,] 0.1770052896 0.3659056213 0.457089089
[50,] 0.1496142683 0.4297282207 0.420657511
[51,] 0.0876507325 0.2147360432 0.697613224
[52,] 0.1826473593 0.4284951138 0.388857527

[53,]	0.2021694935	0.4830879219	0.314742585
[54,]	0.2220126166	0.5292860770	0.248701306
[55,]	0.2384244232	0.5770643962	0.184511181
[56,]	0.1802125365	0.6785745819	0.141212882
[57,]	0.1374857387	0.7534650037	0.109049258
[58,]	0.0532815563	0.8921340782	0.054584366
[59,]	0.0119665515	0.9660824291	0.021951019
[60,]	0.0074155285	0.9737948307	0.018789641

Table S6. Probabilities of 'C8c_CV'. Probabilities of pneumaticity character 'C8c_CV' for each character state ('?', '0', '1') in each of the 60 nodes of the dated phylogeny (referring to the modified 'Carballido & Sander, 2014' phylogeny with the 61 pneumaticity taxa). Calculation performed in *RStudio* using the R code and the data from Table S17 below.

	?	0	1
[1,]	0.3333333	0.3333333	0.3333333
[2,]	0.3333333	0.3333333	0.3333333
[3,]	0.3333333	0.3333333	0.3333333
[4,]	0.3333333	0.3333333	0.3333333
[5,]	0.3333333	0.3333333	0.3333333
[6,]	0.3333333	0.3333333	0.3333333
[7,]	0.3333333	0.3333333	0.3333333
[8,]	0.3333333	0.3333333	0.3333333
[9,]	0.3333333	0.3333333	0.3333333
[10,]	0.3333332	0.3333335	0.3333332
[11,]	0.3333333	0.3333333	0.3333333
[12,]	0.3333325	0.3333350	0.3333325
[13,]	0.3333333	0.3333333	0.3333333
[14,]	0.3333333	0.3333333	0.3333333
[15,]	0.3333333	0.3333333	0.3333333
[16,]	0.3333333	0.3333333	0.3333333

```
[17,] 0.3333333 0.3333334 0.3333333
[18,] 0.3333321 0.3333321 0.3333357
[19,] 0.3332886 0.3332886 0.3334229
[20,] 0.3333333 0.3333333 0.3333334
[21,] 0.3333333 0.3333333 0.3333333
[22,] 0.3333333 0.3333333 0.3333333
[23,] 0.3333333 0.3333333 0.3333333
[24,] 0.3333333 0.3333333 0.3333333
[25,] 0.3333333 0.3333333 0.3333333
[26,] 0.3333331 0.3333337 0.3333332
[27,] 0.3333327 0.3333327 0.3333347
[28,] 0.3333333 0.3333334 0.3333333
[29,] 0.3333332 0.3333332 0.3333336
[30,] 0.3333293 0.3333293 0.3333415
[31,] 0.3333330 0.3333340 0.3333330
[32,] 0.3333242 0.3333508 0.3333250
[33,] 0.3333105 0.3333554 0.3333341
[34,] 0.3331182 0.3331247 0.3337570
[35,] 0.3333333 0.3333333 0.3333333
[36,] 0.3333333 0.3333333 0.3333333
[37,] 0.3333333 0.3333333 0.3333333
[38,] 0.3333333 0.3333333 0.3333333
[39,] 0.3333333 0.3333333 0.3333333
[40,] 0.3333333 0.3333333 0.3333333
[41,] 0.3333333 0.3333333 0.3333333
[42,] 0.3333333 0.3333333 0.3333333
[43,] 0.3333333 0.3333333 0.3333333
[44,] 0.3333333 0.3333333 0.3333333
[45,] 0.3333333 0.3333333 0.3333333
[46,] 0.3333333 0.3333333 0.3333333
```

[47,] 0.3333333 0.3333333 0.3333333
[48,] 0.3333336 0.3333332 0.3333332
[49,] 0.3333333 0.3333333 0.3333333
[50,] 0.3333333 0.3333333 0.3333333
[51,] 0.3333324 0.3333324 0.3333352
[52,] 0.3333333 0.3333333 0.3333333
[53,] 0.3333333 0.3333333 0.3333333
[54,] 0.3333333 0.3333333 0.3333333
[55,] 0.3333333 0.3333334 0.3333333
[56,] 0.3333330 0.3333340 0.3333330
[57,] 0.3333248 0.3333505 0.3333248
[58,] 0.3333333 0.3333333 0.3333333
[59,] 0.3331907 0.3331907 0.3336187
[60,] 0.3294652 0.3294652 0.3410697

Table S7. 'Length' vs 'PDI total'. Results of regression analysis in *RStudio* correlating body length and PDI% total average of the 61 sauropodomorph taxa showing moderately good correlation between them. Results refer to the modified 'Carballido & Sander, 2014' phylogeny with the 61 pneumaticity taxa. Calculation performed in *RStudio* using the R code and the data from Table S22 below.

Residuals:
Min 1Q Median 3Q Max
-0.66398 -0.39385 0.06205 0.21384 0.57508
Branch length transformations:
kappa [Fix] : 1.000
lambda [ML] : 0.663
lower bound : 0.000, p = 0.073028
upper bound : 1.000, p = 0.11316
95.0% CI : (NA, NA)
delta [ML] : 1.305
lower bound : 0.000, p = 2.9147e-08
upper bound : 3.000, p = 0.028743

```
    95.0% CI   : (0.314, 2.784)

Coefficients:
            Estimate Std. Error t value Pr(>|t|)
(Intercept) 2.768513   3.321138  0.8336   0.4185
PDI_total   0.116043   0.067681  1.7146   0.1085

Residual standard error: 0.4129 on 14 degrees of freedom
Multiple R-squared: 0.1735, Adjusted R-squared: 0.1145
F-statistic:  2.94 on 1 and 14 DF,  p-value: 0.1085
```

Table S8. 'Mass' vs 'PDI total'. Results of regression analysis in *RStudio* correlating bod y mass and PDI% total average of the 61 sauropodomorph taxa showing moderate correlation between them. Results refer to the modified 'Carballido & Sander, 20 14' phylogeny with the 61 pneumaticity taxa. Calculation performed in *RStudio* using the R code and the data from Table S22 below.

```
Residuals:
    Min      1Q  Median      3Q     Max
-32.606  -6.190   2.696   8.150  27.417

Branch length transformations:

kappa  [Fix]  : 1.000
lambda [ ML]  : 0.974
   lower bound : 0.000, p = 0.010871
   upper bound : 1.000, p = 0.93813
   95.0% CI   : (0.521, NA)
delta  [ ML]  : 3.000
   lower bound : 0.000, p = 1.5045e-09
   upper bound : 3.000, p = 1
   95.0% CI   : (1.071, NA)

Coefficients:
            Estimate Std. Error t value Pr(>|t|)
(Intercept) -165.342   2794.931 -0.0592   0.9537
PDI_total     37.876     59.342  0.6383   0.5336

Residual standard error: 16.23 on 14 degrees of freedom
Multiple R-squared: 0.02828, Adjusted R-squared: -0.04113
F-statistic: 0.4074 on 1 and 14 DF,  p-value: 0.5336
```

Table S9. 'Length' vs 'PDI CV'. Results of regression analysis in *RStudio* correlating body length and cervical PDI% of the 61 sauropodomorph taxa showing a stro ng correlation between them. Results refer to the modified 'Carballido & Sander, 2014' ph ylogeny with the 61 pneumaticity taxa. Calculation performed in *RStudio* using the R code and the data from Table S22 below.

```
Residuals:
    Min      1Q  Median      3Q     Max
```

```
-1.4973 -0.9043 -0.1691  0.4677  1.5171

Branch length transformations:

kappa  [Fix]  : 1.000
lambda [ ML]  : 0.397
   lower bound : 0.000, p = 0.33243
   upper bound : 1.000, p = 0.041905
   95.0% CI   : (NA, 0.989)
delta  [ ML]  : 0.895
   lower bound : 0.000, p = 1.0435e-07
   upper bound : 3.000, p = 0.0044887
   95.0% CI   : (0.148, 2.134)

Coefficients:
            Estimate Std. Error t value Pr(>|t|)
(Intercept) 1.982562   3.552280  0.5581  0.58558
PDI_cerv    0.148762   0.067956  2.1891  0.04603 *
---
Signif. codes:  0 ‘***’ 0.001 ‘**’ 0.01 ‘*’ 0.05 ‘.’ 0.1 ‘ ’ 1

Residual standard error: 0.9448 on 14 degrees of freedom
Multiple R-squared: 0.255,  Adjusted R-squared: 0.2018
F-statistic: 4.792 on 1 and 14 DF,  p-value: 0.04603
```

Table S10. ‘Mass’ vs ‘PDI CV’. Results of regression analysis in *RStudio* correlating bod y mass and cervical PDI% of the 61 sauropodomorph taxa showing a good correlation bet ween them. Results refer to the modified ‘Carballido & Sander, 2014’ phylogeny with the 61 pneumaticity taxa. Calculation performed in *RStudio* using the R code and the data fro m Table S22 below.

```
Residuals:
    Min      1Q  Median      3Q     Max
-7574.2  -370.2  1305.5  2304.9  3923.0

Branch length transformations:

kappa  [Fix]  : 1.000
lambda [ ML]  : 0.000
   lower bound : 0.000, p = 1
   upper bound : 1.000, p = 0.0040168
   95.0% CI   : (NA, 0.600)
delta  [ ML]  : 0.492
   lower bound : 0.000, p = 7.2108e-07
   upper bound : 3.000, p = 0.008303
   95.0% CI   : (0.033, 2.021)

Coefficients:
            Estimate Std. Error t value Pr(>|t|)
```

```
(Intercept) -3274.14    5977.31 -0.5478  0.59248
PDI_cerv      239.20     101.72  2.3516  0.03386 *
---
Signif. codes:  0 ‘***’ 0.001 ‘**’ 0.01 ‘*’ 0.05 ‘.’ 0.1 ‘ ’ 1

Residual standard error: 3230 on 14 degrees of freedom
Multiple R-squared: 0.2831, Adjusted R-squared: 0.2319
F-statistic:  5.53 on 1 and 14 DF,  p-value: 0.03386
```

Table S11. ‘Length’ vs ‘PDI DV’. Results of regression analysis in *RStudio* correlating body length and dorsal PDI% of the 61 sauropodomorph taxa showing weak correlation between them. Results refer to the modified ‘Carballido & Sander, 2014’ phylogeny with the 61 pneumaticity taxa. Calculation performed in *RStudio* using the R code and the data from Table S22 below.

```
Residuals:
     Min       1Q   Median       3Q      Max
-0.27427 -0.02855  0.04628  0.16044  0.31169

Branch length transformations:

kappa  [Fix]  : 1.000
lambda [ ML]  : 0.816
   lower bound : 0.000, p = 0.013951
   upper bound : 1.000, p = 0.30424
   95.0% CI   : (0.277, NA)
delta  [ ML]  : 1.693
   lower bound : 0.000, p = 1.1791e-08
   upper bound : 3.000, p = 0.12176
   95.0% CI   : (0.480, NA)

Coefficients:
            Estimate Std. Error t value Pr(>|t|)
PDI_dorc    0.088287   0.051325  1.7201   0.1074

Residual standard error: 0.1807 on 14 degrees of freedom
Multiple R-squared: 0.1745, Adjusted R-squared: 0.1155
F-statistic: 2.959 on 1 and 14 DF,  p-value: 0.1074
```

Table S12. ‘Mass’ vs ‘PDI DV’. Results of regression analysis in *RStudio* correlating bod y mass and dorsal PDI% of the 61 sauropodomorph taxa showing a negative and weak co rrelation between them. Results refer to the modified ‘Carballido & Sander, 2014’ phylog eny with the 61 pneumaticity taxa. Calculation performed in *RStudio*

using the R code and the data from Table 22 below.

```
Residuals:
    Min      1Q  Median      3Q     Max
-32.981 -16.265   0.342   6.293  26.649

Branch length transformations:

kappa  [Fix]  : 1.000
lambda [ ML]  : 1.000
   lower bound : 0.000, p = 0.007777
   upper bound : 1.000, p = 1
   95.0% CI   : (0.548, NA)
delta  [ ML]  : 3.000
   lower bound : 0.000, p = 1.2211e-09
   upper bound : 3.000, p = 1
   95.0% CI   : (1.214, NA)

Coefficients:
            Estimate Std. Error t value Pr(>|t|)
(Intercept)  181.073   2756.472  0.0657   0.9486
PDI_dorc      23.807     48.304  0.4928   0.6298

Residual standard error: 16.73 on 14 degrees of freedom
Multiple R-squared: 0.01705,      Adjusted R-squared: -0.05316
F-statistic: 0.2429 on 1 and 14 DF,  p-value: 0.6298
```

Table S13. 'Length' vs 'PDI SV'. Results of regression analysis in *RStudio* correlating body length and sacral PDI% of the 61 sauropodomorph taxa showing a weak correlation between them. Results refer to the modified 'Carballido & Sander, 2014' phylogeny with the 61 pneumaticity taxa. Calculation performed in *RStudio* using the R code and the data from Table 22 below.

```
Residuals:
     Min       1Q   Median       3Q      Max
-0.36970 -0.13364  0.03125  0.18484  0.42899

Branch length transformations:

kappa  [Fix]  : 1.000
lambda [ ML]  : 0.670
   lower bound : 0.000, p = 0.12763
   upper bound : 1.000, p = 0.12194
   95.0% CI   : (NA, NA)
delta  [ ML]  : 1.605
   lower bound : 0.000, p = 3.3432e-08
   upper bound : 3.000, p = 0.1833
   95.0% CI   : (0.322, NA)
```

```
Coefficients:
             Estimate Std. Error t value Pr(>|t|)
(Intercept) 6.085424   2.057447  2.9578  0.01039 *
PDI_sacr    0.060658   0.048671  1.2463  0.23311
---
Signif. codes:  0 ‘***’ 0.001 ‘**’ 0.01 ‘*’ 0.05 ‘.’ 0.1 ‘ ’ 1

Residual standard error: 0.2194 on 14 degrees of freedom
Multiple R-squared: 0.09987,      Adjusted R-squared: 0.03557
F-statistic: 1.553 on 1 and 14 DF,  p-value: 0.2331
```

Table S14. ‘Mass’ vs ‘PDI SV’. Results of regression analysis in *RStudio* correlating body mass and sacral PDI% of the 61 sauropodomorph taxa showing a negative and very weak correlation between them. Results refer to the modified ‘Carballido & Sander, 2014’ phylogeny with the 61 pneumaticity taxa. Calculation performed in *RStudio* using the R code and the data from Table S22 below.

```
Residuals:
    Min      1Q  Median      3Q     Max
-33.652 -16.514  -4.030   4.109  26.191

Branch length transformations:

kappa  [Fix]  : 1.000
lambda [ ML]  : 1.000
   lower bound : 0.000, p = 0.013277
   upper bound : 1.000, p = 1
   95.0% CI   : (0.519, NA)
delta  [ ML]  : 3.000
   lower bound : 0.000, p = 1.0313e-09
   upper bound : 3.000, p = 1
   95.0% CI   : (1.301, NA)
Coefficients:
             Estimate Std. Error t value Pr(>|t|)
(Intercept) 1569.457   2038.355  0.7700   0.4541
PDI_sacr     -13.507     61.280 -0.2204   0.8287

Residual standard error: 16.85 on 14 degrees of freedom
Multiple R-squared: 0.003458,      Adjusted R-squared: -0.06772
F-statistic: 0.04858 on 1 and 14 DF,  p-value: 0.8287
```

Table S15. ‘Length’ vs ‘PDI CD’. Results of regression analysis in *RStudio* correlating body length and caudal PDI% of the 61 sauropodomorph taxa showing a stron g correlation between them. Results refer to the modified ‘Carballido & Sander, 2014’ phyl ogeny with the 61 pneumaticity taxa. Calculation performed in *RStudio* using the R code and the data from Table S22 below.

```
pgls(formula = Length ~ PDI_caud, data = pnusize, lambda = "ML",
    delta = "ML")

Residuals:
     Min       1Q   Median       3Q      Max
-0.46482 -0.26556 -0.01756  0.22929  0.72182

Branch length transformations:

kappa  [Fix]  : 1.000
lambda [ ML]  : 0.000
   lower bound : 0.000, p = 1
   upper bound : 1.000, p = 0.035539
   95.0% CI   : (NA, 0.978)
delta  [ ML]  : 1.287
   lower bound : 0.000, p = 1.0176e-06
   upper bound : 3.000, p = 0.047597
   95.0% CI   : (0.027, 2.984)

Coefficients:
            Estimate Std. Error t value  Pr(>|t|)
(Intercept) 7.543821   1.721229  4.3828 0.0006252 ***
PDI_caud    0.170067   0.051433  3.3066 0.0051940 **
---
Signif. codes:  0 ‘***’ 0.001 ‘**’ 0.01 ‘*’ 0.05 ‘.’ 0.1 ‘ ’ 1

Residual standard error: 0.3793 on 14 degrees of freedom
Multiple R-squared: 0.4385, Adjusted R-squared: 0.3984
F-statistic: 10.93 on 1 and 14 DF,  p-value: 0.005194
```

Table S16. ‘Mass’ vs ‘PDI CD’. Results of regression analysis in *RStudio* correlating bod y mass and caudal PDI% of the 61 sauropodomorph taxa showing a strong correlation between them. Results refer to the modified ‘Carballido & Sander, 2014’ phylogeny with the 61 pneumaticity taxa. Calculation performed in *RStudio* using the R co de and the data from Table S22 below.

```
pgls(formula = Mass ~ PDI_caud, data = pnusize, lambda = "ML",
    delta = "ML")

Residuals:
    Min      1Q  Median      3Q     Max
-28.990  -7.676   2.763   8.969  22.280

Branch length transformations:

kappa  [Fix]  : 1.000
lambda [ ML]  : 0.000
   lower bound : 0.000, p = 1
   upper bound : 1.000, p = 0.14124
   95.0% CI   : (NA, NA)
delta  [ ML]  : 3.000
```

```
   lower bound : 0.000, p = 1.1195e-07
   upper bound : 3.000, p = 1
   95.0% CI   : (0.246, NA)

Coefficients:
            Estimate Std. Error t value Pr(>|t|)
(Intercept)  1493.44    1249.66  1.1951 0.251911
PDI_caud      248.81      71.73  3.4687 0.003762 **
---
Signif. codes:  0 ‘***’ 0.001 ‘**’ 0.01 ‘*’ 0.05 ‘.’ 0.1 ‘ ’ 1

Residual standard error: 13.27 on 14 degrees of freedom
Multiple R-squared: 0.4622, Adjusted R-squared: 0.4238
F-statistic: 12.03 on 1 and 14 DF,  p-value: 0.003762
```

Table S17. ‘Neck length’ vs ‘PDI CV’. Results of regression analysis in *RStudio* correlating length of neck and cervical PDI% of the 61 sauropodomorph taxa showing a st rong correlation between them. Results refer to the modified ‘Carballido & Sander, 2014’ p hylogeny with the 61 pneumaticity taxa. Calculation performed in *RStudio* using the R cod e and the data from Table S22 below.

```
Residuals:
     Min       1Q   Median       3Q      Max
-1.24299 -0.17317  0.05798  1.11271  1.75022

Branch length transformations:

kappa  [Fix]  : 1.000
lambda [ ML]  : 0.000
   lower bound : 0.000, p = 1
   upper bound : 1.000, p = 0.00097929
   95.0% CI   : (NA, 0.570)
delta  [ ML]  : 0.228
   lower bound : 0.000, p = 2.586e-06
   upper bound : 3.000, p = 0.00018524

   95.0% CI   : (0.010, 1.063)
Coefficients:
            Estimate Std. Error t value Pr(>|t|)
(Intercept) 1.049741   1.123441  0.9344  0.36594
PDI_cerv    0.040481   0.018432  2.1962  0.04542 *
---
Signif. codes:  0 ‘***’ 0.001 ‘**’ 0.01 ‘*’ 0.05 ‘.’ 0.1 ‘ ’ 1
```

```
Residual standard error: 0.9918 on 14 degrees of freedom
Multiple R-squared: 0.2562, Adjusted R-squared: 0.2031
F-statistic: 4.823 on 1 and 14 DF,  p-value: 0.04542
```

Table S18. 'Trunk length' vs 'PDI DV'. Results of regression analysis in *RStudio* correlating length of trunk and dorsal PDI% of the 61 sauropodomorph taxa showing a we ak correlation between them. Results refer to the modified 'Carballido & Sander, 2014' ph ylogeny with the 61 pneumaticity taxa. Calculation performed in *RStudio* using the R code and the data from Table S22 below.

```
Residuals:
    Min      1Q  Median      3Q     Max
-1.1740 -0.4390  0.1623  0.4206  1.2261

Branch length transformations:

kappa  [Fix]  : 1.000
lambda [ ML]  : 0.000
   lower bound : 0.000, p = 1
   upper bound : 1.000, p = 0.00068444
   95.0% CI   : (NA, 0.529)
delta  [ ML]  : 0.254
   lower bound : 0.000, p = 2.0271e-06
   upper bound : 3.000, p = 0.0091574
   95.0% CI   : (0.012, 1.444)

Coefficients:
            Estimate Std. Error t value Pr(>|t|)
(Intercept) 1.979454   0.833883  2.3738  0.03246 *
PDI_dorc    0.020804   0.013829  1.5044  0.15470
---
Signif. codes:  0 '***' 0.001 '**' 0.01 '*' 0.05 '.' 0.1 ' ' 1

Residual standard error: 0.7283 on 14 degrees of freedom
Multiple R-squared: 0.1392, Adjusted R-squared: 0.07767
F-statistic: 2.263 on 1 and 14 DF,  p-value: 0.1547
```

Table S19. 'Tail length' vs 'PDI CD'. Results of regression analysis in *RStudio* correlating length of tail and caudal PDI% of the 61 sauropodomorph taxa showing a negative and weak correlation between them. Results refer to the modified 'Carballido & Sander, 2014' phylogeny with the 61 pneumaticity taxa. Calculation perform ed in *RStudio* using the R code and the data from Table S22 below.

```
pgls(formula = taill ~ PDI_caud, data = pnusize, lambda = "M
L",
    delta = "ML")

Residuals:
```

```
      Min        1Q    Median        3Q       Max
-0.289204 -0.004229  0.058901  0.082596  0.160947

Branch length transformations:

kappa  [Fix]  : 1.000
lambda [ ML]  : 0.000
   lower bound : 0.000, p = 1
   upper bound : 1.000, p = 0.01697
   95.0% CI   : (NA, 0.958)
delta  [ ML]  : 1.462
   lower bound : 0.000, p = 4.3177e-07
   upper bound : 3.000, p = 0.18422
   95.0% CI   : (0.054, NA)

Coefficients:
            Estimate Std. Error t value Pr(>|t|)
(Intercept) 4.307531   0.694347  6.2037  2.3e-05 ***
PDI_caud    0.020249   0.021903  0.9245   0.3709
---
Signif. codes:  0 ‘***’ 0.001 ‘**’ 0.01 ‘*’ 0.05 ‘.’ 0.1 ‘ ’ 1

Residual standard error: 0.1112 on 14 degrees of freedom
Multiple R-squared: 0.05754,       Adjusted R-squared: -0.009781
F-statistic: 0.8547 on 1 and 14 DF,  p-value: 0.3709
```

Table S20. 'Femur length' vs 'PDI_total'. Results of regression analysis in *RStudio* correlating length of the femur and total average PDI% of the 61 sauropodomorph taxa showing weak correlation between them. Results refer to the modified 'Carballido & Sander, 2014' phylogeny with the 61 pneumaticity taxa. Calculation performed in *RStudio* using the R code and the data from Table S22 below.

```
pgls(formula = FL ~ PDI_total, data = pnusize, lambda = "ML"
,
    delta = "ML")

Residuals:
      Min        1Q    Median        3Q       Max
-0.099747 -0.045284 -0.024032  0.000904  0.121187

Branch length transformations:

kappa  [Fix]  : 1.000
lambda [ ML]  : 0.571
   lower bound : 0.000, p = 0.14792
   upper bound : 1.000, p = 0.0339
   95.0% CI   : (NA, 0.985)
delta  [ ML]  : 1.111
   lower bound : 0.000, p = 6.5939e-08
   upper bound : 3.000, p = 0.009713
   95.0% CI   : (0.209, 2.451)

Coefficients:
             Estimate Std. Error t value Pr(>|t|)
(Intercept) 0.3408802  0.3297799  1.0337   0.3188
PDI_total   0.0089299  0.0065471  1.3640   0.1941

Residual standard error: 0.0584 on 14 degrees of freedom
Multiple R-squared: 0.1173, Adjusted R-squared: 0.05425
F-statistic:  1.86 on 1 and 14 DF,  p-value: 0.1941
```

Table S21. 'Estimated First Appearance Date (FAD)' vs 'PDI_total'.
Results of regression analysis in *RStudio* correlating evolutionary time in the form of first appearance date and total average PDI% of the 61 sauropodomorph taxa showing a very strong correlation between them. Results refer to the modified 'Carballido & Sander, 2014' phylogeny with the 61 pneumaticity taxa. Calculation performed in *RStudio* using the R code and the data from Table S22 below.

```
pgls(formula = FAD ~ PDI_total, data = pnusize, lambda = "ML
",
    delta = "ML")

Residuals:
     Min       1Q   Median       3Q      Max
-1.39535 -0.18468  0.06935  0.27504  1.27414

Branch length transformations:
```

```
kappa  [Fix]  : 1.000
lambda [ ML]  : 1.000
   lower bound : 0.000, p = 2.0657e-07
   upper bound : 1.000, p = 1
   95.0% CI   : (0.916, NA)
delta  [ ML]  : 1.569
   lower bound : 0.000, p = 2.4604e-09
   upper bound : 3.000, p = 0.019675
   95.0% CI   : (0.631, 2.740)

Coefficients:
             Estimate Std. Error t value  Pr(>|t|)
(Intercept) 228.10382    8.98654 25.3828 4.161e-13 ***
PDI_total    -0.39703    0.18532 -2.1424   0.05022 .
---
Signif. codes:  0 ‘***’ 0.001 ‘**’ 0.01 ‘*’ 0.05 ‘.’ 0.1 ‘ ’
1

Residual standard error: 0.7261 on 14 degrees of freedom
Multiple R-squared: 0.2469, Adjusted R-squared: 0.1931
F-statistic:  4.59 on 1 and 14 DF,  p-value: 0.05022
```

Table S22. The "'Sauropod_Data_Table'.csv" data table used in *RStudio*.

Taxon	FAD	LAD	Length	Mass	PDI_cerv	PDI_dorc	PDI_sacr	PDI_caud	PDI_total	C1c_CV	C8c_CV	neckl	trunkl	taill	FL
Efraasia	215.5	212	6.5	700	0	0	NA	NA	0	0	0	2.61	3.05	6.1	0.226
Plateosaurus	215.5	201.3	8.5	1073	53	75	39	0	59	0	0	1	1.8	3.5	0.75
Ruehleia	228	208.5	10	1000	49	49	39	0	49	0	0	1.2	2	5	N/A
Eucnemesaurus	228	201.3	6	500	0	47	NA	NA	47	0	0	1.5	2.7	5.5	N/A
Thecodontosaurus	208.5	190.8	2.6	24.6	49	39	0	0	47	0	0	1.2	1.5	3	0.28
Camelotia	208.5	201.3	10	2500	0	49	NA	NA	49	0	0	0.5	1	1.1	0.98
Massospondylus	228	190.8	4	136.7	0	0	0	0	0	0	0	2.3	2.5	5	0.33
Aardonyx	201.3	190.8	6.5	1000	0	45	10	NA	39	0	0	1	2	1	0.68
Seitaad	190.8	174.1	2.8	80	NA	39	NA	NA	39	?	?	1.4	1.62	3.25	N/A
Antetonitrus	228	201.3	12.2	5000	0	43	NA	NA	43	0	0	0.5	0.7	1.4	0.794
Vulcanodon	201.3	199.3	6.5	3500	79	NA	0	10	39	1	0	1.4	1.62	3.25	1.1
Tazoudasaurus	190.8	174,1	9.5	5000	10	25	NA	NA	23	0	0	2	2.25	4.5	N/A
Barapasaurus	199.3	182.7	12	7000	49	75	NA	NA	69	1	0	2.6	3	6	1.36
Kotasaurus	199.3	182.7	9	5000	23	25	0	0	23	0	0	2	2.25	4.5	1.13
Spinophorosaurus	174.1	163.5	13	7000	37	39	0	0	37	1	0	2.85	3.25	6.5	N/A
Rhoetosaurus	170.3	168.3	15	9000	67	67	NA	NA	67	1	1	7.65	8	8	N/A
Cetiosaurus	171.6	122.4	16	15800	79	59	0	10	53	1	0	3.45	3.75	7.5	1.61
Shunosaurus	168.3	166.1	8.7	4793.5	67	67	NA	NA	67	1	1	4	4	8	1.25
Omeisaurus	168.3	163.5	20	11796	60	60	65	59	60	1	1	3	2.5	3.2	1.31
Jobaria	174.1	145	24	16000	65	35	NA	39	53	1	1	7.3	6.2	6.5	1.8
Patagosaurus	166.1	163.5	15	9435	79	71	NA	10	59	1	0	3.72	4.12	8.24	1.54
Mamenchisaurus	163.5	152.1	21	18169.7	77	100	NA	NA	90	1	1	5.5	4.75	4.75	0.86
Tehuelchesaurus	157.3	150.8	15	9000	NA	67	90	NA	71	?	?	9	6	6	1.53
Haplocanthosaurus	157.3	145	14	14528.6	35	63	49	NA	47	1	0	4	3	7	1.74
Amphicoelias	157.3	150.8	25	18170	57	39	NA	79	63	1	1	8.3	8.3	16.6	1.77
Australodocus	152.1	145	17	4000	55	NA	NA	NA	55	1	1	5.2	5.5	10.3	N/A
Apatosaurus	157.3	150.8	21	22407.2	69	55	90	55	63	0	1	3.45	3.75	7.5	2.5
Suuwassea	155.7	145	15	5950	47	39	NA	0	45	0	1	6.5	6.5	13	N/A
Barosaurus	157.3	145	26	20039.5	59	79	NA	NA	59	1	1	12	10	18	1.44
Seismosaurus	157.3	145	40	49275.5	NA	NA	NA	51	51	?	?	6	6	13.7	N/A
Diplodocus	157.3	150.8	25.7	19654.6	69	69	59	47	63	0	0	6	6.25	12.5	1.54
Tornieria	155.7	145	25	20000	79	NA	43	69	60	0	0	4	3	5	1.36
Dicraeosaurus	163.5	150.8	12	5700	55	49	60	45	53	1	1	3.13	3.43	6.86	1.22
Amargasaurus	129.4	122.4	10,3	6852.9	60	51	NA	0	59	1	0	2	2.25	4.5	1.05
Nigersaurus	118	110	9	2000	53	80	NA	67	69	0	1	2.6	3	6	N/A
Amazonsaurus	125	100.5	12	5000	NA	71	NA	67	73	?	?	2.6	3	6	N/A
Cathartesaura	99.6	89.8	12	5000	55	NA	NA	51	55	0	0	6.9	3.75	4.35	1.38
Klamelisaurus	163.5	157.3	15	5000	79	79	NA	NA	79	1	0	5.3	5.6	5.6	1.2
Camarasaurus	157.3	150.8	15.4	18413	75	90	79	10	75	1	1	6	4.27	5.13	1.8
Euhelopus	129.4	112	11	4000	67	75	96	NA	75	1	0	5.5	2.75	2.55	0.95
Europasaurus	157.3	152.1	6,2	800	59	55	59	65	59	1	1	3.1	1.55	1.55	0.316
Tendaguria	152.1	145	30	48000	NA	49	NA	NA	49	?	?	8	7	6	N/A
Brachiosaurus	157.3	150.8	21	28264.6	NA	100	79	10	90	?	?	9	8	7	2
Giraffatitan	157.3	150.8	24	38000	73	63	0	55	69	1	1	7.5	3.75	3.45	1.91
Erketu	100.5	86.3	15	5000	63	45	NA	NA	59	0	0	7.5	3.75	3.45	N/A
Ornithopsis	164.7	122.4	15	8000	NA	90	NA	NA	90	?	?	7.5	3.75	3.45	N/A
Eucamerotus	164.7	122.4	15	8000	NA	65	NA	NA	65	?	?	5.6	5.6	5.6	N/A
Pleurocoelus	166.1	125	15	12000	10	69	10	NA	45	0	0	9.5	10	10	N/A
Huanghetitan	100.5	86.3	22	32000	NA	NA	10	10	10	?	?	6	6.3	6.3	N/A
Sauroposeidon	125	113	27	40000	60	NA	NA	NA	60	0	1	5	5.3	5.3	N/A
Janenschia	152.1	145	17	10000	51	NA	NA	10	45	1	1	12	7.5	7.5	1.33
Phuwiangosaurus	129.4	112	19	17000	60	57	55	49	57	1	0	3.45	3.75	7.5	1.25
Malawisaurus	125	113	16	10000	55	NA	NA	47	51	0	0	7	7	8	N/A
Andesaurus	100.5	93.9	18	7000	NA	90	0	29	84	?	?	5.7	6	6	1.55
Dongyangosaurus	100.5	88	15	7000	NA	45	NA	39	45	?	?	4.8	5	5	N/A
Futalognkosaurus	93.5	85.8	30	45000	65	51	NA	67	63	0	0	9.5	10	10	N/A
Neuquensaurus	86.3	72.1	7,5	3500	55	67	0	10	60	0	0	2.3	2.5	2.5	0.7
Saltasaurus	70.6	66	12	4000	92	90	100	100	96	0	0	3.8	4	4	0.87
Puertasaurus	70.6	66	30	45000	33	29	NA	NA	31	0	0	9.5	10	10	N/A
Rapetosaurus	72.1	66	15	8000	57	57	51	39	55	0	1	4.8	5	5	0.68
Alamosaurus	83.5	66	20	16000	79	96	NA	0	88	1	0	6.6	6	7	N/A

Tree figures

Tracing of 8 more pneumaticity characters; C1c (pleurocoel in centrum) for the dorsal vertebrae and C8c (pleurocoelous fossa in centrum) for the cervical and dorsal regions, C1c and C33ns (foramen on the neural spine) for the sacral region, C3c (foramen in centrum) and C4c (fossa in centrum) for the caudal region and D2 (foramen in ilium)] can be viewed in Figures 26b-26i below. The justification to choose this phylogeny is none other than the fact that this tree contains the largest number of taxa in a tree so far, hence it will reveal a broader spectrum of the occurrence and evolution of certain key pneumaticity characters.

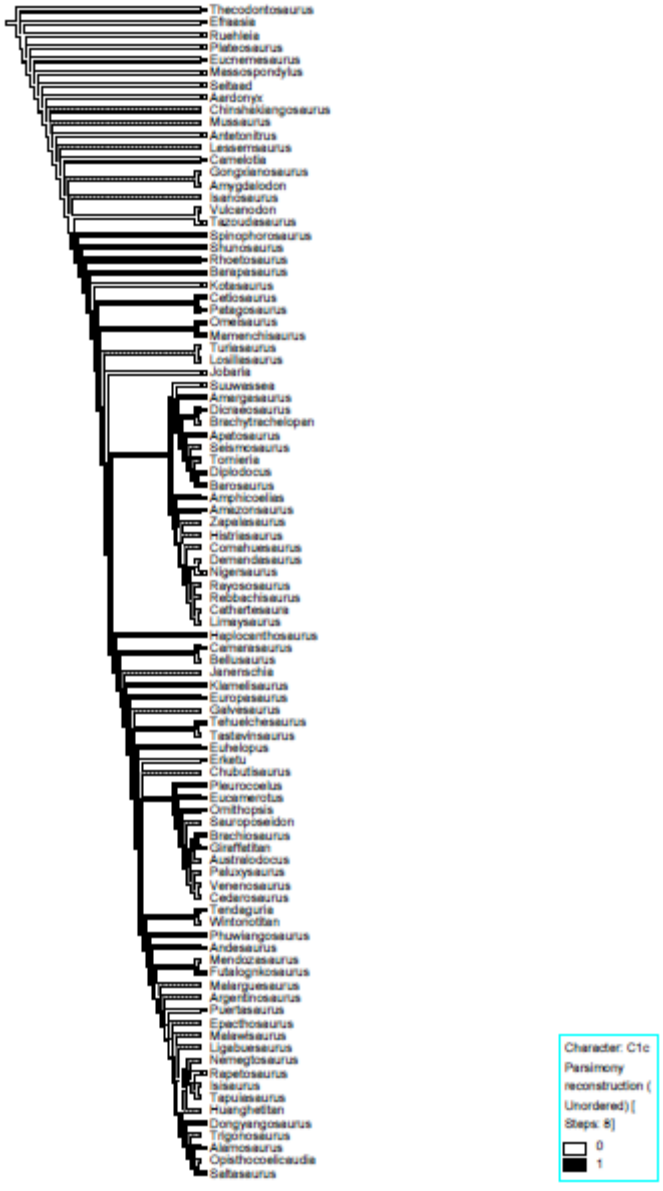

Figure 26b. Evolution of character ‘C1c’ (dorsal) in the composite extended phylogeny of ‘Carballido & Sander (2014)’ across 95 taxa under parsimony. Grey branches indicate ‘unknown’ data.

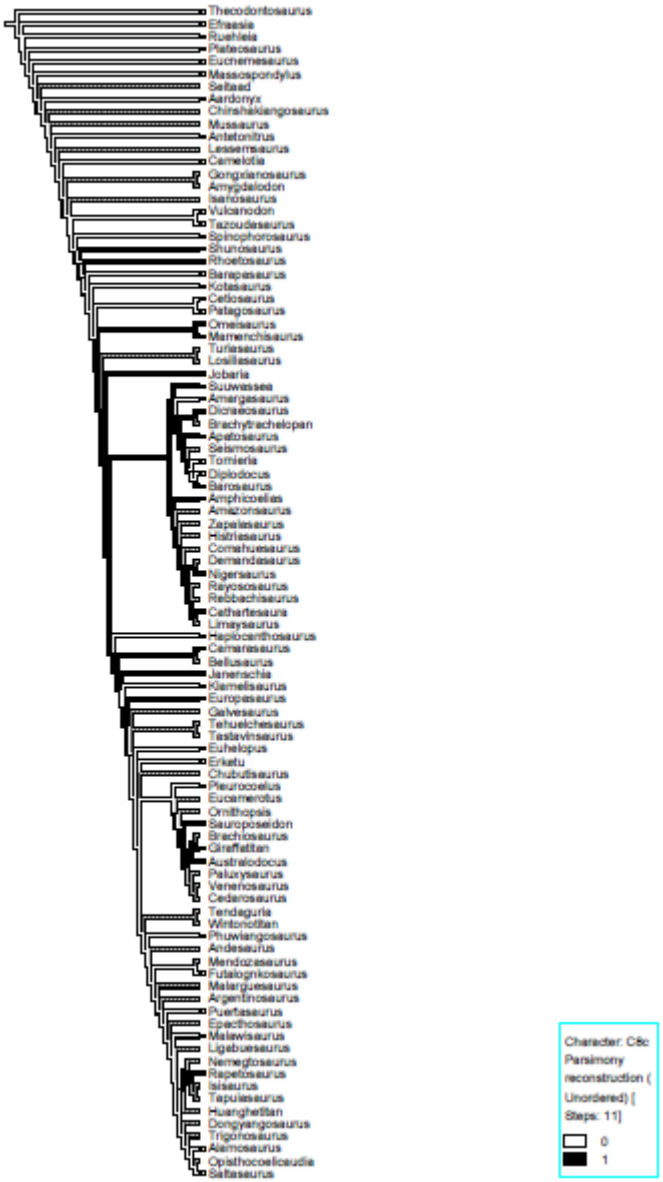

Figure 26c. Evolution of character ‘C8c’ (cervical) in the composite extended phylogeny of ‘Carballido & Sander (2014)’ across 95 taxa under parsimony. Grey branches indicate ‘unknown’ data.

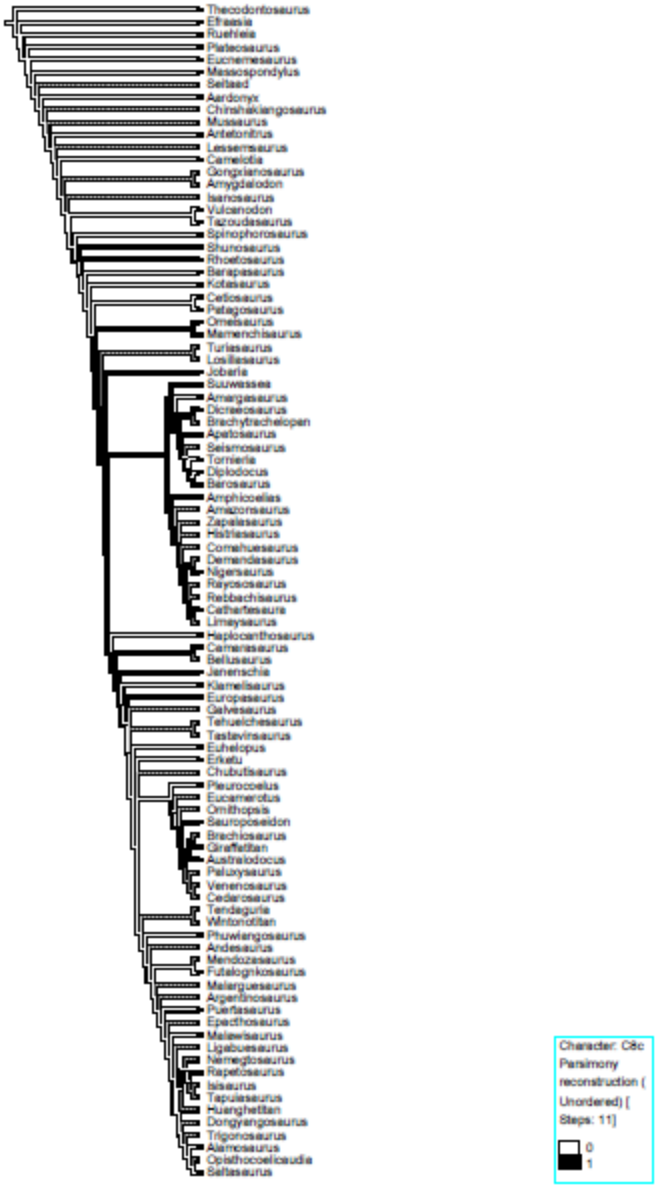

Figure 26d. Evolution of character ‘C8c’ (dorsal) in the composite extended phylogeny of ‘Carballido & Sander (2014)’ across 95 taxa under parsimony. Grey branches indicate ‘unknown’ data.

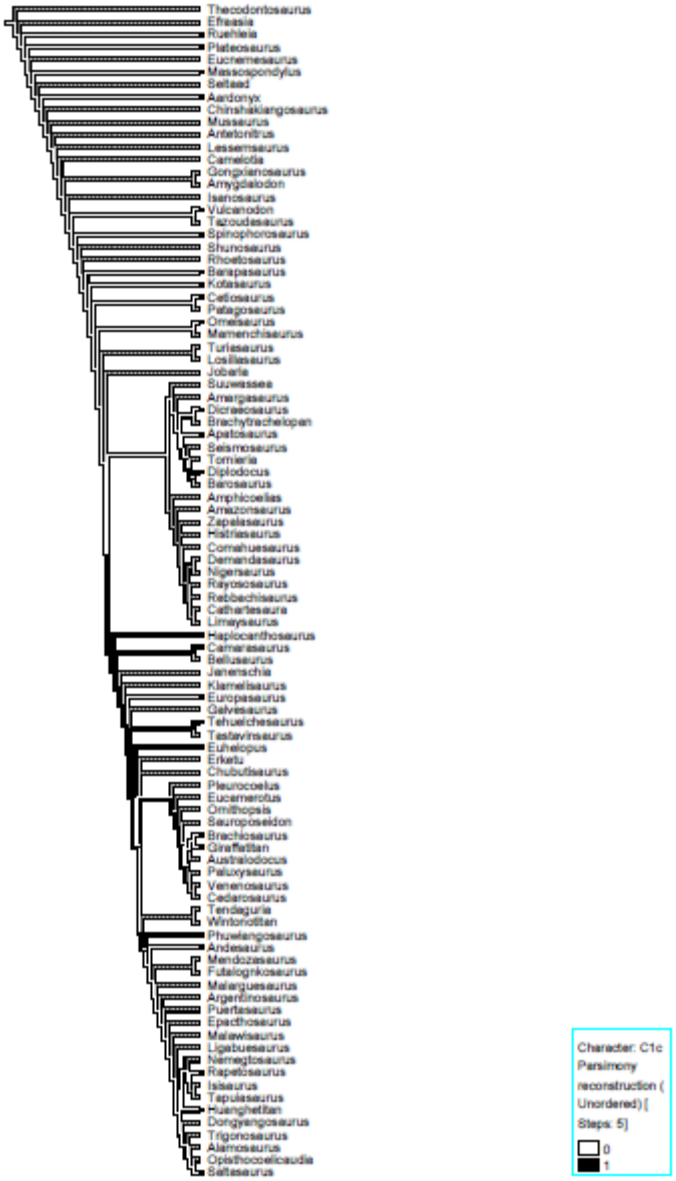

Figure 26e. Evolution of character ‘C1c’ (sacral) in the composite extended phylogeny of ‘Carballido & Sander (2014)’ across 95 taxa under parsimony. Grey branches indicate ‘unknown’ data.

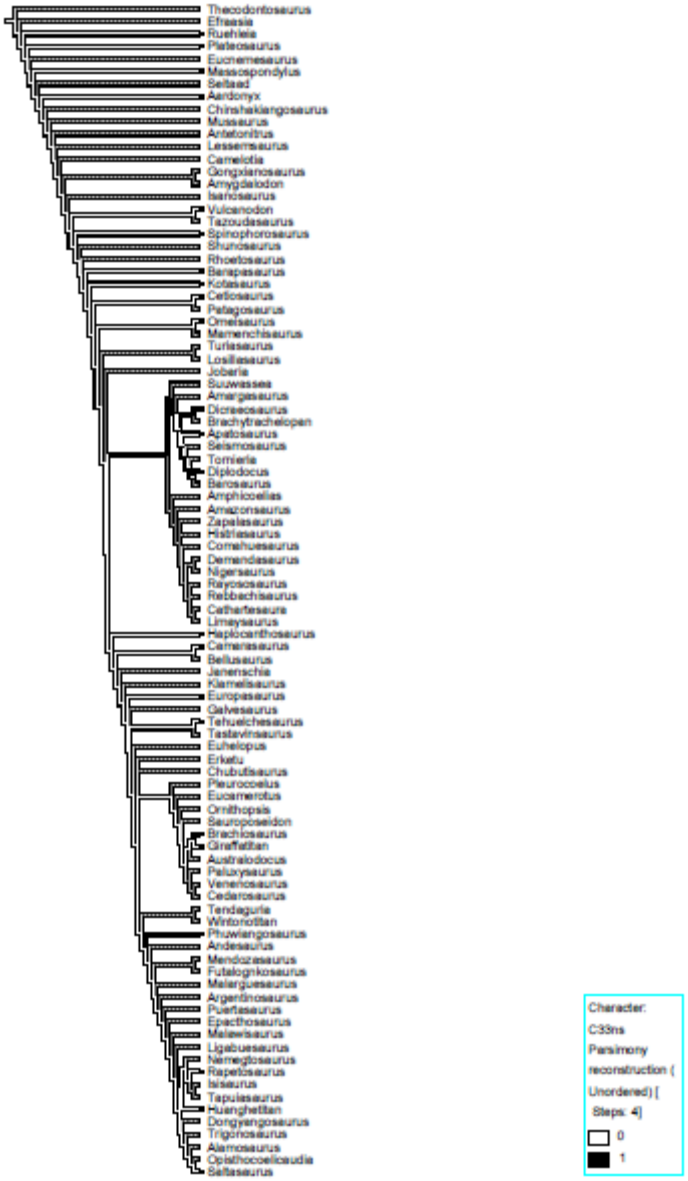

Figure 26f. Evolution of character ‘C33ns’ (sacral) in the composite extended phylogeny of ‘Carballido & Sander (2014)’ across 95 taxa under parsimony. Grey branches indicate ‘unknown’ data.

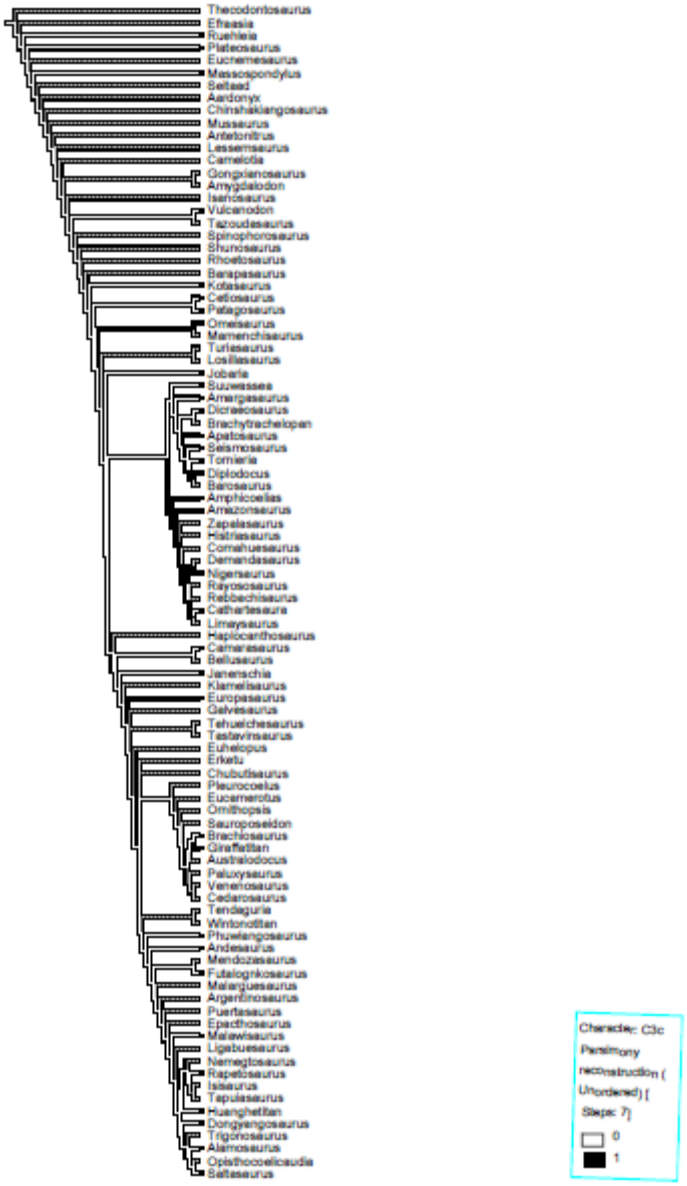

Figure 26g. Evolution of character ‘C3c’ (caudal) in the composite extended phylogeny of ‘Carballido & Sander (2014)’ across 95 taxa under parsimony. Grey branches indicate ‘unknown’ data.

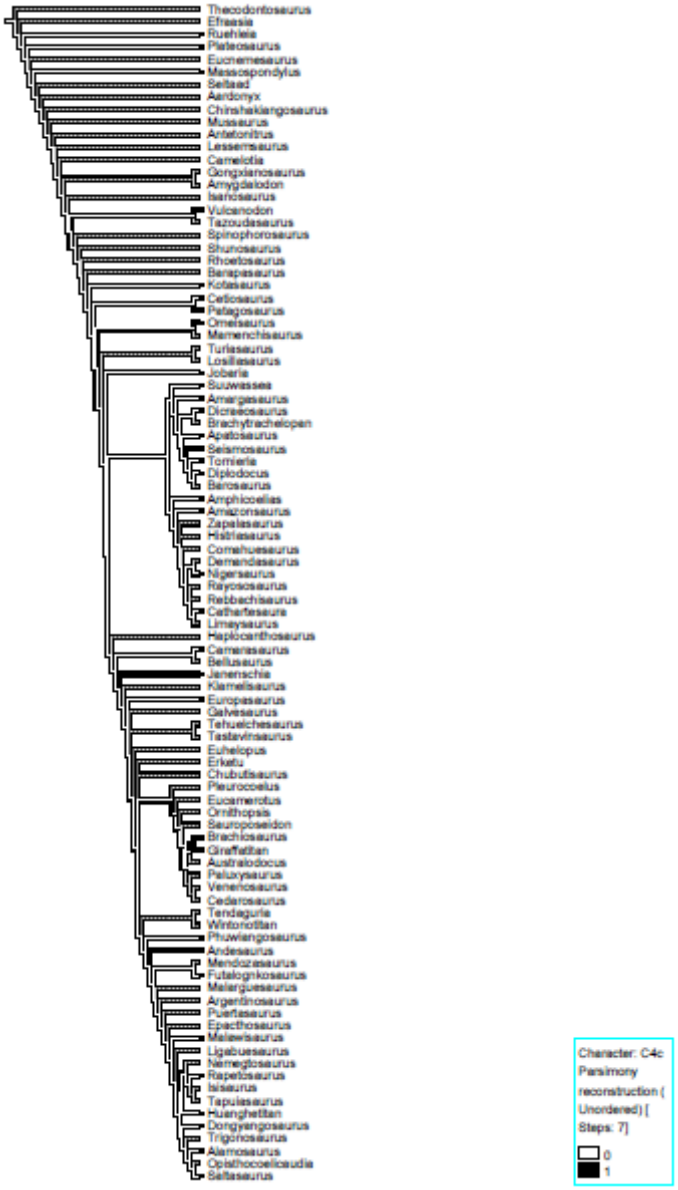

Figure 26h. Evolution of character ‘C4c’ (caudal) in the composite extended phylogeny of ‘Carballido & Sander (2014)’ across 95 taxa under parsimony. Grey branches indicate ‘unknown’ data.

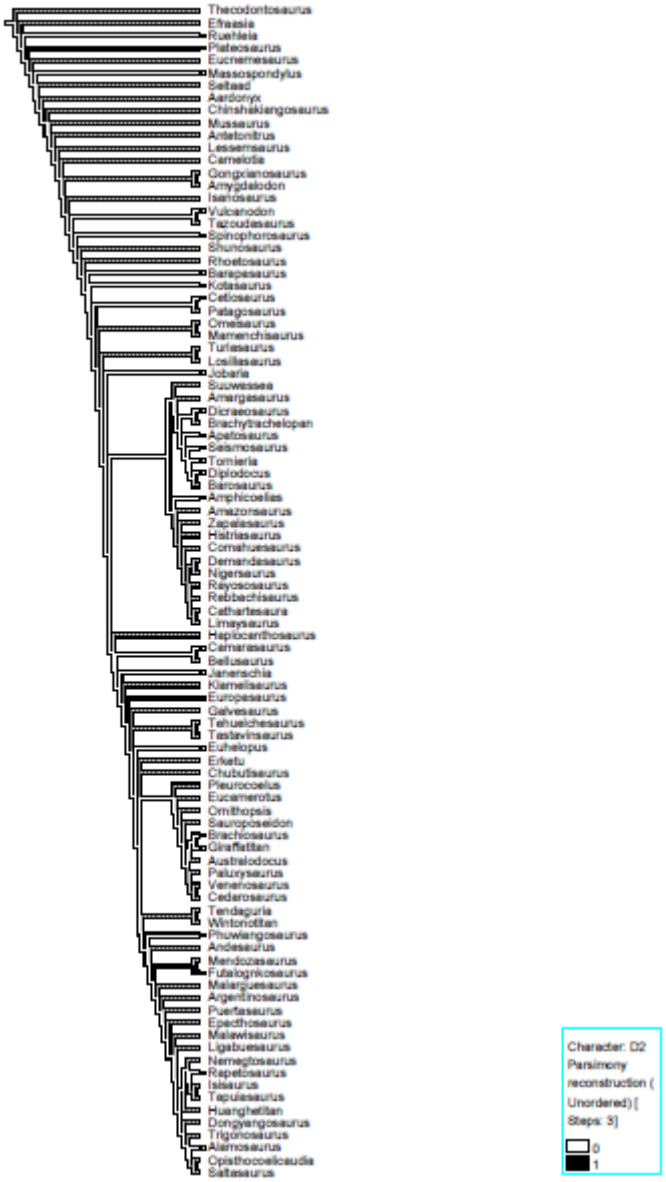

Figure 26i. Evolution of character ‘D2’ (pelvic) in the composite extended phylogeny of ‘Carballido & Sander (2014)’ across 95 taxa under parsimony. Grey branches indicate ‘unknown’ data.

Below are presented 8 more pneumaticity characters [(C1c (pleurocoel in centrum) for the dorsal vertebrae and C8c (pleurocoelous fossa in centrum) for the cervical and dors al regions, C1c and C33ns (foramen on the neural spine) for the sacral region, C3c (foram en in centrum) and C4c (fossa in centrum) for the caudal region and D2 (foramen in ilium)] seen in Figures 42b-42i below. This will provide a concise and thorough view of the oc currence and evolution of pneumaticity of this project’s 61 studied sauropodomorph taxa under a phylogenetic scope.

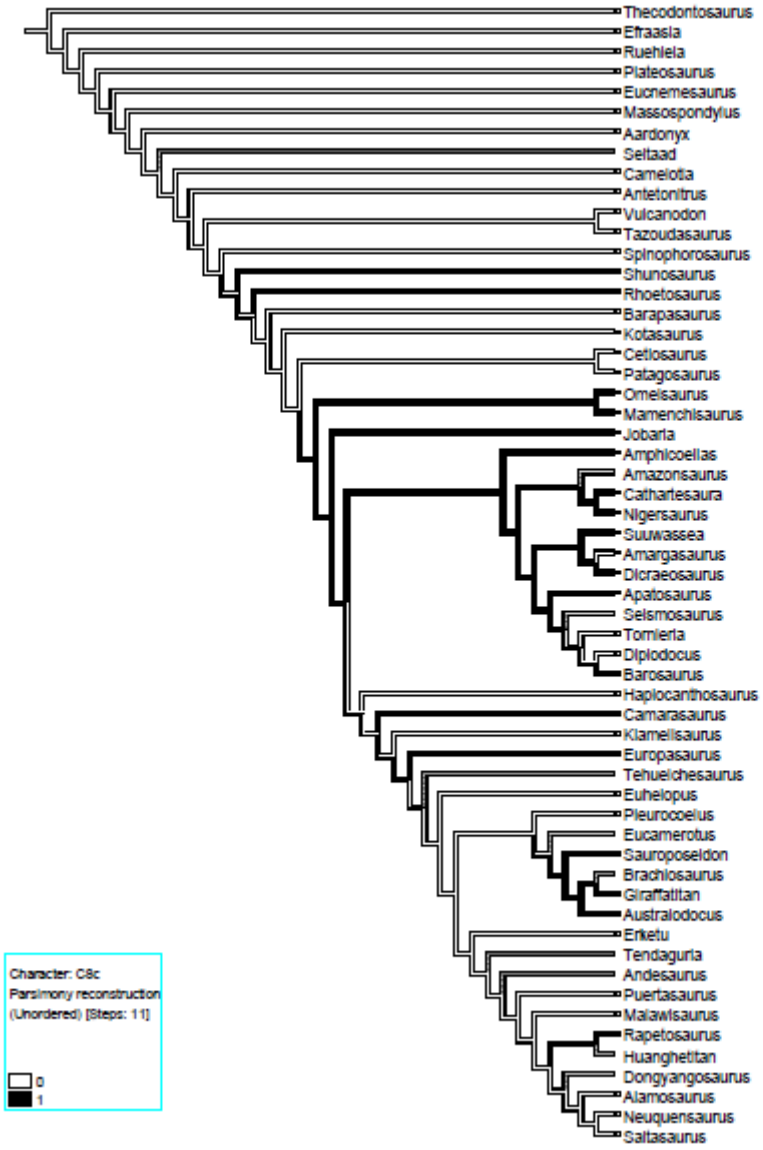

Figure 41b. Reconstruction of character ‘C8c’ (cervical) on the 61 pneumatically studied taxa, placed in a phylogeny based on ‘Carballido & Sander (2014)’. Grey branches indicate ‘unknown’ data.

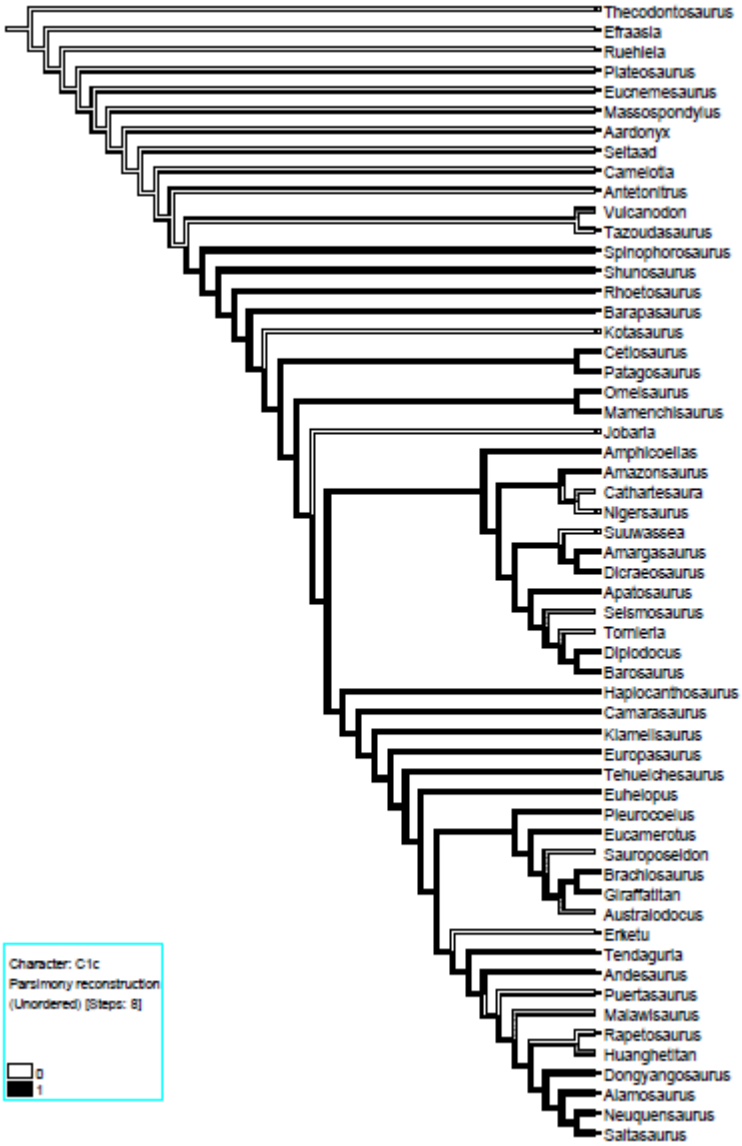

Figure 41c. Reconstruction of character ‘C1c’ (dorsal) on the 61 pneumatically studied taxa, placed in a phylogeny based on ‘Carballido & Sander (2014)’. Grey branches indicate ‘unknown’ data.

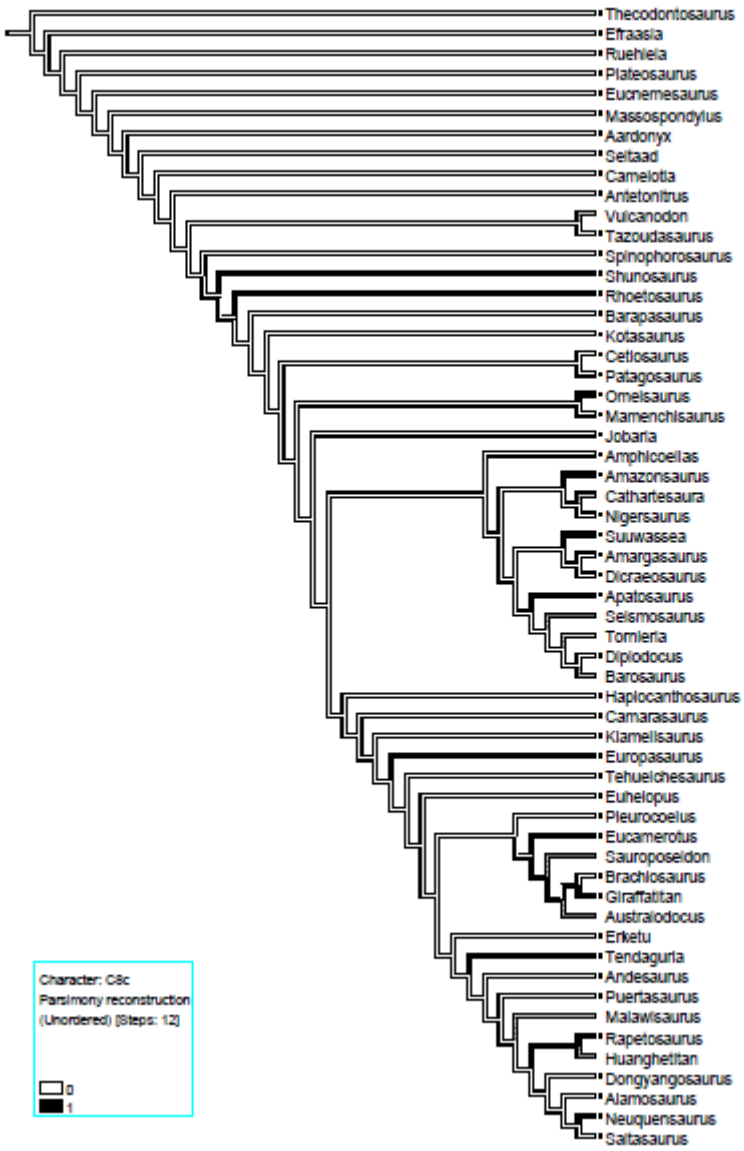

Figure 41d. Reconstruction of character ‘C8c’ (dorsal) on the 61 pneumatically studied taxa, placed in a phylogeny based on ‘Carballido & Sander (2014)’. Grey branches indicate ‘unknown’ data.

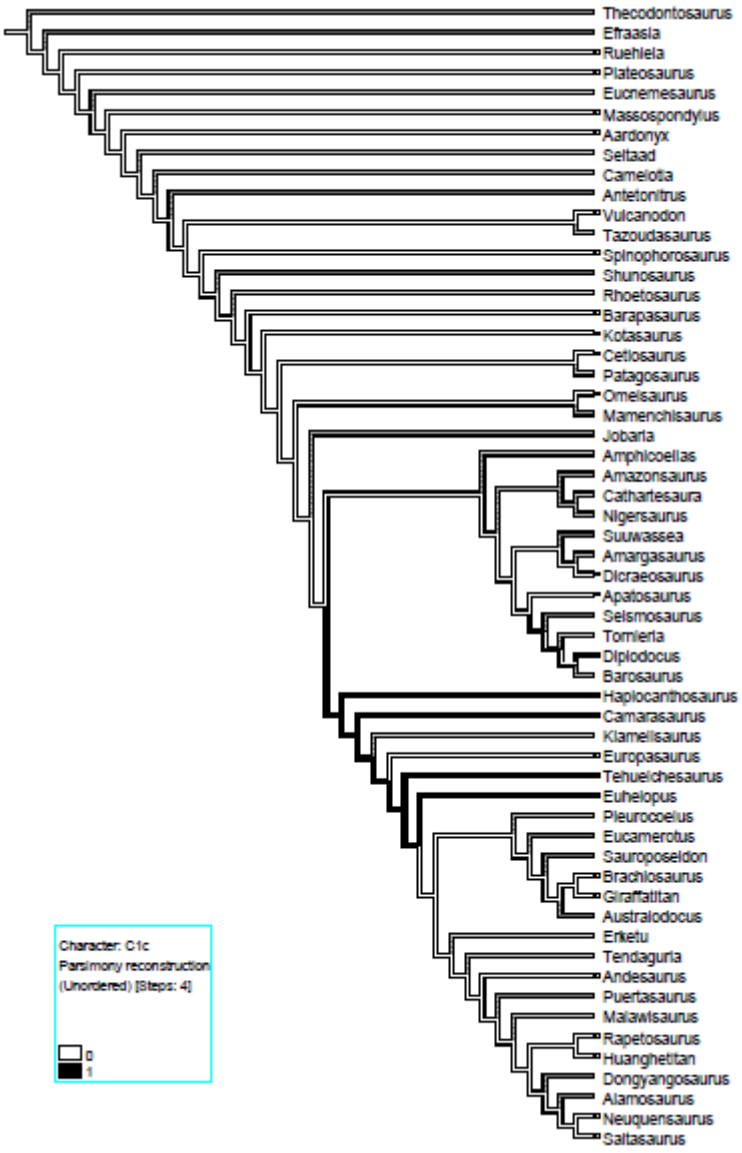

Figure 41e. Reconstruction of character ‘C1c’ (sacral) on the 61 pneumatically studied taxa, placed in a phylogeny based on ‘Carballido & Sander (2014)’. Grey branches indicate ‘unknown’ data.

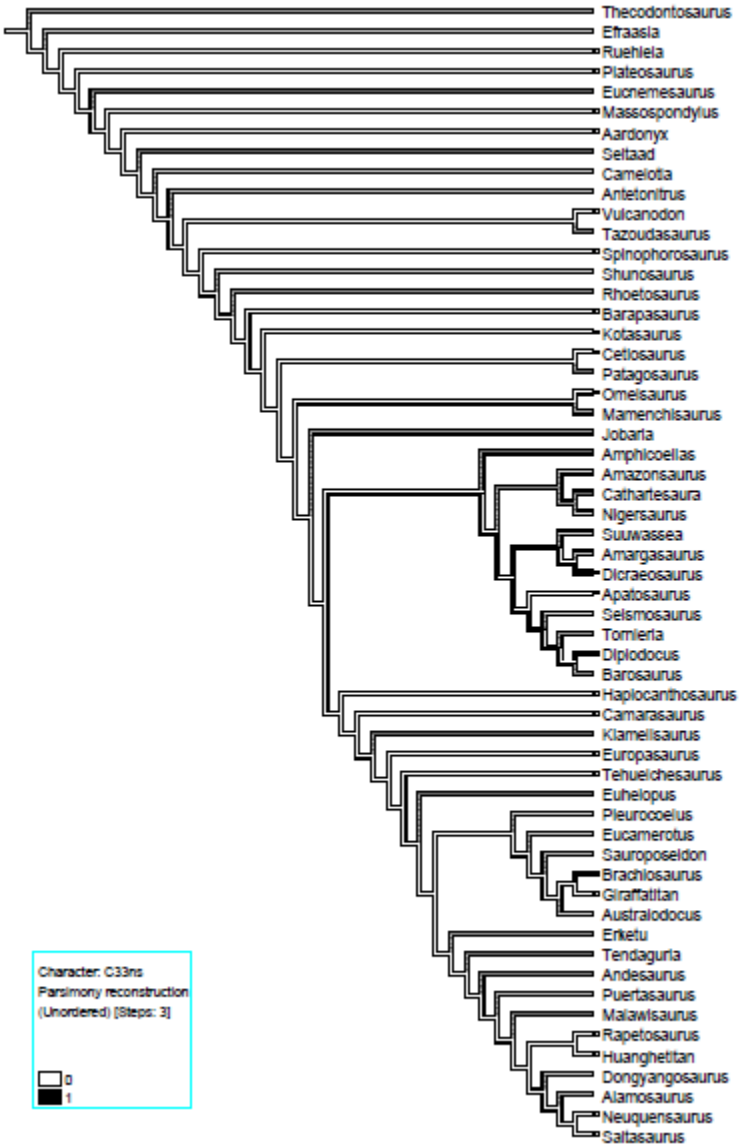

Figure 41f. Reconstruction of character ‘C33ns’ (sacral) on the 61 pneumatically studied taxa, placed in a phylogeny based on ‘Carballido & Sander (2014)’. Grey branches indicate ‘unknown’ data.

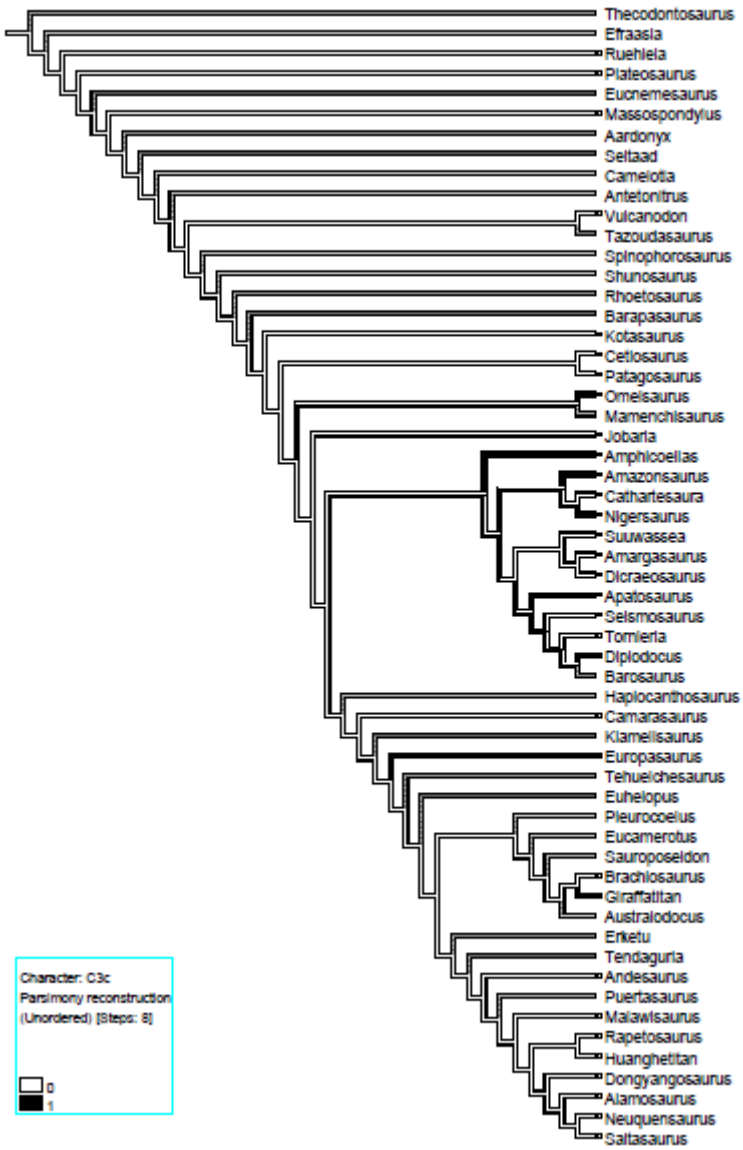

Figure 41g. Reconstruction of character ‘C3c’ (caudal) on the 61 pneumatically studied taxa, placed in a phylogeny based on ‘Carballido & Sander (2014)’. Grey branches indicate ‘unknown’ data.

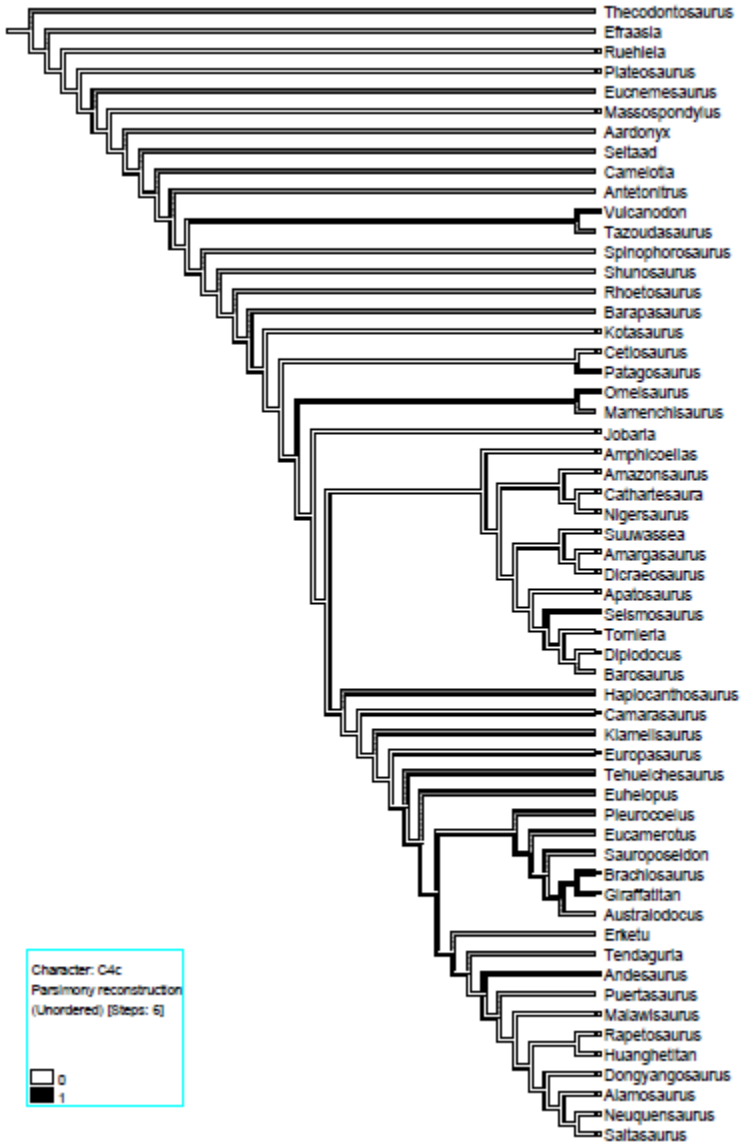

Figure 41h. Reconstruction of character ‘C4c’ (caudal) on the 61 pneumatically studied taxa, placed in a phylogeny based on ‘Carballido & Sander (2014)’. Grey branches indicate ‘unknown’ data.

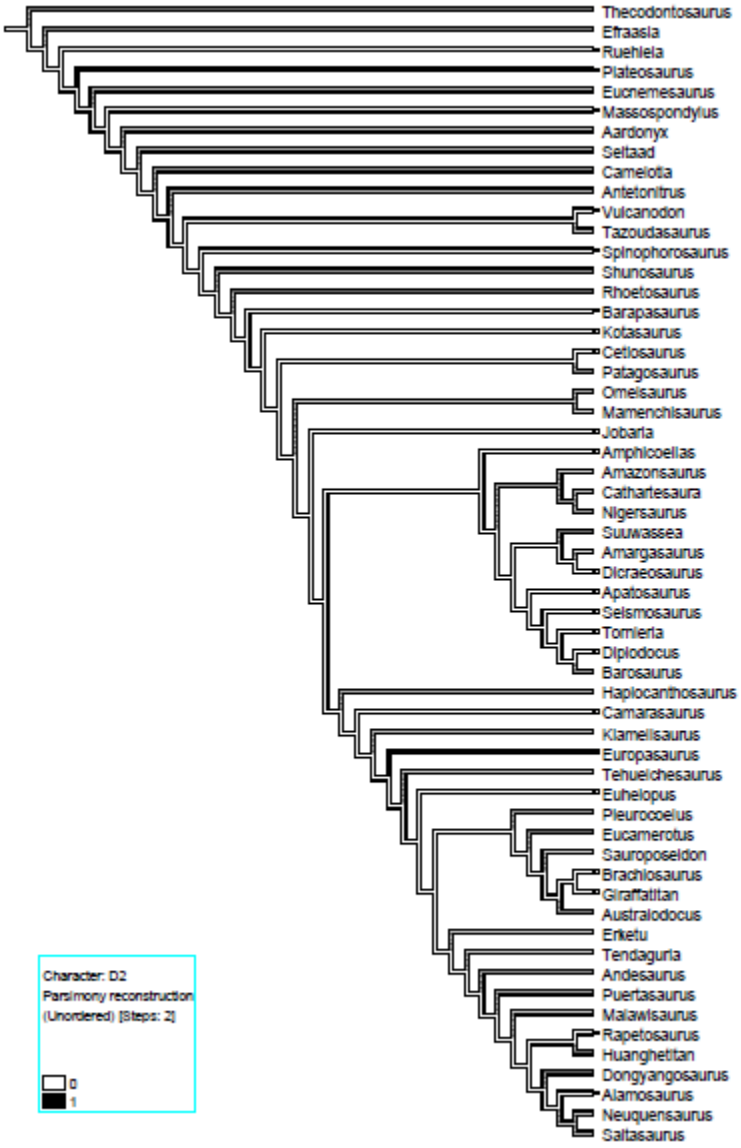

Figure 41i. Reconstruction of character ‘D2’ (pelvic) on the 61 pneumatically studied taxa, placed in a phylogeny based on ‘Carballido & Sander (2014)’. Grey branches indicate ‘unknown’ data.

R Code in *RStudio*

```
# Download R studio from:
# https://www.rstudio.com/products/RStudio/
# Install and load the necessary packages
# Any additional packages can be installed using the "install.packages()" command

library(ape)
library(geiger)
library(paleotree)
library(caper)
library(strap)
library(phytools)
library(data.table)

setwd("C:/Users/Naomi/Desktop/R phylogenetics/C-S")

# Load the tree in .tre (Newick) format
tree<-read.tree("my61sauropods R tree Newick.tre")

# Plot the phylogeny inside R
plot.phylo(tree, cex = 0.5)
# read the character data
sauropods<-read.csv("Sauropod_data_revisedcsv", header=TRUE, sep=";",
row.names=1)

#####################
# Tip-date phylogeny
#####################
```

```
# Separate FAD from sauropods


FAD_LAD<-as.matrix(sauropods[,c(1,2)])

# Assign row names to FAD

row.names(FAD_LAD)<-row.names(sauropods)

row.names(FAD_LAD)

## view dates

FAD_LAD


# run the tip-date estimate routine & create multitree

mbltree<-timePaleoPhy(tree, FAD_LAD, type="mbl", vartime=1,
dateTreatment='randObs', add.term=T,  randres=T, ntrees=25)


#plot tree from multitree

plot.phylo(mbltree[[6]])


write.tree(mbltree, file="multitree.tre")


#################################

#Ancestral state reconstruction

#################################


#First separate out the discrete characters from your data set in to separate objects:

C1c_CV<-sauropods[,10]


# Now run an ancestral state reconstruction the character data

# This uses the 10th iteration in the dated multitree object generated above

asrC1c_CV<-ace(C1c_CV, mbltree[[10]], type="discrete", method="ML", CI=TRUE,
model="ER")
```

```
# Next, tabulate the probabilities of each character state at each node

tableC1c_CV<-asrC1c_CV$lik.anc


# Now to plot the results. First, run the following to find node numbers:

plotTree(mbltree[[1]], node.numbers=T)


# Identify the node of interest and enter it's number here:

node_number<-62


# Now run the following to generate a pie-chart of character state probability

# Note that the colours are presented in the same order as the column headings in the tables: Grey=? White=0 Black=1

pie(tableC8c_CV[node_number-61,], labels="", main=NULL, col=c("Grey", "White", "Black"))

# You can now add the pie charts to the nodes of interest using an image processor

#Same procedure for character C8c_CV

C8c_CV<-sauropods[,11]

asrC8c_CV<-ace(C8c_CV, mbltree[[10]], type="discrete", method="ML", CI=TRUE, model="ER")

tableC8c_CV<-asrC8c_CV$lik.anc

plotTree(mbltree[[1]], node.numbers=T)

node_number<-62

pie(tableC8c_CV[node_number-61,], labels="", main=NULL, col=c("Grey", "White", "Black"))

##################################

# Phylogenetic regression

##################################

# read in the data set again, but this time do not set the row names:

sauropods<-read.table("Sauropod_data_table.csv", sep=";", header=TRUE)
```

```
# run the phylogenetic correction on the data, using one iteration of the multitree
pnusize <- comparative.data(mbltree[[10]], sauropods, Taxon, vcv=TRUE, vcv.dim=3)

# now run the regression analysis
stat1 <- pgls(Length ~ PDI_total, data=pnusize, lambda='ML', delta='ML')
# finally, return the output of the analysis
summary(stat1)

#Same procedure for the remaining correlations
stat2 <- pgls(Mass ~ PDI_total, data=pnusize, lambda='ML', delta='ML')
summary(stat2)
stat3 <- pgls(Length ~ PDI_cerv, data=pnusize, lambda='ML', delta='ML')
summary(stat3)
stat4 <- pgls(Mass ~ PDI_cerv, data=pnusize, lambda='ML', delta='ML')
summary(stat4)
stat5 <- pgls(Length ~ PDI_dorc, data=pnusize, lambda='ML', delta='ML')
summary(stat5)
stat6 <- pgls(Mass ~ PDI_dorc, data=pnusize, lambda='ML', delta='ML')
summary(stat6)
stat7 <- pgls(Length ~ PDI_sacr, data=pnusize, lambda='ML', delta='ML')
summary(stat7)
stat8 <- pgls(Mass ~ PDI_sacr, data=pnusize, lambda='ML', delta='ML')
summary(stat8)
stat9 <- pgls(Length ~ PDI_caud, data=pnusize, lambda='ML', delta='ML')
summary(stat9)
stat10 <- pgls(Mass ~ PDI_caud, data=pnusize, lambda='ML', delta='ML')
summary(stat10)
stat11 <- pgls(neckl ~ PDI_cerv, data=pnusize, lambda='ML', delta='ML')
```

```
summary(stat11)
stat12 <- pgls(trunkl ~ PDI_dorc, data=pnusize, lambda='ML', delta='ML')
summary(stat12)
stat13 <- pgls(taill ~ PDI_caud, data=pnusize, lambda='ML', delta='ML')
summary(stat13)
stat14 <- pgls(FL ~ PDI_total, data=pnusize, lambda='ML', delta='ML')
summary(stat14)
stat15 <- pgls(FAD ~ PDI_total, data=pnusize, lambda='ML', delta='ML')
summary(stat15)

##################################
# Model fitting
##################################
# Create a new data matrix containing the continuous data from the data set
character_data<-as.matrix(sauropods[,10])

# Assign this single column with row names
row.names(character_data)<-row.names(sauropods)

# Fit the data to the following models
brownian_m<-fitContinuous(mbltree[[10]], character_data, model="BM")
stasis<-fitContinuous(mbltree[[10]], character_data, model="white")
early_burst<-fitContinuous(mbltree[[10]], character_data, model="EB")
directional_trend<-fitContinuous(mbltree[[10]], character_data, model="trend")
ornstein_uhlenbeck<-fitContinuous(mbltree[[10]], character_data, model="OU")

# compute the output AICC scores in to Akaike weights
akaike_scores<-c(brownian_m$opt$aicc, stasis$opt$aicc, early_burst$opt$aicc,
directional_trend$opt$aicc, ornstein_uhlenbeck$opt$aicc)
```

```
names(akaike_scores)<-c("BM","Stasis","Early Burst","Trend","OU")

akaike_weights<-aicw(akaike_scores)
```

List of removed vertebral pneumaticity characters from the original matrices

McPhee et al. (2014) – Yates et al. (2009); Both used the characters from Yates (2007)

122. Shallow, dorsally facing fossa on the atlantal neurapophysis bordered by a dorsally everted lateral margin: absent (0) or present (1) (Yates and Kitching 2003).

129. Dorsal excavation of the cervical parapophyses: absent (0) or present (1) (Upchurch 1998).

147. Lateral surfaces of the dorsal centra: with at most vague, shallow depressions (0), with deep fossae that approach the midline (1), or with invasive, sharp-rimmed pleurocoels (2) (Gauthier 1986). Ordered.

148. Oblique ridge dividing pleural fossa of cervical vertebrae: absent (0) or present (1) (Wilson and Sereno 1998).

152. Laminae bounding triangular infradiapophyseal fossae (chonae) on dorsal neural arches: absent (0) or present (1) (Wilson 1999).

158. Prezygodiapophyseal lamina and associated anterior triangular fossa (chonos): present on all dorsals (0) or absent in mid-dorsals (1) (Yates 2003b).

161. Accessory lamina dividing posterior chonos from postzygapophysis: absent (0) or present (1).

162. Lateral pneumatic fenestra in middle chonos of middle and posterior dorsal vertebrae opening into neural cavity: absent (0) or present (1) (Wilson and Sereno 1998).

D'Emic (2012)

17. Presacral vertebrae, pneumatopores in centra (pleurocoels): absent (0); present (1). (Wilson, 2002.)

18. Presacral neural arch bone texture: camerate, with a few, large cavities (0); spongy, with centimetre-scale internal cells and walls, 'semicamellate' (Wedel et al., 2000b) (1); camellate to somphospondylous, with subcentimetre-scale cells and walls (2). (Wilson, 2002.)

21. Cervical pneumatopores (pleurocoels), shape: complex, divided by bony septa (0); simple, undivided (1). (Wilson, 2002.)

56. Anterior and middle caudal vertebrae, blind fossae in lateral centrum: absent (0); present, often sporadically along the vertebral series (1).

63. Dorsal ribs, proximal pneumatocoels: absent (0); present (1). (Wilson & Sereno, 1998).

Whitlock (2011)

76. Presacral bone texture: solid (0); spongy, with large internal cells (camellate) (1).

77. Cervical pneumatopores (pleurocoels): absent (0); present (1).

81. Cervical vertebrae, pneumatization of lateral surface of centra: large, divided pleurocoel over approximately half of centrum (0); reduced, large fossa but sharp-bordered coel, if present, restricted to area above parapophysis (1).

82. Cervical vertebrae, pleurocoel: undivided (0); with lamina dividing pleurocoel (1).

83. Cervical vertebrae, second lateral pneumatic fossa: absent (0); shallow, anteroposteriorly elongate fossa present, posteroventral to pleurocoel (1).

85. Atlantal neural arch: without foramen (0); with foramen (1).

88. Anterior cervical vertebrae, pleurocoel extending onto dorsal surface of parapophysis: absent (0); present (1).

89. Anterior cervicals, paired pneumatic fossae on ventral surface: absent (0); present (1).

95. Mid- and posterior cervical vertebrae, pleurocoel extending onto dorsal surface of parapophysis: present (0); absent (1).

103. Dorsal pneumatopores (pleurocoels): present (0); absent (1).

106. Dorsal neural arches, paired, subdivided pneumatic chambers dorsolateral to neural canal: absent (0), present (1).

111. Mid- and posterior dorsal vertebrae, lateral pleurocoels present in centra: absent (0); present (1).

122. Caudal neural spines, elliptical depression between spinodiapophyseal lamina and postspinal lamina on lateral neural spine: absent (0); present (1).

133. Anterior caudal centra, ventral surface: without irregularly placed foramina (0); irregular foramina present on some anterior caudals (1).

134. Anterior caudal centra, pneumatopores (pleurocoels): absent (0); present (1).

Carballido & Sander (2014)

114. Cervical centra, pleurocoels: absent (0); present with well-defined anterior, dorsal, and ventral edges, but not the posterior one (1); present, with well-defined edges; present but very reduced in size (3). (Carballido et al., in press)

115. Cervical centra, pleurocoels: singles without division (0); with a well defined anterior excavation and a posterior smooth fossa (1); divided by a bone septum, resulting in an anterior and a posterior lateral excavation (2); divided in three or more lateral excavations, resulting in a complex morphology (3); with a well-defined anterior excavation and a posterior smooth fossa (Modified from Salgado et al., 1997; Wilson, 2002; Harris, 2006)

120. Cervical centra, internal pneumaticity: absent (0); present with singles and wide cavities (1); present, with several small and complex internal cavities (2). (Modified from Carballido et al., 2011)

124. Middle cervical vertebrae, lateral fossae on the prezygapophysis process: absent (0); present (1). (Harris, 2006).

135. Dorsal centra, pleurocoels: absent (0); present (1). (Wilson, 2002:ch. 78; Upchurch et al. 2004:128)

139. Dorsal centra, pneumatic structures: absent, dorsal centra with solid internal structure (0); present, dorsal centra with simple and big air spaces (1); present, dorsal centra with small and complex air spaces (2). (Modified from Carballido et al., 2011)

144. Dorsal vertebrae with single neural spines, middle single fossa projected throughout the midline of the neural spine: present (0); absent (1). (Carballido et al., in press)

145. Dorsal vertebrae with single neural spines, middle single fossa, projected through the midline of the neural spine: relatively wide median simple fossa (0); a thin median simple fossa (1); extremely reduced median simple fossa (2). (Carballido et al., in press)

147. Anterior and middle dorsal centra, pleurocoels: have rounded caudal margins (0); have tapering, acute caudal margins (1). (Salgado et al., 1997; Upchurch, 1998:ch. 06; Upchurch et al., 2004:ca 127)

179. Dorsal ribs, proximal pneumatopores: absent (0); present (1). (Wilson, 2002:ch. 141)

186. Pleurocoels in the lateral surfaces of sacral centra: absent (0); present (1). (Upchurch et al., 2004:ch. 165)

194. Anterior caudal centra, pleurocoels: absent (0); present (1). (Wilson, 2002:ch. 119)

List of uninformative characters from the composite pneumatic examined matrices

McPhee et al. (2014) – Yates et al. (2009)

Uninformative characters (26): **3** [Relative height of the rostrum at the posterior margin of the naris: more than (0), or less than (1), 0Æ6 of the height of the skull at the middle of the orbit (Langer 2004)]**, 9** [Posteromedial process of the premaxilla: absent (0) or present (1) (Rauhut 2003a)]**, 35** [Arrangement of lateral maxillary neurovascular foramina: linear (0) or irregular (1) (modified from Sereno 1999)]**, 48** [Jugal-lachrymal relationship: lachrymal overlapping lateral surface of jugal or abutting it dorsally (0), or jugal overlapping lachrymal laterally (1) (Sereno et al. 1993)]**, 51** [Dorsal process of the anterior jugal: present (0) or absent (1) (modified from Rauhut 2003a)]**, 56** [Postfrontal bone: present (0) or absent (1) (Sereno et al. 1993)]**, 70** [Exposure of the lateral surface of the quadrate head: absent, covered by lateral sheet of the squamosal (0) or present (1) (Sereno et al. 1993)]**, 77** [Orientation of the paroccipital processes in occipital view: slightly dorsolaterally directed to horizontal (0) or ventrolaterally directed (1) (Rauhut 2003a)]**, 79** [Size of the post-temporal fenestra: large fenestra (0) or a small hole that is much less than half

the depth of the paroccipital process (1)]**, 80** [Exit of the mid-cerebral vein: through trigeminal foramen (0) or through a separate foramen anterodorsal to trigeminal foramen (1) (Rauhut 2003a).]**,127** [Length of the anterior cervical centra (cervicals 3–5): no more than (0), or greater than (1), the length of the axial centrum.]**, 140** [Shape of cervical rib shafts: short and posteroventrally directed (0) or longer than the length of their centra and extending parallel to cervical column (1) (Sereno 1999)]**,182** [Posterior and anterior expansion of the transverse processes of the first and second primordial sacral vertebrae, respectively, partly roofing the intercostal space: absent (0) or present (1) (Langer 2004)]**, 206** [Shape of the deltopectoral crest: subtriangular (0) or subrectangular (1) (Gauthier 1986)]**, 221** [Ossification of the fifth distal carpal: present (0) or absent (1)]**, 241** [Shape of the unguals of manual digits two and three: straight (0), or strongly curved with tips projecting well below flexor margin of proximal articular surface (1) (Sereno et al. 1993).]**, 271** [Shape of distal ischium: broad and plate-like, not distinct from obturator region (0) or with a discrete rod-like distal shaft (1)]**, 287** [Projection of the lesser trochanter: just a scar upon the femoral surface (0) or a raised process (1).]**, 303** [Proximal end of tibia with a flange of bone that contacts the fibula: absent (0) or present (1) (Gauthier 1986)]**, 319** [Shape of the ascending process of the astragalus: anteroposteriorly deeper than transversely wide (0) or transversely wider than anteroposteriorly deep (1).]**, 366** [C33ns-foramen in neural sacral spine or '?']**, 367** [C3c-foramen in caudal centrum or '?']**, 368** [C3c-fossa in caudal centrum] or '?'**, 370** [D2-foramen in ischium or '?']**, 371** [D11-foramen in ilium or '?']**, 372** [D20-foramen in pubis or '?']**.**

D'Emic (2012) - Whitlock (2011)

Uninformative characters (17): **118** [D'Emic's: ? /Whitlock's: Dorsal neural spine (not including arch), height: less than two times centrum length (0); two times centrum length (1); four times centrum length (2)], **136** [D'Emic's: ? /Whitlock's: Anterior caudal vertebrae, anterior face shape: cylindrical (0); quadrangular (1)], **138** [D'Emic's: ? /Whitlock's: Anterior caudal neural spines, sprl: absent (0); present, extending onto lateral aspect of neural spine (1)], **139** [D'Emic's: ? /Whitlock's: Anterior caudal neural spines, shape: single (0); slightly bifurcate anteriorly (1)], **144** [D'Emic's: ? /Whitlock's: Anterior and mid-caudal centra, ventral longitudinal hollow: absent (0); present (1)], **145** [D'Emic's: ? /Whitlock's: Mid-caudal vertebrae, ratio of centrum length to height: less than 2 : 1 (0); greater than or equal to 2 : 1 (1)], **159** [D'Emic's: ? /Whitlock's: Scapular glenoid, orientation: relatively flat or laterally facing (0); strongly bevelled medially (1)], **161** [D'Emic's: ? /Whitlock's: Humerus, midshaft cross-section, shape: circular, major and minor axes subequal (0); elliptical, major axis twice width of minor axis (1)], **162** [D'Emic's: ? /Whitlock's: Humerus, pronounced proximolateral corner: absent (0); present (1)], **166** [D'Emic's: ? /Whitlock's: Metacarpal I, length: shorter than IV (0); longer than IV (1)], **167** [D'Emic's: ? /Whitlock's: Carpus, number of carpal bones: more than two (0); two or fewer (1)], **169** [D'Emic's: ? /Whitlock's: Pubis, ambiens process development: small, confluent with anterior margin of pubis (0); prominent, projecting anteriorly (1)], **170** [D'Emic's: ? /Whitlock's: Pubis, length of puboischial contact: one-third total length of pubis (0); one-half total length of pubis (1)], **173** [D'Emic's: ? / Whitlock's: Ischium, iliac peduncle: iliac peduncle straight or widening in smooth curve distally (0); narrow, with distinct 'neck' (1)], **183** [D2-foramen in ischium], **184** [D11-foramen in ilium], **185** [D20-foramen in pubis].

Carballido & Sander (2014)

Uninformative characters (17): Uninformative characters and positions after removal of pneumaticity characters: **62** [Palatine, lateral ramus shape: plate-shaped (long maxillary contact) (0); rod-shaped (narrow maxillary contact) (1). (Wilson, 2002:ch. 40)], **80** [Occipital region of skull, shape: anteroposteriorly deep, paroccipital processes oriented posterolaterally (0); flat, paroccipital processes oriented transversely (1). (Wilson, 2002:ch. 54)], **92** [Splenial posterodorsal process: present, approaching margin of adductor chamber (0); absent (1). (Wilson, 2002:ch. 63)], **93** [Coronoid, size: extending to dorsal margin of jaw (0); reduced, not extending dorsal to splenial (1); absent (2). (Wilson, 2002:ch. 64)], **98** [Lateral plate: absent (0); present (1). (Upchurch et al., 2004:ch. 9)], **104** [Enamel surface texture: smooth (0); wrinkled (1). (Wilson, 2002:ch.71)], **169** – 9 positions (114-…-147) -> **160** [Middle and posterior dorsal neural arches, prezygoparapophyseal lamina (PRPL): absent (0); present (1). (Wilson, 2002:ch. 97)], **173** - 9 positions (114-…-147) -> **164** [Middle and posterior dorsal vertebrae, spinodiapophyseal lamina (SPDL): absent (0); present (1). (Upchurch et al., 2004:ch. 157)], **188** – 11 positions (114-…-186) -> **177** [Cervical ribs, distal shafts of longest cervical ribs: are elongate and form overlapping bundles (0); are short and do not project beyond the caudal end of the centrum to which they are attached (1). (Wilson, 2002:ch. 140)], **209** – 12 positions (114-…194) -> **197** [Anterior and middle caudal vertebrae, triangular lateral process on the neural spine: absent (0); present (1). (Whitlock, 2011:ch. 123)], **215** – 12 positions (114-…194) -> **203** [Anterior caudal vertebrae, hyposphene ridge: absent (0); present (1). (Upchurch et al., 2004:ch. 187)], **238** – 12 positions (114-…194) -> **226** [Chevron haemal canal, depth: short, approximately 25% (0); or long, approximately 50% chevron length (1). (Wilson, 2002:ch. 146)], **266** – 12 positions (114-…194) -> **254** [Humeral deltopectoral crest, shape: relatively narrow throughout length (0); markedly expanded distally (1). (Wilson, 2002:ch.161)], **300** – 12 positions (114-…194) -> **288** [Puboischial contact, length: approximately one third total length of pubis (0); one-half total length of pubis (1). (Wilson, 2002:ch. 191)], **338** – 12 positions (114-…194) -> **326** [Metatarsal I distal condyle, transverse axis orientation: perpendicular to (0); angled dorsomedially to axis of shaft (1). (Wilson, 2002:ch. 219)], **339** – 12 positions (114-…194) -> **327** [Metatarsal I distal condyle, posterolateral projection: absent (0); present (1). (Wilson, 2002:ch. 220)], **340** – 12 positions (114-…194) -> **328** [Metatarsal I, minimum shaft width: less than that of metatarsals IIIV (0); or greater than that of metatarsals IIIV (1). (Wilson, 2002:ch. 221)]